



Kanungnuch Keawsupsak

**Enhancing Flame Retardancy
of Polymer Nanocomposites**

A Thesis Presented for the Degree of Doctor of Philosophy

2021

Enhancing Flame Retardancy of Polymer Nanocomposites

Kanungnuch Keawsupsak

**A thesis submitted in fulfillment of the requirements for
the Degree of Doctor of Philosophy**

Department of Materials Science and Engineering

Faculty of Engineering

The University of Sheffield, UK

September 2021

Acknowledgements

This research could not successful the goals if it is without the assistance of many people. First of all, I would like to espress my gratitude to the Royal Thai Government for the financial support and the Thailand Institute of Scientific and Technological Research for the educational opportunity.

Further, I am deeply grateful to my supervisor, Dr. Joel Foreman, who always provided the guidance, support and encouragement throughout this research. I would like to give special thank you to Dr. Simon A Hayes, Dr. Chris Holland and Dr. Frederik Claeysens for the comments and recommendations of research.

Thanks also to member's staff at the deparment of materials science and engineering, Uninersity of Sheffield for the assistance of experimnts. The front line of the staff are Dr. Lisa Holland and Neil Hind, who support for working in the Qurral Laboratory, Dr. Oday Hussein and Sylwester Mikula, who provide the assistance of FTIR and TGA testing and Tes Monaghan who assist for using the grinder.

During my PhD study, I would like to thank to my colleagues under the Joel's PhD team: Dr. Olga A Amariutei, Dr. Roderick T Ramsdale-Capper, Dr. Ying Lan Ang and Euan Gray. They provided the valuable ideas for the research and the thesis and give the encouragement throughout the PhD study. Finally, I wish to espress a special thanks to my family and frinds for their patience and encouragement through the intense academic years.

Abstract

Layered double hydroxides (LDHs) are nano-layers materials used as fillers for epoxy resins to enhance fire resistant performance. The LDHs were modified with four different anions based on organophosphate ester compounds, namely bis-2 ethyl hexyl phosphate (BEHP), phytate (Phy), glycerophosphate (GP) and diphenyl phosphate (DPP). All the LDHs were prepared by a co-precipitation method. For the LDHs synthesis, the decarbonation, pH, aging time and precipitating agent affected the formation of LDHs.

The layers of the modified LDHs are based on hydroxides of magnesium and aluminium. For the modification with the BEHP, GP or DPP anions, they intercalated in the interlayer spaces of LDHs. Meanwhile, the modification of LDH with the Phy anions resulted in the exfoliation of layers. The water molecules also were adsorbed on the surface of LDHs and intercalated among the metal hydroxides layers.

Afterwards, the 1 wt%, 5 wt% and 10 wt% of the pristine LDHs and the modified LDHs were incorporated into epoxy resins of diglycidyl ether of bisphenol A (DGEBA) cured with 4,4'-diamino diphenylmethane (DDM) or 4,4'-diamino diphenyl sulfone (DDS). The LDHs did not influence significantly on the mechanical properties and the interference with the polymer chains movement. However, they increased the storage modulus and the loss modulus in the glassy state of the epoxy nanocomposites. Furthermore, the modified LDHs were able to decrease the thermal decomposition temperature of epoxy resins. The increase of LDHs contents contributed to the rise of char residues.

In the DDM curing system, the loadings of modified LDHs at 5 wt% were sufficient for the stop of combustion. Meanwhile, the 5 wt% modified LDHs could delay the combustion of epoxy resins cured with DDS; however, they were not self-extinguished. It needed to load the modified LDHs at 10 wt% to provide the survived epoxy nanocomposites.

Table of Contents

Acknowledgements		i
Abstract		ii
List of Figures		vii
List of Tables		xxi
Abbreviation and Acronyms		xxxii
Chapter 1	Introduction	1
	1.1 Introduction	2
	1.2 Aim and Objectives	4
	1.3 Thesis Structure	4
Chapter 2	Background	8
	2.1 Combustion of Polymers	9
	2.2 Thermal Degradation of Epoxy Resins	11
	2.3 Flame Retardancy Mechanism of Fillers	15
	2.4 Enhancement of Flame Retardancy in Polymers	16
	2.5 Types of Flame Retardant Fillers	17
	2.6 Characterisation of Combustion Behaviour of Polymers	29
	2.7 Summary	30
Chapter 3	Literature Review	35
	3.1 Structure of LDHs	36
	3.2 Synthesis methods of LDHs	38
	3.3 Characterisation of LDHs	56
	3.4 Polymer Nanocomposites	62
	3.5 Characterisation of Burning of Fire Behaviours of Polymers	64
	3.6 LDHs for Flame Retardant Applications	67
	3.7 Overview of Flame Retardancy Efficiency of LDHs for Polymer Nanocomposites	70
	3.8 Summary	90
Chapter 4	Experimental Procedure	100
	4.1 Materials	101

	4.2 Synthesis of LDHs	102
	4.3 Particle Size Reduction of LDHs	109
	4.4 Preparation of Epoxy Resin Nanocomposites	110
	4.5 Characterisations of Prepared LDHs	113
	4.6 Characterisations of Epoxy Resin Nanocomposites	117
	4.7 Summary	124
Chapter 5	Synthesis and Characterisation of LDHs	127
	5.1 Preparation of LDHs by Co-precipitation	128
	5.2 Characterisation of Pristine LDHs Prepared by the Method of Co-precipitation	130
	5.3 Preliminary Experiment on LDH Modification with Organic Anions	151
	5.4 Characterisation of Organophosphate Ester-Based Compounds Used as Anionic Modifying Agents for LDHs	158
	5.5 Characterisation of LDHs modified with Organophosphate Ester-Based Anions	169
	5.6 Thermal stability of LDHs	191
	5.7 Structural Models of LDHs	201
	5.8 Particle sizes of LDHs	206
	5.9 Summary	210
Chapter 6	Characterisation of Epoxy Resin/LDHs Nanocomposites Cured with DDM	217
	6.1 Curing Mechanism of DGEBA/DDM	218
	6.2 Preparation of EP/LDHs Nanocomposites Cured with the DDM	219
	6.3 Effect of Mixing Procedures on Visual Characteristics and Flexural Properties of EP/DDM Nanocomposites Incorporated with LDHs	220
	6.4 Flexural Properties of EP/LDHs Nanocomposites Cured with DDM	229
	6.5 Dynamic Mechanical Properties of the Pure EP and EP/LDHs Nanocomposites in DDM Curing System	231

	6.6 Thermal Stability of Epoxy Resin/LDHs Nanocomposites Cured with DDM	246
	6.7 Combustion Behaviors of Epoxy Resin Nanocomposites Cured with DDM	263
	6.8 Summary	277
Chapter 7	Characterisation of Epoxy Resin/LDHs Nanocomposites Cured with DDS	282
	7.1 Mechanism of DDS Curing with DGEBA	283
	7.2 Visual Characteristics of EP/DDS Nanocomposites Incorporating LDHs	285
	7.3 Flexural Properties of Pure EP and EP/LDHs Nanocomposites in DDS Curing System	286
	7.4 Dynamic Mechanical Properties of the Pure EP and the EP/LDHs Nanocomposites in DDS Curing System	289
	7.5 Thermal Stability of Epoxy Resin/LDHs Nanocomposites in DDS Curing System	303
	7.6 Combustion Behaviors of Epoxy Resin Nanocomposites Cured with DDS	320
	7.7 Summary	332
Chapter 8	Conclusions and Recommendations for future Works	335
	8.1 Conclusions	336
	8.2 Future work	342
Appendix I	Flexural Behaviours of Pure Epoxy Resin and its Nanocomposites Containing the LDHs in DDM Curing System	344
Appendix II	Burning Test of Pure Epoxy Resin and its Nanocomposites Containing the LDHs in DDM Curing System	357
Appendix III	Flexural Behaviours of Pure Epoxy Resin and its Nanocomposites Containing the LDHs in DDS Curing System	365

List of Figures

Figure 2.1	Schematic diagram of polymer combustion mechanism	11
Figure 2.2	Chemical configurations of epoxy resins	12
Figure 2.3	Representatives of amine compounds employed as curing agents for epoxy resins	13
Figure 2.4	Thermal combustion of DGEBA/4,4 DDS	14
Figure 2.5	Thermal decomposition of DGEBA/DDS	15
Figure 2.6	Chemical structures of brominated flame retardants	18
Figure 2.7	Structural representatives of the organophosphorus-based compounds used as flame retardants	19
Figure 2.8	Formation of pyrophosphate structure from the condensed phosphoric acid	20
Figure 2.9	Structure of phosphorus flame retardants	20
Figure 2.10	Reaction of epoxy resin and triphenyl phosphate	21
Figure 2.11	Thermal decomposition of melamine	22
Figure 2.12	Schematic configuration of 2:1 nanolayered silicate clays	27
Figure 2.13	Schematic configuration of polymer/clay nanocomposites	28
Figure 3.1	Schematically chemical structure of brucite	36
Figure 3.2	Schematic representative of LDH	37
Figure 3.3	Schematic diagram of LDH compositions	37
Figure 3.4	Representatives of pH ranges used for LDH synthesis with various types of divalent and trivalent cations	39
Figure 3.5	Schematic mechanism of LDH formation proposed by Yang et al.	41
Figure 3.6	Schematic diagram of the phase transformation of brucite to high crystallinity of Mg/Al LDH	42
Figure 3.7	XRD patterns of Mg/Al LDHs prepared with the difference of NaOH concentrations: (a) 0.75, (b) 0.9, (c) 1.0 and (d) 1.25 M NaOH	43
Figure 3.8	XRD patterns of Mg/Al LDHs prepared by the co-precipitation with the different precipitating agents: (a) NaOH and (b) NH ₄ OH	45

Figure 3.9	Concentration of metal ions in the mixed solution with the variation of pH: Mg ²⁺ (black line) and Al ³⁺ (gray line)	46
Figure 3.10	XRD patterns of Mg/Al LDHs with the variation of pH	46
Figure 3.11	Interlamellar distance of (003) and (110) reflections for the Ni/Al LDHs synthesised in the different pH	47
Figure 3.12	Average particle size and scanning electron micrographs of synthesis Mg/Al-CO ₃ LDHs with the variation of reaction temperatures: (a) 100°C, (b) 120°C and (c) 150°C	51
Figure 3.13	TGA and DTA results of MgAl-CO ₃	53
Figure 3.14	XRD patterns of MgAl-CO ₃ calcined at different temperatures	53
Figure 3.15	Uptake of Phe into the LDH calcined at 500°C in the variation of reaction temperature: ● = 0°C, ○ = room temperature, □ = 40°C, Δ = 60°C and ◇ = 80°C	55
Figure 3.16	Size distribution of Mg/Al-CO ₃ LDH particles synthesised by the calcination and rehydration method with the difference of rehydrated time (0, 5 min, 1 h, 24 h, 5 days and 28 days)	55
Figure 3.17	X-ray diffraction patterns of synthesised LDHs in different symmetries: (a) rhombohedral, and (b) hexagonal structures	58
Figure 3.18	XRD pattern of Mg ₃ Al(OH) ₈ (CO ₃) _{0.5} ·2H ₂ O	59
Figure 3.19	XRD patterns of Mg/Al LDHs with: (a) unmodified anion, (b) dodecyl sulfate and (c) dodecyl benzene sulfonate	59
Figure 3.20	FTIR spectra of Mg/Al LDHs intercalated with different anions: (a) nitrate, (b) dodecyl sulfate and (c) dodecyl benzene sulfonate	60
Figure 3.21	Thermogram of MgAl-CO ₃ LDH	62
Figure 3.22	Experimental setup of cone calorimeter	65
Figure 3.23	Schematic diagram of LOI measurement	66
Figure 3.24	Experimental setup of the horizontal burning test	67
Figure 3.25	Experimental setup of the vertical burning test	67
Figure 3.26	Schematic thermal decomposition of Mg/Al-CO ₃	69

Figure 3.27	HRR curves of PMMA nanocomposites with incorporation of Ni/Al, Zn/Al and Co/Al LDHs in different contents: (a) 5% loading and (b) 10% loading	71
Figure 3.28	HRR curves of EVA/LDH nanocomposites with the different LDHs: (a) Mg/Al LDH and (b) Zn/Al LDH	72
Figure 3.29	TGA curves and their derivatives of pristine ABS and ABS/LDH nanocomposites	73
Figure 3.30	Values of PHRR and MAHRE of pristine PVC and their composites with addition of LDHs	74
Figure 3.31	Mass loss of EVA polymer composites analysed from the cone calorimeter	75
Figure 3.32	HRR curves of EVA/LDH nanocomposites with addition of different LDHs: (a) Mg/Al-borate and (b) Zn/Al-borate	76
Figure 3.33	Formation of char residue after the combustion test of PP/LDH composites: (a) Pure PP, (b) PP/6% Mg/Al-borate and PP/6% Zn/Al-borate	77
Figure 3.34	HRR curves of pure PP and PP/12 phr LDH-H ₂ PO ₄	78
Figure 3.35	HRR curves of neat LDPE and its nanocomposites adding the 5 phr loading of LDHs intercalated with the nitrate, DS and SA	79
Figure 3.36	Characteristics of neat epoxy resin and epoxy resin nanocomposites after the flame testing: E1 (neat epoxy resin), E2 (Epoxy resin/MPP), E3 (Epoxy resin/MPP/1 g LDH-DS) and E4 (Epoxy resin/MPP/5 g LDH-DS)	80
Figure 3.37	HRR curves of LDH-DBS, LDH-CD-DBS with low content double bonds (LDB), LDH-CD-DBS with high content double bond (HDB)	81
Figure 3.38	Schematic chemical structure of Phy	86
Figure 3.39	Flammability of the neat PP and the PP composites	87
Figure 4.1	Experimental Setup for LDH synthesis	100
Figure 4.2	The chemical structures of various organophosphate compounds employed for modification of Mg/Al LDHs:	107

	bis(2-ethyl hexyl) phosphate (BEHP), phytate (Phy), diphenyl phosphate (DPP) and β -glycerophosphate (GP)	
Figure 4.3	The schematic of attrition milling	109
Figure 4.4	The curing profile of DGEBA and DDM	111
Figure 4.5	The curing profile of DGEBA and DDS	111
Figure 4.6	The schematic diagram of mixing among DGEBA, LDH and hardener with the mechanical stirring	112
Figure 4.7	The schematic diagram of EP/LDHs nanocomposite preparation with using the solvent and the sonication.	113
Figure 4.8	The schematic diagram of the incident and scattered X-rays beam on the crystal planes of sample	114
Figure 4.9	The schematic of the three-point bending test	118
Figure 4.10	The relative diagram of the applied stress and the measured strain during dynamic mechanical testing	119
Figure 4.11	The schematic single cantilever bending mode	120
Figure 4.12	Schematic of flammability test in horizontal direction	122
Figure 4.13	Schematic of flammability test in vertical direction	122
Figure 5.1	The XRD patterns of pristine Mg/Al LDHs synthesised at 60°C for 24 h in the different aging pH	128
Figure 5.2	The comparison of XRD patterns between the LDH synthesised at pH10 and 60°C for 24 h and the PDF number 04-015-1683	131
Figure 5.3	The FTIR spectra of inorganic anion intercalated Mg/Al LDHs synthesised at 60°C for 24 h in the different aging pH	133
Figure 5.4	The XRD patterns of Mg/Al LDHs prepared at pH 9 and 60°C for 24 h in the different decarbonation process.	136
Figure 5.5	The comparison of XRD patterns between the LDH prepared by using the N ₂ and the carbonised water and the reference databases	137
Figure 5.6	The XRD patterns of the unmodified LDHs prepared by using the vacuumed oven and the rotovap	139

Figure 5.7	The XRD patterns of inorganic anion intercalated Mg/Al LDHs in the different pH precipitated using the NaOH solution	141
Figure 5.8	The XRD patterns of pristine Mg/Al LDHs in the different pH precipitated using the NH ₄ OH solution	144
Figure 5.9	The comparison of XRD patterns of the sample prepared in the NH ₄ OH at pH 7 and the reference databases	145
Figure 5.10	The XRD patterns of MgAl LDHs with the variation of aging times under the NaOH solution at pH 9 and 60°C	147
Figure 5.11	The lattice parameters of c and a of LDH samples with the variation of aging times under the NaOH solution at pH 9 and 60°C	148
Figure 5.12	The XRD patterns of Mg/Al LDHs prepared at pH 10 and 60°C with the variation of aging times	149
Figure 5.13	The XRD patterns of Mg/Al LDHs in the various aging time and the use of NH ₄ OH solution under the controlled conditions at pH10 and 60°C	150
Figure 5.14	The lattice parameters of c and a of Mg/Al LDHs prepared in the different aging times using NH ₄ OH solution.	151
Figure 5.15	The XRD patterns LDH-NO ₃ and LDH-DS prepared using without and with the decarbonation and precipitated by NaOH	153
Figure 5.16	The characteristic XRD pattern of MgAl LDH intercalated with DS in the study of Kaul et al	153
Figure 5.17	The XRD patterns of Mg/Al-DS prepared in the different precipitating agents: NaOH (red line) and NH ₄ OH (blue line)	154
Figure 5.18	The FTIR spectra of MgAl LDHs intercalated with the DS and prepared in the base solutions of NaOH and NH ₄ OH	155
Figure 5.19	The XRD patterns of Pural [®] MG70 and reference database with PDF number 04-015-1684	157
Figure 5.20	The XRD patterns of Pural [®] MG70 calcined at 500°C for 5 h and reference database with PDF number 00-004-0829	157

Figure 5.21	The XRD patterns of LDH-DS prepared by the co-precipitation and the rehydration	158
Figure 5.22	The chemical structures of organophosphate ester-based compounds used as the reactants for the anion modification of LDH: BEHP, Phy, GP and DPP.	159
Figure 5.23	The TGA curve and its derivative of BEHP reactant used as modifying agent for LDH	161
Figure 5.24	The proposed thermal decomposition mechanism of BEHP reactant	162
Figure 5.25	The TGA curve and its derivative of Phy reactant used as modifying agent for LDH	163
Figure 5.26	The proposed thermal decomposition mechanism of Phy reactant	164
Figure 5.27	The TGA curve and its derivative of GP reactant used as modifying agent for LDH	166
Figure 5.28	The proposed thermal decomposition mechanism of GP reactant	167
Figure 5.29	The TGA curve and its derivative of DPP reactant used as modifying agent for LDH	168
Figure 5.30	The proposed thermal decomposition mechanism of DPP reactant	169
Figure 5.31	The comparison of XRD patterns of LDH-NO ₃ and LDHs-BEHP without and with the decarbonation of used water and NaOH	171
Figure 5.32	The XRD patterns of the pristine LDH and LDH-BEHP prepared in the NaOH and NH ₄ OH solutions	173
Figure 5.33	The FTIR spectra of the BEHP, the pristine LDH and the BEHP intercalated LDH prepared in the NaOH and NH ₄ OH	174
Figure 5.34	The XRD patterns of LDH-BEHP prepared in the NaOH with the variation of aging time: 5h, 15h and 24h	175
Figure 5.35	The XRD patterns of LDH-BEHP prepared in the NH ₄ OH with the variation of aging time: 5 h, 15 h and 24 h	175

Figure 5.36	The c and a lattice parameters and the crystal size in c direction of LDH-BEHP prepared in the NaOH with the variation of aging time: 5h, 15h and 24h	176
Figure 5.37	The c lattice parameters and the crystal size in c direction of LDH-BEHP prepared in the NH ₄ OH with the variation of aging time: 5h, 15h and 24h	177
Figure 5.38	The XRD patterns of commercial LDH (MG70) and CMG70-BEHP prepared in NaOH without and with the decarbonisation	178
Figure 5.39	The comparison of XRD patterns of CLDH-BEHP prepared in the different base solutions	179
Figure 5.40	The XRD patterns of the pristine LDH and the LDHs-Phy without the decarbonation in the used water and NaOH in the different reaction time	180
Figure 5.41	The FTIR spectra of the phytic acid, the pristine LDH and the LDH-Phy without the decarbonisation in the used water and NaOH	181
Figure 5.42	The XRD patterns of the pristine LDH and the LDH modified with Phy in the various reaction times	183
Figure 5.43	The FTIR spectra of LDHs-Phy prepared under the conditions with carbonate and the exclusion of carbonate and maintained at pH 9 and 60°C for 24 h	184
Figure 5.44	The Chemical structure of glycine and phylalanine	184
Figure 5.45	The XRD patterns of the pristine LDH and the LDHs-Phy precipitated in the NaOH and the NH ₄ OH solutions	186
Figure 5.46	The XRD patterns of the pristine LDH and the LDH-GP prepared in the NaOH and the NH ₄ OH solutions.	187
Figure 5.47	The FTIR spectra of the pure GP, the pristine LDH and the LDH-GP	188
Figure 5.48	The XRD patterns of the pristine LDH and the LDH-DPP prepared in the NaOH and the NH ₄ OH solutions	189
Figure 5.49	The FTIR spectra of the pure DPP, the pristine LDH and the LDH-DPP	190

Figure 5.50	The TGA curve and its derivative of LDH-CO ₃	192
Figure 5.51	The TGA curve and its derivative of LDH-NO ₃	193
Figure 5.52	The TGA curves and their derivatives of the BEHP, LDH-NO ₃ and LDH-BEHP	194
Figure 5.53	The TGA curves and their derivatives of the Phy, LDH-NO ₃ and LDH-Phy	196
Figure 5.54	The TGA curves and their derivatives of the GP, LDH-NO ₃ and LDH-GP	197
Figure 5.55	The TGA curves and their derivatives of the DPP, LDH-NO ₃ and LDH-DPP	198
Figure 5.56	The TGA curves and their derivatives of the pristine LDH and the LDHs modified with BEHP, Phy, GP and DPP	199
Figure 5.57	The simulated structure of nitrate anion	202
Figure 5.58	The possible structural model of LDH-NO ₃ speculated from the molecule size of nitrate simulated by the Avogadro software and the d-spacing of LDH-NO ₃ determined by the XRD	202
Figure 5.59	The simulated structure of BEHP anion	203
Figure 5.60	The possible structural model of LDH-BEHP speculated from the molecule size of BEHP simulated by the Avogadro software and the d-spacing of LDH-BEHP determined by the XRD	203
Figure 5.61	The simulated structure of Phy anion	204
Figure 5.62	The possible structural model of LDH-Phy speculated from the molecule size of nitrate simulated by the Avogadro software and the d-spacing of LDH-Phy determined by the XRD	204
Figure 5.63	The simulated structure of GP anion	205
Figure 5.64	The possible structural model of LDH-GP speculated from the molecule size of nitrate simulated by the Avogadro software and the d-spacing of LDH-GP determined by the XRD	205
Figure 5.65	The simulated structure of DPP anion	206

Figure 5.66	The possible structural model of LDH-DPP speculated from the molecule size of nitrate simulated by the Avogadro software and the d-spacing of LDH-DPP determined by the XRD	206
Figure 5.67	The particle size distribution curves of Pural MG70 before and after the milling at the rotating speed of 250 rpm and the different milling times	208
Figure 5.68	The particle size distribution curves of MG70 milled at 400 rpm	209
Figure 6.1	Schematic curing reaction of DGEBA monomers and DDM	219
Figure 6.2	The flexural strength and flexural modulus of the neat epoxy resin cured with the DDM and the nanocomposites containing the LDH-CO ₃	223
Figure 6.3	The flexural strength and flexural modulus of the neat epoxy resin cured with the DDM and the nanocomposites containing the LDH-NO ₃	224
Figure 6.4	The flexural strength and flexural modulus of the neat epoxy resin cured with the DDM and the nanocomposites containing the LDH-BEHP	225
Figure 6.5	The flexural strength and flexural modulus of the neat epoxy resin cured with the DDM and the nanocomposites containing the LDH-Phy	226
Figure 6.6	The flexural strength and flexural modulus of the neat epoxy resin cured with the DDM and the nanocomposites containing the LDH-GP	227
Figure 6.7	The flexural strength and flexural modulus of the neat epoxy resin cured with the DDM and the nanocomposites containing the LDH-DPP	228
Figure 6.8	The flexural strengths and flexural modulus of the pure EP/DDM and its nanocomposites incorporating the different anionic-modified LDHs	229
Figure 6.9	The storage modulus, loss modulus and tan δ of the pure DGEBA/DDM	232

Figure 6.10	The storage modulus, loss modulus and $\text{Tan } \delta$ of the DGEBA/DDM and its nanocomposites containing the varied contents of LDH-CO ₃	234
Figure 6.11	The storage modulus, loss modulus and $\text{Tan } \delta$ of the DGEBA/DDM and its nanocomposites containing the varied contents of LDH-NO ₃	235
Figure 6.12	The storage modulus, loss modulus and $\text{Tan } \delta$ of the DGEBA/DDM and their nanocomposites containing the varied contents of LDH-BEHP	238
Figure 6.13	The storage modulus, loss modulus and $\text{Tan } \delta$ of the DGEBA/DDM and its nanocomposites containing the varied contents of LDH-Phy	239
Figure 6.14	The storage modulus, loss modulus and $\text{Tan } \delta$ of the DGEBA/DDM and its nanocomposites containing the varied contents of LDH-GP	240
Figure 6.15	The storage modulus, loss modulus and $\text{Tan } \delta$ of the DGEBA/DDM and its nanocomposites containing the varied contents of LDH-DPP	241
Figure 6.16	The storage modulus of the pure EP and its nanocomposites containing the 5 wt% loading volume of LDH-CO ₃ , LDH-NO ₃ , LDH-BEHP, LDH-Phy, LDH-GP and LDH-DPP in the curing system of DDM	244
Figure 6.17	The loss modulus of the pure EP and its nanocomposites containing the 5% loading volume of LDH-CO ₃ , LDH-NO ₃ , LDH-BEHP, LDH-Phy, LDH-GP and LDH-DPP in the curing system of DDM	244
Figure 6.18	The $\text{tan } \delta$ of the pure EP and its nanocomposites containing the 5% loading volume of LDH-CO ₃ , LDH-NO ₃ , LDH-BEHP, LDH-Phy, LDH-GP and LDH-DPP in the curing system of DDM	245
Figure 6.19	The TGA curves and their derivatives of the LDH-CO ₃ , pure EP/DDM and nanocomposites with adding the LDH-CO ₃ in the flowing N ₂	247

Figure 6.20	The TGA curves and their derivatives of the pure EP/DDM and its nanocomposites with adding the LDH-NO ₃ under the flowing N ₂	250
Figure 6.21	The TGA curves and derivatives of the BEHP, LDH-BEHP, pure EP/DDM and nanocomposites with adding the LDH-BEHP under N ₂ atmosphere	252
Figure 6.22	The TGA curves and derivatives of the Phy, LDH-Phy, pure EP/DDM and nanocomposites with adding the LDH-Phy under N ₂ atmosphere	253
Figure 6.23	The TGA curves and derivatives of the GP, LDH-GP, pure EP/DDM and nanocomposites with adding the LDH-GP under N ₂ atmosphere	254
Figure 6.24	The TGA curves and derivatives of the DPP, LDH-DPP, pure EP/DDM and nanocomposites with adding the LDH-DPP under N ₂ atmosphere	255
Figure 6.25	The TGA curves and their derivatives of the pure EP and the EP/LDHs nanocomposites with the different types of LDHs under N ₂	259
Figure 6.26	The TGA curves and their derivatives of the pure EP and the EP/LDHs nanocomposites with the different types of LDHs under air	261
Figure 6.27	The horizontal burning test in the K04 laboratory	265
Figure 6.28	The horizontal burning test in the Quarrell Laboratory	266
Figure 6.29	The experimental setting of vertical flammability test in the K04 laboratory	267
Figure 6.30	The digital photos of the pure DGEBA/DDM and its nanocomposites with the 5% LDHs during the UL-94 test	270
Figure 6.31	The char characteristics after the flame test of the pure DGEBA/DDM and its composites with the 5% LDHs	272
Figure 6.32	The digital photos of the pure DGEBA/DDM and its nanocomposites with the 10% LDHs during the UL-94 test	273
Figure 6.33	The char characteristics after the flame test of the the pure DGEBA/DDM and its composites with the 10% LDHs	275

Figure 7.1	Schematic curing reaction of DGEBA monomers and DDS	284
Figure 7.2	The flexural strength of the pure EP and the EP/LDHs nanocomposites cured with the DDS	287
Figure 7.3	The flexural modulus of the pure EP and the EP/LDHs nanocomposites cured with the DDS	284
Figure 7.4	The storage modulus, loss modulus and Tan δ of the pristine EP cured with the DDS or DDM	290
Figure 7.5	The storage modulus, loss modulus and Tan δ of the DGEBA/DDS and its nanocomposites containing the variation of LDH-CO ₃ contents	292
Figure 7.6	The storage modulus, loss modulus and Tan δ of the DGEBA/DDS and its nanocomposites containing the variation of LDH-NO ₃ contents	293
Figure 7.7	The storage modulus, loss modulus and Tan δ of the DGEBA/DDS and its nanocomposites containing the variation of LDH-BEHP contents	295
Figure 7.8	The storage modulus, loss modulus and Tan δ of the DGEBA/DDS and its nanocomposites containing the variation of LDH-Phy contents	296
Figure 7.9	The storage modulus, loss modulus and Tan δ of the DGEBA/DDS and its nanocomposites containing the variation of LDH-GP contents	297
Figure 7.10	The storage modulus, loss modulus and Tan δ of the DGEBA/DDS and its nanocomposites containing the variation of LDH-DPP contents	298
Figure 7.11	The storage modulus of the pure EP and its nanocomposites containing the 5 wt% loading contents of LDH-CO ₃ , LDH-NO ₃ , LDH-BEHP, LDH-Phy, LDH-GP and LDH-DPP in the curing system of DDS	301
Figure 7.12	The loss modulus of the pure EP and its nanocomposites containing the 5 wt% loading contents of LDH-CO ₃ , LDH-NO ₃ , LDH-BEHP, LDH-Phy, LDH-GP and LDH-DPP in the curing system of DDS	301

Figure 7.13	The Tan δ of the pure EP and its nanocomposites containing the 5 wt% loading contents of LDH-CO ₃ , LDH-NO ₃ , LDH-BEHP, LDH-Phy, LDH-GP and LDH-DPP in the curing system of DDS	302
Figure 7.14	The TGA and DTG curves of the pure EP cured with the DDS and DDM	304
Figure 7.15	The TGA curves and their derivatives of LDH-CO ₃ , pure EP/DDS and EP/LDH-CO ₃ nanocomposites with the variation of LDH-CO ₃ contents under N ₂ flow	306
Figure 7.16	The TGA curves and their derivatives of LDH-NO ₃ , pure EP/DDS and the EP/LDH-NO ₃ nanocomposites with the variation of LDH-NO ₃ contents under N ₂ flow	307
Figure 7.17	The TGA curves and their derivatives of BEHP reactant, LDH-BEHP, pure EP/DDS and the EP/LDH-BEHP nanocomposites with the variation of LDH-BEHP contents under N ₂ flow	309
Figure 7.18	The TGA curves and their derivatives of Phy reactant, LDH-Phy, pure EP/DDS and the EP/LDH-Phy nanocomposites with the variation of LDH-Phy contents under N ₂ flow	310
Figure 7.19	The TGA curves and their derivatives of GP reactant, LDH-GP, pure EP/DDS and the EP/LDH-GP nanocomposites with the variation of LDH-GP contents under N ₂ flow	311
Figure 7.20	The TGA curves and their derivatives of DPP reactant, LDH-DPP, pure EP/DDS and the EP/LDH-DPP nanocomposites with the variation of LDH-DPP contents under N ₂ flow	312
Figure 7.21	The TGA curves and their derivatives of the pure EP/DDS and the EP/DDS-LDHs nanocomposites containing the 5 wt% loading of the various LDHs under N ₂ atmosphere	316
Figure 7.22	The TGA curves and their derivatives of the pure EP/DDS and its nanocomposites with the 5 wt% loading of the various LDHs under air	318
Figure 7.23	The digital photos of the pure DGEBA/DDS and its nanocomposites with the 5 wt% LDHs during the UL-94 test	323

Figure 7.24	The char characteristics after the flame test of the pure DGEBA/DDS and its nanocomposites with the 5 wt% LDHs	326
Figure 7.25	The digital photos of the pure DGEBA/DDS and its nanocomposites with the 10% LDHs during the UL-94 test	328
Figure 7.26	The char characteristics after the flame test of the pure DGEBA/DDS and its nanocomposites with the 10 wt% LDHs	331

List of Tables

Table 2.1	Representatives of components in intumescent flame retardants	23
Table 3.1	Crystallite size of Mg/Al-CO ₃ LDHs prepared with the co-precipitation method at various pH	47
Table 3.2	Average crystallite size in the peaks of (006) and (110) and the particle size of Zn/Al LDHs prepared at the different pH and aging temperature	49
Table 3.3	Average crystallite size in the peaks of (006) and (110) and the particle size of Zn/Al LDHs prepared at pH 10 and 100°C in the various aging times	50
Table 3.4	Values of LOI and smoke density of EVA nanocomposites with addition of LDHs intercalated with carbonate and borate anions	75
Table 3.5	Values of LOI and time to dripping of PP/LDH-H ₂ PO ₄ nanocomposites in different contents of fillers	78
Table 3.6	Results obtained the cone calorimeter of neat LDPE and various LDPE 5 phr LDH nanocomposites	80
Table 3.7	Fire behaviours of the pure EP and the EP/LDH nanocomposites	82
Table 3.8	Flammability behavior of the PMMA nanocomposites with incorporating the Mg/Al LDHs modified by the long-chain alkyl carboxylates	83
Table 3.9	Flammability behaviours of the PS nanocomposites with incorporating the Mg/Al LDHs modified by the long-chain alkyl carboxylates	84
Table 3.10	Fire behaviours of the neat PUF and the composites with the loading of 3 pphp LDHs	85
Table 3.11	Combustion behaviours of the neat PP and the PP composites	87
Table 3.12	Combustion properties of the neat PLA and the composites	87
Table 3.13	Summary of fire retardancy performance of organic anion modified LDHs for polymers	88

Table 4.1	The summaries of the temperatures of mixing, degassing and initial curing for the curing of DGEBA resin with the DDM and the DDS	112
Table 4.2	Criteria and classification of vertical burning behaviour following by ASTM:D3801	123
Table 5.1	The XRD characteristics of the $Mg_{0.83}Al_{0.17}(CO_3)_{0.08}(OH)_2(H_2O)_{0.75}$, PDF card number 04-015-1683.	132
Table 5.2	The peak positions and the d-spacing at the (003) plain of the LDHs prepared in the different pH values	133
Table 5.3	The XRD characteristics of the $Mg_{0.73}Al_{0.27}(OH)_2(NO_3)_{0.27} \cdot 0.5H_2O$ with the PDF Number: 00-062-0583	137
Table 5.4	The 2θ positions and the d-spacing of LDH samples prepared under the decarbonated processes and the varied pH with the NaOH solution	142
Table 5.5	The comparison of Mg/Al LDH chemical formulae synthesised in this work with the previous studies	143
Table 5.6	The mass of Pural [®] MG70 before and after the calcination and their mass loss percentage	156
Table 5.7	The mass loss data of BEHP decomposition (MW of BEHP = 322.39 g/mol)	161
Table 5.8	The mass loss data of Phy decomposition (MW of Phy = 660.04 g/mol)	163
Table 5.9	The mass loss data of GP decomposition (MW of GP = 315.10 g/mol)	166
Table 5.10	The mass loss data of DPP decomposition (MW of DPP = 250.19 g/mol)	168
Table 5.11	The 2θ positions and the d-spacings of the pristine LDH and the LDHs-BEHP without and with the decarbonation of the used water and NaOH	171

Table 5.12	The summary of (003) reflections and d-spacings of the pristine LDH and the LDH-BEHP prepared in the existing and the non-existing carbonate.	178
Table 5.13	The charred yield of LDHs	200
Table 5.14	The d-spacing and gallery height of the pristine LDH and the organophosphate modified LDHs	201
Table 5.15	and after the grinding with the rotating speed of 250 rpm and the different milling times.	209
Table 5.16	The size distribution in the different total percentages and the width of the size distribution of MG70 before and after the milling at 400 rpm for 1 and 2 h	210
Table 6.1	The cut edge of EP/DDM nanocomposites incorporating the LDHs by the method of mechanical stirring	221
Table 6.2	The cross-sections of EP/DDM nanocomposites incorporating the LDHs by the method of sonication, and mechanical stirring	221
Table 6.3	The T_{β} , T_g , storage modulus at the rubbery state and cross-link density of the pure EP, EP/LDH-CO ₃ and EP/LDH-NO ₃ cured with the DDM in the different contents of LDHs	236
Table 6.4	The T_{β} , T_g and cross-link density of the pure EP and EP nanocomposites containing the BEHP, Phy, GP or DPP modified LDHs cured with the DDM in the different contents of LDHs	242
Table 6.5	The $T_{10\%}$, $T_{50\%}$, T_{max} and the residual mass at 800°C of the pure EP/DDM and its nanocomposites with adding the LDH-CO ₃ under N ₂	247
Table 6.6	The $T_{10\%}$, $T_{50\%}$, T_{max} and the residual mass at 800°C of the pure EP/DDM and its nanocomposites with adding the LDH-NO ₃ under N ₂	251
Table 6.7	The $T_{10\%}$, $T_{50\%}$, T_{max} and the residue at 800°C under N ₂ atmosphere of the pure EP/DDM and its nanocomposites containing the LDH-BEHP	252

Table 6.8	The $T_{10\%}$, $T_{50\%}$, T_{\max} and the residue at 800°C under N_2 atmosphere of the pure EP/DDM and its nanocomposites containing the LDH-Phy	253
Table 6.9	The $T_{10\%}$, $T_{50\%}$, T_{\max} and the residue at 800°C under N_2 atmosphere of the pure EP/DDM and its nanocomposites containing the LDH-GP	254
Table 6.10	The $T_{10\%}$, $T_{50\%}$, T_{\max} and the residue at 800°C under N_2 atmosphere of the pure EP/DDM and its nanocomposites containing the LDH-DPP	255
Table 6.11	The $T_{10\%}$, $T_{50\%}$, T_{\max} and residue at 800°C under N_2 of the pure EP and its nanocomposites containing the different types of LDHs at 5 wt% loading	259
Table 6.12	The $T_{10\%}$, $T_{50\%}$, T_{\max} and residue at 800°C under air of the pure EP and its nanocomposites containing the different types of LDHs at 5 wt% loading	261
Table 6.13	The combustion time and burning characteristics of the pure DGEBA/DDM and its nanocomposites incorporating the 5% wt LDHs	268
Table 6.14	Criteria and classification of vertical burning behaviour following by ASTM:D3801	272
Table 6.15	The combustion time and burning characteristics of the pure DGEBA/DDM and its nanocomposites incorporating the 10% wt LDHs	275
Table 7.1	The cross-sections of EP/DDS nanocomposites incorporating the various LDHs	285
Table 7.2	The comparison of flexural properties of pure EPs cured with different aromatic diamines	286
Table 7.3	The T_{β} , T_g , storage modulus at the rubbery state and cross-link density of the pure EP, EP/LDH- CO_3 and EP/LDH- NO_3 cured with the DDS in the different contents of LDHs	294
Table 7.4	The T_{β} , T_g and cross-link density of the pure EP and its nanocomposites containing the BEHP, Phy, GP or DPP	300

	modified LDHs cured with the DDS in the different contents of LDHs	
Table 7.5	The $T_{10\%}$, $T_{50\%}$, T_{\max} and residue at 800°C of the pure EP/DDS and its nanocomposites with the variation of LDH-CO ₃ or LDH-NO ₃ contents under N ₂ flow	308
Table 7.6	The $T_{10\%}$, $T_{50\%}$, T_{\max} and residue percentage at 800°C of the pure EP/DDS and its nanocomposites incorporating the variation contents of modified LDHs	314
Table 7.7	The thermal degradation of the pure EP/DDS and the EP/LDHs nanocomposites under N ₂ atmosphere	317
Table 7.8	The thermal oxidative degradation of the pure EP/DDS and the EP/LDHs nanocomposites under air	319
Table 7.9	The combustion time and burning characteristics of the pure DGEBA/DDS and its nanocomposites with the 5 wt % LDHs	321
Table 7.10	The combustion time and burning characteristics of the pure DGEBA/DDS and its nanocomposites incorporating the 10 wt % LDHs	327
Table I-1	The flexural strength of the pure DGEBA and its nanocomposites containing the LDH-CO ₃ in the DDM curing system prepared with the mechanical stirring	345
Table I-2	The flexural modulus of the pure DGEBA and its nanocomposites containing the LDH-CO ₃ in the DDM curing system prepared with the mechanical stirring	345
Table I-3	The flexural strength of the pure DGEBA and its nanocomposites containing the LDH-NO ₃ in the DDM curing system prepared with the mechanical stirring	346
Table I-4	The flexural modulus of the pure DGEBA and its nanocomposites containing the LDH-NO ₃ in the DDM curing system prepared with the mechanical stirring	346

Table I-5	The flexural strength of the pure DGEBA and its nanocomposites containing the LDH-BEHP in the DDM curing system prepared with the mechanical stirring	347
Table I-6	The flexural modulus of the pure DGEBA and its nanocomposites containing the LDH-BEHP in the DDM curing system prepared with the mechanical stirring	347
Table I-7	The flexural strength of the pure DGEBA and its nanocomposites containing the LDH-Phy in the DDM curing system prepared with the mechanical stirring	348
Table I-8	The flexural modulus of the pure DGEBA and its nanocomposites containing the LDH-Phy in the DDM curing system prepared with the mechanical stirring	348
Table I-9	The flexural strength of the pure DGEBA and its nanocomposites containing the LDH-GP in the DDM curing system prepared with the mechanical stirring	349
Table I-10	The flexural modulus of the pure DGEBA and its nanocomposites containing the LDH-GP in the DDM curing system prepared with the mechanical stirring	349
Table I-11	The flexural strength of the pure DGEBA and its nanocomposites containing the LDH-DPP in the DDM curing system prepared with the mechanical stirring	350
Table I-12	The flexural modulus of the pure DGEBA and its nanocomposites containing the LDH-DPP in the DDM curing system prepared with the mechanical stirring	350
Table I-13	The flexural strength of the pure DGEBA and its nanocomposites containing the LDH-CO ₃ in the DDM curing system prepared with the solvent, sonication and mechanical stirring	351
Table I-14	The flexural modulus of the pure DGEBA and its nanocomposites containing the LDH-CO ₃ in the DDM curing	351

	system prepared with the solvent, sonication and mechanical stirring	
Table I-15	The flexural strength of the pure DGEBA and its nanocomposites containing the LDH-NO ₃ in the DDM curing system prepared with the solvent, sonication and mechanical stirring	352
Table I-16	The flexural modulus of the pure DGEBA and its nanocomposites containing the LDH-NO ₃ in the DDM curing system prepared with the solvent, sonication and mechanical stirring	352
Table I-17	The flexural strength of the pure DGEBA and its nanocomposites containing the LDH-BEHP in the DDM curing system prepared with the solvent, sonication and mechanical stirring	353
Table I-18	The flexural modulus of the pure DGEBA and its nanocomposites containing the LDH-BEHP in the DDM curing system prepared with the solvent, sonication and mechanical stirring	353
Table I-19	The flexural strength of the pure DGEBA and its nanocomposites containing the LDH-Phy in the DDM curing system prepared with the solvent, sonication and mechanical stirring	354
Table I-20	The flexural modulus of the pure DGEBA and its nanocomposites containing the LDH-Phy in the DDM curing system prepared with the solvent, sonication and mechanical stirring	354
Table I-21	The flexural strength of the pure DGEBA and its nanocomposites containing the LDH-GP in the DDM curing system prepared with the solvent, sonication and mechanical stirring	355

Table I-22	The flexural modulus of the pure DGEBA and its nanocomposites containing the LDH-GP in the DDM curing system prepared with the solvent, sonication and mechanical stirring	355
Table I-23	The flexural strength of the pure DGEBA and its nanocomposites containing the LDH-DPP in the DDM curing system prepared with the solvent, sonication and mechanical stirring.	356
Table I-24	The flexural strength and flexural modulus of the pure DGEBA and its nanocomposites containing the LDH-DPP in the DDM curing system prepared with the solvent, sonication and mechanical stirring.	356
Table II-1	The combustion time and characteristics of the pure DGEBA cured with the DDM	358
Table II-2	The combustion time and characteristics of the DGEBA/5% LDH-CO ₃ cured with the DDM	358
Table II-3	The combustion time and characteristics of the DGEBA/10% LDH-CO ₃ cured with the DDM.	359
Table II-4	The combustion time and characteristics of the DGEBA/5% LDH-NO ₃ cured with the DDM	359
Table II-5	The combustion time and characteristics of the DGEBA/10% LDH-NO ₃ cured with the DDM	360
Table II-6	The combustion time and characteristics of the DGEBA/5% LDH-BEHP cured with the DDM.	360
Table II-7	The combustion time and characteristics of the DGEBA/10% LDH-BEHP cured with the DDM	361
Table II-8	The combustion time and characteristics of the DGEBA/5% LDH-Phy cured with the DDM	361
Table II-9	The combustion time and characteristics of the DGEBA/10% LDH-Phy cured with the DDM	362

Table II-10	The combustion time and characteristics of the DGEBA/5% LDH-GP cured with the DDM	362
Table II-11	The combustion time and characteristics of the DGEBA/10% LDH-GP cured with the DDM	363
Table II-12	The combustion time and characteristics of the DGEBA/5% LDH-DPP cured with the DDM	363
Table II-13	The combustion time and characteristics of the DGEBA/10% LDH-DPP cured with the DDM	364
Table III-1	The flexural strength of the pure DGEBA and its nanocomposites containing the LDH-CO ₃ in the DDM curing system prepared with the solvent, sonication and mechanical stirring	366
Table III-2	The flexural modulus of the pure DGEBA and its nanocomposites containing the LDH-CO ₃ in the DDM curing system prepared with the solvent, sonication and mechanical stirring	366
Table III-3	The flexural strength of the pure DGEBA and its nanocomposites containing the LDH-NO ₃ in the DDM curing system prepared with the solvent, sonication and mechanical stirring	367
Table III-4	The flexural modulus of the pure DGEBA and its nanocomposites containing the LDH-NO ₃ in the DDM curing system prepared with the solvent, sonication and mechanical stirring	367
Table III-5	The flexural strength of the pure DGEBA and its nanocomposites containing the LDH-BEHP in the DDS curing system prepared with the solvent, sonication and mechanical stirring	368
Table III-6	The flexural modulus of the pure DGEBA and its nanocomposites containing the LDH-BEHP in the DDS	368

	curing system prepared with the solvent, sonication and mechanical stirring	
Table III-7	The flexural strength of the pure DGEBA and its nanocomposites containing the LDH-Phy in the DDM curing system prepared with the solvent, sonication and mechanical stirring	369
Table III-8	The flexural modulus of the pure DGEBA and its nanocomposites containing the LDH-Phy in the DDM curing system prepared with the solvent, sonication and mechanical stirring	369
Table III-9	The flexural strength and flexural modulus of the pure DGEBA and its nanocomposites containing the LDH-GP in the DDM curing system prepared with the solvent, sonication and mechanical stirring	370
Table III-10	The flexural strength and flexural modulus of the pure DGEBA and its nanocomposites containing the LDH-GP in the DDM curing system prepared with the solvent, sonication and mechanical stirring	370
Table III-11	The flexural strength of the pure DGEBA and its nanocomposites containing the LDH-DPP in the DDM curing system prepared with the solvent, sonication and mechanical stirring	371
Table III-12	The flexural modulus of the pure DGEBA and its nanocomposites containing the LDH-DPP in the DDM curing system prepared with the solvent, sonication and mechanical stirring	371
Table IV-1	The combustion time and characteristics of the pure DGEBA cured with the DDS	373
Table IV-2	The combustion time and characteristics of the DGEBA/5% LDH-CO ₃ cured with the DDS	373

Table IV-3	The combustion time and characteristics of the DGEBA/10% LDH-CO ₃ cured with the DDS	374
Table IV-4	The combustion time and characteristics of the DGEBA/5% LDH-NO ₃ cured with the DDS	374
Table IV-5	The combustion time and characteristics of the DGEBA/10% LDH-NO ₃ cured with the DDS	375
Table IV-6	The combustion time and characteristics of the DGEBA/5% LDH-BEHP cured with the DDS	375
Table IV-7	The combustion time and characteristics of the DGEBA/10% LDH-BEHP cured with the DDS	376
Table IV-8	The combustion time and characteristics of the DGEBA/5% LDH-Phy cured with the DDS	376
Table IV-9	The combustion time and characteristics of the DGEBA/10% LDH-Phy cured with the DDS	377
Table IV-10	The combustion time and characteristics of the DGEBA/5% LDH-GP cured with the DDS	377
Table IV-11	The combustion time and characteristics of the DGEBA/10% LDH-GP cured with the DDS	378
Table IV-12	The combustion time and characteristics of the DGEBA/5% LDH-DPP cured with the DDS	378
Table IV-13	The combustion time and characteristics of the DGEBA/10% LDH-DPP cured with the DDS	379

Abbreviations and Acronyms

A	Anions
AAPP	Ammonium alcohol polyvinyl phosphate
ABS	acrylonitrile-butadiene-styrene
Al(NO ₃) ₃	Aluminium nitrate
Al ₂ O ₃	Aluminium oxide
Al ³⁺	Aluminium ion
APP	Ammonium polyphosphate
ATH	Aluminium trihydroxide, Al(OH) ₃
a ₀	Distance between adjacent cation centre in the x-axis
Å	Angstrom
BEHP	Bis(2-ethylhexyl) phosphate (BEHP)
BDP	bisphenol A bis(diphenyl phosphate)
Br ⁻	Bromide ion
b ₀	Distance between adjacent cation centre in the y-axis
Ca	Calcium
Ca ²⁺	Calcium ion
CD	dextrin
CEPPA	2-carboxylethyl-phenyl-phosphinic acid
CH ₃ (CH ₂) _n COO ⁻	Linear-chain alkyl carboxylates
Cl ⁻	Chloride ion
CNT	Carbon nanotube
Co	Cobalt
CO	Carbon monoxide
CO ₂	Carbon dioxide
CO ₃ ²⁻	Carbonate ion
CrO ₄ ²⁻	Chromate ion
Cu	Copper
c ₀	Length from the middle of one layer to the neighbouring layer (basal spacing)
C ₆₀	Fullerene
°C	Degree Celsius

-CO-	Carbonyl
-COOH	Carboxyl
DBS	Dodecyl benzene sulfonate
DCPDDO	Dicyclopentadiene dioxide
DDM	Diamino diphenyl methane
DDS	4,4-diamino diphenyl sulfone
DGEBA	Bisphenol A diglycidyl ether
DiDOPO	10-dihydro-9-oxa-10-phosphaphenanthrene-10-oxide
DP	Diglycidyl phthalate
DPHPA	N-(2-(5,5-dimethyl-1,3,2-dioxaphosphinyl-2-ylamino)-N-hexylformamide-2-propenyl acid
DPP	Diphenyl phosphate
DOPO	9,10-dihydro-9-oxa-10-phosphaphenanthrene-10-oxide
DS	Dodecyl sulfate
DTA	Differential thermal analyser
d_{hkl}	The d-spacing of the Miller indices (h, k and l)
EP	Epoxy resin
EVA	Ethyl-vinyl acetate
FR	Flame retardants
FTIR	Fourier transformed infrared spectroscopy
F ⁻	Fluoride ion
GP	Glycerophosphate
GO	Graphene oxide
h	Hour
HBCD	Hexabromocyclododecane
HBr	Hydrogen bromide
HCl	Hydrogen chloride
HPO [·]	Hydrogen peroxide radical
HPO ₄ ²⁻	Hydrogen phosphate ion
HRC	Heat release capacity
HRR	Heat release rate
HX	Hydrogen halides

H ₂ O	Water
H ₂ PO ₄	Dihydrogen phosphate
H [·]	Hydrogen free radical
kg	Kilogram
kJ	Kilojoule
kW	kilowatt
L	Litre or a burned length
LDH	Layered double hydroxide
LDH-AAPP	Layered double hydroxide intercalated with AAPP anions
LDH-BA	Layered double hydroxide intercalated with BA anions
LDH-BEHP	Layered double hydroxide intercalated with BEHP anions
LDH-CD	Layered double hydroxide intercalated with CD anions
LDH-CD-DBS-Phy	Layered double hydroxide intercalated with multifunctional anions of CD, DBS and Phy
LDH-CD-DBS-T	Layered double hydroxide intercalated with multifunctional anions of CD, DBS and T
LDH-CEPPA	Layered double hydroxide intercalated with CEPPA
LDH-CO ₃	Layered double hydroxide intercalated with carbonate anions
LDH-DBS	Layered double hydroxide intercalated with DBS anions
LDH-DPHPA	Layered double hydroxide intercalated with DPHPA anions
LDH-DPP	Layered double hydroxide modified with DPP anions
LDH-DOPO	Layered double hydroxide modified with DOPO anions
LDH-DS	Layered double hydroxide modified with DS anions
LDH-SA	Layered double hydroxide modified with SA anions
LDH-GP	Layered double hydroxide modified with GP anions

LDH-HPO ₄	Layered double hydroxide intercalated with hydrogen phosphate anions
LDH-H ₂ PO ₄	Layered double hydroxide intercalated with dihydrogen phosphate anions
LDH-NO ₃	Layered double hydroxide intercalated with nitrate anions
LDH-Phy	Layered double hydroxide modified with Phy anions
LDH-PO ₄	Layered double hydroxide intercalated with phosphate anions
LDH-SPP	Layered double hydroxide intercalated with SPP anions
LDH-T	Layered double hydroxide intercalated with T anions
LOI	Limiting oxygen index
LDPE	Low-density polyethylene
M	Molar
MARHE	maximum average rate of heat emission
MC	Melamine cyanurate
MDH	Magnesium dihydroxide, Mg(OH) ₂
MgAl ₂ O ₄	Magnesium aluminium oxide
Mg/Al LDHs	Layered double hydroxides based on magnesium oxides and aluminium oxides
Mg(NO ₃) ₂	Magnesium nitrate
MgO	Magnesium oxide
Mg(OH) ₂	Brucite
Mg ²⁺	Magnesium ion
MG70	Commercial layered double hydroxide intercalated with carbonate anion
min	minute
MMT	Montmorillonite
mmol	Millimole
mol	Mole
MoO ₄ ²⁻	Molybdate

MPP	Melamine salt of pentaerythritol diphosphate
MWNT	Multi-walled carbon nanotube
m ²	Metre squared
M ²⁺	Divalent metal cations
M ³⁺	Trivalent metal cations
4MgCO ₃ ·Mg(OH) ₂ ·4H ₂ O	Hydromagnesite
n	Valence electron of anions or diffraction order
N	Nitrogen
NaOH	Sodium hydroxide
Na ₂ CO ₃	Sodium carbonate
Na ⁺	Sodium ion
NH ₄ OH	Ammonium hydroxide
Ni	Nickel
nm	Nanometre
NO	Nitrogen oxide
NO ₂	Nitrogen dioxide
NO ₃ ⁻	Nitrate ion
N ₂	Nitrogen gas
-N-	Tertiary amine
-NH-	Secondary amine
-NH ₂	Primary amine
O ₂	Oxygen gas
OH·	Hydroxyl free radical
-OH	Hydroxyl
P	Phosphorus
PBDE	Polybrominated diphenyl ether
PER	Pentaerythritol
Phe	Phenylalanine
phr	Part per hundred
pHRR	Peak heat release rate
Phy	Phytate
PLA	Poly(lactic acid)
PMMA	Poly(methyl methacrylate)

POSS	Polyhedral oligomeric silsesquioxane
PP	Poly propylene
pphp	part per hundred parts polyol
PO·	Phosphorus oxide radical
PO ₂ ·	Phosphorus dioxide radical
PO ₄ ³⁻	Phosphate ion
PS	Polystyrene
PUF	Polyurethane foam
PVC	poly(vinyl chloride)
RDP	Resorcinol bis(diphenyl phosphate)
RP	Red phosphorus
SA	Stearate
Si	Silicon
SiO ₂	Silicon dioxide
SO ₄ ²⁻	Sulfate ion
SPP	Sodium phenyl phosphate
t	Burning time
TBBPA	Tetrabromobisphenol-A
TBPA	Tetrabromophthalate anhydride
TGA	thermogravimetric analyser
TGDDM	Tetraglycidyl diamino diphenyl methane
THR	Total heat released
TiO ₂	Titanium dioxide
T _p	Pyrolysis temperature
TOC	Time of combustion
TPP	Triphenyl phosphate
TTI	Time to ignition
V	Burning rate
XRD	X-ray diffraction
y	Amount of water in LDH structure
Zn	Zinc
Zn/Al LDHs	Layered double hydroxides based on zinc oxides and aluminium oxides

ZnO	Zinc oxide
0D nanostructure	Zero-dimensional nanostructure
1D nanostructure	One-dimensional nanostructure
2D nanostructure	Two-dimensional nanostructure
γ -AlOOH	Boehmite or Oxide-hydroxide aluminium
μm	Micrometre
λ	A wavelength of an X-ray source
θ	A detected reflection angle

Chapter 1

Introduction

1.1 Introduction

Polymer composites are multi-phase materials combining polymers and reinforcing fillers. The properties of polymer composite differ from the original polymer. The general forms of fillers employed for the reinforcement of polymers are fibres and particles. As the polymer composites possess excellent strength, fatigue resistance, vibration damping, good chemical resistance and light-weight, they have been intensively utilised in various applications in industries such as aerospace, transportation (e.g. car, train and ship) and construction [1]. However, they are low flame resistance because of the high contents of hydrocarbons in the polymeric chains. The hydrocarbon chains are easily cleavage by flame, causing rapid burning. The combustion of polymers can produce an extensive amount of flame, heat and smoke that results in harm to human health, environment and property [1, 2]. To protect serious damage resulting from the combustion of polymers, there have been attempts to enhance the flame retardancy of polymers.

Incorporating flame retardant additives into the polymer is one of the common methods used extensively to improve fire retardancy since it is not a complicated fabrication process and a low production cost [3]. Nowadays, there are several kinds of flame retardant additives such as compounds based on halogen [3, 4], phosphorus [3, 5], and nitrogen [3, 6], intumescent flame retardants [3, 7], mineral flame retardants [3, 8] and nano-flame retardants [3, 9]. The five first types of additives are the traditional flame retardants used for over a century [10]. Meanwhile, nanocomposites have been researched and developed across five decades [11].

For the first one, the halogenated compounds have been broadly employed as flame retardants due to the high level of fire retardancy efficiency at the low loading content and cheap price [12]. However, a considerable volume of smoke and corrosive gas consisting of halogen elements, e.g. HBr and HCl, are emitted during burning of halogen flame retardants. These released by-products impact on health and environmental problems. Therefore, the use of halogenated compounds has been concerned with the toxicology and the environment [3, 4]. These are crucial reasons prompting the use of non-halogenated flame retardants in the industries [4].

In the case of phosphorus and/or nitrogen-based compounds, they have high fire retardancy efficiency and are non-halogenated flame retardant additives. As there are many phosphorus compounds utilised as flame retardants, they can dominate in many industrial applications. On the other hands, some nitrogen compounds have been employed [5-7]. Another type of flame retardant used widely is a mineral filler. Metal hydroxides such as magnesium hydroxide and aluminium hydroxide represent mineral fillers that are the most commonly used type in the industry. The disadvantage of this flame retardant type is to the significant reduction of strength and toughness. Several industries have attempted to solve this issue by applying fine fillers, especially nano-sized particles [8].

In the last decades, layered double hydroxides (LDHs), two dimensional (2D) nanoparticles, have been researched rapidly to use as flame retardants fillers. The structure of LDHs comprises layered di- and trivalent metal cations and anions interacted in the interlayers [12]. Usually, the most commonly used metal cations are Mg^{2+} and Al^{3+} . Both cations exist in their hydroxide forms, similar to chemical compounds of mineral flame retardant fillers. For the applications of flame retardants, the anionic compounds can be categorised into two fundamental groups: inorganic compounds (e.g. carbonate, nitrate, borate, phosphate and dihydrogen phosphate) and organic compounds (e.g. dodecyl sulphate, stearate, cyclodextrin, bis(2-ethyl hexyl) phosphate and phytate).

From the literature on phosphorus flame retardants, the organic compounds containing phosphate ester groups were recognised as flame retardant additives [13]. Due to the diversity of compounds and active phosphate ester groups in the chemical structures, organic compounds containing phosphate esters would be selected to modify the LDHs structure. Hence, this research is interested in the modification of LDHs with four types of organophosphate ester compounds: bis(2-ethylhexyl) phosphate (BEHP), phytate (Ph), glycerophosphate (GP) and diphenyl phosphate (DPP) to enhance flame retardancy efficiency for polymers. Although the flame retardant efficiency of the BEHP and Ph-modified LDHs had been reported in a few polymers, there was no research on the epoxy resin. Meanwhile, both the GP and DPP were the novel organophosphate ester compounds used to modify LDHs. In this research, the

epoxy resin of bisphenol A diglycidyl ether (DGEBA) was used as the representative of polymers.

1.2 Aim and Objectives

The reducing flammability of polymer composites with the loading of organophosphate-modified LDHs has been published in a few articles [14-18]. Although there were studies in various polymers, they had not researched epoxy resins. This thesis aimed to enhance the flame retardancy efficiency of epoxy resin by incorporating organophosphate ester-modified LDH fillers.

There were four objectives to achieve the aim of the thesis:

- 1) To modify LDHs with different compounds containing organophosphate esters.
- 2) To analyse the characteristics of the crystalline phase, chemical structure, and thermal decomposition behaviours of synthesised LDHs.
- 3) To evaluate the flame retardancy efficiency of modified LDHs preparing epoxy resin nanocomposites
- 4) To determine the thermal behaviours and flammability of epoxy resin nanocomposites containing the modified LDHs, including visual and mechanical properties.

1.3 Thesis Structure

The dissertation is composed of eight themed chapters. The overview of each chapter follows.

Chapter 1 introduces the motivation for the enhancement of flame retardancy of polymers. The representative of polymers used for the study is epoxy resins. Besides, it provides the aim, practical objectives and thesis outline of the thesis.

Chapter 2 provides general knowledge in the combustion process of polymers, particularly to epoxy resins. The common flame-retardant fillers used for the inhibition of combustion in polymers are also described: halogenated flame retardants,

phosphorus-based flame retardants, nitrogen-based flame retardants, intumescent flame retardants, mineral flame retardants and nano-flame retardants.

Chapter 3 reviews literature regarding layered double hydroxides (LDHs), one of the intensively attractive flame-retardant fillers for polymers. The typical structure, preparation and characterisation of LDHs are explained. Then, there are reviews of flame retardancy mechanism and efficiency of LDHs in polymer nanocomposites.

Chapter 4 presents the experimental procedures for synthesising unmodified and organophosphate-modified LDHs and preparing cured epoxy resin/LDHs nanocomposites. It also describes techniques used for analysing the properties of the synthesised LDHs and the prepared resin nanocomposites.

Chapter 5 investigates the influence of synthesis parameters on the characteristics of unmodified and modified LDHs in the first part. The crystalline phases, chemical structures, and thermal behaviours of the LDHs are also discussed. Then, there are the presences of particle size of LDHs in both the before and after a grinding process. Finally, the structural models of both unmodified and modified LDHs are speculated using all the characterised results of the LDHs.

Chapter 6 compares two blending methods for the cured resin/LDHs nanocomposites: only mechanical stirring and a using of solvent, sonication, and mechanical stirring. This chapter focuses on resin curing with diamino diphenyl methane (DDM). It also investigates the effect of unmodified and modified LDHs on the visual, flexural, dynamic mechanical properties, thermal stability and flammability of the resin/LDHs nanocomposites.

Similarity, Chapter 7 investigates the effect of unmodified and modified LDHs on the resin/LDHs nanocomposites properties. In this chapter, however, the resin samples are cured with 4,4-diamino diphenyl sulfone (DDS)

Chapter 8 concludes the experimental results from the studies and gives suggestions for future works.

References

- [1] R.-M. Wang, S.-R. Zheng and Y.-P. Zheng, "Polymer Matrix Composites and Technology", Woodhead Publishing Limited, USA, 2011
- [2] M. Bar, R. Alagirusamy and A. Das, "Flame Retardant Polymer Composites", *Fiber. Polym.*, 2015, **16(4)**, 705-717
- [3] A. B. Morgan and J. W. Gilman, "An Overview of Flame Retardancy of Polymeric Materials: Application, Technology, and Future Directions", *Fire. Mater.*, 2013, **37(4)**, 259-279
- [4] J. W. Mitchell, "The History and Future Trends of Non-Halogenated Flame Retarded Polymers," in "Non-Halogenated Flame Retardant Handbook", eds. A. B. Morgan and C. Wilkie, Scrivener Publishing LLC, Canada, 2014, pp 1-16
- [5] S. V. Levchik and E. D. Weil, "Thermal Decomposition, Combustion and Flame-retardancy of Epoxy Resins-A Review of the Recent Literature", *Polym. Inter.*, 2004, **53(12)**, 1901-1929
- [6] M. Klatt, "Nitrogen-based Flame Retardants," in "Non-halogenated Flame Retardant Handbook", eds. A. B. Morgan and C. A. Wilkie, Scrivener Publishing LLC, Canada, 2014, pp 143-168
- [7] D. Duquesne and T. Futterer, "Intumescent Systems," in "Non-halogenated Flame retardant Handbook", eds. A. B. Morgan and C. A. Wilkie E, Scrivener Publishing LLC, Canada, 2014, pp 293-346
- [8] R. Sauerwein, "Mineral Filler Flame Retardants," in "Non-halogenated Flame Retardant Handbook", eds. A. B. Morgan and C. A. Wilkie, Scrivener Publishing LLC, Canada, 2014, pp 75-142
- [9] G. Beyer and T. Lan, "Polymer Nanocomposites: A nearly Universal FR Synergist," in "Non-halogenated Flame Retardant Handbook", eds. A. B. Morgan and C. A. Wilkie, Scrivener Publishing LLC, Canada, 2014, pp 243-292
- [10] S. Bourbigot and S. Duquesne, "Fire Retardant Polymers: Recent Developments and Opportunities" *J. Mater. Chem.*, 2007, **17(22)**, 2283-2300
- [11] J. W. Gilman, C. L. Jackson, A. B. Morgan, R. Harris, E. Manias, E. P. Giannealis, M. Wuthenow, D. Hilton, S. H. Phillips, "Flammability

- Properties of Polymer-Layered-Silicate Nanocomposites. Polypropylene and Polystyrene Nanocomposites", *Chem. Mater.*, 2000, **12(7)**, 1866-1873
- [12] Y. Gao, J. Wu, Q. Wang, C. A. Wilkie and D. Hare, "Flame Retardant Polymer/Layered Double Hydroxide Nanocomposites", *J. Mater. Chem. A*, 2014, **2(29)**, 10996-11016
- [13] F. Laoutid, L. Bonnaud, M. Alexandre, J. M. Lopez-Cuesta and P. Dubois, "New Prospects in Flame Retardant Polymer Materials: From Fundamentals to Nanocomposites", *Mater. Sci. Eng.*, 2009, **63(3)**, 100-125
- [14] P. Ding, B. Kang, J. Zhang, J. Yang, N. Song, S. Tang, L. Shi, "Phosphorus-containing Flame Retardant Modified Layered Double Hydroxides and their Applications on Polylactide Film with Good Transparency", *J. Colloid. Interface. Sci.*, 2015, **440**, 46-52
- [15] P. K. Kaul, A. J. Samson, G. T. Selvan, I. Enoch and P. M. Selvakumar, "Synergistic Effect of LDH in the Presence of Organophosphate on Thermal and Flammable Properties of an Epoxy Nanocomposite", *Appl. Clay Sci.*, 2017, **135**, 234-243
- [16] X. Jin, X. Gu, C. Chen, W. Tang, H. Li, X. Liu, S. Bourbigot, Z. Zhang, J. Sun and S. Zhang, "The Fire Performance of Polylactic Acid Containing a Novel Intumescent Flame Retardant and Intercalated Layered Double Hydroxides", *J. Mater. Sci. Lett.*, 2017, **52(20)**, 12235-12250
- [17] L. Qiu, Y. Gao, C. Zhang, Q. Yan, D. O'Hare and Q. Wang, "Synthesis of Highly Efficient Flame Retardant Polypropylene Nanocomposites with Surfactant Intercalated Layered Double Hydroxides", *Dalton Trans.* 2018, **47(9)**, 2965-2975
- [18] E. N. Kalali, A. Montes, X. Wang, L. Zhang, M. E. Shabestari, Z. Li and D.-Y. Wang, "Effect of Phytic Acid-Modified Layered Double Hydroxide on Flammability and Mechanical Properties of Intumescent Flame Retardant Polypropylene System", *Fire Mater.*, 2018, **42(2)**, 213-220

Chapter 2

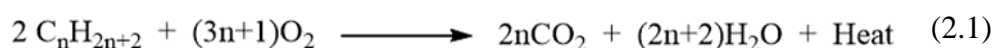
Background

This chapter describes the fundamental combustion and the thermal degradation of polymer materials, especially epoxy resins. It also provides various fundamental techniques used for enhancing the flame retardancy for polymers. One technique employed significantly is the incorporation of flame retardant fillers to the polymer matrix. There are several types of compounds employed as flame retardants explained in this chapter.

2.1 Combustion of Polymers

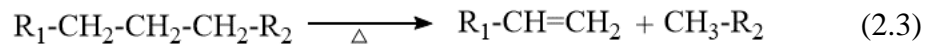
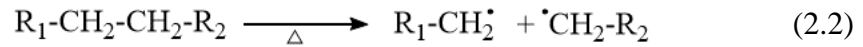
Polymers are macromolecule materials combining long chains of repeating monomers with covalent bonds [1]. They consist of mainly carbon and hydrogen, called hydrocarbons [2]. Each carbon atoms link together to build backbone chains of polymers. Despite the components of hydrocarbons, some elements such as oxygen, nitrogen and sulfur can include in the backbone chains. It is well acknowledged that materials comprising hydrocarbons possess high flammability since they are combustible elements [1].

The burning reaction with oxygen gas is called combustion. The general combustion reaction of alkane, which contains the hydrocarbon, produces carbon dioxide, water and heat. Equation 2.1 shows the basic stoichiometric combustion of alkane [3]. Parameters affecting materials' flammability rely on their chemical components, structural arrangement, and molecular size [2].



In a polymers' thermal degradation process, thermal energy from an ignition source should be higher than covalent bonding energy in polymer chains to break the bonds linked between atoms. The cleavage of bonds takes place at the weakest bonds in the chains. The mechanisms of thermal polymer degradation can be divided into two types: non-oxidising and oxidising thermal degradations. The former is the thermal degradation in condition without oxygen. The scission of polymer chains occurs when the heat of materials increases to pyrolysis temperature (T_p) of materials. As a result, there is a formation of active free-radicals, dehydrogenation or both within polymer

chains. Equation 2.2 and 2.3 show the representatives of non-oxidising thermal degradation reactions in polymers with the formation of free-radicals and dehydrogenation, respectively [4].



In contrast, the thermal decomposition process with using oxygen in the air is an oxidising thermal degradation. The bond scission in polymers with this reaction promotes many products containing different functional groups such as carboxyl (-COOH), carbonyl (-CO-) and hydroxyl (-OH). Moreover, free radicals of H[·] and OH[·] have generated the duration of the decomposition process. These active radicals of macromolecules can recombine to build new bonds [4].

The combustion mechanism of polymers occurs through oxidising thermal degradation. Three significant sources supporting the ignition of any materials are heat, combustible gas (e.g. oxygen in air), and combustible materials (e.g. polymers). When thermal energy transmits to polymer substrate by radiation, convection and conduction, polymer temperature rises gradually to its T_p . In this stage, the polymer chains are degraded, producing combustible and incombustible gases, vaporising substances, condensed liquids, and carbonaceous residues. Among the heat flux, specific heat and thermal conductivity of polymer influence temperature change. The ignited polymer reacts with the early produced combustible gases and vapours with oxygen in air. This stage induces a rapid increase of the temperature in the burning system, leading to combustion. The products generated from the combustion are an extensive amount of heat, light and smoke. They can be applied in the combustion process again, contributing to the propagation of burn. The fire propagation depends on the flammability and supply of polymer and the environment of combusting area [2, 5]. Figure 2.1 illustrates the simplified diagram of the combustion mechanism in polymers.

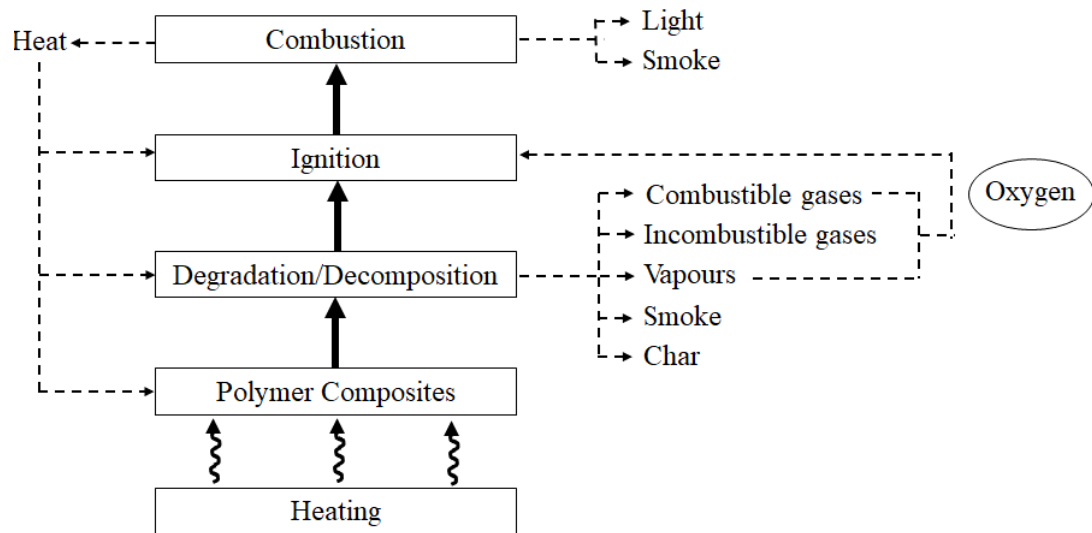


Figure 2.1 Schematic diagram of polymer combustion mechanism [5].

2.2 Thermal Degradation of Epoxy Resins

Epoxy resin (EP) is a broad term used to refer to pre-polymers containing reactive epoxy groups. If EP reacts with a curing agent (hardener) at room temperature or elevated temperature, it will promote three-dimensional networks in the polymer structure, resulting in thermoset polymer. The temperature in the curing process depends on the sorts of EPs and curing agents. After the complete curing, it provides the hardened resin. Hence, the term EP can also be referred to as cured EP [6, 7].

There are two principal types of epoxies, namely glycidyl and non-glycidyl epoxies. The former is further divided in glycidyl ether, glycidyl ester and glycidyl amine. Examples of those epoxies are diglycidyl ether of bisphenol A (DGEBA), diglycidyl phthalate (DP) and tetraglycidyl diamino diphenyl methane (TGDDM), respectively. The latter is cycloaliphatic epoxies such as dicyclopentadiene dioxide [8, 9]. Figure 2.2 displays the chemical structures of epoxy representatives

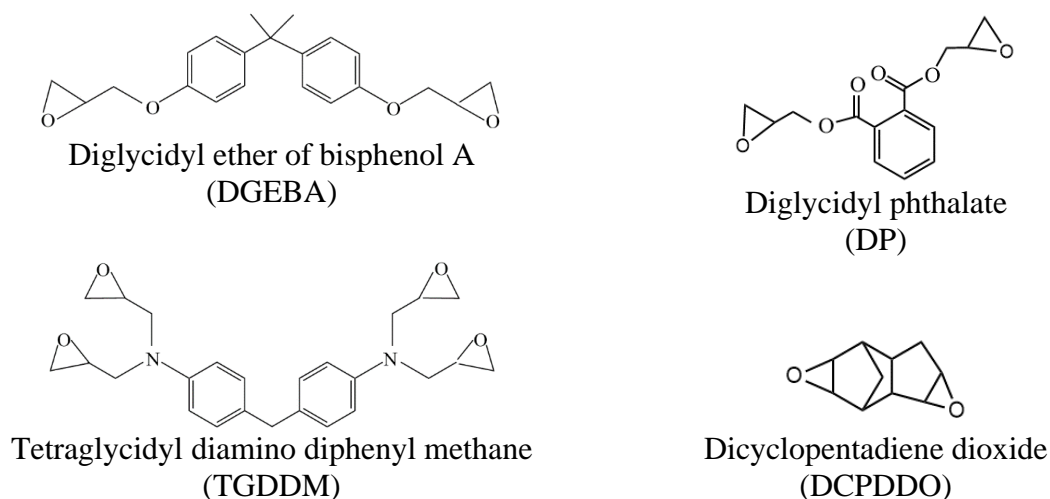
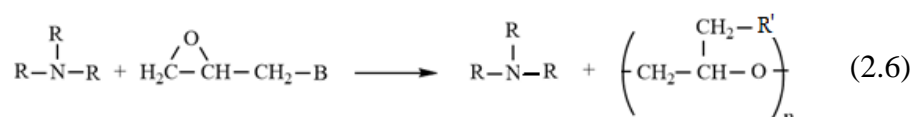
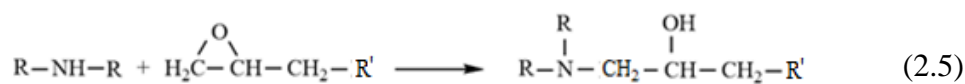
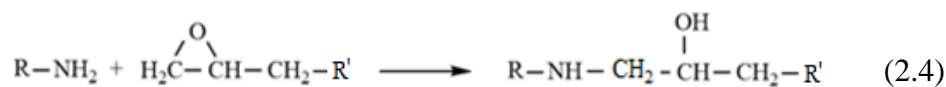


Figure 2.2 Chemical configurations of epoxy resins

One of the epoxies, which is most widely used in composites as the matrix, is DGEBA because of its excellent performance characteristics, e.g., good mechanical properties, thermal resistance and chemical corrosion. Besides, DGEBA can react with a variety of curing agents [10]. Hence, this study was concentrating on DGEBA as epoxy representative for composites.

Production of three-dimensional crosslinked networks in epoxy resins requires curing agents. There are many types of curing agents, such as compounds based on amines, anhydrides and phenol-formaldehydes. Most curing agents used for epoxy curing are amines because they have diverse compounds that provide a wide range of properties for cured epoxy resins. The existence of primary amine ($-\text{NH}_2$) and secondary amine ($-\text{NH}-$) in curing agents reacts with epoxy groups in resins. Meanwhile, tertiary amine ($-\text{N}-$) did not contain active-hydrogen, thereby, it doesn't react with the epoxy group. However, tertiary amine influence as a catalyst for self polymerisation of epoxy groups [9-11]. Equation 2.4-2.6 show reactions of primary, secondary and tertiary amines with epoxides, respectively [11].



Considering the structural characteristics of amine-based curing agents, they can be categorised into three principal groups of amines: aliphatic amines, cycloaliphatic amines and aromatic amines. For aliphatic amine curing agents, their structures are based on linear aliphatic chains that can react with epoxies at room temperature. Meanwhile, cycloaliphatic amine curing agents contain cyclic aliphatic chains that increase glass transition temperatures and chemical resistance of cured epoxy resins. In aromatic amine curing agents, the compounds have aromatic groups that increase glass transition temperature. Epoxy resins cured with aromatic amines are higher thermal and chemical resistance than that with cycloaliphatic amines [6, 12]. The representatives of each amine type used as curing agents are provided in Figure 2.3.

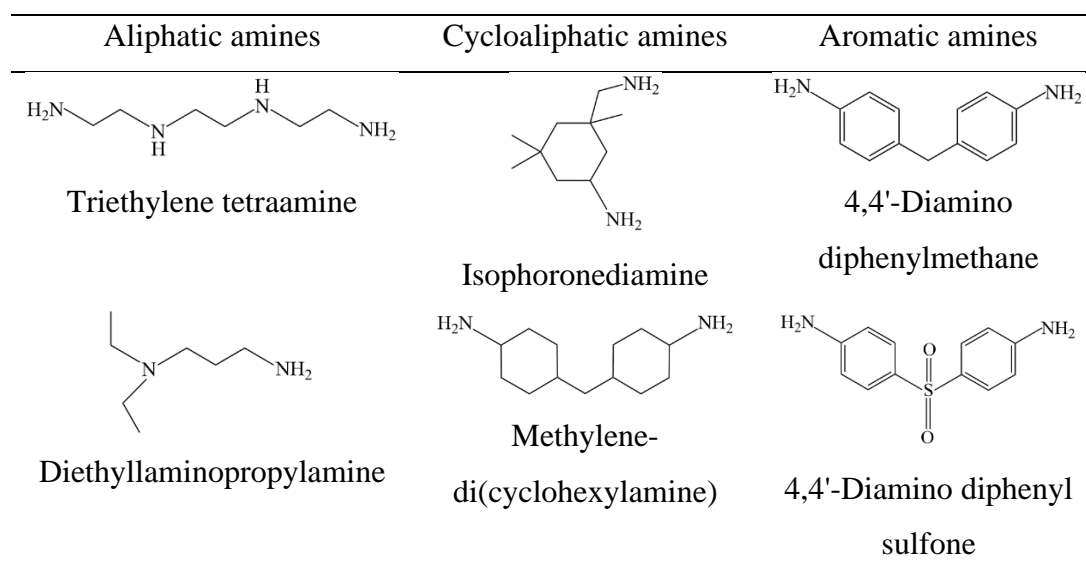
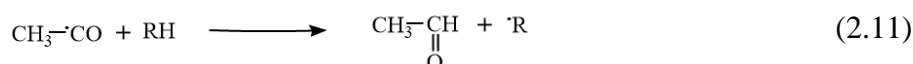
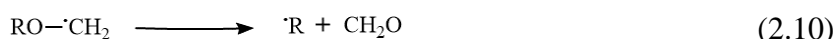
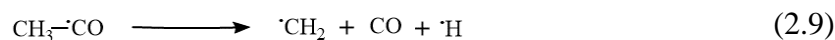
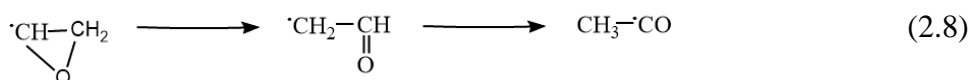
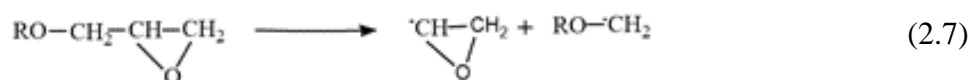


Figure 2.3 Representatives of amine compounds employed as curing agents for epoxy resins.

Nowadays, many researchers have focused on the thermal decomposition mechanism of epoxy resins [13-17]. The thermal stability and flammability of epoxy resins associate with epoxy monomers and hardeners' structure and the crosslink density of cured epoxy resins [18]. Neřman et al. [13] suggested that the chemical bonds of epoxy resins broke at high temperature, generating the epoxy and alkyl free-radicals (Equation 2.7). The epoxy free-radical was isomerised to vinyloxy and acetyl radicals, respectively (Equation 2.8). The produced acetyl radical decomposed to methyl radical and carbon monoxide (Equation 2.9). For the alkyl radicals, they broke down to create the formaldehyde and acetaldehyde compounds (Equation 2.10-2.11).



In a case of thermal degradation of DGEBA cured with 4,4'-diamino diphenyl sulfone (DDS), the nitrogen bonds in the EP was broken in the initial stage of pyrolysis because the binding energy of the aliphatic carbon-nitrogen (305 kJ/mol) is lower than that of the aliphatic carbon-oxygen (358 kJ/mol) and the aliphatic carbon-carbon (346 kJ/mol) [15, 19, 20]. Then, there was the random scission of polymeric chains, promoting the formation of various gaseous products (e.g. sulfur dioxide, phenol, methylaniline) and bisphenol A. At the higher temperature, char residues, carbon monoxide and methane are formed. Figure 2.4 illustrates the thermal decomposition of the EP/DDS [15].

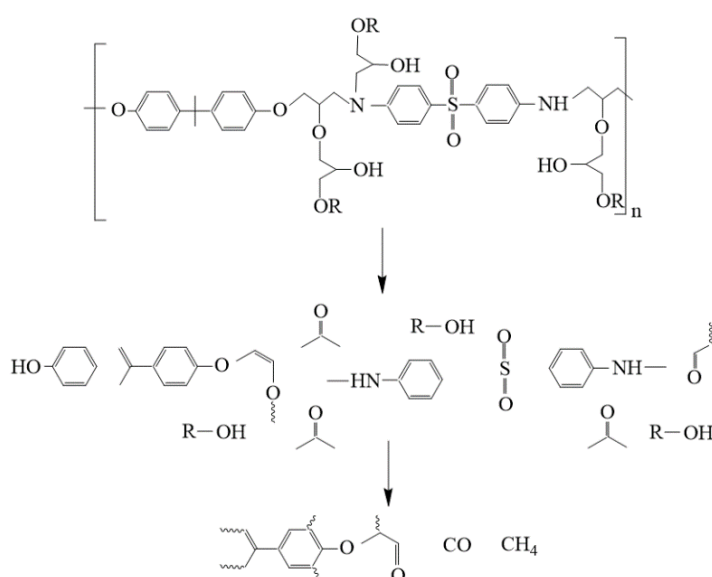


Figure 2.4 Thermal combustion of DGEBA/4,4 DDS [15].

Similarly, Zhang et al. [17] demonstrated that there were the degradation of C-O bonds in the main chains of the DGEBA and the decomposition of DDS in the initial process. The consequences of thermal degradation produced the free-radicals and sulfur dioxide, respectively. This stage is called ignition. After, the scission of bonds takes place randomly to contribute to the large amounts of active radicals. These radicals can recombine to build the new crosslinks. Due to the release of many combustible substances, the rate of degradation reaction grows remarkably, generating the propagating combustion of the resin. At the termination stage, there was the formation of char residues resulting from the thermal oxidation. The mechanism of thermal degradation of DGEBA/DDS is presented in Figure 2.5.

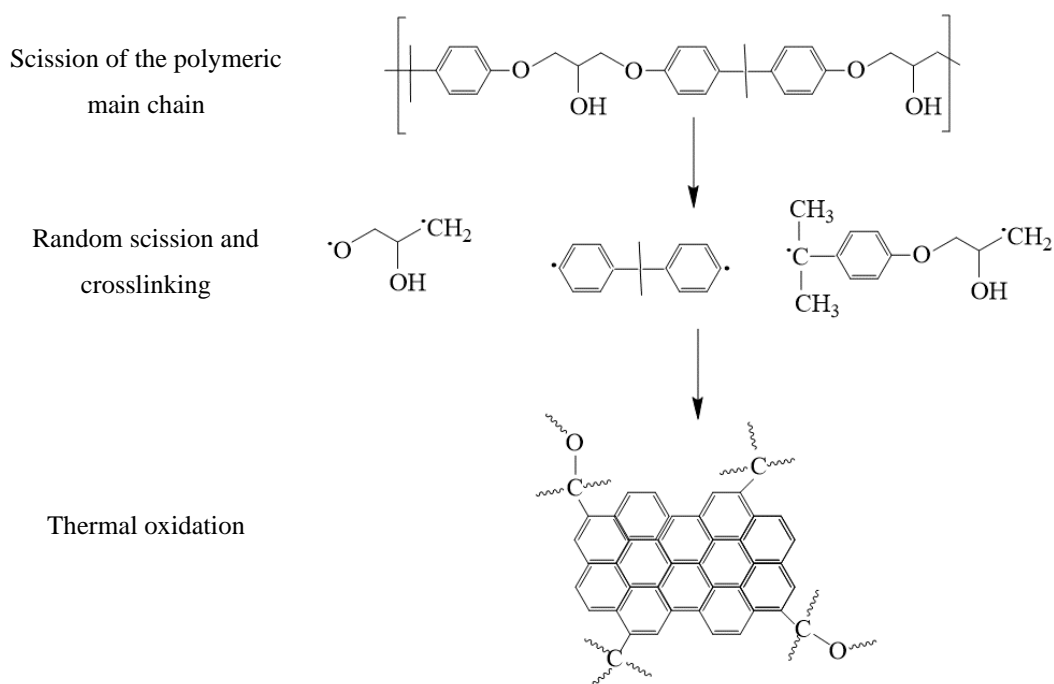


Figure 2.5 Thermal decomposition of DGEBA/DDS [17].

2.3 Flame Retardancy Mechanism of Fillers

The combustion cycle can be interrupted by three different mechanisms: heat sink, gas phase and condense phase. The different flame retardants possess the distinction in the mechanisms of actions in the prohibition of flame propagation [4, 5, 21].

2.3.1 Heat Sink Mechanism

The endothermic decomposition of flame retardants can cool substrate of combustible materials. The examples of flame retardant fillers with this action mode are metal hydroxides, metal carbonates and metal hydrates. Besides, the decomposition of flame retardants release of non-flammable gases such as H₂O and CO₂, which dilute the combustible gas and reduce the temperature of combustion system. The inorganic residue producing from the decomposition also acts as a physical barrier to inhibit the transmission of heat and combustible gas through the polymer substrate. These actions lead to the delay of pyrolysis. [21, 22].

2.3.2 Gas Phase Mechanism

The release of non-flammable gases obtaining from the thermal decomposition of flame retardants dilutes concentration of combustible gas (e.g. O₂) in burning area. This flame retardancy method is called gas phase mechanism. The fillers with this flame retardancy mechanism are compounds-based halogen or phosphorus [5, 21, 22]. The dilution of flammable volatile products contributes to reduction of heat transfer to polymers, leading to the decrease of degradation rate. Thus, the gas phase mechanism delays combustion of polymers [23].

2.3.3 Condensed Phase Mechanism

The char residues produced from the degradation process have a function of physical barrier. It can impede the transmission of heat and flammable gases to the burned area. This phenomenon is a condensed phase mechanism. The examples of flame retardant fillers acting this mechanism are intumescent and nanocomposites [5, 21].

2.4 Enhancement of Flame Retardancy in Polymers

As polymers have high flammability, many studies and industries have intensively studied to improve this property. There are three basic methods applied for reducing the flammability of polymers. The first method is to use high-performance polymers

with inherent flame retardancy such as polyimides, poly(tetrafluoroethylene), and poly(ether-ether ketone). These polymers possess a degradation temperature over 350°C, which are high heat resistant materials. However, they are high production cost since their manufacturing process is relatively complicated. Another strategy is grafting in the backbone or on the surface of polymers with compounds containing phosphorus (P), nitrogen (N) and/or silicon (Si). The modification, however, influences the mechanical properties of the obtained polymers. The last technique is incorporating flame retardants into polymers, which is the most extensive use enhancing fire retardancy. The advantages of this method are simple operation and low cost [24, 25]. Therefore, the increase of flame retardancy of polymers in this thesis focuses solely on incorporating flame retardant additives.

2.5 Types of Flame Retardant Fillers

A variety of additives are used as a fire retardant, namely compounds with the compositions of halogen, phosphorus and/or nitrogen, intumescent, minerals, and nanomaterials. This section will explain the characteristics of individual flame retardants.

2.5.1 Halogenated Flame Retardants

Compounds containing halogen elements are acceptable as flame retardants for polymers [21]. The efficiency of halogen flame retardants depends on the halogen elements. Since fluorinated compounds are higher thermal stable than polymers, the fluorine radicals cannot release at the decomposing temperature of polymers. In contrast, the thermal stability of iodinated compounds is lower than that of polymers, that the species of iodine may decompose during polymer processing. From the decomposition behaviours of both the elements, they have been limited to use in the applications. For chemicals comprising bromine, they have attracted considerable attention as flame retardants because the additives can decompose with polymers' combustion. The examples of brominated flame retardants are hexabromocyclododecane (HBCD), tetrabromophthalate anhydride (TBPA),

tetrabromobisphenol-A (TBBPA) and polybrominated diphenyl ether (PBDE). Their structures are provided in Figure 2.6 [4, 12].

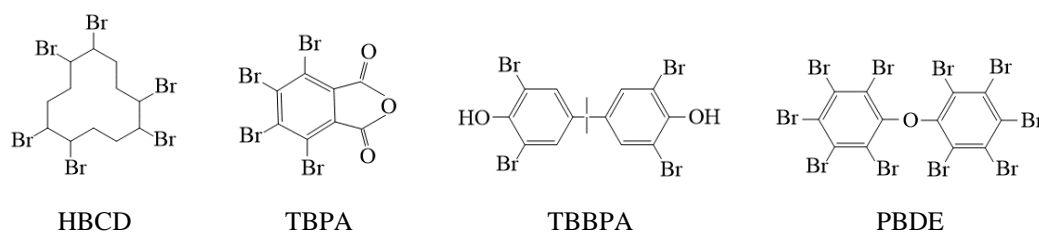
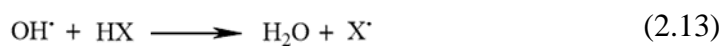
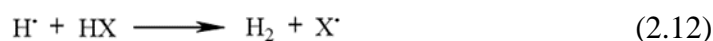


Figure 2.6 Chemical structures of brominated flame retardants.

Many studies explained the fire retardancy mechanism of halogenated additives (RX, R=alkyl groups and X=halogen elements) incorporated in polymer matrix composite. The hydrogen halides (HX) released from the thermal decomposition of halogenated flame retardants can protect the dispersion and dilute flammable gases' concentration. Afterwards, high-active hydrogen radicals ($H\cdot$) and hydroxyl radicals ($OH\cdot$), occurring in the polymer degradation, reacting with the HX molecules (Equation 2.12 and 2.13). This process leads to the formation of non-flammable volatile layer (e.g. H_2O) that can protect the permeation of heat and gases to the combustible surface of polymers. [4] In this process, the halogen flame retardant presents the gas phase mechanism.

The next step is an abstraction of hydrogen; the halogen radicals attack the hydrogen in the polymers. This action contributes to the alkyl radical and hydrogen halide (Equation 2.14) [4]. The alkyl radical can re-bond to form char, which delays the transmission of heat, flame and combustible gases to the burning area. This is the characteristic of condensed mechanism. Meanwhile, the hydrogen halide can be used in the combustion cycle.



Although the halogenated compounds have been widely applied as flame retardant additives for polymers, their disadvantages are releasing enormous amounts of smoke and corrosive gas such as HBr and HCl during combustion. These products cause human health and air pollution problems concerned significantly. Thus, halogenated flame retardants are limited usage in the industries [21, 26].

2.5.2 Phosphorus-based Flame Retardants

One of the halogen-free flame retardants used extensively is phosphorus-based compounds involving inorganic compounds (e.g. red phosphorus and metal phosphates), semi-organic compounds (e.g. metal salts of organophosphinic acids and phosphonium salts) and organic compounds (e.g. phosphinates, phosphonate and phosphate esters) [18]. The organophosphate-based compounds are the most use of phosphorus-containing flame retardants [27]. Figure 2.7 presents the chemical structure representatives of organophosphate compounds.

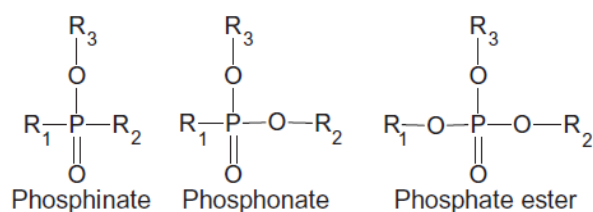


Figure 2.7 Structural representatives of the organophosphorus-based compounds used as flame retardants [27].

Levchik [28] stated that phosphorus flame retardants are more effective with polymers containing oxygen or nitrogen. Most phosphorus-based compounds provide the condensed phase mechanism. During the thermal decomposition of phosphorus flame retardants, phosphoric acid molecules are decomposed significantly and condensed rapidly. The by-products of the condensation are pyrophosphoric acid and water, as displayed in Figure 2.8. The former decomposed to high-active species of PO^\cdot , PO_2^\cdot and HPO^\cdot and they interacted with the radicals of H^\cdot and OH^\cdot . This process contributed to char production. The pyrophosphoric acid can accelerate the formation of crosslinked and carbonaceous residues. Meanwhile, the volatile latter can reduce the concentration of flammable gas around the combustion area.

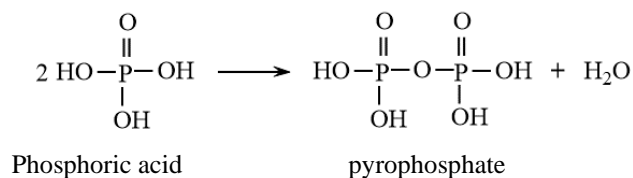


Figure 2.8 Formation of pyrophosphate structure from the condensed phosphoric acid.

The review of Laoutid et al. [4] reported that the flame retardancy efficiency of phosphorus compound was five and ten times as high as that of brominated and chlorinated flame retardants, respectively. The common phosphate-based compounds applied in polymeric matrix composites are red phosphorus (RP), ammonium polyphosphate (APP), resorcinol bis(diphenyl phosphate) (RDP) and bisphenol A bis(diphenyl phosphate) (BDP), that their molecular structures can be seen in Figure 2.9.

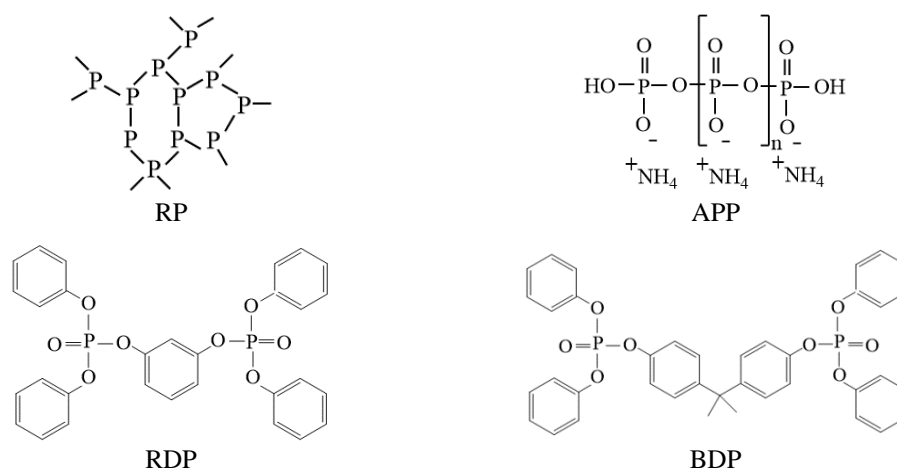


Figure 2.9 Structure of phosphorus flame retardants.

Moreover, the phosphorus compounds have also been used as plasticisers for polymers, especially phosphate ester-containing compounds (e.g. tributyl phosphate and triphenyl phosphate) [27]. Besides, the organophosphorus-based flame retardants can react with polymer chains, providing the structure of three-dimensional networks in the polymer composites. The study of Mariappan et al. [29] showed that the phosphate ester groups in the triphenyl phosphate could interact with the hydroxyl groups in the epoxy resin of DGEBA by the reaction of trans-esterification. The

crosslinked derivatives of alkyl phenyl phosphite were produced by the reaction, presenting in Figure 2.10.

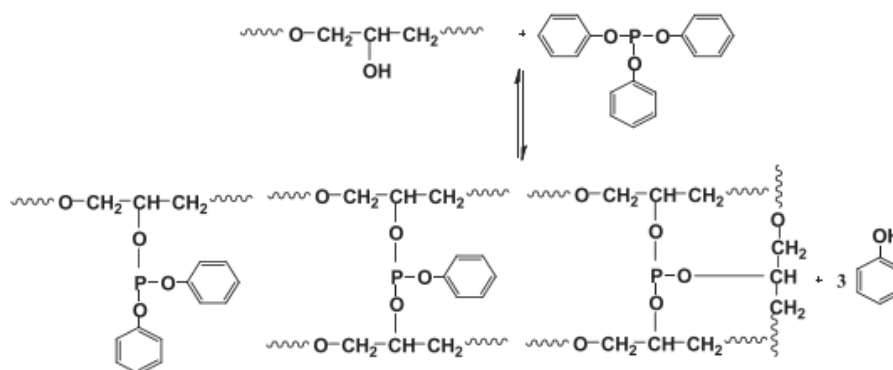


Figure 2.10 Reaction of epoxy resin and triphenyl phosphate [29].

From the above information, phosphorus-based compounds can be widely used as flame retardants, particularly the organophosphate esters. They can act as plasticisers and crosslinking agents for polymers.

2.5.3 Nitrogen-based Flame Retardants

The incorporation of nitrogen-based compounds into the polymer matrix is another alternative used to reduce the flammability of the composites. The fillers do not provide hazardous gases during thermal combustion [30]. Typically, nitrogen-based flame retardants can be classified in terms of fire retardancy action into two groups [31].

The first group is compounds containing either ammonia or melamine. This group's thermal decomposition can absorb the heat and release non-flammable gases (e.g. nitrogen and ammonia) [31]. This process is the flame retardancy of heat sink mechanism. For instance, melamine can sublime at around 350°C, affecting energy absorption. The combustion temperature of the polymer, therefore, decreases with the addition of melamine. At a high temperature, the decomposition of melamine emits ammonia. The produced gases can dilute combustible gases. Subsequently, there are the formations of melam, melem and melon in the condensed phase. These actions diminish the heat in the combusting area [4]. Figure 2.11 displayed the thermal decomposition of melamine.

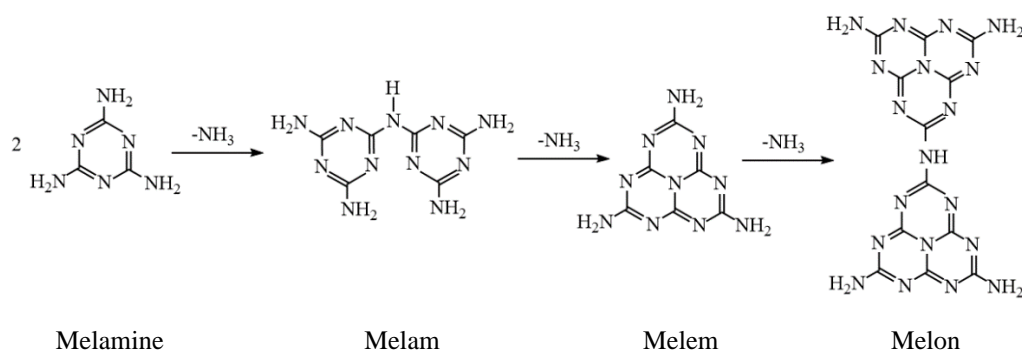


Figure 2.11 Thermal decomposition of melamine [4].

Despite the pure melamine, its salts (e.g. melamine cyanurate, melamine phosphate and melamine pyrophosphate) are also utilised as flame retardants. The melamine salts have the same fire retardancy mechanism as the neat melamine. The more melamine content is, the higher flame retardancy performance is [4].

The other nitrogen-based flame retardants are compounds following condensed phase mechanism, such as N-alkoxy hindered amines. This type of flame retardants interacts with the polymer during combustion, accounting for the char formation. The nitrogen flame retardants are practically combined with phosphorus flame retardants to increase condensed phase action [31].

2.5.4 Intumescent Flame Retardants

Phenomena of intumescent flame retardants is an expansion of carbonised layer on the degraded polymer surface during combustion. With the burning of materials containing intumescent flame retardant, ingredients of intumescent system decompose leading to formation of carbonaceous char and viscous liquids. The formation of char residue from the thermal decomposition of intumescent presents the flame retardancy mechanism of condensed phase. Then, there is a releasing of inert gases trapped in the viscous liquids. This results in an expansion of materials. The formed char layer plays a vital role in the thermal insulator leading to reduced heat transformation from the heat source to the polymer surface [4].

The general components of intumescent flame retardants should consist of acid source, carbonising agent, and blowing agent. Table 2.1 shows the representatives of

each intumescent components. If the additives are heated, there is an explosion of acid at 150°C to 215°C, depending on the acid type. The acidic substances accelerate the dehydration rate of the carbon source. As a result, char formation increases significantly. Meanwhile, the blowing agent in the combusting condition emits some inert gases, inducing polymer expansion and the swelling of carbonised layer [4, 21, 25].

Table 2.1 Representatives of components in intumescent flame retardants [4, 32].

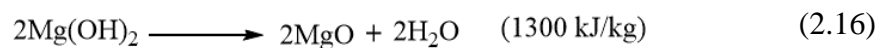
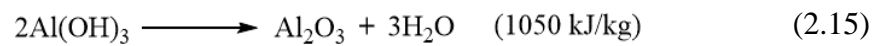
Inorganic acid source	Carbonising agent	Blowing agent
- Phosphoric acid	- Starch	- Urea
- Sulfuric acid	- Dextrins	- Urea-formaldehyde
- Boric acid	- Sorbital	- Melamine
- Ammonium salts	- Char former polymers	- Polyamide
- Phosphate of amine and amide (e.g. melamine phosphate)	(e.g. Polyamide, polycarbonate)	
- Organophosphate compounds (e.g. tricresyl phosphate)		

2.5.5 Mineral Flame Retardants

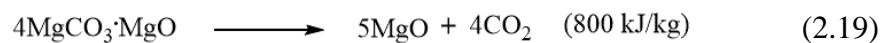
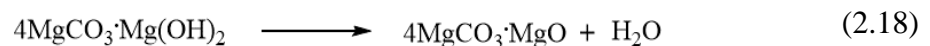
Another traditional flame retardants are mineral additives, including metal hydroxides, metal carbonates hydroxides and metal oxides. These additives can provide endothermic energy during the combustion, which is the characteristic of heat-sink mechanism. Besides, the gradation of mineral fillers generates the char and gases, presenting the characteristics of gas phase and condensed phase mechanism, respectively. [4, 21]

The primary metal hydroxides used extensively to enhance the fire retardancy of polymers are aluminium trihydroxide (ATH, $\text{Al}(\text{OH})_3$) and magnesium dihydroxide (MDH, $\text{Mg}(\text{OH})_2$). For the decomposition of ATH, alumina (Al_2O_3) and water vapour are produced at the temperature of 180°C to 200°C. The alumina acts as a thermal

insulating barrier, while the water molecule can dilute the flammable gases and induces the formation of a protective gas layer. Despite the produced chemicals, the thermal degradation of ATH also absorbs heat the surrounding. This can cool the temperature of combustion system. Likewise, the thermal degradation of MDH at 300°C to 340°C promotes magnesium oxide (MgO) and volatile water formation. The fire retardancy mechanism of MDH is similar to ATH. [4, 21] The endothermic reactions of both metal hydroxides are shown in Equation 2.15-2.16.



In the case of metal carbonate hydroxide, the example of this type is hydromagnesite ($4\text{MgCO}_3 \cdot \text{Mg}(\text{OH})_2 \cdot 4\text{H}_2\text{O}$) used frequently as a flame retardant additive. It attributes the production of magnesium hydroxy carbonate, magnesium carbonate, water and carbon dioxide, and the endothermic energy around 800 kJ/kg during the combustion at 200-500°C, as presented in Equation 2.17-2.19 [4, 21].



For the metal oxides, borate compounds (e.g. $2\text{ZnO} \cdot 3\text{B}_2\text{O}_3 \cdot 3.5\text{H}_2\text{O}$) are interesting to use as flame retardants for polymers. The boric acid, boron oxide and water molecules are formed after their thermal decomposition between 290°C and 450°C. The produced boron oxide acts as a layered physical barrier. Moreover, the formation of the carbonised layer in the combustion process increases dramatically with the formation of boric acid. During the combustion, there is energy absorption at 503 kJ/kg. Hence, the burning of the polymer is interrupted by incorporating the inorganic fillers [4, 21].

Although the advantages of mineral additives are low emission of smoke and toxic gases and inexpensive cost, they are low-performance flame retardancy. They can

delay the burning, but they cannot completely stop the combustion. To achieve the high efficiency of flame retardancy, it is necessary to use the high loading of the additives over 50-70%. However, the high loading of the fillers affects the decrease of polymer composite mechanical properties [21].

2.5.6 Nano-flame Retardants

Another alternative type of flame retardant is nanomaterials, which are substances with the dimension of 1-100 nm. The typical nanostructure can be categorised into three types, following by the dimension: zero-, one- and two-dimensional structures. The zero-dimensional nanostructure (0D) is a particulate material or spherical nanoparticles. The one-dimensional nanostructure (1D) is a fibrous material or needle-like structure. The two-dimensional nanostructure (2D) is a layered material or plate-like structure.

Several studies established that the blending of nanomaterials can improve mechanical properties, thermal behaviours and fire resistance of polymers [4, 33]. The incorporation of nanofillers in polymer composites is a novel technique for the application of flame retardants, that gets much attention. Much of researchers showed that nano-flame retardants have more effective than any other traditional flame retardants. There are three principal types of nanomaterials employed as flame retardant additives, namely nano-sized particles, nanocarbon fillers and nano-clays. The characteristics of each nano-flame retardants will explain in the following section.

2.5.6.1 Nano-sized Particulate Additives

The nanoparticles of metal oxides and polyhedral oligomeric silsesquioxane (POSS) have been used as fire retardants. The traditional metal oxides with the particle size in the dimension of nanometer used in the applications are zinc oxide (ZnO), titanium dioxide (TiO₂), silicon dioxide (SiO₂) and aluminium oxide (Al₂O₃). The flame retardancy mechanism of nanoparticles is similar to the microparticles; however, nanoparticles' efficiency is higher than larger molecules. The small contents of nanoparticles increased the thermal stability and reduced the rate of heat release in the combustion of the polymer [4, 12].

2.5.6.2 Carbon Nano-additives

In addition to the nanoparticulate, the flammability of polymer composites can be reduced with the incorporation of nanocarbon additives. The carbon molecules used in flame retardants are carbon nanotube (CNT), graphene oxide (GO) and fullerene (C₆₀) [34].

The CNT, which is a macromolecule of carbon, is a cylinder of graphene. Due to the outstanding conductivity, thermal and mechanical properties of CNT, it has been used in various applications, especially high-performance flame retardants. As the network layered structure of CNT can shield the dispersion of heat and combustible gases to the burning area, the CNT presents the flame retardancy mechanism of condensed phase. Furthermore, the unique network structure and the composition of CNT contribute to the increase of thermal stability. It causes the increase of thermal stability. The review of Ma et al. [33] reported that the fire retardancy efficiency of multi-walled carbon nanotube (MWNT) was higher than silicate nanoclay. The heat release rate and mass loss rate of composite declined with adding the CNT.

For the GO flame retardant, its configuration contains the stacked graphene sheets modified with the hydroxyl, carbonyl and ether groups. It causes good compatibility with polar polymers. The increasing of char content and thermal stability in polymer nanocomposites with loading the GO reduces the polymer flammability [34].

The other nanocarbon with a unique structure is fullerene. It possesses the molecule of 60 carbon atoms with hollow shape. Thus, during the polymer combustion, the macromolecule and the free radicals produced from the degradation of polymer can be trapped by the C₆₀ molecules. Subsequently, the gelled ball network is created, influencing the increase of melted polymeric viscosity. This phenomenon results in the inhibition of combustion [33, 35].

2.5.6.3 Nano-layered Materials

Nanomaterials with layered structure have attracted remarkable attention in use as flame retardants for polymers. The reviews of Yue et al. [36] reported that the heat

release rate and mass loss rate of composites containing nano-layered materials were more decreased than spherical and tubular structures. The two vital types of layered nanoparticles used widely for flame retardant applications are layered silicates and layered double hydroxides [37].

Layered silicates are groups of clays, including tetrahedral silicon dioxide (SiO_2) layers and octahedral aluminium oxide (Al_2O_3) layers. The structural arrangement of layered silicates depends on a proportion of tetrahedral to octahedral layers. If the ratio is 1:1, the structure has an alternation of one tetrahedral layer and one octahedral layer. For the 2:1 type, one octahedral layer intermediate between two tetrahedral layers [38]. Each clay layer joins together with van der Waals force and electrostatic force. Some of Al^{3+} in the octahedral layers are substituted with Mg^{2+} , contributing to the negative charge of the silicate layer surface. The excess negative charges connect with inorganic cations, e.g., Na^+ or Ca^{2+} to neutralise the charge of the layer structure. As these inorganic cations can absorb water, it encourages hydrophilicity in clay [37, 39, 40].

The common layered silicates employed for polymer nanocomposites is montmorillonite (MMT) with 2:1 phyllosilicate. The layer thickness and lateral dimensions of MMT is 0.96 nm and 200-300 nm, respectively. Therefore, an aspect ratio, a ratio of length to thickness, is approximately 200-300 [37, 39, 41]. Figure 2.12 provides the schematic structure of nanolayered MMT.

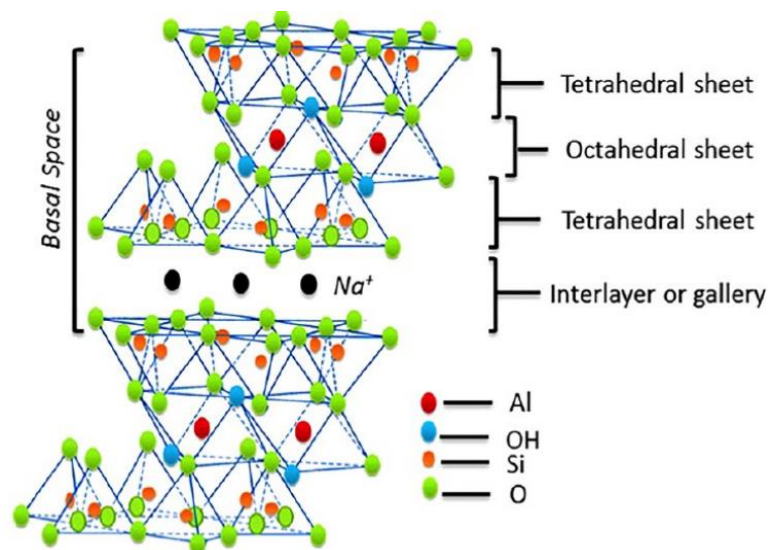


Figure 2.12 Schematic configuration of 2:1 nanolayered silicate clays [40].

The principal models of polymer nanocomposite incorporated with the nano-layered materials are phase separation, intercalation and exfoliation, illustrated in Figure 2.13. When the polymer cannot intercalate in the interlayers of nanoclays, this phenomenon is called a phase-separated configuration. Because of the low interaction between the polymer and the clay, the nanocomposite obtains low mechanical properties. Meanwhile, if the galleries of clay are extended with polymer but the layers still maintain, this composite structure is named intercalated configuration. For the exfoliated structure, the clay lamellar are entirely separated and dispersed in the polymer matrix, promoting the high interaction of matrices. Hence, the nanocomposite with exfoliation has the highest mechanical properties than the other structures [24, 39, 41, 42].

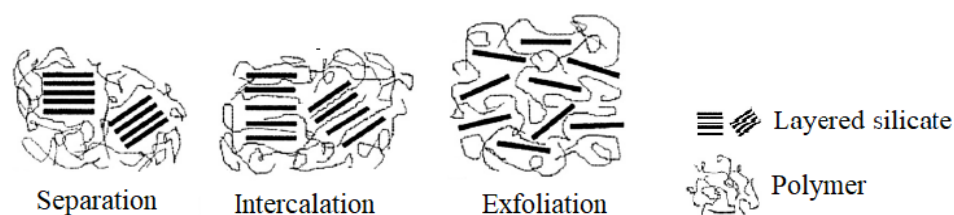


Figure 2.13 Schematic configuration of polymer/clay nanocomposites [39].

Numerous studies have shown that nanoclays achieve enhanced polymer fire retardancy [43-45]. The layered materials can reduce the heat release rate and also increase the char formation during combustion. Qin et al. [46] suggested the fire retardancy mechanism of the silicate clays for polymer nanocomposite. The degradation of silicate clays generated acid sites on the surface of clay lamellar. They can accelerate the initial reaction of thermal decomposition. This process results in the decrease of ignition time, the increase of initial heat release rate, and carbonised layer formation on the surface. It presents the flame retardancy mechanism of condensed phase. Besides, the dehydrogenation and the crosslinking of polymer chains are catalysed by the active sites. Thus, the nanocomposites' thermal and oxidative stabilities increase; however, the peak heat rate decreases.

Another type of nanolayered clay obtaining great attention as flame retardants is layered double hydroxides (LDHs). The compositions of LDHs are positively charged layers of metal hydroxides and anions, and water in the interlayer regions. According

to the unique components of LDHs, heat and combustible gas in the combustion process can be reduced by releasing water vapour in LDHs. This action is the flame retardancy mechanism of gas phase. Besides, the decomposition of metal hydroxide layers in LDHs provides the metal oxides acting as the physical layers to protect the dispersion of heat, flame and combustible gases to the burn substrate. It is the condensed phase mechanism. The addition of LDHs also accelerates the residual formation in the thermal decomposition process and enhances the thermal stability of polymer composites.

As the flame retardancy mechanisms of LDHs are both gas phase and condensed phase, they are better than other flame retardants. In addition, the chemical structure of LDHs can be modified by various compounds to develop their properties. Therefore, this thesis is interested in using the additives of layered double hydroxides as the flame retardants for the polymer. The literature on the characteristics and the flame retardancy efficiency of LDHs will be reviewed in Chapter 3.

2.6 Characterisation of Combustion Behaviour of Polymers

Several techniques are used to study the combustion behaviours of polymers. One technique that has attracted attention widely is cone calorimetry since it exhibits high performance for combustion behaviours. The instrument analyses a value of heat release rate (HRR), peak heat release rate (pHRR), total heat released (THR), time to ignition (TTI), time of combustion (TOC) and heat release capacity (HRC) during the combustion process of polymers. The mass loss, released content of CO and CO₂ and total smoke are also detected in the combustion test period [4, 47].

Another test is a determination of limiting oxygen index (LOI), which is a value showing the minimum concentration of oxygen used during the combustion of materials in the mixture system between oxygen and nitrogen. However, the LOI test is the simulation of combustion, which is not the actual situation. It is just used for the classification of combustible or self-extinguishing materials.

Furthermore, the standard method used to estimate the flammability of materials is a burning test in horizontal and vertical positions. This test measures combusting time and observes characteristics of combustion, e.g. flame dripping.

2.7 Summary

Overall, polymers are high flammability due to their compositions of hydrocarbons in the polymeric chains. The combustion of polymers provides large amounts of heat, smoke, gases and residue char. To inhibit and stop the combustion of polymers, the various flame retardant additives are used in the applications: the compounds containing halogen, phosphorus and/or nitrogen, the minerals and the nanomaterials. As the thermal decomposition of halogenated flame retardants releases corrosive gases, they cannot be used in industries. Thus, non-halogenated flame retardants are used significantly. The flame retardancy mechanisms of additives are the gaseous and condensed phase actions, depending on the types of flame retardants.

One of the excellent flame retardants is layered double hydroxides, which is the 2D nanostructure since it comprises the cationic layers of metal hydroxides, the anions intercalated between the layers and the water molecules. These can block the permeation of heat and flammable gases to the combustible surface of polymers. This study is interested in using layered double hydroxides as the flame retardant additives for polymers.

References

- [1] A. Kumar and R. K. Gupta, "Fundamentals of Polymer Engineering (Mechanical Properties)", McGraw-Hill, USA, 2003
- [2] H. Macskásy and G. Palyi, "Plastics: Their Behaviour in Fires", Elsevier Science, New York, 1991
- [3] K. P. C. Volhardt, "Chapter 3: The Reactions of Alkanes Pyrolysis and Dissociation Energies, Combustion and Heat Content, Free-Radical Halogenation, and Relative Reactivity", in "Organic Chemistry", W.H. Freeman and Company, USA, 1987

- [4] F. Laoutid, L. Bonnaud, M. Alexandre, J. M. Lopez-Cuesta and P. Dubois, "New Prospects in Flame Retardant Polymer Materials: From Fundamentals to Nanocomposites", *Mater. Sci. Eng.*, 2009, **63(3)**, 100-125
- [5] M. Bar, R. Alagirusamy and A. Das, "Flame Retardant Polymer Composites", *Fiber. Polym.*, 2015, **16(4)**, 705-717
- [6] B. Ellis, "Introduction to the Chemistry, Synthesis, Manufacture and Characterization of Epoxy Resins" in "Chemistry and Technology of Epoxy Resins", Springer Science and Business Media Dordrecht, Bath, 1993, pp 1-36
- [7] B. Dewprashad and E. Eisenbraun, "Fundamentals of Epoxy Formulation", *J. Chem. Educ.*, 1994, **71(4)**, 290-294
- [8] N. Saba, M. Jawaid, O. Y. Alothman, M. T. Paridah and A. Hassan, "Recent Advances in Epoxy Resin, Natural Fiber-reinforced Epoxy Composites and their Applications", *J. Reinf. Plast. Comp.*, 2016, **35(6)**, 447-470
- [9] S. Pradhan, P. Pandey, S. Mohanty and S. K. Nayak, "Insight on the Chemistry of Epoxy and Its Curing for Coating Applications: A Detailed Investigation and Future Perspectives", *Polym. Plast. Technol. Eng.*, 2016, **55(8)**, 862-877
- [10] K. B. Tator, "Epoxy Resins and Curatives", in "Protective Organic Coating", ASM International, 2015, **5B**, 63-79
- [11] M. A. Boyle, C. J. Martin and J. D. Neuner, "Epoxy Resins," in "Composites", ASM International, 2001, **21**, 78-89
- [12] A. Kausar, I. Rafique, Z. Anwar and B. Muhammad, "Recent Developments in Different Types of Flame Retardants and Effect on Fire Retardancy of Epoxy Composite", *Polym. Plast. Tech. Eng.*, 2016, **55(14)**, 1512-1535
- [13] M. B. Neĭman, B. M. Kovarskaya, L. I. Golubenkova, A. S. Strizhkova, I. I. Levantovskaya and M. S. Akutin, "The Thermal Degradation of Some Epoxy Resins", *J. Polym. Sci.*, 1962, **56(164)**, 383-389
- [14] D. Puglia, L. B. Manfredi, A. Vazquez and J. M. Kenny, "Thermal Degradation and Fire Resistance of Epoxy-Amine-Phenolic Blends", *Polym. Degrad. Stabil.*, 2001, **73(3)**, 521-527
- [15] U. Braun, A. I. Balabanovich, B. Schartel, U. Knoll, J. Artner, M. Ciesielski, M. Döring, R. Perez, J. K. W. Sandler, V. Altstädt, T. Hoffmann and D. Pospiech, "Influence of the Oxidation State of Phosphorus on the

- Decomposition and Fire Behaviour of Flame-retarded Epoxy Resin Composites", *Polym.*, 2006, **47(26)**, 8495-8508
- [16] B. Perret, B. Schartel, K. Stöß, M. Ciesielski, J. Diederichs, M. Döring, J. Krämer, V. Altstädt, "Novel DOPO-Based Flame Retardants in High-performance Carbon Fibre Epoxy Composites for Aviation", *Eur. Polym. J.*, 2011, **47(5)**, 1081-1089
- [17] W. Zhang, X. Li and R. Yang, "The Degradation and Charring of Flame Retarded Epoxy Resin During the Combustion", *J. Appl. Polym. Sci.*, 2013, **130(6)**, 4119-4128
- [18] S. V. Levchik and E. D. Weil, "Thermal Decomposition, Combustion and Flame-Retardancy of Epoxy Resins-A Review of the Recent Literature", *Polym. Inter.*, 2004, **53(12)**, 1901-1929
- [19] S. V. Levchik, G. Camino, M. P. Luda, L. Costa, G. Muller and B. Costes, "Epoxy Resins Cured with Aminophenylmethylphosphine Oxide-II. Mechanism of Thermal Decomposition", *Polym. Degrad. Stabil.*, 1998, **60(1)**, 169-183
- [20] C. T.L., *The Strengths of Chemical Bonds*. London: Butterworths, 1958.
- [21] A. B. Morgan and J. W. Gilman, "An Overview of Flame Retardancy of Polymeric Materials: Application, Technology, and Future Directions", *Fire. Mater.*, 2013, **37(4)**, 259-279
- [22] P. R. Hornsby, "Fire Retardant Fillers for Polymers", *Inter. Mater. Rev.*, 2001, **46(4)**, 199-210
- [23] G. Camino and L. Costa, "Performance and Mechanisms of Fire Retardants in Polymers—A Review", *Polym. Degrad. Stab.*, 1988, **20(3)**, 271-294
- [24] S. Bourbigot and S. Duquesne, "Fire Retardant Polymers: Recent Developments and Opportunities", *J. Mater. Chem.*, 2007, **17(22)**, 2283-2300
- [25] C. Gerard, G. Fontaine, and S. Bourbigot, "New Trends in Reaction and Resistance to Fire of Fire-retardant Epoxies", *Mater.*, 2010, **3**, 4476-4499
- [26] J. W. Mitchell, "The History and Future Trends of Non-Halogenated Flame Retarded Polymers", in "Non-halogenated Flame Retardant Handbook", eds. A. B. Morgan and C. Wilkie, Scrivener Publishing LLC, Canada, 2014, pp 1-16

- [27] I. van Der Veen and J. de Boer, "Phosphorus Flame Retardants: Properties, Production, Environmental Occurrence, Toxicity and Analysis", *Chemosphere*, 2012, **88(10)**, 1119-1153
- [28] S. Levchik, "Phosphorus-based FRs", in "Non-Halogenated Flame Retardant Handbook", eds. A. B. Morgan and C. A. Wilkie, Scrivener Publishing LLC, Cannada, 2014, pp 17-74
- [29] T. Mariappan, Y. Zhou, J. Hao and C. A. Wilkie, "Influence of Oxidation State of Phosphorus on the Thermal and Flammability of Polyurea and Epoxy Resin", *Eur. Polym. J.*, 2013, **49(10)**, 3171-3180
- [30] H. Horacek and R. Grabner, "Advantages of Flame Retardants Based on Nitrogen Compounds", *Polym. Degrad. Stab.*, 1996, **54(2-3)**, 205-215
- [31] M. Klatt, "Nitrogen-based Flame Retardants," in "Non-Halogenated Flame Retardant Handbook", eds. A. B. Morgan and C. A. Wilkie, Scrivener Publishing LLC, Canada, 2014, pp 143-168
- [32] J. Alongi, Z. Han and S. Bourbigot, "Intumescence: Tradition Versus Novelty. A Comprehensive Review", *Prog. Polym. Sci.*, 2015, **51**, 28-73
- [33] H. Ma, P. Song and Z. Fang, "Flame Retarded Polymer Nanocomposites: Development, Trend and Future Perspective", *Sci. China Chem.*, 2011, **54(2)**, 302-313
- [34] H. D. Lu, L. Song and Y. Hu, "A Review on Flame Retardant Technology in China. Part II: Flame Retardant Polymeric Nanocomposites and Coatings" *Polym. Adv. Technol.*, 2011, **22(4)**, 379-394
- [35] P. Song, H. Liu, Y. Shen, B. Du, Z. Fang and Y. Wu, "Fabrication of Dendrimer-like Fullerene (C60)-Decorated Oligomeric Intumescent Flame Retardant for Reducing the Thermal Oxidation and Flammability of Polypropylene Nanocomposites", *J. Mater. Chem.*, 2009, **19(9)**, 1305-1313
- [36] X. Yue, C. Li, Y. Ni, Y. Xu and J. Wang, "Flame Retardant Nanocomposites Based on 2D Layered Nanomaterials: A Review", *J. Mater. Sci.*, 2019, **54(20)**, 13070-13105
- [37] G. Beyer and T. Lan, "Polymer Nanocomposites: A nearly University FR Synerist", in "Non-Halogenated Flame Retardant Handbook", eds. A. B. Morgan and C. A. Wilkie, Scrivener Publishing LLC, Canada, 2014, pp 243-292

- [38] M. Khajeh, S. Laurent and K. Dastafkan, "Nanoadsorbents: Classification, Preparation, and Applications (with Emphasis on Aqueous Media)", *Chem. Rev.*, 2013, **113(10)**, 7728-7768
- [39] P. Kiliaris and C. D. Papaspyrides, "Polymer/Layered Silicate (Clay) Nanocomposites: An Overview of Flame Retardancy", *Prog. Polym. Sci.*, 2010, **35(7)**, 902-958
- [40] M. Nuruzzaman, M. M. Rahman, Y. Liu and R. Naidu, "Nanoencapsulation, Nano-guard for Pesticides: A New Window for Safe Application", *J. Agric. Food Chem.*, 2016, **64(7)**, 1447-1483
- [41] M. Alexandre and P. Dubois, "Polymer-Layered Silicate Nanocomposites: Preparation, Properties and Uses of a New Class of Materials", *Mater. Sci. Eng. R.*, 2000, **28(1)**, 1-63
- [42] D. Porter, E. Metcalfe and M. Thomas, "Nanocomposite Fire Retardants-A Review", *Fire Mater.*, 2000, **24(1)**, 45-52
- [43] H. T. Kahraman, H. Gevgilili, E. Pehlivan and D. M. Kalyon, "Development of an Epoxy Based Intumescent System Comprising of Nanoclays Blended with Appropriate Formulating Agents", *Prog. Org. Coat.*, 2015, **78**, 208-219
- [44] G. Huang, J. Gao, Y. Li, L. Han and X. Wang, "Functionalizing Nano-Montmorillonites by Modified with Intumescent Flame Retardant: Preparation and Application in Polyurethane", *Polym. Degrad. Stabil.*, 2010, **95(2)**, 245-253
- [45] X. Li, Z. Yang, J. Yao and Y. Zhang, "Organic Nano-montmorillonite for Simultaneously Improving the Flame Retardancy, Thermal Stability and Mechanical Properties of Intumescent Flame-retardant Silicone Rubber Composites", *J. Macromol. Sci. Part B*, 2015, **54(10)**, 1282-1296
- [46] H. Qin, S. Zhang, C. Zhao, G. Hu and M. Yang, "Flame Retardant Mechanism of Polymer/Clay Nanocomposites Based on Polypropylene", *Polym.*, 2005, **46(19)**, 8386-8395
- [47] J. H. Koo, S. C. Lao and J. C. Lee, "Flame-retardancy Characterization of Polymer Nanocomposites", in "Characterization Techniques for Polymer Nanocomposites", eds. V. Mittal, Wiley-VCH, Germany, 2012, pp 33-74

Chapter 3

Literature Review

Layered double hydroxides (LDHs) are a group of two-dimensional nano-layered materials. The first LDH discovered over a century ago is mineral hydrotalcite, comprising a hydroxycarbonate of magnesium and aluminium. Its chemical formula is $[\text{Mg}_6\text{Al}_2(\text{OH})_{16}]\text{CO}_3 \cdot 4\text{H}_2\text{O}$. Later, there was an attempt to synthesis the hydrotalcite-like compounds to use as LDH representative. Thus, LDHs are also assigned as hydrotalcite-like compounds [1-4]. To date, LDH is a novel flame retardant for polymeric materials that provides inhibition of fire propagation process. The objectives of this chapter are to present fundamental structure, synthesis, characterisation of LDHs. Besides, there were the presences of brief polymer nanocomposites and the state of the art modifications of LDH structure to enhance fire retardancy for polymers, especially epoxy resin nanocomposites.

3.1 Structure of LDHs

The base layered configuration of LDHs is brucite ($\text{Mg}(\text{OH})_2$). The crystal structure of brucites possessed hydroxide anions (OH^-) in hexagonal close packing and magnesium ions (Mg^{2+}) occupied in octahedral sites. The hydroxide layers stacks along a vertical direction that is combined with van der Waals force. Figure 3.1 illustrates a schematic configuration of brucite. In the literature on the brucite crystal, the distance between adjacent cation centre in the x-axis (a_0) is 0.314 nm which is equal to that in the y-axis (b_0), while the length from the middle of one layer to that in the neighbouring layer (basal spacing, c_0) is 0.477 nm [2-4].

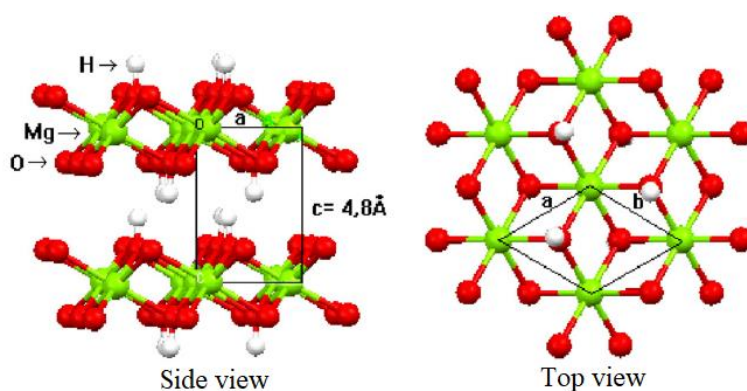


Figure 3.1 Schematically chemical structure of brucite [3].

For LDH structure, some divalent metal cations in the brucite structure are substituted by trivalent metal cations (M^{3+}). It results in an excess positive charge in the metal layers. To neutralise the charge in the layer structure, anions are intercalated in the interlamellar region. Besides, molecules of water intercalate the interlayer space of LDH. The water molecules combine to the metal hydroxide layers and the anions with hydrogen bonds [2-4]. Figure 3.2 and 3.3 display a schematic structure and a diagram of LDH representation, respectively.

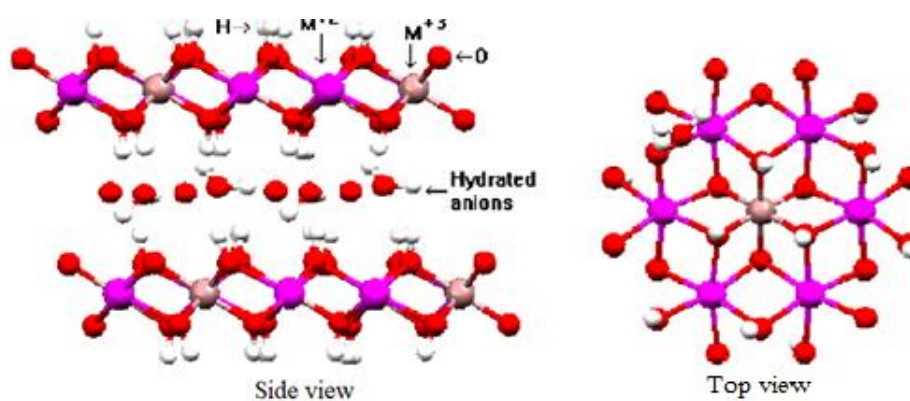


Figure 3.2 Schematic representative of LDH [5].

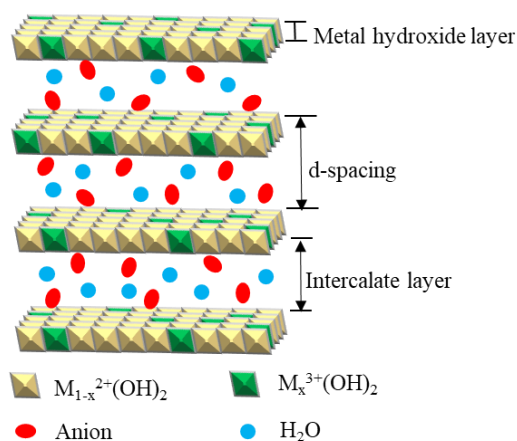


Figure 3.3 Schematic diagram of LDH compositions [6].

As the arrangement of LDH lattices is stacked by the metal hydroxide layers along the basal axis, it is defined as the 2D nanomaterials. The interaction between atoms in the layer is bound by covalent bonds, and each neutralised layer connected through van der Waals force. The common empirical formula of the LDH group is $[M_{1-x}^{2+}M_x^{3+}(OH)_2]^{x+}[A^{n-}]_{x/n}\cdot yH_2O$, where M^{2+} is the divalent cation (e.g. Mg^{2+} and Zn^{2+}), M^{3+} is the trivalent cation (e.g. Al^{3+} and Fe^{3+}), A is a counter anion with valency

n (e.g. CO_3^{2-} and NO_3^-), x is a value of the molar ratio of $\text{M}^{2+}/(\text{M}^{2+}+\text{M}^{3+})$, and y is the amount of water in the structure [2-4].

As mentioned previously, the values of a_0 and b_0 relate to the average distance between adjacent cations on the metal lamellae, whereas the value of c_0 corresponds to the length of basal spacing (d-spacing) in the layered structure. For LDHs based Mg and Al ions (Mg/Al LDHs), the approximate value of a_0 varies around 0.302 nm and 0.307 nm. It is small by comparison with the a_0 value of brucite (0.314 nm) due to the reduction of atomic size. The atomic size of Al^{3+} (0.0675 nm) substituting in the metal hydroxide layers of LDHs is smaller than Mg^{2+} (0.0860 nm). Meanwhile, LDHs possess intercalated anions and water molecules in the interlayer space, resulting in an enlargement of gallery distance. Therefore, the c_0 value of LDHs is higher than the brucite (0.477 nm), depending on the types of intercalating anions [3]. For instance, the d-spacing of Mg/Al LDHs intercalated with CO_3^{2-} or NO_3^- is 0.78 nm and 0.89 nm, respectively [7, 8].

3.2 Synthesis Methods of LDHs

Since the properties of mineral LDH discovered in nature are limited to industrial applications, numerous studies have attempted to synthesis LDHs with achieving the desired properties. There are several techniques used for LDH preparations in recent years, classified into direct and indirect methods. The direct method is a synthesis of LDHs in one technique such as co-precipitation and urea hydrolysis. It does not need to use LDHs as a precursor for the modification of LDHs. On the other hand, the indirect is a multi-technique used for LDHs synthesis, which needs to use LDHs as a precursor for the synthesis. The examples of indirect methods are anion exchange and reconstruction by memory effect [1, 4, 6, 9]. Ritchetta et al. (2017, cited in Daneil and Thomas, 2020) [4] reported that the types of cationic and anionic ions and the physical properties of LDHs influence the choice of the synthesis methods. This section will describe the details in each preparing method.

3.2.1 Co-precipitation

The most frequently used technique for LDH synthesis is co-precipitation. This method is a one-pot direct synthesis for preparing LDHs [4, 9]. In this synthesis method, an aqueous solution of mixed metal salts containing both the divalent and trivalent cations with an appropriate ratio is slowly added into an alkaline solution consisting of target anions under vigorous stirring. The excess hydroxide concentration contributes to the hydroxylation and the precipitation of the two metal salts. During the addition of the metal salt solution, the pH value of the mixed solution decreases steadily. Therefore, to control the pH of the precipitation, a dilute basic solution of sodium hydroxide, potassium hydroxide or ammonium hydroxide is dropped into the mixed solution. The typical pH during the synthesis is maintained between 7 and 10, depending on the types of metal salts [1, 3, 4, 6, 9]. Figure 3.4 displayed the examples of pH values used for LDHs synthesis with a difference of metal cations.

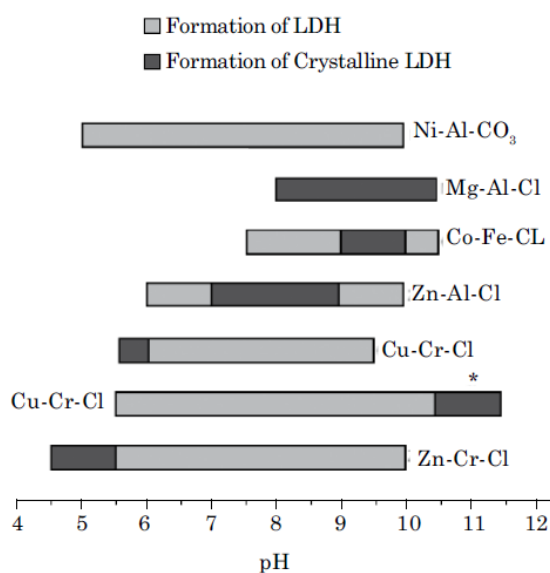


Figure 3.4 Representatives of pH ranges used for LDH synthesis with various types of divalent and trivalent cations [10].

Although the LDHs crystals can be formed at room temperature, thermal treatment of the suspended solution is necessary to the synthesis process because it can increase the crystallinity and yield of the synthesised LDH. The simple technique used for the thermal treatment is to ageing the solution at 60-100°C for a few hours to over several days [1, 9]. After the ageing process, the precipitate is washed with water and dried at 70°C [1].

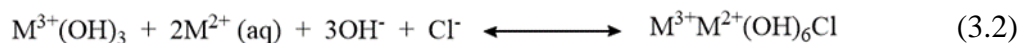
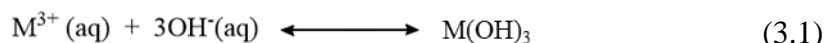
According to the study of He et al. [9], the desired anions intercalated in the interlayers ought to introduce a potent attraction to the metal hydroxide lamellae and to have a large amount for the intercalation. For these reasons, nitrate or chloride salts of divalent and trivalent cationic metals are used as precursors for LDHs preparation since they have a low affinity comparing to the desired anion. The synthesis conditions on LDHs should be without contamination of carbon dioxide (CO₂), carbonate ions (CO₃²⁻), or both. They are high affinity that can interact speedily with the cationic layers of metal hydroxides. This interrupts the interaction of desired anions with the layers. Thus, nitrogen gas (N₂), an inert gas, is flowed into a reactor during the synthesis process to protect the absorption of CO₂.

3.2.1.1 Mechanism of Crystalline LDH Formation Prepared by Co-precipitation Method

Even if many LDH synthesis studies via the co-precipitation method have attracted wide attention, there are just a few published works on the mechanism of crystalline LDH formation. The two primary mechanisms of the LDH formation are nucleation and growth of LDH crystallites [11-13]. A comprehensive study by Tathode and Gazit [13] stated that when the first drop of the metal precursor solution was added to the alkaline solution, it generated a negligible amount of LDH nuclei in the mixed solution. The further drop of metal salt solution contributed to either the growth of formed nuclei, new nuclei production, or both. The particle size distribution varied in a broad range in the initial co-precipitation. Once the complete addition of the metal precursor solution, many nuclei increased dramatically, but the growth of the particles reduced. This stage attributed to the reduction of the size distribution. The increase of nucleation rate was exponential, whereas the growth rate rose by a linear curve. After the co-precipitation, the solution was heated, leading to the crystal growth, agglomeration and stacking of the LDH layers. Some small particles can re-dissolve to the solution and agglomerate to produce the larger particles during ageing. This action is known as an Ostwald ripening mechanism.

Moreover, the study of Bocclair and Braterman proposed the chemical reaction of LDH formation [14]. In the first step, the dropping of the mixed metal salt solution containing both M²⁺ and M³⁺ ions to the saturated alkaline solution resulted in trivalent

metal hydroxide ($M^{3+}(\text{OH})_3$) presented in Equation 3.1. Then, the M^{2+} ions interacted with the M^{3+} -rich LDH phase and the anions e.g. chloride (Cl^-) were intercalated in the structure. Equation 3.2 shows the equilibrium reaction of the LDH formation.



Yang et al. [15] reported that the amorphous aluminium hydroxide was precipitated at the beginning of synthesis because the pH for the precipitation of Al^{3+} was lower than that of Mg^{2+} . Further, an accumulation of the amorphous aluminium hydroxide took place in the solution inducing a formation of lamellar boehmite (oxide-hydroxide aluminium, $\gamma\text{-AlOOH}$). Then, the Mg^{2+} were absorbed on the boehmite's surface and incorporated in the boehmite layers, resulting in an unbalance of charge in the structure. The anions (e.g. carbonate and nitrate) were combined in the interlayers to balance the unstable-ionic layers. Afterwards, there was the stacking of layers along the c-direction, contributing to the LDH structure. The crystallinity of LDH increased with the crystal growth process until the appearance of perfect LDH. Figure 3.5 illustrates the mechanism of the LDH formation proposed in this study.

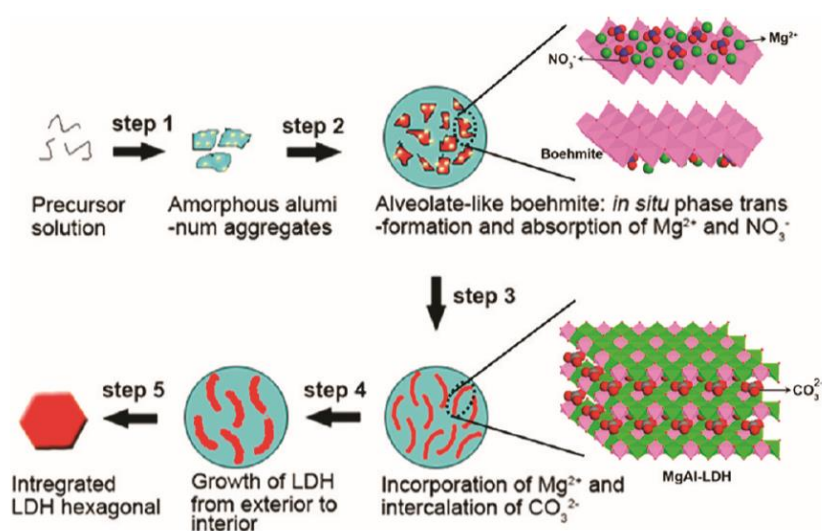


Figure 3.5 Schematic mechanism of LDH formation proposed by Yang et al. [15]. In contrast, some researchers argued that the LDH formation mechanism resulted from the diffusion of M^{3+} ions into the divalent hydroxide structure [16, 17]. Shin et al. [17] suggested that the mechanisms of LDH formation had three critical stages.

The first stage of LDH formation was a warming-up stage. In the initial time of 1.5 h, the boehmite molecules were attached to the brucite layers, resulting in the slight expansion along with the c-axis from 4.75 Å for the pristine brucite to 4.80 Å for the heat-treated brucite. Subsequently, the boehmite diffused into the brucite lamellar, causing the dissolution, re-precipitation and substitution of Mg^{2+} . In the meantime, the CO_3^{2-} ions combined with the excess cations on the metal hydroxide layers to compensate for the charge in the layered structure. This circumstance accounted for the phase transformation from the brucite phase to the low crystalline LDH in the period of 1.5-2.3 h. At the last stage, the low crystalline LDH was growing both the c-axis and the ab-plane. It promoted the increase of crystallinity and the growth of crystal size. This process is called the crystal growth and ordering stage. Figure 3.6 illustrates the schematic diagram of the phase transformation of brucite to high crystallinity of LDH.

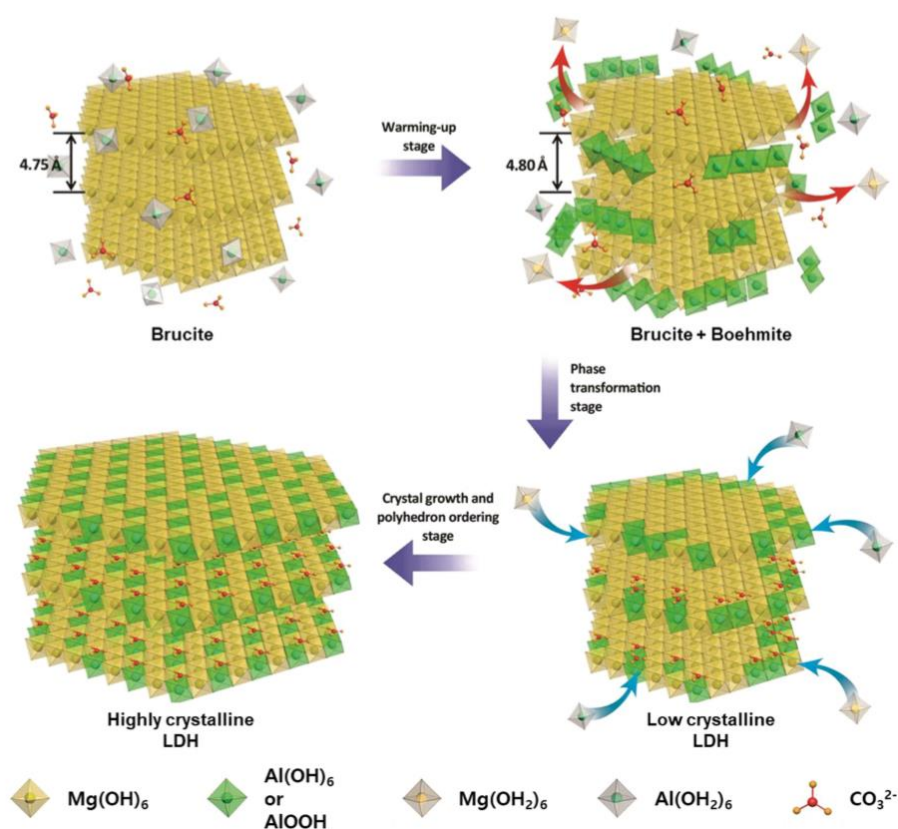


Figure 3.6 Schematic diagram of the phase transformation of brucite to high crystallinity of Mg/Al LDH [17].

3.2.1.2 Effect of Parameters on LDH Formation

To date, numerous researches have studied the effect of parameters on the LDH formation prepared by the co-precipitation method, for example, precipitating agents [12, 18], pH of solution [12, 19-21] and aging temperature and time [22-24].

3.2.1.2.1 Precipitating Agents

The general basic solution used as a precipitating agent for the co-precipitation is the sodium hydroxide (NaOH) aqueous solution. Kameda and Umetsu established that the concentration of the NaOH solution affected the crystallinity of LDHs. From the XRD results in Figure 3.7, it can be observed that the intensity and sharpness of crystalline peaks increased obviously with using the high concentration of NaOH. This result was evidence of crystalline increase [18]. These results related to the prior research that the higher NaOH concentration used, the larger crystalline size of Mg/Al LDHs obtained [12].

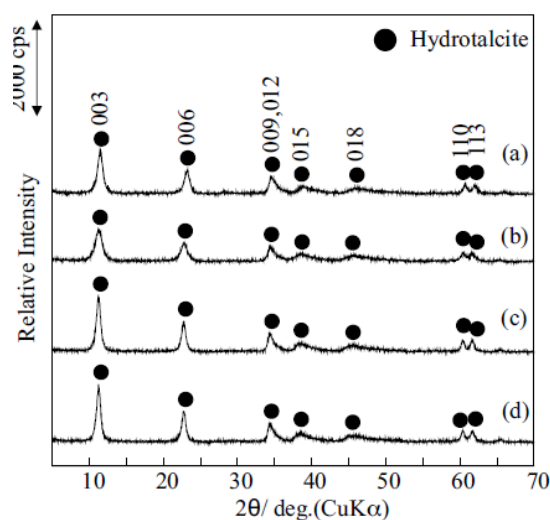


Figure 3.7 XRD patterns of Mg/Al LDHs prepared with the difference of NaOH concentrations: (a) 0.75, (b) 0.9, (c) 1.0 and (d) 1.25 M NaOH [18].

With the characterisation of ion concentration during the synthesis, the small amount of Mg^{2+} existed in the mixed solution as the pH maintained with the low NaOH concentration (0.75 and 0.9 M NaOH). It indicated that the low concentration of NaOH could not precipitate the Mg^{2+} to form the $Mg(OH)_2$. The applying of the higher concentration of NaOH, nevertheless, encouraged the precipitation of Mg^{2+} .

Meanwhile, the precipitation of Al^{3+} ions could take place in all the concentrations of the base solution.

After the complete precipitation and aging processes, the suspension was filtered and washed with the water until neutralisation. In case of LDH synthesis with using the low NaOH concentration, the filtrate may contain some Mg^{2+} . It was necessary to remove the Mg^{2+} in the filtrate for wastewater treatment. On the contrary, if the high NaOH concentration was used in the LDH synthesis, it must consume a large amount of water in the washing process for the remove of excess NaOH and the neutralisation of residue [18]. Hence, the selection of appropriate NaOH concentration is important for the LDH synthesis with this method.

Besides the NaOH solution, another basic solution for LDH synthesis with the co-precipitation method is an aqueous ammonium hydroxide solution (NH_4OH). Olanrewaju et al. [8] compared the performance of different base precipitating agents. The XRD results in Figure 3.8 demonstrated that the d-spacing at the lowest angle of the crystalline peak of LDHs prepared using the NaOH and NH_4OH solutions were 7.8 Å and 8.8 Å, respectively. According to the prior studies, the LDH with the d-spacing was 7.6-7.8 Å, attributing to the intercalation of carbonate ions between the inter-lamellar of metal hydroxide layers, whereas the d-spacing of 8.5-8.8 Å represents the existence of nitrate form in the interlayer region of LDH [7, 8]. Hence, the use of NaOH induced the intercalation of carbonate forms, while the LDH presented the nitrate forms in the interlayers of LDHs using the NH_4OH solution [8].

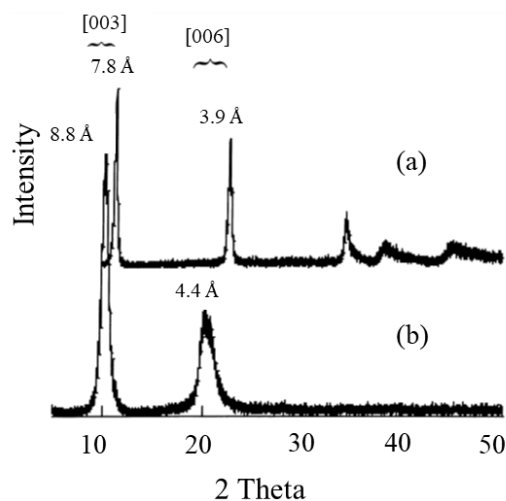


Figure 3.8 XRD patterns of Mg/Al LDHs prepared by the co-precipitation with the different precipitating agents: (a) NaOH and (b) NH_4OH [8].

3.2.1.2.2 pH Values

For the co-precipitation method, controlling pH value in the suspended solution with adding alkaline solution is necessary to the co-precipitation of the two metal salts [9]. Most LDH synthesis studies maintained the pH of the mixed solution at 10. However, there was no explanation of why the LDH synthesis needs to use this condition. The only research of Seron and Delorme [19] considered the concentration of Mg^{2+} and Al^{3+} in the suspended solution for the LDH synthesis by the co-precipitation without a maintained pH. The solution of NaOH and Na_2CO_3 was dropped into a solution of $\text{Mg}(\text{NO}_3)_2$ and $\text{Al}(\text{NO}_3)_3$ with a constant rate until the solution obtained to pH 13.2. The reaction of the metal salts and the NaOH contributed to the reduction of pH. The sampling of suspension in the various pH was carried out to measure the concentration of Mg^{2+} and Al^{3+} in the liquid phase, as presented in Figure 3.9. It could be seen that at the pH less than 7.1, the concentration of Al^{3+} decreased rapidly, but the concentration of Mg^{2+} reduced gradually. This result stated that the hydroxide forms of the trivalent cations were generated in the initial precipitation. At the pH over 7.1, there was not found the Al^{3+} ions in the solution.

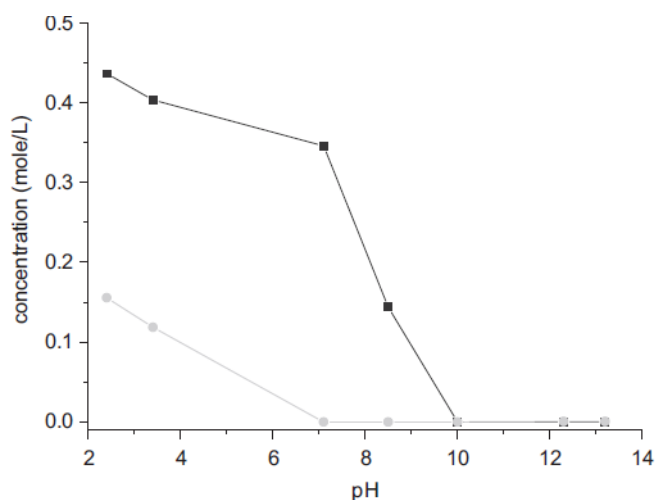


Figure 3.9 Concentration of metal ions in the mixed solution with the variation of pH: Mg²⁺ (black line) and Al³⁺ (gray line) [19].

Meanwhile, the contents of the Mg²⁺ ions dropped significantly and disappeared in the solution at pH 10 that may produce the magnesium hydroxides. This condition led to the formation of Mg/Al LDHs verified by the XRD patterns in Figure 3.10. Thereby, the pH controlling of the suspension at 10 was probably appropriate to form the LDH.

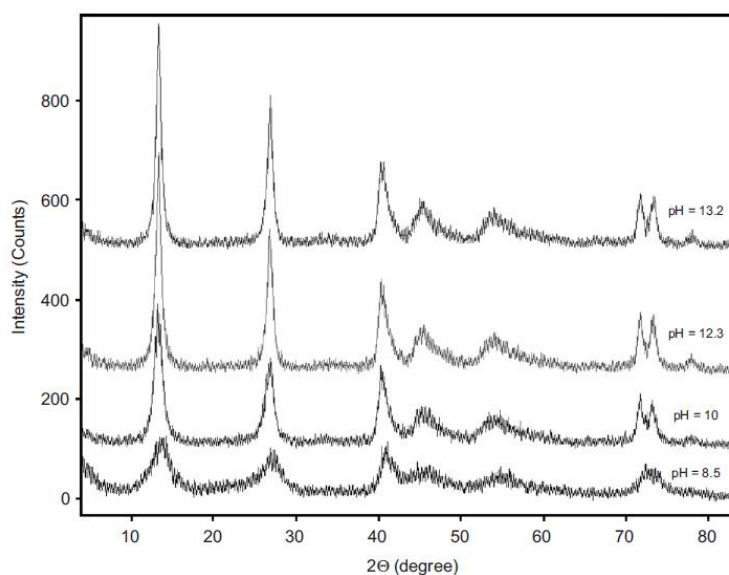


Figure 3.10 XRD patterns of Mg/Al LDHs with the variation of pH [19].

Furthermore, the XRD peak intensity of LDHs increased significantly with increasing the pH values related to the published research of Ay et al. [21]. Besides, Panda et al.

[12] affirmed that the LDH preparation at the higher pH affected the larger crystallite size, displayed in Table 3.1.

Table 3.1 Crystallite size of Mg/Al-CO₃ LDHs prepared with the co-precipitation method at various pH [12].

Molar concentration of NaOH (M)	Average crystallite size (Å)		
	pH9	pH10	pH11
0.10	1.97	2.85	2.24
0.25	1.65	2.43	2.59
0.50	2.08	2.45	3.10
1.00	2.42	2.57	-

According to the study of Li et al. [20] on the phase transformation of LDHs with the variation of pH, it could be noticed that the LDH prepared under pH 6 presented the intercalation of nitrate forms while the LDH preparation at higher pH was intermediate with the carbonate forms. These results were confirmed from the d-spacing of (003) peaks in the XRD patterns, as presents in Figure 3.11. As described above, the interlayer distance of 8.8 Å and 7.8 Å was assigned to the intercalation of nitrate and carbonate ions, respectively. This phenomenon showed the phase transformation from the nitrate to carbonate forms with the increase of pH.

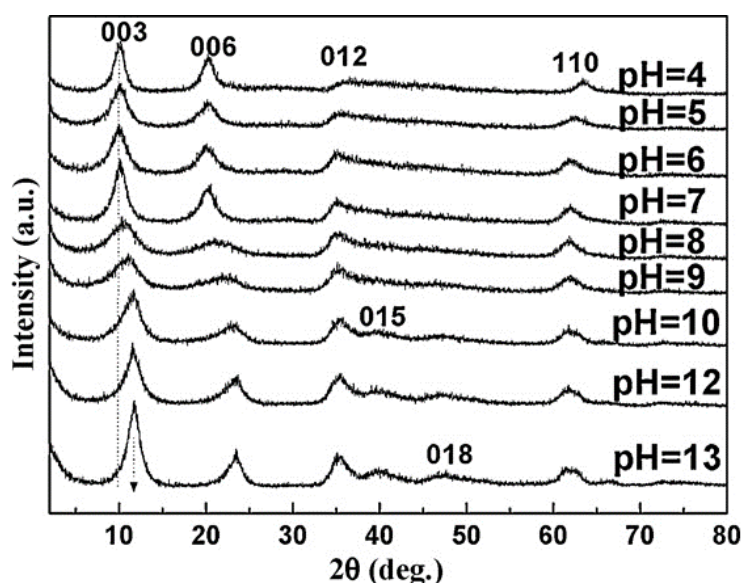
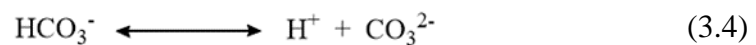
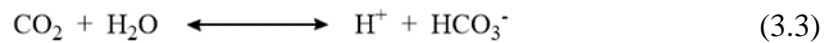


Figure 3.11 Interlamellar distance of (003) and (110) reflections for the Ni/Al LDHs synthesised in the different pH [20].

Considering the solubility of CO₂ in water, the CO₂ can react with water, resulting in bicarbonate anion formation (HCO₃⁻). Then the anions decompose to the carbonate ion. The reversible reactions of CO₂ dissolution in water are presented in Equation 3.3 and 3.4. The values of acid ionisation constants for K_{a1} and K_{a2} at 25°C of both equations are given in Equation 3.5 and 3.6, respectively.



$$K_{a1} = \frac{[\text{HCO}_3^-] \cdot [\text{H}^+]}{[\text{H}_2\text{CO}_3]} = 10^{-6.352} \text{ mol/L} \quad (3.5)$$

$$K_{a2} = \frac{[\text{CO}_3^{2-}] \cdot [\text{H}^+]}{[\text{HCO}_3^-]} = 10^{-10.329} \text{ mol/L} \quad (3.6)$$

From the equations, when the calculation of carbonate concentration is at around pH 5, it equaled 10⁻⁶ mol/L. It presented that the low concentration of acid in the solution at pH5. Therefore, the carbonate ions could not be in the LDH structure. However, if the solution was pH10, the carbonate concentration increased remarkably in the system of LDH synthesis. As the carbonate possesses a high affinity, it leads to the replacement of nitrate with carbonate ions in the LDH structure.

3.2.1.2.3 Aging Temperature and Time

The ageing of the precipitated solution is the process that is important to enhance the crystallinity of synthesised LDHs. This information is confirmed by Galvão et al. [24], who studied the effect of ageing temperature on the crystallite characteristics of Zn/Al LDHs. The data in Table 3.2 shows that the higher temperature, the larger crystallites and particle size of LDHs. The increase in the temperature also influenced the decrease in surface areas of LDHs [8].

Table 3.2 Average crystallite size in the peaks of (006) and (110) and the particle size of Zn/Al LDHs prepared at the different pH and ageing temperature [24].

Sample (Conditions)	Crystallite size in (006) (nm)	Crystallite size in (110) (nm)	Particle size (nm)
At pH 8.5			
50°C	17 ± 2	31 ± 3	345 ± 15
70°C	22 ± 2	35 ± 3	448 ± 16
100°C	30 ± 2	48 ± 3	445 ± 10
At pH 10			
50°C	19 ± 2	30 ± 3	341 ± 21
70°C	20 ± 2	29 ± 3	362 ± 14
100°C	26 ± 2	49 ± 3	400 ± 11
120°C	43 ± 2	50 ± 3	913 ± 111

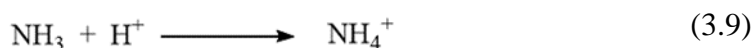
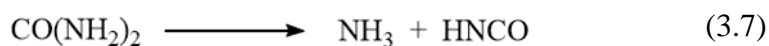
Another factor for the thermal treatment was the time for the aging process. The study of Galvão et al. [24] also investigated the influence of the crystallisation time on the crystallite and particle size of Zn/Al-NO₃ LDHs. All the results were shown in Table 3.3. It was found that there was no significant difference in crystalline size and particle size in the first few hours of thermal treatment. These results could be explained in terms of stable hydrodynamic materials during the co-precipitation. It produced small amorphous particles with high surface energy in the initial heat treatment. They possessed low hydrodynamic stability. Thus, the particles could be consecutively dissolved until they obtained high thermal stability. After the two hours of ageing, both the sizes of crystals and particles increased significantly with the longer crystallisation times due to the growth of the LDH crystals. The results were similar to the other researches [22, 23].

Table 3.3 Average crystallite size in the peaks of (006) and (110) and the particle size of Zn/Al LDHs prepared at pH 10 and 100°C in the various ageing times [24].

Sample (Conditions)	Crystallite size in (006) (nm)	Crystallite size in (110) (nm)	Particle size (nm)
0 h	15 ± 2	28 ± 3	342 ± 11
1 h	15 ± 2	28 ± 3	331 ± 17
2 h	15 ± 2	34 ± 3	333 ± 8
4 h	26 ± 2	49 ± 3	400 ± 11
6 h	38 ± 2	50 ± 3	678 ± 28

3.2.2 Urea Hydrolysis

Urea has been used for the precipitation of metal hydroxides. It is interesting to apply urea into the aqueous solution of mixed-valence metallic salts to obtain the hydrolysis reaction and the LDH formation. The mixed solution is re-fluxed under the controlled temperature [4, 9]. Equation 3.7-3.9 present the hydrolysis reactions of urea. The by-product of the reactions is ammonium hydroxide that can interact with the required metal ions [3]. The reaction rate relies on the applied temperature that affects the particle size of LDH.



Ogawa and Kaiho [25] indicated that the average particle size of LDH decreased with the high reaction temperature, as displayed in Figure 3.12. The particle size decreased by 0.9 μm for 150°C from 2.9 μm for 100°C. Furthermore, the review of He et al. [9] claimed that the LDHs prepared by the urea hydrolysis methods had a larger particle size than by any other methods.

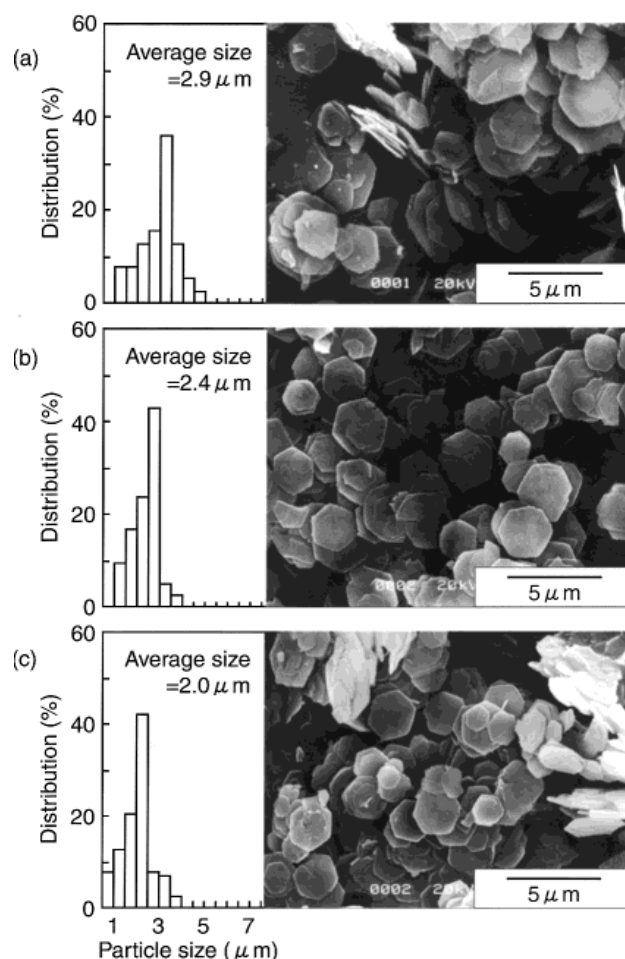


Figure 3.12 Average particle size and scanning electron micrographs of synthesis Mg/Al-CO₃ LDHs with the variation of reaction temperatures: (a) 100°C, (b) 120°C and (c) 150°C [26].

Nevertheless, another product liberated from the hydrolysis of urea is CO₂. It can react with the water, providing the carbonate ions. This reason may contaminate the produced LDH or obstruct the interaction of desired anions because the CO₃²⁻ is high affinity. Hence, this method is preferred for synthesis of LDHs-CO₃ [3, 25]. As most organic anions are lower affinity than the carbonate anion, the urea hydrolysis method may not be suitable for the preparation of LDH intercalated with organic compounds.

3.2.3 Anion Exchange

Another method used for the synthesis of LDH is the anion exchange, known as the indirect method. An LDH precursor is vigorously stirred in a solution containing desired anions. During the preparation process, an exchange of existing anions

intercalated in the interlamellar regions of the LDH precursor with the desired anions in an aqueous solution. The proportion of desired anions should be higher than the anions in the precursor LDHs. The possibility of the ion exchange reaction is proposed in Equation 3.10 [4, 6, 9, 27].



The efficiency of anion exchange depends on the electrostatic forces between positive charges on the metal hydroxide lamellae and negative charges of exchanging anions [6, 9, 28]. The anions with the high charge provide stronger the interaction force with the metal hydroxide layer than that with low charge [28]. The order of affinity in various sorts of anions with the LDH lamellae is $\text{NO}_3^- < \text{Br}^- < \text{Cl}^- < \text{F}^- < \text{OH}^- < \text{MoO}_4^{2-} < \text{SO}_4^{2-} < \text{CrO}_4^{2-} < \text{HPO}_4^{2-} < \text{CO}_3^{2-}$ [4]. For this reason, the exchange of anions in the LDHs preparation was limited with using LDH intercalated with divalent or trivalent cations as precursors. Practically, the LDHs intercalated with NO_3^- or Cl^- are used as precursors for the synthesis since they provide a weak affinity with the metal hydroxide layers. Thus, the host anions are substituted with the guest anions in the interlayer space [6, 9].

3.2.4 Reconstruction by Structural Memory Effect

One of the unique characteristics of LDH is the presence of a memory effect. The structure of LDH can reconstruct after the LDH is calcined at high temperature and suspended in an aqueous solution with the composition of desired anions. The two fundamental LDH synthesis processes with this method are calcination and rehydration [6, 9].

3.2.4.1 Calcination

For the calcination, the pristine LDH- CO_3 is dehydrated by a thermal treatment in a furnace leading to the liberation of interlayer water molecules and anions and hydroxyl species. This stage produced mixed metal oxides [6, 9]. The study of Millange et al. [29] described the thermal decomposition of Mg/Al- CO_3 by using a thermogravimetric analyser (TGA) and differential thermal analyser (DTA). Figure

3.13 show the TGA curve and its derivative of Mg/Al-CO₃. The results indicated that there were two main stages of thermal decomposition. The first peak of the weight loss at 220°C was assigned to the loss of water molecules adsorbed on the surface of LDH and intercalated in the gallery regions of LDH. At the temperature range of 240-480°C, the mixed metal hydroxides in the LDH layers were dehydrated, resulting in metal oxides such as MgO and MgAl₂O₄.

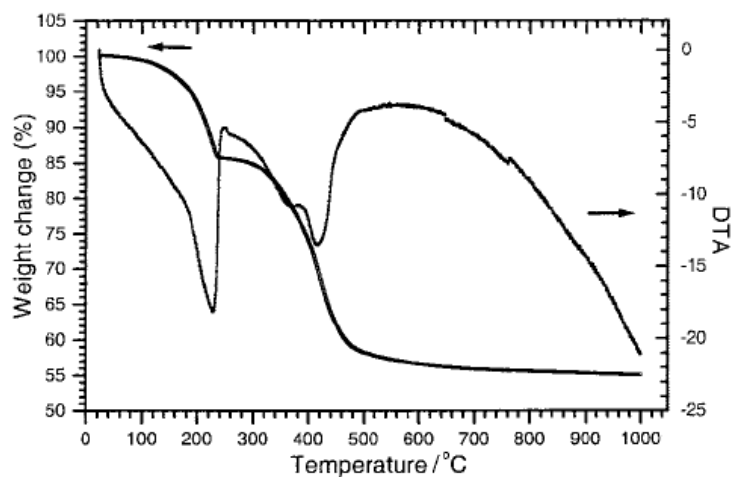


Figure 3.13 TGA and DTA results of MgAl-CO₃ [29].

In the meantime, the decarboxylation could be observed due to the decomposition of carbonate anions intermediated between the layers. The thermal behaviours of LDH-CO₃ correlated to the XRD results, displayed in Figure 3.14.

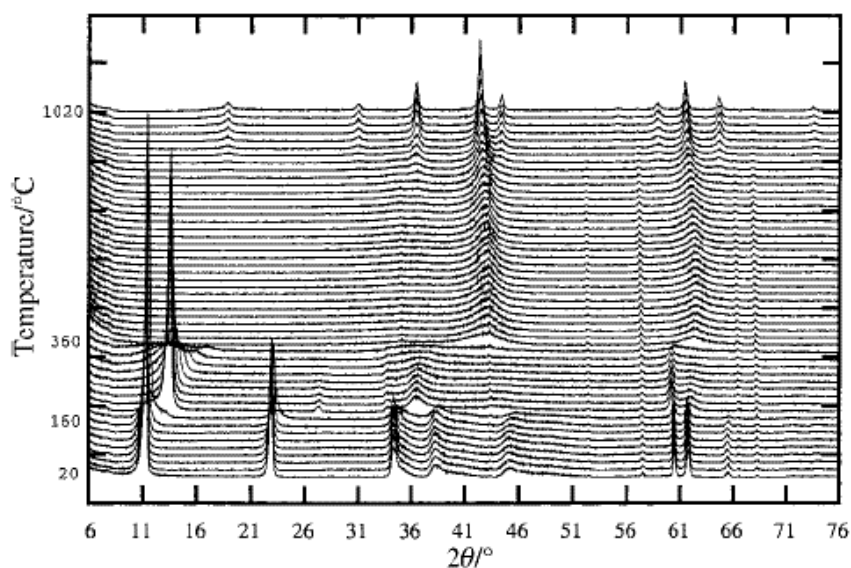


Figure 3.14 XRD patterns of MgAl-CO₃ calcined at different temperatures [29].

From the XRD diffraction patterns, it can be seen that the calcinations of LDHs at temperatures below 160°C did not affect the transition of the crystalline phase; the samples provided the crystalline LDHs. Between 160°C and 360°C, the d-spacing of the calcined LDHs at the crystalline plane (003) shifted from 7.8 Å to 6.8 Å. It corresponded to the decrease of the interlamellar spacing. These results occurred in the processes of dehydroxylation and decarboxylation during the heating. Moreover, the intensity of XRD peaks reduced, especially the reflection of (006).

Meanwhile, the diffraction peak around 60°, corresponding to the metal-metal distance in the layer broadens due to the disordered structure. For the calcination over 360°C, the XRD patterns being characteristic of LDHs structure were not completely obtained. However, three broad peaks correlated to the mixture of oxide phases such as MgO and Al ions in the lattice. Besides, there was an increase of sharpness at the higher temperature of calcination. It determined the increase of crystallinity resulting from the sintering of calcined crystals. At the calcination temperature of 1020°C, it provided the spinel-like compound (MgAl_2O_4) [29].

3.2.4.2 Rehydration

For rehydration, the layer structure of LDH can be regenerated by a hydration reaction of the calcined LDH. The calcined LDH contacts with the target anions in an aqueous solution. As a result, the metal oxides produced from the calcination of pristine LDHs are rehydrated by absorption of water in the solution, contributing to the re-formation of the metal hydroxide lamellae. In the meantime, the desire anions are intercalated in the interlamellar galleries of the layers [6, 9].

Nakayama et al. (2004) [30] reported the effect of rehydration temperature on the intercalation of phenylalanine (Phe) into the interlayers of the calcined LDH at 500°C. The amount of Phe used in the rehydrating period is observed, as shown in Figure 3.15. The uptake of Phe increased rapidly with the temperature rising (0 to 40°C), and the rate of uptake is stable at above 40°C. The amount of the saturated Phe used during the reaction is 2.5 mmol.

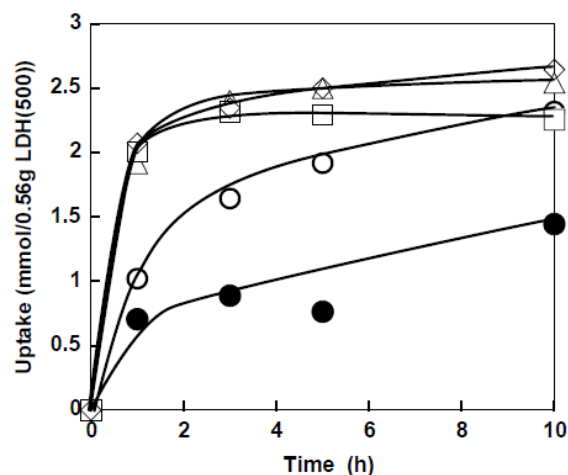


Figure 3.15 Uptake of Phe into the LDH calcined at 500°C in the variation of reaction temperature: ● = 0°C, ○ = room temperature, □ = 40°C, △ = 60°C and ◇ = 80°C [30].

Furthermore, Delorme et al. [31] studied the effect of rehydration time on the reconstruction of LDHs in the Na_2CO_3 solution. Figure 3.16 exhibits the size distribution of the particles both before and after the soaking in the Na_2CO_3 for 5 min, 1 h, 24 h, 5 days and 28 days. It can be seen that three populations of particle diameter, namely, 0.36, 1.7 and 4.9 μm presented for the soaking time for 5 min to 5 days. However, the primary particle size of the heat-treated Mg/Al LDH soaked in the Na_2CO_3 solution for 28 days is 1.7 μm .

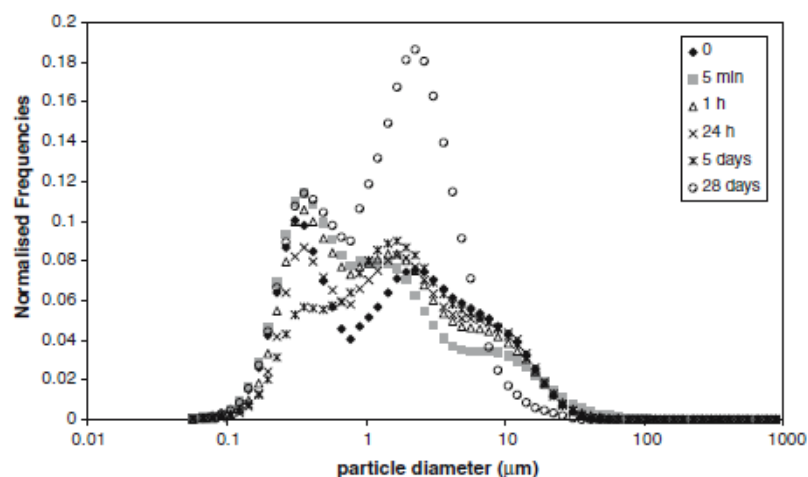


Figure 3.16 Size distribution of Mg/Al- CO_3 LDH particles synthesised by the calcination and rehydration method with the difference of rehydrated time (0, 5 min, 1 h, 24 h, 5 days and 28 days) [31].

3.3 Characterisation of LDHs

The characterisation of synthesised LDHs is essential to understanding their structure and properties and approaching the optimum conditions of the synthesis. There are several scientific techniques used for the analysis of LDH properties, such as X-ray diffractometry (XRD), Fourier transformed infrared spectroscopy (FTIR) and thermogravimetric analysis (TGA) [3, 4, 32]. Therefore, this section will explain some methods for LDH characterisation.

3.3.1 X-Ray Diffractometry

The most technique for characterisation of LDH crystalline phase is X-ray diffractometry (XRD). The X-ray reflections of LDH can be categorised into three groups. For the first series, the sharp peaks are apparent at low angles in (00*l*) reflections, determining the stacking of layers along the c-axis. The positions of these angles relate to the thickness of basal spacing (c_0), which is the distance from one metal hydroxide layer to an adjacent interlayer space [2]. The basal spacing or d-spacing is calculated by using Bragg's Equation:

$$n\lambda = 2d \sin\theta \quad (3.11)$$

where n is a diffraction order, λ is a wavelength of an X-ray source, and θ is a detected reflection angle [10].

For the higher-order reflections (00*n*), their spacing is equal to $c_0/2$ and $c_0/3$ for $n = 2$ and 3, respectively. However, if the stacking of layers disorders, the spacings do not correspond to this relationship [2, 32]. The interlayer spacing of LDH can be calculated from d-spacing and thickness of the metal hydroxide layer. The distance between the lamellae relies on the size and orientation of intercalated anionic molecules. Generally, the thickness of the metal hydroxide layer is approximately 0.48 nm [3, 32]. Many studies reported that the gallery height of LDHs was 0.38-0.40 nm [7, 8, 21] and 0.29-0.32 nm [7, 8] with the intercalation of NO_3^- and CO_3^{2-} ,

respectively. A lattice parameter of the unit cell in the c-axis for the n-layers (c) is equal to multiple of c_0 [2].

The second peak position at around 60° with using Cu K_α radiation as an X-rays source can be observed corresponding to a reflection (110). The d-spacing of (110) reflection is used to determine lattice parameter a_0 from the formula of $a_0 = 2d(110)$. The calculated a_0 displays the cationic radii [2].

For the last peak positions, the reflections of (01l) and/or (10l) display between the prior peak positions. These peaks determine the stacking patterns of the metal hydroxide layers. As the lattice system of metal atoms in the LDH layers possesses hexagonal unit cell, the number of stacked layers can be calculated from a relationship in Equation 3.12:

$$\frac{1}{d_{(hkl)}^2} = \frac{4}{3} \left(\frac{h^2 + hk + k^2}{a_0^2} \right) + \frac{l^2}{c^2} \quad (3.12)$$

where d_{hkl} is the d-spacing of the Miller indices (h, k and l) and a_0 and c are the lattice parameters. The stacking orientation of the LDH structure can be determined by using systematic absences. The two possible symmetric structure are rhombohedral and hexagonal symmetries. If the result of $-h+k+l$ is equal to $3n$, it corresponds to the rhombohedral structure. However, unless that relationship is equivalent, it indicates the hexagonal structure. For instance, considering the diffraction patterns of a synthesised hydrotalcite ($Mg_6Al_2(OH)_{16}(CO_3) \cdot 4H_2O$) in Figure 3.17a. The pattern showed that the LDH structure has three layers of stacking along the c-axis in rhombohedral symmetry with the lattice parameters of $a_0 = 0.306$ nm, $c_0 = 0.78$ nm and $c = 2.34$ nm. Meanwhile, the diffraction of manasseite mineral, which is the same formula as the hydrotalcite, in Figure 3.17b presents the stacking of two layers with hexagonal symmetry with the unit cell values of $a_0 = 0.306$, $c_0 = 0.78$ and $c = 1.56$ nm. [2]

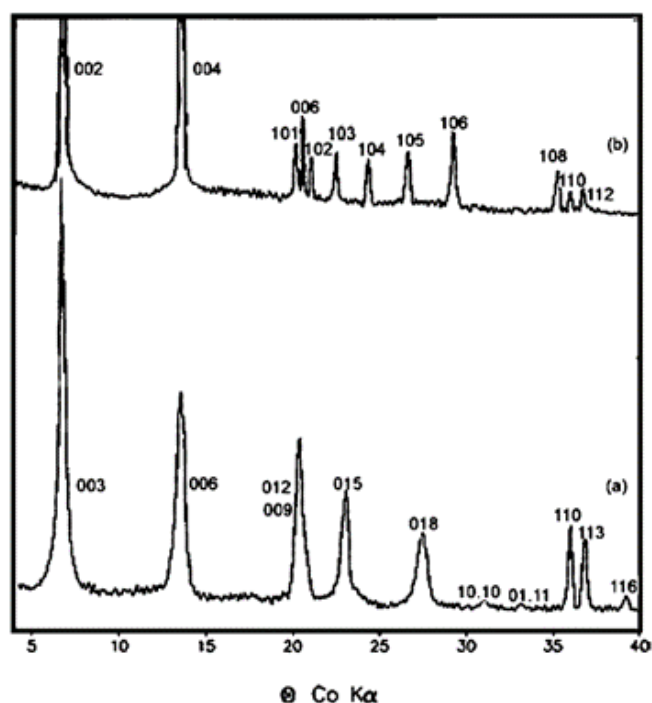


Figure 3.17 X-ray diffraction patterns of synthesised LDHs in different symmetries: (a) rhombohedral, and (b) hexagonal structures [2].

Figure 3.18 displayed the XRD pattern of LDH- CO_3 . Millange et al. [29] investigated the XRD pattern of the prepared Mg/Al- CO_3 LDH with the chemical formula of $\text{Mg}_3\text{Al}(\text{OH})_8(\text{CO}_3)_{0.5}\cdot 2\text{H}_2\text{O}$. The patterns provided the strong peaks at low angles presented the (003), (006) and (009) reflections. Due to the overlap with the (102) reflection, the peak at the same (009) reflection was a little broad. Furthermore, the pattern showed the (110) and (113) reflections between 60° and $63^\circ 2\theta$. Considering the characteristic of the pattern, it presented the high intensity with broad shape for the (00 l) reflections. This consequence showed that the prepared LDH had high crystallinity but small crystallites. The d-spacing of (003), (006) and (009) planes were 7.8, 3.9 and 2.6 Å, respectively. From the calculation of the unit cell parameters from the plane of (003) and (110), the value of the c_0 was 2.332 nm and that of the a_0 was 0.306 nm. The calculated interlayer space was 0.777 nm, corresponding to the location of the carbonate anions.

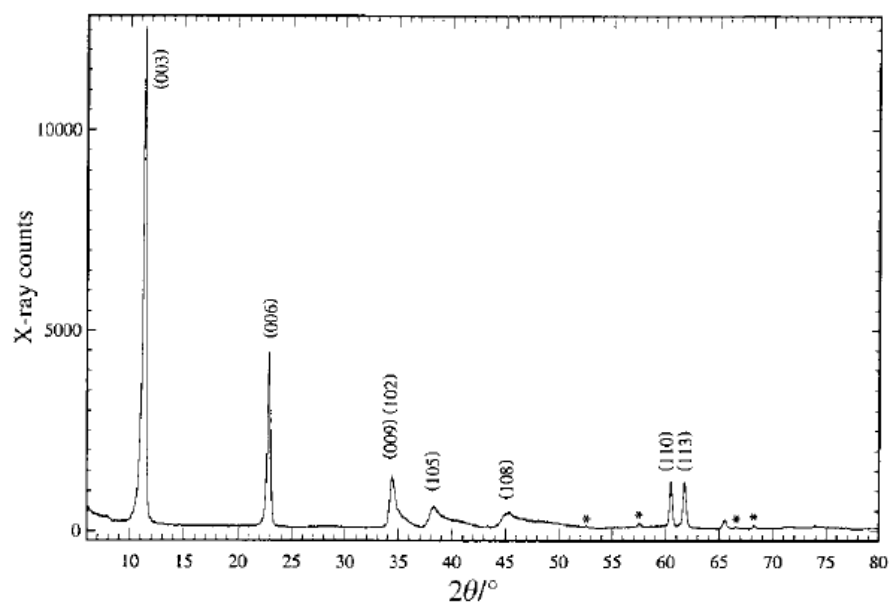


Figure 3.18 XRD pattern of $\text{Mg}_3\text{Al}(\text{OH})_8(\text{CO}_3)_{0.5}\cdot 2\text{H}_2\text{O}$ [29].

For the intercalation of desired anions, many studies established that the peak intensity of modified LDHs reduces compared to the unmodified LDHs. For the modified LDH with organic anions intercalated into the interlayers, the (003) reflection was shifted to the lower angle, compared to the unmodified LDH. For example, the intercalation of Mg/Al LDHs with dodecyl sulfate (DS) and dodecyl benzene sulfonate (DBS) is showed in Figure 3.19. The basal spaces of LDHs increase from 8.71 Å for nitrate ions to 24.2 Å for DS and 29.6 Å for DBS [33].

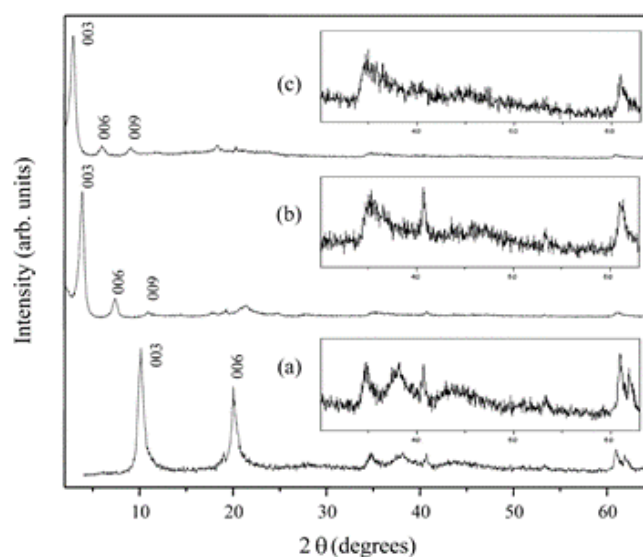


Figure 3.19 XRD patterns of Mg/Al LDHs with: (a) unmodified anion, (b) dodecyl sulfate and (c) dodecyl benzene sulfonate [33].

3.3.2 Fourier Transformed Infrared Spectroscopy

A technique used to characterise the chemical structures of LDH, particularly to molecules intercalated in the intermediate metal hydroxide lamellae, is Fourier transformed infrared spectroscopy (FTIR). The bands in the region of 400-1000 cm^{-1} attribute to the metal-oxygen-metal vibrations in the layers. A broad peak at 3500-3600 cm^{-1} is shown in the spectrum regarding a stretching vibration of the OH group in the metal hydroxide layers and the water molecules. The shoulder peak around 3000 cm^{-1} can be observed because of the characteristic of the hydrogen bond between water molecules and anions in the interlamellar region. Besides, bending vibration of the interlayered water displays at 1600-1650 cm^{-1} [1, 32].

For the intercalated anions, the vibrations of anions and metal-oxygen can be observed in the range of 200-2000 cm^{-1} , however, the main bands show between 1000 and 1800 cm^{-1} . With the intercalation of CO_3^{2-} anions in the interlayers, the spectrum provides the bands at 1350-1380 cm^{-1} , 850-880 cm^{-1} and 670-690 cm^{-1} . For the interaction of anionic NO_3^- , there are the appearance of 1380 cm^{-1} and 830 cm^{-1} in the spectrum [1, 32]. If the carbonate or nitrate ions are replaced with other anions, the intensity of bands at 1380 cm^{-1} decreases.

Venugopal et al. [33] presented the FTIR spectra of Mg/Al LDHs intercalated with the nitrate, dodecyl sulfate (DS) and dodecyl benzene sulfonate (DBS) anions, as presented in Figure 3.20. The spectra of LDH-DS and LDH-DBS differed from the LDH- NO_3 in the bands around 3000 cm^{-1} , 1180 cm^{-1} , presenting the stretching vibration of C-H in the alkyl chain and the stretching absorption of S=O in the SO_4 group, respectively. The spectrum of LDH-DBS also exhibited the characteristics of C-H stretching absorption in the aromatic ring at 3030 cm^{-1} . Compared to the LDH- NO_3 , the band at 1381 cm^{-1} , corresponding to the nitrate group, was not absorption in the LDH-DS and LDH-DBS. These results confirmed that the the nitrate anions were replaced with the organic anions.

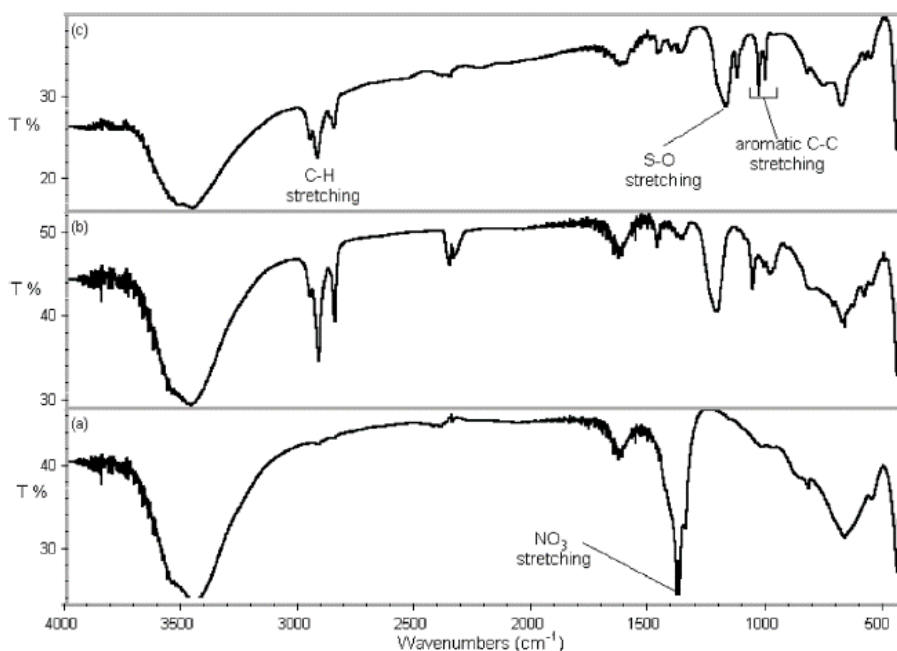


Figure 3.20 FTIR spectra of Mg/Al LDHs intercalated with different anions: (a) nitrate, (b) dodecyl sulfate and (c) dodecyl benzene sulfonate [33].

3.3.3 Thermal Analysis

Thermogravimetric analysis can characterise LDH thermal behaviour. The mass loss of the thermally decomposed LDH is plotted as a function of temperature. The decomposition curve performs several stages, relying upon the type of LDH, rate of heat and atmosphere of heating e.g. N_2 or air. There are two stages of the decomposition: the mass loss of water in the LDH structure with the temperature range from room temperature to about 200°C and the decomposition of hydroxyl groups in the lamellar and intercalated anions in between 200°C and 800°C [3, 10].

However, Hickey et al. [34] described that the TGA curve of the Mg/Al- CO_3 LDH (hydrotalcite) presented three crucial stages of the weight loss. The first stage occurred at the temperature between room temperature and 150°C corresponding to the absorbed water loss. In the further step, the interlamellar water was completely decomposed at 235°C . The last stage was the dehydroxylation of the hydroxyl group in the lamellar and the decomposition of carbonate in the interlayers. The complete decomposition of the LDH performs at 430°C . For the DTA curve, the three maximum

peaks were observed at around 140, 225 and 310°C. Figure 3.21 presents both the thermogram and its derivative of the Mg/Al-CO₃ LDH.

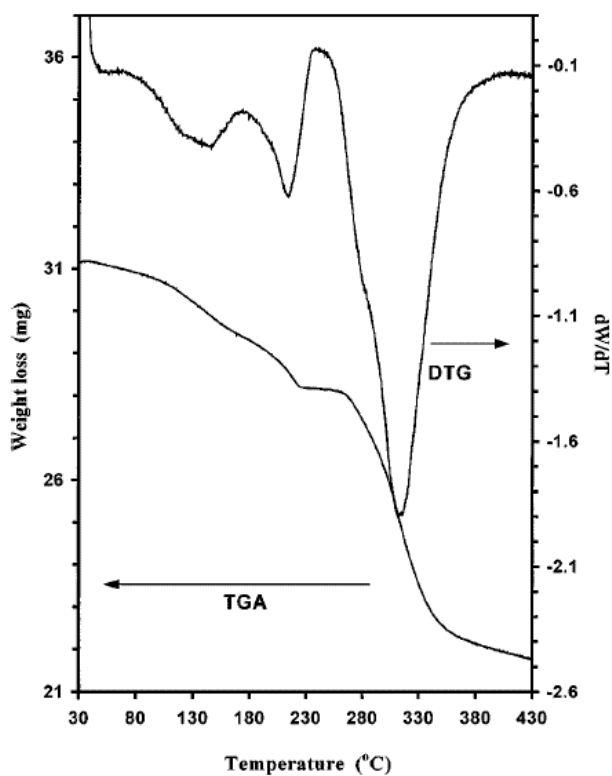


Figure 3.21 Thermogram of MgAl-CO₃ LDH [34].

3.4 Polymer Nanocomposites

Polymer nanocomposites are polymeric materials consisting of polymer matrix (e.g. thermoplastics or thermosetting plastics) and nanomaterials (e.g. nanoparticle or nanofiber) [35]. Thermoplastics are polymers that melt with heating and re-solidify with cooling and can be repeated in processing several times. In the meanwhile, thermosetting plastics are polymers solidified by a formation of three-dimensional networks in molecules, thus cannot be repeated in processing [36]. For polymer nanocomposites, nanomaterials are embedded in the polymer matrix.

The existence of nanomaterials in polymer matrix improves many properties such as mechanical properties, gas barrier, chemical resistance, thermal stability and flame retardancy. However, the addition of nanomaterials increases viscosity, which limits processability and may provide optical issues due to agglomeration and sedimentation

of nanomaterials. The properties of polymer nanocomposites depend on characteristics of polymer matrix (e.g. molecular weight, chemical compositions and crystallinity), types of nanomaterials (e.g. montmorillonite organoclays, carbon nanofibers and carbon nanotube) and morphology of polymer nanocomposites. [37]

3.4.1 Fabrication Method of Polymer Nanocomposites

The dispersion of nanomaterials in the polymer matrix affects the physical, mechanical and chemical properties of polymer nanocomposites. It is determined by the fabrication method of polymer nanocomposites. There are two common fabrication methods of polymer nanocomposites: a liquid phase and a solvent phase. For the former, the fillers were dispersed in liquid monomers and the mixture was polymerised. Meanwhile, the latter used a solvent as a reaction medium to dissolve monomers or polymers, resulting in the reduction of viscosity of monomers or polymers. Then, the nano-fillers were added in to the reduced viscosity monomers or polymers [38].

3.4.2 Characterisation of Polymer Nanocomposites

Generally, characterisation of polymer nanocomposites can be categorised, namely structure and property analysis. Structure of polymer nanocomposites is analysed by using a variety of microscopes and spectrometers, whereas properties of polymer nanocomposites are characterised with various techniques depending on the individual application. The common techniques used for characterisation of polymer nanocomposites are X-ray diffraction (XRD), transmission electron microscopy (TEM), scanning electron microscopy (SEM), thermal gravimetric analysis (TGA), differential scanning calorimetry (DSC) and dynamic mechanical thermal analysis (DMTA). Besides, an universal testing machine (UTM) is employed to characterise tensile, flexural and compressive properties. For flammability, it is determined by using a cone calorimeter and UL-94 test. [37]

3.4.3 Mechanical and Thermal Properties of Polymer Nanocomposites

Generally, the incorporation of nano-layered materials enhances tensile strength and modulus for polymer nanocomposites due to the high degree of exfoliation in the nano-layered materials. The exfoliation of layered materials in the composites are an increase of surface area interacting between the polymer matrix and the incorporating layers. The modification of nano-layered materials with organic compounds enhanced a compatibility with the polymer matrix [37].

As mentioned in the chapter 2, the nanomaterials used as the flame retardants were nano-sized particulates, nano-carbon additives and nano-layered materials. The thermal stability and flame retardancy of polymer nanocomposites containing the nano-layered materials were greater than other flame retardants because of the increase of char residue. The increased exfoliation of the layers resulted in a self-extinguishing behavior, leading to the stop of burning [37].

3.5 Characterisation of Burning of Fire Behaviours of Polymers

As mentioned in Chapter 2, the cone calorimetry, limiting oxygen index and burning test are the common techniques used to estimate fire burning behaviours of polymers. The details of each method would be explained in this section.

3.5.1 Cone Calorimetry

Cone calorimetry is the most well-known test used to study the fire behaviours of materials as following the standard test of ASTM E1354 and ISO 5660. The schematic diagram of the cone calorimeter is illustrated in Figure 3.22. The sample is ignited by a cone heater within a combustion chamber, resulting in the flame propagation of the sample. The by-products from the burning are gathered by an exhaust hood and separated by an exhaust blower. The concentrations of O₂, CO and CO₂ and their gas release rate and smoke density produced during the combustion of the specimen are detected. These measurements can be used for the calculation of heat release rate (HRR), peak heat release rate (pHRR), total heat released (THR), time to ignition

(TTI), time of combustion (TOC) and heat release capacity (HRC) as a function of time. Besides, the instrument detects the CO and CO₂ contents and total smoke released during the burning test [39, 40].

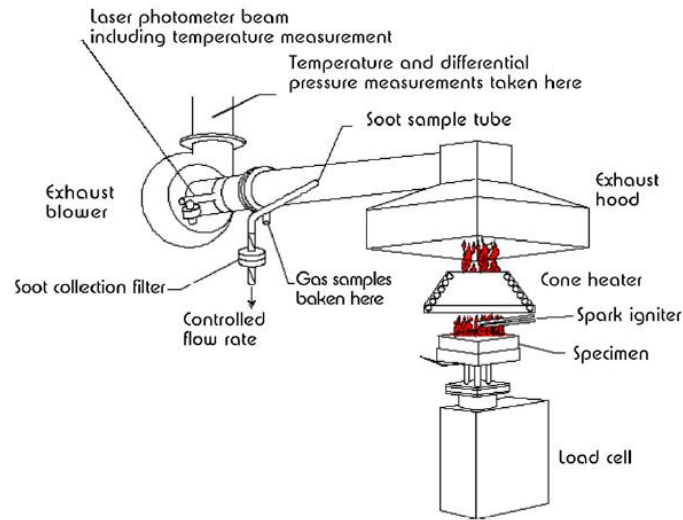


Figure 3.22 Experimental setup of cone calorimeter [39]

From the above information, the cone calorimetry is the high-performance technique for study the fire behaviours of materials since it can detect the released products through the combustion process. Thus, this technique is widely used for the test in bench-scale [39].

3.5.2 Limiting Oxygen Index

It is well-known that the combustion process requires oxygen (O₂) in the air to use in the burning reaction. The measurement of minimum O₂ volume used in the combustion is considered to classify the types of the materials: combustible materials or self-extinguishing materials. The estimation of combustible ability is defined in a term of limiting oxygen index (LOI). It presents the minimum concentration of O₂ consumed in mixture condition of oxygen and nitrogen (O₂/N₂) deriving from combusting simulation. Figure 3.23 provides the schematic setup of LOI measurement, and Equation 3.13 shows the calculation of LOI value.

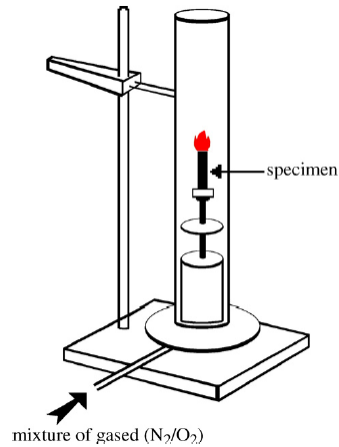


Figure 3.23 Schematic diagram of LOI measurement [39]

$$\text{LOI} = \left(\frac{[\text{O}_2]}{[\text{O}_2] + [\text{N}_2]} \right) \times 100 \quad (3.13)$$

However, the LOI test is the simulation of combustion, which is not the actual situation. It is just used for the screening, which is not reported in statistics. According to ISO 4589, materials are classified into two groups as the LOI value. If the value is below 21, they are defined as combustible materials. If that is over 21, they are categorised into self-extinguishing materials. The LOI value is a direct variation with the used volume of O₂. Hence, materials with the high LOI are implied the high flame retardants [39, 40]

3.5.3 UL-94 Test

The Underwriters Laboratories (UL-94) is the standard used to classify the flammability of materials. The burning test in this standard is a preliminary screening of the fire performance of materials by measuring and observing the response to the applied heat and flame. The general burning test can carry out both in horizontal and vertical directions by following the standards of the ASTM D635 [41] and the ASTM D3801 [42], respectively. The testing setups of both are illustrated in Figure 3.24 and 3.25.

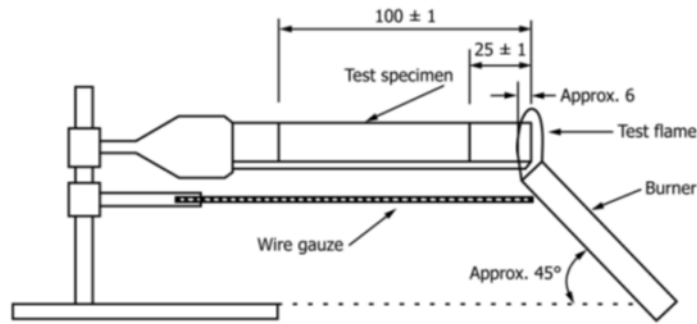


Figure 3.24 Experimental setup of the horizontal burning test [41].

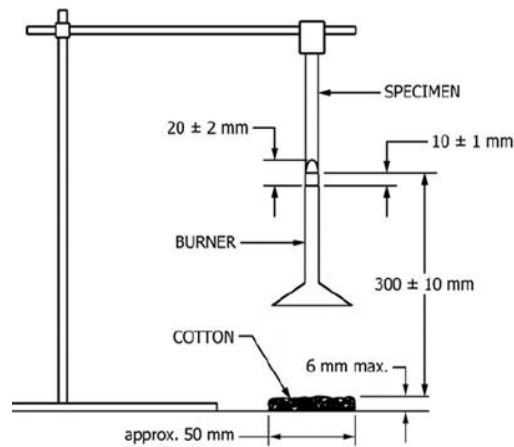


Figure 3.25 Experimental setup of the vertical burning test [42].

For the brief procedure, the sample is clamped on one side while the fire source applies to the other side. During the test, the ignition time, combustion time and flame dripping are measured and observed. Most of the horizontal burning test is processed to determine the burning rate (V) by using Equation 3.14, where L is the burned length and t is the burning time.

$$V = \frac{60 L}{t} \quad (3.14)$$

3.6 LDHs for Flame Retardant Applications

The fundamental structure of LDH comprises the metal hydroxide layers with the intercalation of anions and water molecules in the interlayers. In general, Mg^{2+} and Al^{3+} are widely used as the divalent and trivalent metals in the lamellae, respectively [1, 2]. As the LDHs are the same chemical composition as the mineral flame retardants

(MgOH_2 and AlOH_3), they have attracted remarkable attention as flame retardants for polymers [3, 43].

3.6.1 Flame Retardant Mechanism of LDHs

In the recent years, much published studies have reported the fire retardancy process of LDHs in polymer composites. The burn on polymer/LDH composites results in the degradation of polymer matrix and the decomposition of LDH additives. The former is rapidly degraded by heating whereas some molecules produced from the latter decomposition can retard the ignition and reduce the fire spreading. The published review of Gao et al. [44] noted that the liberation of water molecules and CO_2 and the formation of char during the thermal decomposition of LDH can decrease the released heat, dilute the concentration of flammable gas and suppress smoke in the combustion system. The burning process is suspended unless the amount of fuel is sufficient for the combustion.

In 2004, Zhang et al. [45] studied the mechanism of flame retardancy of $\text{Mg}/\text{Al}-\text{CO}_3$ for polymers (polystyrene, acrylonitrile-butadiene-styrene copolymer, polyethylene and poly (vinyl chloride)). The polymer fractions degraded at around 200°C . For the degradation of LDH, the adsorbed and interlayered water molecules were removed under 100°C and at the temperature range of $110\text{-}260^\circ\text{C}$, respectively. The liberated water can diminish the surface temperature of polymers during the combustion. Besides, the produced water vapor supported the dilution of O_2 concentration in the combustion area. The water removal did not destroy the layer structure of LDH. Afterwards, the hydroxyl groups in the metal hydroxide layers decomposed at $260\text{-}360^\circ\text{C}$ for the aluminium hydroxides and at $360\text{-}480^\circ\text{C}$ for magnesium hydroxides. The dehydroxylation of layers contributed to the releasing of water, the collapse of layers and the formation of Al_2O_3 and MgO . The formed metal oxide can absorb the toxic gases released during the combustion of polymers such as NO , NO_2 and HCl . For the decomposition of CO_3^{2-} intercalated in the interlayers, it happened at $480\text{-}700^\circ\text{C}$. This process promoted the CO_2 gas that can dilute the concentration of combustible gas. The schematic thermal decomposition of $\text{LDH}-\text{CO}_3$ is presented in Figure 3.26. The proposed flame retardant mechanism of LDH in this study also corresponded to other literature [46-48].

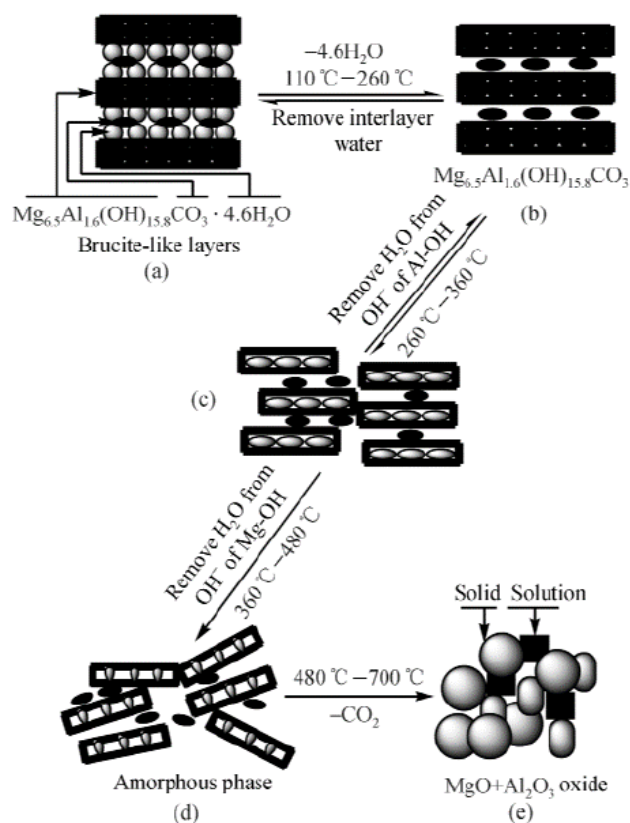


Figure 3.26 Schematic thermal decomposition of Mg/Al-CO₃ [45].

The study of Camino et al. reviewed by Gao et al. [46] noted that the combustion of LDH at around 200°C generated the release of interlayered water molecules. Subsequently, the decompositions of intercalated CO₃²⁻ anions and layered metal hydroxides were presented at 291°C and 416°C, respectively. The by-products of thermal decomposition of the metal hydroxides were magnesium oxide (MgO) and magnesium aluminium oxide (MgAl₂O₃). These produced metal oxides can inhibit the dispersion of oxygen in the air through the combustion area.

For the flame behaviours of MgAl-PO₄ [49] and MgAl-H₂PO₄ [50], they were not only the production of large amount of H₂O and char during the burning but also the release of PO₄⁻ free radicals. The phosphate radicals interacted with the OH[·] and H[·] radicals, resulted from the degradation of polymer. This stage led to the char formation. Thus, the LDHs containing the phosphate compounds can disrupt the combustion.

Likewise, the flammability of epoxy resin composite was decreased with incorporating the Mg/Al LDH intercalated with phenethyl-bridged 9,10-dihydro-9-oxa-10-phosphaphenanthrene-10-oxide (DiDOPO). The thermal decomposition of DiDOPO liberated the PO[·] radicals, and then they combined with the OH[·] and H[·] radicals. Besides the PO[·], it produced some acid molecules of phosphorus compounds during the decomposition of DiDOPO. These formed acids could accelerate the rate of char formation. Thus, the combustion of epoxy resin (EP) was inhibited and stopped [51]. Compared to the Mg/Al-CO₃ to Mg/Al-PO₄, the flame retardant efficiency of the latter was higher than the former [49].

3.7 Overview of Flame Retardancy Efficiency of LDHs for Polymer Nanocomposites

The last two decades have seen the rapid development of LDHs to use in many applications, especially flame-retardant additives for polymers. There have been used LDHs as flame retardants since the 1970s, reported in a review of Qiu and Qu [52]. To improve flame retardancy efficiency of LDHs, the metal cations and intercalated anions in LDH structures have been modified with a variety of chemicals [44, 52]. This section will review flammability of polymers nanocomposites with incorporation of LDHs in previous published researches.

3.7.1 Modification of Metal Cations in LDHs

As the thermal decomposition of metal hydroxide layers in LDHs can encourage the inhibition of polymeric combustion, the selection of metal cations is a significant importance to flame retardancy of polymers [44]. Some researchers have attempted to study the role of both divalent and trivalent cations in metal hydroxide layers of LDHs in flame-retardant performance of polymer/LDHs nanocomposites. The representatives of divalent and trivalent cations used widely are Mg²⁺ and Al³⁺, respectively. The other divalent cations used to study the efficiency of flame retardants were Zn, Ni, Co, Cu and Ca.

In 2008, Manzi-Nshuti et al. [53] investigated the effect of LDHs with different divalent cations (Ni, Zn and Co) on the properties of poly(methyl methacrylate) (PMMA) nanocomposites. The controlled trivalent cations and the interlayer anions were Al^{3+} ions and undecanoate molecules, respectively. The results of cone calorimeter showed that both PHRR and THR of all composites was hardly change with the loading of 1% LDHs compared to the pure PMMA. However, the loading of 5 and 10% LDHs had an influence on the fire behaviours of PMMA/LDHs nanocomposites, particularly PHRR presented in Figure 3.23. At 5% LDHs loading (Figure 3.27(a)), the PHRR of PMMA/ZnAl₂ LDH and PMMA/CoAl₂ reduced slightly, but the curve could not be observed the change in PMMA/NiAl₂. Considered at 10% loading of the LDHs, the PHRR of PMMA/CoAl₂, PMMA/ZnAl₂ and PMMA/NiAl₂ decreased significantly by 41, 26 and 16% from the 1057 kWm^{-2} for the pure PMMA.

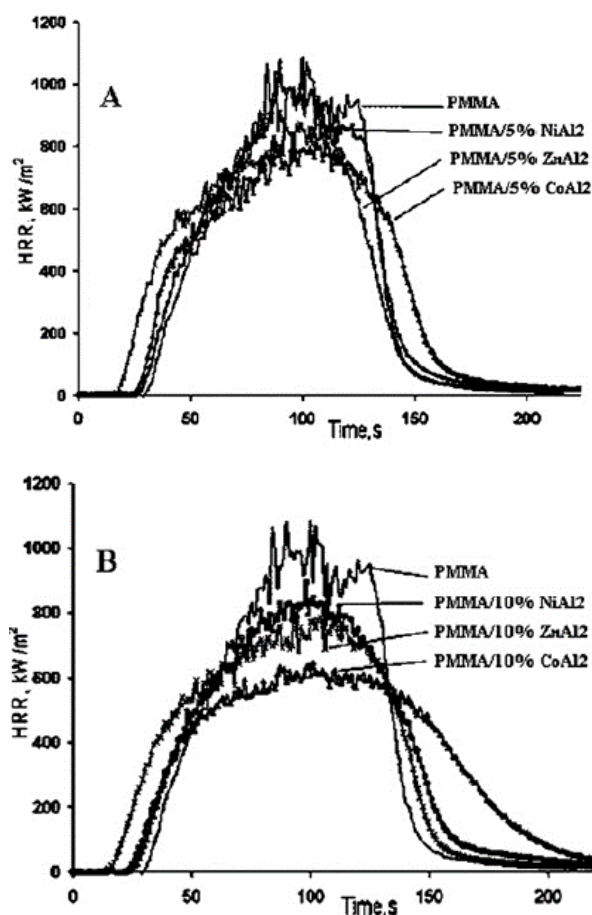


Figure 3.27 HRR curves of PMMA nanocomposites with incorporation of Ni/Al, Zn/Al and Co/Al LDHs in different contents: (a) 5% loading and (b) 10% loading [53].

A year later, Manzi-Nshuti et al. [54] had studied more in the flame retardancy of PMMA nanocomposites with the loading of LDHs-based Mg/Al, Ni/Al, Cu/Al, Zn/Al and Ca/Al. At the 6% LDH loading, the percentage of PHHR reduced to 36% for Ca/Al and Ni/Al LDH, 24% for Mg/Al LDH, 16% for Zn/Al LDH and 0% for Cu/Al LDH. Another study compared the efficiency of flame-retardant properties of Mg/Al and Zn/Al LDHs intercalated with oleate in ethyl-vinyl acetate (EVA) [55]. The performance of the Mg/Al LDH was higher than Zn/Al LDH due to the larger reduction of PHHR, especially the loading at 10%. The HRR curves of EVA/LDH nanocomposites are shown in Figure 3.28. And also, the time to ignition of composite containing Mg/Al LDH was longer than that of Zn/Al LDH. After the cone calorimeter test, the observed dripping of the composites reduced obviously and the char residue of composites with loading of Mg/Al LDH was more than Zn/Al LDH.

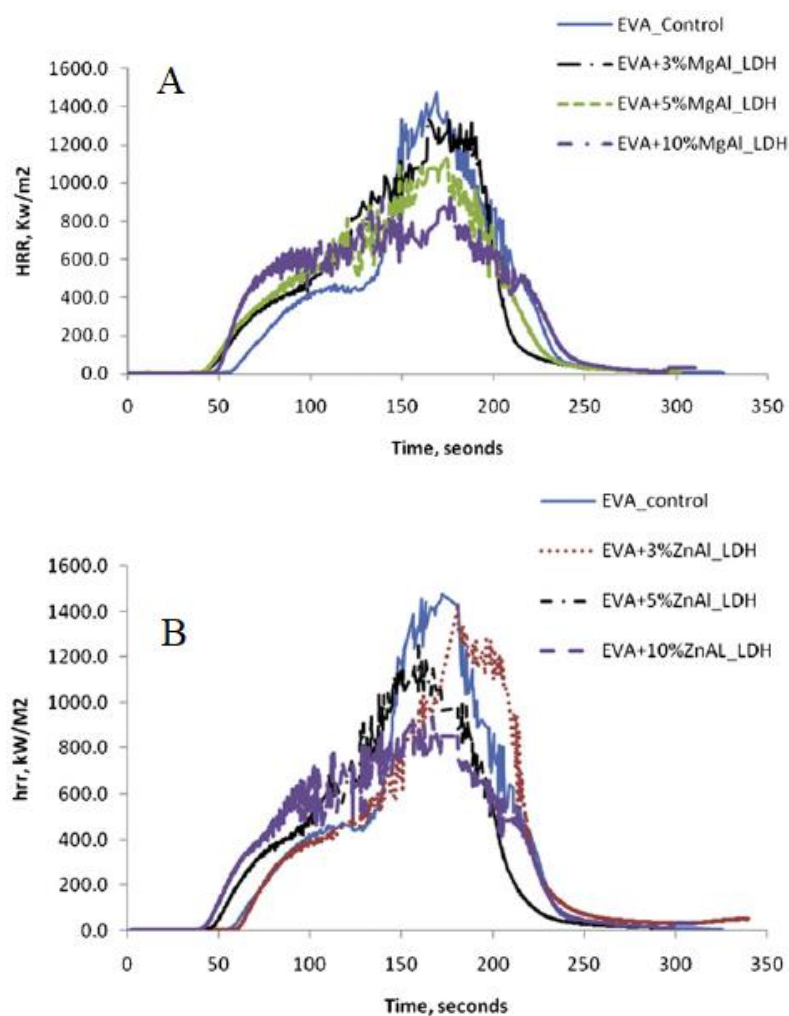


Figure 3.28 HRR curves of EVA/LDH nanocomposites with the different LDHs: (a) Mg/Al LDH and (b) Zn/Al LDH [55].

Moreover, there were modification of LDHs by partial or full substitution of Mg and Al atoms in the metal hydroxide layers with other metals to enhance flame retardancy. Xu et al. [56] synthesised the Mg/Al and Zn/Mg/Al LDHs and studied their fire retardancy in acrylonitrile-butadiene-styrene (ABS). From the TGA curves and their first derivative shown in Figure 3.29, both the composites displayed the thermal decompositions at below 300°C and around 430°C, whereas the pristine ABS presented the only decomposition at 430°C. These results demonstrated the decomposition temperature of composites decreased with adding of LDHs. The loading of both Mg/Al and Zn/Mg/Al LDHs also induced the considerable increase of the char residues. Comparing the flammability test with the pristine ABS, both the composites provided an increase of LOI values, a suppression of smoke density and a declination of PHHR.

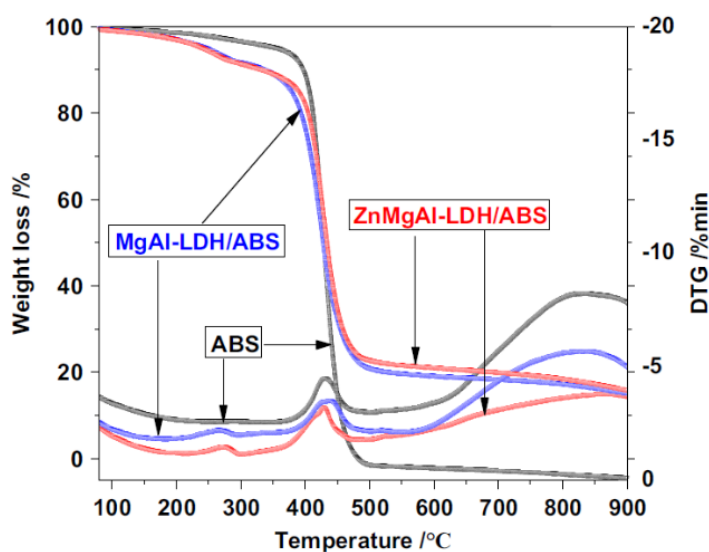


Figure 3.29 TGA curves and their derivatives of pristine ABS and ABS/LDH nanocomposites [56].

Similarly, the loading of LDH-CO₃ contained among Mg, Al and Fe attributed the high flame-retardant performance to poly(ethylene-vinyl acetate) EVA nanocomposite compared to the LDH without the composition of Fe³⁺. Jiao et al. [57] suggested that Fe³⁺ can accelerate the rate of char layer formation and can react with flammable free radicals produced during the combustion. Moreover, Labuschagné et al. [58] showed that the partial and full replacement of Mg and Al with Ca, Cu, Zn and Fe could improve the flame retardancy of poly(vinyl chloride) (PVC). Besides the

reduction of PHRR, the maximum average rate of heat emission (MARHE) also decreased dramatically, presented in Figure 3.30.

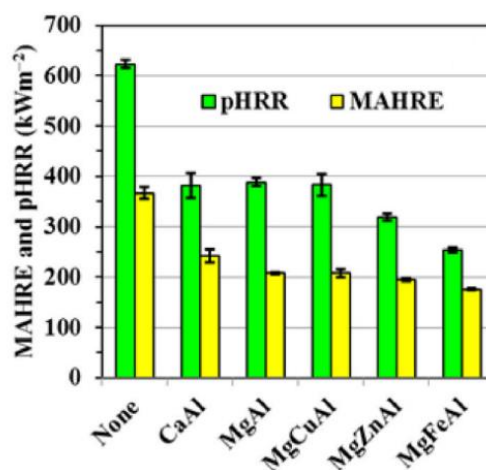


Figure 3.30 Values of PHRR and MAHRE of pristine PVC and their composites with addition of LDHs [58].

Overall, there seems to be some evidence to indicate that modification of metal cations in metal hydroxide layers of LDHs with Mg, Ni, Zn, Co, Ca and Fe can improve flame retardancy of polymers depending on the types of metal cations. However, LDHs based on Mg²⁺ and Al³⁺ cations are still widely used as flame retardant additives.

3.7.2 Modification of Intercalated Anions in LDHs

3.7.2.1 Incorporation of LDHs Intercalated with Inorganic Anions

The most common method used widely to develop fire-retardant efficiency of LDHs is to modify intercalated anions in the interlayers. The types of anions intermediate between the lamellae are inorganic and organic anions. The first LDH used for reducing flammability of polymers is intercalated with carbonate ion [44]. Camino et al. [46] compared fire retardant effectiveness of hydrotalcite (Mg/Al-CO₃ LDH) in EVA polymer. At the 50% loading of fillers, the composite with the LDH provided the longest time to ignition and the lowest peak of gas temperature, as shown in Figure 3.31. Furthermore, the results also presented that the LDH could delay the maximum of heat release rate of the polymer combustion since the thermal decomposition of

LDH took place in the wide temperature range of 200-500°C. The results corresponded to the research of Zhang et al. [45].

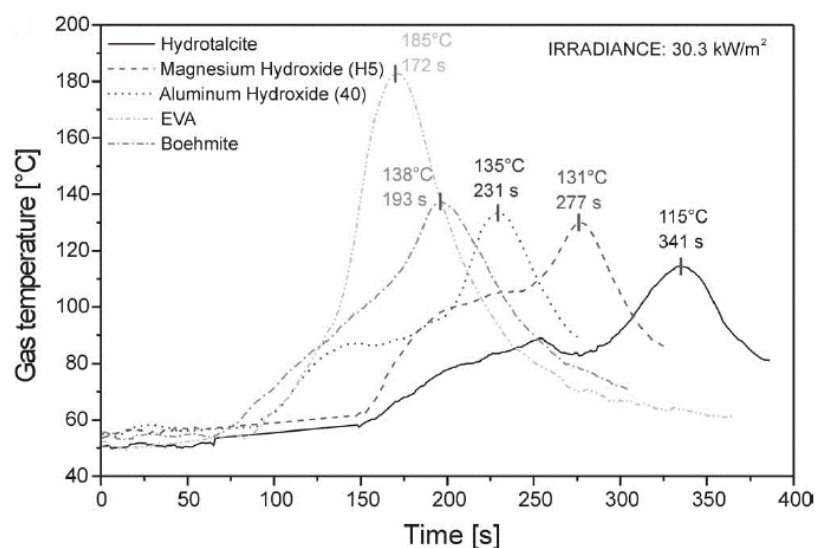


Figure 3.31 Mass loss of EVA polymer composites analysed from the cone calorimeter [46].

According to the limitation of metal hydroxide flame retardants, zinc borate is blended with metal hydroxides (e.g. magnesium hydroxide and aluminium hydroxide) to improve smoke-suppressing properties. Shi et al. [59] investigated the loading of 60 wt% Mg/Al LDHs intercalated with carbonate and borate (Mg/Al-borate) as flame retardants for EVA. The LOI values of both EVA/LDHs nanocomposites were more than that of the pure EVA. By considering the smoke density during the combustion, the addition of Mg/Al-borate reduced the smoke density by 45% from the pure EVA that was better than that of Mg/Al-carbonate. All the results of LOI and smoke density are presented in Table 3.4.

Table 3.4 Values of LOI and smoke density of EVA nanocomposites with addition of LDHs intercalated with carbonate and borate anions [59].

Samples	Limiting oxygen index (%)	Smoke density
EVA	21.3	187.4
EVA/LDH-CO ₃	30.0	133.1
EVA/LDH-borate	29.2	102.9

In 2005, Nyambo et al. [60] compared the flame retardant performance of MgAl LDHs and ZnAl intercalated with borate in EVA polymer. The cone calorimetry results indicated that the PHHR of composites decreases obviously with addition of both LDHs. For example, the PHHR of EVA composites is reduced by 42% for the loading of 3% MgAl-borate and by 36% for the loading of 3% ZnAl-borate. The more LDHs loaded, the greater reduction of PHHR obtained. The decrease of PHHR for addition of the two LDH types did not display a significant difference. The HHR curves are shown in Figure 3.32.

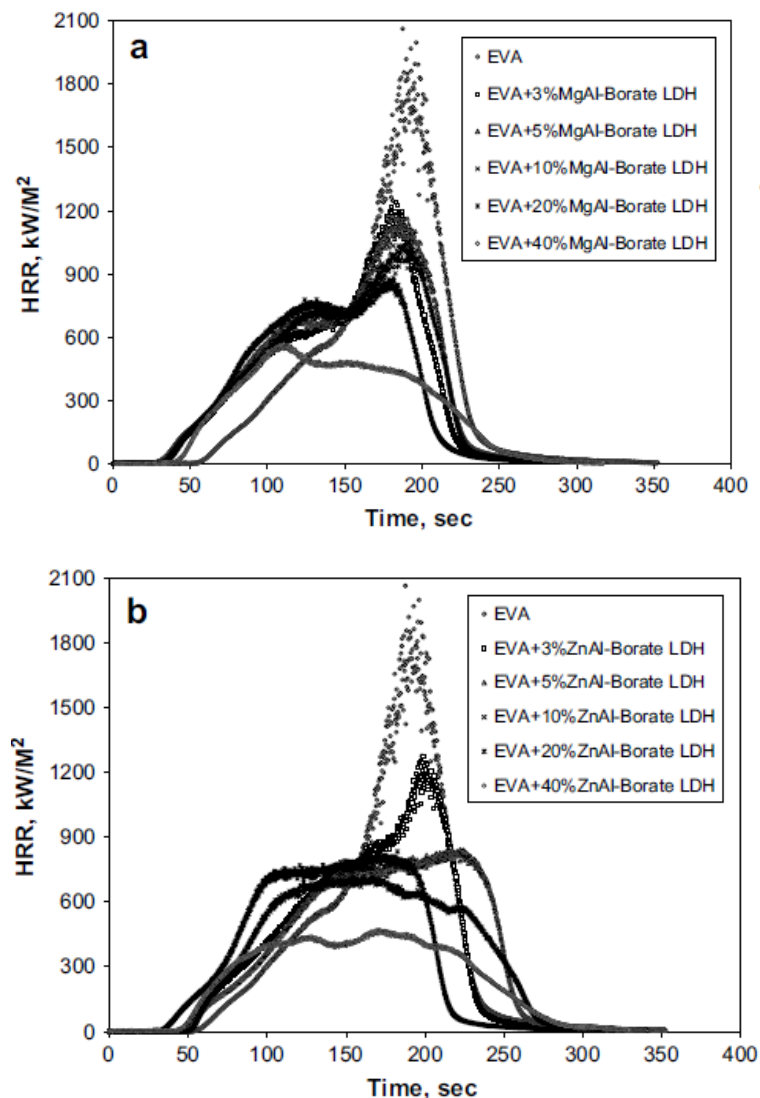


Figure 3.32 HHR curves of EVA/LDH nanocomposites with addition of different LDHs: (a) Mg/Al-borate and (b) Zn/Al-borate [60].

In contrast, the study of Wang et al. [61] reported that the flame-retardant effective of Zn/Al-borate was higher than Mg/Al-borate because the PHHR of the former (1186.9

kW/m^2) was less than the latter (1290.3 kW/m^2) for the loading of 6% LDHs. Not only the PHHR but also the total heat release and the average mass loss rate of PP/ZnAl composites were decreased compared to the pure PP. After the combustion test of the polymer composites, the characteristic of char residue was observed. At the same proportion of LDH, the char quantity of the composite with addition of Zn/Al LDH was more than that of Mg/Al LDH, as displayed in Figure 3.33.

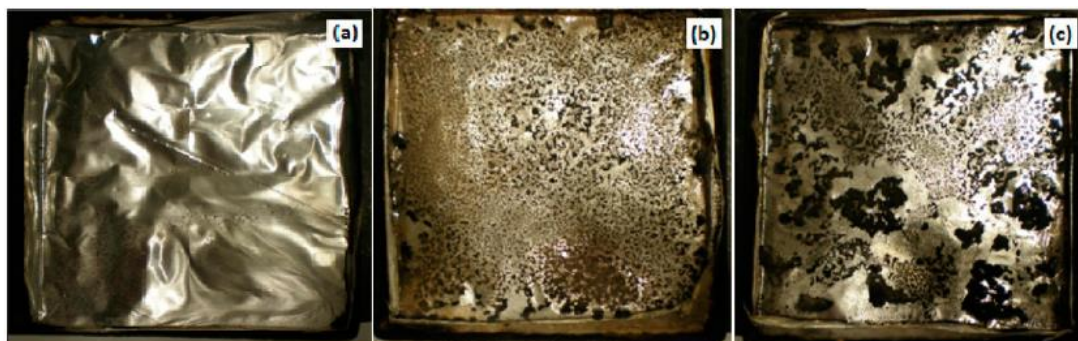


Figure 3.33 Formation of char residue after the combustion test of PP/LDH composites: (a) Pure PP, (b) PP/6% Mg/Al-borate and PP/6% Zn/Al-borate [61].

Furthermore, there was a synergy between phosphorus-based flame retardants and metal hydroxide flame retardants in the polymer matrix. The content of char residue after the combustion of composites increased. The char layers prevented the diffusion of heat and flammable gases through the combustion area. They can delay and stop the burning process of polymers. Thus, the intercalation of phosphate compounds between the metal hydroxide layers of LDHs has significant interesting for development of flame retardancy of LDHs [49].

Ye et al. [49] established that the flame retardancy of the EVA composites with the loading of Mg/Al- PO_4 was higher than that with Mg/Al- CO_3 . To achieve the V-0 rating for the UL-94 test, it needed to add both types of LDH to the polymer matrix to 60 wt%. The PO_4^{3-} ions in the interlayers was oxidised to various derivatives of phosphoric acid that they accelerated the thermal decomposition of polymer and interacted with free radicals of combustion of polymer. This process produced the structure of char comprising P-O-C and P-O-P complexes during the combustion of polymer. These actions had the disappearance in the thermal decomposition of Mg/Al- CO_3 .

Liu et al. [50] synthesised the LDH modified with H_2PO_4^- and prepared the PP/LDH composites. The flammability tests were found that the LOI value of composites increased slightly with the loading of 3-12 phr LDH- H_2PO_4 . Besides, the addition of LDH- H_2PO_4 also prolonged the dripping time of polymer combustion and decreased significantly the PHHR, average HRR and THR. The values of LOI and time to dripping are shown in Table 3.5 and the curves of HRR are presented in Figure 3.34. The flame-retardant mechanism of LDH- H_2PO_4 was similar to the LDH- PO_4 .

Table 3.5 Values of LOI and time to dripping of PP/LDH- H_2PO_4 nanocomposites in different contents of fillers [50].

Content of LDH- H_2PO_4 (phr)	LOI (%)	Time to dripping (s)
0	17.8 ± 0.1	3 ± 1
3	18.4 ± 0.1	9 ± 1
6	18.8 ± 0.2	15 ± 1
9	19.5 ± 0.1	30 ± 1
12	21.2 ± 0.2	38 ± 2

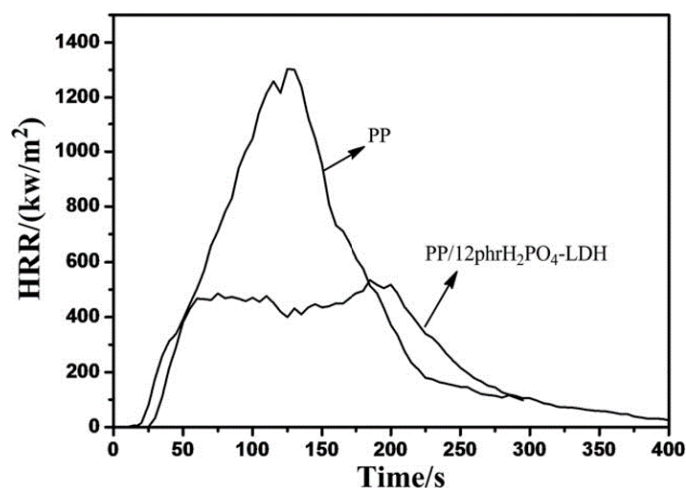


Figure 3.34 HRR curves of pure PP and PP/12 phr LDH- H_2PO_4 [50].

All the above evidence insisted that the LDHs modified with inorganic anions including carbonate, borate and phosphate are high potential flame retardants for polymers. The flame retardancy of LDHs with the borate and phosphate are higher than that with carbonate. As LDHs intercalated with inorganic anions have high charge density in the metal hydroxide lamellae, strong hydrophilicity on the layer

surface and small distance between interlayers (< 1 nm), they are poorly compatible with hydrophobic polymers. To increase hydrophobicity and enlarge the interlayer space of LDHs, organic anions are considered to modify LDHs [43, 44]. In the present, many studies have been developed LDHs modified with various hydrophobic organic anions.

3.7.2.2 Incorporation of LDHs Intercalated with General Organic Anions

Ye and Wu [62] investigated the flame-retardant properties of low-density polyethylene (LDPE)/LDH nanocomposites that the LDHs were modified with dodecyl sulfate (DS) and stearate (SA). The combustion calorimetry results are shown in Figure 3.35 and Table 3.6. The PHRR reduced dramatically with the loading of 5 phr LDHs, especially LDHs modified with the DS and SA. The THR and T_{HRR} of the polymer nanocomposites also presented a downward trend with adding of LDHs. In a subsequent publication, Qiu et al. [63] prepared the PP/Mg₃Al-DS and PP/Mg₃Al-SA nanocomposites and studied their flammability. The results present the same trend as the previous research.

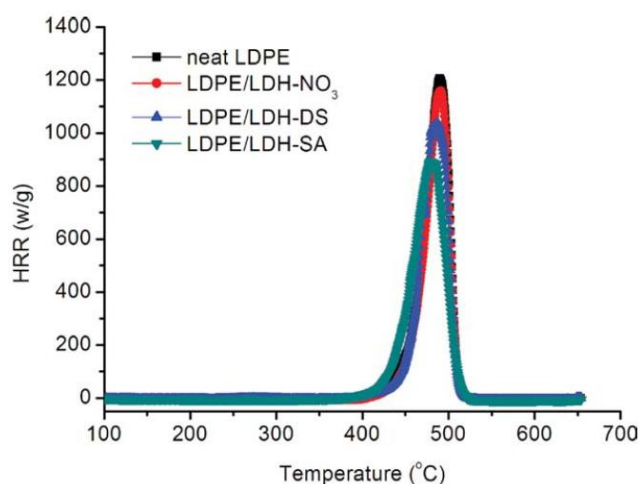


Figure 3.35 HRR curves of neat LDPE and its nanocomposites adding the 5 phr loading of LDHs intercalated with the nitrate, DS and SA [62].

Table 3.6 Results obtained the cone calorimeter of neat LDPE and various LDPE/5 phr LDH nanocomposites [62].

Sample	PHRR (w/g)	PHRR reduction with respect to LDPE (%)	THR (kJ/g)	TpHRR (°C)
Neat LDPE	1230	-	43.3	491
LDPE/LDH-NO ₃	1170	5	41.5	488
LDPE/LDH-DS	1051	14.5	40.4	483
LDPE/LDH-SA	898	27	40.1	481

Moreover, Kaul et al. [64] synthesised epoxy resin nanocomposites blended with Mg/Al-DS and melamine salt of pentaerythritol diphosphate (MPP). The MPP acted as an intumescent agent. From the UL-94 tests in the vertical direction, the combustion time of the composite with Mg/Al-DS (E-3 and E-4 samples) was less than the neat epoxy resin (E1 sample) and the epoxy resin and MPP (E2 sample). Figure 3.36 displays the characteristic of samples after the burning test.



Figure 3.36 Characteristics of neat epoxy resin and epoxy resin nanocomposites after the flame testing: E1 (neat epoxy resin), E2 (Epoxy resin/MPP), E3 (Epoxy resin/MPP/1 g LDH-DS) and E4 (Epoxy resin/MPP/5 g LDH-DS) [64].

Dodecyl benzyl sulfate (DBS) modified LDH has also been used as a flame retardant for polymers. Wang et al. [65] reported the burning behaviours of polylactic acid (PLA) composites with synergy between a mixture flame retardant (FR) containing ammonium polyphosphate (APP), pentaerythritol (PER), and melamine cyanurate

(MC) and LDH-DBS. Comparing the neat PLA with the PHHA of 436 kW/m^2 , the percentages of PHHR reduction decreased by 65% and 62% for PLA/FR and PLA/FR/Zn/Al-DBS, respectively. Meanwhile, the addition of both FR and LDH resulted in the significant decline of THR, but the considerable increase of char yield.

Some studies have developed LDHs with using cyclodextrin (CD)-based compounds [47, 66, 67]. Kang and Wang [66] modified the LDH with anions of β -cyclodextrin functionalised with the DBS. The synthesis of modified LDH had controlled the amount of carbon-carbon double bond in the structure. From the HRR curves in Figure 3.37, the PHHR values of LDHs intercalated with CD-DBS decreased remarkably compared with the LDH-DBS.

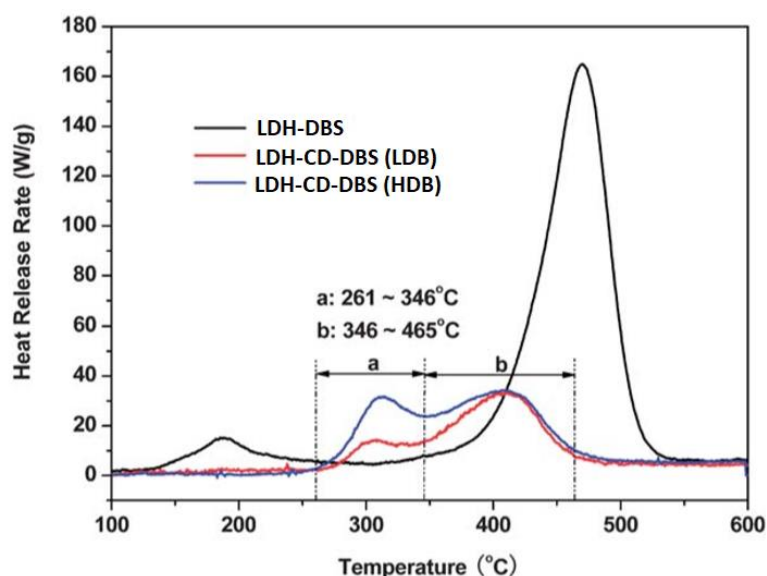


Figure 3.37 HRR curves of LDH-DBS, LDH-CD-DBS with low content double bonds (LDB), LDH-CD-DBS with high content double bond (HDB) [66].

Kalali et al. [47] compared the flammability of epoxy resin/6 wt% LDH nanocomposites to the pure epoxy resin. The LDHs were intercalated with CD (LDH-CD), taurine (LDH-T) and multifunctional anions of CD, DBS and T (LDH-CD-DBS-T). The observation of combustion behaviours was found that all the composites with LDHs provided the small increase of LOI values with the comparison with the pure epoxy resin. However, there was only EP/ LDH-CD-DBS-T obtaining the V-0 rating for the UL-94 test. In addition, the TTI and PHRR decrease dramatically with the addition of LDH-CD-DBS-T, whereas it provided the increase of char residual after

the burning. The combustion results are shown in Table 3.7. Subsequently, Kalali et al. [67] synthesised the LDH modified with CD, DBS and phytate (Phy) (LDH-CD-DBS-Phy) and prepared the EP/LDH nanocomposites. The results exhibited the same trend as the prior study. The modified LDH was a highly efficient flame retardant.

Table 3.7 Fire behaviours of the pure EP and the EP/LDH nanocomposites [47].

Sample	LOI (%)	UL-94	TTI (s)	PHHR (kW/m ²)	Char residual (%)
Pure EP	23.0	No-rating	58 ± 1	931 ± 12	14.3 ± 0.3
EP-LDH-NO ₃	25.2	No-rating	65 ± 3	621 ± 26	21.4 ± 1.2
EP-LDH-T	24.0	No-rating	61 ± 3	491 ± 19	26.0 ± 0.9
EP-LDH-CD	23.5	V-2	37 ± 2	525 ± 18	24.0 ± 1.4
EP-LDH-CD-DBS-T	26.8	V-0	40 ± 3	318 ± 23	30.0 ± 0.8

Another types of anions modified in the interlayers of LDHs was linear-chain alkyl carboxylates ($\text{CH}_3(\text{CH}_2)_n\text{COO}^-$ where $n = 8, 10, 12, 14, 16, 18, 20$ and 22) [48, 68, 69], oleate [70], and adipate [71]. Nyambo et al. [48] studied the fire retardancy of PMMA and PS with incorporating the Mg/Al LDHs intercalated with the various long chain linear alkyl carboxylates. The thermal stability of the polymer composites increased with the addition of the modified LDHs. The Cone calorimetry results are presented in Table 3.8 and Table 3.9 for the PMMA and PS nanocomposites, respectively. The results showed that the increase of Mg/Al LDH loading from 3 wt% to 10 wt% affected the reduction of the PHRR, THR, average mass loss and smoke formation during the combustion of the polymer nanocomposites. The loading of 10% LDHs intercalated with the decanoate (C10) was the highest effective for the PHRR reduction that was 58% for the PMMA nanocomposite and 56% for the PS nanocomposite. The results corresponded to other studies [68, 69].

Table 3.8 Flammability behavior of the PMMA nanocomposites with incorporating the Mg/Al LDHs modified by the long-chain alkyl carboxylates [48].

Sample	PHRR (kW/m ²)	PHRR Reduction (%)	THR (MJ/m ²)
Pure PMMA	1043 ± 50	-	92 ± 2
PMMA+3% MgAl-C10	788 ± 63	24	64 ± 28
PMMA+5% MgAl-C10	631 ± 57	40	70 ± 31
PMMA+10% MgAl-C10	442 ± 22	58	85 ± 10
PMMA+3% MgAl-C12	665 ± 34	36	86 ± 1
PMMA + 5% MgAl-C12	550 ± 19	47	84 ± 1
PMMA+10% MgAl-C12	448 ± 83	57	79 ± 2
PMMA+3% MgAl-C14	774 ± 14	26	82 ± 3
PMMA+5% MgAl-C14	635 ± 24	39	80 ± 2
PMMA+10% MgAl-C14	484 ± 37	54	74 ± 3
PMMA+3% MgAl-C16	746 ± 29	29	83 ± 2
PMMA+5% MgAl-C16	728 ± 30	30	81 ± 1
PMMA+10% MgAl-C16	485 ± 31	54	73 ± 5
PMMA+3% MgAl-C18	786 ± 32	25	85 ± 1
PMMA+5% MgAl-C18	699 ± 27	33	83 ± 2
PMMA+10% MgAl-C18	515 ± 15	51	78 ± 4
PMMA+3% MgAl-C22	847 ± 31	19	84 ± 3
PMMA+5% MgAl-C22	714 ± 45	32	87 ± 0
PMMA+10% MgAl-C22	534 ± 28	49	83 ± 1

Table 3.9 Flammability behaviours of the PS nanocomposites with incorporating the Mg/Al LDHs modified by the long-chain alkyl carboxylates [48].

Sample	PHRR (kW/m ²)	PHRR Reduction (%)	THR (MJ/m ²)
Pure PS	1116 ± 25	-	97 ± 5
PS+3% MgAl-C10	778 ± 47	30	96 ± 1
PS+5% MgAl-C10	678 ± 19	39	99 ± 4
PS+10% MgAl-C10	491 ± 31	56	96 ± 17
PS+3% MgAl-C12	831 ± 43	26	104 ± 1
PS+5% MgAl-C12	704 ± 32	37	105 ± 1
PS+10% MgAl-C12	540 ± 12	52	100 ± 3
PS+3% MgAl-C14	781 ± 15	30	105 ± 1
PS+5% MgAl-C14	726 ± 51	35	107 ± 2
PS+10% MgAl-C14	591 ± 15	47	103 ± 1
PS+3% MgAl-C16	805 ± 25	28	105 ± 4
PS+5% MgAl-C16	749 ± 18	33	108 ± 2
PS+10% MgAl-C16	736 ± 34	34	108 ± 9
PS+3% MgAl-C18	921 ± 81	17	113 ± 2
PS+5% MgAl-C18	885 ± 20	21	116 ± 3
PS+10% MgAl-C18	908 ± 54	19	114 ± 1
PS+3% MgAl-C22	1083 ± 87	3	118 ± 4
PS+5% MgAl-C22	1001 ± 48	10	114 ± 2
PS+10% MgAl-C22	883 ± 67	21	1165

3.7.2.3 Incorporation of LDHs Intercalated with Organophosphate Anions

According to the high flame retardancy of LDHs intercalated with inorganic phosphate anions, a variety of organic phosphate-containing compounds has been interesting to use as intercalated agents in the presents. Gómez-Fernández et al. [72] compared the flame retardant properties of polyurethane foam (PUF) with the loading of Mg/Al LDH modified with bis(2-ethylhexyl phosphate) (BEHP) to the pure PUF, PUF/LDH-CO₃, PUF/LDH-HPO₄. At the loading of 3 part per hundred parts polyol (pphp) LDHs, the LDH-BEHP had the highest effective reduction of PHRR and heat

release capacity as presented in Table 3.10. The LDH modified BEHP was also used as the flame retardant in PMMA and PS nanocomposites [73].

Table 3.10 Fire behaviours of the neat PUF and the composites with the loading of 3 pphp LDHs [72].

Sample	PHHR at the first stage (W/g)	PHHR at the second stage (W/g)	Heat release capacity (J/gK)
Neat PUF	144.7 ± 6.5	382.2 ± 6.8	420.3 ± 22.5
PUF/LDH-CO ₃	136.4 ± 5.5	333.5 ± 10.9	371.7 ± 11.2
PUF/LDH-HPO ₄	138.4 ± 6.5	327.2 ± 2.2	345.7 ± 2.1
PUF/LDH-BEHP	133.2 ± 11.0	309.9 ± 2.3	334.5 ± 0.7

Ding et al. [74] investigated the flammability of PLA nanocomposites containing Ni/Al LDHs intercalated with 2-carboxylethyl-phenyl-phosphinic acid (CEPPA). The addition of 10 wt% LDH-CEPPA resulted in the significant increase of PHRR to 404.2 W/g from 294.9 W/g for the pure PLA. It was suggested that the thermal degradation rate of composite increased with incorporating the LDH. However, the LDH-CEPPA affected the reduction of THR of composites. The THR value of composite adding 10% LDH-CEPPA was 9.7 kJ/g, that was less than the pure PLA of 12.0 kJ/g. Thus, the LDH-CEPPA can be used in flame retardant applications. Gao et al. [75] studied the effect of ammonium polyvinyl phosphate (APP) modified between the layers of LDHs on the properties of PP composites. At the loading of 20 wt% LDH-APP, the PHRR reduced by 55% from 1585 W/g for the neat PP while the THR decreased from 47.6 kJ/g for the neat PP to 34.0 kJ/g for the addition of modified LDH.

Dong et al. [76] proved that the ammonium alcohol polyvinyl phosphate (AAPP) intercalated LDH could enhance the flame retardancy properties of epoxy resin nanocomposites. The LOI values of composites increased moderately with increasing of the LDHs from 23.2% to 29.0% for the 10% and 40% additions of LDHs, respectively. The loading of the LDH-AAPP over 30 wt% can provide the V-0 rating of UL-94 test. Huang et al. synthesised the LDH modified with N-(2-(5,5-dimethyl-1,3,2-dioxaphosphinyl-2-ylamino)-N-hexylformamide-2-propenyl acid (DPHPA) to

use as a flame retardant for PMMA [77] and EVA [78] with loading of 5 wt% modified LDH.

Another phosphate-based compound used for modification in the intermediate region of LDH layers to improve flame retardancy is a phytate (Phy). Figure 3.38 illustrates the schematic chemical structure of Phy.

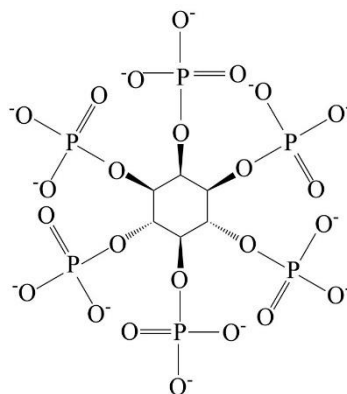


Figure 3.38 Schematic chemical structure of Phy.

Kalali et al. [79] synthesised the LDH intercalated with Phy and prepared the PP nanocomposites containing the APP and LDH-Phy. The LOI value of PP/APP/LDH-Phy increased by 8% from 19% for the neat PP, as presented in Figure 3.39. The combustion and flammability behaviours of the neat PP and composites are shown in Table 3.11. The loading of LDH-Phy led to the significant reduction of TTI and PHRR, but the significant increase of char residue. For the UL-94 tests, the composites with loading of 2% LDH-Phy provided the V-0 rating, while the other composites presented the V-1 rating. Therefore, the PP/APP/2% LDH-Phy was the optimum proportion for the composite production with high flame retardancy.

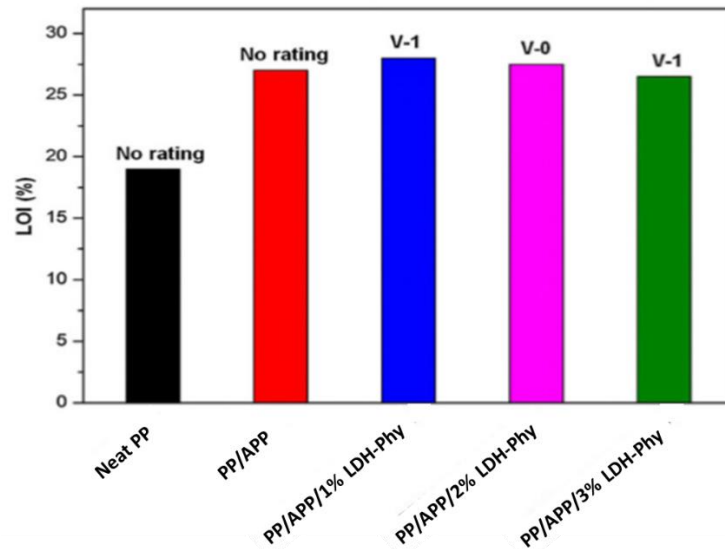


Figure 3.39 Flammability of the neat PP and the PP composites [79].

Table 3.11 Combustion behaviours of the neat PP and the PP composites [79].

Sample	TTI (s)	PHRR (kW/m ²)	Char residues
Neat PP	34 ± 1.6	1294 ± 39	0.2
PP/APP	21 ± 1.2	306 ± 28	41.7
PP/APP/1% LDH-Phy	20 ± 1.9	200 ± 24	58.6
PP/APP/2% LDH-Phy	19 ± 1.7	291 ± 18	57.2
PP/APP/3% LDH-Phy	18 ± 1.3	327 ± 23	57.9

Likewise, Jin et al. [80] found that there were the decreases of TTI, PHR and THR, but the increases of smoke and char formation with the loading of 1% LDH-Phy in the PLA blended with intumescent flame retardant containing diethylenetriamine penta(methylenephosphonic) acid and melamine (PLA/FR/LDH-Phy). Table 3.12 presents the cone calorimetry results of the polymer composites.

Table 3.12 Combustion properties of the neat PLA and the composites [80].

Sample	TTI (s)	PHRR (kW/m ²)	THR (MJ/m ²)	Total smoke production (m ²)	residues (%)
Neat PLA	38	812 ± 41	112 ± 6	0.23	0
PLA/FR	20	300 ± 15	76 ± 4	1.69	5.5
PLA/FR/LDH-CO ₃	21	385 ± 19	70 ± 4	1.32	6.5
PLA/FR/LDH-Phy	21	301 ± 15	64 ± 3	0.81	8.2

Moreover, there has been used 9,10-dihydro-9-oxa-10-phosphaphenanthrene-10-oxide (DOPO) [51] and sodium phenyl phosphate (SPP) [81] as modifying agents for LDHs to reduce flammability of epoxy resin. With the addition of 10% Mg/Al-DOPO, the PHRR of epoxy resin composite reduced by 390 kW/m^2 from the 781 kW/m^2 for the neat epoxy resin [51]. For incorporating of Cu/Al-SPP LDH, Ding et al. [81] suggested that the loading of 4% LDH-SPP decreased the PHRR to 663 kW/m^2 from 1493 kW/m^2 for the pure epoxy resin. Therefore, the LDH-SPP could improve the fire hazards of epoxy resins.

Considering these circumstances, the modification of intercalated anions with various inorganic and organic anions can significantly enhance the fire-retardant efficiency. The carbonate, borate and phosphate anions are used as inorganic intercalating agents. For the modification of organic anions, the compounds based on the sulfate (e.g. DS and DBS), cyclodextrin, long-chain alkyl carboxylates (e.g. decanoate and stearate), phosphate (e.g. BEHP and Phy). In the combustion of polymer nanocomposites, the addition of modified LDHs reduces the PHRR and THR, but the increase of LOI value and char residues. The PHRR reduction performances of polymer nanocomposites containing the different organic anion modified LDHs are summarised in Table 3.13.

Table 3.13 Summary of fire retardancy performance of organic anion modified LDHs for polymers

Metal cations	Organic anions	Polymers	PHRR reduction (%) (at the loading amount of LDHs)	References
Mg/Al	DS	LDPE	15 (5%)	[62]
Mg/Al	BA	LDPE	27 (5%)	[62]
Mg ₃ /Al	DS	PP	58 (20%)	[63]
Mg ₃ /Al	SA	PP	61 (20%)	[63]
Zn/Al	DBS	PLA	62 (2%)	[65]
Mg/Al	CD	EP	44 (6%)	[47]
Mg/Al	T	EP	47 (6%)	[47]
Mg/Al	CD-DBS-T	EP	66 (6%)	[47]
Mg/Al	CD-DBS-Phy	EP	72 (7%)	[67]
Mg/Al	Decanoate	PMMA	58 (10%)	[48]

Table 3.13 Summary of fire retardancy performance of organic anion modified LDHs for polymers (continued)

Metal cations	Organic anions	Polymers	PHRR reduction (%) (at the loading amount of LDHs)	References
Mg/Al	Laurate	PMMA	57 (10%)	[48]
Mg/Al	Myristate	PMMA	54 (10%)	[48]
Mg/Al	Palmitate	PMMA	54 (10%)	[48]
Mg/Al	Stearate	PMMA	51 (10%)	[48]
Mg/Al	Beherate	PMMA	49 (10%)	[48]
Zn/Al	Undecenoate	PMMA	45 (10%)	[68]
Mg/Al	Palmitate	PMMA	68 (20%)	[69]
Mg/Al	BEHP	PUF	19 (3%)	[72]
Mg/Al	DBS	PMMA	45 (10%)	[73]
Mg/Al	EHS	PMMA	27 (10%)	[73]
Mg/Al	BEHP	PMMA	37 (10%)	[73]
Ni/Al	CEPPA	PLA	-37 (10%)	[74]
Mg3/Al	APP	PP	55 (20%)	[75]
Mg/Al	DPHPA	PMMA	35 (5%)	[77]
Mg/Al	DPHPA	EVA	43 (5%)	[78]
Mg/Al	Phy	PP	78 (2%)	[79]
Mg/Al	Phy	PLA	63 (1%)	[80]
Mg/Al	DOPO	EP	50 (10%)	[51]
Cu/Al	SPP	EP	56 (4%)	[81]

It can be seen that the various organic compounds are applied between the interlayers of LDHs to enhance the flame retardancy in polymers, especially the organophosphate compounds. Therefore, this research concentrates on the enhancement of flame retardancy of Mg/Al LDHs with the use of different organophosphate-based compounds, namely bis(2-ethylhexyl phosphate) (BEHP), phytate (Phy), glycerophosphate (GP) and diphenyl phosphate (DPP). The BEHP and Phy have been used to modify LDHs, whereas the GP and DPP are novel organophosphate compounds used as the modifying agent for LDHs.

3.8 Summary

LDHs is the 2D nanomaterial containing the metal hydroxide layers and anions intercalated between the layers. In addition to the anions, water molecules also exist in the interlayer space. The synthesis of LDHs can carry on several methods: co-precipitation, urea hydrolysis, salt-oxide, anion exchange, and reconstruction by structural memory effect. The co-precipitation method is remarkably used for LDH synthesis because it is the direct method and provides high crystallinity. Besides, it is suitable for anionic modification of LDHs. The characterisation of LDHs can use the XRD, FT-TR, and TGA to analyse crystalline phenomena, chemical structure, and thermal decomposition, respectively.

According to the literature, the incorporation of LDHs had efficiency in inhibiting the combustion process of polymers since the releasing of water vapour can reduce the heat and dilute the concentration of combustible gases, and the formation of metal oxide and carbonaceous residues can obstruct the heat and combustible gases passing through the combustion surface of the polymer matrix. To enhance the flame retardancy efficiency of LDHs, the alternative method was the modification of anions in LDHs with organic compounds such as DS, DBS, linear-chain alkyl carboxylates and organophosphate-based compounds (e.g. DOPO, BEHP and Phy)

Considering the composition of organo-anionic modifying agents, the organophosphate-based compounds contained the phosphate ester groups in the structures correlated to the phosphorus flame retardants. The phosphate ester group is high reactivity, and their compounds have been used as flame retardants. This research had attempted to modify LDHs with organophosphate-based compounds. There were four types of organophosphate-based compounds used as modifying agents for LDHs, namely BEHP, Phy, GP and DPP. It expects that all the LDHs modified with the organophosphate-based compounds would enhance the flame retardancy of epoxy resins.

References

- [1] F. Cavani, F. Trifirò and A. Vaccari, "Hydrotalcite-Type Anionic Clays: Preparation, Properties and Applications", *Catalysis Today*, 1991, **11(2)**, 173-301
- [2] D. G. Evans and R. C. T. Slade, "Structural Aspects of Layered Double Hydroxides", in "Structure and Bonding", eds. M. D.M.P., Springer, Germany, 2006, pp1-87
- [3] G. G. C. Arizaga, K. G. Satyanarayana and F. Wypych, "Layered Hydroxide Salts: Synthesis, Properties and Potential Applications", *Solid State Ionics*, 2007, **178(15)**, 1143-1162
- [4] S. Daniel and S. Thomas, "Layered Double Hydroxides: Fundamentals to Applications" in "Layered Double Hydroxide Polymer Nanocomposites", eds. S. Thomas and S. Daniel, Elsevier, UK, 2020, pp 1-76
- [5] S. Denis, D.E. L. Vieira, A. Zarkov, M. G. S. Ferreira, A. Beganskiene, V.V. Rubanik, A. D. Shilin, A. Kareiva and A.N. Salak "Sonication Accelerated Formation of Mg-Al-Phosphate Layered Double Hydroxide via Sol-gel Prepared Mixed Metal Oxides", *Scientific Reports*, 2019, **9(1)**, 1-9
- [6] G. Mishra, B. Dash and S. Pandey, "Layered Double Hydroxides: A Brief Review from Fundamentals to Application as Evolving Biomaterials", *Appl. Clay Sci.*, 2018, **153**, 172-186
- [7] G. W. Brindley and S. Kikkawa, "Formation of Mixed Mg Al Hydroxides with Interlayer Nitrate and Carbonate Ions", *Thermochim. Acta*, 1978, **27(1-3)**, 385-386
- [8] J. Olanrewaju, B. L. Newalkar, C. Mancino and S. Komarneni, "Simplified Synthesis of Nitrate form of Layered Double Hydroxide", *Mater. Lett.*, 2000, **45(6)**, 307-310
- [9] J. He, M. Wei, B. Li, Y. Kang, D. G. Evans and X. Duan, "Preparation of Layered Double Hydroxides", in "Structure and Bonding", eds., D. M. P. Mingos, Springer, Verlag Berlin Heidelberg, 2006, pp 89-119
- [10] L. P. F. Benicio, R. A. Silva, J. A. Lopes, D. Eulálio, R. M. M. Santos, L. A. Aquino, L. Vergütz, R. F. Novais, L. M. Costa, F. G. Pinto and J. Tronto,

- "Layered Double Hydroxides: Nanomaterials for Applications in Agriculture", *Rev. Bras. Cienc. Solo*, 2015, **39**, 1-13
- [11] Y. Zhao, F. Li, R. Zhang, D. G. Evans and X. Duan, "Preparation of Layered Double-Hydroxide Nanomaterials with a Uniform Crystallite Size Using a New Method Involving Separate Nucleation and Aging Steps", *Chem. Mater.*, 2002, **14(10)**, 4286-4291
- [12] H. Panda, R. Srivastava and D. Bahadur, "Synthesis and in situ Mechanism of Nuclei Growth of Layered Double Hydroxides", *Bull. Mater. Sci.*, 2011, **34(7)**, 1599-1604
- [13] A. P. Tathod and O. M. Gazit, "Fundamental Insights into the Nucleation and Growth of Mg-Al Layered Double Hydroxides Nanoparticles at Low Temperature", *Crys. Growth Des.*, 2016, **16(12)**, 6709-6713
- [14] J. W. Boclair and P. S. Braterman, "Layered Double Hydroxide Stability. 1. Relative Stabilities of Layered Double Hydroxides and their Simple Counterparts", *Chem. Mater.*, 1999, **11(2)**, 298-302
- [15] Y. Yang, X. Zhao, Y. Zhu and F. Zhang, "Transformation Mechanism of Magnesium and Aluminum Precursor Solution into Crystallites of Layered Double Hydroxide", 2012, **24**, 81-87
- [16] A. Eliseev, A. Lukashin, A. Vertegel, V. Tarasov and Y. Tret'yakov, "A Study of Crystallization of Mg-Al Double Hydroxides", *Dokl. Chem.*, 2002, **387(4)**, 339-343
- [17] J. Shin, C. J. Choi, T. H. Kim and J. M. Oh, "Phase Transformation from Brucite to Highly Crystalline Layered Double Hydroxide through a Combined Dissolution-Reprecipitation and Substitution Mechanism", *Crys. Growth Des.*, 2018, **18(9)**, 5398-5405
- [18] T. Kameda and Y. Umetsu, "Effect of Preparation Method on Particle Properties of Carbonate-Type Magnesium-Aluminum Layered Double Hydroxides", *J. Ind. Eng. Chem.*, 2017, **53**, 105-110
- [19] A. Seron and F. Delorme, "Synthesis of Layered Double Hydroxides (LDHs) with Varying pH: A Valuable Contribution to the Study of Mg/Al LDH Formation Mechanism," *J. Phys. Chem. Solid.*, 2008, **69(5)**, 1088-1090
- [20] K. Li, N. Kumada, Y. Yonesaki, T. Takei, N. Kinomura, H. Wang and C. Wang, "The pH Effects on the Formation of Ni/Al Nitrate form Layered

- Double Hydroxides (LDHs) by Chemical Precipitation and Hydrothermal Method", *Mater. Chem. Phys.*, 2010, **121(1)**, 223-229
- [21] A. Ay, B. Zumreoglu-Karan, A. Temel and L. Mafra, "Layered Double Hydroxides with Interlayer Borate Anions: A Critical Evaluation of Synthesis Methodology and pH-Independent Orientations in Nano-Galleries", *Appl. Clay Sci.*, 2011, **51(3)**, 308-316
- [22] Z. P. Xu, G. Stevenson, C.-Q. Lu and G. Q. M. Lu, "Dispersion and Size Control of Layered Double Hydroxide Nanoparticles in Aqueous Solutions," *J. Phys. Chem. B*, 2006, **110(34)**, 16923-16929
- [23] X. Sun and S. K. Dey, "Insights into the Synthesis of Layered Double Hydroxide (LDH) Nanoparticles: Part 2. Formation Mechanisms of LDH", *J. Colloid Interf. Sci.*, 2015, **458**, 160-168
- [24] T. L. P. Galvão, C. S. Neves, A.P.F. Caetano, F. Maia, D. Mata, E. Malheiro, M. J. Ferreira, A. C. Bastos A. N. Salak, J. R.B. Gomes, J. Tedim and M. G. S. Ferreira, "Control of Crystallite and Particle Size in the Synthesis of Layered Double Hydroxides: Macromolecular Insights and a Complementary Modeling Tool", *J. Colloid Interf. Sci.*, 2016, **468**, 86-94
- [25] M. Ogawa and H. Kaiho, "Homogeneous Precipitation of Uniform Hydrotalcite Particles", *Langmuir*, 2002, **18(11)**, 4240-4242
- [26] S. Naito, K. Nitoh, A. Ayril and M. Ogawa, "Preparation of Finite Particles of Nitrate Forms of Layered Double Hydroxides by pH Adjustment with Anion Exchange Resin", *Ind. Eng. Chem. Res.*, 2012, **51(44)**, 14414-14418
- [27] B. Saifullah and M. Hussein, "Inorganic Nanolayers: Structure, Preparation, and Biomedical Applications", *Int. J. Nanomed.*, 2015, **10**, 5609-5633
- [28] S. V. Prasanna and P. V. Kamath, "Anion-Exchange Reactions of Layered Double Hydroxides: Interplay between Coulombic and H-Bonding Interactions", *Ind. Eng. Chem. Res*, 2009, **48(13)**, 6315-6320
- [29] F. Millange, R. I. Walton and D. O'Hare, "Time-Resolved in situ X-ray Diffraction Study of the Liquid-Phase Reconstruction of Mg-Al-Carboate Hydrotalcite-Like Compounds", *J. Mater. Chem.*, 2000, **10(7)**, 1713-1720
- [30] H. Nakayama, N. Wada and M. Tshako, "Intercalation of Amino Acids and Peptides into Mg-Al Layered Double Hydroxide by Reconstruction Method", *Int. J. Pharm.*, 2004, **269(2)**, 469-478

- [31] F. Delorme, A. Seron, M. Bizi, V. Jean-Prost, and D. Martineau, "Effect of Time on the Reconstruction of the $Mg_4Al_2(OH)_{12}CO_3 \cdot 3H_2O$ Layered Double Hydroxide in a Na_2CO_3 Solution", *J. Mater. Sci.*, 2006, **41(15)**, 4876-4882
- [32] K.-H. Goh, T.-T. Lim and Z. Dong, "Application of Layered Double Hydroxides for Removal of Oxyanions: A Review", *Water Res.*, 2008, **42(6)**, 1343-1368
- [33] B. R. Venugopal, C. Shivakumara and M. Rajamathi, "Effect of Various Factors Influencing the Delamination Behavior of Surfactant Intercalated Layered Double Hydroxides," *J. Colloid Interf. Sci.*, 2006, **294(1)**, 234-239
- [34] L. Hickey, J. Klopogge and R. Frost, "The Effects of Various Hydrothermal Treatments on Magnesium-Aluminium Hydrotalcites", *J. Mater. Sci.*, 2000, **35(17)**, 4347-4355
- [35] S. Peeterbroeck, M. Alexandre, and P. Dubois, "Processing of Polymer Nanocomposites: New Developments and Challenges", in "Recent Advances in Polymer Nanocomposites: Synthesis and Characterisation", eds. T. S., Z. G.E., V. S.V., and A. P. Meera, IDC, Netherlands, 2010, pp. 19-48
- [36] R. D. Deanin, "Thermosets," in "Handbook of Plastics Technologies", eds. C. A. Harper, McGraw-Hill, USA, 2006, pp. 3.1-3.76
- [37] J. H. Koo, "Polymer Nanocomposites: Processing, Characterization, and Applications (An Overview of Nanoparticles)". McGraw-Hill, USA, 2006
- [38] F. Delogu, G. Gorrasi, and A. Sorrentino, "Fabrication of polymer nanocomposites via ball milling: Present status and future perspectives", *Progress in materials science*, 2017, **86**, 75-126
- [39] F. Laoutid, L. Bonnaud, M. Alexandre, J. M. Lopez-Cuesta and P. Dubois, "New Prospects in Flame Retardant Polymer Materials: From Fundamentals to Nanocomposites", *Mater. Sci. Eng.*, 2009, **63(3)**, 100-125
- [40] J. H. Koo, S. C. Lao and J. C. Lee, "Flame-Retardancy Characterization of Polymer Nanocomposites", in "Characterization Techniques for Polymer Nanocomposites", eds. V. Mittal, Wiley-VCH, Germany, 2012, pp 33-74
- [41] ASTM:D635 Standard Test Method for Rate of Burning and/or Extent and Time of Burning of Plastics in a Horizontal Position, A. International, US, 2014

- [42] ASTM:D3801 Standard Test Method for Measuring the Comparative Burning Characteristics of Solid Plastics in a Vertical Position, A. International, US, 2010
- [43] Z. Matusinovic and C. A. Wilkie, "Fire Retardancy and Morphology of Layered Double Hydroxide Nanocomposites: A review", *J. Mater. Chem.*, 2012, **22(36)**, 18701-18704
- [44] Y. Gao, J. Wu, Q. Wang, C. A. Wilkie and D. Hare, "Flame Retardant Polymer/Layered Double Hydroxide Nanocomposites", *J. Mater. Chem. A*, 2014, **2(29)**, 10996-11016
- [45] Z. Zhang, C. Xu, F. Qiu, X. Mei, B. Lan and S. Zhang, "Study on Fire-Retardant Nanocrystalline Mg-Al Layered Double Hydroxides Synthesized by Microwave-Crystallization Method", *Sci China Ser. B: Chem.*, 2004, **47(6)**, 488-498
- [46] G. Camino, A. Maffezzoli, M. Braglia, M. De Lazzaro and M. Zammarano, "Effect of Hydroxides and Hydroxycarbonate Structure on Fire Retardant Effectiveness and Mechanical Properties in Ethylene-Vinyl Acetate Copolymer", *Polym. Degrad. Stabil.*, 2001, **74(3)**, 457-464
- [47] E. N. Kalali, X. Wang and D.-Y. Wang, "Functionalized Layered Double Hydroxide-Based Epoxy Nanocomposites with Improved Flame Retardancy and Mechanical Properties", *J. Mater. Chem. A*, 2015, **3(13)**, 6819-6826
- [48] C. Nyambo, P. Songtipya, E. Manias, M. M. Jimenez-gasco and C. A. Wilkie, "Effect of MgAl-Layered Double Hydroxide Exchanged with Linear Alkyl Carboxylates on Fire-Retardancy of PMMA and PS", *J. Mater. Chem.*, 2008, **18(40)**, 4827-4838
- [49] L. Ye and B. Qu, "Flammability Characteristics and Flame Retardant Mechanism of Phosphate-Intercalated Hydrotalcite in Halogen-Free Flame Retardant EVA Blends", *Polym. Degrad. Stabil.*, 2008, **93(5)**, 918-924
- [50] X. Liu, X. Gu, S. Zhang, Y. Jiang, J. Sun and M. Dong, "Effects of Dihydrogen Phosphate Intercalated Layered Double Hydroxides on the Crystal Behaviors and Flammability of Polypropylene", *J. Appl. Polym. Sci.*, 2013, **130(5)**, 3645-3651
- [51] W. Yan, J. Yu, M. Zhang, S. Qin, T. Wang, W. Huang and L. Long, "Flame-Retardant Effect of a Phenethyl-Bridged DOPO Derivative and Layered Double Hydroxides for Epoxy Resin", 2017. *RSC Adv.*, **7(73)**, 46236-46245

- [52] L. Qiu and B. Qu, "Polymer/Layered Double Hydroxide Flame Retardant Nanocomposites", 2011, pp. 332-356.
- [53] C. Manzi-nshuti, D. Wang, J. M. Hossenlopp and C. A. Wilkie, "Aluminum-Containing Layered Double Hydroxides: the Thermal, Mechanical, and Fire Properties of (Nano)Composites of Poly(methyl methacrylate)", *J. Mater. Chemistry*, 2008, **18(26)**, 3091-3102
- [54] C. Manzi-Nshuti, D. Chen, S. Su and C. A. Wilkie, "The Effects of Intralayer Metal Composition of Layered Double Hydroxides on Glass Transition, Dispersion, Thermal and Fire Properties of their PMMA Nanocomposites", *Thermochim. Acta*, 2009, **495(1)**, 63-71
- [55] X. Wang, R. Rathore, P. Songtipya, M. D. M. Jimenez-Gasco, E. Manias and C. A. Wilkie, "EVA-Layered Double Hydroxide (Nano) Composites: Mechanism of Fire Retardancy", *Polym. Degrad. Stabil.*, 2011, **96(3)**, 301-313
- [56] S. Xu, L. Zhang, Y. Lin, R. Li and F. Zhang, "Layered Double Hydroxides Used as Flame Retardant for Engineering Plastic Acrylonitrile-Butadiene-Styrene (ABS)", *J. Phys. Chem. Solid.*, 2012, **73(12)**, 1514-1517
- [57] C. M. Jiao, Z. Z. Wang, X. L. Chen and Y. Hu, "Synthesis of a Magnesium/Aluminum/Iron Layered Double Hydroxide and its Flammability Characteristics in Halogen-Free, Flame-Retardant Ethylene/Vinyl Acetate Copolymer Composites", *J. Appl. Polymer Sci.*, 2008, **107(4)**, 2626-2631
- [58] J. Labuschagné, D. Molefe, W. W. Focke and O. Ofosu, "Layered Double Hydroxide Derivatives as Flame Retardants for Flexible PVC", *Macromol. Symp.*, 2019, **384(1)**, 1800148
- [59] L. Shi, D. Li, J. Wang, S. Li, D. Evans and X. Duan, "Synthesis, Flame-Retardant and Smoke-Suppressant Properties of a Borate-Intercalated Layered Double Hydroxide", *Clays Clay Miner.*, 2005, **53(3)**, 294-300
- [60] C. Nyambo and C. A. Wilkie, "Layered Double Hydroxides Intercalated with Borate Anions: Fire and Thermal Properties in Ethylene Vinyl Acetate Copolymer", *Polym. Degrad. Stabil.*, 2009, **94(4)**, 506-512
- [61] Q. Wang, J. P. Undrell, Y. Gao, G. Cai, J. -C. Buffet, C. A. Wilkie, D. ÓHare, "Synthesis of Flame-Retardant Polypropylene/LDH-Borate Nanocomposites", *Macromolecules*, 2013, **46(15)**, 6145-6150

- [62] L. Ye and Q. Wu, "Effects of an Intercalating Agent on the Morphology and Thermal and Flame-Retardant Properties of Low-Density Polyethylene/Layered Double Hydroxide Nanocomposites Prepared by Melt Intercalation", *J. Appl. Polym. Sci.*, 2012, **123(1)**, 316-323
- [63] L. Qiu, Y. Gao, C. Zhang, Q. Yan, D. O'Hare and Q. Wang, "Synthesis of Highly Efficient Flame Retardant Polypropylene Nanocomposites with Surfactant Intercalated Layered Double Hydroxides", *Dalton Trans.*, 2018, **47(9)**, 2965-2975
- [64] P. K. Kaul, A. J. Samson, G. T. Selvan, I. Enoch and P. M. Selvakumar, "Synergistic Effect of LDH in the Presence of Organophosphate on Thermal and Flammable Properties of an Epoxy Nanocomposite", *Appl. Clay Sci.*, 2017, **135**, 234-243
- [65] D.-Y. Wang, A. Leuteritz, Y.-Z. Wang, U. Wagenknecht and G. Heinrich, "Preparation and Burning Behaviors of Flame Retarding Biodegradable Poly(lactic acid) Nanocomposite Based on Zinc Aluminum Layered Double Hydroxide", *Polym. Degrad. Stabil.*, 2010, **95(12)**, 2474-2480
- [66] N.-j. Kang and D.-y. Wang, "A Green Functional Nanohybrid: Preparation, Characterization and Properties of a - Cyclodextrin Based Functional Layered Double Hydroxide", *J. Mater. Chem. A*, 2013, **1(37)**, 11376-11383
- [67] E. N. Kalali, X. Wang and D.-Y. Wang, "Multifunctional Intercalation in Layered Double Hydroxide: Toward Multifunctional Nanohybrids for Epoxy Resin", *J. Mater. Chem. A*, 2016, **4(6)**, 2147-2157
- [68] C. Manzi-Nshuti, J. M. Hossenlopp and C. A. Wilkie, "Fire Retardancy of Melamine and Zinc Aluminum Layered Double Hydroxide in Poly(methyl methacrylate)", *Polym. Degrad. Stabil.*, 2008, **93(10)**, 1855-1863
- [69] C. Nyambo, D. Chen, S. Su and C. A. Wilkie, "Does Organic Modification of Layered Double Hydroxides Improve the Fire Performance of PMMA?," *Polym. Degrad. Stabil.*, 2009, **94(8)**, 1298-1306
- [70] C. Manzi-Nshuti, P. Songtipya, E. Manias, M. M. Jimenez-Gasco, J. M. Hossenlopp and C. A. Wilkie, "Polymer Nanocomposites Using Zinc Aluminum and Magnesium Aluminum Oleate Layered Double Hydroxides: Effects of LDH Divalent Metals on Dispersion, Thermal, Mechanical and Fire Performance in Various Polymers", *Polym.*, 2009, **50(15)**, 3564-3574

- [71] C. M. C. Pereira, M. Herrero, F. M. Labajos, A. T. Marques and V. Rives, "Preparation and Properties of New Flame Retardant Unsaturated Polyester Nanocomposites Based on Layered Double Hydroxides", *Polym. Degrad. Stabil.*, 2009, **94(6)**, 939-946
- [72] S. Gómez-Fernández, L. Ugarte, C. Peña-Rodríguez, M. Zubitur, M. Á. Corcuera and A. Eceiza, "Flexible Polyurethane Foam Nanocomposites with Modified Layered Double Hydroxides", *Appl. Clay Sci.*, 2016, **123**, 109-120
- [73] L. Wang, S. Su, D. Chen and C. A. Wilkie, "Variation of Anions in Layered Double Hydroxides: Effects on Dispersion and Fire Properties", *Polym. Degrad. Stabil.*, 2009, **94(5)**, 770-781
- [74] P. Ding, B. Kang, J. Zhang, J. Yang, N. Song, S. Tang, L. Shi, "Phosphorus-Containing Flame Retardant Modified Layered Double Hydroxides and their Applications on Polylactide Film with Good Transparency", *J. Colloid Interf. Sci.*, 2015, **440**, 46-52
- [75] Y. Gao, Q. Wang and W. Lin, "Ammonium Polyphosphate Intercalated Layered Double Hydroxide and Zinc Borate as Highly Efficient Flame Retardant Nanofillers for Polypropylene", *Polym.*, 2018, **10(10)**, 1114
- [76] Y. Dong, Y. Zhu, X. Dai, D. Zhao, X. Zhou, Y. Qi and J. H. Koo, "Ammonium Alcohol Polyvinyl Phosphate Intercalated LDHs/Epoxy Nanocomposites", *An International Forum for Thermal Studies*, 2015, **122(1)**, 135-144
- [77] G. Huang, A. Zhuo, L. Wang and X. Wang, "Preparation and Flammability Properties of Intumescent Flame Retardant-Functionalized Layered Double Hydroxides/Polymethyl Methacrylate Nanocomposites", *Mater. Chem. Phys.*, 2011, **130(1)**, 714-720
- [78] G. Huang, Z. Fei, X. Chen, F. Qiu, X. Wang and J. Gao, "Functionalization of Layered Double Hydroxides by Intumescent Flame Retardant: Preparation, Characterization, and Application in Ethylene Vinyl Acetate Copolymer", *Appl. Surf. Sci.*, 2012, **258(24)**, 10115-10122
- [79] E. N. Kalali, A. Montes, X. Wang, L. Zhang, M. E. Shabestari, Z. Li and D. - Y. wang, "Effect of Phytic Acid-Modified Layered Double Hydroxide on Flammability and Mechanical Properties of Intumescent Flame Retardant Polypropylene System", *Fire Mater.*, 2018, **42(2)**, 213-220

- [80] X. Jin, X. Gu, C. Chen, W. Tang, H. Li, X. Liu, S. Bourbigot, Z. Zhang, J. Sun and S. Zhang "The Fire Performance of Polylactic Acid Containing a Novel Intumescent Flame Retardant and Intercalated Layered Double Hydroxides", *J. Mater. Sci. Lett.*, 2017, **52(20)**, 12235-12250
- [81] J. Ding, Y. Zhang, X. Zhang, Q. Kong, J. Zhang, H. Liu and F. Zhang, "Improving the Flame-Retardant Efficiency of Layered Double Hydroxide with Disodium Phenylphosphate for Epoxy Resin", *J. Therm. Anal. Calorim.*, 2019, **140(1)**, 149-156

Chapter 4

Experimental Procedure

As the aim of the research is to enhance the fire retardancy of polymers by incorporating nanomaterials of layered double hydroxides (LDHs), the synthesis of LDHs and the preparation of polymer nanocomposites containing the LDHs would be implemented. The LDHs would be modified with the four different organophosphate compounds, while the representative of polymers used in this research was the epoxy resin (EP) of bisphenol A diglycidyl ether (DGEBA).

This chapter provides details of methodologies for the LDHs synthesis and the EP nanocomposite preparations incorporating the synthesised LDHs. Firstly, the materials employed as precursors for the experiments are presented. The second to fourth sections describe the experimental setup and procedures for LDHs preparation intercalated with inorganic anions and modified with the organic anions, the reduction of LDH particle size and the characterisation of LDHs, respectively. In the following section, the curing processes of epoxy resin composites are detailed. The last section explains techniques used to estimate the performance of the LDHs and the pristine EP, and the EP/LDHs nanocomposites.

4.1 Materials

For the synthesis of LDHs, the inorganic metal salt precursors were magnesium nitrate hexahydrate ($\text{Mg}(\text{NO}_3)_2 \cdot 6\text{H}_2\text{O}$, 98% purity) and aluminum nitrate nonahydrate ($\text{Al}(\text{NO}_3)_3 \cdot 9\text{H}_2\text{O}$, ACS reagent), purchased from Acros Organics. The modifying agents for the LDHs were sodium dodecyl sulfate ($\geq 98\%$ purity), bis(2-ethyl hexyl) phosphate (97% purity), phytic acid solution (50% w/w in water), β -glycerophosphate disodium salt hydrate ($\geq 98\%$ purity) and diphenyl phosphate (99% purity). All the organic anion compounds were supplied from Sigma-Aldrich. Sodium hydroxide (NaOH) pellets (98% purity) and ammonium hydroxide (NH_4OH) solution (25% in water) employed as precipitating agents were purchased from VWR chemicals and Merck, respectively. Pural[®] MG70, a commercial Mg/Al LDHs with the chemical formula of $\text{Mg}_{2x}\text{Al}_2(\text{OH})_{4x+4}\text{CO}_3 \cdot n\text{H}_2\text{O}$, was acquired from the Sasol company. The proportion of $\text{MgO}:\text{Al}_2\text{O}_3$ in the commercial LDH was 70:30.

In preparing epoxy resin nanocomposites, the DGEBA (Epikote828) purchased from Hexion was used as a based polymer. Two hardeners of 4,4'-diamino diphenylmethane (DDM, 97% purity) and 4,4'-diamino diphenylsulfone (DDS, 97% purity) employed for the epoxy curing were supplied from Sigma-Aldrich and Acros Chemicals, respectively.

4.2 Synthesis of LDHs

As described in Section 3.2 of the literature review chapter, several methods are used to synthesise LDHs. They can be divided into two major groups: direct and indirect methods. The most common direct method used for LDH synthesis is the co-precipitation. The advantages of this route are that ease of the process and production of high crystallinity of LDHs. Besides, the co-precipitation method has been applied for preparing LDHs intercalated with organic anions. For these reasons, this research interested in synthesising the LDHs modified with the organic compounds by using the co-precipitation method.

Another method used for the synthesis of LDHs was the dehydration-rehydration. It was chosen because few studies published about the modification of LDHs with organic anions by this method. To compare the characteristics of modified LDHs, the pristine LDHs, which had no modifying of the organic compounds, were also prepared.

4.2.1 Synthesis of Pristine LDHs by Co-precipitation Method

For the preparation of Mg/Al LDHs by the co-precipitation method, the mole fraction of Mg^{2+} to Al^{3+} was 2:1 [1]. The experimental setup of LDH synthesis is displayed in Figure 4.1. A flat flange reaction vessel was covered with a five-neck flat flange lid connected to two pressure dropping funnels, a reflux condenser and a pH probe. Within the dropping funnels, one contained a mixed metal salt solution of 0.025 mol (6.41 g) of $Mg(NO_3)_2 \cdot 6H_2O$ and 0.0125 mol (4.69 g) $Al(NO_3)_3 \cdot 9H_2O$ in 25 ml distilled water, whereas the other one contained an aqueous solution of 1M NaOH.

Besides, an alkaline solution of NaOH derived from a dissolution of 0.0626 mol (2.5 g) NaOH pellets in 30 ml distilled water was in the reaction vessel.

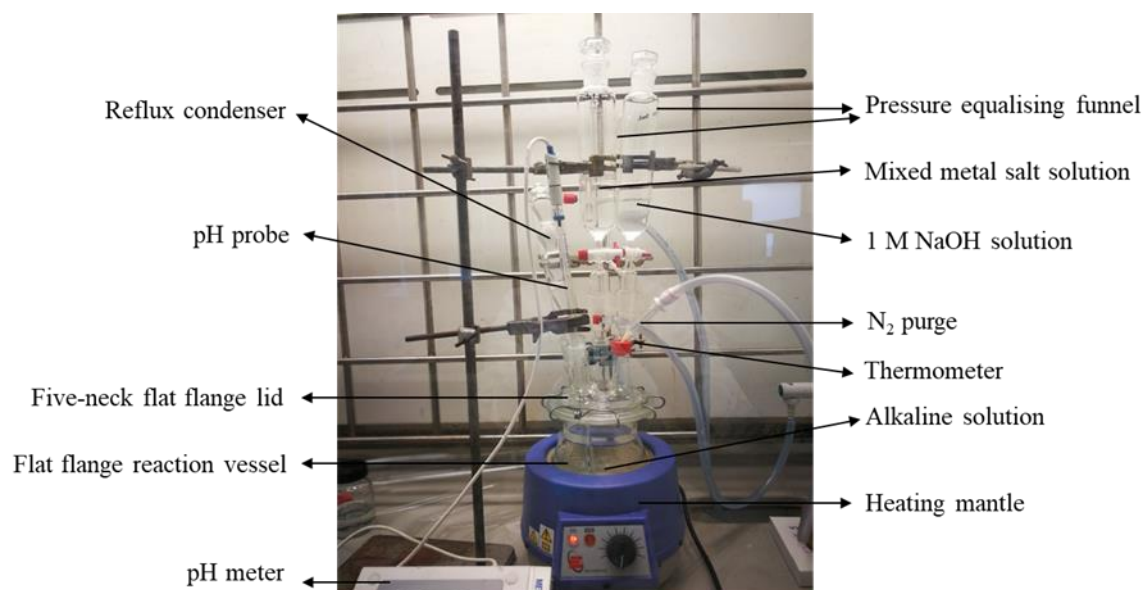


Figure 4.1 Experimental Setup for LDH synthesis.

At the beginning of synthesis, the mixed metal salt solution was slowly added to the alkaline solution in the reaction vessel. During the solution dropping, the mixture solution was vigorously stirred at room temperature. The dropping rate of the mixed metal salt solution was approximately 2 ml/min. As a result, the white precipitate was immediately formed and suspended in the mixture solution. The entire precipitation process was performed under a nitrogen (N_2) atmosphere to prevent carbon dioxide (CO_2) contamination in the air spread to the reactor.

In the meantime, the reaction between the metal salts and NaOH in the mixture solution resulted in a rapid decrease of pH. To maintain the pH value of the solution, the 1 M NaOH in the dropping funnel was added to the suspension. Then, it was stirred and heated at $65^\circ C$ for 24 h. The temperature of mixture was measured by a thermometer. Afterwards the hydrothermal aging process, the particles in the solution were separated by a vacuum filtration using a cellulose filter paper with particle retention of 5-13 μm . The residue on the filter paper was washed with a large amount of distilled water until the filtrate's pH was neutral to remove all the supernatant liquid and the non-reactive chemicals. The drying of samples was subsequently carried out by using an air oven at $50^\circ C$ for 24 h. The dried samples were ground by using a

mortar to reduce the particle size, and then the various sizes of particles were separated by sieves with opening sizes of 1 mm, 200 μm and 100 μm . The particles with a size smaller than 100 μm were used for property testing.

The influence of pH and aging time on the formation of LDHs were studied in this research. Both the parameters were varied to determine the optimum conditions for the synthesis of LDHs. In the case of the pH study, the mixture solutions were maintained at 60°C for 24 h. Meanwhile, the mixture solutions were controlled at pH 9 and 60°C for the time effect study.

As there was a problem of carbonate contamination in the synthesis process (discussed in Chapter 5), the exclusion of CO_3^{2-} poisoning is necessary to synthesis the LDHs. Therefore, this research also studied methods of decarbonation in the distilled water and the NaOH used for the LDH synthesis. There were two assumed methods of decarbonation in the water, namely a vacuuming in a vacuum oven and a boiling with an rotary evaporator (rotovap). For the first method, the water was bubbled in the vacuum oven under low pressure. The pressure gauge pointed at -1 bar, which was lower than the zero point of ambient atmospheric pressure. The negative sign presented the vacuum. Therefore, the bubbling of water in the oven took place under vacuum. An extensive number of bubbles was performed in the water during the vacuuming. This process was operated continuously at room temperature until the disappearance of the gas bubbles. For the second method, the water was boiled with the rotovap under the pressure of 0.3 bar at 80°C for 20 min. The pH values of the water were measured both before and after the bubbling processes.

In the case of the used NaOH pellet, its chemical specification sheet presents an impurity of 1% sodium carbonate (Na_2CO_3). It may be a source of carbonate toxicity for the LDH synthesis. The decarbonation process of the NaOH was carried out by a preparation of 50 wt% NaOH in an aqueous solution, which is a high concentration. The 250 g of NaOH pellets were contained in a 500 ml of volume metric flask. And then, the decarbonated and distilled water was added to the flask until the solution reached a volume level of the container. Afterwards, the solution in the flask was swirled in order to dissolve the NaOH. The consequence of NaOH dissolving generated an obvious production of minute white particles that were suspended in the

solution. The suspended particles were probably Na_2CO_3 . Subsequently, the base solution was poured into a polyethylene bottle and kept in a fume hood. The bottle was left for at least three weeks without moving. As a result, the white solids settled to the bottom of the liquid. The top of the liquid was pipetted to use for the LDH synthesis.

In addition to the 1 M NaOH used as another precipitating agent for the LDH synthesis, an aqueous solution of NH_4OH was employed the same act as the NaOH solution. The solution of NaOH in the reaction vessel and in the additional funnel was replaced with the 2M NH_4OH .

4.2.2 Synthesis of LDHs Modified with Organic Anions

The modification of LDHs with anions of organophosphate compounds was expected to improve the flame retardancy of LDHs. This research attempted to use several organophosphate-based compounds, namely bis(2-ethyl hexyl) phosphate (BEHP), phytate (Phy), β -glycerophosphate (GP) and diphenyl phosphate (DPP) as modifying agents for the modification of LDHs. To confirm the accuracy of the preparing procedure, the preliminary modification of LDHs used dodecyl sulfate (DS) as the anionic modifying agent because the clear instruction of LDH-DS preparation has been described in a number of published journals [2-4].

4.2.2.1 Preliminary Modification of Mg/Al LDHs with Dodecyl Sulfate

4.2.2.1.1 Preparation of LDH-DS by the Co-precipitation Method

The process of the preliminary modification of LDH-DS was followed by the previous study [2]. The $\text{Mg}(\text{NO}_3)_2 \cdot 6\text{H}_2\text{O}$ (0.025 mol, 6.41 g) and $\text{Al}(\text{NO}_3)_3 \cdot 9\text{H}_2\text{O}$ (0.0125 mol, 4.69 g) were dissolved in 40 ml of the distilled water. The mixed metal salt solution was dropped slowly to 60 ml of a homogenised aqueous solution of sodium dodecyl sulfate (SDS) (0.025 mol, 7.20 g). During the mixing, the solution was simultaneously stirred at room temperature and constantly kept at pH 9 by using the stock base solution (1M NaOH or 2M NH_4OH). After the complete addition of the salt solution, the mixture solution was still stirred and heated at 60°C for 24h. The modified LDH

was prepared under the flow of N₂ gas [2]. Then the obtained precipitate was filtered, washed with the distilled water and dried in the oven overnight at 50°C. The synthesised sample was named LDH-DS. The preparation of LDH-DS was repeated, but the decarbonated and distilled water was utilised in the process instead.

4.2.2.1.2 Preparation of LDH-DS by the Dehydroxylation-rehydration Method

First of all, the LDH precursor must be heated at high temperature to calcined the LDH. This process was called the calcination. In the experiment, the 15 g of the dried Pural[®] MG70 LDH was put in an alumina crucible. It was heated in a furnace at 500°C for 5 h under the air with a heating rate of 10°C/min. The mass of LDH both before (M_0) and after (M_1) the heat treatment were recorded to calculate the percentage of mass loss by employing Equation 4.1.

$$\text{Percentage of mass loss} = \left(\frac{M_0 - M_1}{M_0} \right) \times 100 \quad (4.1)$$

The calcined commercial LDH (CLDH) was used as the precursor for the synthesis of modified LDHs. The 1.00 g of CLDH was dispersed in 100 ml of an aqueous solution of 0.005 mol (1.44 g) SDS. The colloid solution was maintained in the conditions at 60°C for 24 h [5]. After that, the solid was collected by the filtering, washing and drying. The decarbonated and distilled water and the gaseous N₂ were applied through the synthesis. The abbreviation of the DS modified LDH produced from this method was CLDH-DS.

4.2.2.2 Synthesis of LDHs Modified with the Different Organophosphate-based Compounds

To improve the flame retardancy potential of LDHs, the compounds of bis(2-ethyl hexyl) phosphate, phytic acid, diphenyl phosphate and β -glycerophosphate disodium salt hydrate were used as the precursors of modifying anions for the LDH preparations. The modification of LDHs with the two first organophosphates have been reported in the previous studies [6-9]. Meanwhile, the other compounds are novel modifying agents applied in the interlayer galleries of LDHs.

The synthesis method of LDHs modified with the various organic phosphate types resembled the preparation process of LDH-DS. However, most of the initial substances of produced anions were neutral molecule, which were low reactivity. Therefore, the deprotonation of the organic compounds before beginning the reaction with the metal salt solution was essential for modifying the LDHs. The details of the deprotonation of organophosphate compounds and the preparation of modified LDHs would be described in this section.

4.2.2.2.1 Conversion of organophosphate compounds to their salts

At the beginning of the synthesis, the phosphate compounds were deprotonated by a reaction with the alkaline solution (1 M NaOH or 2 M NH₄OH) in order to induce the formation of anions in their compounds. The chemical structures of all anionic organophosphate compounds are presented in Figure 4.2

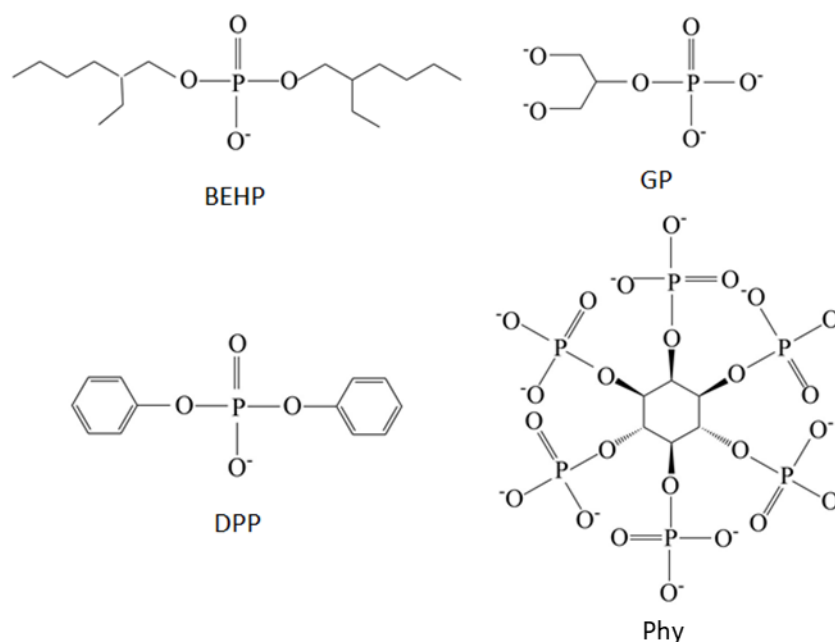


Figure 4.2 The chemical structures of various organophosphate compounds employed for modification of Mg/Al LDHs: bis(2-ethyl hexyl) phosphate (BEHP), phytate (Phy), diphenyl phosphate (DPP) and β -glycerophosphate (GP).

The initial precursor with phosphate groups was dissolved in the NaOH or NH₄OH solutions in the reaction vessel. The mixture was vigorously stirred under the reaction

conditions. Due to the different number of phosphate groups in each compound, the quantities of the base solutions used for the deprotonation were not equivalent. For the deprotonation of bis(2-ethyl hexyl) phosphate (BEHP), the 0.025 mol of BEHP was dissolved in the 20 ml of the NaOH or NH₄OH aqueous solution. The obtained solution was heated at 60°C for 1 h. Meanwhile, the OH groups in the phytic acid (Phy) were dehydrolysed by combining the 4 ml of 50% w/w phytic acid in water with the 25 ml of the base solution. The phytate solution was heated to 60°C and hold it for 3 h.

Likewise, the deprotonation of diphenyl phosphate (DPP) could be carried out by the reaction with the aqueous solutions of NaOH and NH₄OH. The quantities of whole chemicals were equivalent to that of the bis(2-ethyl hexyl) phosphate and the base solutions used to prepare the LDH-BEHP. The phosphate compound was included in the base solutions at 60°C for 1h. In case of the preparation of β -glycerophosphate anions (GP), it could be prepared by the dissolution of the 0.025 mol of β -glycerophosphate disodium salt hydrate in 20 ml of the decarbonated and distilled water. This phosphate precursor was unnecessary to react with the base solutions due to its possession on the salt form.

4.2.2.2.2 Preparation of Organophosphates Modified LDHs by Co-precipitation Method

After the complete deprotonation, the pH of the organophosphate salt solution was adjusted at 9 by adding the 1M NaOH or 2M NH₄OH, depending on the base types applied in the deprotonation process. For example, if the phosphate compound was deprotonated by using the NaOH, the LDH synthesis would apply that base to control the pH solution. Then, the same compositions of mixed metal salt solution used in the synthesis of LDH-DS were added slowly drop-wise into the aqueous solution of phosphate salts. The mixture solution was vigorously stirred, and its pH value was constantly controlled at the same initial pH during the dropping. Then, the obtained slurry was aged at 60°C for 24 h. Subsequently, the product was filtered and washed by the distilled water until the neutralised filtrate. To dry the produced sample, it was brought into the oven at 50°C for 24 h. The prepared LDH samples modified with the

various phosphate anions of BEHP, Phy, DPP and GP were named the LDH-BEHP, LDH-Phy, LDH-DPP and LDH-GP, respectively.

4.2.2.2.3 Preparation of Organophosphates Modified LDHs by Rehydration

Method

An alternative technique used for the preparation of modified LDHs was the calcination and rehydration method. The former method was explained in Section 4.2.2.1. For the latter method, when the solution containing the salt form of phosphate compounds was prepared already, the 1 g of the calcined LDH was dispersed in the phosphate solution in the reaction vessel. The pH of the solution was maintained at pH 9 and pH 10 for the use of 1M NaOH and 2 M NH₄OH, respectively. In the reaction's period, the mixture solution was stirred continuously under the N₂ atmosphere.

4.3 Particle Size Reduction of LDHs

The LDH samples were ground by an attritor (Union Process, Szegvazi Model11). The schematic attritor is illustrated in Figure 4.3. The 20 g of LDHs was contained in a vertical stationary tank with impellers inside it. In addition to the powder samples, the 800 g of polystyrene beads with 3 mm in diameters and isopropanol (IPA) were added into the container, used as the ball mills and a grinding media, respectively. The samples were milled with a speed rotation of 250 rpm at different times (1, 2 and 3 h). After the grinding process, the IPA in the solution was evaporated by heating in the oven at 50°C for 48 h. To compare particle size's change, the particle sizes of both before and after milling were measured by using a laser diffraction analysis.

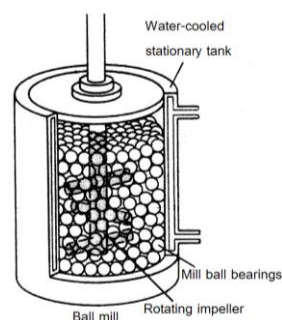


Figure 4.3 The schematic of attrition milling [10].

4.4 Preparation of Epoxy Resin Nanocomposites

The representative of polymers used in this study was the epoxy resin of DGEBA cured by the hardeners of DDM and DDS. The proportion of epoxy resin and hardener was different, depending on the type of hardener. The ratio of DGEBA and DDM was 100:23.9, while the ratio of DGEBA and DDS was 100:30. To evaluate the efficiency of the modified LDHs used as the flame-retardant additives for the polymers, they would be incorporated in the epoxy resin with variation of loading contents (1 wt %, 5 wt % and 10 wt %). The epoxy resin nanocomposites with the incorporation of LDHs can be prepared by two different methods: mechanical stirring and sonicated solvent and stirring.

4.4.1 Preparation of Pristine Epoxy Resin

The chemical proportion and procedure of epoxy resin curing were followed by the previous study [11]. The DGEBA and the hardener were weighted separately in a 250 ml of beaker and a paper cup. For the initial curing of EP, the beaker of DGEBA was heated in an oil bath with the setting temperature at 80°C and 140°C for the curing via the DDM and DDS, respectively. The general temperature of the oil in the bath was higher than that of the resin in the beaker approximately 20°C. During the heating of the epoxy resin, it was vigorously stirred by using a mechanical stirrer. The curing agent was included in the epoxy resin. The mixture was still stirred at that temperature until the curing agent was dissolved completely, becoming the homogeneous mixture.

During the stirring, the viscous mixture can trap the surrounding air, leading to bubbles forming within the resin mixture. It was degassed by using a preheated vacuum oven under the pressure of -1 bar. The degassing temperatures were 70°C and 100°C for the curing systems of the DDM and the DDS, respectively. The degassing process was carried out until the mixture stopped bubbling. Subsequently, the resin mixture was taken out from the vacuum oven, and then it was poured on a preheated flat glass plate with coating a mould releasing agent (Frekote 770-NC, Loctite). The viscous resin was thermally cured following by a curing profile that the resin was hardened. The thermal profiles for the DDM and the DDS curing are presented in

Figure 4.4 and 4.5, respectively. The temperatures of mixing, degassing, and initial curing for the resin curing were also summarised in Table 4.1. The cured epoxy resins were kept in a zip-lock plastic bag and put in a desiccator with phosphorus pentoxide (P_2O_5) used as a high performance of desiccant.

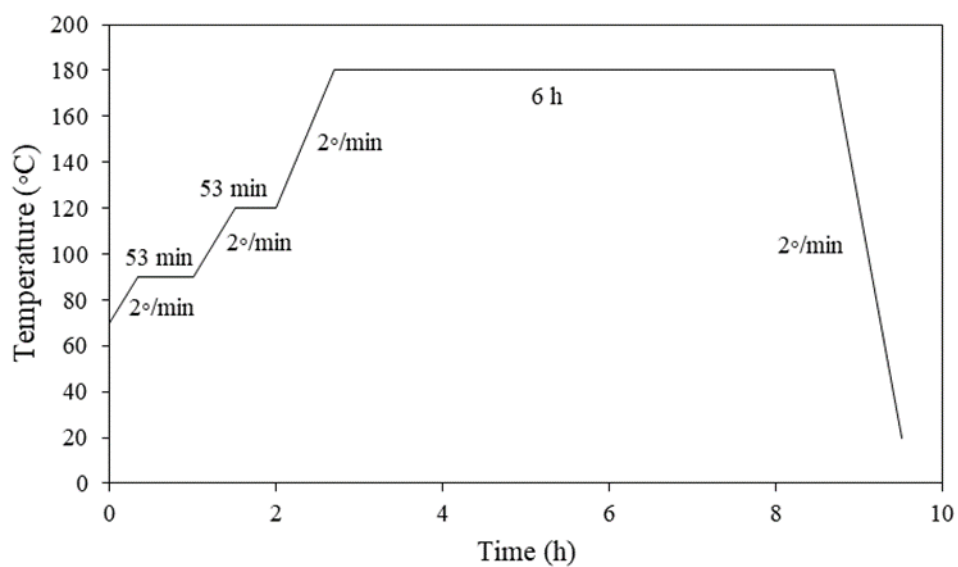


Figure 4.4 The curing profile of DGEBA and DDM [11].

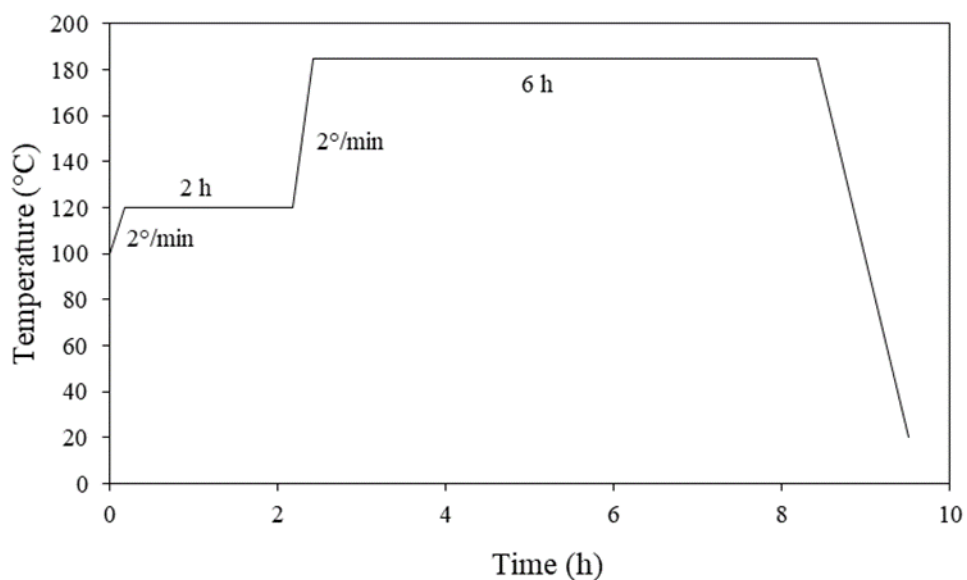


Figure 4.5 The curing profile of DGEBA and DDS [11].

Table 4.1 The summaries of the temperatures of mixing, degassing and initial curing for the curing of DGEBA resin with the DDM and the DDS.

Data	Types of hardeners	
	DDM	DDS
Stoichiometric ratio of DGEBA and hardener	100:23.9	100:30
Mixing temperature (°C)	80	140
Degassing temperature (°C)	70	100
Initial curing temperature (°C)	70	100

4.4.2 Preparation of EP/LDHs Nanocomposites by Method of Mechanical Stirring

After the weighing of DGEBA, LDH filler and hardener, the epoxy resin in the beaker was stirred and applied the heat in the oil bath at the same temperature as the preparation of the pristine EP. Then, the dried LDH was dispersed in the resin part by stirring continuously for 1 h. After the blending, the hardener was added to the mixture of DGEBA and LDH. The blend was mixed until the hardener was dissolved completely. As the epoxy mixture was cloudy with the addition of LDH, it was difficult to observe the dissolution of hardener. This step used the same mixing conditions as the preparation of pristine epoxy resin. Further, the EP mixture was degassed and cured in the oven, following by the pristine EP preparation. Figure 4.6 displays a schematic diagram of EP nanocomposite preparation via the mechanical stirring.

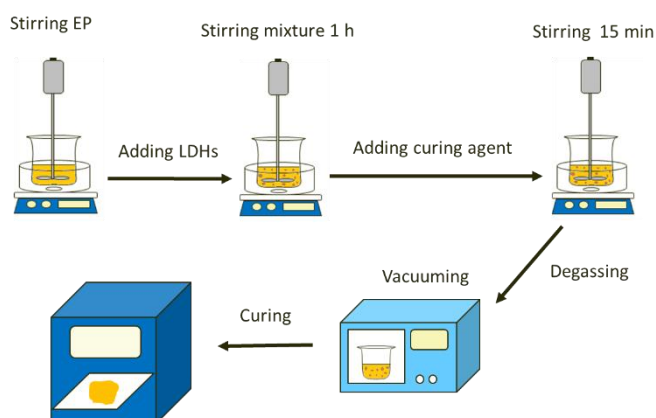


Figure 4.6 The schematic diagram of mixing among DGEBA, LDH and hardener with the mechanical stirring.

4.4.3 Preparation of EP/LDHs Nanocomposites by Using the Solvent, Sonication, and Stirring

At the first step, the LDH was dispersed in an organic solvent by using a magnetic stirrer for 10 min. The container of slurry was covered with parafilm in order to avoid the evaporation of the solvent. In this work, the organic solvent of acetone was employed because of the ease of evaporation. The proportion between the LDH and acetone was 1g of the LDH to 10 ml of acetone. Then the slurry was sonicated in an ultrasonic bath (Elmasonic S 10 (H), Fisherbrand™) at the room temperature for 1 h. For the next step, the solution comprising the LDH was poured into the beaker of DGEBA in the oil bath. The beaker was concealed with aluminium foil. To homogenise the mixture, it was blended at the room temperature for 1 h. Further, the foil was unwrapped, and the homogenised mixture was warmed at 45°C for an hour to evaporate the acetone. After that, it was heated to 80°C to ready for the dissolving of DDM or to 120°C for the dissolving of DDS, and the hardener was blended in the mixture. The degassing and the curing processes were carried out the same condition as the preparation of the pristine EP. The schematic diagram of EP nanocomposite preparation for using the solvent and the sonication is presented Figure 4.7.

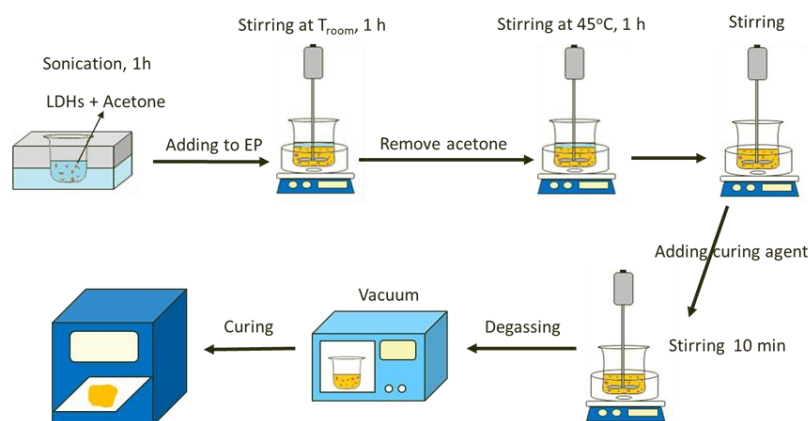


Figure 4.7 The schematic diagram of EP/LDHs nanocomposite preparation with using the solvent and the sonication.

4.5 Characterisations of Prepared LDHs

The characteristics of LDHs were analysed by various techniques. The crystalline phase, the distances between the interlayer, the lattice parameter and the crystal size

of the synthesised LDHs were determined by using the X-ray diffractometer (XRD). Their chemical structure and thermal behaviour were analysed by the Fourier transform infrared spectrometer (FTIR) and the thermogravimetry analyser (TGA), respectively. The laser diffraction analyser was used for the determination of particle sizes. The procedure of characterisation will be detailed in the below sections.

4.5.1 X-Ray Diffractometry

Typically, X-ray diffraction is a technique used for characterisations of crystallographic structure, crystal size and orientation distribution of crystalline samples. When the incident X-rays with a monochromatic wavelength reach the crystal planes of the sample, the X-rays are scattered with the same wavelength as the incident x-rays. In addition, the angles (θ) of the incident beam are equal to that of the scattered beam. The scattered X-rays reflected in an X-ray diffraction pattern. [12] The characteristic of the X-rays scattering is shown in Figure 4.8.

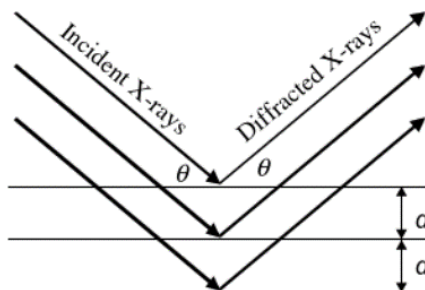


Figure 4.8 The schematic diagram of the incident and scattered X-rays beam on the crystal planes of sample [12].

In this study, the crystalline patterns of LDHs were determined by the XRD diffractometer (D2 phaser, Bruker) with an X-ray source of $\text{CuK}\alpha$ radiation ($\lambda=0.154$ nm). The powder sample of LDH was put in a specimen holder and the height level of sample was adjusted by using a glass slide. Then, the sample holder was brought into the XRD machine with a slit gap of 1 mm. The XRD patterns were detected in the 2θ range of $5\text{-}70^\circ$ with a step size of 0.02° and a scan speed of $3^\circ/\text{min}$. The XRD patterns of samples were used to characterise the crystalline phases by matching with reference data of the International Centre for Diffraction Data (ICDD) in a Sleve+

programme. Furthermore, the XRD data can be used for the calculation of d-spacing, lattice parameter and crystal size.

The d-spacing and the crystallite size of LDH can be calculated by using the Bragg's and the Scherrer equation, displayed in Equation 4.2 and 4.3, respectively:

$$n\lambda = 2d \sin\theta \quad (4.2)$$

$$D = \frac{K\lambda}{\beta \cos\theta} \quad (4.3)$$

where n is a diffraction order, λ is the X-ray source wavelength, θ is the Bragg's angle, D is the crystal size, K is a constant (0.89), β is the full width at half maximum intensity of the peak (FWHM).

4.5.2 Fourier Transform Infrared Spectroscopy

Fourier transform infrared spectroscopy (FTIR) is a technique correlating to absorption of electromagnetic radiation in IR regions. There are three regions of IR: 400-10 cm^{-1} for far IR, 4000-400 cm^{-1} for mid-IR and 14285-4000 cm^{-1} for near IR. When the IR form a radiation source through a sample, the IR radiation is absorbed. As a result, it leads to vibration and rotation of functional groups in the molecule of the sample. The vibrational mode can be classified into two transitions: stretching and bending. The former is a change of bond length, which can be symmetry or asymmetry. The latter is a change of bond angle, which is deformation in the same or the opposite directions[13]

In this experiment, the FTIR spectra of samples were obtained by the FTIR spectrometer (Frontier, Perkin Elmer) in the wavenumber range of 4000 to 400 cm^{-1} with a resolution of 2 cm^{-1} . The testing procedure of the powder sample was carried out a standard KBr pellet method. The 0.002 g of fine sample and the 0.2 g of potassium bromide (KBr) were ground and mixed with an agate mortar. The mixture was then transferred into a stainless-steel mould and compressed into a disk by using a manual hydraulic press at 1 ton and 10 tons for 1min each. The homogeneous and

transparent disk sample was taken apart by the mould and inserted in a sample holder for the characterisation. For the liquid sample (BEHP and phytic acid), it was analysed by an attenuated total reflectance (ATR) technique. The samples were dropped on a diamond crystal plate.

4.5.3 Thermogravimetric Analysis

Thermogravimetric analysis (TGA) is a technique measuring the change of mass as a function of temperature under the desired atmosphere. With the elevated temperature, the mass loss of samples can be observed from the thermogram [13]. This study used the TGA (Pyris1 TGA, Perkin Elmer) for the characterisation of thermal behaviours of samples. Before the testing, the sample was dried in an oven at 50°C for 24 h. The powders or small pieces of samples were weighed in an aluminum pan and heated between 30°C and 800°C with a heating rate of 10°C/min under the nitrogen atmosphere at 20 ml/min. The mass loss of the sample was recorded with the change of heating as displayed in the thermogram. Besides, the first derivatives of thermograms (DTG) were also plotted.

4.5.4 Prediction of Structural Models of LDHs

The results of LDHs characteristics obtained from the XRD, FT-IR and TGA can be used to predict orientations of organophosphate anions in the LDH structures. The general factors affecting the arrangements of LDHs are the thickness of metal hydroxide layers and the size and orientation of anions. The general Mg/Al LDHs possess the thickness of layers around 0.48 nm. For the size of anionic compounds, they were measured from the molecules simulated with a software of Avogadro. The parameters used for the structure optimisation were the Universal Force Field (UFF) and the steepest descent algorithm. According to the data of interlayer space getting from the XRD and the size of anions, the orientation of anions were expected. All the data can be used to propose the structural models of the pristine LDH and the modified LDHs.

4.5.5 Particle Size Measurement

In the present, there are a variety of techniques used for the measurement of particle size such as sieving, microscopy and laser diffraction. The last method is a well-known technique for particle size measurement in industry. The principal of laser diffraction for measurement of particle size is to a passing of monochromatic laser to a suspension containing particles. It results in the diffraction angle, relating to the particle size [14]. The particle sizes of the obtained LDHs were measured by a particle size analyser (Mastersizer 3000, Malvern Analytical). The wet dispersion process was used for the testing. The particle sample was added in the water used as a dispersant with stirring and ultrasonic. The laser diffraction of samples was detected for the measurement of particle size and its distribution.

4.6 Characterisations of Epoxy Resin Nanocomposites

The visual, flexural, dynamic thermal, thermal degradable and flammable properties of the pristine EP and their nanocomposites were characterised by a microscope, flexural tester, dynamic thermal analyser, thermogravimetric analyser and burn tester, respectively.

4.6.1 Visual Properties

To observe the dispersion of LDHs in the resin matrix, the samples were cut, and the sides of samples were polished with abrasive grinding papers with different grit sizes of 240, 600, 1200 and 2500. The tops and the bottoms would not be polished. The polished sides of samples were observed by a portable microscope with a magnification of 1000 times.

4.6.2 Flexural test

One of the common methods used for the determination of flexural properties is a three-point bending test. The samples were tested by the three-point bending by a universal testing machine (TA500, Lloyd) with a 500 N load cell. According to the

ASTM D790-17 [15], the required dimension of polymeric specimen for the flexural testing is approximately 12.7 mm of width, 60 mm of length and 1.6 mm of thickness. The surfaces of samples were ground by a manual grinder with using the grinding paper of 240 grit size until they reached the desired dimension.

The drive systems of the bending machine always display a compliance, estimated by the difference between the applied crosshead displacement and the displacement given to the specimen. Therefore, this compliance was measured to subtract from the test data. As a result, the corrected data had accuracy. For the procedure of compliance, a thick steel disc was placed on the supports, and then the crosshead was pressed slowly down to the steel. The reported data of loads and deflections was plotted a line graph. The slope of the plotted line was used for the collection of deflections.

For the test, the specimens were placed on two roller supports with a span of 25 mm. The preload of 0.1 N applied to the centre of specimens. Figure 4.9 shows the schematic of the three-point bending test. The loads and the deflections of the tested specimens were recorded during the applied load until the specimens were fractured. The obtained data of the deflections were corrected by using the compliance value before the use for calculation. The flexural stress and modulus of elasticity were calculated by using the corrected data, followed by Equation 4.4 and 4.5, respectively.

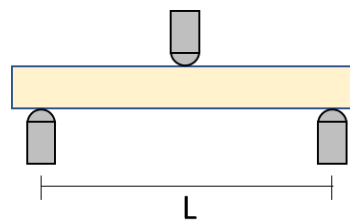


Figure 4.9 The schematic of the three-point bending test.

$$\sigma_f = \frac{3PL}{2bd^2} \quad (4.4)$$

$$E_B = \frac{L^3m}{4bd^3} \quad (4.5)$$

Where σ_f is the flexural stress (MPa), P is the load given on the curve of load-deflection (N), L is support span (mm), b is the width of the specimen (mm), d is the thickness of specimen (mm), E_B is the modulus of elasticity (MPa), m is an initial slope of the load-deflection curve in the straight line (N/mm).

4.6.3 Dynamic Mechanical Analysis

Dynamic mechanical analysis (DMA) characterises the mechanical properties of a specimen as a function of temperature. A sinusoidal oscillating force applied to the specimen, corresponding to the stress as followed by Equation 4.6:

$$\sigma(t) = \sigma_{\max} \sin \omega t \quad (4.6)$$

where $\sigma(t)$ is the stress at a time (t), σ_{\max} is the maximum stress and ω is the frequency (f) of oscillation that is equal to $2\pi f$. The applied force resulted in the displacement, determining the strain (ϵ). The ratio of stress to strain was Young's modulus (E). [16]

For the materials with the imperfect elasticity, the measured strain responds slowly to the applied stress by the phase difference (δ), as illustrated in Figure 4.10. The ratio of the peak stress and the peak strain provides the complex modulus consisting of the storage modulus (E') and the loss modulus (E''). The storage modulus derives from the applied stress, correlating to the elastic section of materials. Meanwhile, the loss modulus results from the differentiated strain, representing the viscous behaviour of materials. The mechanical damping factor ($\tan \delta$) can be derived from the ratio of E'' to E' , as present in Equation 4.7. The $\tan \delta$ is an analysis of deformational energy with heating. [16]

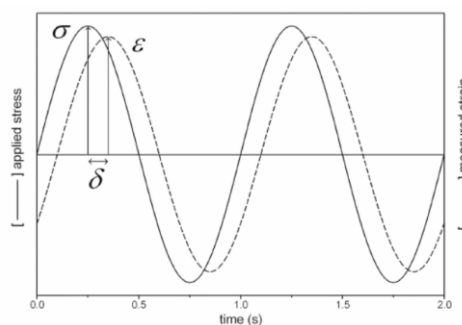


Figure 4.10 The relative diagram of the applied stress and the measured strain during dynamic mechanical testing [16].

$$\tan \delta = \frac{E''}{E'} \quad (4.7)$$

The dynamic mechanical properties of the cured polymers were analysed by the DMA (DMA8000, Perkin Elmer). The samples were tested in a geometry mode of single cantilever bending, which is the mode used for polymeric bar samples. Figure 4.11 shows the schematic geometry mode of single cantilever bending. The cast samples were cut by a tile saw and ground by a grinder with using a grinding paper of P240 to get the dimensions of 10 mm width, 30 mm length and 1.5 mm thickness. Due to the manual process, the dimensions of samples varied between 0.2 mm.

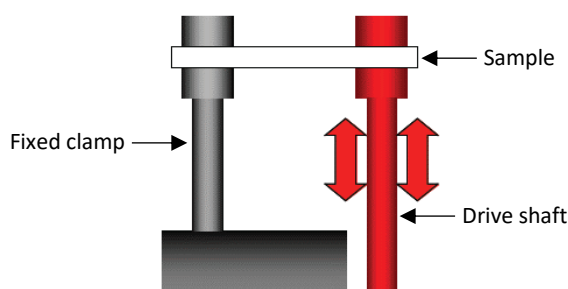


Figure 4.11 The schematic single cantilever bending mode [16].

Most of the beta and gamma transitions of polymers show at the lower room temperature. Thus, the study of dynamic mechanical properties was operated in the range of cooling temperature and high temperature. For the cooling system, liquid nitrogen was used as a cooling agent because it can cool down to -190°C .

The samples were run in the temperature scan mode (-190°C to 300°C) with a heating rate of $3^{\circ}\text{C}/\text{min}$. The tests occurred under a displacement of 0.05 mm and a multi-frequency of 1, 5, 10 and 50 Hz. The two specimens of each sample were repeated for the tests. The obtained results were averaged and plotted by the OriginPro software.

Moreover, the data of storage modulus in the rubbery state was used to calculate the crosslink density (ν_c) in the sample by following an Equation 4.8,

$$\nu_c = \frac{E'_{\text{Rubbery}}}{3RT} \quad (4.8)$$

where E' rubbery is the storage modulus at the temperature above the T_g at 30°C , T is T_g+30 and R is a universal gas constant [17].

4.6.4 Thermogravimetric Analysis

The thermal stabilities of the pristine EP and their nanocomposites with the loading of LDHs were analysed by TGA. The small pieces of the samples were employed for the characterisation. The testing conditions were the same as the LDHs, i.e. the temperature range of 30°C to 800°C with the heating rate of $10^\circ\text{C}/\text{min}$ under the N_2 or air.

4.6.5 Burning Test

According to the Section 3.6 in the Chapter 3, it was found that the cone calorimetry was the main technique used considerably to investigate the burning behaviors of polymers. This technique reflected the phenomenon of combustion such as heat release rate (HRR), total heat released (THR), time to ignition (TTI), time of combustion (TOC) and total smoke released (TSR). It was the best technique for the characterisation of burning test, thereby this study has planned to use a cone calorimeter at the University of Bolton for the test.

In the early 2020, there has been the COVID-19 pandemic across the UK. The Government announced the national lockdown a long period of time to stop the spread of COVID-19. It has impacted the close contact with anyone and the travelling. From these reasons, the plan of burning test with the cone calorimeter at the University of Bolton were cancelled. Therefore, this work looked for an alternative technique for the estimation of combustion behaviors.

The literature review in the Section 3.5.2.2 presented the relatives between the results obtained from the cone calorimeter test and the Underwriters Laboratories (UL-94) test. In the former, the materials with high flame retardancy provided the reduction of TTI and peak of HRR (PHRR) and the increase of time to PHRR and char residue, compared to the flammable materials. For the later, the TTI and burning time decreased for materials with high flame retardancy that did not display the flame

dripping during the test. From the relating results of both the combustion test, the UL-94 test was selected to characterise the burning behaviours in this study, replacing the cone calorimeter test.

Fire behaviours of samples were estimated by the UL-94 in the horizontal and vertical positions. The ASTM:D635 is for the burning test in the horizontal direction [18] and the ASTM:D3801 is for the burning test in the vertical direction [19]. Figure 4.12 and 4.13 present the schematic setups of both tests, respectively. The dimension of specimens for the tests was 125 mm x 13 mm x 3 mm. The five specimens in each sample were run and averaged.

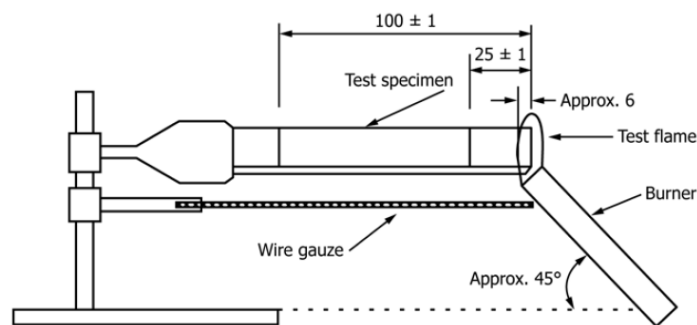


Figure 4.12 Schematic of flammability test in horizontal direction [18].

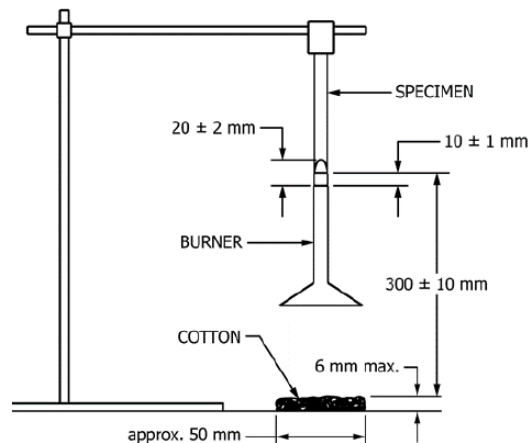


Figure 4.13 Schematic of flammability test in vertical direction [19].

For the testing in horizontal position, the specimens were marked with two lines perpendicular to the length of strip bars from the ends of 25 mm and 100 mm. The specimen was clamped with another side without the mark. The flame from a burner applied to the free end of the specimen for 30 s at the same position. Then, the burner

was moved out of the specimen. It could be burned until it reached to the first reference mark. The time of burning (t) in the unit of second was recorded by a timer. The burning was carried out until it stopped. The burned length (L) in mm was measured. From the obtained data, they were used for a calculation of burning rate (V).

$$V = \frac{60 L}{t} \quad (4.7)$$

However, if the burning cannot approach the first reference line after the flame is removed, the flammability test in horizontal direction may not be suitable for the sample.

For the test in vertical position, the clamped specimen was ignited at the bottom by applying the flame for 10 s, and then it was to move away from the specimen. As a result, the specimen continued to burn. The burn time after moving the burner was recorded (t_1). When the burn stops, the second flame was applied immediately to the specimen for 10 s. Then, the burner was removed, and the burned time was recorded (t_2). Besides, the flame burning behaviours and the flame dripping of the specimen were observed.

Meanwhile, the test in vertical position is used for the classification of flammability of materials into three groups: V-0, V-1 and V-2. The criteria of each class are presented in Table 4.2

Table 4.2 Criteria and classification of vertical burning behaviour following by ASTM:D3801 [20].

Requirement	Categories		
	V-0	V-1	V-2
t_1 for each specimen	≤ 10 s	≤ 30 s	≤ 30 s
T_2 for each specimen	≤ 30 s	≤ 60 s	≤ 60 s
Total time of t_1 and t_2 for five specimens	≤ 50 s	≤ 250 s	≤ 250 s
Burning processes to the holding clamp	No	No	No
Dropping of flame particles	No	No	Yes

4.7 Summary

This chapter described the preparing procedure of the pristine LDHs and LDHs modified with the organophosphate anions, namely the BEHP, Phy, GP and DPP. The obtained LDHs were analysed the crystalline characteristics, chemical structure and thermal behaviours by the XRD, FTIR and TGA, respectively. To reduce the particle size of the LDHs, they were ground by the attrition mill. And then, there was the analysis of particle size of LDHs by the particle size analyser.

The LDHs were used as the fillers for the EP nanocomposites in the curing system of DDM and DDS. The EP nanocomposites contained the 1, 5 and 10 wt%. of LDHs. Besides, the pure EPs were prepared to compare the properties with their nanocomposites. All the cured epoxy samples were observed in the visual cross-section characteristics by the microscope. The influences of LDHs loadings on the flexural, dynamic thermal and thermal properties were tested by the three-point bending tester, DMA and TGA, respectively.

Additionally, the most crucial test in the research was the burning test to estimate the flammability of the cured samples. The pure EPs and their nanocomposites containing the pristine LDHs and the modified LDHs were tested the burning in the horizontal and vertical position. The results of LDHs characterisation were discussed in Chapter 5. Meanwhile, the characteristics of EP/LDHs nanocomposites cured with the DDM and DDS were evaluated in Chapter 6 and 7, respectively.

References

- [1] T. T. X. Hang, T. A. Truc, N. T. Duong, P. G. Vu and T. Hoang, "Preparation and Characterization of Nanocontainers of Corrosion Inhibitor Based on Layered Double Hydroxides", *Appl. Clay Sci.*, 2012, **67-68**, 18-25
- [2] P. K. Kaul, A. J. Samson, G. T. Selvan, I. Enoch and P. M. Selvakumar, "Synergistic Effect of LDH in the Presence of Organophosphate on Thermal and Flammable Properties of an Epoxy Nanocomposite", *Appl. Clay Sci.*, 2017, **135**, 234-243

- [3] S. Lv, Y. Yuan and W. Shi, "Strengthening and Toughening Effects of Layered Double hydroxide and Hyperbranched Polymer on Epoxy Resin," *Prog. Org. Coat.*, 2009, **65(4)**, 425-430
- [4] L. Ye and Q. Wu, "Effects of an Intercalating Agent on the Morphology and Thermal and Flame-Retardant Properties of Low-Density Polyethylene/ Layered Double Hydroxide Nanocomposites Prepared by Melt Intercalation", *J. Appl. Polym. Sci.*, 2012, **123(1)**, 316-323
- [5] M. Bouraada, M. Lafjah, M. S. Ouali, and L. C. de Menorval, "Basic Dye Removal from Aqueous Solutions by Dodecylsulfate-and Dodecyl Benzene Sulfonate-Intercalated Hydrotalcite", *J. Hazard. Mater.*, 2008, **153(3)**, 911-918
- [6] L. Wang, S. Su, D. Chen and C. A. Wilkie, "Variation of Anions in Layered Double Hydroxides: Effects on Dispersion and Fire Properties", *Polym. Degrad. Stabil.*, 2009, **94(5)**, 770-781
- [7] S. Gómez-Fernández, L. Ugarte, C. Peña-Rodríguez, M. Zubitur, M. Á. Corcuera and A. Eceiza, "Flexible Polyurethane Foam Nanocomposites with Modified Layered Double Hydroxides", *Appl. Clay Sci.*, 2016, **123**, 109-120
- [8] X. Jin, X. Gu, C. Chen, W. Tang, H. Li, X. Liu, S. Bourbigot, Z. Zhang, J. Sun and S. Zhang, "The Fire Performance of Polylactic Acid Containing a Novel Intumescent Flame Retardant and Intercalated Layered Double Hydroxides", *J. Mater. Sci. Lett.*, 2017, **52(20)**, 12235-12250
- [9] E. N. Kalali, A. Montes, X. Wang, L. Zhang, M. E. Shabestari, Z. Li and D.-Y. Wang, "Effect of Phytic Acid-Modified Layered Double Hydroxide on Flammability and Mechanical Properties of Intumescent Flame Retardant Polypropylene System", *Fire Mater.*, 2018, **42(2)**, 213-220
- [10] C. L. De Castro and B. S. Mitchell, "Nanoparticles from Mechanical Attrition," in "Synthesis, Functionalization and Surface Treatment of Nanoparticles", eds. M.-I. Baraton, American Scientific Publishers, USA, 2003, pp 1-15
- [11] T. Young, "Tailoring the Natural Toughness of Epoxy Resins," Master, Materials Science and Engineering, University of Sheffield, UK, 2018.
- [12] B. B. He, "Two-dimensional x-ray diffraction", John Wiley & Sons, USA, 2009

- [13] O. J. Rees, "Fourier Transform Infrared Spectroscopy: Developments, Techniques and Applications", Nova Science Publishers, New York, 2010
- [14] M. Rhodes, "Particle Size Analysis" in "Introduction to Particle Technology", John Wiley & Sons, England, 2008, pp. 1-450
- [15] D790-17 Standard Test Methods for Flexural Properties of Unreinforced and Reinforced Plastics and Electrical Insulating Materials A. International, US.
- [16] P. J. Haines and C. "Royal Society of, Principles of Thermal Analysis and Calorimetry" in "Thermal analysis and calorimetry", Royal Society of Chemistry, Cambridge, UK, 2002
- [17] R. Ramsdale-Capper and J. P. Foreman, "Internal Antiplasticisation in Highly Crosslinked Amine Cured Multifunctional Epoxy Resins", *Polym.*, 2018, **146**, 321-330
- [18] D635-14 Standard Test Method for Rate of Burning and/or Extent and Time of Burning of Plastics in a Horizontal Position, A. International, US.
- [19] D3801-10 Standard Test Method for Measuring the Comparative Burning
- [20] ASTM:D3801 Standard Test Method for Measuring the Comparative Burning Characteristics of Solid Plastics in a Vertical Position, A. International, US, 2010.

Chapter 5

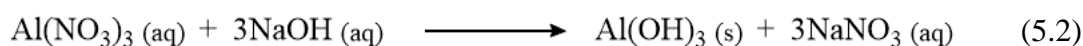
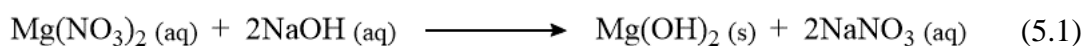
Synthesis and Characterisation of LDHs

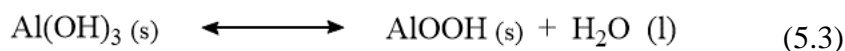
This chapter focuses on the preparation of layered double hydroxides (LDHs) via the co-precipitation and the rehydration methods. The first section presents the results of pristine LDHs preparation with variations of pH, ageing time and bases. The later section discusses the preparation of LDHs modified with various organophosphate ester-based anions. All the LDHs are characterised crystalline structure, chemical structures, thermal stability with proper instruments. Besides, the data obtained from the characterisations of LDHs and the structural simulation of anionic compounds are used for speculation of LDHs structural models. The last section provided the effect of LDHs milling on the particle size.

5.1 Preparation of LDHs by the Co-precipitation

During the co-precipitation for the LDH synthesis, the white insoluble solids were produced immediately after adding the small drops of the mixed metal nitrate salt solutions comprising the magnesium nitrate $\text{Mg}(\text{NO}_3)_2$ and aluminium nitrate $\text{Al}(\text{NO}_3)_3$ to the base solution of sodium hydroxide (NaOH). It was assumed that the insoluble solids produced from the co-precipitation process were magnesium dihydroxide ($\text{Mg}(\text{OH})_2$) and aluminium trihydroxide ($\text{Al}(\text{OH})_3$).

Since $\text{Mg}(\text{NO}_3)_2$ and $\text{Al}(\text{NO}_3)_3$ used as the reactants for the LDH synthesis were soluble in water, the aqueous solution contained the ions of Mg^{2+} , Al^{3+} , NO_3^- , Na^+ and OH^- . Generally, the positively charged cation interacts with the negative charge in anion to form an ionic compound. In this experiment, the possible ionic interactions were the Mg^{2+} and Al^{3+} with the OH^- and the Na^+ with the NO_3^- . According to the solubility guideline for ionic compounds, most metal hydroxides are insoluble in water, while the nitrates of alkali metal cations can dissolve in water [1]. Hence, the $\text{Mg}(\text{OH})_2$ and $\text{Al}(\text{OH})_3$ suspended in the aqueous solution, and the sodium nitrate (NaNO_3) was soluble in there. For the solid of $\text{Al}(\text{OH})_3$, it can rearrange the structure to boehmite (AlOOH) during the co-precipitation [2]. The balance equations for the precipitation reactions present in Equation 5.1-5.3.





As mentioned in Chapter 3 of the literature review, there were two different concepts of LDH formation mechanisms. A few studies suggested that the Mg(OH)_2 formed the layer structure of brucite in the early step, and then the AlOOH diffused in the layers. It contributed to the replacement of some Mg(OH)_2 with the AlOOH . This circumstance led to the unbalance of charges on the layered structure. Thus, the anions in the solution, e.g., NO_3^- and/or other desired anions, combined to the cations of metal hydroxide layers [3, 4].

On the other hand, the previous study claimed that the layers of AlOOH produced in the initial co-precipitation process, then the Mg^{2+} cations were adsorbed and diffused into the boehmite lamellae. This action affected the unbalancing charges of layers. It caused an attachment of anionic compounds to the cationic lamellae. The product in the stage was the low crystalline LDHs. To increase the crystallinity, the LDHs were aged in the solution for the desired time [2]. This thesis also studied the effect of aging times on LDH formation. It will be discussed in the following section.

After the crystallisation process, the precipitate was separated from the solution by the filtration. The residue was washed with the decarbonised and distilled water until the pH of the filtrate was neutral. It was then dried in the oven. The characteristic of the dried sample was a white flaky solid. The LDH was ground using the mortar to reduce the particle size and then was sieved to separate particles' sizes. The analysis of LDHs used the synthesised sample with a particle size of fewer than 100 μm . All the prepared LDH samples were stored in small glass vials. They should not keep in the desiccator because the high active desiccant (P_2O_5) might remove the water molecules in the LDH structures. Therefore, they were kept in the cupboard at the room temperature.

5.2 Characterisation of Pristine LDHs Prepared by the Method of Co-precipitation

To determine the optimum conditions for the LDH preparation via the co-precipitation method, the pristine LDHs, which were unmodified by the organic compounds, were prepared in the various aging conditions (pH and time) and the different precipitating agents. The characteristics of LDHs were analysed by the x-ray diffractometry (XRD), fourier transform infrared (FTIR) and thermogravimetry analysis (TGA). As the procedure of pristine LDH followed to the previous study, the obtained result was the LDH intercalated with nitrate. Therefore, the initial experiment was aiming the nitrate intercalated LDH as the pristine LDH.

5.2.1 Effect of pH on the Formation of LDHs

For the preparation of LDHs with the co-precipitation method under the N₂ atmosphere, the solution of the mixed metal salts was added to the base solution. The combination of both solutions resulted in the formation of the white precipitated solid and the reduction of the pH value in the solution. The mixture solution's pH remained at the desired pH (9, 10, 11 and 12) by adding the 1M NaOH under the controlled conditions at 60°C for 24 h. The XRD patterns of LDH samples prepared in different pH are shown in Figure 5.1. It can be seen that the peak positions did not change with increasing the pH. Hence, the variation of pH did not affect the crystalline phases of samples.

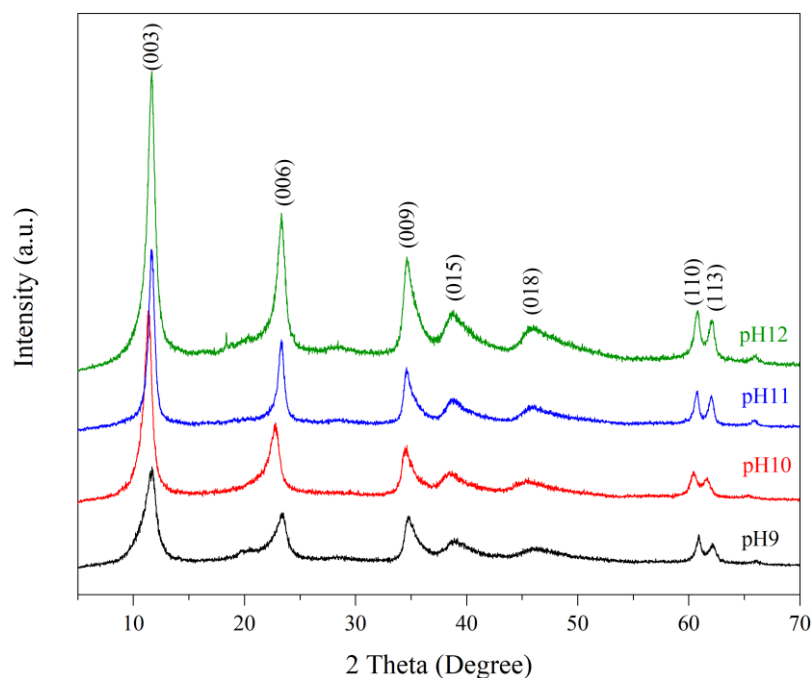


Figure 5.1 The XRD patterns of pristine Mg/Al LDHs synthesised at 60°C for 24 h in the different aging pH.

As the identification of crystalline phases by using the reference databases of the International Centre for Difference Data (ICDD), the patterns of samples matched with a crystal structure of magnesium aluminium carbonate hydroxide hydrate with the chemical formula of $\text{Mg}_{0.83}\text{Al}_{0.17}(\text{CO}_3)_{0.08}(\text{OH})_2(\text{H}_2\text{O})_{0.75}$ (the powder diffraction file number: 04-015-1683). Figure 5.2 compares the XRD patterns of the LDH sample prepared at pH 10 with the LDH reference. The peak positions of the synthesised samples (red line) shifted slightly from the database reference (blue line). It might result from the orientation of imperfect crystals in the synthesised samples including the lower purity of crystals.

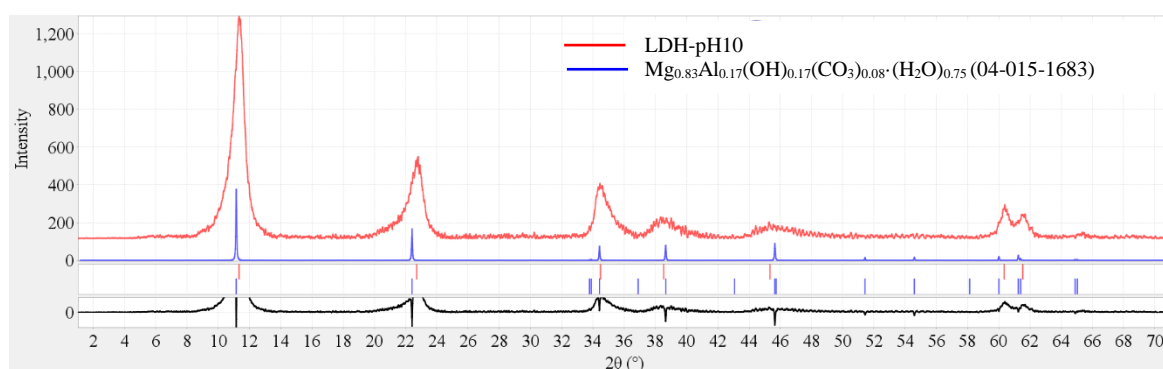


Figure 5.2 The comparison of XRD patterns between the LDH synthesised at pH10 and 60°C for 24 h and the PDF number 04-015-1683.

Although the peak position of the LDH sample was shifting from the reference LDH, the LDH sample's three first strongest peaks ($2\theta = 11.33^\circ$, 22.71° and 34.49°) matched this reference database. From the above XRD results, it indicated that the crystalline phase of obtained samples was the layers of magnesium and aluminium hydroxide with the intercalation of carbonate anions in the interlayer area. The diffraction characteristics of the reference database are presented in Table 5.1.

Table 5.1 The XRD characteristics of the $Mg_{0.83}Al_{0.17}(CO_3)_{0.08}(OH)_2(H_2O)_{0.75}$, PDF card number 04-015-1683.

2θ	d (nm)	(I/I _s) x 100 *	h	k	l
11.15	0.79	100	0	0	3
22.41	0.40	44.9	0	0	6
34.42	0.26	23.7	0	0	9
38.66	0.23	25.8	0	1	5
45.65	0.20	28.0	0	1	8
60.01	0.15	7.40	1	1	0
61.25	0.15	9.71	1	1	3

* Remark: I is an intensity of diffraction peak

I_s is an intensity of the strongest diffraction peak

Following the previous literature on the characterisation of LDHs, the distance of one layer to one adjacent interlayer space (d-spacing) at the lowest 2θ the (003) reflection of LDHs can determine anion type intercalated in the interlayer space. The LDH with d-spacing around 0.78 nm is assigned to the intercalation of CO_3^{2-} anions between the layers of metal hydroxides [5, 6]. In the experiment, the d-spacing of samples at the lowest peak position (2θ around 11.6°) was approximate 0.76 nm, as presented in Table 5.2. The expected value of d-spacing was 0.87 nm, which was the characteristic of nitrate intercalation. Nevertheless, the d-spacing values of the synthesised LDHs were almost equivalent to the results in the previous studies. It was the characteristic of the carbonate anions intercalated between the metal hydroxide layers of LDHs. Thus, this implied that there was the intercalation of CO_3^{2-} in the interlayer galleries.

Table 5.2 The peak positions and the d-spacing at the (003) plain of the LDHs prepared in the different pH values.

Sample	2θ ($^\circ$)	d(003) (nm)	Anion
LDH-pH9	11.60	0.76	CO_3^{2-}
LDH-pH10	11.37	0.78	CO_3^{2-}
LDH-pH11	11.60	0.76	CO_3^{2-}
LDH-pH12	11.60	0.76	CO_3^{2-}

Considering the FTIR spectra of LDHs in Figure 5.3, all the spectra presented bands at 3443, 1637, 1382, 836, 671, 550 and 450 cm^{-1} . The broad peak in the region of 3700-3300 cm^{-1} , centred around 3443 cm^{-1} , was attributed to the O-H stretching vibration in the metal hydroxide layers and the interlayer water molecules. The shoulder band at around 3065 cm^{-1} could be assigned to the interaction between the water molecules and the carbonate anions in the interlayer gallery, particular hydrogen bonds. This position can be observed in the samples, especially at the high pH 11 and pH 12. The characteristic of the O-H bending in the water molecules presented at 1637 cm^{-1} . The metal and oxygen interaction (M-O and O-M-O) in the metal hydroxide layers was reflected in the band range of 800 to 450 cm^{-1} [7, 8].

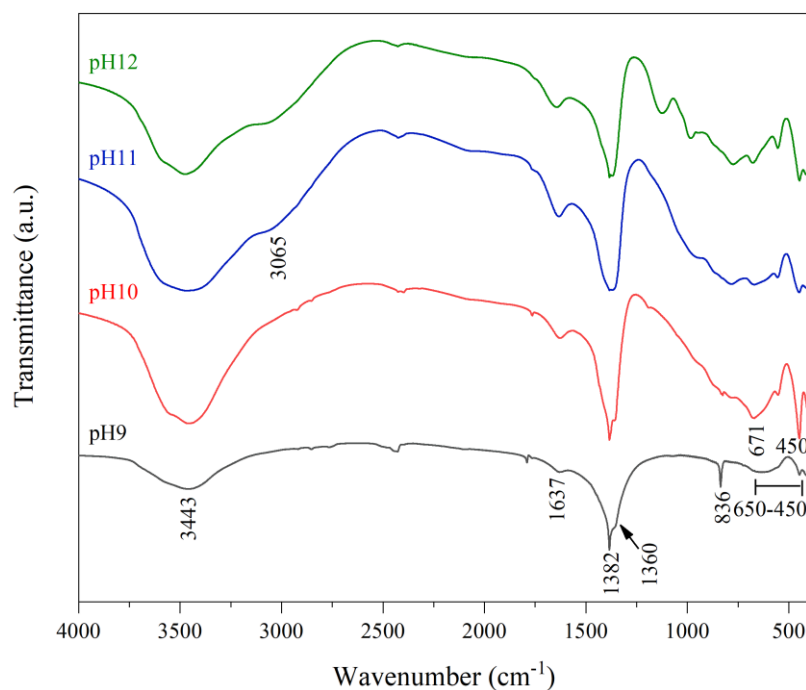


Figure 5.3 The FTIR spectra of inorganic anion intercalated Mg/Al LDHs synthesised at 60°C for 24 h in the different aging pH.

Due to the carbonate intercalated LDHs, the characteristic spectra of samples provided three modes of IR active bands of CO_3^{2-} . The asymmetric stretching mode (ν_3), bending non-planar mode (ν_2) and bending angular mode (ν_4) were displayed at 1382, 836 and 671 cm^{-1} , respectively [9]. The increase in pH values reduced the sharpness of the band at 1382 cm^{-1} . It might occur an increase of carbonate volume in the LDHs at the higher pH.

However, the anion type intercalated in the LDHs differed from the prior research, prepared with the same synthesis procedure and chemical proportions. From the results of the LDH synthesis of Hang et al., the d-spacing of (003) in the XRD pattern was 0.81 nm and the strong transmittance peak at 1383 cm^{-1} in the IR spectrum. This evidence presented the existence of nitrate anions in the interlayer spacing of LDH [10]. Thus, the ambient conditions of LDH synthesis were contamination with carbonates.

Even though there was the flowing of the inert gas in the reaction vessel through the synthesis, it might not be sufficient to exclude CO_2 and CO_3^{2-} from the experimental conditions. The toxic carbonate sources might come from either the distilled water or the NaOH pellets used to prepare LDHs or both. The next section will present and discuss the influence of decarbonation in both sources on the formation of LDHs.

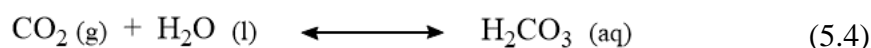
Overall, the preparation of the pristine LDH under the flowing N_2 provided the carbonate in the LDH structure. This experiment followed a previously published procedure that the result obtained from the prior study was the nitrate intercalated LDH [10]. It was noticeable that the result of the experiment was dissimilar to the previous research although there was the resemblance of preparing procedure between both. This state that the carbonate might contaminate within the synthesising conditions. In the prior study, it did not give advice about decarbonation in the process of LDH synthesis. Two possibilities of carbonate sources were the distilled water and the NaOH pellets used for the LDH synthesis.

5.2.2 Effect of Decarbonation on Formation of LDHs

Due to the high affinity of CO_3^{2-} ions, if it exists in the preparing system of LDH, it will disrupt the intercalation of desire anions with the low affinity. Therefore, the exclusion of carbonate from the synthesised system is necessary for the preparation of LDHs. The general method used to eliminate carbonate in the reaction system is to the flow of N_2 gas to the reaction vessel through the synthesis process. [11]

According to the XRD and FTIR consequences in the previous section, the pristine LDHs prepared under the N_2 atmosphere possessed the intercalation of carbonate anions in the interlayer galleries. Theoretically, the CO_3^{2-} should not display in the structure of LDHs. These results indicated that there was contamination of the toxic species in the system of LDH synthesis. The sources of CO_2 and/or CO_3^{2-} might be in the distilled water and the NaOH pellets applied to prepare LDHs.

The first assumption was the existence of CO_2 in the used water. Considering the electronegativities of CO_2 and H_2O , the former is non-polar, whereas the latter is polar. However, the oxygen atoms in CO_2 belong to high electronegativity that produces the small polarity within the CO_2 molecule. In the principal theory of solubility, it is that like dissolves like. The chemicals with a resemblance of chemical characteristics can dissolve in each other. As both CO_2 and H_2O are polar, one can dissolve in the other [12]. The reversible reaction of both molecules is presented in Equation 5.4. The by-product of this reaction is carbonic acid (H_2CO_3) [13].



The eradication of CO_2 dissolved in the distilled water could be carried out by using the vacuum oven. The water was vacuumed under low pressure at room temperature. During the vacuuming process, it could observe the bubbling in water that the bubbles were probably dissolved CO_2 boiling off. This process was conducted continuously until the disappearance of gas bubbles in the vacuumed water. The pH of the water was measured both before and after the vacuuming process. It was found that the pH values elevated slightly from 6.02 for the before vacuum to 6.82 for the after vacuum. This result was likely to reduce the carbonic acid concentration produced from the dissolution of CO_2 in water. Thus, the vacuum of water might be able to take the CO_2 gas out of the water.

After the decarbonation of the distilled water, it was utilized for the synthesis of pristine LDH with aging at pH 9 and 60°C for 24h. The LDH sample was precipitated by using the NaOH solution. With the observation of the XRD pattern in Figure 5.4, the peak positions of the (003) reflections in the sample (red line) presented at 10.04° with the d-spacing of (003) of 0.88 nm. The prior studies reported that the LDHs with the d(003) of 0.88 nm obtained the intercalation of nitrate anions in the interlayer area [14, 15].

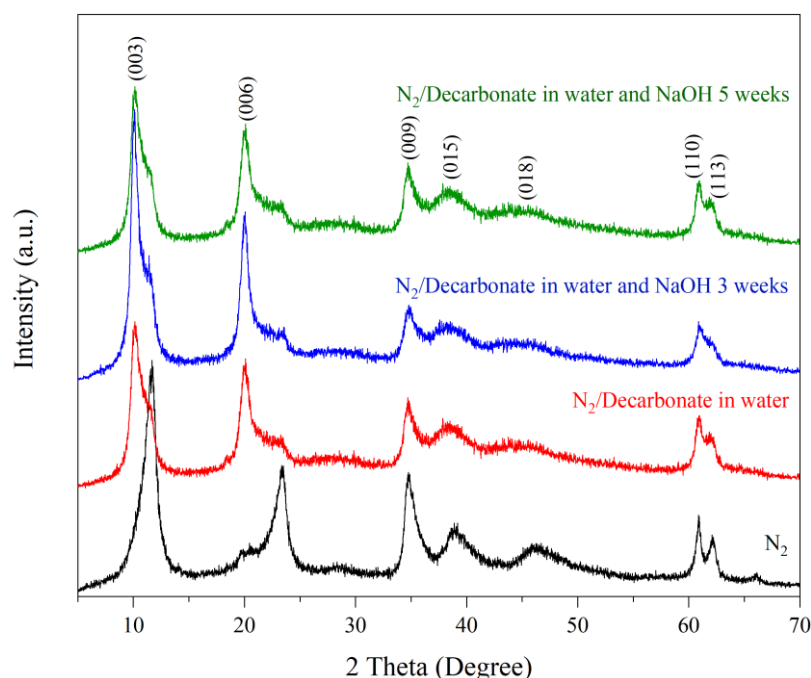


Figure 5.4 The XRD patterns of Mg/Al LDHs prepared at pH 9 and 60°C for 24 h in the different decarbonation process.

Moreover, the identification of the crystalline phase of the sample using N₂ and the decarbonated water confirmed the intercalation of NO₃⁻ species in the LDH structure. The diffraction pattern of the sample was related to the crystalline phase of Mg_{0.73}Al_{0.27}(OH)₂(NO₃)_{0.27}·0.5H₂O (PDF Number: 00-062-0583), as presented in Figure 5.5. The diffraction characteristics of the Mg/Al LDH-NO₃ reference database is provided in Table 5.3. The results indicated that the vacuum of distilled water could exclude the CO₂ in the water, reducing carbonate poisoning in the synthesis process of LDH.

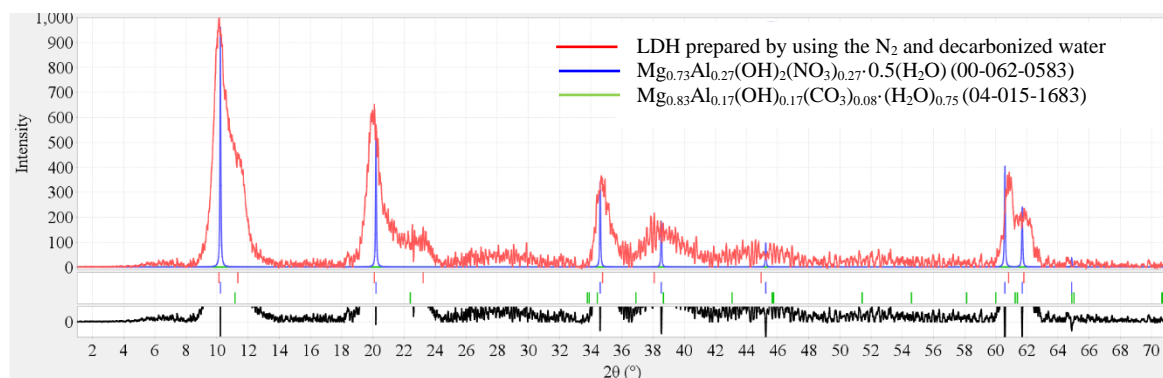


Figure 5.5 The comparison of XRD patterns between the LDH prepared by using the N_2 and the carbonised water and the reference databases.

Table 5.3 The XRD characteristics of $Mg_{0.73}Al_{0.27}(OH)_2(NO_3)_{0.27} \cdot 0.5H_2O$ with the PDF Number: 00-062-0583.

2θ	d (nm)	$(I/I_s) \times 100^*$	h	K	l
10.217	0.8651	100	0	0	3
20.207	0.4391	54	0	0	6
34.605	0.2590	35	0	1	2
38.525	0.2335	19	0	1	5
45.234	0.2003	10	0	1	8
60.590	0.1527	42	1	1	0
61.708	0.1502	25	1	1	3

* Remark: I is an intensity of diffraction peak

I_s is an intensity of the strongest diffraction peak

However, the peaks of (003) and (006) reflections still showed their shoulder peaks that were the same position as the LDH intercalated with the CO_3^{2-} anions (the black line in Figure 5.4). It seemed that a small amount of CO_3^{2-} existed in the LDH preparing system. The NaOH pellets were one of the carbonate source assumptions due to their impurity in containing the Na_2CO_3 .

This study attempted to purify NaOH with the preparation of 50 wt% NaOH and left it for three weeks. Subsequently, the high concentration of 50 wt% NaOH diluted to 1M NaOH in the aqueous solution for use in the LDH preparation. The diffraction pattern of the LDH prepared under N_2 flowing and using the purified water and NaOH

is presented in a blue line of Figure 5.4. It can be seen that there was a similarity of the XRD pattern of LDH synthesised by the use of N_2 and the decarbonised water (the red line in Figure 5.4). This result demonstrated the appearance of CO_3^{2-} anions in the LDH.

From the observation in the 50 wt% NaOH solution after the preparation for three weeks, it could observe the small white particles settle in the bottom of the solution and suspended in the solution. The insoluble particles in the aqueous solution might be particles of Na_2CO_3 produced at the high concentration of NaOH. The contamination of Na_2CO_3 in the LDH synthesis could occur during the transferring of 50 wt% NaOH to prepare the diluted NaOH solution. This process was complicated for the separation of the suspended small particles from the solution. However, when the use of the highly concentrated NaOH solution extended the leaving time to another two weeks, the XRD pattern of the sample displayed the reduction of crystalline peaks corresponding to carbonate interaction (the green line in Figure 5.4). The main intercalating anions in the LDH were nitrate anions.

The results indicated that the vacuuming process was adequate for the removal of CO_2 in the water. The pristine LDHs presented the nitrate anions intercalated the metal hydroxide layers. However, the small amounts of carbonate anions still contaminated between the interlayers. Additionally, the water's degassing in the vacuum oven might damage the vacuum pump because of some vapour water through the pump. Thus, the vacuum of the water may be not suitable for decarbonisation.

This study improved the distilled water decarbonation using the rotary evaporator (rotovap) under the pressure of 300 mbar at $80^\circ C$. With the efficiency comparison between the vacuum oven and the rotovap, the pH of water after using the rotovap for 20 min (pH = 7.15) was slightly higher than that after using the vacuum oven (pH = 6.82). This evidence can be believed that the rotary evaporation was more effective than the vacuum for the removal of carbon dioxide dissolved in the water. It was worth noting that the pH of distilled water after using the rotovap was more than 7 that the pH of pure water is equal to 7. Basically, distilled water is water purified by boiling and condensation. These processes can separate inorganic compounds and non-volatile organic molecules from the water. The pH of water measured from the

experiment was little higher than 7 that might be a calibration error of pH meter. However, the calibration result was acceptable.

Considering the XRD pattern of the pristine LDH prepared by using the water decarbonated by the rotovap and the purified NaOH (the red line of Figure 5.6), the diffraction pattern showed the crystalline planes of (003) and (006) at 10.04° and 20.07° , respectively. This pattern was the crystalline characteristic of nitrate anions intercalated LDH without the intermediate of carbonate anions. Both the shoulder peaks did not present in the XRD pattern with using the rotovap, but they could be observed with using the vacuum oven (the black line of Figure 5.6). This circumstance established that the decarbonation of water using the rotovap was more effective than the vacuum oven.

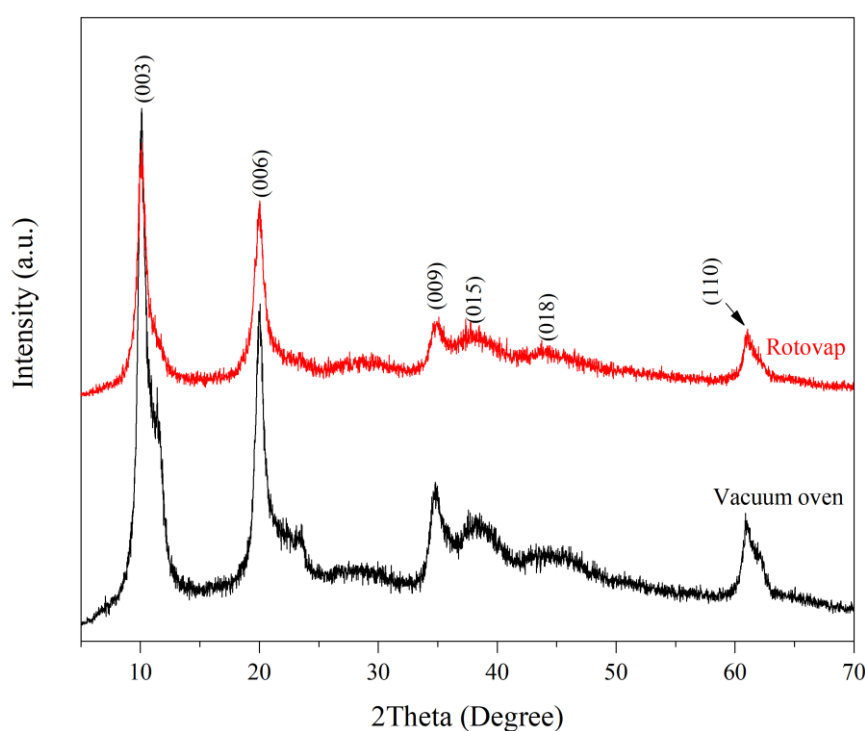


Figure 5.6 The XRD patterns of the unmodified LDHs prepared by using the vacuum oven and the rotovap.

The differences of two decarbonation methods were the temperature and pressure. The water decarbonated with the rotovap was applied the heat under the pressure of 0.3 bar, whereas the decarbonation of water with using the vacuum oven was carried out at the room temperature in the lower atmospheric pressure of 1 bar. In general, the gas

solubility in liquids reduce as high temperature, low pressure or both. Therefore, the amount of CO₂ gas dissolved in the water removed with the rotovap was more than that with the vacuuming process. Besides, the decarbonation of water with the vacuum oven did not apply the heat. As the water heated in the oven would result in the evaporation of water, affecting the damage of vacuum pump. Hence, the suitable method for the decarbonation of water was the use of rotovap with applying the heat and pressure.

Overall, the experimental condition of LDH synthesis should be without the contamination of CO₂ and/or CO₃²⁻ since the carbonate anions providing high affinity can easily combine with the cations of the metal hydroxide layers. In the process of LDH synthesis, the purged N₂ gas, the decarbonated water, and the purified NaOH dramatically reduced the toxicity of carbonate. Thus, all the three operations were carried out in the further experiment to reduce carbonate contamination risk.

5.2.3 Effect of pH on Formation of LDHs Prepared under Decarbonated System

5.2.3.1 Precipitation with the NaOH Solution

The experiment of pH variations was repeated using the decarbonised and distilled water and the purified NaOH in the synthesis process. The diffraction patterns of new LDH samples prepared with the different pH values are shown in Figure 5.7. All the samples presented at the same peak positions in the 2 Theta range of 25-70°, attributing to the metal hydroxide layer structure of LDHs. On the contrary, there was the distinction of reflections between 10° and 25° with the variation of pH correlating with the anion types in the interlayer galleries of LDHs. These results implied that the pH had no effect on the layer structure formation but affected the types of anions intercalated in the metal hydroxide lamellae.

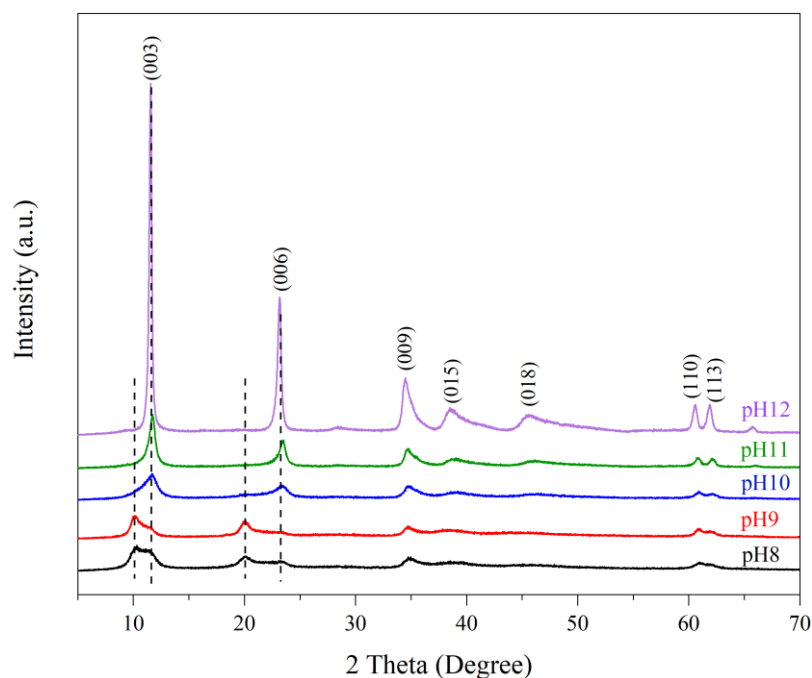


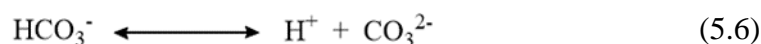
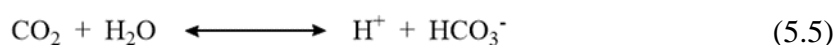
Figure 5.7 The XRD patterns of inorganic anion intercalated Mg/Al LDHs in the different pH precipitated using the NaOH solution.

Observing Figure 5.7, it can be seen that there were similar to the XRD patterns of LDHs prepared at pH 8-9 and pH 10-12. The samples prepared at pH 8 and 9 provided the (003) and (006) reflection at 10.04° and 20.50° , respectively. The diffractions were the characteristics of the LDHs intercalated with the nitrate groups in the interlayers [14, 15]. However, the peak intensity of pH 9 was higher than that of pH 8, presenting the increase of LDH crystallinity. For the higher pH, the (003) and (006) reflections of LDHs synthesised at pH 10, 11 and 12 displayed approximate 11.60° and 23.18° , respectively. The results insisted on the intercalation of carbonate in the LDHs prepared under the high pH values [14, 15]. Table 5.4. reports the peak positions and the d-spacing of (003) and (006) reflection in each sample prepared with the various pH. From the results, it was found that the nitrate forms were substituted for the carbonate forms with the increase of pH.

Table 5.4 The 2θ positions and the d-spacing of LDH samples prepared under the decarbonated processes and the varied pH with the NaOH solution.

Sample	2θ (003) ($^\circ$)	d (003) (nm)	2θ (006) ($^\circ$)	d (006) (nm)	Anion
pH8	10.20	0.87	20.07	0.44	NO_3^-
pH9	10.04	0.88	20.50	0.43	NO_3^-
pH10	11.68	0.76	23.42	0.38	CO_3^{2-}
pH11	11.76	0.75	23.45	0.38	CO_3^{2-}
pH12	11.60	0.76	23.18	0.38	CO_3^{2-}

These consequences were in agreement with the study of Li et al. [16], described in Chapter 3. The previous research reported that the crystalline phase's transformation from the NO_3^- to the CO_3^{2-} took place with the preparation of LDHs under the higher pH conditions (pH 8-13). According to the equilibrium reactions of CO_2 in water in Equation 5.4, it transferred to the H_2CO_3 , which was the acid form. The H_2CO_3 decomposed to the ions of H^+ and HCO_3^- (Equation 5.5), and the HCO_3^- decomposed to the ions of H^+ and CO_3^{2-} (Equation 5.6). The acid ionisation constants of both equations show in Equation 5.7 and 5.8, respectively. From the Equation 5.8, the $[\text{H}^+]$ is $\frac{[\text{HCO}_3^-]}{[\text{CO}_3^{2-}]} \times 10^{-10.329}$. In theory, the pH value of a solution is determined by Equation 5.9.



$$K_{a1} = \frac{[\text{HCO}_3^-] \cdot [\text{H}^+]}{[\text{H}_2\text{CO}_3]} = 10^{-6.352} \text{ mol/L} \quad (5.7)$$

$$K_{a2} = \frac{[\text{CO}_3^{2-}] \cdot [\text{H}^+]}{[\text{HCO}_3^-]} = 10^{-10.329} \text{ mol/L} \quad (5.8)$$

$$\text{pH} = -\log [\text{H}^+] \quad (5.9)$$

The replacement of $[\text{H}^+]$ in the above equation was provided in Equation 5.10 and 5.11.

$$\text{pH} = -\log\left(\frac{[\text{HCO}_3^-]}{[\text{CO}_3^{2-}]}\right) \times 10^{-10.329} \quad (5.10)$$

$$\text{pH} = -\log[\text{HCO}_3^-] + \log[\text{CO}_3^{2-}] + 10.329 \quad (5.11)$$

Considering Equation 5.11, it can be seen that the pH value is a direct variation with the concentration of CO_3^{2-} . This cause resulted in a large amount of carbonate in the aqueous solution at the high pH. Therefore, the preparation of LDHs under the high pH (>9) attributed to the carbonate forms in the LDHs. Furthermore, the peak intensity of diffraction increased considerably with the increase of pH, demonstrating the increase of LDH crystallinity, especially at pH 12. This study supported the previous researches [17, 18].

For the crystalline phase of LDH intercalated with the nitrate, it matched with a phase of $\text{Mg}_{0.73}\text{Al}_{0.27}(\text{OH})_2(\text{NO}_3)_{0.27} \cdot 0.5\text{H}_2\text{O}$ (PDF card number: 00-062-0583). The empirical formulae of synthesised LDH differed from the other studies, as shown in Table 5.5. The causes of difference might occur the proportion of chemicals, the arrangement of atoms and the maintained conditions of, e.g., pH, temperature and time.

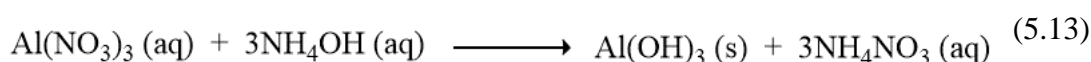
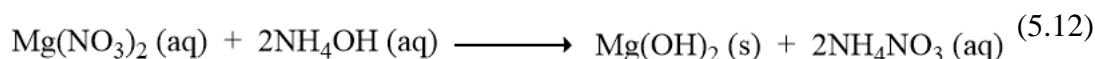
Table 5.5 The comparison of Mg/Al LDH chemical formulae synthesised in this work with the previous studies.

Chemical formula	PDF number	Reference
$\text{Mg}_{0.73}\text{Al}_{0.27}(\text{OH})_2(\text{NO}_3)_{0.27} \cdot 0.5\text{H}_2\text{O}$	00-062-0583	This study
$\text{Mg}_{0.66}\text{Al}_{0.33}(\text{OH})_2(\text{NO}_3)_{0.33} \cdot n\text{H}_2\text{O}$	N/A	[19]
$\text{Mg}_{0.68}\text{Al}_{0.32}(\text{OH})_2(\text{NO}_3)_{0.32} \cdot 1.2\text{H}_2\text{O}$	N/A	[20]

From the above results, the pH contributing to the formation of carbonate was not selected for the synthesis of LDHs. If the system of LDH preparation contaminates carbon dioxide or carbonate, it will obstruct the intercalation of desired anion with the lower affinity than the carbonate. Thus, the pH 9 adjusted with the NaOH solution was the most suitable for the LDH synthesis since it could induce the nitrate forms and the high crystallinity.

5.2.3.2 Precipitation with the NH₄OH Solution

The optional precipitating agent used for the preparation of LDHs by the co-precipitation was the NH₄OH solution. The chemical reactions between the metal nitrate salts and the NH₄OH were displayed in Equation 5.12 and 5.13. The products generated from the reactions were the hydroxide forms of metals. Afterwards, these metal hydroxides would form the structural layers. The mechanism of LDH formation was similar to the preparation with the NaOH solution.



During the reaction, the pH of the mixture solution was maintained at 7, 8, 9 and 10 by adding the NH₄OH solution. The X-ray diffractions of these samples are presented in Figure 5.8. All the patterns showed the characteristic peaks of layered magnesium and aluminium hydroxide with the intercalation of nitrate species between the layers due to the presence of lowest peak position at 2θ of 10.02. Additionally, the sharpness of diffraction peaks increased with the rise of pH, particularly at pH 10; these results related to the other works [14, 15].

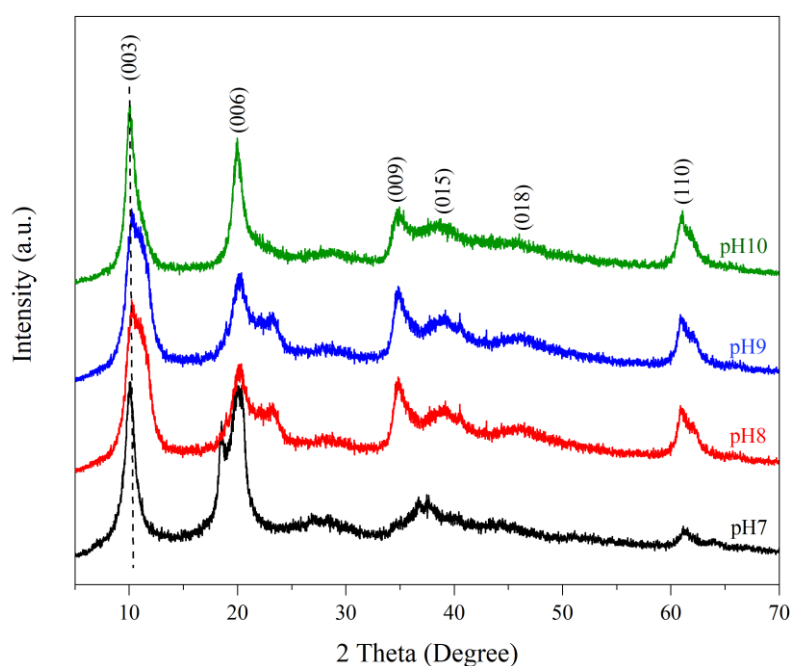


Figure 5.8 The XRD patterns of pristine Mg/Al LDHs in the different pH precipitated using the NH₄OH solution.

Nevertheless, the sample at pH 7 included the nitrate intercalated LDH phase and the crystalline phase of aluminium hydroxide ($\text{Al}(\text{OH})_3$), correlated to the reference database with the PDF number 00-038-0376. Figure 5.9 exhibits the comparison of the sample's diffraction patterns at pH 7 with that of the reference databases. This study indicated that the pH 7 maintained by adding NH_4OH solution was not proper for forming a single LDH crystal.

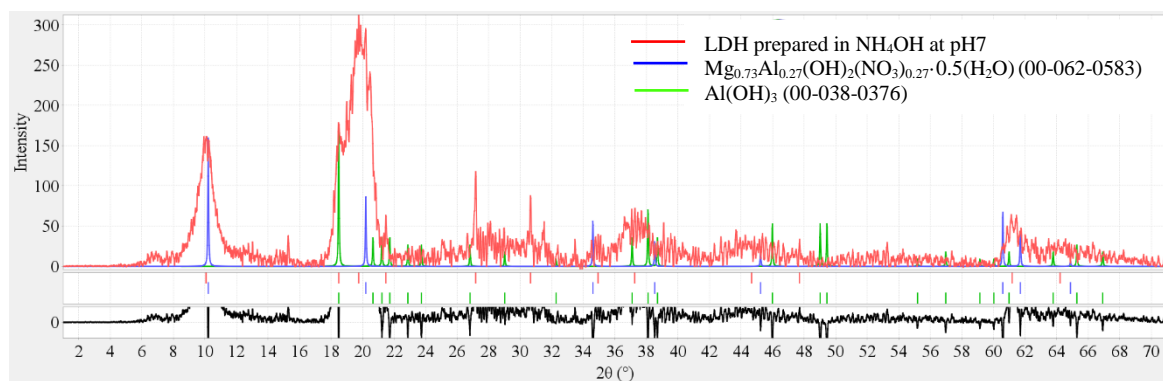


Figure 5.9 The comparison of XRD patterns of the sample prepared in the NH_4OH at pH 7 and the reference databases.

By the comparison of the LDHs prepared with the different precipitating agents, the use of NaOH solution could induce the partial carbonate forms, while the use of NH_4OH solution provided the intercalation of nitrate. These results were consistent with Olanrewaju et al. [15], who reported using NH_4OH solution to prepare the anionic intercalated LDHs. The NH_4OH solution induced the nitrate forms in the LDHs under the conditions without the decarbonation in the used water. The strong base may affect the dissolution of CO_2 in the base solution. It was well known that NaOH is a strong base, whereas NH_4OH is a weak base. Thus, NaOH can be more active in interaction with CO_2 than NH_4OH [21]. This reason might cause the existence of CO_2 in the NaOH solution.

To sum up, the results of this study confirmed that the pH influenced the LDH formation. Using the NaOH solution as the precipitating agent, the preparation of LDHs under the $\text{pH} \leq 9$ provided the nitrated forms intercalated in the interlayer galleries, whereas that under the $\text{pH} > 9$ generated the replacement of nitrate forms with the carbonate forms. On the contrary, the intercalated nitrate anions were in the

LDH with using the precipitating agent of NH_4OH solution. The synthesis of LDH at pH 10 under the NH_4OH condition provided the highest phase crystallinity. Therefore, the optimum pH for the LDH preparation was at pH 9 for NaOH solution and pH 10 for applying the NH_4OH solution.

5.2.4 Effect of Aging time on Formation of LDHs

5.2.4.1 Precipitation with NaOH Solution

In the LDH preparation process using the NaOH, the mixture solution containing the metal salts and the alkaline solution was aged under pH 9 at 60°C . This work carried out the determination of optimum aging time for the LDH synthesis. The aging time was varied at 5, 10, 15 and 24 h. The X-ray diffraction patterns of samples with the variation of treatment times were shown in Figure 5.10. It was found that the longer aging time resulted in the increase of peak sharpness and intensity. The aging for 24 h provided the highest sharpness and intensity of peaks. However, there was not a difference of crystalline peak positions with the variation of aging times. The (003) reflections of all samples exhibited at the 2θ of 10° with the d-spacing of 0.87 nm. These results were the characteristics of the nitrate forms in the LDHs. It was the positive consequence for the preparation of LDHs with the majority intercalation of nitrate anions in the interlayers.

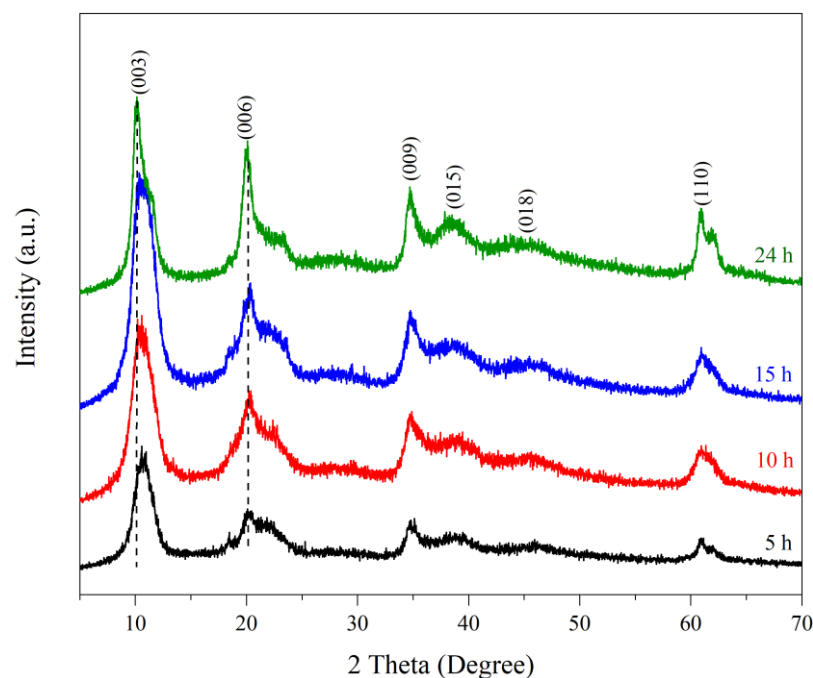


Figure 5.10 The XRD patterns of MgAl LDHs with the variation of aging times under the NaOH solution at pH 9 and 60°C.

Regarding the lattice constants of LDH crystals, the a and c parameters can be calculated by using the d -spacing of (110) and (003), respectively. The literature pointed out the correlation between the d -spacing and lattice parameter, as presented in Equation 5.14 and 5.15. The lattice parameter of a represents the distance between two metal ions in the layers, which is equal to $2d(110)$. In the case of the lattice parameter of c , it can refer to the distance in the c direction of crystals. The c parameter depends on the thickness of metal hydroxide layers, the size and orientation of interlayer anions, and the water contents. The c value is equivalent to the $d(003)$ multiplied by the ordering number (n) of hydroxide layers [6].

$$a = 2 d(110) \quad (5.14)$$

$$c = n d(003) \quad (5.15)$$

With considering the calculated lattice parameters of a (black line) and c (red line) in Figure 5.11, it was noticeable that the lattice parameters of a were level off at 0.3 nm with a difference in the ranges of thermal treatment times 5 to 24 h. In the meantime, the value of c rose gradually by 0.12 nm for 24 h from 2.50 nm for 5 h. These results

indicated that the increase of aging time was not significant to the crystal growth in the ab plain in the unit cell, but had the influence of the layer stacking of crystals along the c-axis. For the results of crystal size (blue line), there was an increasing tendency for the crystal size with the increase of aging time. The longer aging time obtained an opportunity to grow of crystals.

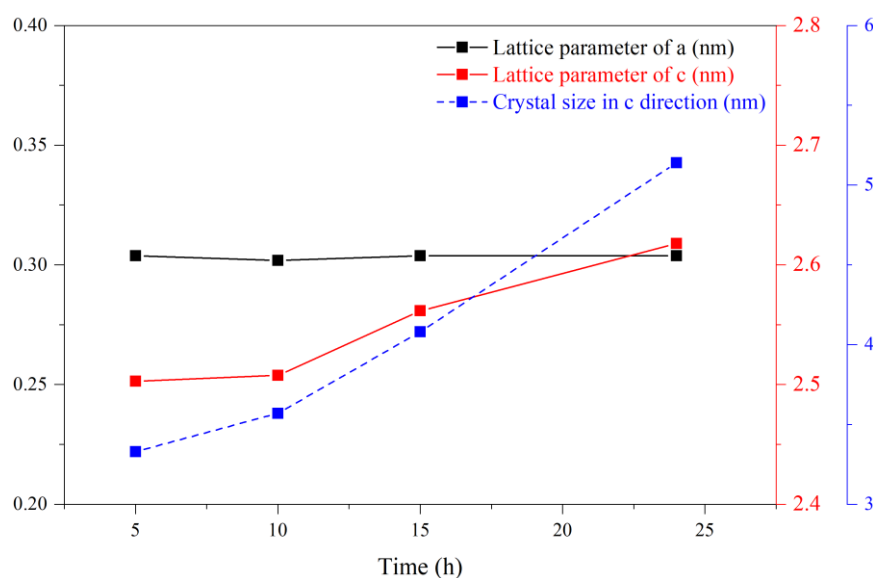


Figure 5.11 The lattice parameters of c and a of LDH samples with the variation of aging times under the NaOH solution at pH 9 and 60°C.

In addition, the lattice parameter, the pH influenced on the crystal size (D) of LDHs. The crystal size could be determined by using Equation 5.16, where K is a constant (0.89), λ is the X-ray source wavelength, β is the full width at half maximum intensity of the peak (FWHM) θ is the Bragg's angle.

$$D = \frac{K\lambda}{\beta \cos\theta} \quad (5.16)$$

The plotted crystal sizes of LDHs in the c direction with the different aging times were displayed in the blue line of Figure 5.11. The crystal size reduced slightly with increasing the time from 5 h to 15 h. And then, it increased remarkably to 5.14 nm. These results were presented in the blue line of Figure 5.10. The results of the calculated crystal size related to the growth of crystals in the c direction. The aging of mixture solution for 24 h provided the highest crystal growth. Hence, the aging of the

mixture solution at 60°C for 24 h under pH 9 was the appropriate condition for the synthesis of Mg/Al LDHs.

Nevertheless, the variation of aging time for the LDH preparation maintained at pH10 and 60°C, there was a change of the X-ray diffraction between the degree range of 10° to 25°, observed in Figure 5.12. For the aging for 5 h, the d-spacing of (003) reflection was 0.85 nm, represented to the nitrate forms in the LDH. When the time equaled to 10 h, the crystalline peak of (003) exhibited at 10.39° and its shoulder peak at 11.20°. The former and the latter represented the existence of NO_3^- and CO_3^{2-} , respectively. These results indicated that both anions formed in the intermediate layers of LDH prepared at pH 10 and 60°C for 10 h. Subsequently, the CO_3^{2-} species involved in the LDH structure with the aging for 15 and 24 h. The replacement of nitrate with carbonate may cause the high solubility of CO_2 in the aqueous solution at pH10, as explained in the previous section. The increase of aging time could induce the formation of carbonate in the interlayer regions at pH10.

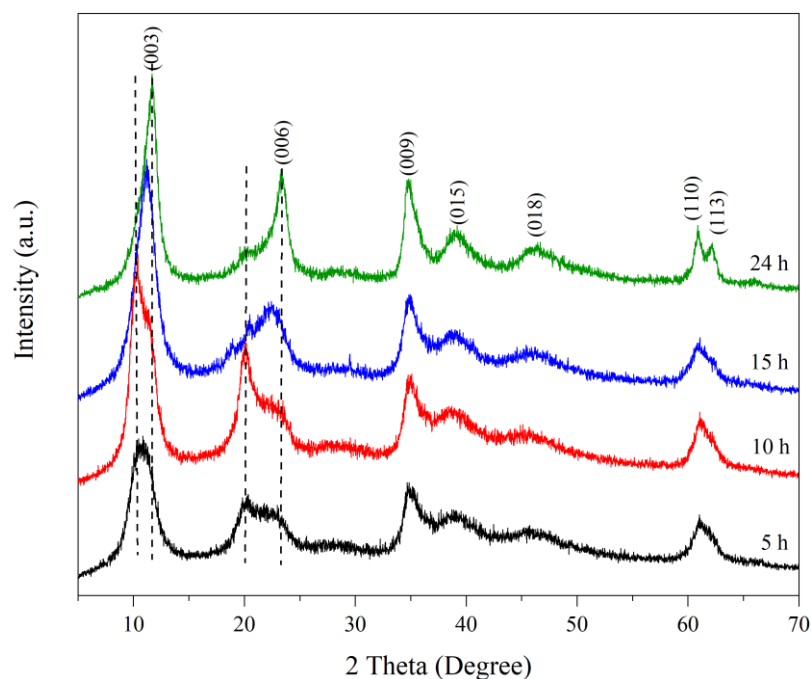


Figure 5.12 The XRD patterns of Mg/Al LDHs prepared at pH 10 and 60°C with the variation of aging times.

5.2.4.2 Precipitation with NH_4OH Solution

In the case of the NH_4OH solution employed as the precipitating agent for the LDH synthesis, all the samples prepared with the different aging times possessed the crystalline phase of the metal hydroxide layer with the intercalation of nitrate anions in the intermediate layers. The results can be observed from the X-ray diffraction patterns in Figure 5.13. The intensity and the sharpness of the peaks of X-ray diffraction increased with the increase of aging times. The reason may result from the growth of LDH crystals along the c -axis during the mixture solution's aging.

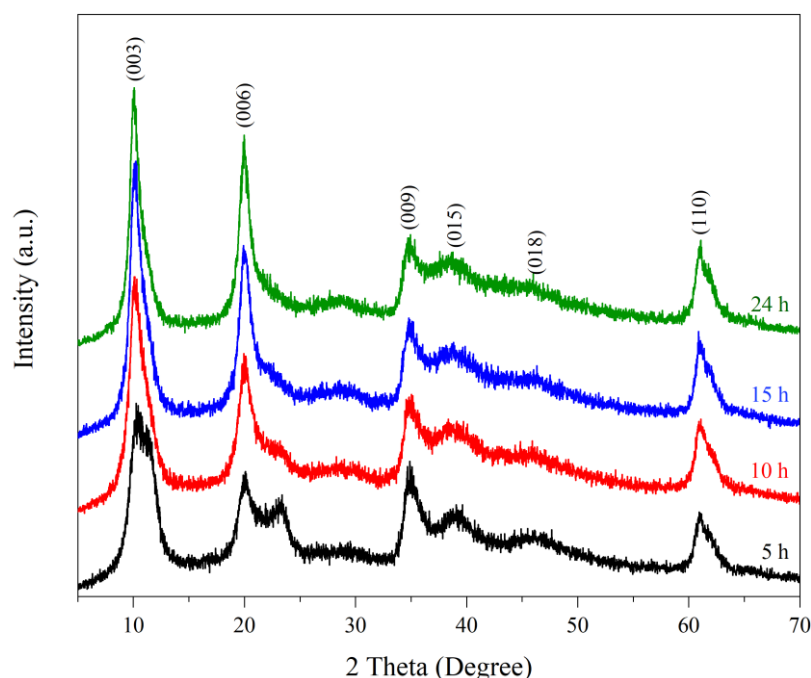


Figure 5.13 The XRD patterns of Mg/Al LDHs in the various aging time and the use of NH_4OH solution under the controlled conditions at pH10 and 60°C .

The calculated lattice parameters supported this assumption, as exhibited in Figure 5.14. The a lattice constants remained steadily at 0.30 nm; however, the c lattice constants fluctuated slightly in the range of 2.58 to 2.63 nm with increasing the treatment times. As considered the crystal size in the c direction, the crystal sizes of LDHs prepared using the NH_4OH showed an upward trend. The crystal sizes at 5, 10, 15 and 14 h were 3.20, 4.56, 6.09 and 7.43 nm, respectively. The crystal growth of LDHs by using NH_4OH had the same trend as that of NaOH . The preparation of LDH under the NH_4OH at 60°C for 24 h induced the highest crystallinity and crystal growth.

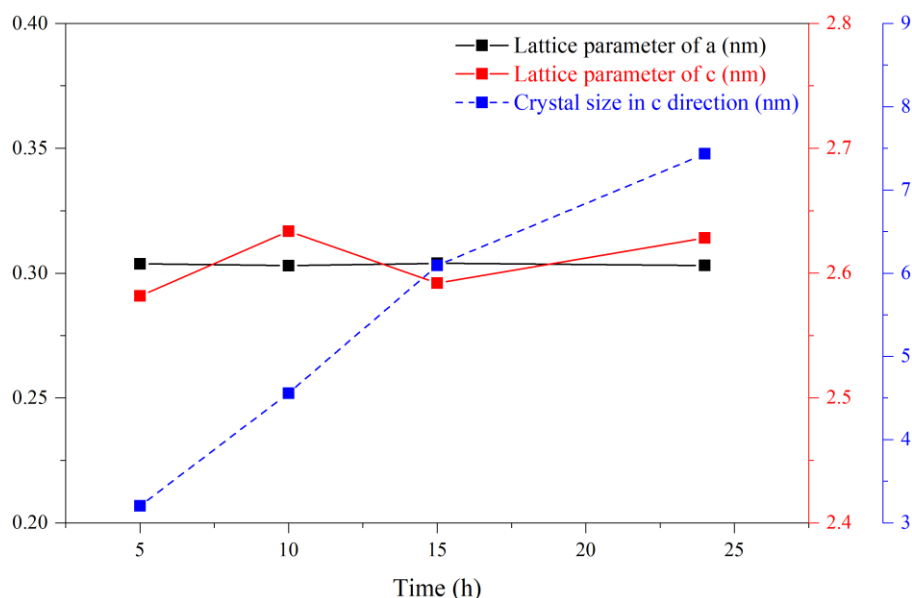


Figure 5.14 The lattice parameters of c and a of Mg/Al LDHs prepared in the different aging times using NH_4OH solution.

Overall, there was the growth of LDH crystals along the c-axis with the increase of treatment times. All the LDHs prepared using both the NaOH and NH_4OH solutions provided the nitrate forms with the time variation. The optimum aging time for LDH synthesis was 24 h because it induced the nitrate within the LDH structure and provided the highest crystallinity and crystal size.

5.3 Preliminary Experiment on LDH Modification with Organic Anions

According to the Section 3.5.2.2 in the Chapter 3, the LDHs interacted with the various organic anions had high performance flame retardants for polymers. As the combustion of the organic-intercalated LDHs contributed to the dehydroxylation of LDHs and the decomposition of intercalated organic compounds, it produced the water, metal oxide, non-flammable gases and char residues, All the obtained products could restrict the distribution of heat, flame and combustible gases through the combustion area. Furthermore, the Section 2.4.2 in the Chapter 2 stated that the organophosphate ester-based compounds were high performance of fire retardancy by accelerating the char formation.

To enhance the fire retarding ability of LDHs, this work attempted to modify LDH structure by using organophosphate ester-based compounds as the anionic modifying agents. They would be intercalated in the intermediate lamellar structure. There were four types of modifying agents used in this study. The two kinds of phosphate ester anions that had been used for the modification of LDHs were the bis(2-ethyl hexyl) phosphate (BEHP) and the phytate (Phy). Meanwhile, the β -glycerophosphate (GP) and the diphenyl phosphate (DPP) were the novel compounds used as intercalating agents for the LDHs and utilised for flame retardant applications. The properties of the modified LDHs would be analysed and discussed in the later section.

Before modifying with the desiring organophosphate-based compounds, the experimental setting and the procedure would be validated by following the process studied in the previous works. One of the typical anionic surfactants used widely for the functionalisation of LDHs was the dodecyl sulfate (DS). Therefore, the DS was selected as the organo-modifying agent for the preliminary experiment.

5.3.1 Co-precipitation Method

As above mentioned, the preliminary synthesis of organoanion-intercalated LDHs was the preparation of LDH intercalated with the DS (LDH-DS). The preparing methods of LDH intercalated with DS have been reported in numerous published researches [22-25]. Most modified LDHs were prepared by the co-precipitation method. In this work, the modifying procedure of LDH with DS was followed by the previous studies. The X-ray diffraction patterns and the IR spectra of the obtained LDH-DS were compared with the pristine LDH.

Figure 5.15 shows the diffraction patterns of the pristine LDH and the LDHs-DS. The pristine LDH (the black line) presented the lowest angle of the crystal peak presented at 10.04° with the basal spacing of 0.88 nm. This was the characteristic of nitrate intercalation between the layers. For the XRD pattern of LDH-DS prepared without the decarbonation in water and NaOH solution (the red line), the lowest peak shifted to lower degree at 6.97° with the d-spacing of 1.27 nm. It was noticed that the distance between the metal hydroxide layers of LDH-DS was wider than the pristine LDH. This consequence insisted on the intercalation of DS molecules in the interlayer

galleries, although it was prepared under the carbonate contamination in both water and NaOH. The XRD patterns of LDH-DS synthesised in this work was a significant resemblance to the study of Kaul et al. [22]. The crystalline pattern of Mg/Al LDH-DS reported in the literature is exhibited in Figure 5.16.

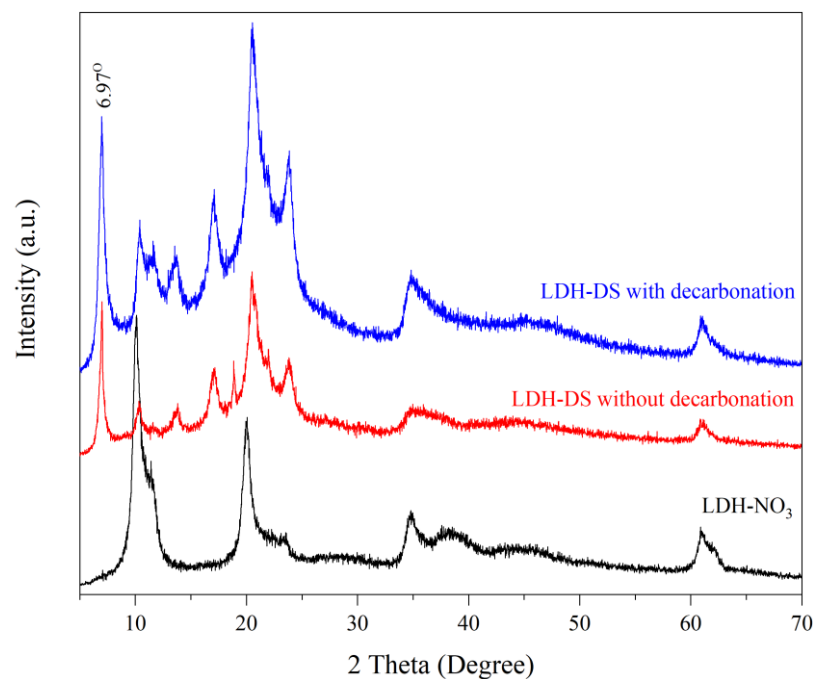


Figure 5.15 The XRD patterns LDH-NO₃ and LDH-DS prepared using without and with the decarbonation and precipitated by NaOH.

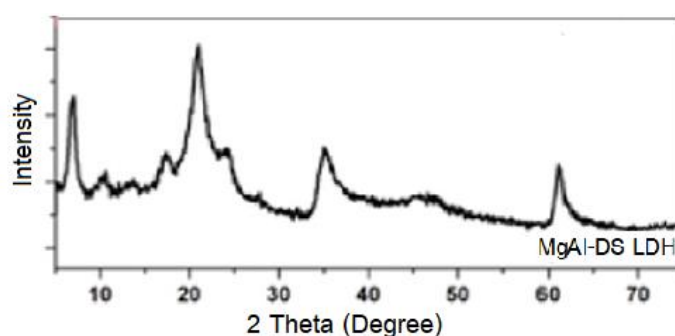


Figure 5.16 The characteristic XRD pattern of MgAl LDH intercalated with DS in the study of Kaul et al. [22].

In the theory, the modification of LDHs with desired anions requires the conditions without the CO_3^{2-} contamination in the process of synthesis to avoid carbonate formation in the LDHs. However, it was worth noting that the DS anions could intercalate between the cationic metal hydroxide lamellae, prepared under the CO_3^{2-}

contamination. That means the affinity of DS anion might be stronger than the CO_3^{2-} anion.

When the LDH-DS synthesis was reprocessed using the decarbonated water and NaOH, the sample's diffraction pattern was similar to the preparation without the decarbonation. The blue line in Figure 5.15 shows the XRD pattern of LDH-DS prepared under the decarbonation conditions. The synthesis with the decarbonation contributed to higher peak intensities. Thus, the decarbonation process is significantly essential to the synthesis of LDHs.

In addition to the use of NaOH solution for the LDH-DS synthesis, the NH_4OH solution was used as the precipitating agent. Figure 5.17 compares the XRD patterns of LDH-DS prepared in the different precipitating agents. The pattern of LDH-DS precipitated in the NH_4OH (blue line) was similar to that in the NaOH (red line). It indicated that the NH_4OH solution could be also used for the synthesis of LDH-DS.

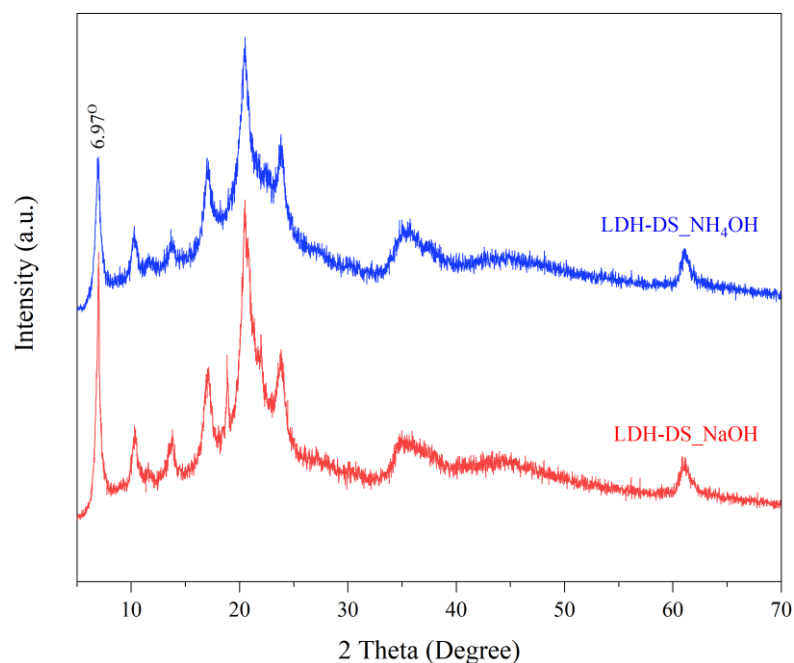


Figure 5.17 The XRD patterns of Mg/Al-DS prepared in the different precipitating agents: NaOH (red line) and NH_4OH (blue line)

The LDH-DS structures prepared by both the NaOH and the NH_4OH were evaluated using the FTIR spectra, as presented in Figure 5.18. The former spectrum (red line) was comparable to that of the latter (blue line). The broad band at around 3526 cm^{-1}

can be assigned to the stretching vibration of hydroxyl groups in the layered magnesium aluminium hydroxides and the intercalated water molecules in the LDH. The bending vibration of water molecules contributed to the band at 1637 cm^{-1} . The bands between 450 and 650 cm^{-1} can be attributed to the vibration of metal-oxygen, e.g. M-O and O-M-O. All bands can also be observed in the LDH- NO_3 (black line).

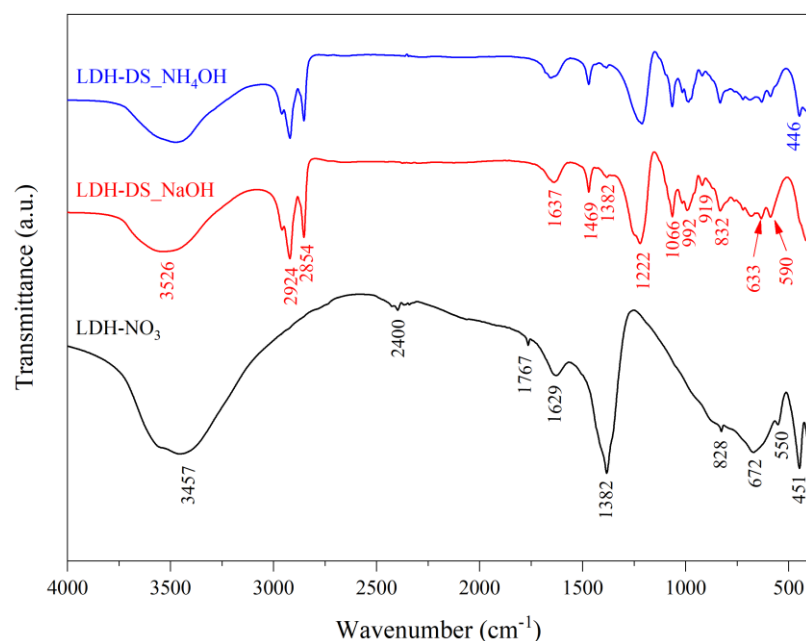


Figure 5.18 The FTIR spectra of MgAl LDHs intercalated with the DS and prepared in the base solutions of NaOH and NH_4OH .

Due to the involving of DS in the LDH, there were the presences of C-H stretching vibration at 2924 and 2854 cm^{-1} and C-H bending vibration at 1469 cm^{-1} . Additionally, the vibrations of S=O showed at 1222 cm^{-1} for the asymmetric mode and at 1066 cm^{-1} for the symmetric mode. It was noticeable that the IR intensity of the band at 1382 cm^{-1} reduced significantly with the incorporation of DS in the LDHs [22]. This band was the characteristic of existing NO_3^- in the structure. These results proved the replacement of nitrate anions with the DS anions in the lamellae's intermediate area.

From the above results, there has been a successful synthesis of LDH-DS by the co-precipitation method. The experimental results corresponded to the prior study. Hence, the procedure of LDH modification with the organic anion was the accuracy.

5.3.2 Rehydration Method

Another method used for the modification of LDH was the rehydration of the calcined LDH. The unmodified LDH were heated at a high temperature. This process was called the calcination. Subsequently, the calcined LDH were treated in the aqueous solution containing the desired anions to rehydrate the structure. This process was called the rehydration. The details in each process would be discussed below this.

5.3.2.1 Calcination Process

When the Pural[®] MG70, the commercial LDH-CO₃, was calcined at 500°C for 5 h, the mass loss percentage was calculated using the sample mass before and after calcination. The whole data were shown in Table 5.6. It was found that there was a decrease in mass around 39.55 % after the heat treatment.

Table 5.6 The mass of Pural[®] MG70 before and after the calcination and their mass loss percentage.

Information	Number of measurements		
	1	2	3
Mass before calcination (M ₀) (g)	15.0512	15.1192	15.1255
Mass after calcination (M ₁) (g)	9.1153	9.1281	9.1404
Mass loss (%)	39.44	39.63	39.57
Average mass loss (%)	39.55		

The study of thermal decomposition of LDHs in the prior research [26] reported that the water molecules adsorbed on the surface and intercalated in the interlayers liberated at the below temperature 200°C. The magnesium and aluminium hydroxides in the layers were dehydrated, and the carbonate anions intercalated the interlamellar were decomposed in the temperature between 200°C and 400°C. As a consequence of these decompositions promoted the formation of Mg_{1-x}Al_xO(OH)_x phases and CO₂. At 400-600°C, the dehydration of magnesium and aluminium hydroxides still maintained and generated the phase of Mg_{1-x}Al_xO_{1+x/2}. Hence, both the dehydration

and the decomposition were the possible reasons for the mass loss in the calcination process.

The identification of the LDH crystalline phases both before and after the heat treatment was analysed using the characteristics of X-ray diffraction. Figure 5.19 displays the XRD pattern of Pural[®] MG70 with the matching of the reference database. The crystalline phase of MG70 correlated to the phase of hydrotalcite ($\text{Mg}_{0.64}\text{Al}_{0.36}(\text{CO}_3)_{0.18}(\text{OH})_2(\text{H}_2\text{O})_{0.46}$) with the PDF number of 04-015-1684. When the MG70 was heated at 500°C for 5 h, the crystalline phase became the magnesium oxide (MgO) due to the dehydration of Mg-Al hydroxides. The XRD pattern matched the crystalline phase of MgO reference data with the number 00-004-0829, presented in Figure 5.19. The Al^{3+} ions can dissolve in the lattice of MgO. This result was related to the previous study [26, 27].

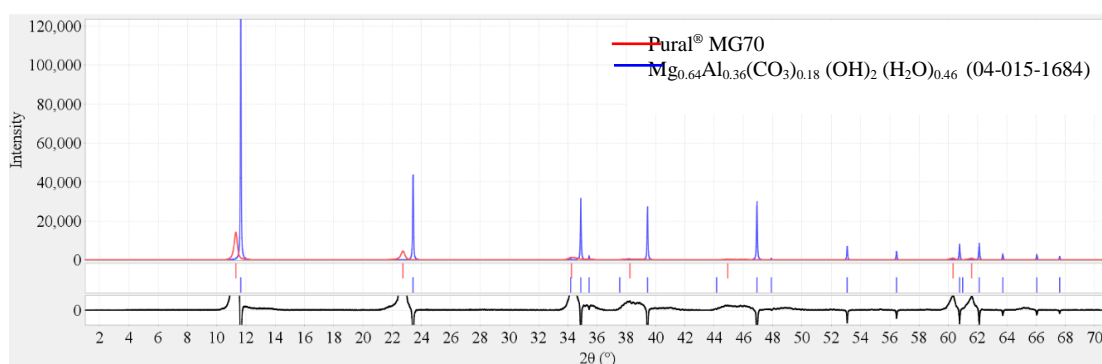


Figure 5.19 The XRD patterns of Pural[®] MG70 and reference database with PDF number 04-015-1684.

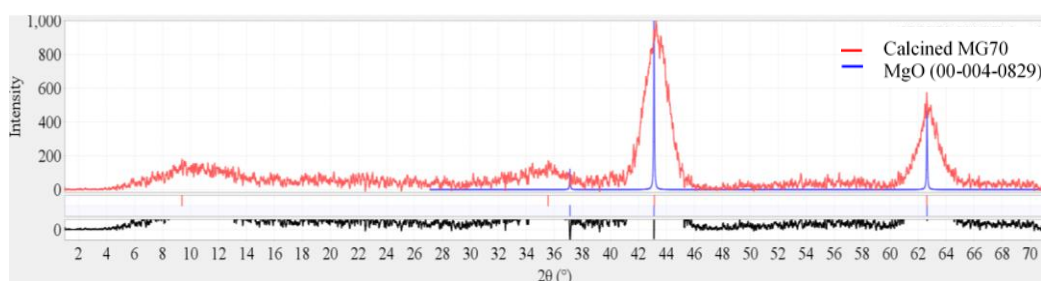


Figure 5.20 The XRD patterns of Pural[®] MG70 calcined at 500°C for 5 h and reference database with PDF number 00-004-0829.

When the calcined LDH was soaked in the aqueous solution of DS for 24h, the metal hydroxide layers were reformed by the adsorption of water. The DS anions

and water were also incorporated into the interlayer spaces. Comparing the XRD pattern of LDH-DS synthesised in the different methods presenting in Figure 5.21. There was a similarity of the XRD pattern of LDH-DS prepared with the co-precipitation (the black line) and the rehydration (the red line). This was a confirmation of DS in the interlayer regions. However, the peak intensity of rehydration was much lower than that of co-precipitation. Thus, the preparation of LDH-DS with the co-precipitation method was more suitable than that with the rehydration.

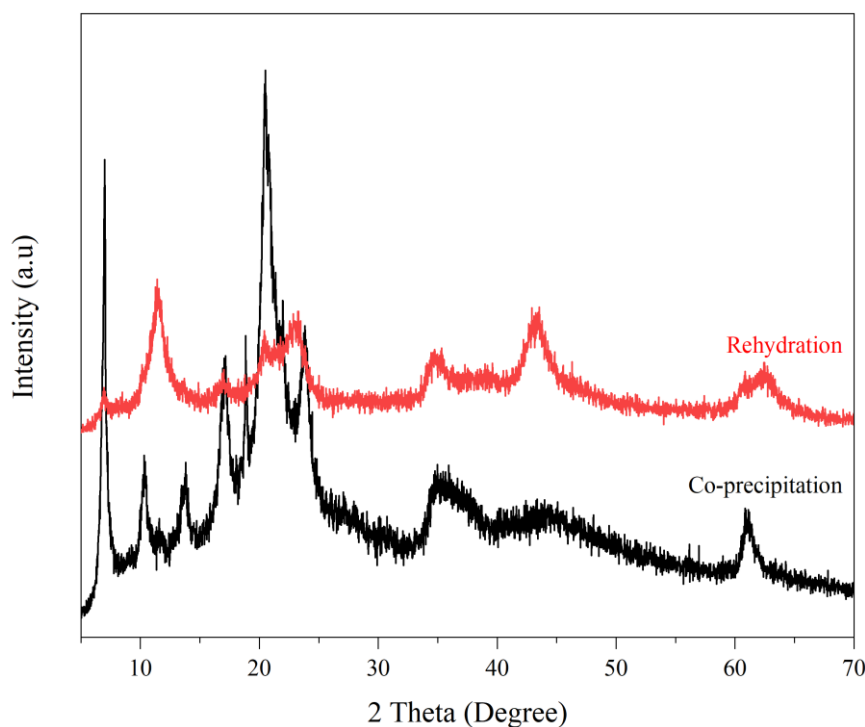


Figure 5.21 The XRD patterns of LDH-DS prepared by the co-precipitation and the rehydration.

Overall, the experiment had achieved success in the LDH-DS synthesis. The co-precipitation method was more appropriate than the rehydration method. Also, the results indicated that the experimental setting and the procedure for the LDH modification validated.

5.4 Characterisation of Organophosphate Ester-Based Compounds Used as Anionic Modifying Agents for LDHs

As described in the Chapter 1, the objective of this research was the modification of the LDH with various anions of organophosphate ester-based compounds. The four types of organic compounds containing the phosphate ester groups selected as modifying agents for LDH were bis(2-ethylhexyl) phosphate (BEHP), phytic acid (Phy), glycerophosphate (GP) and diphenyl phosphate (DPP). Their chemical structures are exhibited in Figure 5.22.

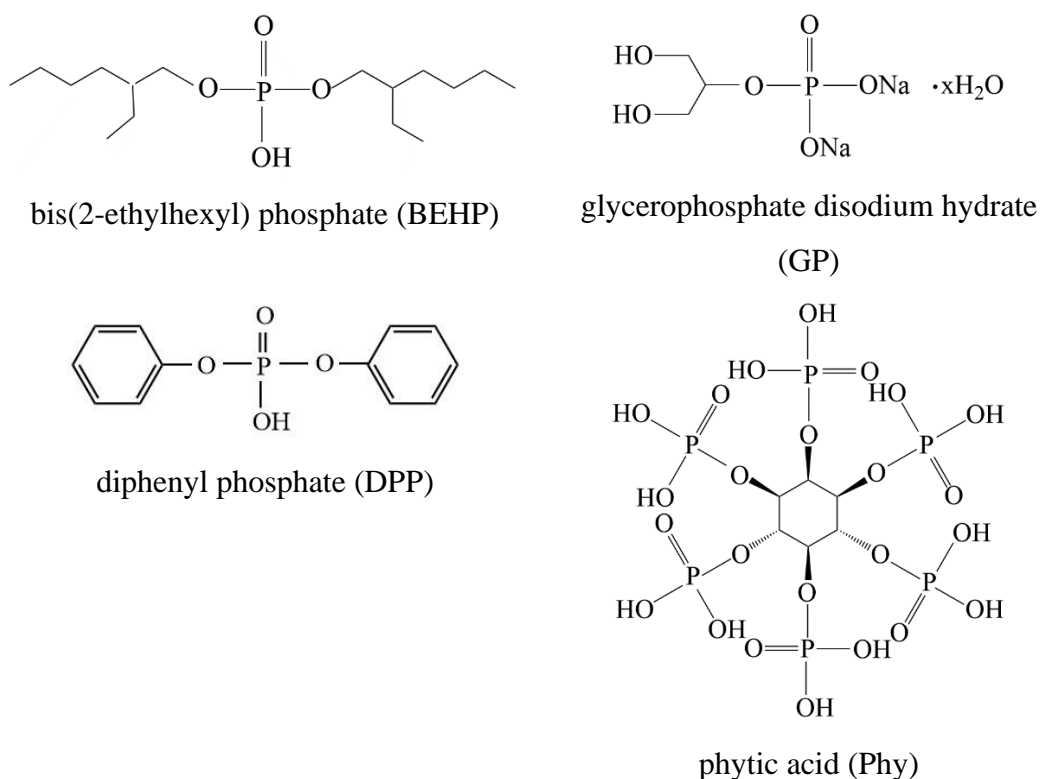


Figure 5.22 The chemical structures of organophosphate ester-based compounds used as the reactants for the anion modification of LDH: BEHP, Phy, GP and DPP.

All the organophosphate ester-based compounds contain acidic groups with the base solutions, leading to the formation of anions in the compounds. The organic anions can bond with the cations on the layered metal hydroxides. Both the BEHP and DPP provided monohydrogen phosphate ester but have different side groups. Their side groups are two alkyl and aryl groups, respectively. In the case of the Phy, it contains a six-fold dihydrogen phosphate ester, which has the largest molecule employed in this research. The smallest molecule of organophosphate ester compound is the GP, which consists of only one alkyl group.

For the flame retardant applications, the LDH intercalated with the BEHP and Phy anions has been studied in the prior works, whereas the GP and DPP modified LDHs have been not published in any paper. Besides, the previously published works did not compare the flame retardancy efficiency of different organophosphate ester intercalated LDHs. From these reasons, this research studied the effectiveness of the LDHs modified with the diverse organophosphate compounds.

As the combustion was associated with the thermal degradation, the study of thermal decomposition can support the understand of combustion phenomenon. The thermal decompositions of all organic reactants were analysed by the TGA. The fundamental of TGA is the measurement of mass of materials as the increasing temperature. The applied heat results in the decomposition of components. The testing result shows a thermogram of thermal decomposition of sample that can provide one, two, or multi-stages of mass-loss change, depending on the reactant's thermal behaviours.

Moreover, the mass change in the TGA result correlates to the mass of a volatile fractions, determining the molecular weight of volatile compounds. This information can be used for an expectation of thermal decomposition of materials. The TGA thermograms of BEHP, Phy, GP and DPP reactants were compared in Figure 5.23-5.26, respectively

For the thermogram of BEHP reactant in Figure 5.23, it presented two stages of mass loss in the ranges of 150-350°C and 350-800°C with the maximum mass loss rates at 260.0°C and 639.4°C, respectively. The mass loss content of the first decomposing stage was 75.9%, while the mass loss content of the second stage was 19.4%. With the conversion of mass loss content to the mass, they were equal to 244.70 g for the early stage and 62.54 g for the last stage. The molecular weight (MW) of BEHP reactant is 322.39 g/mol. Generally, the molecular weight of the decomposed gas molecules should be nearly the calculated mass.

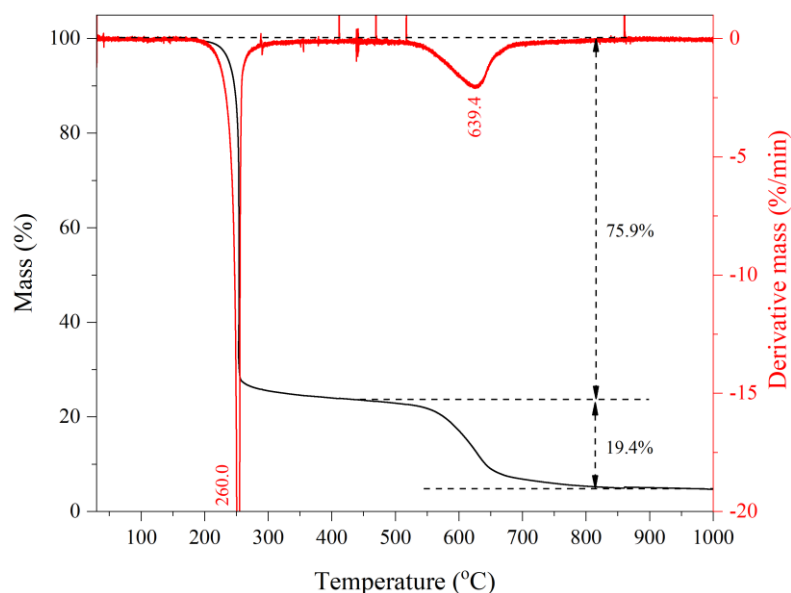


Figure 5.23 The TGA curve and its derivative of BEHP reactant used as modifying agent for LDH

From the study on the pyrolysis of organophosphate ester compound in the previous work, it decomposed to form alkene products and phosphoric acid compounds [28]. The phosphoric acid can decompose in the range of 400-800°C [29]. This work proposes that the initial decomposition of BEHP reactant might generate gas fragments of hydrocarbon and liquid fragment of phosphoric acid (H_3PO_4). At the same temperature range, the acidic liquid could also be decomposed to vapour water and liquidous P_2O_5 . The calculated weight of gaseous products was equal to 260.42 g. With the increasing temperature, the liquid phase of P_2O_5 would be transformed to its gas phase with the calculated weight of 70.97 g. Both the weights of gaseous products derived from the calculation were nearby the tested values. Figure 5.24 presented the thermal decomposition reactions of BEHP reactant. The comparison between the tested values and the calculated values of mass loss for the thermal decomposition of BEHP reactant were summarised in Table 5.7.

Table 5.7 The mass loss data of BEHP decomposition (MW of BEHP= 322.39 g/mol)

Range of decomposition temperature (°C)	Experiment		Calculation	
	Mass loss (%)	Mass loss (g)	Mass loss (%)	Mass loss (g)
150-350	75.9	244.70	78.0	260.42
350-800	19.4	62.54	22.0	70.97

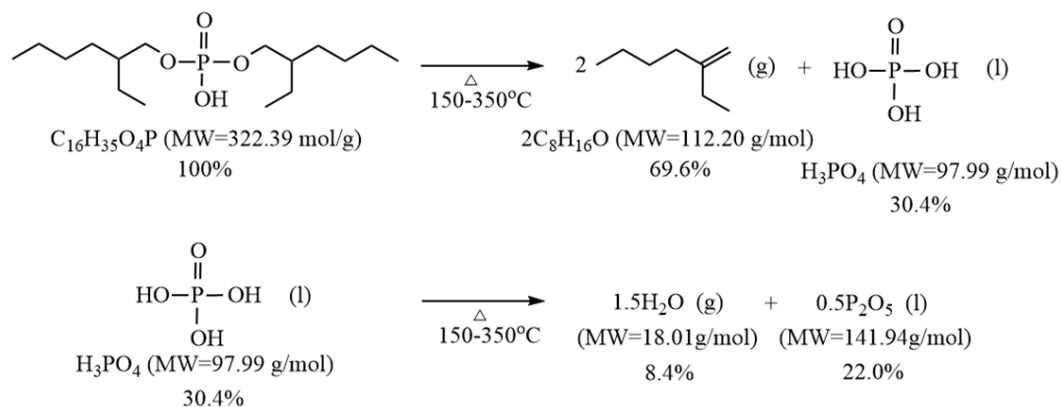
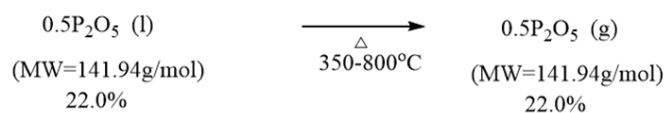
1st Stage of decomposition2nd Stage of decomposition

Figure 5.24 The proposed thermal decomposition mechanism of BEHP reactant [28, 29]

In the case of the Phy, the 50% phytic acid solution in water was used as the reactant for the modification of LDH. Figure 5.25 displayed the TGA curve and its derivative of Phy reactant. As the chemical was dried in the oven so as to get rid of the water, the TGA curve did not appear to lose water at below 100°C. The thermogram of phytic acid provided four mass loss stages: 100-200°C, 200-300°C, 300-400°C and 550-1000°C. The thermal behaviour of phytic acid had been reported in the previous study. Daneluti and Matos [30] suggested that the hydroxyl groups in the phosphate can be decomposed that induce the dehydration at the ranges of 162-292°C and 248-447°C. Then, the decomposition of phytate groups and carbon compound formed in the previous stage between 447°C and 863°C.

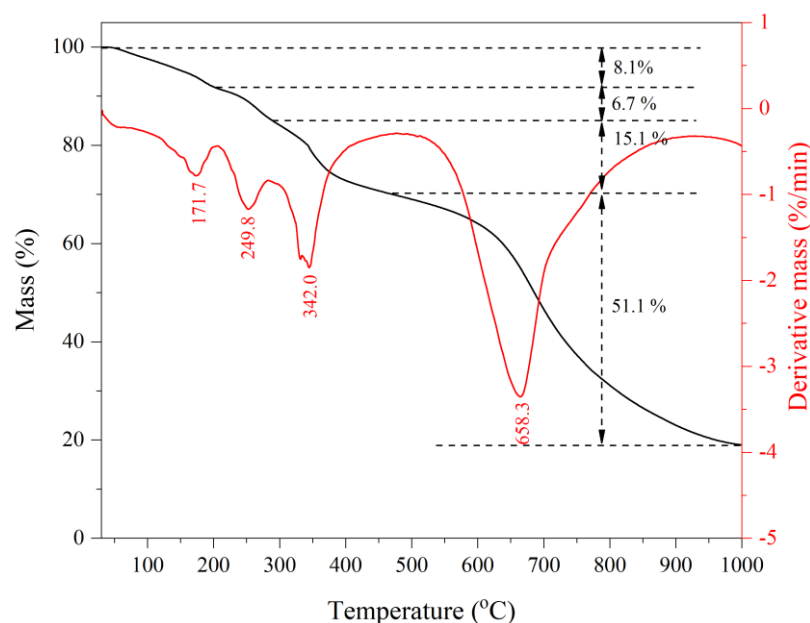


Figure 5.25 The TGA curve and its derivative of Phy reactant used as modifying agent for LDH

To estimate the gas products released during the heat, the mass loss percentage in each stage was considered. From the data in a specification document, the molecular weight of phytic acid is 660.04 g/mol. The thermogram of phytic acid in this work provided the mass loss of 8.1%, 6.7% and 15.1%, associating with the dehydration in the first three curve stages. Despite the water molecules, the P_2O_5 in the liquid state could also be promoted during the heating. Subsequently, they might be evaporated to provide the gas phase. The residue at the end of heat might be the formation of carbon compound. The important data of the mass loss derived from the decomposition of Phy reactant was presented in Table 5.8. The possible degradation mechanism of phytic acid is shown in Figure 5.26.

Table 5.8 The mass loss data of Phy decomposition (MW of Phy = 660.04 g/mol)

Range of decomposition temperature (°C)	Experiment		Calculation	
	Mass loss (%)	Mass loss (g)	Mass loss (%)	Mass loss (g)
100-200	8.10	53.46	8.2	54.03
200-300	6.70	44.22	4.1	27.02
300-400	15.10	99.66	12.3	81.04
550-1000	51.10	337.28	64.5	425.82

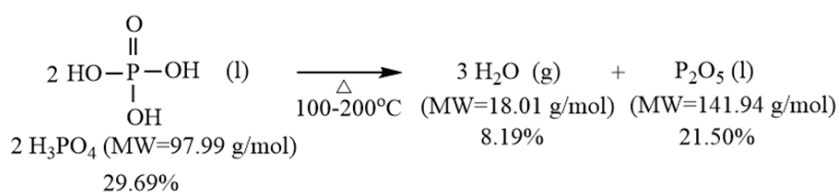
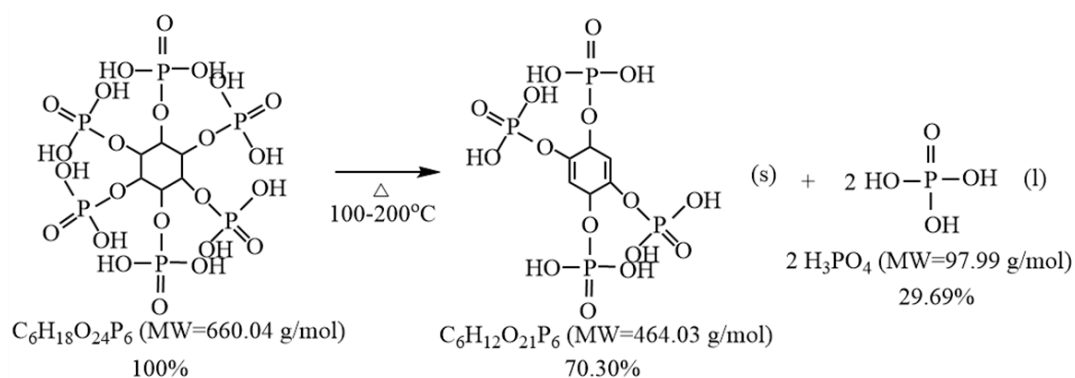
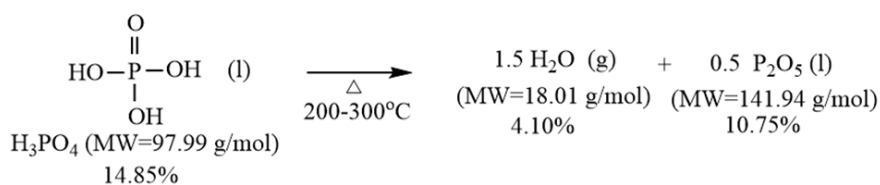
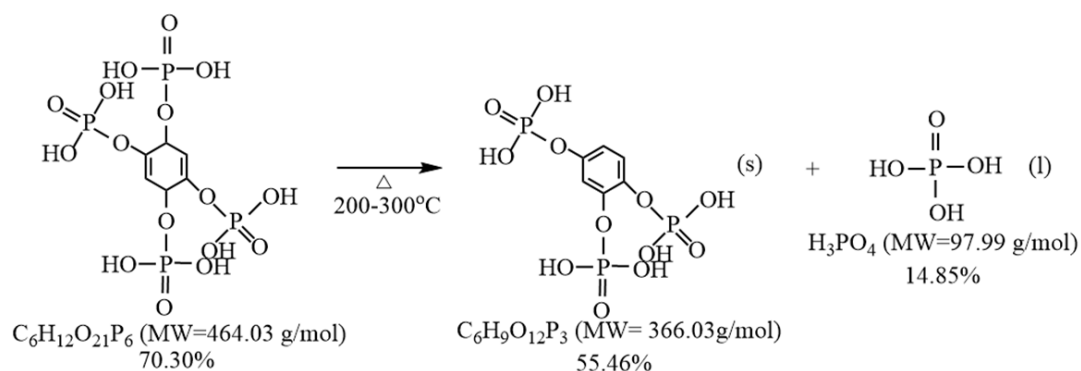
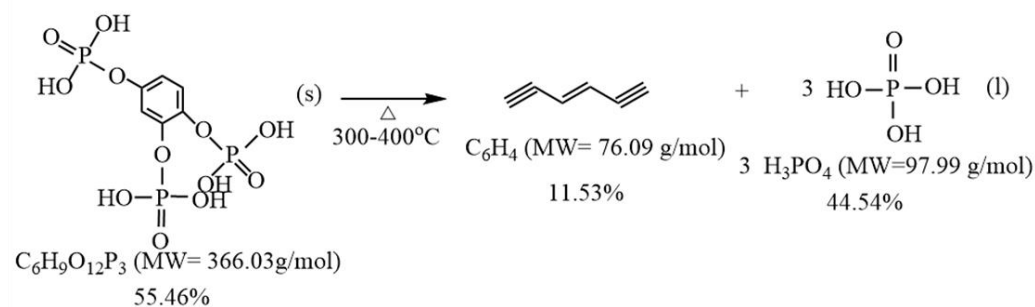
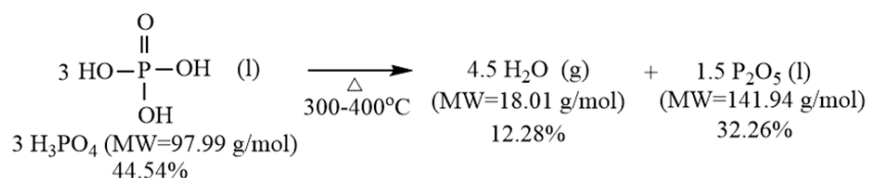
1st Stage of decomposition2nd Stage of decomposition3rd Stage of decomposition

Figure 5.26 The proposed thermal decomposition mechanism of Phy reactant. [30]



4st Stage of decomposition

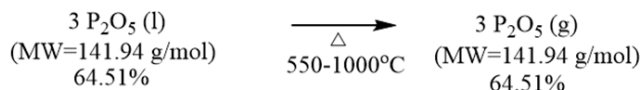


Figure 5.26 The proposed thermal decomposition mechanism of Phy reactant. [30]

(continued)

For the GP, the reactant was the sodium salt hydrate form with the molecular weight of 315.10 g/mol. The TGA curve of GP reactant displayed three steps of thermal decomposition, as presented in Figure 5.27. The first step took place between 70°C and 1120°C with the mass loss of 24.8%. As the component of GP reactant was the water, this decomposing step was attributed to the evaporation of water in the GP structure. The calculated mass loss of this stage was 25.7%. For the later step in the range of 250-320°C, there was the mass loss at 15.0%. At the final step, the decomposition occurred at the range of 320-400°C with the mass loss of 14.4%. According to the study of Piotr et al. [31], the initial thermal decomposition of disodium glycerophosphate provided sodium hydrogen glycerophosphate and sodium hydroxide. Then, the sodium hydrogen glycerophosphate decomposed to dihydrogen glycerophosphate and sodium hydroxide. Table 5.9 and Figure 5.28 show the data of mass loss obtained from the decomposition of GP reactant and the suggested decomposition mechanism of GP reactant, respectively.

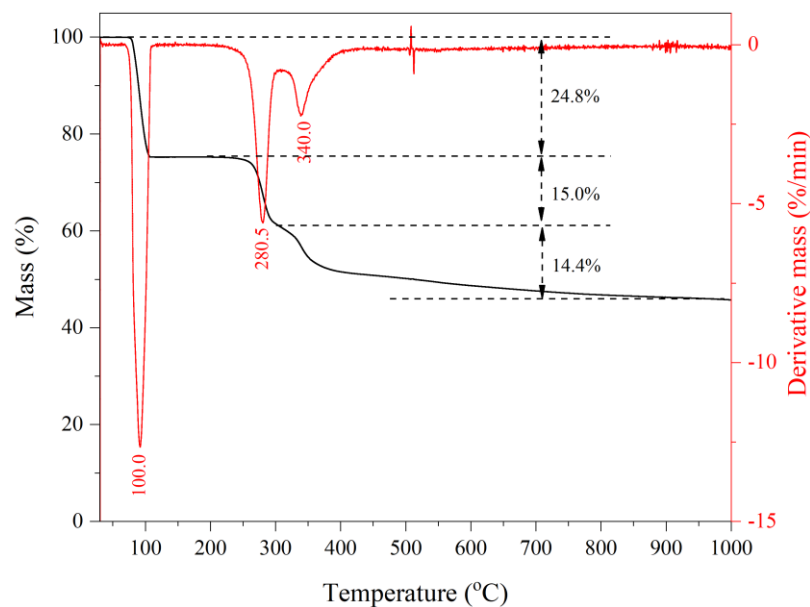


Figure 5.27 The TGA curve and its derivative of GP reactant used as modifying agent for LDH

Table 5.9 The mass loss data of GP decomposition (MW of GP =315.10 g/mol)

Range of decomposition temperature (°C)	Experiment		Calculation	
	Mass loss (%)	Mass loss (g)	Mass loss (%)	Mass loss (g)
100-120	24.8	78.14	25.7	81.04
250-320	15.0	47.27	12.7	40.00
320-400	14.4	45.37	12.7	40.00

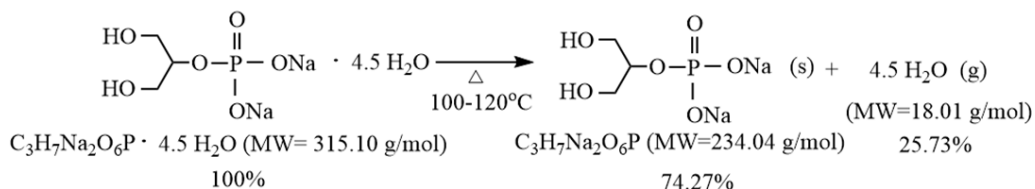
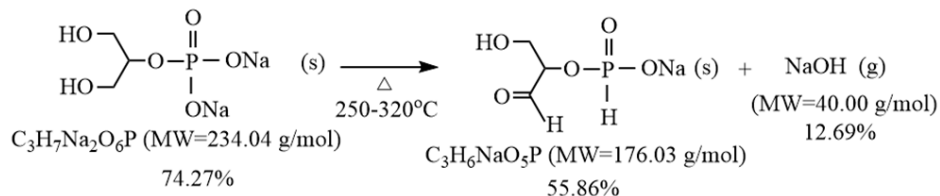
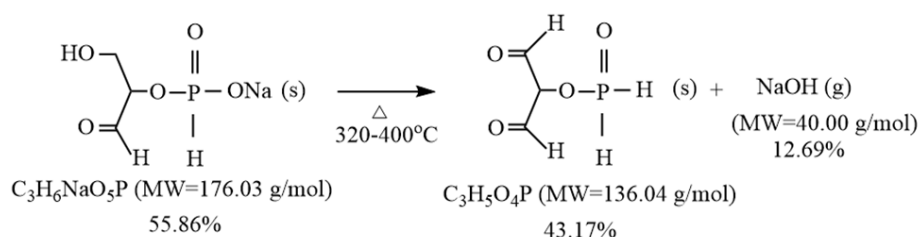
1st Stage of decomposition2nd Stage of decomposition3rd Stage of decomposition

Figure 5.28 The proposed thermal decomposition mechanism of GP reactant [31].

With considering the TGA curve of DPP reactant in Figure 5.29, the thermogram revealed two stages of decompositions at 150-350°C and 350-800°C with the mass loss of 78.3% and 15.7 %, respectively. By comparison with the TGA curve of the BEHP, the pattern of DPP (Figure 5.23) was almost the same due to the similarity of chemical structure. Therefore, the decomposition mechanism of both compounds were expected the similarity. That was a breaking of C-O bonds in the DDP molecule at 150-350°C, promoting hydrocarbon compounds and water in the gas state and the P₂O₅ in the liquid state. Then, the transformation of liquid P₂O₅ to its gas form might be performed in the final process. The tested and calculated mass loss of DPP decomposition are presented in Table 5.10. The thermal decomposition mechanism of the DPP was suggested in Figure 5.30.

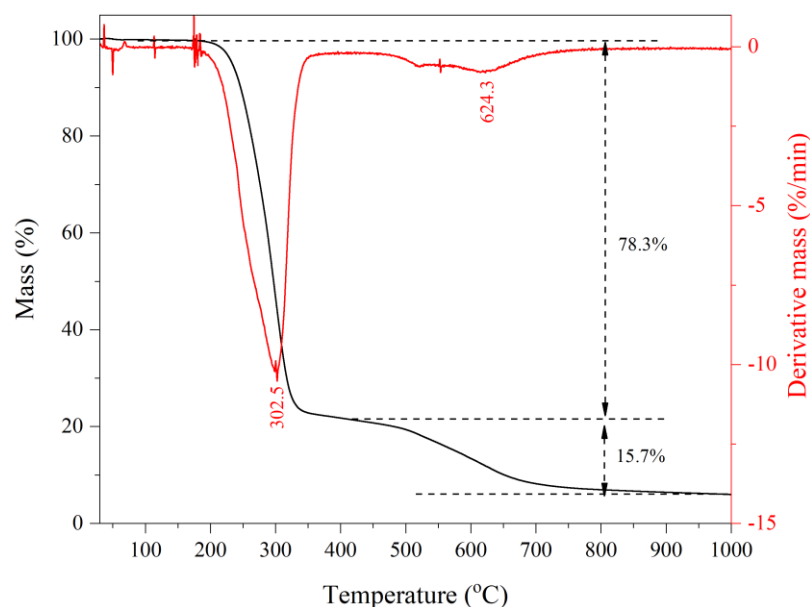
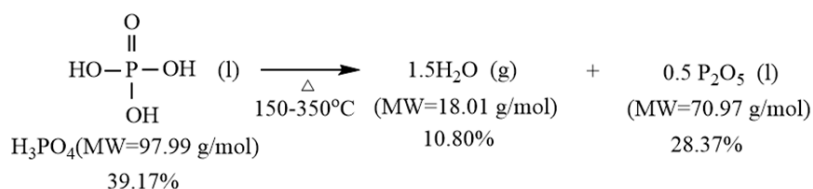
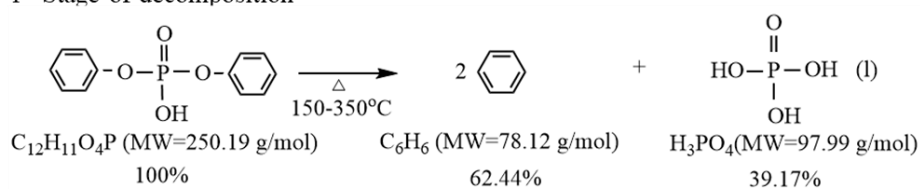


Figure 5.29 The TGA curve and its derivative of DPP reactant used as modifying agent for LDH

Table 5.10 The mass loss data of DPP decomposition (MW of DPP = 250.19 g/mol)

Range of decomposition temperature (°C)	Experiment		Calculation	
	Mass loss (%)	Mass loss (g)	Mass loss (%)	Mass loss (g)
150-350	78.3	195.90	74.8	187.26
350-800	15.7	39.28	14.1	35.49

1st Stage of decomposition



2nd Stage of decomposition

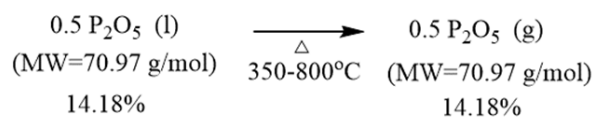


Figure 5.30 The proposed thermal decomposition mechanism of DPP reactant.

From the information in the literature reviews and the characteristics of the organophosphate ester compounds, it can be seen that the selected organic compounds (BEHP, Phy, GP and DPP) decomposed in the wide temperature ranges. Both the char residues and the phosphate oxides produced during the decomposition process may impede and stop the combustion of polymers. Moreover, the structures of the organophosphate ester-based compounds can be deprotonated with the base solutions to form the anions on the structure. These formed anions can interact with the cations on the layers of metal hydroxides. Hence, all the selected organophosphate ester-based compounds were likely to be used as the modifying agents for LDHs and enhance the flame retardancy for polymers.

5.5 Characterisation of LDHs Modified with Organophosphate Ester-Based Anions

As mentioned previously, the four types of organophosphate-based anions used for the modification of LDHs were BEHP, Phy, GP and DPP. The modified LDHs were prepared in the various conditions. The influence of preparing conditions on the X-ray diffraction behaviours functional groups characteristics of the modified LDHs would be discussed in this section.

5.5.1 Modification with Bis(2-Ethyl Hexyl) Phosphate

The LDHs modified with the BEHP were prepared by the co-precipitation and the rehydration with the different conditions. The effect of decarbonation, precipitating agents and aging time on the modification were studied.

5.5.1.1 Synthesis by the Co-precipitation Method

5.5.1.1.1 Effect of Decarbonation

In the initial preparation of LDH-BEHP via the co-precipitation method, there was only the N₂ flow within the reactor to protect against the contamination of CO₂ in the atmosphere. It did not use the decarbonated water and the purified NaOH in the synthesis process. The XRD pattern of LDH-BEHP without the decarbonization in

the water and NaOH is shown in the red line of Figure 5.31. It was found that the lowest degree of the crystallisation peak was 11.68° , corresponding to the d-spacing of 0.76 nm. Meanwhile, the pristine LDH, which was not modified with the organophosphate compound, providing the lowest peak position at 10.04° and the d-spacing of 0.88 nm, as displayed in the black line of Figure 5.31. It can be seen that the d-spacing of the modified LDH was less than the pristine LDH. These results indicated that the BEHP anion was not intercalated in the interlamellar space in the LDH. It seems possible that the CO_2 and/or CO_3^{2-} might be poisoning in the synthesis process.

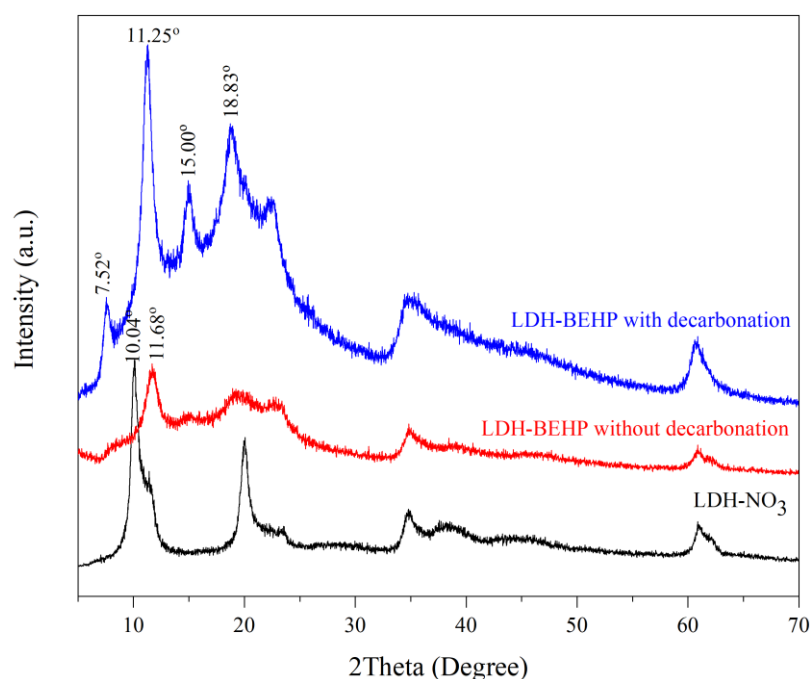


Figure 5.31 The comparison of XRD patterns of LDH-NO₃ and LDHs-BEHP without and with the decarbonation of used water and NaOH.

When the CO_2 and CO_3^{2-} were excluded from the reaction system by using the purified water and NaOH, the diffraction pattern of LDH-BEHP revealed the lowest degree of the peak at the 2θ of 7.52° with the d-spacing of 1.17 nm. This result is presented in the blue line of Figure 5.31. It was noticeable that the d-spacing of LDH-BEHP was considerably enlarged with preparing in the conditions without the CO_2 and CO_3^{2-} toxic. This result established the intercalation of BEHP between the layers of metal hydroxides. Also, the results emphasised the importance of decarbonation. The 2θ

positions and the d-spacings of the synthesised LDH samples at the lowest angle are noted in Table 5.11.

Table 5.11 The 2θ positions and the d-spacings of the pristine LDH and the LDHs-BEHP without and with the decarbonation of the used water and NaOH.

Sample	2θ ($^\circ$)	d-spacing (nm)	Anions
Pristine LDH with decarbonation	10.04	0.88	NO_3^-
LDH-BEHP without decarbonation	11.68	0.76	CO_3^{2-}
LDH-BEHP with decarbonation	7.52	1.17	BEHP

The XRD pattern of the LDH-BEHP in this work resembled the prior study. Costa et al. [24] reported that the (003), (006) and (009) reflections of Mg/Al LDH modified the BEHP showed at 5.81° , 11.06° and 19.30° , respectively. The interlayer distance of (003) was 1.52 nm. However, few published studies suggested that the d-spacings of LDH-BEHP were 2.31 nm [32] and 2.34 nm [33]. Theoretically, interlayer distance in LDH modified with organic compounds depends on the thickness of metal hydroxide layers, the molecular size of intercalated anions and their anionic orientation in the interlayer area [24]. In this case, both the layer thickness and the intercalated anionic size were the same. Thus, the distinction between the two d-spacing lengths could account for the different orientation of BEHP molecules in the interlamellar area. The arrangement of anions in the LDH would be discussed in further section.

5.5.1.1.2 Effect of Precipitating Agent

Figure 5.32 compares the XRD patterns of the pristine LDH to that of the BEHP modified LDHs prepared under the NaOH and NH_4OH solution. They were represented in the black, red and blue line, respectively. With the use of NH_4OH , the lowest peak position displayed at 6.30° , correlated to the d-spacing of 1.40 nm. The reflection peak of NH_4OH shifted to lower diffraction angle by comparison with the NaOH. These results indicated more expansion of distance between the metal hydroxide layers with using the NH_4OH . Also, the peak intensities of NH_4OH were higher than that of NaOH. This means that the crystallinity of the sample increased

with using the NH_4OH . The results demonstrated that the NH_4OH solution was appropriate to the synthesis of LDH-BEHP.

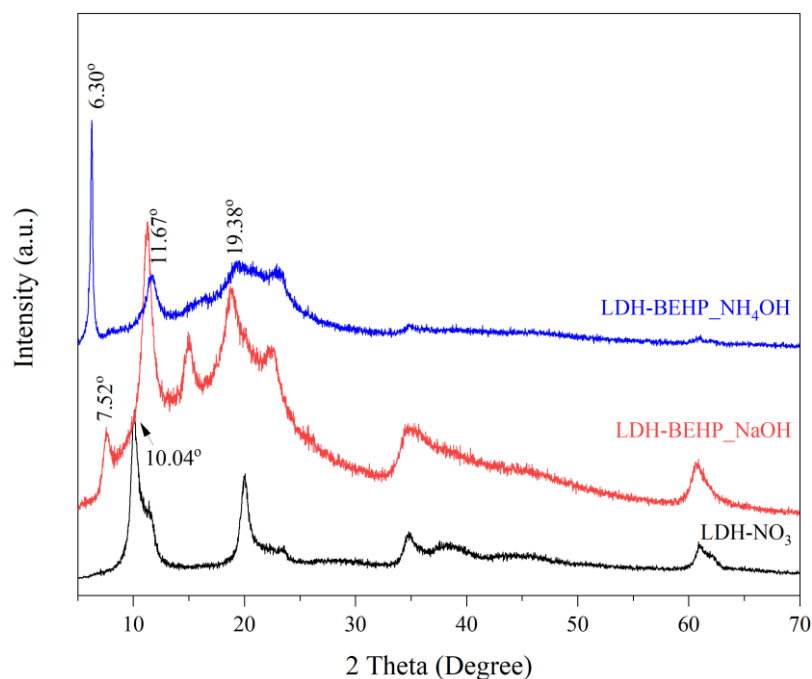


Figure 5.32 The XRD patterns of the pristine LDH and LDH-BEHP prepared in the NaOH and NH_4OH solutions.

The increase of LDH crystallinity with using the NH_4OH could be explained in term of dissociation constants of bases. It is well known that NaOH is a strong base dissociated completely in water, but on the other hand, NH_4OH is a weak base ionized incompletely in water [34]. The rate of precipitation with NaOH was higher than NH_4OH , resulting in a large amount of nuclei in the initial step of precipitation and the low crystalline growth. Meanwhile, the precipitation of LDH with NH_4OH occur slowly, providing the small content of nuclei and the slow crystal growth. Therefore, the use of NH_4OH for the precipitation induced the high crystallinity.

The observation of FTIR spectra of LDH-BEHP also confirmed the existence of BEHP within the LDHs. The IR spectra of the pure BEHP, the pristine LDH and the BEHP modified LDHs prepared in the NaOH and NH_4OH were presented in Figure 5.33.

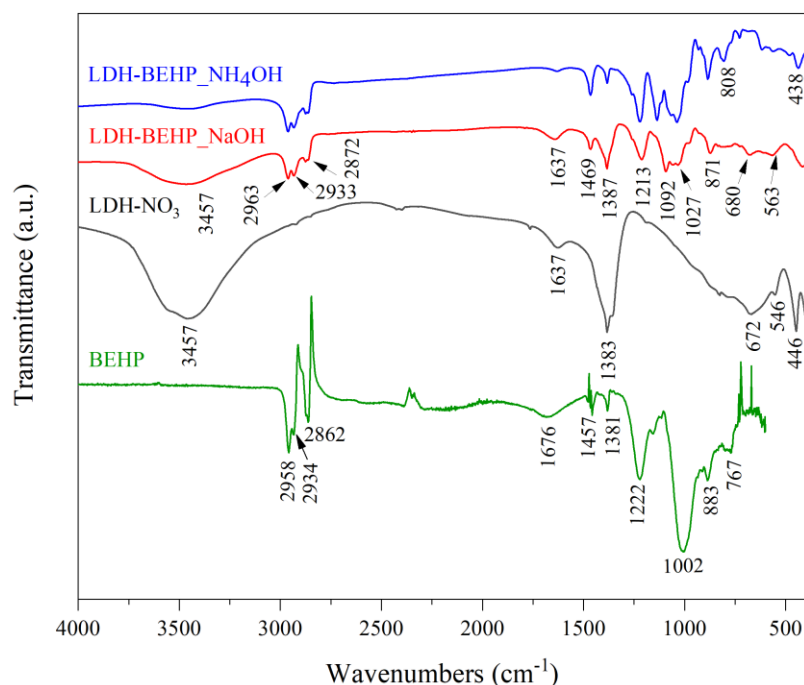


Figure 5.33 The FTIR spectra of the BEHP, the pristine LDH and the BEHP intercalated LDH prepared in the NaOH and NH_4OH .

For the BEHP reactant (the green line), the group bands at 2958, 2934 and 2862 cm^{-1} can be assigned to the asymmetric stretching vibration of C-H, while the bending vibration of C-H presented at 1547 cm^{-1} . The bands at 1222, 1022 and 833 cm^{-1} showed the characteristics of P=O and P-O. Considered the spectra of LDHs-BEHP (the red and green lines), not only the characteristics of the metal hydroxide and the water molecule were presented, but also the all IR bands of the pure BEHP can be found in the LDHs modified with BEHP.

5.5.1.1.3 Effect of Aging Time

The influence of aging time on the formation of LDH-BEHP was also studied in this experiment. The XRD results of LDHs-BEHP prepared with the variation of aging times for 5, 15 and 24 h are shown in Figures 5.34 and 5.35 for the use of NaOH and NH_4OH solutions, respectively. For the LDH-BEHP preparation with the NaOH, the peak intensities and sharpness were likely to increase when the treatment periods increased. Likewise, the longer aging times led to the rise of diffraction intensities of LDH-BEHP prepared with the NH_4OH . Hence, the crystallinity of the modified LDHs increased with the longer aging time.

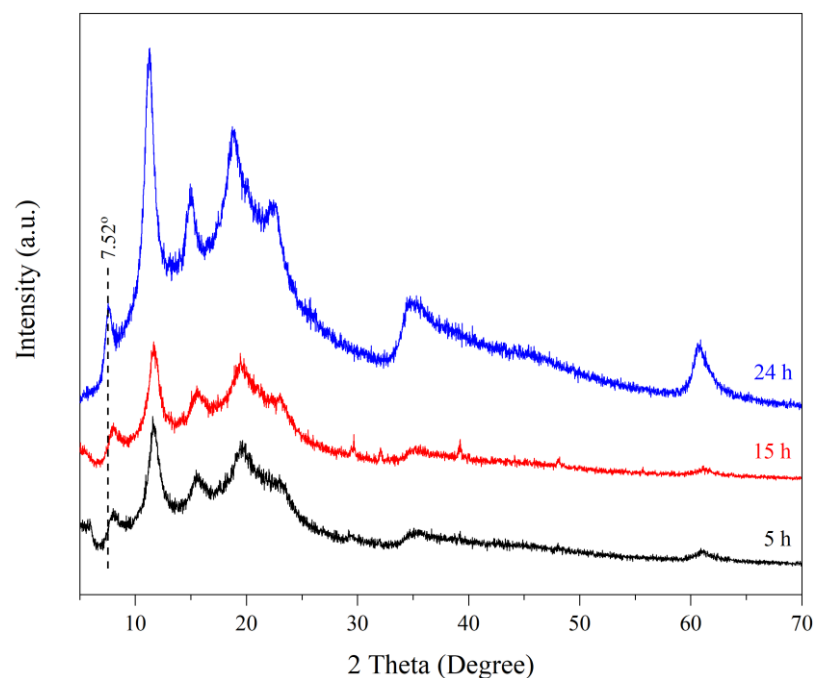


Figure 5.34 The XRD patterns of LDH-BEHP prepared in the NaOH with the variation of aging time: 5h, 15h and 24h.

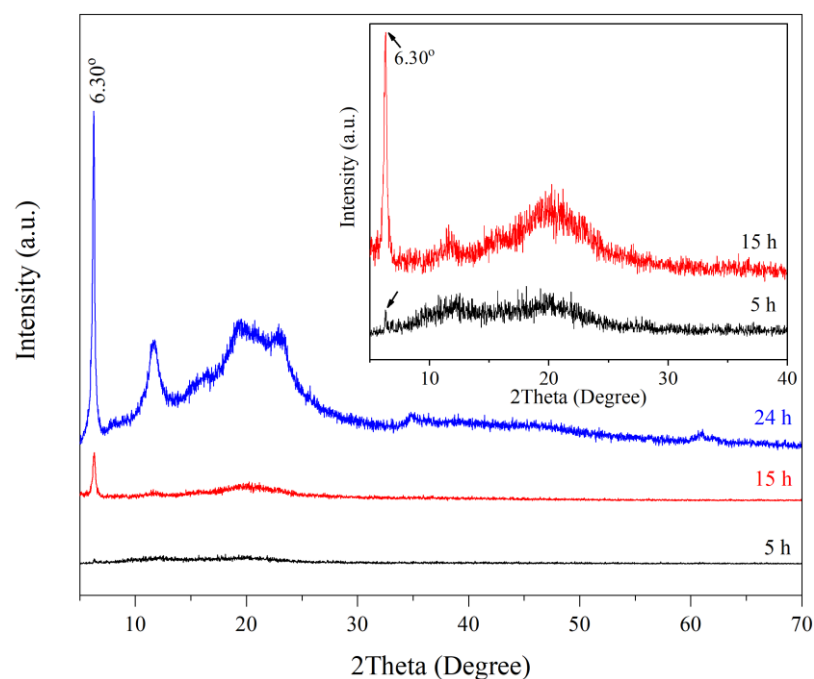


Figure 5.35 The XRD patterns of LDH-BEHP prepared in the NH₄OH with the variation of aging time: 5 h, 15 h and 24 h.

Considering the calculated lattice parameters and the crystal size of the modified LDHs in the NaOH (Figure 5.36), the lattice parameter of *c* (black line) was stable at around 3.3 nm with the aging time of less than 15 h. Then, it rose slightly to 3.51 nm

at the aging time of 24 h. In the meantime, the crystal growth of the ab-plane had constantly maintained at 0.30 nm with the increase of aging periods from 5 h to 24 h (red line). These results can be implied that the increasing of treatment time did not affect the crystal growth in the ab-plane but induced the stacking of crystals along the c direction. Additionally, the crystal size in the c direction also grew gradually from 3.45 nm for 5 h to 4.07 nm and 3.88 nm for 15 h and 24 h, respectively (blue line).

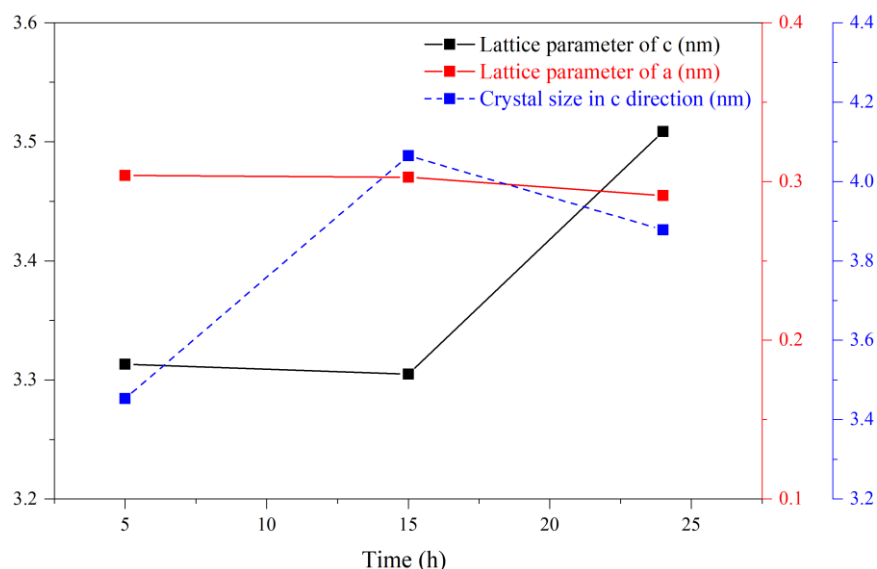


Figure 5.36 The c and a lattice parameters and the crystal size in c direction of LDH-BEHP prepared in the NaOH with the variation of aging time: 5h, 15h and 24h.

In the case of the NH_4OH , the lattice parameter and the crystal size in the c direction were exhibited in Figure 5.37. The lattice parameter of the ab-plane could not define since there was a disappearance of peak position at 2θ 60° . Meanwhile, the c parameters of the modified LDHs seemed stable at around 4.2 nm with increasing times. However, the crystal size reduced significantly, almost 50 % from 65.63 nm for 5 h to 33.49 nm for 24 h. The XRD results indicated that the increase of time led to the increase of crystallinity and crystal size reduction using the NH_4OH .

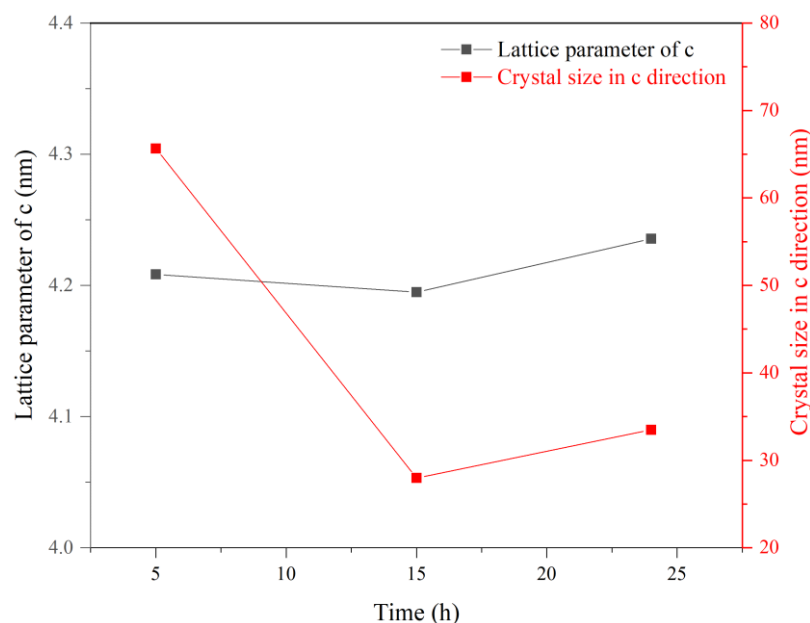


Figure 5.37 The *c* lattice parameters and the crystal size in *c* direction of LDH-BEHP prepared in the NH_4OH with the variation of aging time: 5h, 15h and 24h

5.5.1.2 Synthesis by the Rehydration Method

5.5.1.2.1 Effect of Decarbonation

For the preparation of LDH-BEHP with the rehydration method, the calcined LDH- CO_3 (CLDH) was dispersed in the aqueous solution of BEHP. The slurry was simultaneously stirred through the reaction time. Besides, the pH of the slurry was also controlled by adding the solutions of NaOH or NH_4OH . In the case of NaOH, the CLDH-BEHP prepared in both the existence and the non-existence of CO_3^{2-} in the water and NaOH.

Figure 5.37 displays the XRD patterns of the MG70 LDH and the CLDHs-BEHP prepared in the different conditions. At the lowest peak position, the pristine LDH showed at 11.32° , responding to the *d*-spacing of 0.78 nm (black line). Meanwhile, the CLDHs-BEHP provided the diffraction degree at 7.79° and 5.99° for the non-decarbonation (red line) and the decarbonation (blue line) of water and NaOH, respectively. It was worth nothing that the *d*-spacings of CLDHs-BEHP increased in the comparison with the LDH- CO_3 .

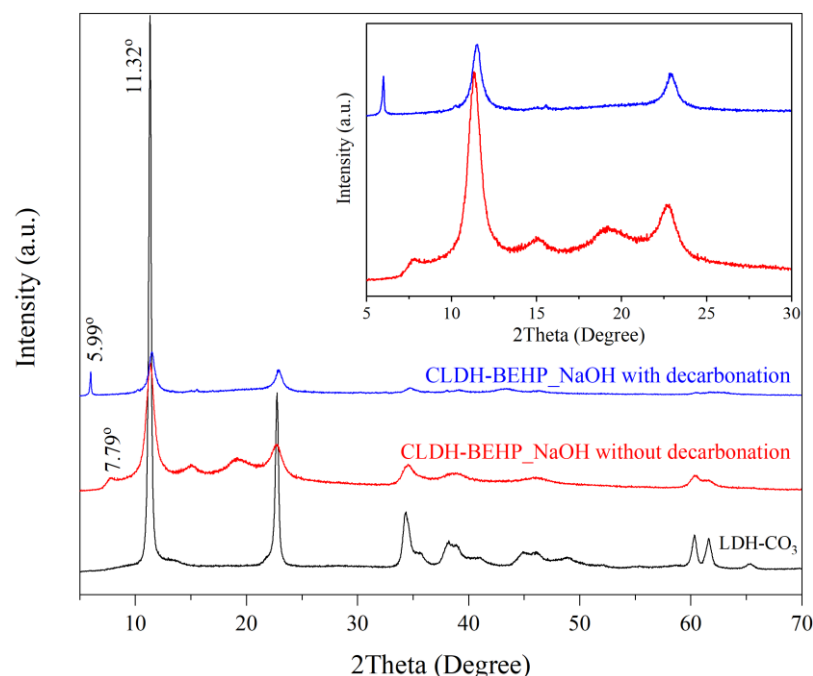


Figure 5.38 The XRD patterns of commercial LDH (MG70) and CMG70-BEHP prepared in NaOH without and with the decarbonisation.

Table 5.12 The summary of (003) reflections and d-spacings of the pristine LDH and the LDH-BEHP prepared in the existing and the non-existing carbonate.

Sample	(003) (°)	d(003) (nm)	Intercalating anion
MG70	11.32	0.78	CO ₃ ²⁻
CMG70-BEHP without the decarbonation (NaOH)	7.79	1.13	BEHP
CMG70-BEHP with the decarbonation (NaOH)	5.99	1.47	BEHP
CMG70-BEHP with the decarbonation (NH ₄ OH)	6.27	1.41	BEHP

The CLDH-BEHP prepared in the solution with the existing carbonate had the d-spacing of 1.13 nm, whereas that with the decarbonation obtained the d-spacing of 1.47 nm. The d-spacing of CLDH-BEHP prepared under the decarbonation was higher than the preparation without the decarbonization. The (003) reflections and d-spacings of the pristine LDH and the LDH-BEHP are summarised in Table 5.12. This result was another evidence to support the importance of decarbonation in the period of LDH modification.

5.5.1.2.2 Effect of Bases

In addition to the rehydration in the NaOH solution, the CLDH-BEHP was also synthesised in the NH_4OH . Figure 5.39 displayed the XRD patterns of CLDH-BEHP prepared with using the NaOH and NH_4OH . For the use of NH_4OH , the lowest peak position exhibited at 6.27° , corresponding to the d-spacing of 1.41 nm. Compared with the use of NaOH, the d-spacing and the crystallinity of NH_4OH were a little less than that of NaOH. Therefore, the preparation of LDH-BEHP with the rehydration method in the NaOH was suitable for the modification of LDH.

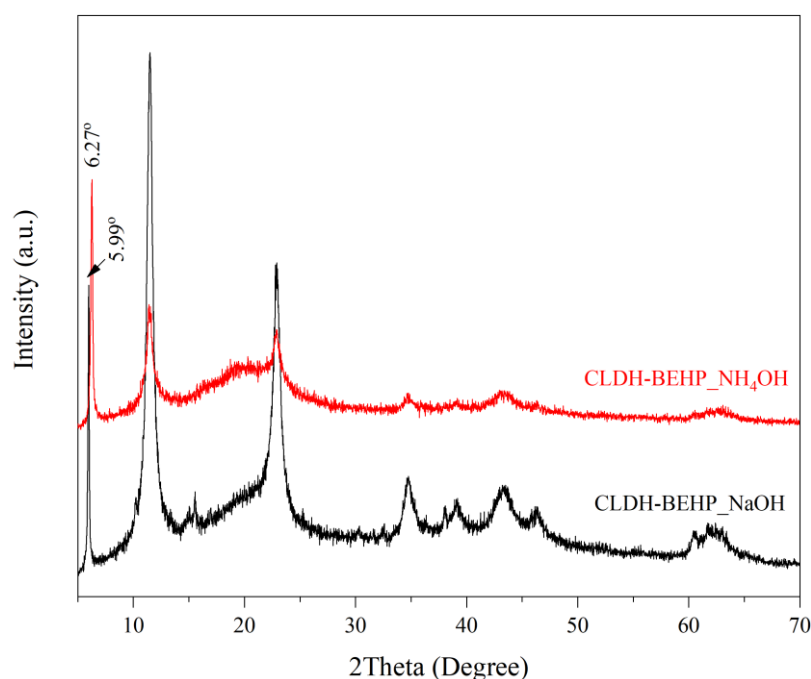


Figure 5.39 The comparison of XRD patterns of CLDH-BEHP prepared in the different base solutions.

5.5.1.3 Evaluation of the preparation methods

From the above results, both the co-precipitation and the rehydration were able to induce the intercalation of BEHP anions in the interlamellar galleries of LDHs. The co-precipitation method was the direct method (one process) for the synthesis of LDH, that was a convenience for the synthesis. Hence, the proper conditions for the synthesis of LDH-BEHP were the preparation at pH 9 and 60°C for 24h under the NH_4OH solution.

5.5.2 Modification with the Phytic Acid

In recent years, a few published research have reported the preparation of phytate intercalated LDH (LDH-Phy) by the methods of co-precipitation [35, 36] and ions exchange [37, 38]. This study selected the preparation of LDH-Phy with the co-precipitation. The preparing procedure and the used chemical proportion were followed by the description in the prior research [35].

5.5.2.1 Effect of Decarbonation

The XRD result of LDH-Phy acquired from the preliminary preparation is shown in the red line of Figure 5.40. The LDH-Phy displayed the same XRD pattern as the LDH intercalated with CO_3^{2-} anions (the black line in Figure 5.39). As there was no change of peak positions, especially in the range of low diffraction angles, it suggested that the phytate might not be inserted between the lamellae of the LDH. From the crystalline phase analysis, it was surprising that the significant intercalated anion between the interlayers of LDH was carbonate, although the LDH was prepared under the phytate solution.

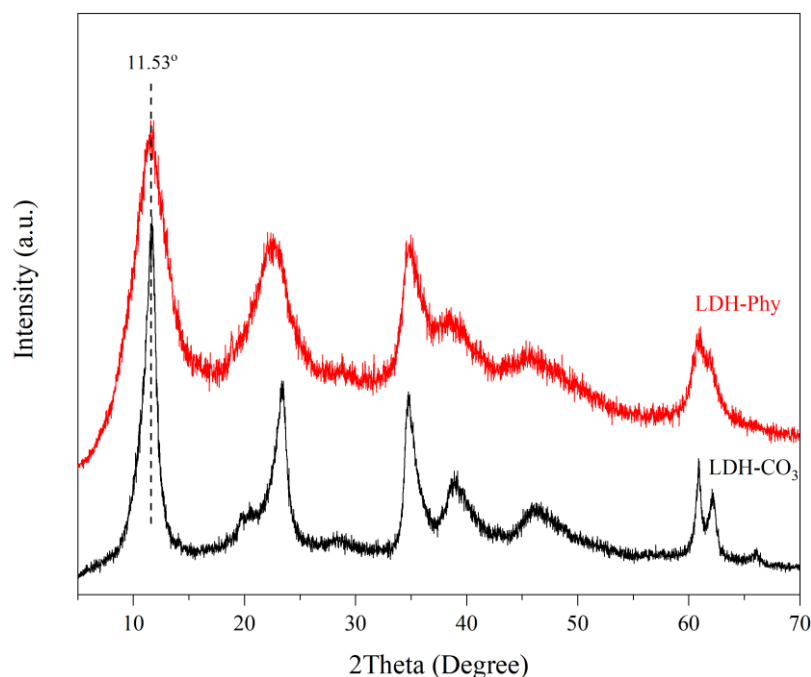


Figure 5.40 The XRD patterns of the pristine LDH and the LDHs-Phy without the decarbonation in the used water and NaOH in the different reaction time.

As mentioned earlier, the synthesis method of LDH-Phy carried out following the previous study [35]. However, the result obtained from the experiment was contrary to the researched result. Kalali et al. [36] reported that the first diffraction peak of LDH-Phy displayed at 7.30° , correlating with the interlamellar distance of 1.13 nm. It indicated the intercalation of phytate molecules in the interlayer area. This conflicting synthesis result could be associated with CO_2 and/or CO_3^{2-} contamination in the experiment. The previous study did not explain the procedure of decarbonation during the synthesis of LDH.

From the observation of FTIR results in Figure 5.41, the spectra of the pure phytic acid, the pristine LDH and the LDH-Phy were presented in the black, red and blue lines, respectively. As the phytic acid is a liquid phase, the ATR mode of FTIR was used for the test of the phytic acid. Meanwhile, the FTIR of both the pristine LDH and LDH-phy, which were solid phase, were analysed by using the KBr method. For this reason, the spectrum characteristic of phytic acid was different from the others. The intensities of FTIR bands obtained from the ATR mode were lower than that from the KBr method.

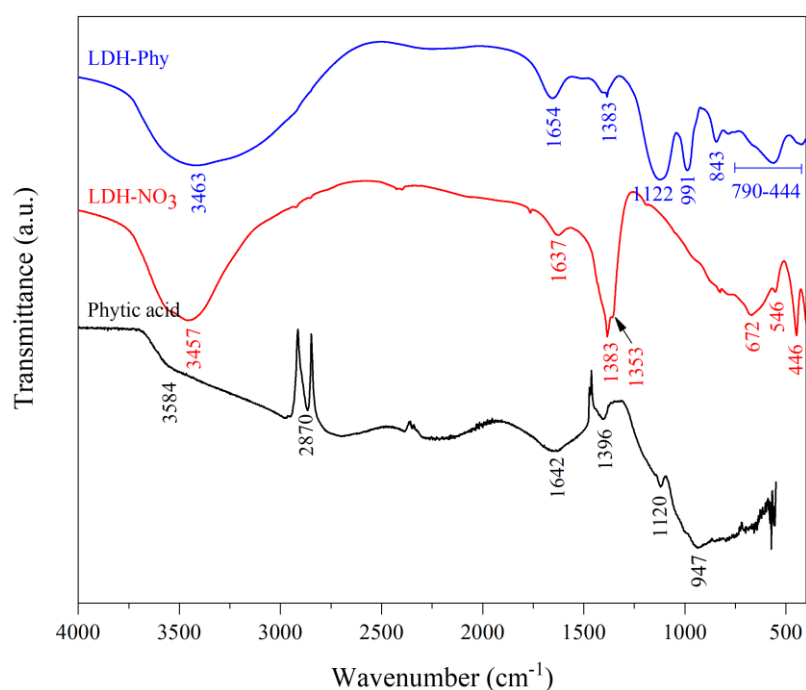


Figure 5.41 The FTIR spectra of the phytic acid, the pristine LDH and the LDH-Phy without the decarbonisation in the used water and NaOH.

The spectrum of LDH-Phy included the characteristics of both the pristine LDH and the phytic acid. The broad band at around 3463 cm^{-1} could be assigned to the -OH functional groups in the LDH and the small band at 1654 cm^{-1} belonged to the interaction of water molecules. The band range of $400\text{--}800\text{ cm}^{-1}$ could be attributed to the bonds between the metal and oxygen atoms. For the phytate characteristics, the PO_3^{2-} groups presented at 1122 cm^{-1} and the interaction bond of P-O-C displayed at 991 and 843 cm^{-1} . The resultant analysis was supported by previous studies [37, 38]. However, the pure phytic acid presented the band at 2870 cm^{-1} , corresponding to the C-H stretching vibration. It could not be observed in the spectrum of LDH-Phy.

According to the XRD result of LDH-Phy, it indicated no intercalation of phytate anions in the interlayer galleries of LDH. However, the FTIR result as above described indicated the existence of phytate molecules in the LDH structure. This means the phytate might just be adsorbed on the surface of LDH. As discussed previously, the existence of carbonate in the synthesis process might obstruct the intercalation of phytate to the metal hydroxide lamellae.

When the distilled water and the NaOH were decarbonated before utilising the synthesis process, the modification of LDH with Phy anions was carried out again at the same experimental conditions. The X-ray diffractions of LDH-Phy prepared under the decarbonising conditions with the variation of reaction times (5, 15 and 24 h) are presented in Figure 5.42.

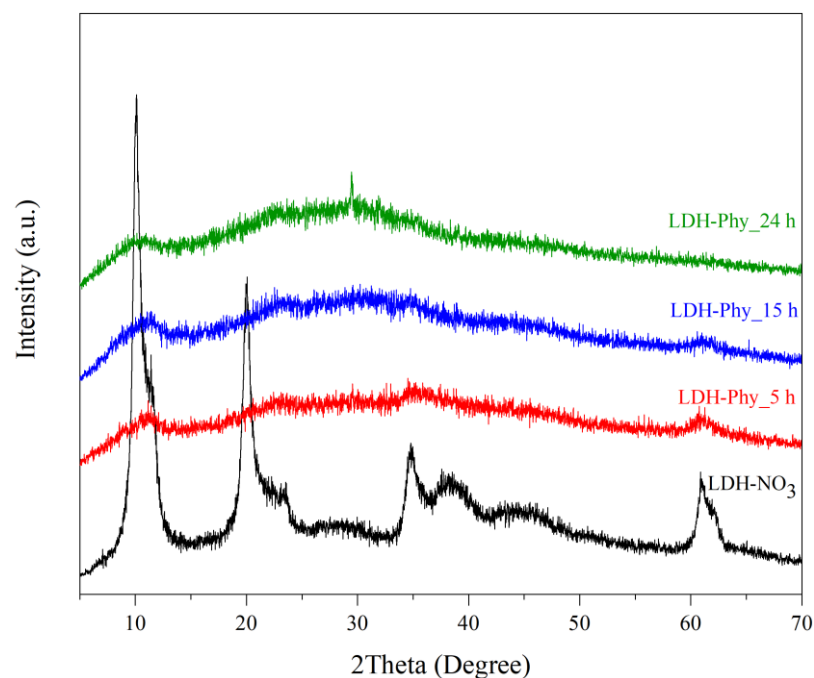


Figure 5.42 The XRD patterns of the pristine LDH and the LDH modified with Phy in the various reaction times

It was apparent that all the XRD patterns of LDHs-Phy prepared in the different reaction times did not show the low intensity of diffraction peak, indicating the reduction of crystallinity with the modification of Phy. These results suggested that there could be delamination of the modified LDHs. The layers of metal hydroxides in the LDHs might be exfoliated with the phytate molecules. Figure 5.43 compares the FTIR spectra of LDHs-Phy prepared under the carbonation and the decarbonation. This result supported the existence of phytate molecules in the LDH structure.

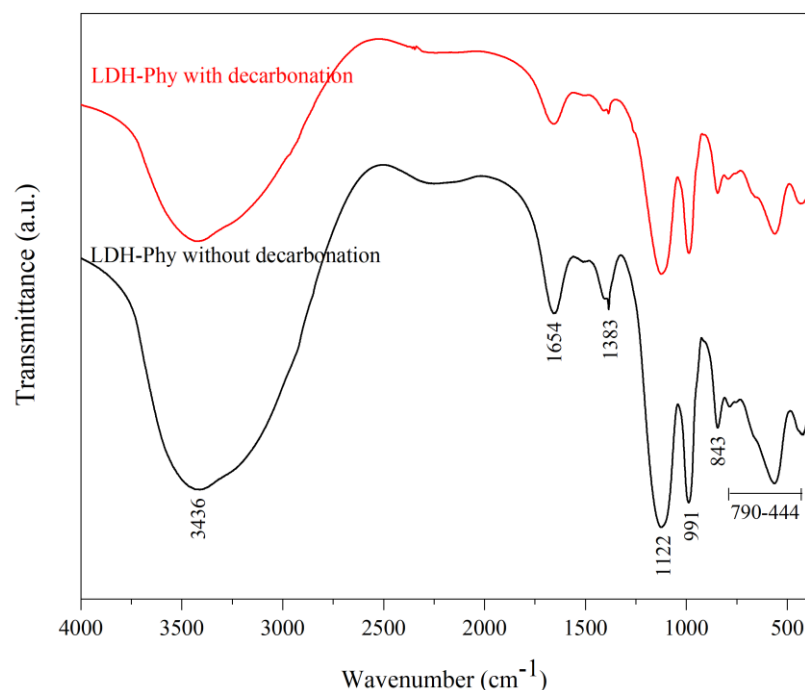


Figure 5.43 The FTIR spectra of LDHs-Phy prepared under the conditions with carbonate and the exclusion of carbonate and maintained at pH 9 and 60°C for 24 h.

In the literature, there was an explanation of delamination in LDH modified with bulky organic anions. Hibino [39] described the delamination of LDHs containing amino acid e.g. phenylalanine and glutamine that was associated with the hydrogen bonds. The chemical structures of both amino acids are displayed in Figure 5.43. The anionic molecules of amino acid bonded among themselves and with the cationic layers via hydrogen bonds. The anions of amino acids connected to both above and below LDH layers. As much of hydrogen bonds were produced during the synthesis, that obstructed the interaction of amino acid molecules. Besides, the side chains of amino acid were hydrophobic that repelled the H₂O molecule in the LDHs. This might also result in the delamination,



Figure 5.44 The Chemical structure of glycine and phenylalanine.

Even if the LDH-Phy in this experiment was prepared in the same condition as the previous study, the XRD patterns of both still were different. Considering the used chemicals for the preparation of LDH-Phy, there were similarities between the experiment and literature, except the phytic acid salts. The literature used the commercial product of phytic acid sodium salt, a chemical formulation of $C_6H_{18}O_{24}P_6 \cdot xNa^+ \cdot yH_2O$. The specification data of this phosphate compound does not report the exact number of sodium substituting in the compound.

Meanwhile, this experiment carried out the conversion of phytic acid to its sodium salt by adding the 1M NaOH solution under 100°C for 5 h. The amount of NaOH solution used for the conversion related to the total number of hydrogen atoms in the OH groups of the compound, as the equivalent chemical equation of the reaction. It was anticipated that the six phosphates in the phytic acid could be deprotonated with the NaOH solution.

Consequently, it resulted in the formation of negative ions of phytate dissolved in the aqueous solution. With the formation of cationic layers of magnesium and aluminium hydroxides, the one negative charge of phytate interacted with the one positive charge on the layers to stabilise the charges within the LDH structure. Due to the excess negative charges of phytate molecules, the phytate molecules might connect with the nearest neighbor. This induced the formation of bulk molecules. These reasons might lead to a significant increase in distance between the layers, inducing the exfoliation of layers.

5.5.2.2 Effect of Precipitating Agents

Likewise, the XRD pattern of the LDH-Phy synthesised using the NH_4OH displayed the broad peaks, presented in the blue line of Figure 5.45. This result was similar to the LDH-Phy preparation under the NaOH (red line, Figure 5.45). However, some diffraction positions of the NH_4OH at around 38° and 61° was more intensity than that of the NaOH. It might occur the partial exfoliation of layers in the modified LDH.

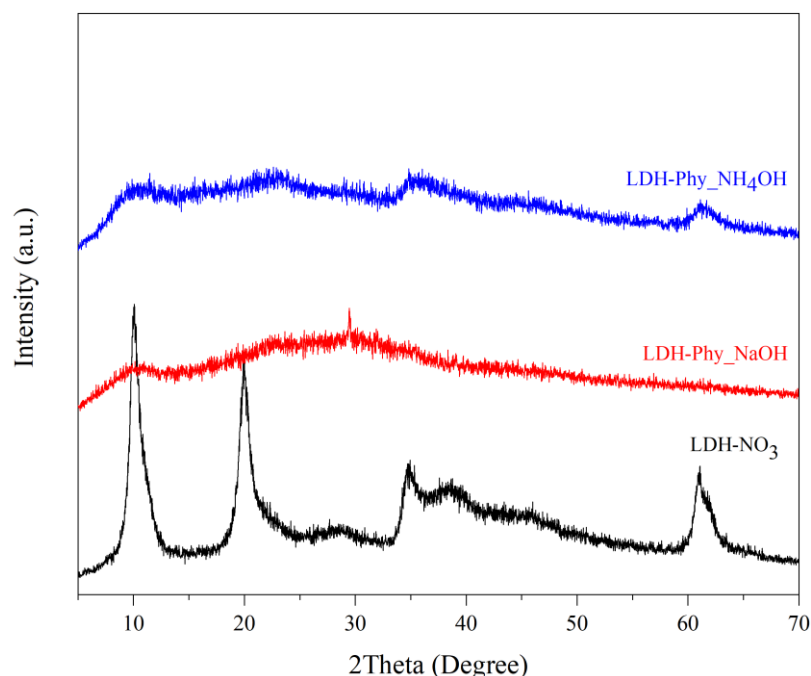


Figure 5.45 The XRD patterns of the pristine LDH and the LDHs-Phy precipitated in the NaOH and the NH_4OH solutions.

Overall, the phytate anions encouraged the exfoliation of metal hydroxide layers in the LDHs with the co-precipitation method. Both the NaOH and the NH_4OH solutions were appropriate for the preparation of LDH-Phy.

5.5.3 Modification with the β -Glycerophosphate

The alternative organophosphate ester compound used as the modifying agent of LDH was a compound with a small molecular size so as to compare the performance with the LDH modified with the larger molecular sizes. This study chose the glycerophosphate (GP) because it consists of a short alkyl chain connecting to the phosphate sodium salts. As the reactant of GP is already in the sodium salt form, the anionic species of GP can produce by the dissolution in the water. The preparing process of GP intercalated LDH (LDH-GP) was not necessary to convert the phosphate compound to its salt form, which was different from the synthesis of the other modified LDHs.

Figure 5.46 showed the XRD patterns of the pristine LDH and the LDH-GP precipitated in the NaOH and the NH_4OH solutions. The results stated that the peak

intensities of the obtained LDHs decreased obviously with the modification of the GP. Furthermore, the lowest reflection peak's degrees shifted slightly to the lower angles for the LDHs-GP at around 9.03° - 9.56° comparing the pristine LDH at 10.09° . As a result, the d-spacing of LDH-GP increased to 0.92-0.98 nm from 0.89 nm for the pristine LDH. The expanded d-spacing of LDH-GP indicated the intercalation of GP anions in the interlayers of LDHs. Nevertheless, the LDH-GP prepared in the NaOH displayed the enlargement of the interlamellar regions more than that in the NH_4OH . Therefore, the LDH-GP should be prepared under the NaOH.

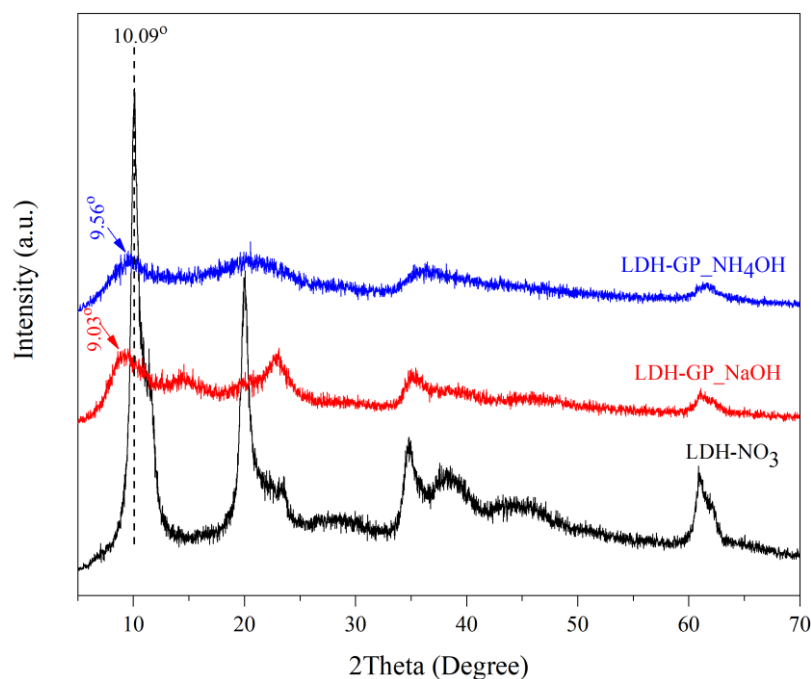


Figure 5.46 The XRD patterns of the pristine LDH and the LDH-GP prepared in the NaOH and the NH_4OH solutions.

With the observation of the FTIR spectra in Figure 5.47, the pure glycerophosphate disodium salt hydrate (GP), the pristine LDH and the LDH-GP were represented in black, red and blue lines, respectively. The glycerophosphate disodium salt hydrate used as the reactant of GP anions showed the stretching vibration bands of C-H at 2938, 2869 and the bending vibration band of C-H at 1461 cm^{-1} , the bands of the P-O-C group at 1117, 1071 and 973 cm^{-1} and the band of P=O group at 1224 cm^{-1} . Due to the water component in the glycerophosphate disodium salt hydrate, its spectrum presented broad bands in the range of $3500\text{-}3000\text{ cm}^{-1}$ and a small band at 1685 cm^{-1} , corresponding to the stretching vibration of OH group and the interaction of H_2O ,

respectively. All of the IR characteristics of GP can be found in the spectrum of the LDH-GP. Moreover, the spectrum also displayed the characteristics of the metal hydroxide layer. These results indicated the presence of the GP anion in the LDH structure.

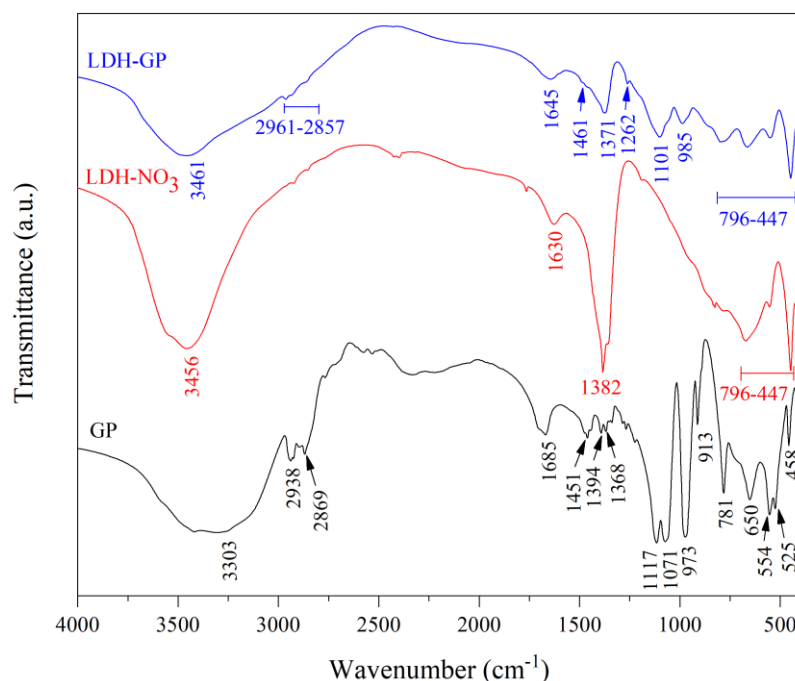


Figure 5.47 The FTIR spectra of the pure GP, the pristine LDH and the LDH-GP.

The obtained results can be summarized that the LDH was intercalated with the GP by using the co-precipitation method. The preparation of LDH-GP under the NaOH provided higher crystallinity and d-spacing than using the NH_4OH as precipitating agents.

5.5.4 Modification with the Diphenyl Phosphate

As described in Section 3.5.2 on the flame retardancy efficiency of LDHs, the BEHP intercalated LDH has been used as the flame retardant for polymers. The chemical structure of BEHP consists of the phosphate ester groups connecting to the two branches of aliphatic hydrocarbons. This study looked for a novel compound of phosphate ester that possesses a structure nearby the BEHP. Therefore, an organophosphate ester compound with an aromatic group was considered for the modification of LDH. The diphenyl phosphate (DPP) was selected since its chemical

structure contains two sides of aromatic groups. It would probably provide the required properties.

The XRD results of the DPP modified LDHs (LDH-DPP) prepared by the co-precipitation using the NaOH solution as the precipitating agents are shown in Figure 5.48. It can be seen that the XRD pattern of LDH-DPP prepared with using NaOH (the red line) differed from the pristine LDH with the intercalation of nitrate anions (the blue line), particular the degree range of 10-25°. There was the broad peak around the degree of 10° for the LDH-DPP prepared. It seemed that the disorder of layer structure in the obtained LDH-DPP.

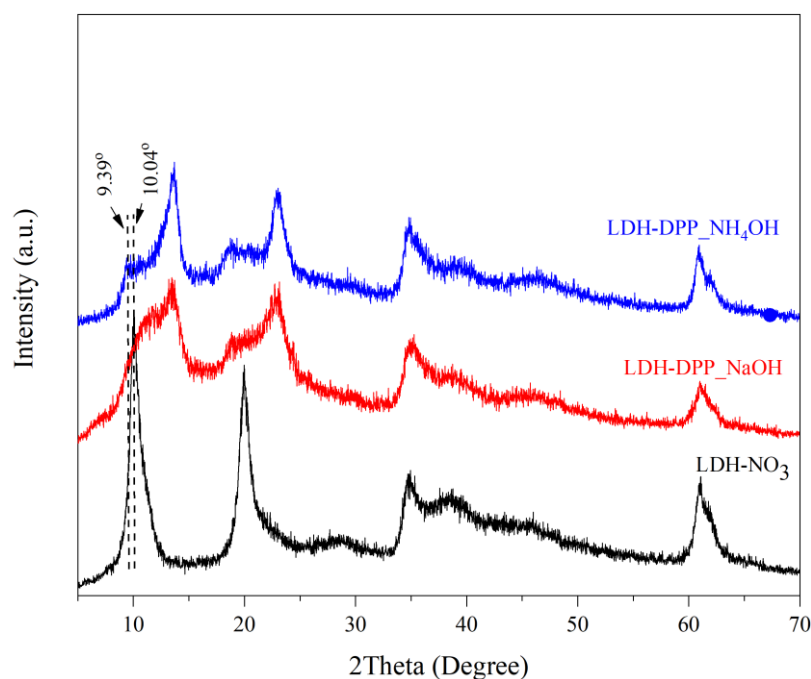


Figure 5.48 The XRD patterns of the pristine LDH and the LDH-DPP prepared in the NaOH and the NH₄OH solutions

Nevertheless, when the LDH-DPP was prepared by using the NH₄OH solution as the precipitating agent, the XRD pattern (the blue line) seemed to a similarity to the LDH-DPP prepared using the NaOH. However, the small reflection peak at 9.39° could be observed in the pattern of the LDH-DPP prepared by using the NH₄OH. This diffraction position shifted to a lower degree than the pristine LDH displayed at 10.04° (black line in Figure 5.48). The calculated d-spacing of DPP modified LDH was 0.94

nm, which was little more than the d-spacing of the pristine LDH (0.88 nm). This result insisted on the intercalation of the DPP in the interlayers of LDH.

In addition, the use of NH_4OH induced more sharp diffraction peaks, corresponding to the increase of crystallinity. As the same reason described in the preparation of LDH-BEHP, it was associated with the dissociation constant of base. The NH_4OH was the weak base, affecting the slow rate of precipitation. Consequently, the growth of crystals was formed slowly leading to the high crystallinity.

To confirm the existence of DPP in the LDH, the LDH-DPP was analysed by the FTIR. Figure 5.49 shows the FTIR spectra of the pure DPP, the pristine LDH and the LDH-DPP, represented in the black, red and blue lines, respectively. The band characteristics of among the hydroxyl groups (around 3400 cm^{-1}), the water interaction (at 1630 cm^{-1}) and the metal-oxide bonds ($800\text{-}450\text{ cm}^{-1}$) in the layers of LDH-DPP have exhibited the same position as the others LDHs, mentioned previously.

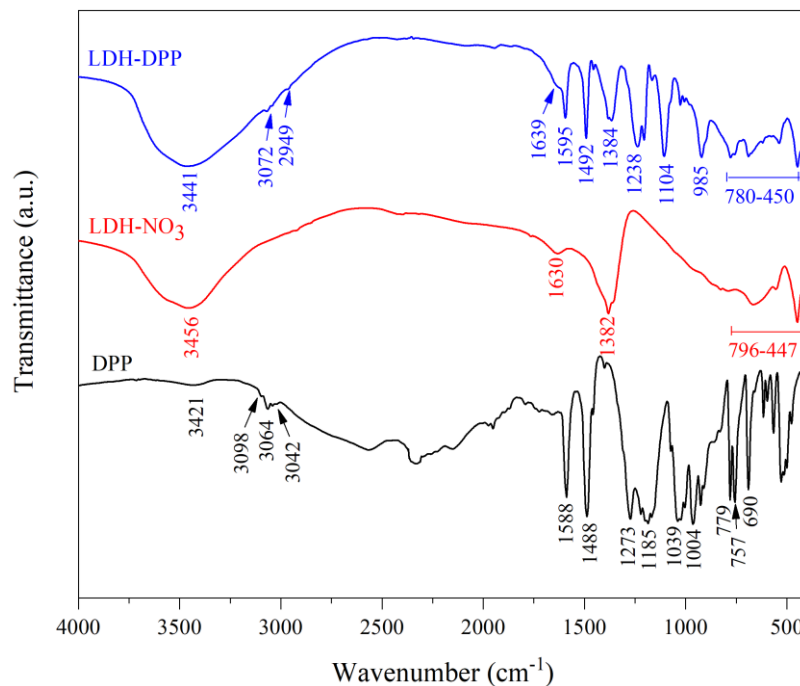


Figure 5.49 The FTIR spectra of the pure DPP, the pristine LDH and the LDH-DPP.

Besides, the IR characteristics of pure DPP can also be observed in the spectrum of the LDH-DPP. The band at 1238 cm^{-1} belonged to the vibration of $\text{P}=\text{O}$, whereas the

bands at 1104 cm^{-1} and 985 cm^{-1} can be assigned the characteristics of the P-O-aromatic group. In the aromatic ring structure, the C-H group showed the bands at 3072 cm^{-1} and 2949 cm^{-1} for the stretching vibration mode and the range band of 900 cm^{-1} to 675 cm^{-1} for the bending vibration mode. For the carbon-carbon bonds' characteristics in the aromatic rings, the C=C group presented at 1595 cm^{-1} , and the C-C group showed at 1492 cm^{-1} and 1384 cm^{-1} .

Overall, the modification of LDH with the DPP, which was the novel LDH, has been successfully prepared by the co-precipitation method. The crystallinity of LDH-DPP prepared in the NH_4OH solution was greater than that in the NaOH.

5.6 Thermal Stability of LDHs

From the above XRD and FTIR results, it established that the modification of LDHs with the organophosphate ester-based compounds have been successfully prepared by the co-precipitation method. The BEHP, DPP and GP were intercalated in the interlayers of the LDHs, whereas the modification of the Phy produced the exfoliation of the lamellae. This study aimed to fire retardancy enhancement of the polymer with the incorporation of modified LDHs. Hence, to approach and understand the flame retardancy mechanisms of the fillers, the thermal decompositions of the modified LDHs were characterised by using the TGA under the N_2 atmosphere.

5.6.1 Thermal Stability of Pristine LDHs

The TGA and derivative curves of the commercial LDH- CO_3 was shown in Figure 5.49. The thermogram displayed two main stages of mass loss in the temperature ranges of $30\text{-}220^\circ\text{C}$ and $220\text{-}800^\circ\text{C}$. In the first region, the mass loss was 15.8%, with the derivative peak at approximately 200°C . It occurred the dehydration of the interlamellar water in the layer structure [5, 40]. Due to the only removal of water, the layered structure of the LDH was not damaged in this stage [40, 41].

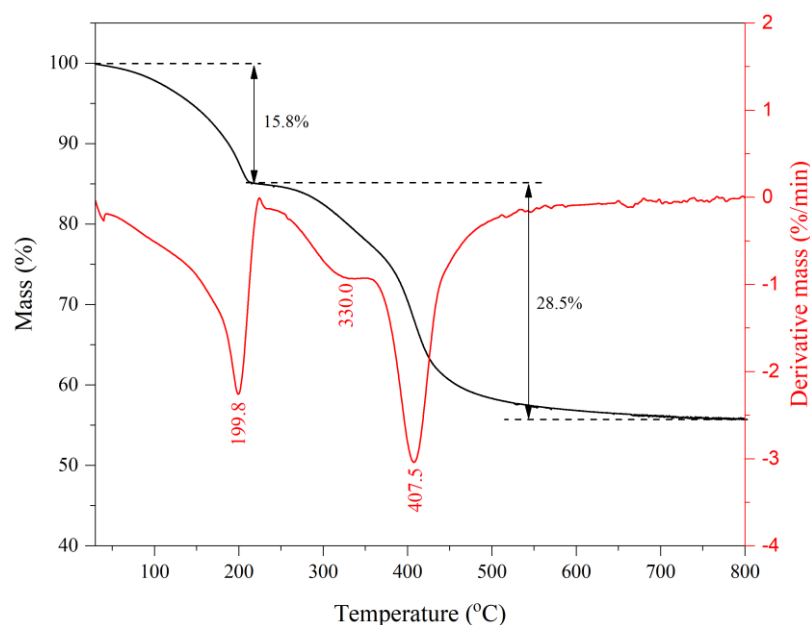


Figure 5.50 The TGA curve and its derivative of LDH-CO₃.

In the second region, the percentage of mass loss was 28.5%. The DTG curve showed the shoulder peak at 330°C and the sharp peak at 407.5°C. This stage was ascribed to the dehydroxylation of metal hydroxide layers. The lower temperature presented the Al-OH decomposition, while the higher temperature displayed the degradation of the Mg-OH [5, 40]. As there was the water removal from the hydroxyl groups in the metal hydroxides, the layer structure of LDH was collapsed in this stage [5, 40, 42]. The consequence of this process was the formation of Al₂O₃ and MgO. A few studies reported the crystalline phases of the metal oxides obtained from the thermal decomposition of LDH-CO₃ [5, 43, 44]. In addition to the dehydroxylation of metal hydroxides, this mass loss stage included the releasing of CO₂ gas due to the decomposition of carbonate anions intercalated in the interlayer gallery of the LDH structure [5, 40].

Likewise, the thermal decomposition of the synthesized LDH-NO₃ provided the three significant regions of mass loss, as exhibits in Figure 5.51. The initial thermal decomposition showed in the range temperature of 30-250°C with the peaks at 123.5°C and 241.0°C. It was ascribed the loss of adsorbed and interlayered water, respectively [33, 45]. The thermal energy used for the loss of water intercalated in the interlayer space was higher than that of water adsorbed on its surface. The total mass loss in this stage was 13.7%.

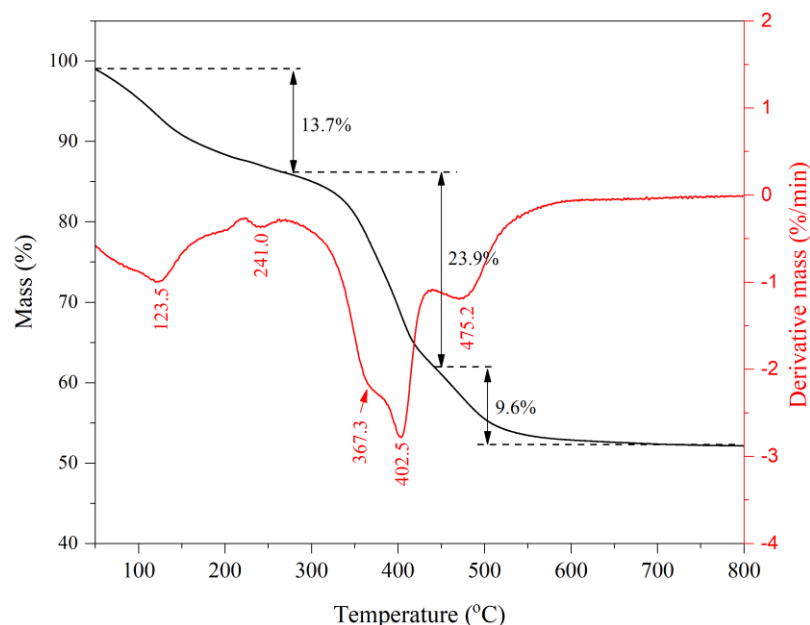


Figure 5.51 The TGA curve and its derivative of LDH-NO₃.

At the second region of mass change, it took place between 250°C and 450°C. The derivative peak in this range presented at 402.5°C, and also showed the shoulder peak at 367.3°C. The percentage of mass loss in this stage was 23.9%. This mass loss was attributed to the thermal degradation of the hydroxide layers, i.e., removing the -OH groups in the metal hydroxides [33, 45]. The final stage in the temperature range of 450-700°C displayed the peak at 475.2°C with the mass loss of nearly 9.6%. Conterosito et al. [45] reported that this stage was the decomposition of nitrate anions intercalated in the interlayered gallery, produced the evolution of NO and NO₂.

5.6.2 Thermal Stability of LDH Modified with Organophosphate Ester-Based Anions

In the case of the organophosphate ester modified LDHs, their thermal decompositions were presented in the blue lines of Figure 5.51-5.54 for the LDH-BEHP, LDH-Phy, LDH-DPP and LDH-GP, respectively. The thermal behaviours of the modified LDHs were also compared with the phosphate ester-based reactants (black line) and the pristine LDH-NO₃ (red lines) in each Figure.

5.6.2.1 Thermal Stability of LDH-BEHP

For the TGA result of the BEHP intercalated LDH (Figure 5.52), the thermogram presented two stages of mass loss. The first stage displayed at the low-temperature range of 30-200°C with the derivative peak at 181.2°C. It was determined the loss of water molecules in the LDHs. At the high temperature of 200-400°C, the peak of mass loss was at 343.7°C and its shoulder peak at 310.7°C.

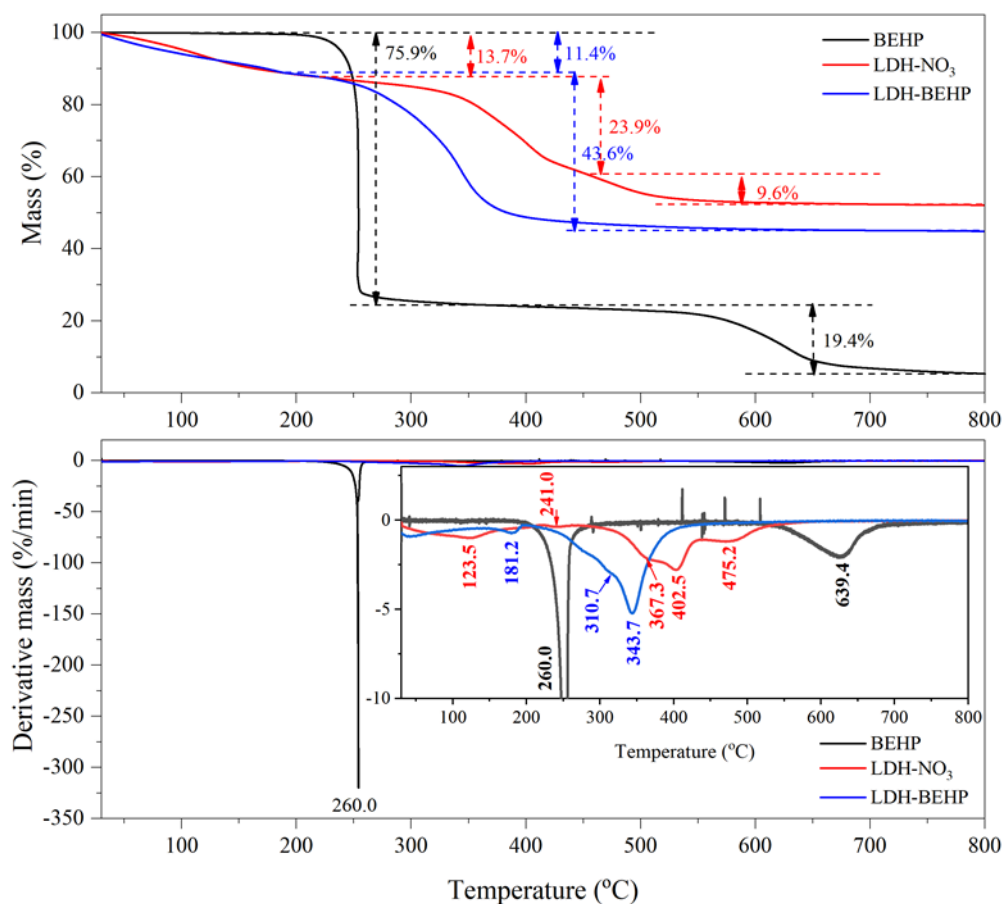


Figure 5.52 The TGA curves and their derivatives of the BEHP, LDH-NO₃ and LDH-BEHP.

In the meantime, the thermogram of pure BEHP between 200°C and 400°C showed the decomposition of the compound. At the same temperature range, besides, the unmodified LDHs provided the dehydroxylation of layered metal hydroxides. Therefore, the mass loss of LDH-BEHP in the range of 200-400°C might result from the degradation of the intercalated BEHP molecules and the metal hydroxides in the layer structure.

At the higher temperature (over 500°C), it was noticeable that the thermogram of LDH-BEHP did not present the mass change; however, there was the mass change of the pure BEHP. The previous section suggested that the high temperature provided the decomposition of the phosphate group, e.g., P_2O_5 in the BEHP. The disappearance of this mass loss in the LDH-BEHP might result from the interaction between the phosphate groups in the BEHP and the metal hydroxide layers, leading to high thermal stability of compounds at the high temperature.

5.6.2.2 Thermal Stability of LDH-Phy

For the TGA of LDH-Phy (Figure 5.53), the thermogram showed two stages of mass loss in the ranges of 30-200°C and over 200°C. Both the stages displayed the derivative peaks at 72.5°C and 331.6°C, respectively. The first stage of decomposition was the loss of water in the LDH. Since the maximum mass loss temperature at this stage was less than 100°C, it indicated the only loss of water adsorbed on the surface of lamellae. This circumstance could be attributed to the exfoliation of layers, causing the adsorption of water molecules on the surface of layers. At the second stage of mass loss, there might be attributed to the thermal decompositions of the phytate intermediated in the interlayers of LDH and the metal hydroxide layers of LDH. This assumption was insisted on the thermograms of phytic acid and the unmodified LDH.

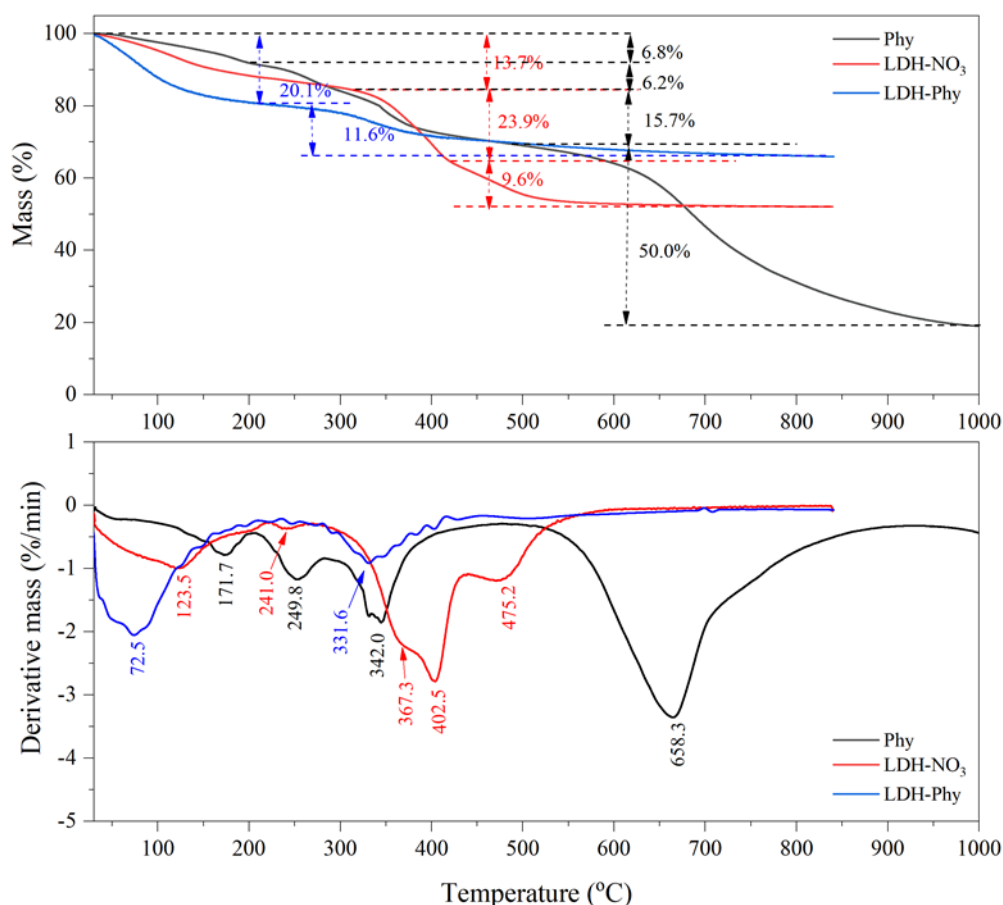


Figure 5.53 The TGA curves and their derivatives of the Phy, LDH-NO₃ and LDH-Phy.

Considering the thermal decomposition of phytic acid reactant, there were four stages of mass loss decomposition in the temperature ranges of 100-200°C, 200-300°C, 300-400°C and 550-1000°C, respectively. The maximum temperature of mass loss in each stage was at 171.7°C, 249.8°C, 342.0°C and 658.3°C. As can be seen from the thermal decomposition study of phytic acid in the previous research, Daneluti and Matos [30] established that the first event related to the loss of water in the phytic acid, the second and third events corresponded to the decomposition of hydrocarbon and hydroxyl groups in the structure of phytic acid, and the last event corresponded to the decomposition of phosphate ester.

By the comparison with the thermograms of LDH-NO₃, it was apparent that the decomposition temperature range of LDH-Phy (250-450°C) occurred in the same decomposition temperatures of the hydrocarbon and hydroxyl groups in phytic acid and the metal hydroxides in the LDH. Furthermore, the thermogram of LDH-Phy had

no phosphate decomposition at around 600°C, which was similar to the LDH-BEHP. This evidence suggested that there were likely to form the strong bond between the phytate and metal oxide.

5.6.2.3 Thermal Stability of LDH-GP

For the LDH-GP, the thermogram in Figure 5.54 presented the four stages of mass loss. The initial stage of mass loss displayed in the range of 100-300°C with the maximum peaks of mass loss at 155.6°C and 275.7°C. This stage was attributed to the evaporation of water in the LDH. Then there was the mass-loss between 300°C and 450°C with the peak of mass loss at 387.5°C. It might be the decomposition of hydrocarbon in the GP and the dehydroxylation of layered metal hydroxides in the LDH. The last decomposition process took place at 450-550°C, which was the maximum mass loss rate at 474.1°C. This stage might be the decomposition of hydrocarbon compounds formed in the previous stage.

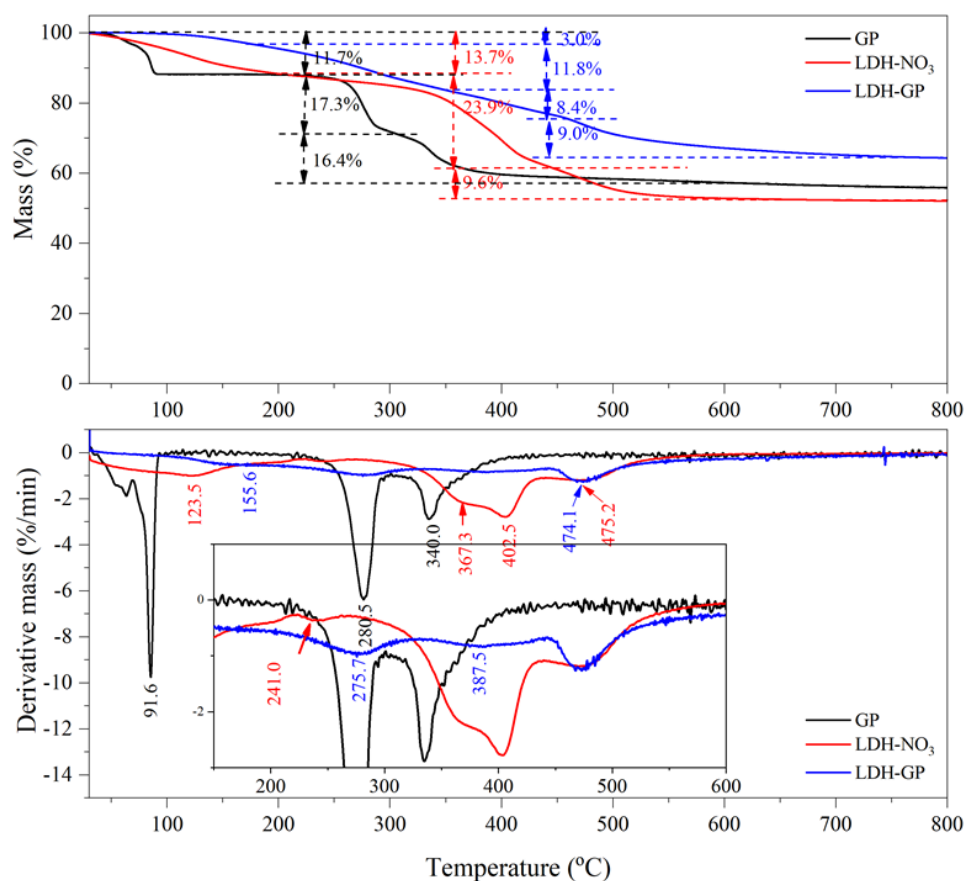


Figure 5.54 The TGA curves and their derivatives of the GP, LDH-NO₃ and LDH-GP.

5.6.2.4 Thermal Stability of LDH-DPP

In the case of LDH-DPP, the three stages of mass loss were displayed in Figure 5.55. The early thermal decomposition stage (30-200°C) provided the volatile of physically adsorbed and intercalated water molecules. It was the same evaporation as the other modified LDHs. The further stage was placed at 200-260°C, matching the decomposition of hydrocarbons in the DPP reactant. At the temperature of 260-500°C, there might be provided with the mass loss of metal hydroxides and the phosphate groups in the DPP.

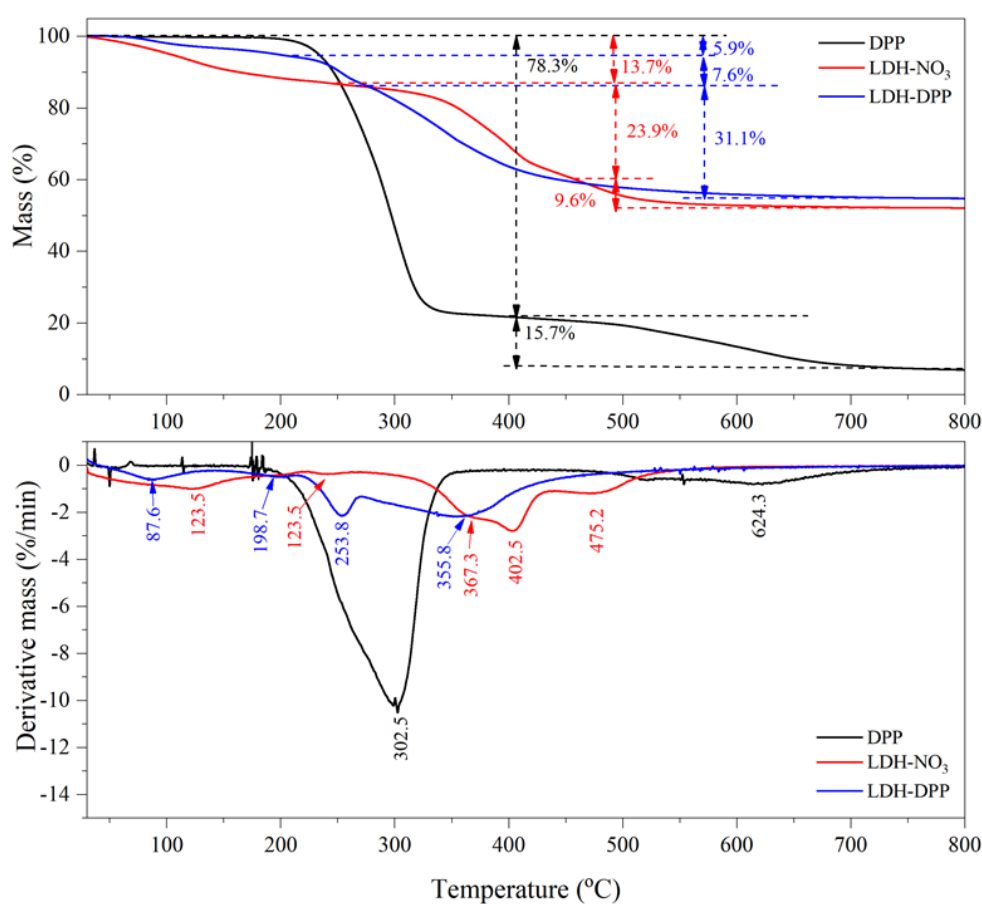


Figure 5.55 The TGA curves and their derivatives of the DPP, LDH-NO₃ and LDH-DPP.

5.6.2.5 Comparison of Thermal Stability in Different LDHs

By comparing the thermal stability of different modified-LDHs, as showed in Figure 5.56, it can be seen that the organic compounds used for the modification of LDHs had a significant influence on the thermal decomposition of LDHs. At the first region of 30-250°C, it was ascribed to the mass loss of physical adsorbed and interlayer water. The total dehydration of the pristine LDHs completed in this stage around at 250°C; however, the modified LDHs took place below 200°C. The results stated that the water in the modified LDHs could be more easily removed than in the pristine LDH. The organophosphate compounds used as modifying agents can reduce the strong interaction of water molecules with hydroxide layers in the interlayer region due to the expansion of gallery space [24, 46].

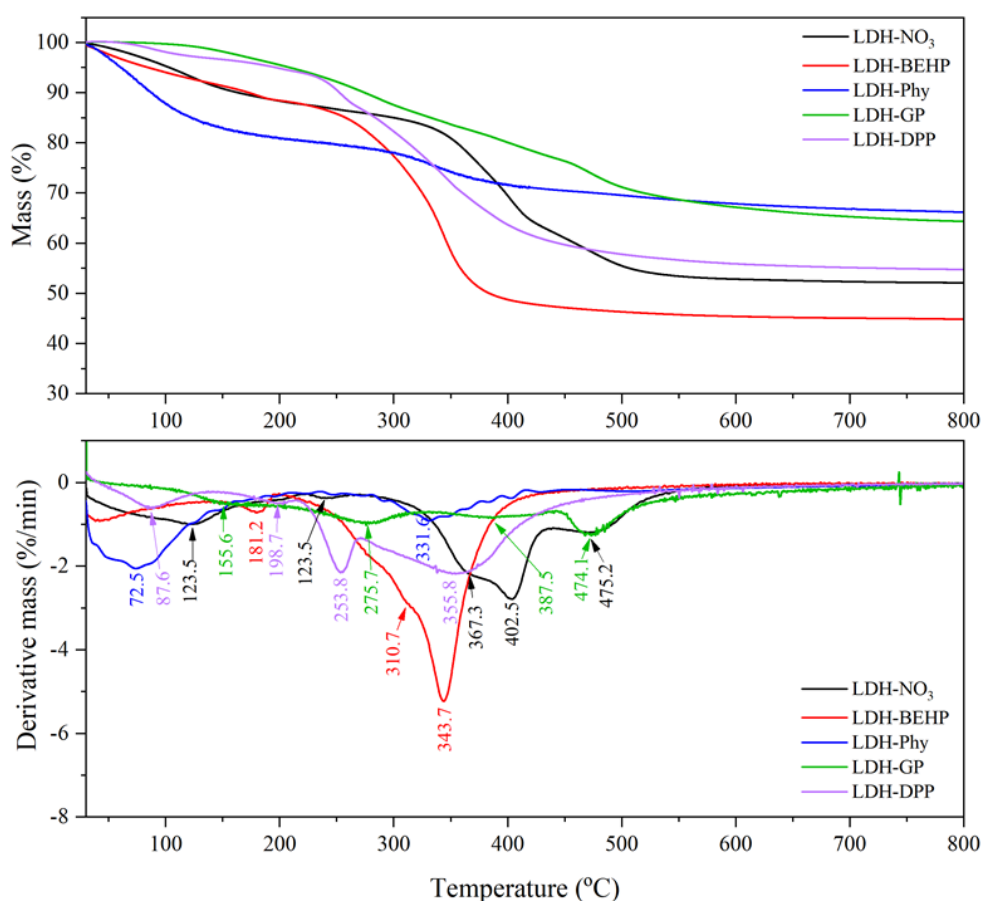


Figure 5.56 The TGA curves and their derivatives of the pristine LDH and the LDHs modified with BEHP, Phy, GP and DPP.

The second stage of mass loss (250-450°C) was attributed to the decomposition of modifying organic compounds and layered metal hydroxides. The maximum decomposition rate peaks of organophosphate-modified LDHs occurred at lower temperatures than that of pristine LDH since the phosphates generated during the heating of the modified LDHs can accelerate the decomposition. The consequence of this was the formation of decomposing residues at the lower temperature. It was a positive result for the flame-retardant application because the char residues can play a role in the barrier so as to protect the diffusion of heat and combustible gas to the burning area.

Considered the initial decomposition temperature of 10% mass loss, the temperature of LDHs increased with the modification of organophosphate compounds, excluding the LDH-Phy. It was implied that the thermal stabilities of LDHs could improve when the LDHs were modified with the organic compounds. Moreover, the modification of LDHs promoted the increase of char content at 800°C. Table 5.13 presented the decomposition temperatures at 10% mass loss and the char contents at 800°C of the pristine LDH and the phosphate modified LDHs.

Table 5.13 The charred yield of LDHs

Sample	Temperature at 10% mass loss (°C)	Char residues at 800°C (%)
LDH-NO ₃	164.0	52.1
LDH-BEHP	173.2	44.9
LDH-Phy	87.1	66.2
LDH-GP	274.7	64.4
LDH-DPP	252.4	54.8

Overall, the study of thermal behaviours of LDHs indicated that the adsorbed and interlayered water and the layer metal hydroxides were evaporated by the dehydration process. For the pristine LDH, the elimination of water in the LDH occurred below 250°C and the dehydration of layer hydroxides took place in the range of 250-450°C. As a result, the metal hydroxides can convert to their oxide forms. The nitrate anions intercalated in the interlayers decomposed at over 450°C.

In the case of the organophosphate modified LDHs, both the water and layered metal hydroxides degraded at the same temperature range as the pristine LDH. However, the curves shifted to the lower temperature due to the decomposition of organophosphate-based compounds at low temperatures. The TGA curves indicated that the thermal stability and the char contents of LDHs had a trend of increase with the modification of organic compounds. Due to the increase of char residues, it was the advantage of flame retardants.

5.7 Structural Models of LDHs

The structural arrangement of metal hydroxide layers, anions and water in the obtained LDHs by using the XRD, FTIR and TGA results. It is well known that the basic structure of LDH consists of the layers of metal hydroxides with the intercalation of anions and water in the interlayer space. The perception of the LDH arrangement can encourage an understanding of the compatibility of polymers and LDHs. The difference in structures of anionic compounds affected the orientation of anions within the LDH structure.

From the XRD results, they provided the d-spacing data of the LDHs. The d-spacing is the total distance from one layer to one interlayer. The distance of interlayer space is determined with the thickness of the metal hydroxide layer and the molecular size, and the orientation of anionic compounds [19, 24]. According to the previous literature, the thickness of the layer containing the Mg and Al hydroxides is 0.48 nm [6]. Thus, the layer thickness's subtraction from the d-spacing contributed to the interlayer distance, as shown in Table 5.14.

Table 5.14 The d-spacing and gallery height of the pristine LDH and the organophosphate modified LDHs.

Sample	d-spacing (nm)	Gallery height (nm)
LDH-NO ₃	0.88	0.40
LDH-BEHP	1.10	0.62
LDH-Phy	NA	NA
LDH-GP	0.98	0.50
LDH-DDP	0.94	0.46

In this study, the molecule sizes of organophosphate anions were estimated by measuring the length of simulated molecules. An Avogadro program was a software used for the geometry simulation of the compounds and the measurement of molecular sizes. The prediction of anionic orientation used both the distances of interlayer galleries and the sizes of anionic compounds.

5.7.1 Structural Model of Pristine LDH

For the pristine LDH-NO₃, the distances of d-spacing and interlayer space were 0.88 nm and 0.40 nm, respectively. From the simulation of nitrate structure, it provided the molecular size of 0.25 nm. The simulated nitrate structure presented in Figure 5.57. Since the gallery height of LDH was almost twice as distance as the size of intercalating anions, the nitrate molecules might orient in the double layers with the slight tilt of the molecules. The prior study suggested that the nitrate anions intercalated in the interlayers and interacted to the layers with inclining at 70° [47]. Despite the FTIR and the TGA results, they indicated the water existed both the outside and inside of LDH. The speculated orientation of LDH-NO₃ was presented in Figure 5.58.

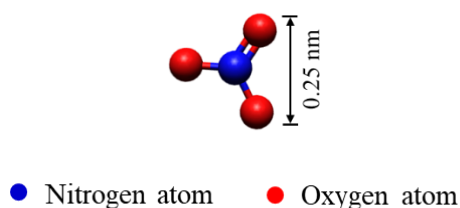


Figure 5.57 The simulated structure of nitrate anion.

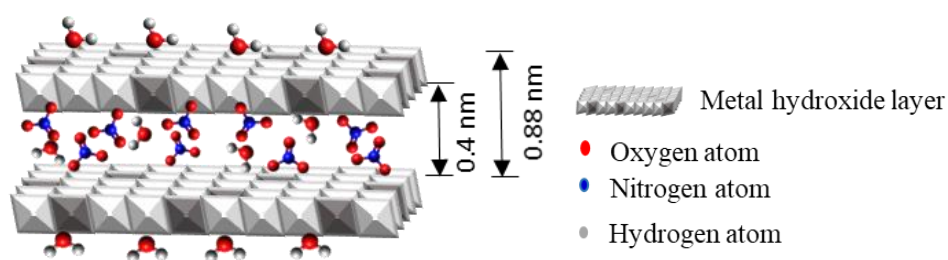


Figure 5.58 The possible structural model of LDH-NO₃ speculated from the molecule size of nitrate simulated by the Avogadro software and the d-spacing of LDH-NO₃ determined by the XRD.

5.7.2 Structural Model of LDH-BEHP

In the case of LDH-BEHP, the gallery height (0.62 nm) was nearly the measured size of BEHP (0.64 nm). The configuration of the BEHP anion was simulated and displayed in Figure 5.59. It can be seen that the distance of the interlamellar space was almost equal to the size of the intercalated anion. Therefore, the molecules of BEHP might arrange in a monolayer form. This assumption related to the study of Costa et al. [24]. The TGA curve presented the water adsorbed on the surface of layers and interacted between the lamellae. From all experimental results, the structural model of LDH-BEHP was proposed in Figure 5.60.

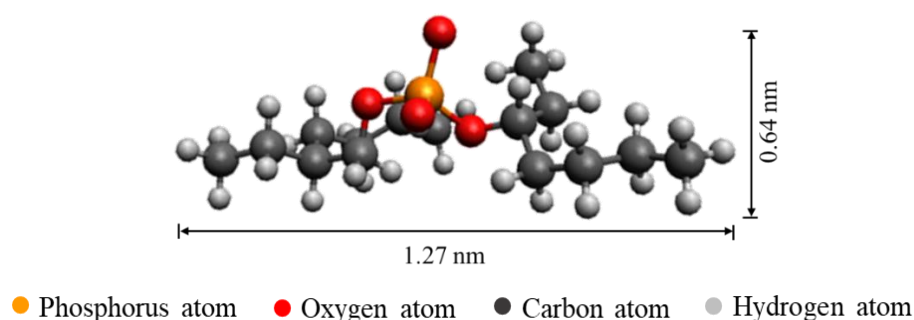


Figure 5.59 The simulated structure of BEHP anion

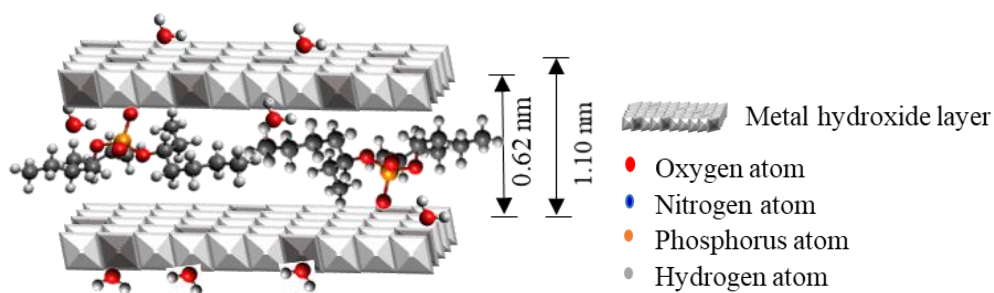


Figure 5.60 The possible structural model of LDH-BEHP speculated from the molecule size of BEHP simulated by the Avogadro software and the d-spacing of LDH-BEHP determined by the XRD.

5.7.3 Structural Model of LDH-Phy

As the XRD pattern of LDH-Phy provided the amorphous characteristic, the layers of metal hydroxides were exfoliated with the Phy molecules. This circumstance also caused the adsorption of much water on the surface of layers. It associated with mass

loss at the below 100°C, corresponding to the evaporation of adsorbed water. The configuration of Phy anion and the LDH-Phy model were proposed in Figure 5.61 and 5.62, respectively.

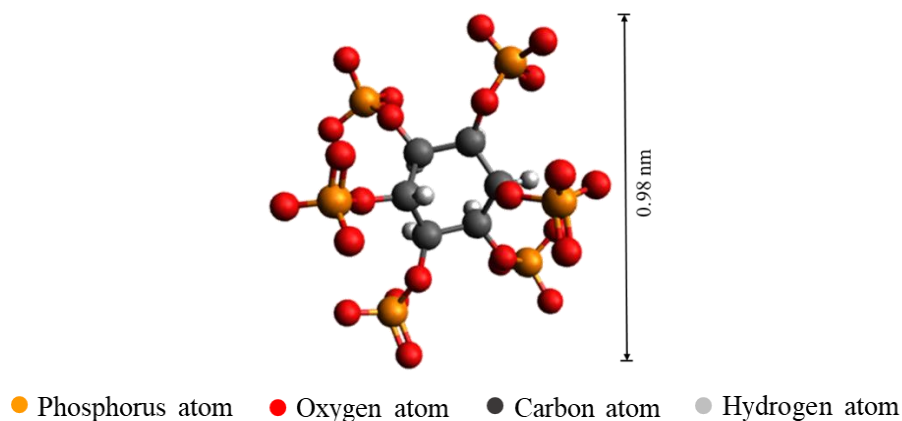


Figure 5.61 The simulated structure of Phy anion.

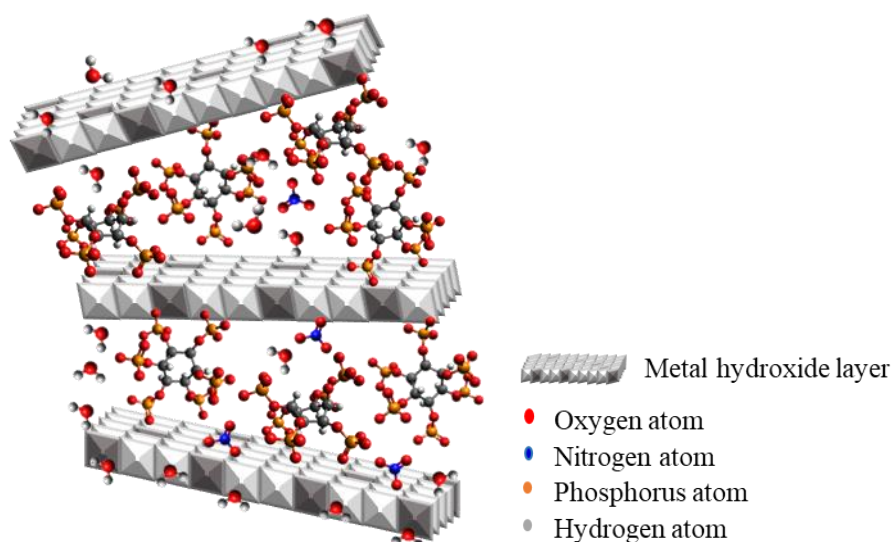


Figure 5.62 The possible structural model of LDH-Phy speculated from the molecule size of nitrate simulated by the Avogadro software and the d-spacing of LDH-Phy determined by the XRD.

5.7.4 Structural Model of LDH-GP

Meanwhile, the LDH-GP provided the gallery height of 0.50 with the GP length of 0.62 nm. Figure 5.63 showed the GP configuration. The gallery height was narrower than the net length of GP. Thus, the GP molecule was likely to intercalate in the

interlayers in the monolayer orientation with the incline of GP. The arrangement of LDH-GP is illustrated in Figure 5.64.

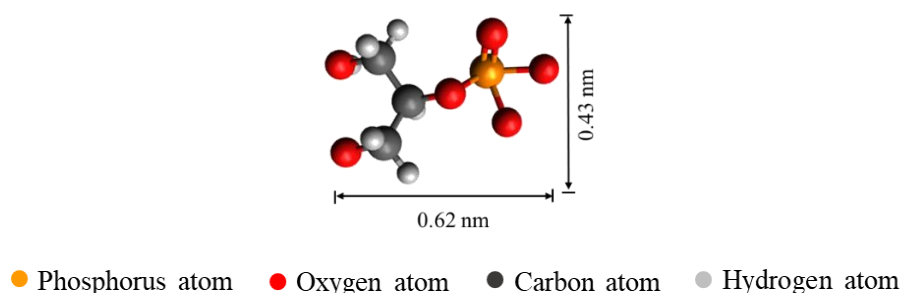


Figure 5.63 The simulated structure of GP anion.

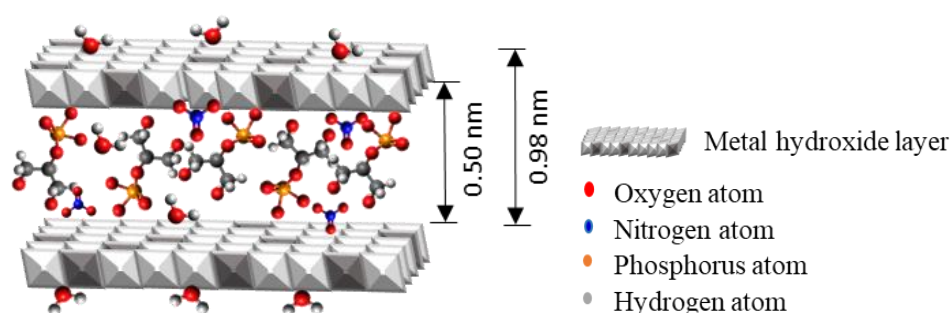


Figure 5.64 The possible structural model of LDH-GP speculated from the molecule size of nitrate simulated by the Avogadro software and the d-spacing of LDH-GP determined by the XRD.

5.7.5 Structural Model of LDH-DPP

For the first novel modified LDHs, the modification of DPP provided the interlamellar space of 0.46 nm. The length of the DPP was 0.49 nm, measured from the simulated configuration in Figure 5.65. Both the interlayer gallery and the DPP size were almost equivalent. The results can be believed that the DPP might arrange the monolayer form in the gallery between the layers. Additionally, there was the adsorption and the intercalation of water in the structures of the LDH-DPP. All the evidence could be used to simulate the LDH-DPP, as presented in Figure 5.66.

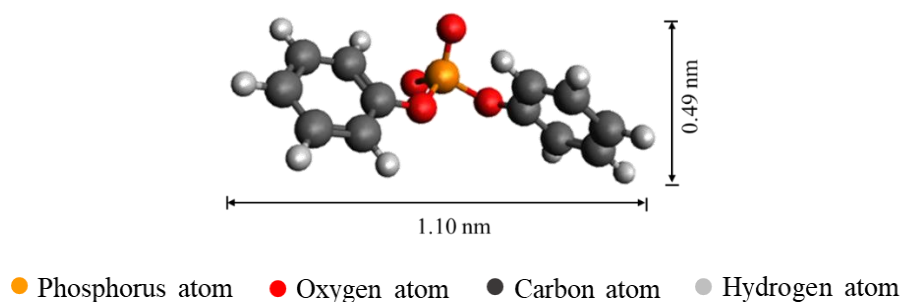


Figure 5.65 The simulated structure of DPP anion.

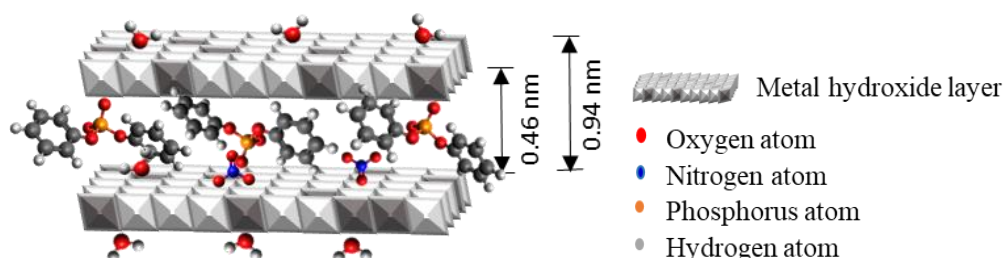


Figure 5.66 The possible structural model of LDH-DPP speculated from the molecule size of nitrate simulated by the Avogadro software and the d-spacing of LDH-DPP determined by the XRD.

Overall, the proposed structural models of the modified LDHs contained the layers of Mg and Al hydroxides with the intercalation of the organophosphate-based anions (BEHP, GP and DPP). Among the intercalating anions were in the monolayer orientation. For the LDH-Phy, the lamellae were separate entirely due to the exfoliation. All the modified LDHs were the component of water adsorbed on the surface of the layer and intercalated in the interlayer, excluding the modification of Phy. The LDH-Phy possessed only the physical adsorption of water. The speculated models can be used for discussion in the preparation of polymer nanocomposites.

5.8 Particle Sizes of LDHs

According to the TGA results, the organophosphate ester-modified LDHs provided the high thermal stability and the increase of residue content. They would be expected to contribute to the high efficiency of flame retardancy for polymers. To prove this assumption, the epoxy resin/LDH nanocomposites would be prepared and tested the flammability.

One of the parameters having a crucial impact on the properties and the blending process of the composites is particle size of nanoparticles. Several studies have been attempted to control the obtained nanoparticle size of LDHs in the synthesis process by controlling either the dropping rate of the metal salt solution to the base solution or the aging process. However, after the drying process, the particulate dimension of obtained LDHs was micro-sized [48]. If the micro-sized LDHs were incorporated in to the polymer matrix, it may result in the significant decrease of mechanical properties and thermal stability for the polymer composites. For the reason of this assumption, the large particulates have low surface area, affecting the reduction of interaction with the polymer matrix. This circumstance induced the decrease of properties for polymer composites. On the other hand, the small particles having high surface area can make more interaction with the polymer matrix than the large particles. To approach the high performance of properties, it was necessary to reduce the particle size of LDHs by grinding process.

Currently, the common method employed for the reduction of particle size is milling. There are a variety of milling techniques such as shaker milling, planetary ball milling and attrition milling. This study selected the attrition mill for the size reduction due to the less operating time. The attrition comprises the stationary tank for the sample, grinding ball and media solution and the rotating impellers. The rotation of impellers at high-speed leads to the particle collision between balls, between balls and wall of container and among balls, shaft, and impellers. As a result, the particles are deformed and fractured, generating the reduction of particle size [49, 50].

In this study, both the commercial LDH and the prepared LDHs were crushed by the attrition mill, and then they would be analyzed the particle size. For the particle size of commercial LDH as showed in Figure 5.67, it can be seen that the distribution curves of the MG70 (commercial LDH-CO₃) transferred to downward size classes with the milling at different times, indicating the reduction of particle sizes with the milling. The grinding for 1 and 2 h exhibited only one distribution at the high-volume density. Meanwhile, the grinding for 3 h appeared the two distributions with the high and low volume densities. It may occur the agglomeration of particles during the long milling time.

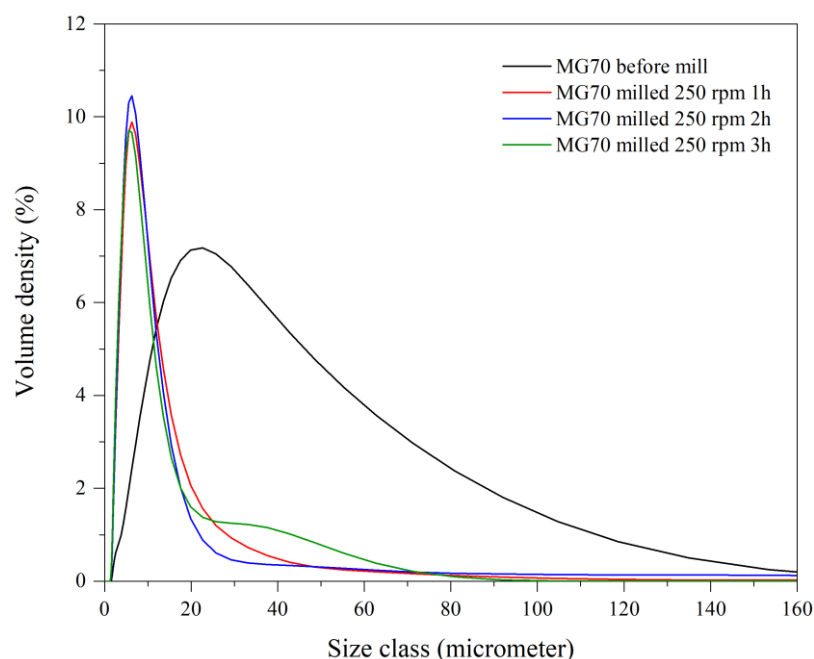


Figure 5.67 The particle size distribution curves of Pural MG70 before and after the milling at the rotating speed of 250 rpm and the different milling times.

Typically, the peak of the distribution curve represents the most frequent size in the sample [51]. The most particle size of MG70 before the milling was 21.7 μm . When the MG70 was milled with the speed of 250 rpm for 1, 2 and 3 h, the milled particle size was 6.28 μm , 6.22 μm and 5.62 μm , respectively.

From the distribution curves, the particle size distributions of the samples at 10% (D_{10}), 50% (D_{50}) and 90% (D_{90}) were measured as presented in Table 5.15. Considering the same distribution percentage, the milled LDH- CO_3 were less than the unmilled LDH- CO_3 without the grinding. The size distribution values of milled LDH- CO_3 were no significant difference with increasing the grinding times. However, the different grinding times affected the width of the size distribution (span). The span can be calculated by $\frac{D_{90}-D_{10}}{D_{50}}$. It was found that the grinding at 250 rpm for 2 h provided the lowest width of distribution, indicating the narrow size class. Therefore, the milling of the LDH sample at 250 rpm for 2 h was probably sufficient for particle size reduction.

Table 5.15 The particle size distributions and their width of the Pural MG70 before and after the grinding with the rotating speed of 250 rpm and the different milling times.

Time of milling (h)	D ₁₀ (μm)	D ₅₀ (μm)	D ₉₀ (μm)	Span
0	6.94	21.7	62.4	2.56
1	2.82	6.37	16.0	2.07
2	3.03	6.33	14.2	1.76
3	2.88	6.23	17.5	2.35

Likewise, the size distribution of MG70 ground with the higher rotating speed at 400 rpm for 1 and 2 h decreased obviously, comparing to the unmilled sample. Figure 5.68 presents the curves of particle size distribution of MG70 both before and after grinding at 400 rpm. At the grinding for 1 h, the curve showed the one broad peak with the highest frequently size of 7.06 μm, which was lower than that of 21.7 μm for the unmilled sample. Besides, there was a reduction of size distributions, as reported in Table 5.16. These results supported the reduction of particle sizes with the milling.

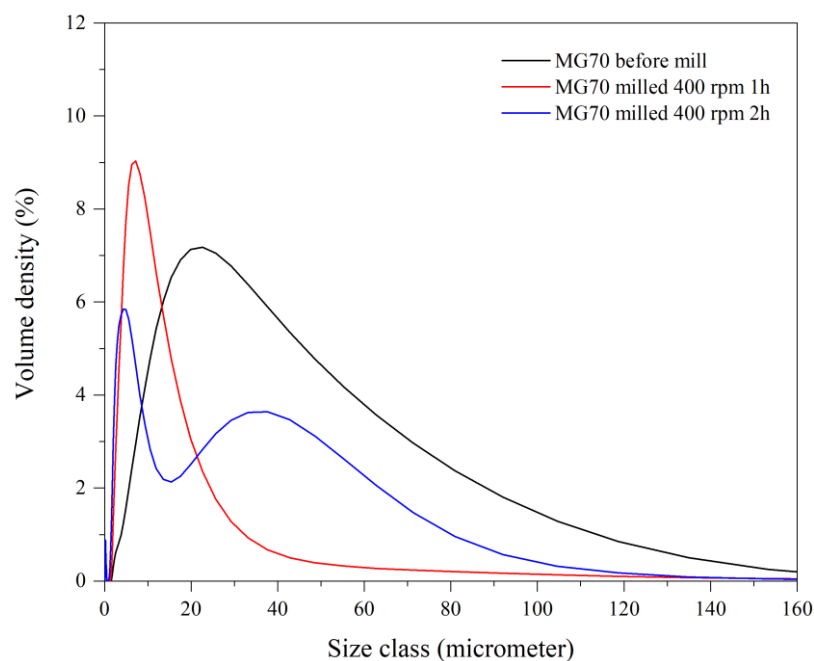


Figure 5.68 The particle size distribution curves of MG70 milled at 400 rpm

Table 5.16 The size distribution in the different total percentages and the width of size distribution of MG70 before and after the milling at 400 rpm for 1 and 2 h.

Time of milling (h)	D ₁₀ (μm)	D ₅₀ (μm)	D ₉₀ (μm)	Span
0	6.94	21.70	62.40	2.56
1	3.24	7.44	19.10	2.13
2	1.92	6.40	44.70	6.68

Nevertheless, the milling of MG70 at 400 rpm for 2 h presented two broad peaks in the distribution curves (the blue line in Figure 5.64). The peak of 2 h with the higher volume was 4.46 μm, which was less than the milling for 1 h. It indicated the reduction of particle size with increasing the grinding time. Meanwhile, the lower volume peak was 35.39 μm, which was more than that of the un-milled MG70. It stated that some particle agglomerated from the milling at the high rotating speed and the long grinding time. Considering the width of size distribution, the milling for 2 h was higher than that for 0 and 1 h. It can be summarized that the grinding of the sample with the high speed and the long time provided both the size reduction and the agglomeration of particles.

The above results found that the optimum conditions for the sample size reduction were the grinding with the attrition mill at 250 rpm for 2 h. It provided the fine particle and the narrow size distribution. Hence, the other modified LDHs were reduced the particles by using the same milling conditions of MG70.

5.9 Summary

Overall, the preparation of Mg/Al LDHs modified with the BEHP, Phy, DPP, or GP had been successful in this study. The characterizations of XRD and FTIR insisted on the existences of the organophosphate ester-based compounds in the LDH structures. Furthermore, the thermal stabilities of LDHs were enhanced with the modification of the organic compounds. The char residues also increased in most of the modified LDHs. These circumstances were the excellent characteristics of flame retardants. From the characterized results, they were used for the speculations of modified LDH

structures. All the LDHs were reduced the particle sizes by the attritor at 250 rpm for 2 h. The tiny particle size of LDH samples would be applied to the epoxy resin to study the effect of the LDHs on the polymers, especially the flammability. The properties of composites would be discussed in the further chapters.

References

- [1] T. L. Brown, H. LeMay, B. Bursten, C. Murphy, P. Woodward, S. Langford, M. Sheppard, A. George and D. Sagatys, "Chemistry: The Central Science", Pearson, Australia, 2014
- [2] Y. Yang, X. Zhao, Y. Zhu and F. Zhang, "Transformation Mechanism of Magnesium and Aluminum Precursor Solution into Crystallites of Layered Double Hydroxide", 2012, **24**, 81-87
- [3] A. Eliseev, A. Lukashin, A. Vertegel, V. Tarasov and Y. Tret'yakov, "A Study of Crystallization of Mg-Al Double Hydroxides", Dokl. Chem., 2002, **387(4)**, 339-343
- [4] J. Shin, C. J. Choi, T. H. Kim and J. M. Oh, "Phase Transformation from Brucite to Highly Crystalline Layered Double Hydroxide through a Combined Dissolution-Reprecipitation and Substitution Mechanism", Crys. Growth Des., 2018, **18(9)**, 5398-5405
- [5] F. Millange, R. I. Walton and D. O'Hare, "Time-Resolved in situ X-ray Diffraction Study of the Liquid-Phase Reconstructim of Mg-Al-Carbooaate Hydrotalcite-Like Compounds", J. Mater. Chem., 2000, **10(7)**, 1713-1720
- [6] D. G. Evans and R. C. T. Slade, "Structural Aspects of Layered Double Hydroxides", in "Structure and Bonding", eds. D.M.P Mingos, Springer, Germany, 2006, 1-87
- [7] F. Cavani, F. Trifirò and A. Vaccari, "Hydrotalcite-Type Anionic Clays: Preparation, Properties and Applications", Catalysis Today, 1991, **11(2)**, 173-301
- [8] K.-H. Goh, T.-T. Lim and Z. Dong, "Application of Layered Double Hydroxides for Removal of Oxyanions: A Review", Water Res., 2008, **42(6)**, 1343-1368

- [9] W. Yang, Y. Kim, P. K. T. Liu, M. Sahimi and T. T. Tsotsis, "A Study by in situ Techniques of the Thermal Evolution of the Structure of a Mg-Al-CO₃ Layered Double Hydroxide", *Chem. Eng. Sci.*, 2002, **57(15)**, 2945-2953
- [10] T. T. X. Hang, T. A. Truc, N. T. Duong, P. G. Vu and T. Hoang, "Preparation and Characterization of Nanocontainers of Corrosion Inhibitor Based on Layered Double Hydroxides", *Appl. Clay Sci.*, 2012, **67-68**, 18-25
- [11] J. He, M. Wei, B. Li, Y. Kang, D. G. Evans and X. Duan, "Preparation of Layered Double Hydroxides", in "Structure and Bonding", eds. D. M. P. Mingos, Springer, Germany, 2006, pp 89-119
- [12] A. Burrows, "Chemistry: Introducing Inorganic, Organic and Physical Chemistry", Oxford University Press, Oxford, 2017
- [13] E. R. Christensen, "Physical and Chemical Processes in the Aquatic Environment", Wiley, 2014
- [14] G. W. Brindley and S. Kikkawa, "Formation of Mixed Mg Al Hydroxides with Interlayer Nitrate and Carbonate Ions", *Thermochim. Acta*, 1978, **27(1-3)**, 385-386
- [15] J. Olanrewaju, B. L. Newalkar, C. Mancino and S. Komarneni, "Simplified Synthesis of Nitrate form of Layered Double Hydroxide", *Mater. Lett.*, 2000, **45(6)**, 307-310
- [16] K. Li, N. Kumada, Y. Yonesaki, T. Takei, N. Kinomura, H. Wang and C. Wang, "The pH Effects on the Formation of Ni/Al Nitrate form Layered Double Hydroxides (LDHs) by Chemical Precipitation and Hydrothermal Method", *Mater. Chem. Phy.*, 2010, **121(1)**, 223-229
- [17] A. Seron and F. Delorme, "Synthesis of Layered Double Hydroxides (LDHs) with Varying pH: A Valuable Contribution to the Study of Mg/Al LDH Formation Mechanism", *J. Phy. Chem. Solid.*, 2008, **69(5)**, 1088-1090
- [18] A. Ay, B. Zumreoglu-Karan, A. Temel and L. Mafra, "Layered Double Hydroxides with Interlayer Borate Anions: A Critical Evaluation of Synthesis Methodology and pH-Independent Orientations in Nano-Galleries", *Appl. Clay Sci.*, 2011, **51(3)**, 308-316
- [19] M. Meyn, K. Beneke and G. Lagaly, "Anion-Exchange Reactions of Layered Double Hydroxides", *Inorg. Chem.*, 1990, **29(26)**, 5201-5207

- [20] J. H. Choy, S. Y. Kwak, J. S. Park, Y. J. Jeong and J. Portier, "Intercalative Nanohybrids of Nucleoside Monophosphates and DNA in Layered Metal Hydroxide", *J. Am. Chem. Soc.*, 1999, **121(6)**, 1399-1400
- [21] N. V. Malanova, V. V. Korobochkin and V. I. Kosintsev, "The Application of Ammonium Hydroxide and Sodium Hydroxide for Reagent Softening of Water", *Procedia chem.*, 2014, **10**, 162-167
- [22] P. K. Kaul, A. J. Samson, G. T. Selvan, I. Enoch and P. M. Selvakumar, "Synergistic Effect of LDH in the Presence of Organophosphate on Thermal and Flammable Properties of an Epoxy Nanocomposite", *Appl. Clay Sci.*, 2017, **135**, 234-243
- [23] M. Bouraada, M. Lafjah, M. S. Ouali and L. C. de Menorval, "Basic Dye Removal from Aqueous Solutions by Dodecylsulfate- and Dodecyl Benzene Sulfonate-Intercalated Hydrotalcite", *J. Hazard. Mater.*, 2008, **153(3)**, 911-918
- [24] F. R. Costa, A. Leuteritz, U. Wagenknecht, D. Jehnichen, L. Häußler and G. Heinrich, "Intercalation of Mg-Al Layered Double Hydroxide by Anionic Surfactants: Preparation and Characterization", *Appl. Clay Sci.*, 2008, **38(3-4)**, 153-164
- [25] S. Lv, Y. Yuan and W. Shi, "Strengthening and Toughening Effects of Layered Double hydroxide and Hyperbranched Polymer on Epoxy Resin" *Prog. Org. Coat.*, 2009, **65(4)**, 425-430
- [26] N. K. Julianti, T. K. Wardani, I. Gunardi and A. Roesyadi, "Effect of Calcination at Synthesis of Mg-Al Hydrotalcite Using Co-Precipitation Method", *J. Pure Appl. Chem. Res.*, 2017, **6(1)**, 7-13
- [27] F. Delorme, A. Seron, M. Bizi, V. Jean-Prost and D. Martineau, "Effect of Time on the Reconstruction of the $Mg_4Al_2(OH)_{12}CO_3 \cdot 3H_2O$ Layered Double Hydroxide in a Na_2CO_3 solution", *J. Mater. Sci.*, 2006, **41(15)**, 4876-4882
- [28] H. E. Baumgarten and R. A. Setterquist, "Pyrolysis of Alkyl Phosphates," *J. Am. Chem. Soc.*, 1957, **79(10)**, 2605-2608
- [29] M. Zięzio, B. Charmas, K. Jedynek, M. Hawryluk, and K. Kucio, "Preparation and Characterization of Activated Carbons Obtained from the Waste Materials Impregnated with Phosphoric Acid(V)", *Appl. Nanosci.*, 2020, **10(12)**, 4703-4716

- [30] A. L. M. Daneluti and J. d. R. Matos, "Study of Thermal Behavior of Phytic Acid", *Braz. J. Pharm. Sci.*, 2013, **49(2)**, 275-283
- [31] P. Owczarz, A. Rył, and J. Sowiński, "Influence of Glycerophosphate Salt Solubility on the Gelation Mechanism of Colloidal Chitosan Systems", *Int J Mol Sci*, 2021, 22(8), 4043
- [32] S. Gómez-Fernández, L. Ugarte, C. Peña-Rodriguez, M. Zubitur, M. Á. Corcuera and A. Eceiza, "Flexible Polyurethane Foam Nanocomposites with Modified Layered Double Hydroxides", *Appl. Clay Sci.*, 2016, **123**, 109-120
- [33] L. Wang, S. Su, D. Chen and C. A. Wilkie, "Variation of Anions in Layered Double Hydroxides: Effects on Dispersion and Fire Properties", *Polym. Degrad. Stabil.*, 2009, **94(5)**, 770-781
- [34] B. G. Cox, "Acids and bases: solvent effects on acid-base strength". Oxford University Press, Oxford, 2013
- [35] E. N. Kalali, A. Montes, X. Wang, L. Zhang, M. E. Shabestari, Z. Li and D.-Y. Wang, "Effect of Phytic Acid-Modified Layered Double Hydroxide on Flammability and Mechanical Properties of Intumescent Flame Retardant Polypropylene System", *Fire Mater.*, 2018, **42(2)**, 213-220
- [36] E. N. Kalali, X. Wang and D.-Y. Wang, "Multifunctional Intercalation in Layered Double Hydroxide: Toward Multifunctional Nanohybrids for Epoxy Resin", *J. Mater. Chem. A*, 2016, **4(6)**, 2147-2157
- [37] X. Jin, X. Gu, C. Chen, W. Tang, H. Li, X. Liu, S. Bourbigot, Z. Zhang, J. Sun and S. Zhang, "The Fire Performance of Polylactic Acid Containing a Novel Intumescent Flame Retardant and Intercalated Layered Double Hydroxides", *J. Mater. Sci. Lett.*, 2017, **52(20)**, 12235-12250
- [38] C. Jin, H. Liu, X. Kong, H. Yan and X. Lei, "Enrichment of Rare Earth Metal Ions by the Highly Selective Adsorption of Phytate Intercalated Layered Double Hydroxide", *Dalton Trans.*, 2018, **47(9)**, 3093-3101
- [39] T. Hibino, "Delamination of Layered Double Hydroxides Containing Amino Acids", *Chem. Mater.*, 2004, **16(25)**, 5482-5488
- [40] Z. Zhang, C. Xu, F. Qiu, X. Mei, B. Lan and S. Zhang, "Study on Fire-Retardant Nanocrystalline Mg-Al Layered Double Hydroxides Synthesized by Microwave-Crystallization Method", *Sci. China Ser. B: Chem.*, 2004, **47(6)**, 488-498

- [41] C. Nyambo, D. Chen, S. Su and C. A. Wilkie, "Does Organic Modification of Layered Double Hydroxides Improve the Fire Performance of PMMA?", *Polym. Degrad. Stabil.*, 2009, **94(8)**, 1298-1306
- [42] L. Ye and B. Qu, "Flammability Characteristics and Flame Retardant Mechanism of Phosphate-Intercalated Hydrotalcite in Halogen-Free Flame Retardant EVA Blends", *Polym. Degrad. Stabil.*, 2008, **93(5)**, 918-924
- [43] G. Camino, A. Maffezzoli, M. Braglia, M. De Lazzaro and M. Zammarano, "Effect of Hydroxides and Hydroxycarbonate Structure on Fire Retardant Effectiveness and Mechanical Properties in Ethylene-Vinyl Acetate Copolymer", *Polym. Degrad. Stabil.*, 2001, **74(3)**, 457-464
- [44] K. Takehira, "Recent Development of Layered Double Hydroxide-Derived Catalysts-Rehydration, Reconstitution, and Supporting, Aiming at Commercial Application ", *Appl. Clay Sci.*, 2017, **136**, 112-141
- [45] E. Conterosito, L. Palin, D. Antonioli, D. Viterbo, E. Mugnaioli, U. Kolb, L. Perioli, M. Milanesio and V. Gianotti, "Structural Characterisation of Complex Layered Double Hydroxides and TGA-GC-MS Study on Thermal Response and Carbonate Contamination in Nitrate- and Organic-Exchanged Hydrotalcites", *Chem. Eur. J.*, 2015, **21(42)**, 14975-14986
- [46] P. Zhang, S. Sago, T. Yamaguchi and G. M. Anilkumar, "Mg-Al Layered Double Hydroxides Containing Glycine Betaine as Low Humidity-Dependent Anion Conducting Electrolyte Materials for Solid State Alkaline Fuel Cell (SAFC)", *J. Power Sources*, 2013, **230**, 225-229
- [47] S. Marappa, S. Radha and P. V. Kamath, "Nitrate-Intercalated Layered Double Hydroxides-Structure Model, Order, and Disorder", *Eur. J. Inorg. Chem.*, 2013, **2013(12)**, 2122-2128
- [48] C. Pagano, F. Marmottini, M. Nocchetti, D. Ramella, and L. Perioli, "Effects of Different Milling Techniques on the Layered Double Hydroxides Final Properties", *Appl. Clay Sci.*, 2018, **151**, 124-133
- [49] C. L. De Castro and B. S. Mitchell, "Nanoparticles from Mechanical Attrition", in "Synthesis, Functionalization and Surface Treatment of Nanoparticles", eds. M.-I. Baraton, American Scientific Publishers, USA, 2003, pp 1-15

- [50] G. Gorrasi and A. Sorrentino, "Mechanical Milling as a Technology to Produce Structural and Functional Bio-Nanocomposites", *Green Chem.*, 2015, **17(5)**, 2610-2625
- [51] M. Rhodes, "Introduction to Particle Technology", 2008, pp 1-450

Chapter 6

Characterisation of Epoxy Resin/LDHs Nanocomposites Cured with DDM

This chapter aims to present the performance of LDHs on the properties of epoxy resin nanocomposites, particularly to the flammability. The representative epoxy resin monomer and curing agent focused on this chapter was diglycidyl ether of bisphenol A (DGEBA) and 4,4'-diamino diphenylmethane (DDM), respectively. The initial section displays the curing mechanism of DGEBA/DDM. The later section estimates the preparing processes of epoxy (EP) nanocomposites with incorporating layered double hydroxides (LDHs) (EP/LDHs) by observing visual characteristics and by testing flexural properties. The LDHs modified with anions of carbonate, nitrate, bis(2-ethyl hexyl) phosphate (BEHP), phytic acid (Phy), β -glycerophosphate disodium (GP) or diphenyl phosphate (DPP) were used as the fillers for the epoxy nanocomposites. The following section evaluates the dynamic mechanical properties and thermal behaviours under N₂ or air of the cured epoxy nanocomposites. The last section will discuss the flammability of the composites, including the flame retardancy mechanism of LDHs for the epoxy resin.

6.1 Curing Mechanism of DGEBA/DDM

Before preparing the EP/LDHs nanocomposites, the neat EP was cured with the reaction between the DGEBA and the DDM to use as a controlling sample. During the heat treatment of the DDM cured EP (EP/DDM) mixture, the active hydrogen on the amine group in the DDM curing agent reacted with the epoxy group in the DGEBA. It encouraged the partial formation of cross-linked networks. The early stage of heat treatment contributed to the growth and branching of molecules, but the molecular size still small. At this stage, the viscous liquid transferred to the gel. Then, numerous larger molecules were produced due to the formation of partially cross-linking networks. The cross-link density increased significantly, inducing the cured solid form of EP [1, 2]. The schematic reaction of the DGEBA and the DDM was presented in Figure 6.1.

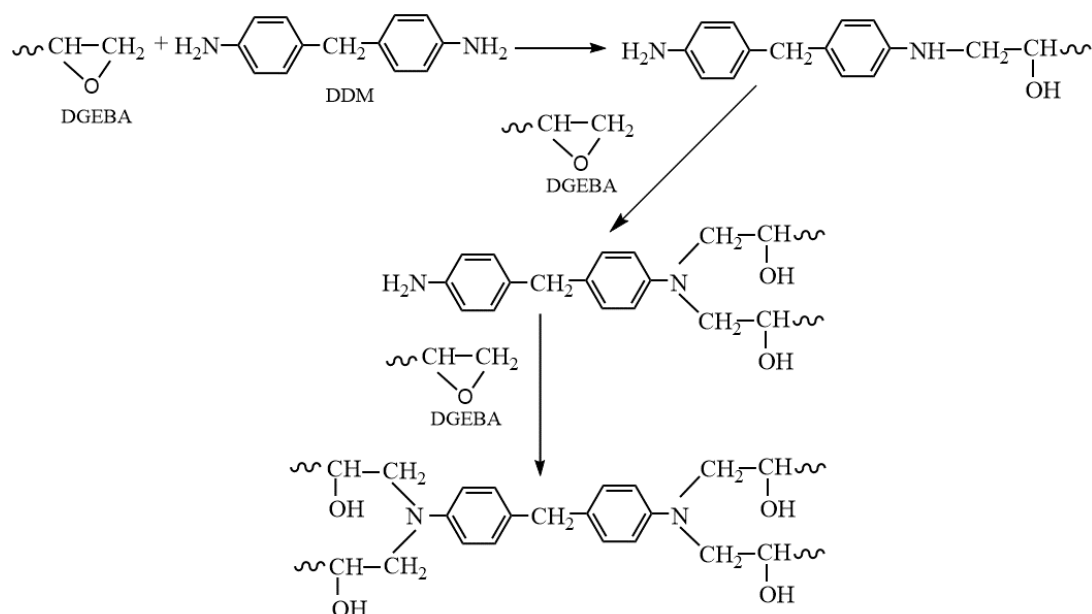


Figure 6.1 Schematic curing reaction of DGEBA monomers and DDM [2].

6.2 Preparation of EP/LDHs Nanocomposites Cured with the DDM

The general incorporation of nanolayered-like fillers, e.g., LDHs into polymer matrix can be carried out with three various methods: 1) intercalation of LDH with monomers, 2) intercalation of LDH with polymers and 3) pre-exfoliation of nanolayered-like fillers, and restacking layers with either monomers or polymers. For the first method, the interlayer space of LDHs is intercalated by monomers at the early stage of the fabrication. After that, the mixture is polymerised, leading to the exfoliation of nanolayers in the polymer matrix. In the second method, there is a similarity with the first fabrication, but the monomers are replaced with polymers. The consequence is the separation of LDH layers because of the intercalation of macromolecular chains of polymers. Lastly, both solvent and sonication are used for the pre-exfoliation of nanolayers. The LDHs are dispersed in acetone solvent and are sonicated. Then, the mixture of LDH and solvent is homogenised with monomers or polymers. This method provides the penetration of monomers or polymers into the layers of LDHs, and then the solvent is evaporated from the composites in the following step. [3]

In this study, the EP/LDHs nanocomposites were prepared by two different mixing routes: 1) the only mechanical stirring and 2) the solvent blending, the sonication, and

the mechanical stirring. For the former, the LDHs were added into the epoxy resin monomers, and the mixture was vigorously stirred with the mechanical stirrer for 1 h. Then, the hardener was added to the mixture of EP/LDHs. In the latter case, the rough procedure was the sonication of the mixture solution containing the LDHs and acetone solvent at room temperature for 1 h. Subsequently, the solution was mixed with the epoxy resin monomer using the mechanical stirrer for 1 h. After that, the mixture was heated for approximately 2 h so as to remove the solvent. The final process was the blend of the DDM curing agent and the EP/LDH mixture. The details of the preparing procedure were described in Section 4.4.3. The comparison of both mixing methods would be discussed in the later section.

6.3 Effect of Mixing Procedures on Visual Characteristics and Flexural Properties of EP/DDM Nanocomposites Incorporated with LDHs

For particulate-filled polymer composites, the dispersion and distribution of particulate fillers in the polymer matrix are considered since they affect the properties of the composites. In this study, the distribution consistency of LDHs in the epoxy resin matrix was investigated from the cut edge of composites, which are cut and polished. The characteristics of the cut edge of samples prepared by the different mixing methods were presented in Table 6.1 for the only mechanical stirring and Table 6.2 for the sonication and stirring. The top and bottom of photos were the sides contacting the air and the glass mould, respectively.

Table 6.1 The cut edge of EP/DDM nanocomposites incorporating the LDHs by the method of mechanical stirring.

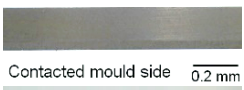
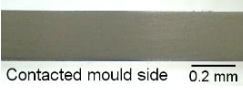

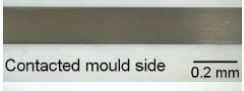
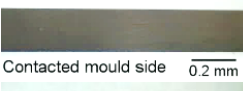
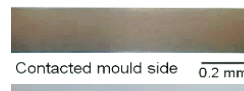
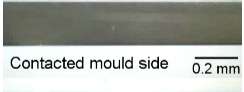
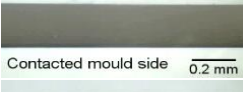

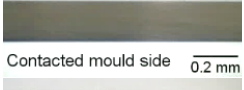
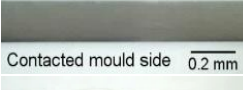
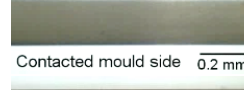
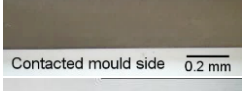
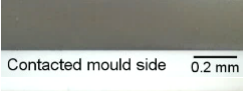
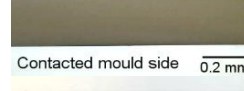
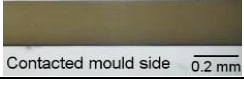
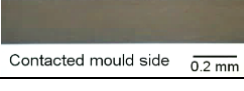
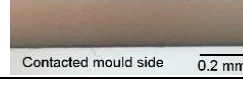
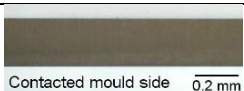
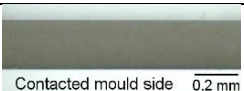
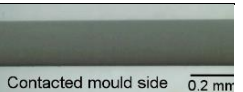
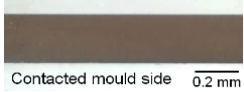
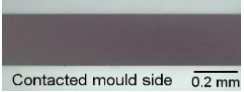
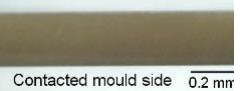
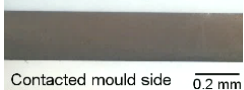
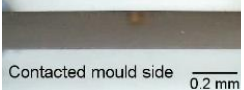
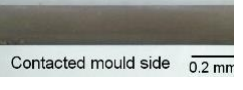
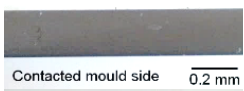
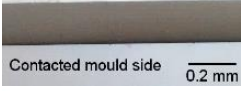
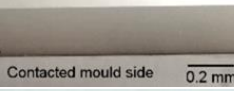
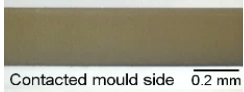
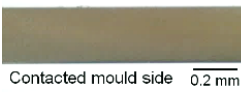
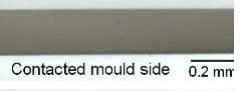
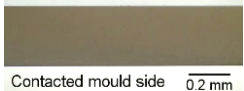
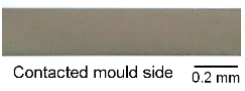
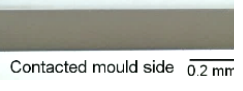
Sample	Contents of LDHs		
	1%	5%	10%
EP/DDM-LDH-CO ₃			
EP/DDM-LDH-NO ₃			
EP/DDM-LDH-BEHP			
EP/DDM-LDH-Phy			
EP/DDM-LDH-GP			
EP/DDM-LDH-DPP			

Table 6.2 The cross-sections of EP/DDM nanocomposites incorporating the LDHs by the method of sonication, and mechanical stirring.

Sample	Contents of LDHs		
	1%	5%	10%
EP/DDM-LDH-CO ₃			
EP/DDM-LDH-NO ₃			
EP/DDM-LDH-BEHP			
EP/DDM-LDH-Phy			
EP/DDM-LDH-GP			
EP/DDM-LDH-DPP			

At the 1 wt% LDHs in both the mixing methods, the cut edge of samples presented the colour consistency. It can assume that the LDHs distributed evenly throughout the epoxy resin matrix. Another assumption was that the addition of the 1 wt% LDHs in

the polymer matrix might be too small. It could not be observed the physical change. When the contents of LDHs increased to 5 wt% and 10 wt%, the cross-sections of the composites still displayed the consistency of colour. These results indicated that the preparation of EP/LDHs nanocomposites with the only stirring and the sonication, and stirring provided the composites with the good distribution of LDHs in the epoxy resin matrix cured by the DDM.

This study estimated the influence of mixing methods on flexural behaviours of the EP/LDHs nanocomposites by using the universal testing machine (UTM). Figure 6.2-6.7 show the flexural strength and flexural modulus of the EP nanocomposites containing the LDH-CO₃, LDH-NO₃, LDH-BEHP, LDH-Phy, LDH-GP and LDH-DPP, respectively. It can be seen that at the same contents of fillers, the flexural strength and flexural modulus of composites prepared from using the solvent and sonication performed slightly greater than the samples prepared by the only stirring method. The results indicated that the interaction between the epoxy matrix and the LDHs improved by using the solvent and sonication in the composite preparation.

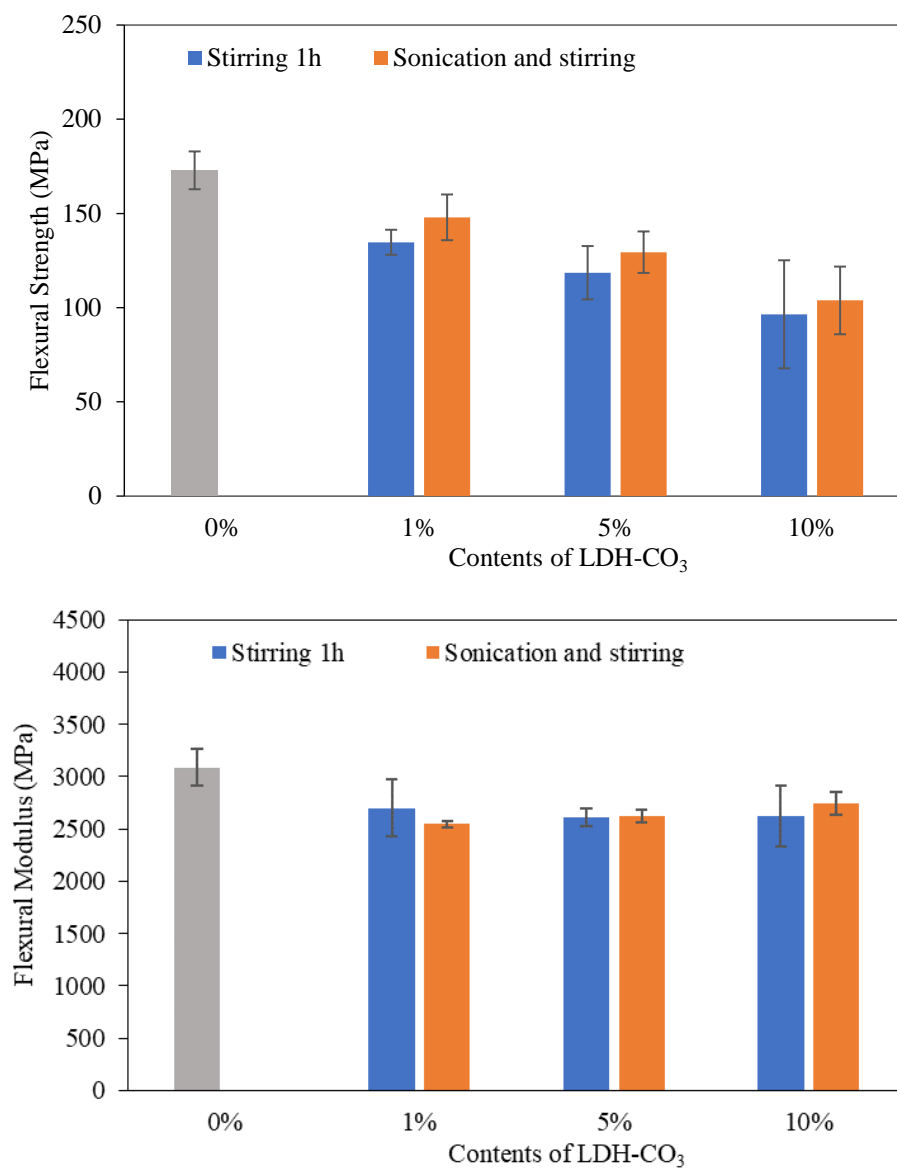


Figure 6.2 The flexural strength and flexural modulus of the neat epoxy resin cured with the DDM and the nanocomposites containing the LDH-CO₃.

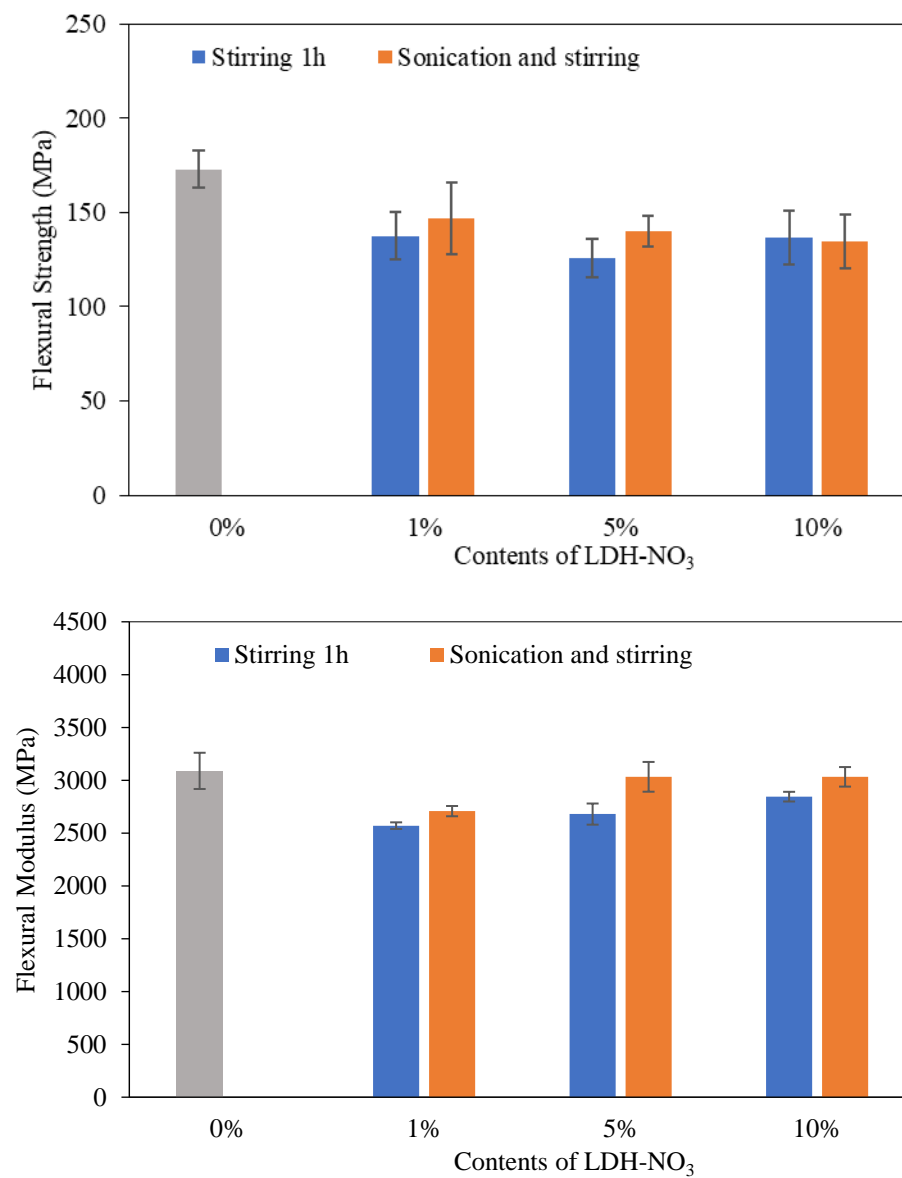


Figure 6.3 The flexural strength and flexural modulus of the neat epoxy resin cured with the DDM and the nanocomposites containing the LDH-NO₃.

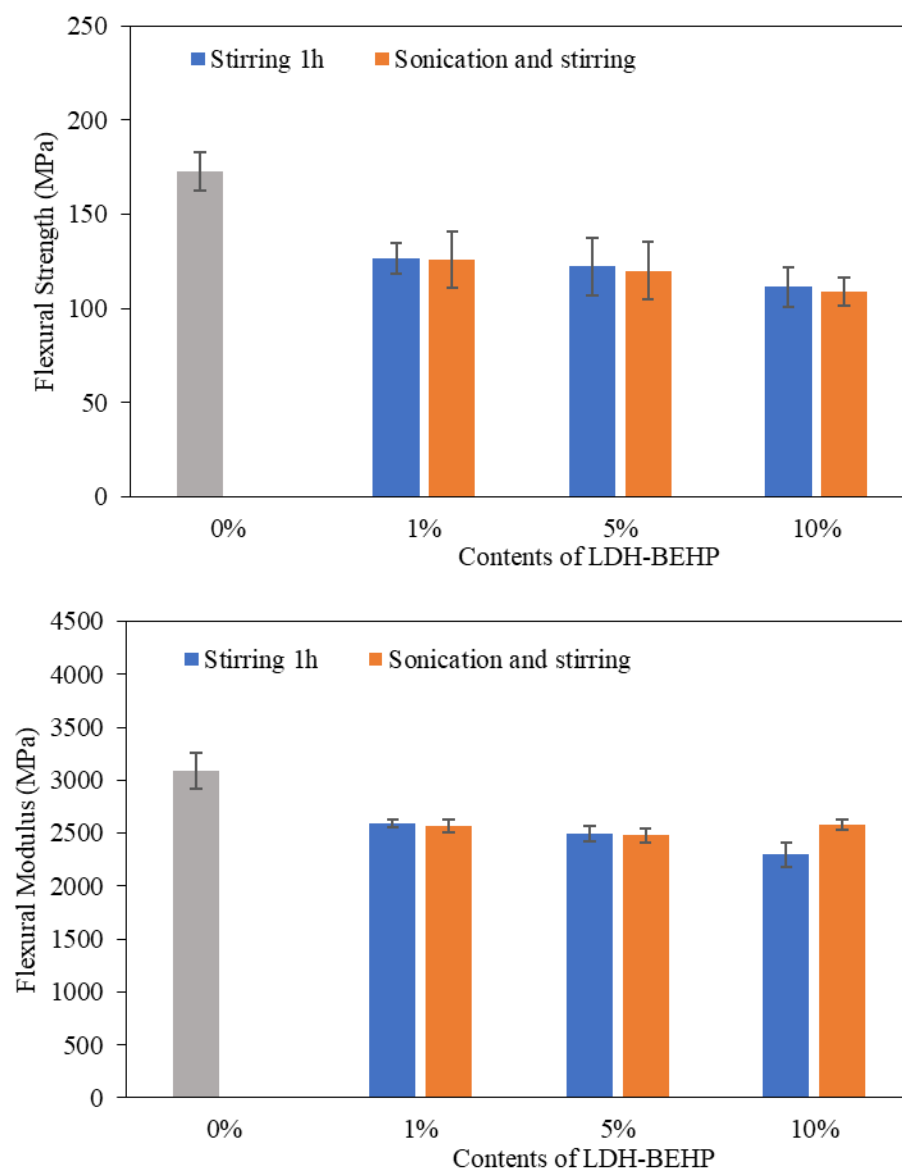


Figure 6.4 The flexural strength and flexural modulus of the neat epoxy resin cured with the DDM and the nanocomposites containing the LDH-BEHP.

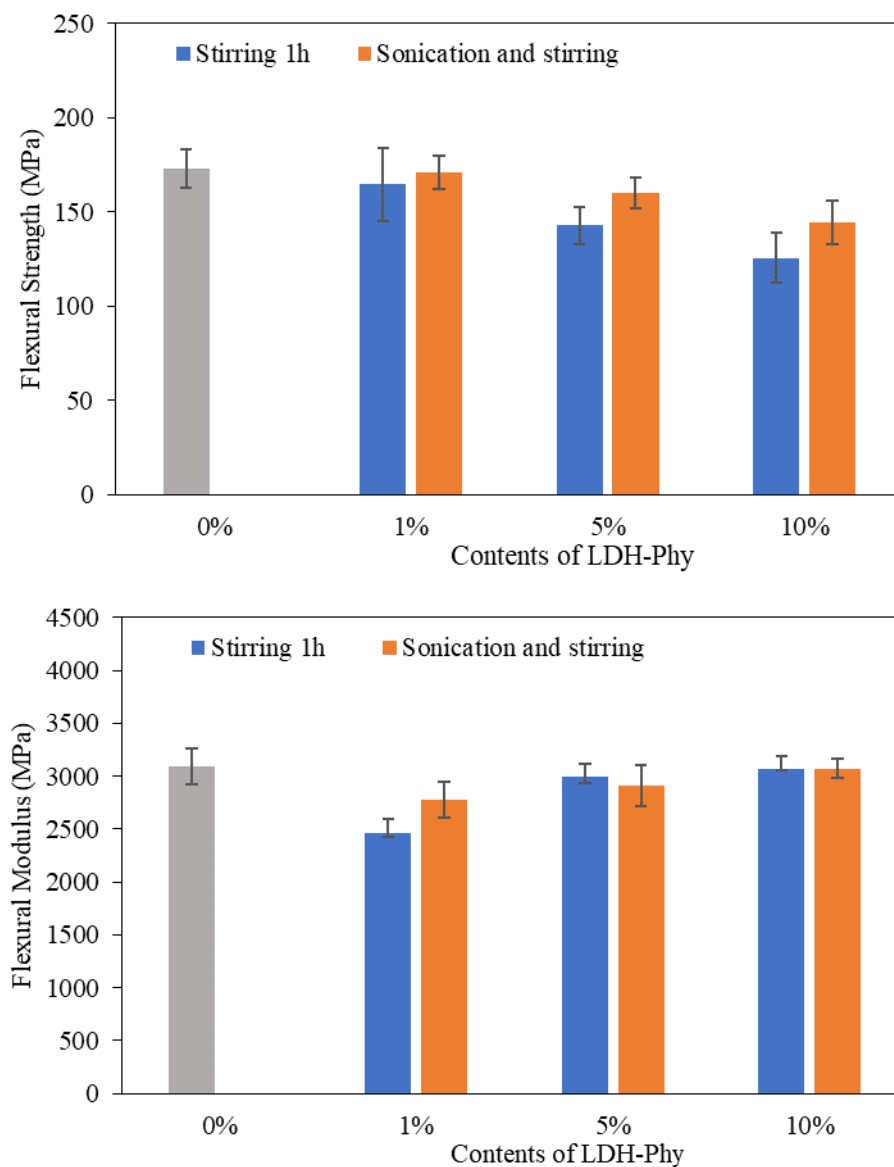


Figure 6.5 The flexural strength and flexural modulus of the neat epoxy resin cured with the DDM and the nanocomposites containing the LDH-Phy.

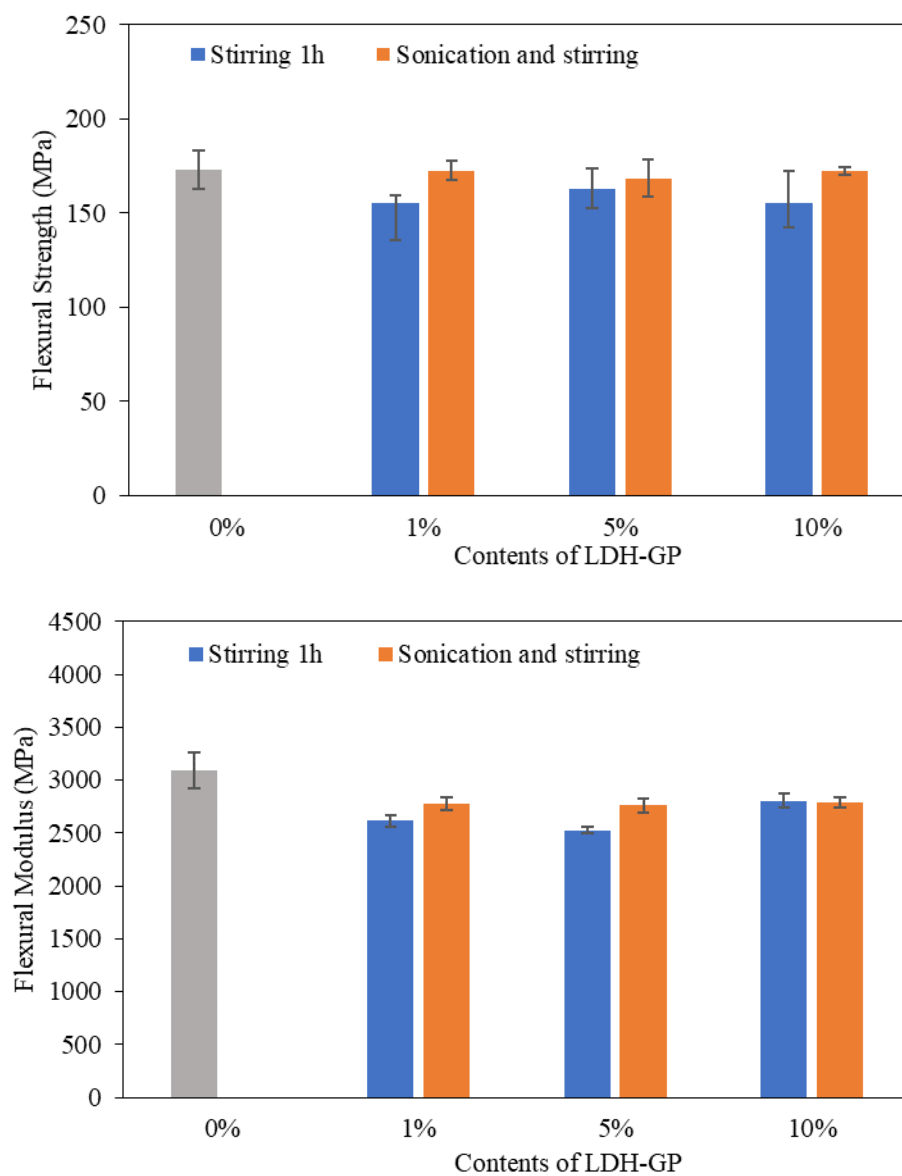


Figure 6.6 The flexural strength and flexural modulus of the neat epoxy resin cured with the DDM and the nanocomposites containing the LDH-GP.

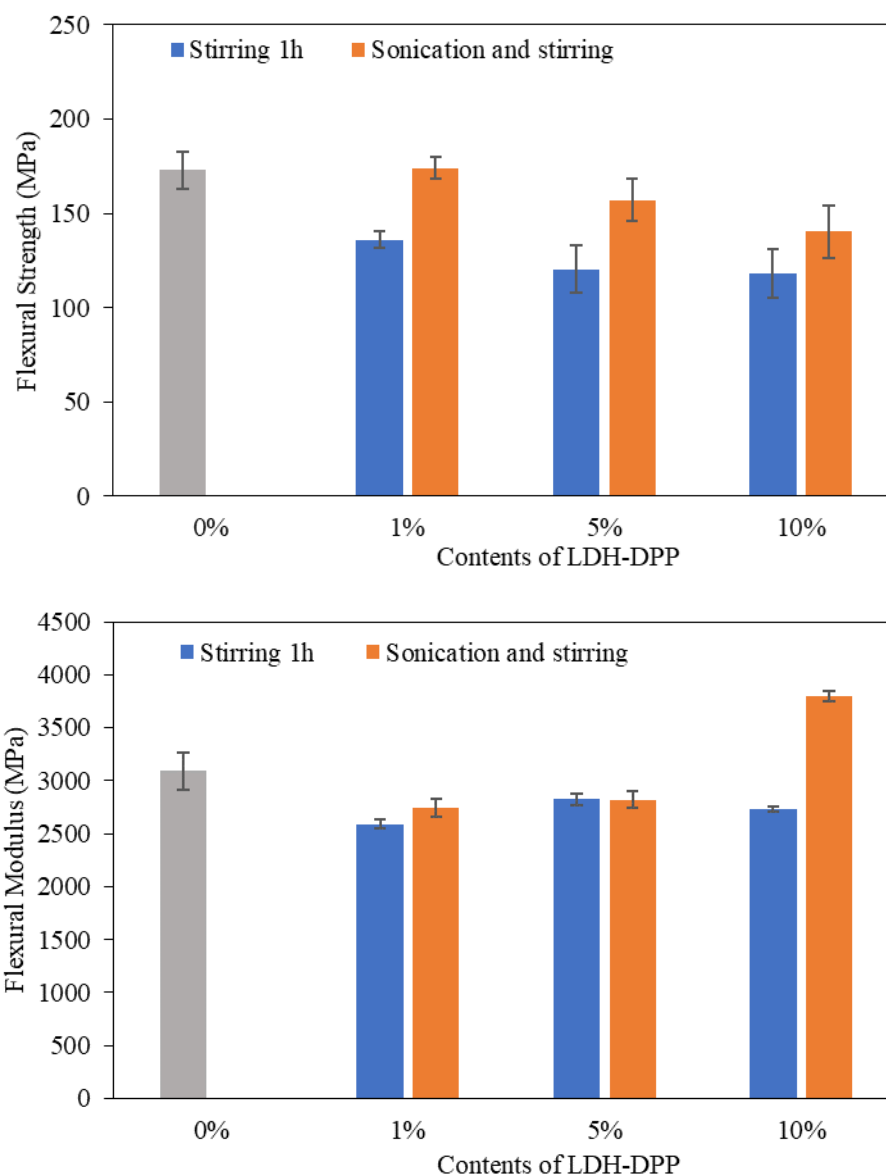


Figure 6.7 The flexural strength and flexural modulus of the neat epoxy resin cured with the DDM and the nanocomposites containing the LDH-DPP.

Since the dispersion of sonicated LDHs in the solvent affected the swelling of metal hydroxide layers, the monomer of epoxy could easily penetrate into the interlayer galleries of LDHs. It increased surface area with the interaction between the fillers and the polymer matrix, including the dispersion and distribution. Hence, the uses of solvent and sonication were the appropriate processes for preparing the epoxy resin nanocomposites.

6.4 Flexural Properties of EP/LDHs Nanocomposites Cured with DDM

The effect of different LDHs on the flexural properties of the EP/DDM nanocomposites were estimated by using the average value of five specimens in each sample. Figure 6.8 shows the flexural strength and modulus of the pure EP/DDM and its nanocomposites with the variation of LDHs loading (1%, 5% and 10% by weight). The results revealed that the addition of LDHs reduced the flexural strength and flexural modulus in the nanocomposites compared to the pure EP.

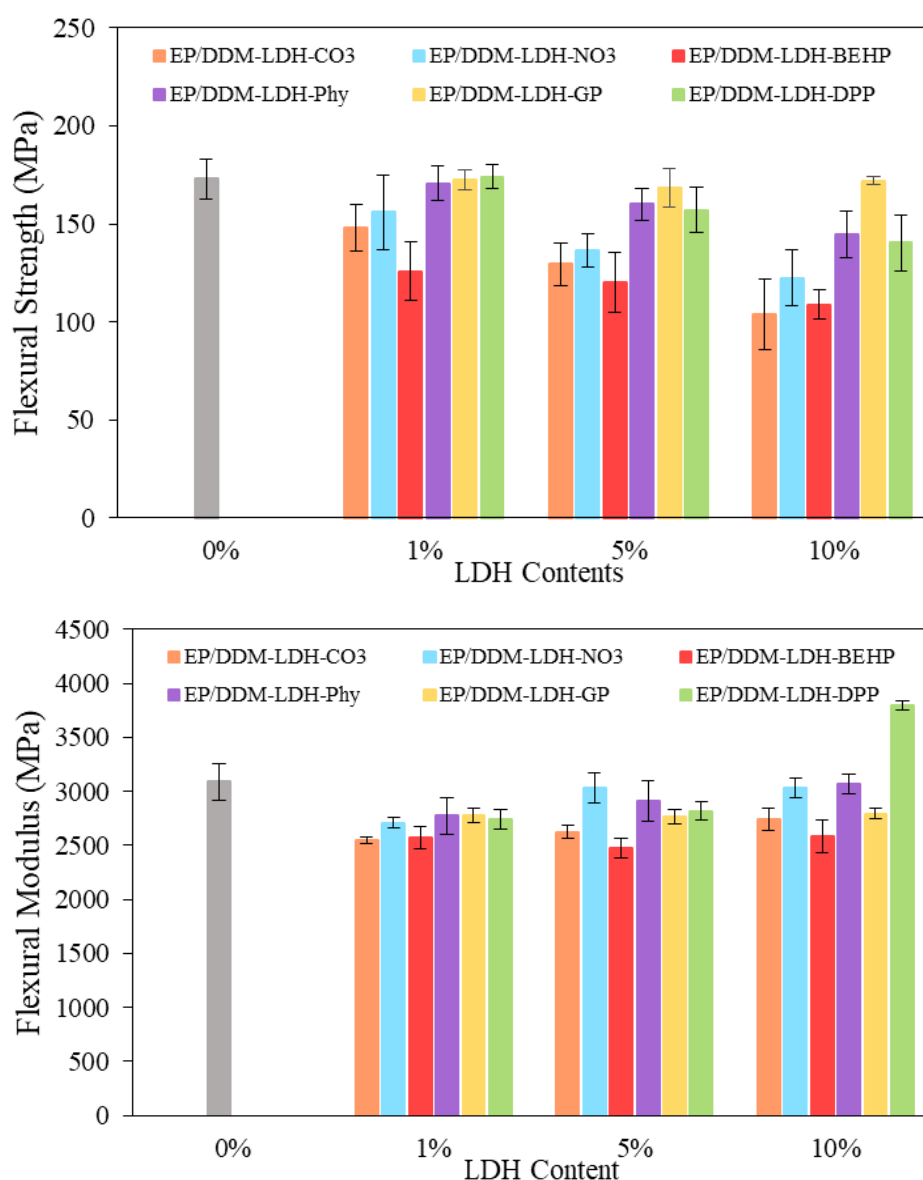


Figure 6.8 The flexural strengths and flexural modulus of the pure EP/DDM and its nanocomposites incorporating the different anionic-modified LDHs.

The reduction of flexural strength in the nanocomposites might occur the existence of microvoids in the epoxy matrix. As the LDHs were the inorganic fillers, they could not be incompatible with the DGEBA in the DDM curing system. This circumstance resulted in many microvoids in the matrix, which were the flaw of the nanocomposites. When the nanocomposite specimen was bent by applying the stress, the cracks were initiated at the voids [4, 5]. In the meantime, the flexural modulus of nanocomposites decreased with the loading of LDHs.

It is noticeable that the poor interface between the fillers and the epoxy matrix was likely the cause of reduction in the mechanical property. The interface between the fillers and the matrix can be improved by considering various factors. First of all, the surface of LDHs should be modified with compounds containing both organic and inorganic sections. The organic part in modifying agents can bond with the epoxy resin whereas the inorganic part in modifying agents can interact with the LDH filler. In the same way, the modifying agent may be added to the mixture of epoxy resin and LDHs. The use of modifying agent can enhance the compatibility and interfacial adhesion between the matrix and fillers. Secondary, the interface between matrix and fillers can be increased by a reduction of LDHs particle size in order to increase the surface area. This can decrease the size of voids, leading to the decrease of crack deflection in the matrix during the flexural test. Lastly, the improvement of interfacial interaction between the matrix and fillers is a use of high shear mixing process for the preparation of epoxy resin nanocomposites. As the LDHs were in the nanolayered form, the use of high shear mixing process may help the exfoliation of the layers in LDHs. From this circumstance, the epoxy matrix can through the layers of LDHs. Thus, the interface between the matrix and fillers increases.

Compared to different LDHs, the flexural properties of the EP nanocomposites containing the LDH-CO₃ and LDH-NO₃ (the pristine LDHs) were less than the composites with the organophosphate ester modified LDHs except adding the LDH-BEHP. From the characterisation of interlayer space on the LDHs in the Chapter 5, the spaces between the layers of the pristine LDHs (0.30-0.38 nm) were less than that of the modified LDHs (0.46-0.62 nm). The intercalation of the epoxy matrix to the pristine LDHs was more difficult than the organic-modified LDHs.

Besides, the pristine LDHs were the fillers with high polarity since they are based on the inorganic compounds. Meantime, the existence of hydroxyl and amine groups on the resin chains accounted for the high polar in the epoxy resin. The difference of polarity between the pristine LDHs and the epoxy resin might be still high. When the organophosphate ester anions were used as the modifying agent for the LDHs, they might be able to reduce the polarity of LDHs. Thus, the polarities of the modified LDHs were likely to be close to the epoxy resin, which were more than the pristine LDHs. The modification of LDHs with the organic compounds could improve the interaction with the epoxy matrix. Therefore, the EP nanocomposites with the addition of the organophosphate ester modified LDHs had flexural properties greater than the composites containing the pristine LDHs.

Overall, the LDHs did not significantly reduce the mechanical properties of the resin. Most polymer composites had a reduction of mechanical properties with loading the additives. As this research aimed to enhance the flame retardancy of epoxy resin, it was expected that the LDHs would be able to improve this property, discussed in the Section 6.7.

6.5 Dynamic Mechanical Properties of the Pure EP and EP/LDHs Nanocomposites in DDM Curing System

Dynamic mechanical analysis (DMA) was utilised to measure the thermal behaviours of polymer materials. The pure EP/DDM and its nanocomposites consisting of the pristine LDHs and the organophosphate ester modified LDHs were investigated the dynamic mechanical properties. The results obtained from the DMA were presented by plotting the storage modulus (E'), loss modulus (E'') and $\tan \delta$ as the function of temperature. The average of two tests was plotted as the DMA results.

6.5.1 Dynamic Mechanical Behaviors of Pure EP Cured with DDM

The storage modulus, loss modulus and $\tan \delta$ of the pure EP/DDM are shown in Figure 6.9. The storage modulus decreased gradually in the range of -150°C to 100°C and then declined rapidly to around 170°C . At the higher temperature of 170°C , the

plotted line was levelled off. The storage modulus corresponds to the elastic modulus of polymers depending on free volume (V_f) in the polymers. The change in V_f determines the thermal transition of the solid-state in polymers. The increasing temperature encouraged a deformation of polymer elasticity and a reduction of stiffness [6, 7]. Thus, there was a reduction of storage modulus at elevated temperature.

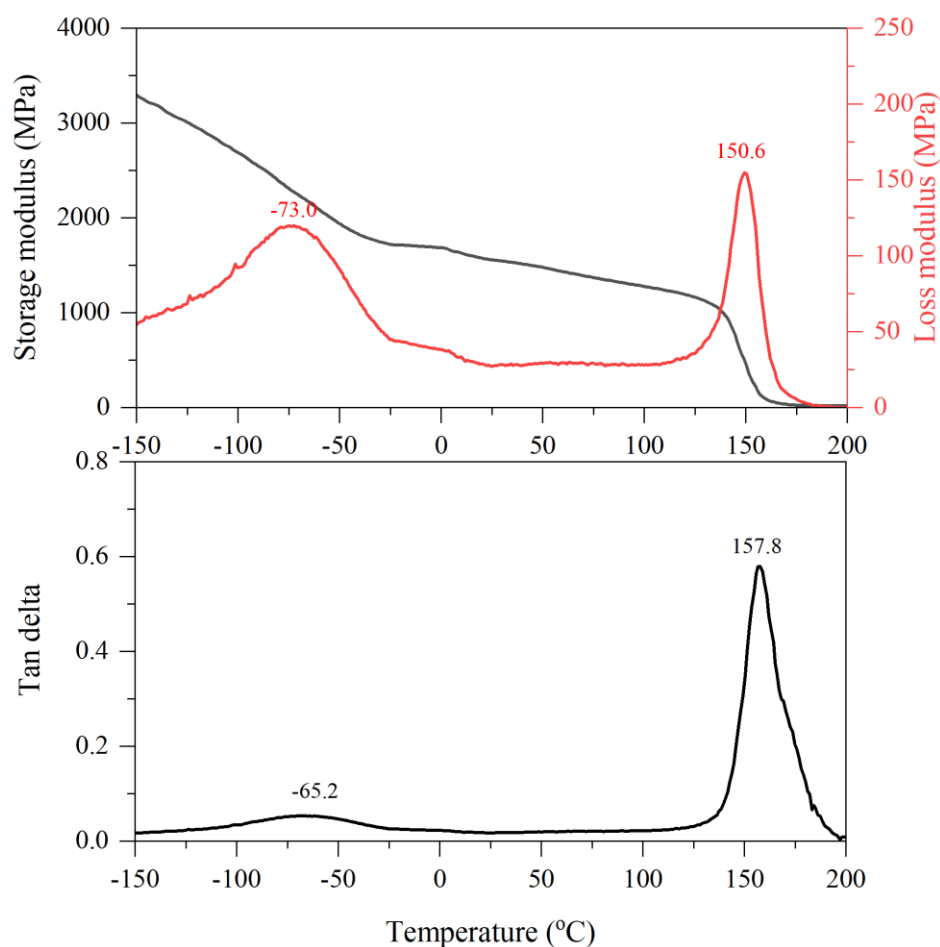


Figure 6.9 The storage modulus, loss modulus and $\tan \delta$ of the pure DGEBA/DDM.

For the loss modulus and $\tan \delta$ curves, they presented two peaks of the minor peak in the range -150°C to 50°C and the major peak in the range of 100°C to 200°C . The obtained peaks in the loss modulus curve were at -58.2°C and 151.7°C , whereas the provided peaks in the $\tan \delta$ curve were at -51.5°C and 159.2°C . As above mentioned, the elevated temperature resulted in the phase transition in polymer chains. The loss modulus measures the energy loss of materials due to the friction caused by the motion

of polymer chains [6]. Meanwhile, $\tan \delta$ was attributed to the relaxation of the polymer matrix [7].

At the very low temperature, the molecule in the polymer was tightly packed. When the temperature of the polymer increased, the material expanded, increasing the free volume. It induced the movement of the localised bonds and side chains or small groups on the backbone of polymer structure, e.g., the units of hydroxy ether and phenyl groups in the polymer by rotation and vibration. This characteristic transition at the low temperature is called the beta transition (T_β). At the higher temperature, it increased the free volume in the polymers, leading to the movement of the polymer backbone. It was associated with the phase transition from the glassy state to the rubbery state. This transition is called the glass transition (T_g). [7, 8]

In general, the characterisation of T_g from the DMA can be determined in at least five ways, such as the peak or the onset of $\tan \delta$ curve, the peak and onset of loss modulus or the onset of storage modulus [7]. The common method often used to define T_g is the peak of $\tan \delta$ curve [9], used in this study. Therefore, the T_g of the pure EP cured with the DDM was 159.2°C.

6.5.2 Dynamic Mechanical Behaviors of EP/Pristine LDHs Nanocomposites Cured with the DDM

The influences of the carbonate and nitrate-intercalated LDHs additions on the dynamic mechanical properties of EP nanocomposites were displayed in Figure 6.10-6.11, respectively. In comparison with the pure EP, the EP/LDHs nanocomposites had a high storage modulus. The increase of LDH-CO₃ and LDH-NO₃ contents generated the enhancement of storage modulus. The CO₃ and NO₃-intercalated LDHs acted as the inorganic fillers for the polymer. The addition of inorganic fillers into the polymer matrix increased the stiffness of composites, contributing to the increase of storage modulus [10, 11].

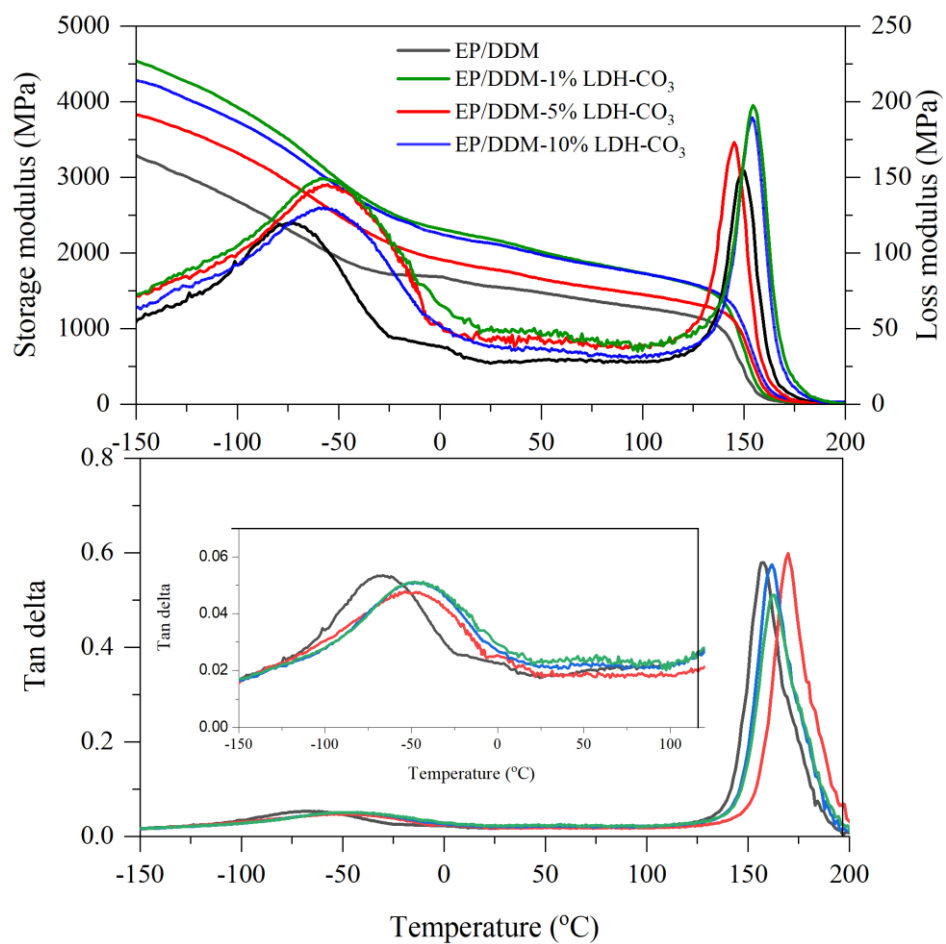


Figure 6.10 The storage modulus, loss modulus and Tan δ of the DGEBA/DDM and its nanocomposites containing the varied contents of LDH-CO₃.

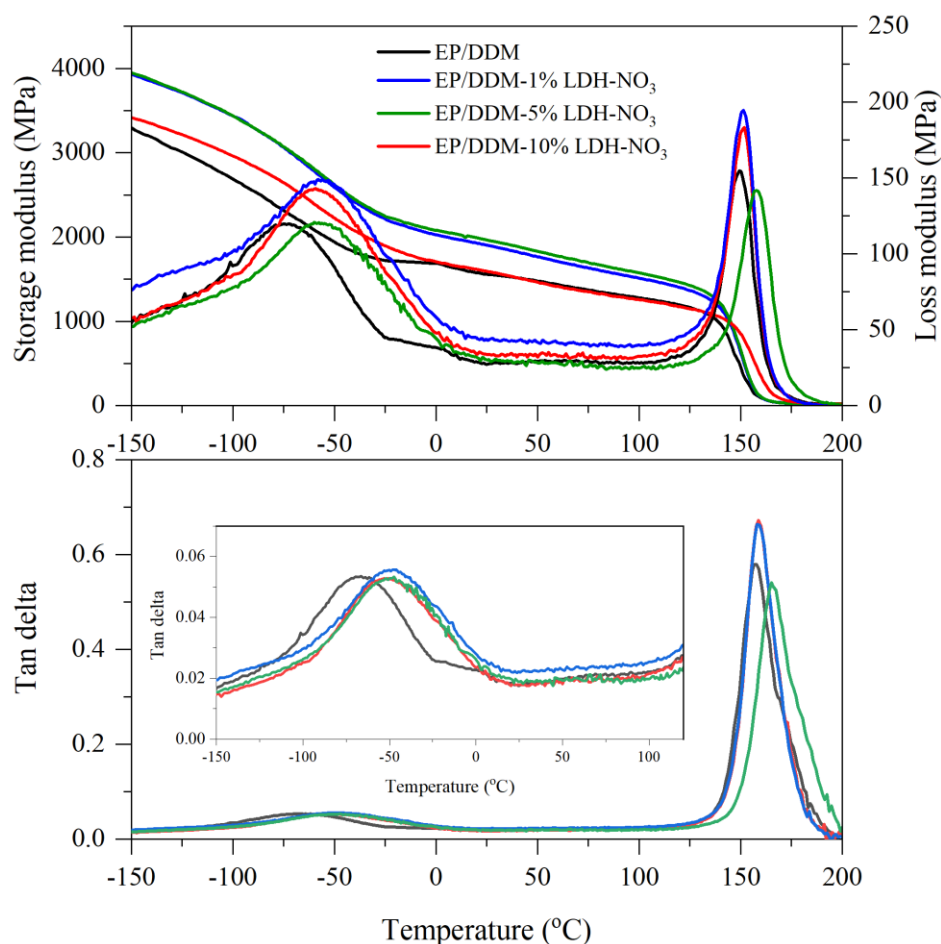


Figure 6.11 The storage modulus, loss modulus and Tan δ of the DGEBA/DDM and its nanocomposites containing the varied contents of LDH-NO₃.

For the E'' and $\tan \delta$ curves of the composites, they provided two peaks of polymer relaxations in the plotted curves. The patterns of EP/LDH-CO₃ and EP/LDH-NO₃ nanocomposites were similar to the pure EP. The peaks at the lower and higher temperatures were attributed to the T_{β} and T_g , respectively. Table 6.3 showed the T_{β} and T_g of the EP nanocomposites containing the LDH-CO₃ or LDH-NO₃ with the variation of percent loading. At the 1% loading of LDH-CO₃ or LDH-NO₃, the EP nanocomposites presented the T_{β} at -51°C and the T_g at 160°C. They closely resemble the T_{β} and T_g of pure EP. With the increase of LDHs contents to 5 wt% and 10 wt% loading, the transition temperatures were slightly changed. As the values of both were in the range of standard deviation, there was no significant difference between the pure EP and the EP/pristine LDHs nanocomposites.

Table 6.3 The T_{β} , T_g , storage modulus at the rubbery state and cross-link density of the pure EP, EP/LDH- CO_3 and EP/LDH- NO_3 cured with the DDM in the different contents of LDHs.

Sample	T_{β} (°C)	T_g (°C)	E' at T_g+30 (MPa)	Crosslink density (mol/m ³)
Pure EP/DDM	-51.7 ± 1.1	159.2 ± 0.5	17.6 ± 3.5	1530 ± 302
EP/DDM-1% LDH- CO_3	-50.9 ± 0.6	160.0 ± 1.1	17.1 ± 2.9	1481 ± 252
EP/DDM-5% LDH- CO_3	-47.5 ± 0.3	161.0 ± 0.7	24.7 ± 1.7	2132 ± 147
EP/DDM-10% LDH- CO_3	-47.2 ± 0.1	162.6 ± 0.1	29.4 ± 3.3	2535 ± 281
EP/DDM-1% LDH- NO_3	-51.1 ± 0.4	159.4 ± 0.8	18.1 ± 2.8	1573 ± 243
EP/DDM-5% LDH- NO_3	-50.3 ± 0.5	158.8 ± 0.9	21.4 ± 2.1	1861 ± 189
EP/DDM-10% LDH- NO_3	-50.2 ± 1.2	158.8 ± 0.4	26.0 ± 1.6	2253 ± 139

As mentioned previously, the motion of side groups in polymer chains reflects T_{β} , and the movement of backbone chains in polymer relates to the T_g . The DMA results indicated that the mobility of the side groups on the polymer chains and the backbone of polymers were insensitive to the addition of LDHs. The lamellae of LDHs might be completely separated in the composites, which did not affect the free volume in the polymer.

When the polymeric samples were heated through their glass transition range, the polymers transformed from the glassy to rubbery state. It induced the reduction of modulus, affecting the stiffness [7]. The storage modulus in the rubbery plateau region above T_g can determine the number of cross-links in the cured epoxy [7]. The cross-link density could be calculated by using Equation 6.1,

$$\nu_c = \frac{E'_{\text{Rubbery}}}{3RT} \quad (6.1)$$

where E' rubbery is the storage modulus at the temperature above the T_g at 30°C, T is T_g+30 and R is a universal gas constant.

The calculated cross-link densities of epoxy resin nanocomposites were also presented in Table 6.3. The cross-link density of the EP nanocomposites tended to increase with the loading of the pristine LDHs. The higher LDHs loading, the more cross-link density.

Generally, the T_g of polymers relates to cross-linking density. In the DMA experiment, however, the addition of LDHs did not affect the T_g change but increased the calculated cross-link density. The possible cause of this circumstance might occur by the reliability of the data. As the DMA is the machine designed for stiffness materials, the region at above T_g appeared fluctuation of $\tan \delta$ more than the region at below T_g . Therefore, the use of rubbery modulus for the calculation of cross-link density might be errored. Another possibility was the effect of inorganic fillers. When the inorganic fillers were incorporated into the polymer materials, it could contribute to the cross-link density change. At the below T_g , both the van der Waals force and cross-links in the cured EP/LDHs nanocomposites were not broken. For the above T_g , the van der Waals force could be destroyed, but the cross-links still remained in the composites because the strength of the covalent bonds in cross-links was more than the interaction of the van der Waals force. The epoxy resin transformed into rubbery instead of melting because the cross-links hold the polymer structure. The elastic modulus allowed to increase with the cross-link density, relating to the stiffness. In general, the added inorganic fillers provide a higher stiffness than the polymer matrix. Hence, the LDHs increased the stiffness and cross-link density of polymer nanocomposites, but did not affect the T_g .

6.5.3 Dynamic Mechanical Behaviors of EP/Modified LDH Nanocomposites Cured with DDM

With adding the BEHP, Phy, GP or DPP modified LDHs, the DMA measurements of the EP/modified LDHs nanocomposites were displayed in Figure 6.12-6.15, respectively. It can be seen that the storage modulus of the epoxy nanocomposites containing the organophosphate ester modified LDHs were higher than that of the pure EP in the glassy state. The increase of the modified LDHs contents also enhanced the stiffness of the epoxy matrix, leading to the increase of storage modulus.

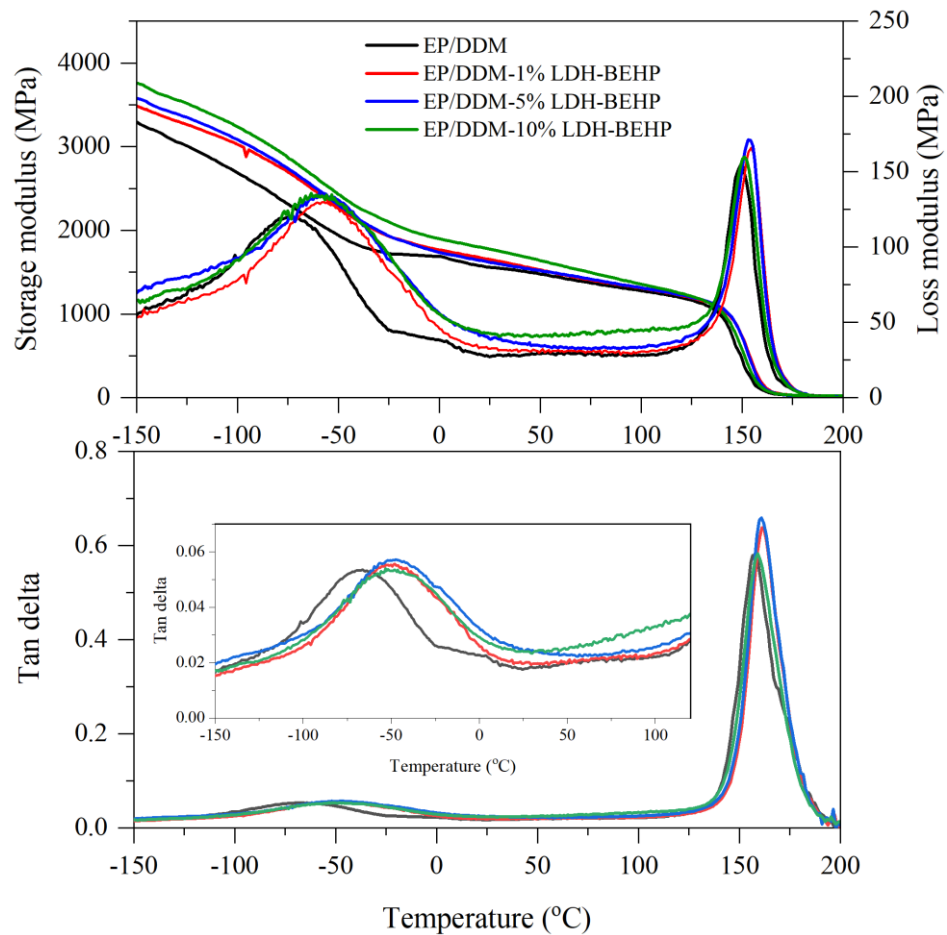


Figure 6.12 The storage modulus, loss modulus and $\text{Tan } \delta$ of the DGEBA/DDM and their nanocomposites containing the varied contents of LDH-BEHP.

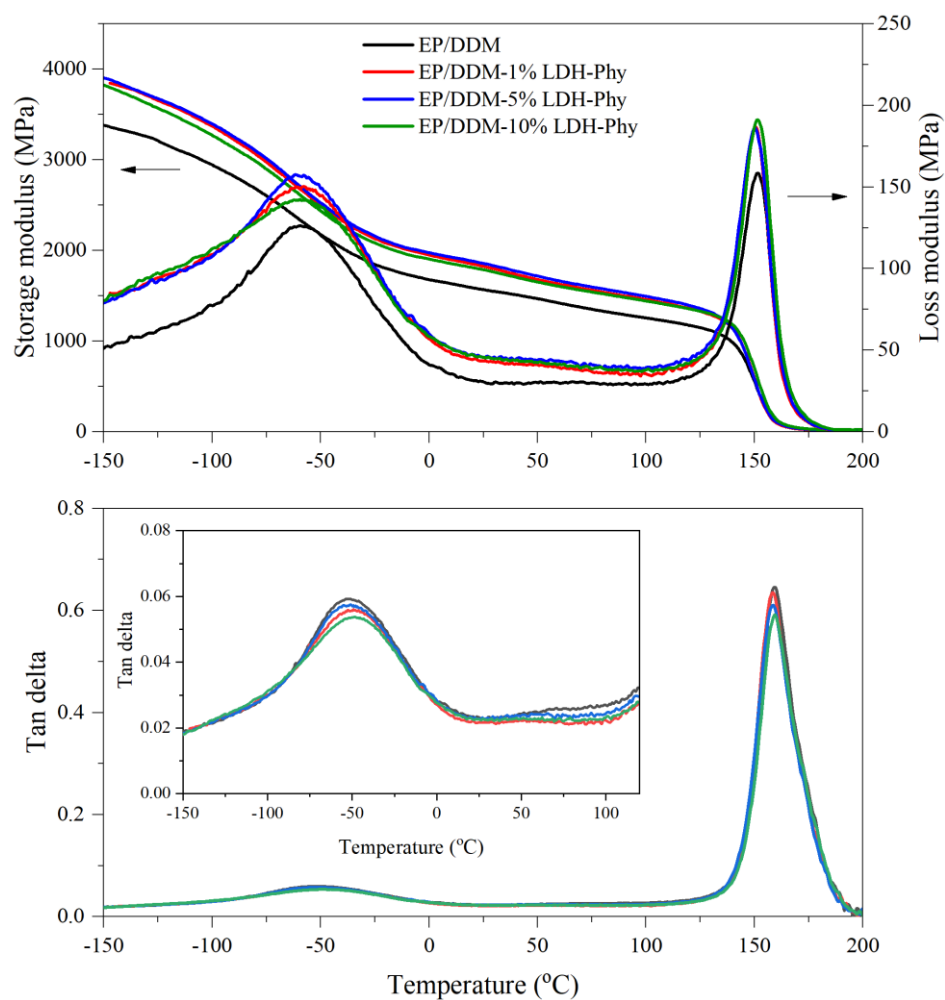


Figure 6.13 The storage modulus, loss modulus and $\text{Tan } \delta$ of the DGEBA/DDM and its nanocomposites containing the varied contents of LDH-Phy.

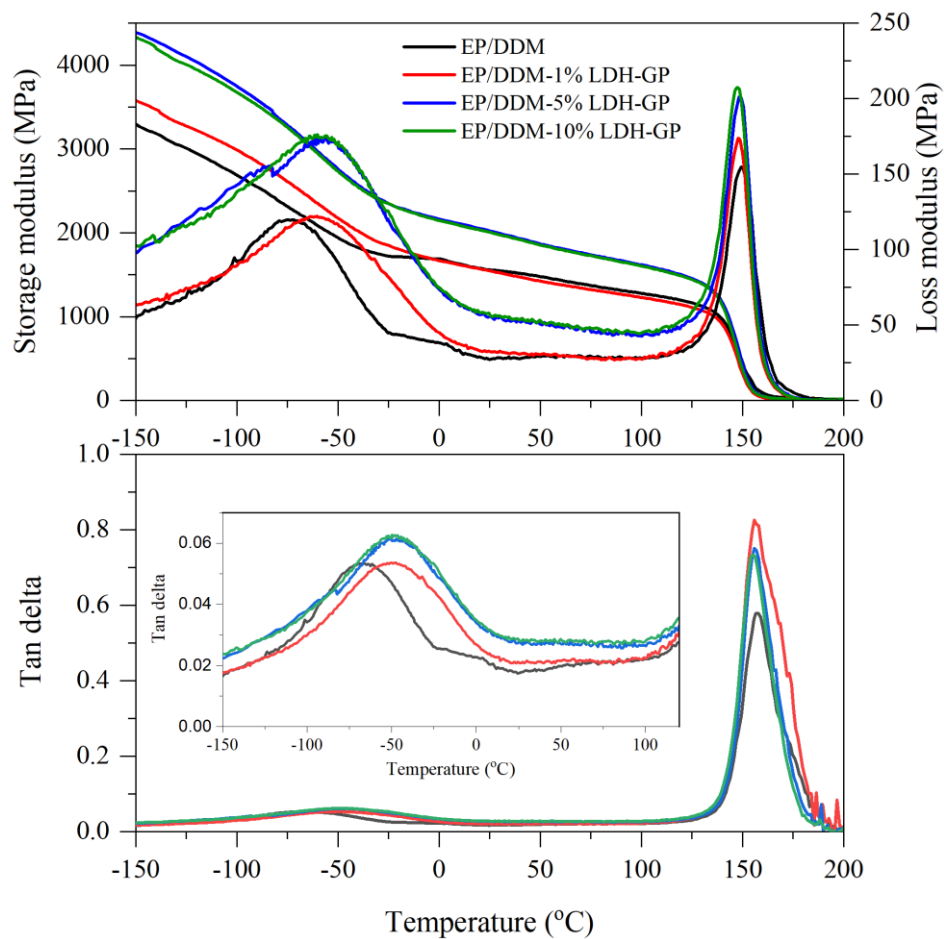


Figure 6.14 The storage modulus, loss modulus and $\text{Tan } \delta$ of the DGEBA/DDM and its nanocomposites containing the varied contents of LDH-GP.

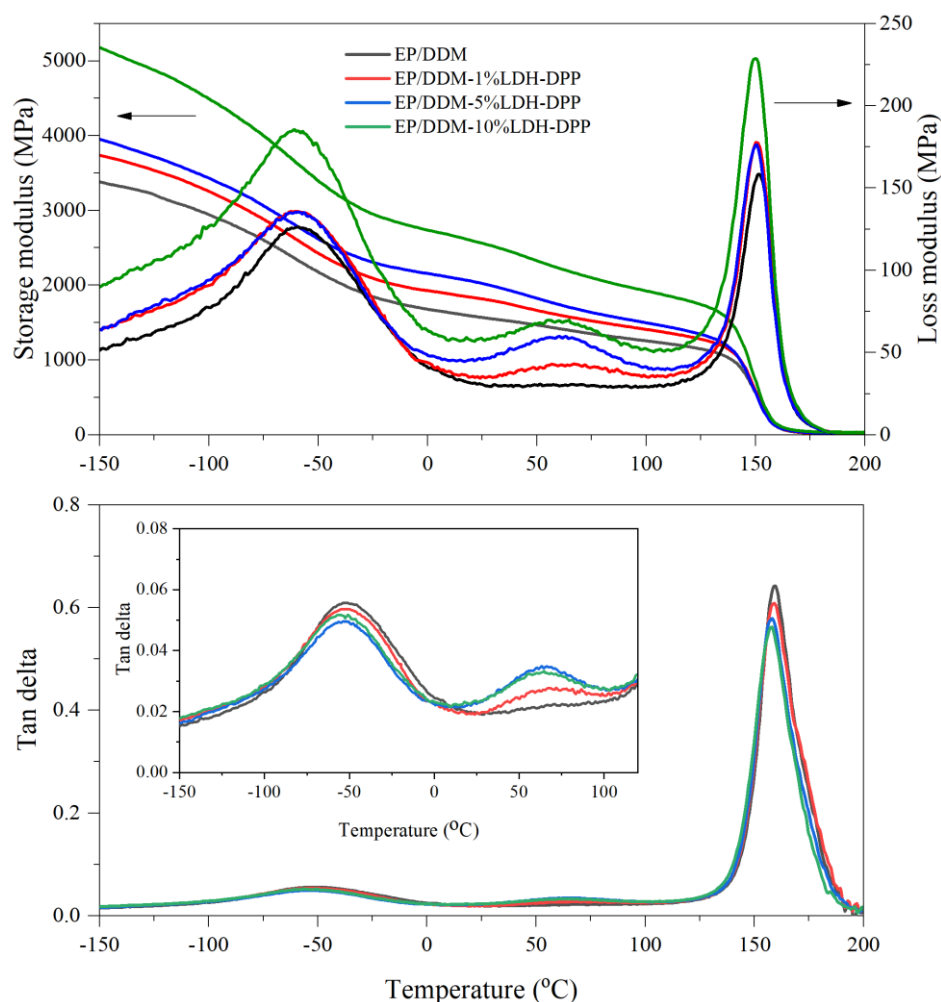


Figure 6.15 The storage modulus, loss modulus and Tan δ of the DGEBA/DDM and its nanocomposites containing the varied contents of LDH-DPP.

For the results of loss modulus and tan δ , the two peaks in the curves can be observed in both the pure EP and the epoxy nanocomposites with adding the LDHs modified the BEHP, Phy or GP. The values of T_{β} and T_g of these composites were reported in Table 6.4. Both the temperatures of the nanocomposites with loading the LDH-BEHP, LDH-Phy or LDH-GP resembled the pure EP and the EP/pristine LDHs. The results stated that the organophosphate ester-modified LDHs did not affect the mobility of side molecules on the EP chains and backbone of EP in the composites.

Table 6.4 The T_{β} , T_g and cross-link density of the pure EP and EP nanocomposites containing the BEHP, Phy, GP or DPP modified LDHs cured with the DDM in the different contents of LDHs.

Sample	T_{β} (°C)	T_{ω} (°C)	T_g (°C)	E' at T_g+30 (MPa)	Crosslink density (mol/m ³)
Pure EP/DDM	-51.7 ± 1.1	-	159.2 ± 0.5	17.6 ± 3.5	1530 ± 302.0
EP/DDM-1% LDH-BEHP	-49.9 ± 0.4	-	161.3 ± 0.2	24.1 ± 0.4	2078.8 ± 30.6
EP/DDM-5% LDH- BEHP	-48.2 ± 1.0	-	160.8 ± 0.4	25.0 ± 5.9	2158.0 ± 507.8
EP/DDM-10% LDH- BEHP	-52.0 ± 1.7	-	159.1 ± 0.3	29.0 ± 6.0	2516.6 ± 524.2
EP/DDM-1% LDH-Phy	-51.0 ± 2.1	-	158.5 ± 0.2	19.0 ± 2.4	1646.1 ± 211.1
EP/DDM-5% LDH-Phy	-51.0 ± 0.2	-	158.3 ± 0.6	22.4 ± 1.8	1948.8 ± 155.1
EP/DDM-10% LDH-Phy	-48.4 ± 0.4	-	159.4 ± 0.4	24.3 ± 2.3	2106.4 ± 203.3
EP/DDM-1% LDH-GP	-49.8 ± 0.9	-	158.5 ± 0.2	14.4 ± 0.7	1254.2 ± 59.7
EP/DDM-5% LDH-GP	-49.1 ± 1.0	-	158.3 ± 0.6	16.8 ± 3.3	1456.6 ± 288.2
EP/DDM-10% LDH-GP	-49.5 ± 0.3	-	159.4 ± 0.4	17.2 ± 0.1	1488.0 ± 9.2
EP/DDM- 1%LDH-DPP	-51.5 ± 0.7	70.9 ± 1.6	159.0 ± 0.1	17.8 ± 0.4	1544.9 ± 32.8
EP/DDM-5% LDH-DPP	-52.4 ± 0.8	63.9 ± 0.1	158.0 ± 0.0	24.9 ± 3.8	2397.2 ± 40.0
EP/DDM-10% LDH-DPP	-50.2 ± 0.4	71.9 ± 0.1	156.7 ± 2.0	33.1 ± 2.1	2882.4 ± 194.3

However, the loss modulus and $\tan \delta$ plots of EP/LDH-DPP nanocomposites in Figure 6.15 were different from the other nanocomposites. The thermograms presented three regions of relaxation. The two of three peaks provided the same maximum temperatures as the other nanocomposites at around -50°C and 150°C , corresponding to T_{β} and T_g , respectively. Meanwhile, another peak took place at the intermediate temperatures between the T_{β} and T_g , observed around 60°C . The previous study calling the phenomenon at this temperature was an omega transition (T_{ω}) [12].

The literature reported that this relaxation reflected the segments of unreacted molecules and/or heterogeneity in the composites resulting from distinctive cross-linking resins [12]. For this reason, the particles of LDH-DPP could not interact with the cured EP/DDM. It has been speculated that the phenyl groups in the DPP intercalated in the LDH layers, which were high stability, might not react with the epoxy matrix. The T_{β} , T_{ω} and T_g of the EP nanocomposites containing the LDH-DPP were reported in Table 6.4.

Considering the calculated cross-link density of the EP nanocomposites in Table 6.4, it increased by adding the high loading of the organophosphate-modified LDHs. The trend of this result was similar to the addition of LDH- CO_3 or LDH- NO_3 . The causes of this circumstance were described previously.

To evaluate the performance of the different LDHs in the EP nanocomposites, the 5wt% LDHs were used for the comparison. The storage modulus, loss modulus and $\tan \delta$ of the samples are plotted in Figure 6.16-6.18, respectively. For all the EP/LDHs nanocomposites, the storage modulus improved over the temperature range compared with the pure EP. The storage modulus of EP/LDH-GP or LDH-DPP nanocomposites was more improved than the EP/LDH- CO_3 or LDH- NO_3 nanocomposites. The results suggested that the layers of the GP or DPP modified LDHs could be exfoliated more than the inorganic compounds-intercalated LDHs. It might increase the surface areas of the modified LDHs, enhancing the stiffness in the EP nanocomposites. Thus, there was the increase of storage modulus with adding the organophosphate-modified LDHs.

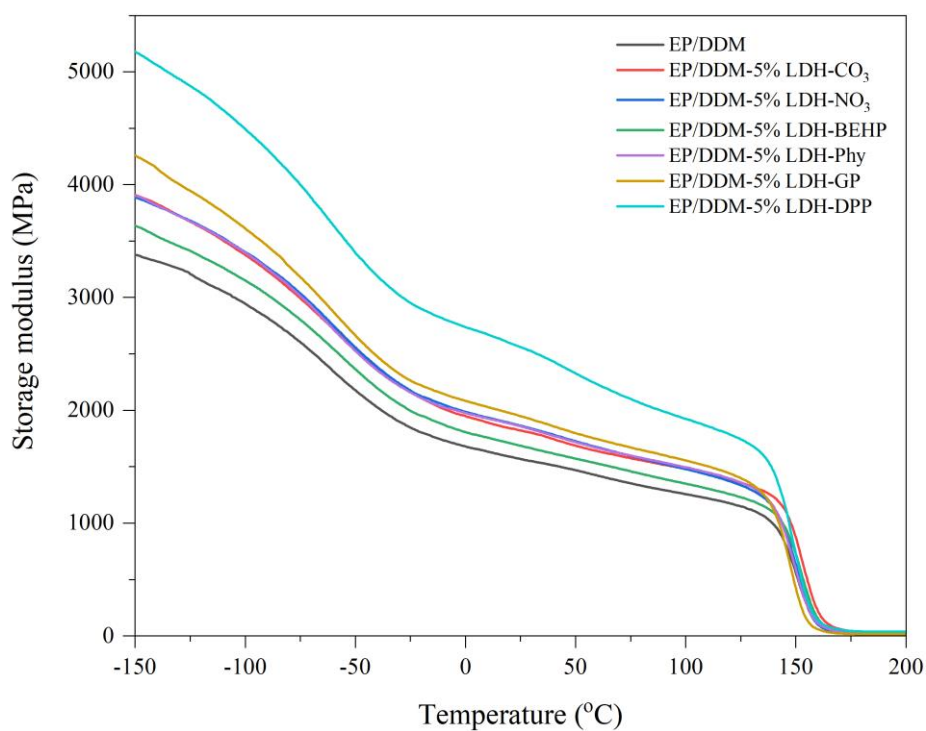


Figure 6.16 The storage modulus of the pure EP and its nanocomposites containing the 5 wt% loading volume of LDH-CO₃, LDH-NO₃, LDH-BEHP, LDH-Phy, LDH-GP and LDH-DPP in the curing system of DDM.

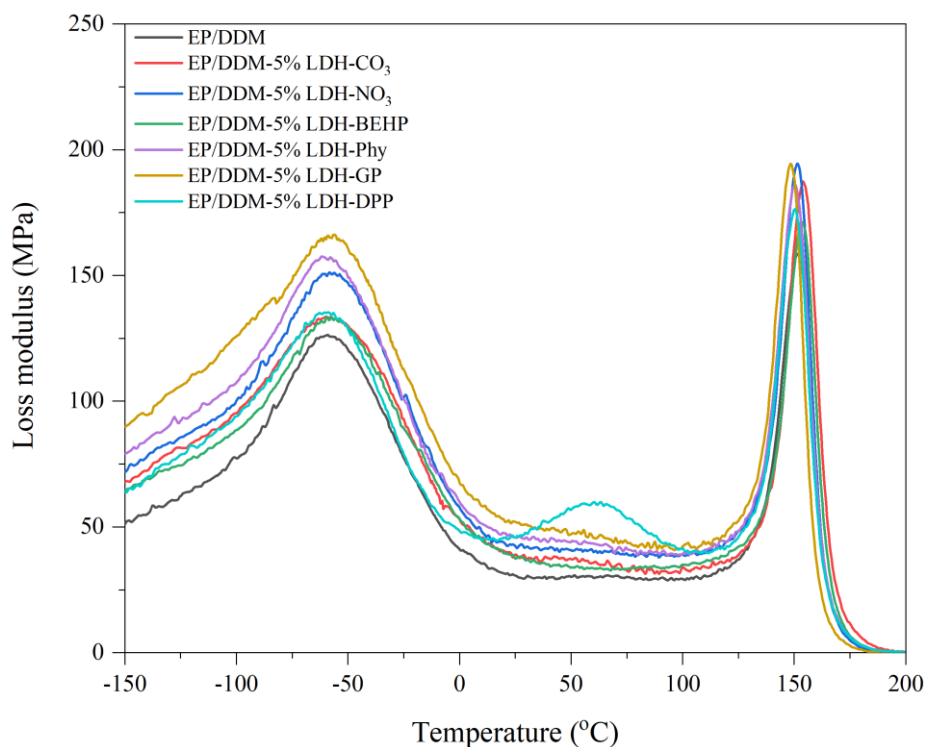


Figure 6.17 The loss modulus of the pure EP and its nanocomposites containing the 5% loading volume of LDH-CO₃, LDH-NO₃, LDH-BEHP, LDH-Phy, LDH-GP and LDH-DPP in the curing system of DDM.

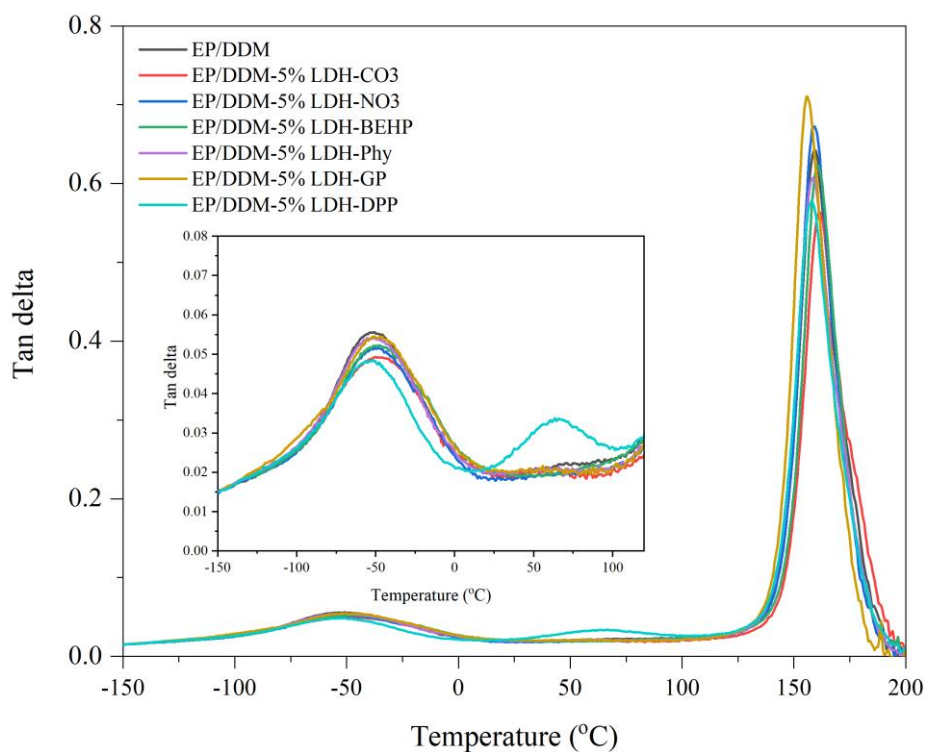


Figure 6.18 The $\tan \delta$ of the pure EP and its nanocomposites containing the 5% loading volume of LDH- CO_3 , LDH- NO_3 , LDH-BEHP, LDH-Phy, LDH-GP and LDH-DPP in the curing system of DDM.

For the EP nanocomposites with the LDH-BEHP loading, the storage modulus was less than the addition of LDH- CO_3 or LDH- NO_3 . Meanwhile, the storage modulus of EP/LDH-Phy compound seemed to be similar to the nanocomposites containing the unmodified LDHs.

According to the flexural strength and modulus results, they indicated the agglomeration of LDHs in the epoxy matrix. The large agglomeration of the fillers might exist in the composites, reducing the surface interaction between the fillers and the matrix. It decreased the elasticity of the epoxy nanocomposites. Nevertheless, there was no change in the peaks for the loss modulus and the tan delta. Although the LDHs interacted with the matrix and agglomerated together, they did not affect the movement of polymer chains.

To enhance the T_g and mechanical properties of resins, the surface of LDHs should be functionalised by interface modifiers e.g. stearic acid. The chemical structure of stearic acid contains a carboxylic group with a long alkyl chain. The carbonyl group

in the stearic acid can interact with the LDH with hydrogen bond, whereas the long alkyl chain of the stearic acid bond to the DGEBA. Therefore, the surface modification of LDH can decrease the surface energy of LDH particulates, protecting the agglomeration of the particulate fillers in the polymer matrix.

6.6 Thermal Stability of Epoxy Resin/LDHs Nanocomposites Cured with DDM

The thermal degradation behaviours of the pure EP and its LDHs nanocomposites were investigated by the thermogravimetric analysis (TGA) measurement both under nitrogen or air. The test under nitrogen was used for studying the decomposition reacting to the only heating [13]. Meanwhile, the test under air was to evaluate the thermal oxidation degradation simulating the decomposition in the actual environment [14]. In general, the thermal stability of samples was mainly determined by a temperature at 10% of the mass loss ($T_{10\%}$), a temperature at mid-point of mass loss ($T_{50\%}$), a temperature of maximum mass loss (T_{max}) and a percentage residue at 800°C [15]. The effect of various types and contents of the pristine and modified LDHs on the thermal stability of DDM cured EP nanocomposites were studied.

6.6.1 Thermal Stability of EP/Pristine LDHs Nanocomposites in the DDM Curing System under the N₂ Atmosphere

Figure 6.19 demonstrated the TGA curves and their derivatives of the LDH-CO₃, pure EP and EP/LDH-CO₃ nanocomposites in the DDM curing system under the N₂ condition. The related data were listed in Table 6.5. With the observation of the thermograms, the pure EP presented one main stage of mass loss between 300°C and 500°C with the T_{max} at 402.3°C. It was ascribed to the random scission of epoxy chains [16] and cross-linked macromolecular networks [17, 18]. Dong et al. [19] suggested that the ether linkage and alkyl fractions in the DDM-cured DGEBA were cleaved during the thermal decomposition process, resulting in the volatile release of phenol, amine, ester, ether, aliphatic hydrocarbons, water, CO₂ and CO. Due to the recombination and rearrangement of degraded bonds during the heating, it induces the

formation of stable charred structure [18]. The residual content of EP/DDM at 800°C was 16.3%.

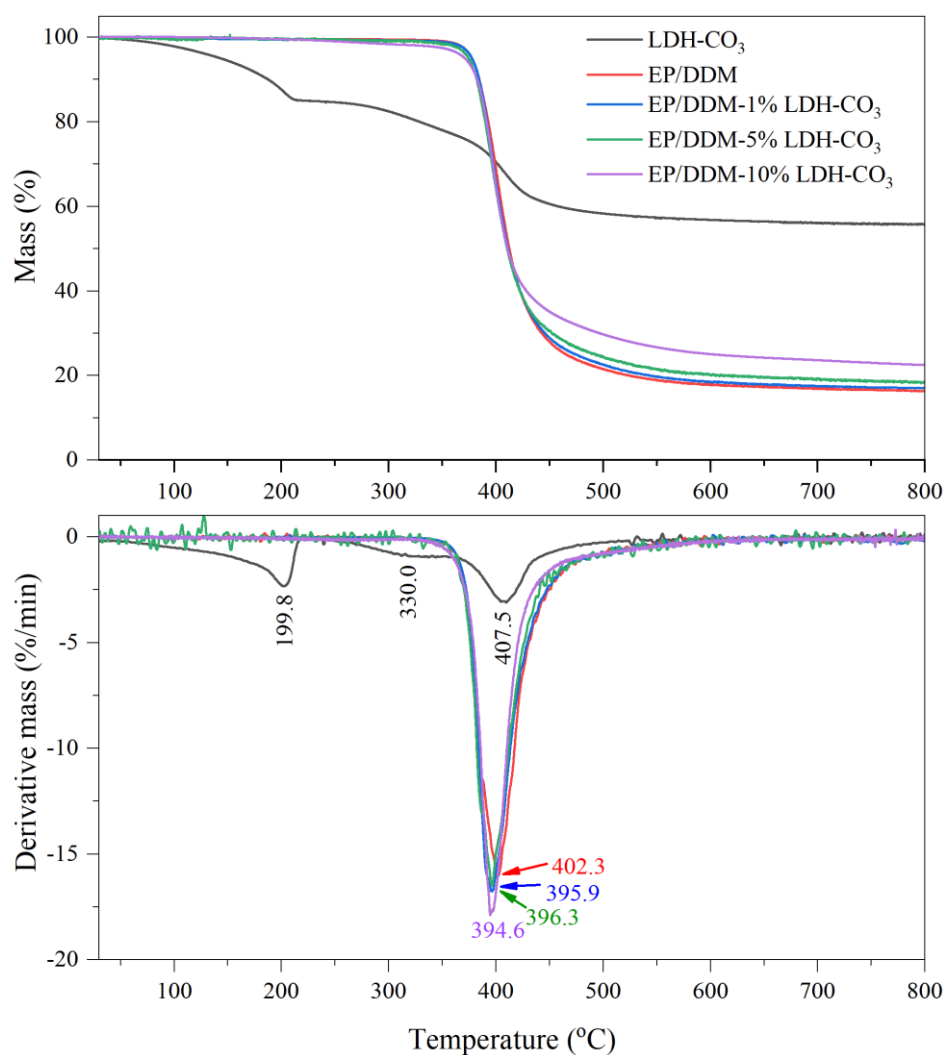


Figure 6.19 The TGA curves and their derivatives of the LDH-CO₃, pure EP/DDM and nanocomposites with adding the LDH-CO₃ in the flowing N₂.

Table 6.5 The T_{10%}, T_{50%}, T_{max} and the residual mass at 800°C of the pure EP/DDM and its nanocomposites with adding the LDH-CO₃ under N₂.

Sample	T _{10%} (°C)	T _{50%} (°C)	T _{max} (°C)	Mass at 800°C (%)
EP/DDM	384.4	412.5	402.3	16.3
EP/DDM-1% LDH-CO ₃	384.4	411.2	395.9	17.1
EP/DDM-5% LDH-CO ₃	382.1	410.4	396.3	18.4
EP/DDM-10% LDH-CO ₃	382.4	410.8	394.6	22.5

When the LDH-CO₃ was incorporated in the resin matrix with a different percentage of loading, all the epoxy nanocomposites exhibited one degradation stage with the same decomposition temperature range as the pure EP. However, the T_{10%} and T_{50%} of all the nanocomposites were lower than the pure EP. At the 1 wt% LDH-CO₃, the T_{10%} and T_{50%} of EP nanocomposite seemed no significant difference from the pure EP. The T_{10%} and T_{50%} of pure EP/DDM were 384.4°C and 412.5°C, respectively.

If the LDH-CO₃ loading increased from 1 wt% to 5 wt% and 10 wt%, there were slight declinations of T_{10%} and T_{50%} by around 2°C from the pure EP. Moreover, the T_{max} of all the nanocomposites shifted to lower temperatures compared to the pure EP. The DTG peak of the pure EP was 402.3°C, whereas the EP nanocomposites containing 1 wt%, 5 wt% and 10 wt% of LDH-CO₃ were 395.9°C, 396.3°C and 394.6°C, respectively. Thus, the T_{10%}, T_{50%} and T_{max} were likely to reduce with increasing the LDH-CO₃ contents in the EP nanocomposites.

Considering the thermal behaviour of LDH-CO₃, it decomposed approximately in the range of 100-500°C, providing the evaporation of water molecules in the LDH, the dehydroxylation of metal hydroxides and the decomposition of CO₂ intercalated in the interlayer spaces. It can be seen that the decomposition of LDH-CO₃ was lower than the pure EP. For this reason, the reduction of temperatures in the EP/LDH-CO₃ nanocomposites was probably associated with the decomposition of LDH-CO₃.

Furthermore, the residue at 800°C increased with loading the LDH-CO₃ from the 16.3% for the pure EP to the 17.1%, 18.4% and 22.5% for the 1 wt%, 5 wt% and 10 wt% LDH-CO₃, respectively. The thermal degradation of LDH-CO₃ produced mixed metal oxides such as MgO and MgAl₂O₄ [20]. Hence, the residue of the composites consisted of carbonaceous char deriving from the degradation of the polymer matrix and mixed metal oxides resulting from the dehydroxylation of LDH. This circumstance caused the enhancement of char yield with the increase of LDH-CO₃ loading.

From the above TGA results, the incorporation of LDH-CO₃ at the higher contents (5 wt% and 10 wt%) in the EP nanocomposites led to the reduction of T_{10%}, T_{50%} and T_{max}, but the elevation of residual volume. These data demonstrated that the LDH-

CO₃ embedded in the resin matrix could accelerate the thermal degradation of the EP nanocomposites and the production of more residues. Nevertheless, the results in this study do not agree with the previous research. Tseng et al. [11] showed that the decomposition temperature at 5% mass loss was increased by adding the LDH-CO₃ in the EP nanocomposites cured with the DDM. It might be because of the curing profile difference, affecting the formation of three-dimensional networks in the material.

Another type of pristine LDH used as filler for the epoxy resin was LDH-NO₃. Figure 6.20 compared the TGA curves and their derivatives of EP/LDH-NO₃ nanocomposites with the LDH-NO₃ and the pure EP. The TGA results of the composites displayed one stage of mass loss in the range of 300-500°C, which were similar to the pure EP. As the main compositions of EP/LDH-NO₃ nanocomposites were the cured epoxy resin, the mass loss of nanocomposites in the TGA curves represented the degradation of cured EP.

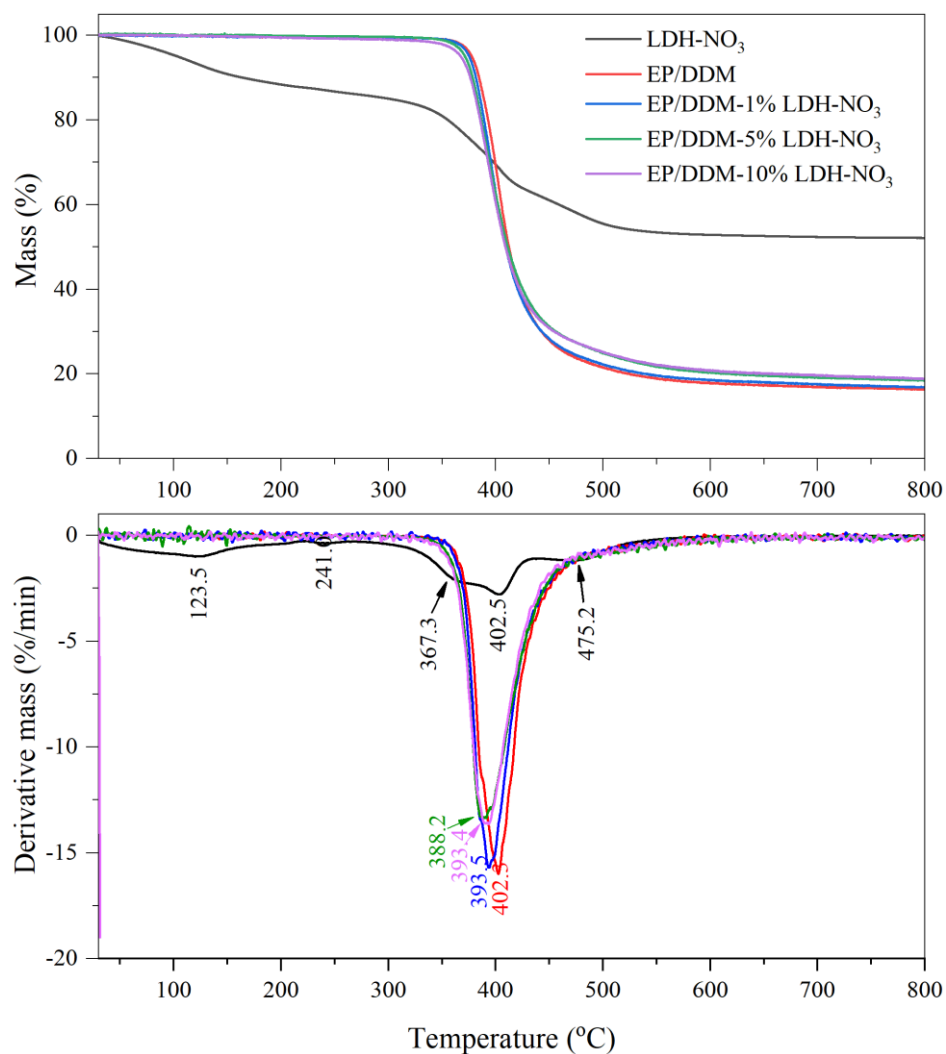


Figure 6.20 The TGA curves and their derivatives of the pure EP/DDM and its nanocomposites with adding the LDH-NO₃ under the flowing N₂.

With the incorporation of 1 wt% LDH-NO₃, there were the slight reductions of T_{10%} and T_{50%} by approximately 3°C for the EP nanocomposite, compared with the unfilled EP. Also, the T_{max} of EP/1% LDH-NO₃ (393.5°C) was much lower than that of the pure EP (402.3°C). When the 5 wt% and 10 wt% of LDH-NO₃ were blended to the resin matrix, the T_{10%}, T_{50%} and T_{max} of the EP nanocomposites depressed gradually. Besides, the addition of LDH-NO₃ at the higher loading caused the increase of the residual yield at 800°C from 16.3% for the pure EP to 18.8% for the 10% loading of unmodified LDH. Table 6.6 summarised the TGA data of the unfilled EP and its nanocomposites containing the different contents of LDH-NO₃.

Table 6.6 The $T_{10\%}$, $T_{50\%}$, T_{\max} and the residual mass at 800°C of the pure EP/DDM and its nanocomposites with adding the LDH- NO_3 under N_2 .

Sample	$T_{10\%}$ ($^{\circ}\text{C}$)	$T_{50\%}$ ($^{\circ}\text{C}$)	T_{\max}	Mass at 800°C (%)
EP/DDM	384.4	412.5	402.4	16.3
EP/DDM-1% LDH- NO_3	381.4	409.4	393.5	16.9
EP/DDM-5% LDH- NO_3	378.4	411.3	388.2	18.4
EP/DDM-10% LDH- NO_3	376.0	409.1	393.4	18.8

Compared with the incorporation of LDH- CO_3 , the EP/LDH- NO_3 nanocomposites provided the same thermal behaviour trend as the LDH- CO_3 . The $T_{10\%}$, $T_{50\%}$ and T_{\max} decreased, but the residue increased with loading the unmodified LDHs at the higher contents. As described previously, the reduction of decomposition temperatures in the nanocomposites occurred under the LDHs loading. This event led to the fast production of char residues. The formation of char at the lower temperature was a good performance for the application of flame-retardant fillers.

6.6.2 Thermal Stability of EP/Modified LDHs Nanocomposites in the DDM Curing System under the N_2 Atmosphere

The influence of LDH modified with the various organophosphate ester-based anions on the thermal stability of EP nanocomposites was studied. The TGA thermograms and their derivatives of EP nanocomposites filling the LDHs modified with the BEHP, Phy, GP and DPP were shown in Figure 6.21-6.24, respectively. The Figures also displayed the TGA results of the organophosphate compounds used as the reagents to modify LDHs, the modified LDHs and the pure EP. For the crucial results in the thermograms of samples, they were presented in Table 6.7-6.10.

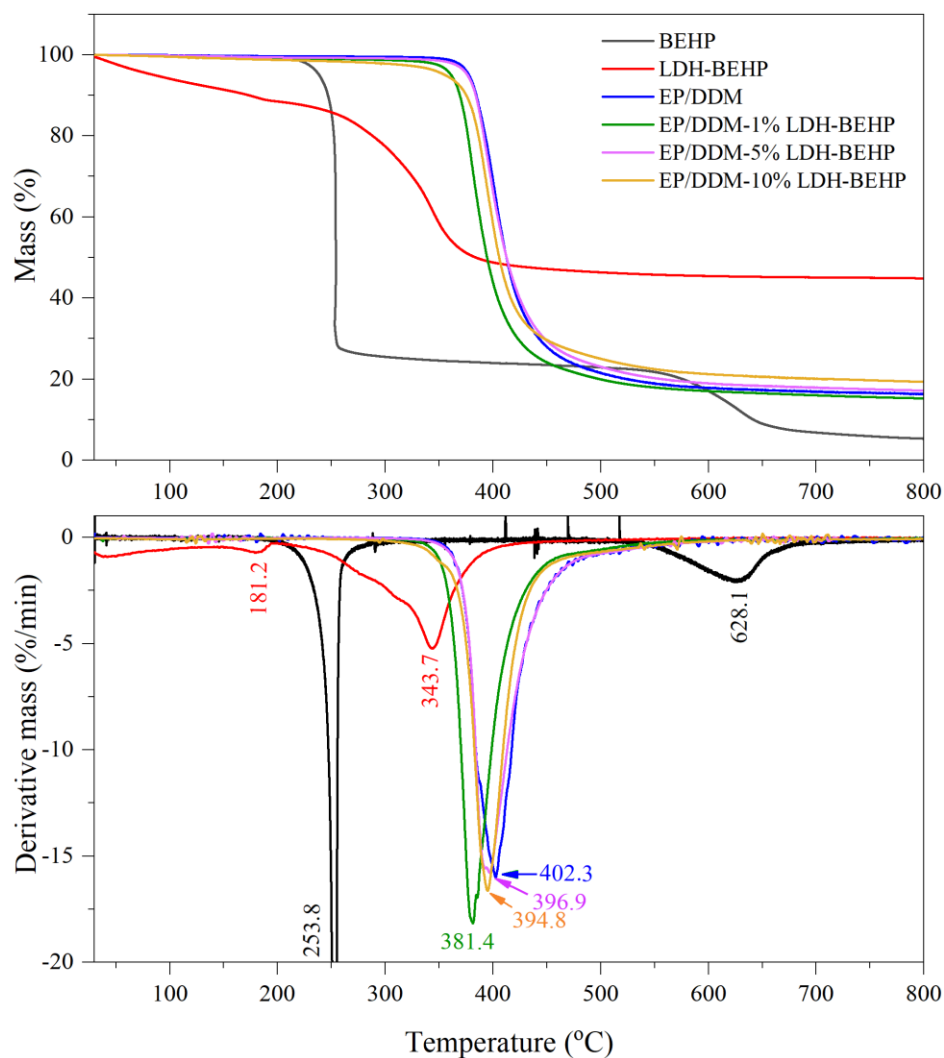


Figure 6.21 The TGA curves and derivatives of the BEHP, LDH-BEHP, pure EP/DDM and nanocomposites with adding the LDH-BEHP under N_2 atmosphere.

Table 6.7 The $T_{10\%}$, $T_{50\%}$, T_{max} and the residue at $800^\circ C$ under N_2 atmosphere of the pure EP/DDM and its nanocomposites containing the LDH-BEHP

Sample	$T_{10\%}$ ($^\circ C$)	$T_{50\%}$ ($^\circ C$)	T_{max}	Mass at $800^\circ C$ (%)
EP/DDM	384.4	412.5	402.4	16.3
EP/DDM-1% LDH-BEHP	369.1	394.5	381.4	15.3
EP/DDM-5% LDH-BEHP	383.8	412.6	396.9	17.2
EP/DDM-10% LDH-BEHP	375.1	405.8	395.0	24.3

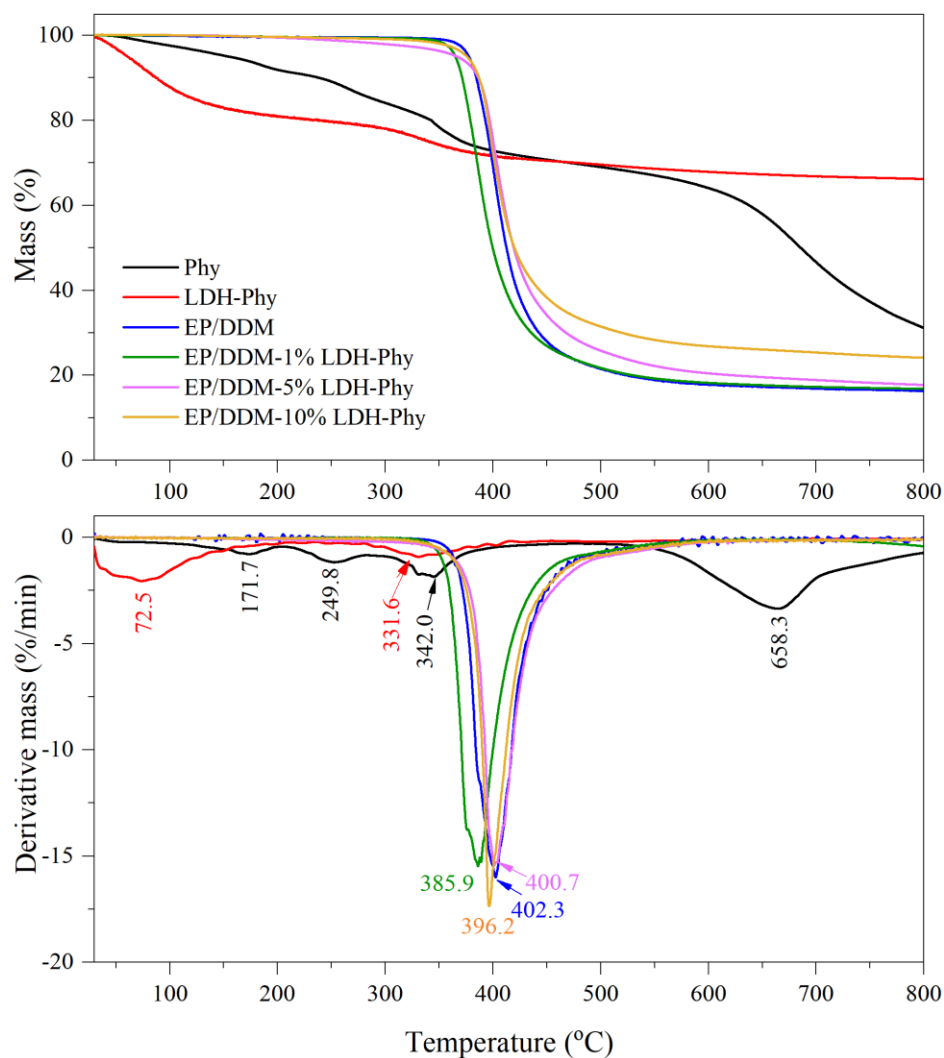


Figure 6.22 The TGA curves and derivatives of the Phy, LDH-Phy, pure EP/DDM and nanocomposites with adding the LDH-Phy under N_2 atmosphere.

Table 6.8 The $T_{10\%}$, $T_{50\%}$, T_{max} and the residue at $800^\circ C$ under N_2 atmosphere of the pure EP/DDM and its nanocomposites containing the LDH-Phy

Sample	$T_{10\%}$ ($^\circ C$)	$T_{50\%}$ ($^\circ C$)	T_{max}	Mass at $800^\circ C$ (%)
EP/DDM	384.4	412.5	402.4	16.3
EP/DDM-1% LDH-Phy	371.3	399.6	385.9	16.9
EP/DDM-5% LDH-Phy	386.4	419.1	400.8	17.7
EP/DDM-10% LDH-Phy	386.9	419.8	396.1	24.1

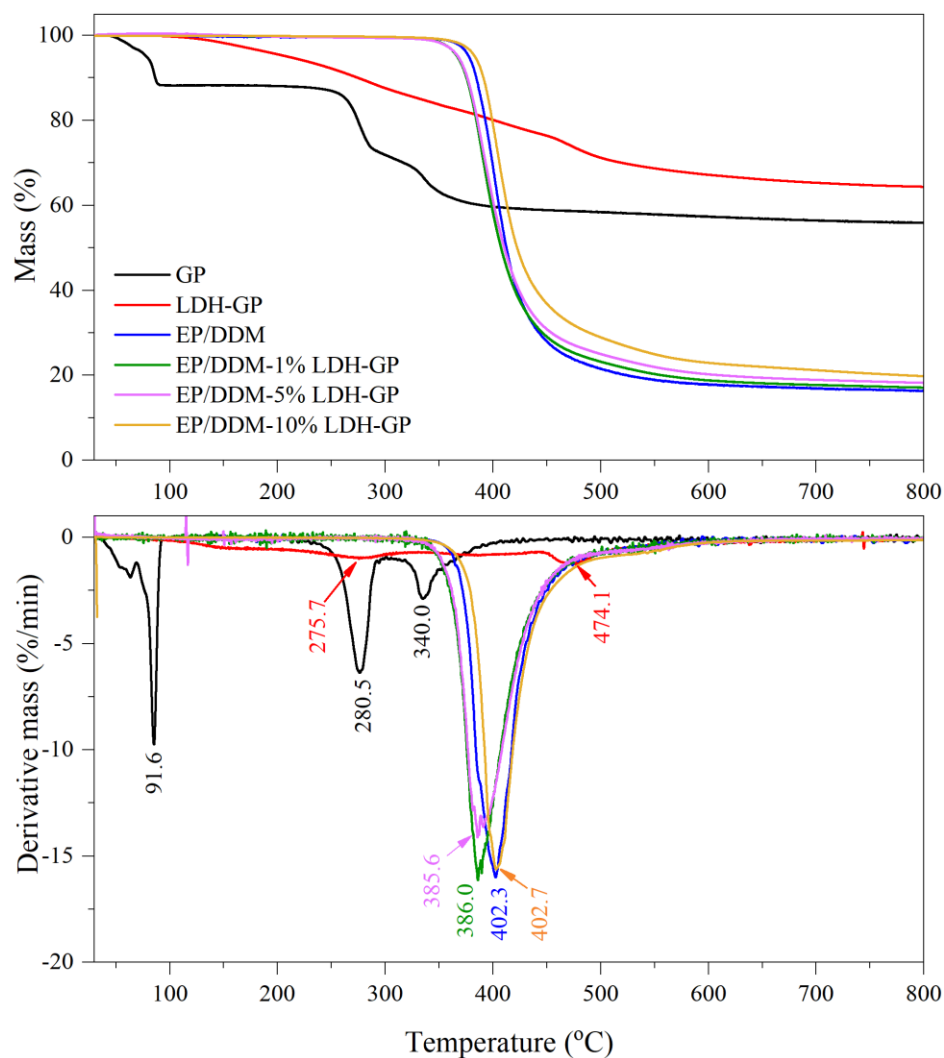


Figure 6.23 The TGA curves and derivatives of the GP, LDH-GP, pure EP/DDM and nanocomposites with adding the LDH-GP under N_2 atmosphere.

Table 6.9 The $T_{10\%}$, $T_{50\%}$, T_{max} and the residue at $800^\circ C$ under N_2 atmosphere of the pure EP/DDM and its nanocomposites containing the LDH-GP

Sample	$T_{10\%}$ ($^\circ C$)	$T_{50\%}$ ($^\circ C$)	T_{max}	Mass at $800^\circ C$ (%)
EP/DDM	384.4	412.5	402.4	16.3
EP/DDM-1% LDH-GP	375.4	407.4	387.5	17.1
EP/DDM-5% LDH-GP	376.2	410.4	385.6	18.2
EP/DDM-10% LDH-GP	391.0	422.5	402.7	19.8

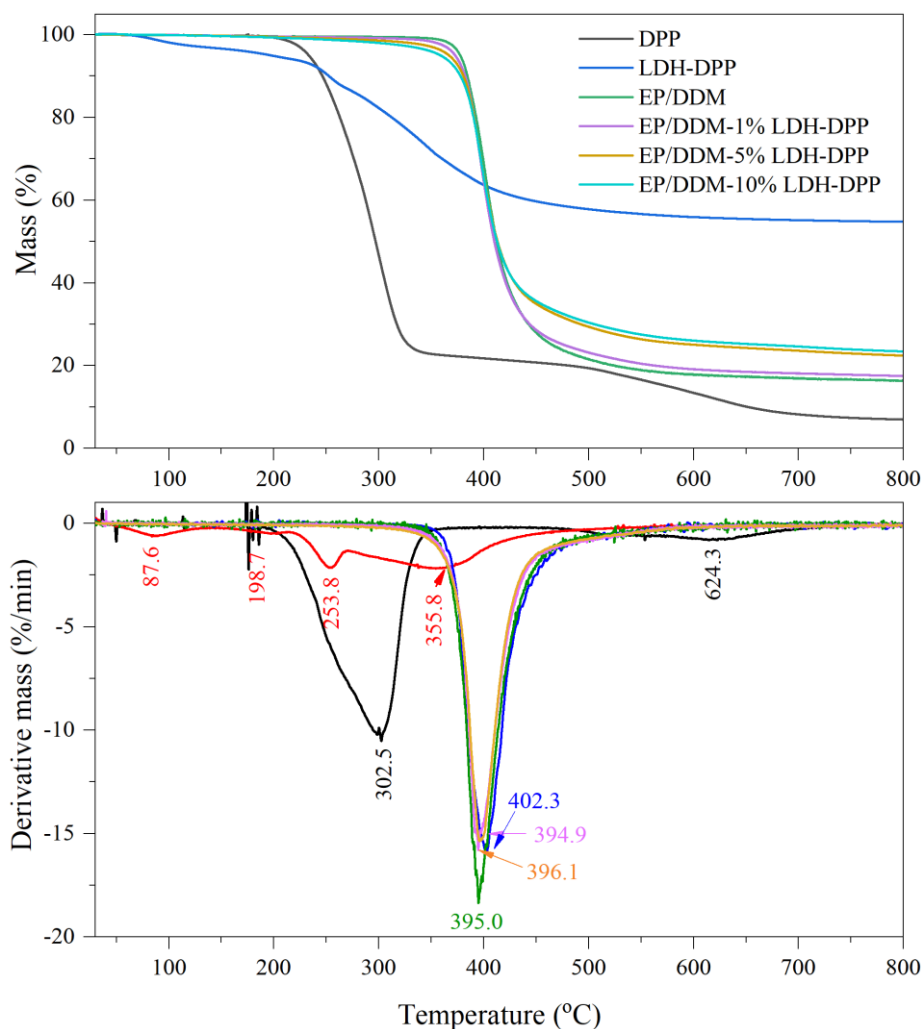


Figure 6.24 The TGA curves and derivatives of the DPP, LDH-DPP, pure EP/DDM and nanocomposites with adding the LDH-DPP under N_2 atmosphere.

Table 6.10 The $T_{10\%}$, $T_{50\%}$, T_{max} and the residue at $800^\circ C$ under N_2 atmosphere of the pure EP/DDM and its nanocomposites containing the LDH-DPP

Sample	$T_{10\%}$ ($^\circ C$)	$T_{50\%}$ ($^\circ C$)	T_{max}	Mass at $800^\circ C$ (%)
EP/DDM	384.4	412.5	402.4	16.3
EP/DDM-1% LDH-DPP	382.3	410.1	395.0	17.5
EP/DDM-5% LDH-DPP	380.6	413.1	394.9	22.4
EP/DDM-10% LDH-DPP	377.8	412.7	395.9	23.4

The thermograms of all EP/modified LDH nanocomposites displayed one step of weight loss between $300^\circ C$ and $500^\circ C$. The decomposed temperature ranges of each composite were nearby the thermal degradation temperature of pure EP. However, the

$T_{10\%}$, $T_{50\%}$, and T_{\max} were shifts in the epoxy nanocomposites with the variation of LDH contents and types compared to the pure EP. The mass loss in all the composites can be attributed to the random breakage of bonds within the cured epoxy resin.

The addition of 1 wt% modified LDHs reduced the $T_{10\%}$, $T_{50\%}$ and T_{\max} from the pure EP. The temperatures at 10% mass loss were 369.1°C, 371.3°C, 375.4°C and 382.3°C and the temperatures at 50% mass loss were 394.5 °C, 399.6°C, 407.4°C and 410.1°C for the loading of 1 wt% LDHs modified with the BEHP, Phy, GP and DPP, respectively. The T_{\max} of resin composites containing the 1 wt% LDH-BEHP, LDH-Phy, LDH-GP and LDH-DPP were lower than that of pure EP (402.3°C) by 20.9°C, 16.4°C, 16.3°C and 7.3°C, respectively.

Considering the mass loss in the pure organophosphate ester-based reactants and the LDHs modified with those compounds, both decomposed in the range of 100°C to 650°C. It can be seen that the decomposition temperatures of all the pure organophosphate compounds and the modified LDHs were lower than that of the pure EP. The reduction of decomposition temperatures in the EP nanocomposites might cause the thermal decomposition of the organophosphate compounds intercalated in the layers of LDH and the metal hydroxides in the lamellae.

When the loading contents of modified LDHs increased to 5 wt%, all the three temperatures of most nanocomposites still were lower than those of the pure EP but higher than the EP/1% LDHs nanocomposites. This trend excluded the addition of LDH-Phy. The degradation of the organic compounds and the layers in the modified LDHs might affect the decrease of $T_{10\%}$. However, the temperatures at the mid-point decomposition of all EP/5%LDHs nanocomposites increased slightly. The results could imply that the initial thermal degradations of the EP nanocomposites provided the decomposition of modified LDHs, inducing the reduction at the $T_{10\%}$. Afterwards, the organophosphate-modified LDHs can impede the degradation of EP nanocomposites. That meant the thermal stability of EP compounds enhanced with the component of modified LDHs.

Meanwhile, the addition of 10 wt% modified LDHs encouraged the increase of $T_{10\%}$ in some EP nanocomposites containing the Phy and GP. At the mid-point percentage

of mass loss, the temperatures of the EP nanocomposites were higher than the pure EP. It was the same reason as in the addition of the 5% modified LDHs, described above. In addition to the enhancement of decomposition temperatures, the high loading contents of LDHs in the resin matrix led to the gradual increase of the percentage residues at 800°C. As the thermal decomposition at the high temperature of the organophosphate ester-based anions in the LDHs could produce the carbonaceous char, and the layers of LDHs could promote the metal oxides, the mass of residue in the EP nanocomposites increased.

As observed in the literature, one published paper on the efficiency of LDHs intercalated the BEHP and Phy on the thermal stability of polymers. Wang et al. [21] indicated that the addition of 10% LDH-BEHP could improve the thermal stability of PMMA composites due to the slight increases of decomposition temperatures at 10% and 50% mass loss. On the contrary, the thermal stability of PS composite with the 10% loading of LDH-BEHP reduced.

For the Phy intercalated LDH, the initial decomposition at 5% mass loss of the PP composites combining ammonium polyphosphate (APP) and LDH-Phy took place at the lower temperature than the PP/APP composite [22]. Furthermore, the incorporation of LDH-Phy enhanced the thermal stability of polymer composites-based PLA and intumescent flame retardant [23]. From the literature, it can be seen that the influence of LDH-BEHP and LDH-Phy on the thermal behaviors of epoxy resin was not studied. However, the thermal behaviors of epoxy resin nanocomposites containing the LDH-BEHP or LDH-Phy obtained from this study presented the same trend as the previously studied polymers. The incorporation of both modified LDHs enhanced the thermal stability of epoxy resin. At the higher content of LDHs, the nanocomposites exhibited the higher temperature of decomposition and the more content of char residues. The increases of thermal stability and char content were positive results for the enhancement of flame retardancy of epoxy resin nanocomposites. Hence, it is possible to use the LDH-BEHP and LDH-Phy as the flame retardants for the epoxy resin.

6.6.3 Comparison of Thermal Behaviours of EP/DDM Nanocomposites with the Addition of LDHs Modified with Different Organophosphate Ester-Based Anions

The efficiency of LDHs modified with the various types of organophosphate ester-based anions on the thermal stability of EP nanocomposites was compared under N₂ or air flows, respectively. The 5 wt% loadings of LDHs were used for the efficiency comparison.

6.6.3.1 TGA Test under N₂ Atmosphere

The thermal behaviours of the pure EP and the epoxy nanocomposites containing the different LDHs in the flowing N₂ were shown in Figure 6.25, and the vital data from the TGA were presented in Table 6.11. It was found that the additions of the unmodified and modified LDHs resulted in the reduction of the T_{10%} and T_{50%} in all the EP nanocomposites except the incorporation of LDH-Phy. The decomposition temperature of EP/5% LDH-Phy composites was higher than the pure EP by 2.0°C and 6.6°C for the T_{10%} and T_{50%}, respectively. Moreover, the temperature of maximum mass loss rate in the EP/modified LDHs nanocomposites presented the same trend as the T_{10%} and T_{50%}.

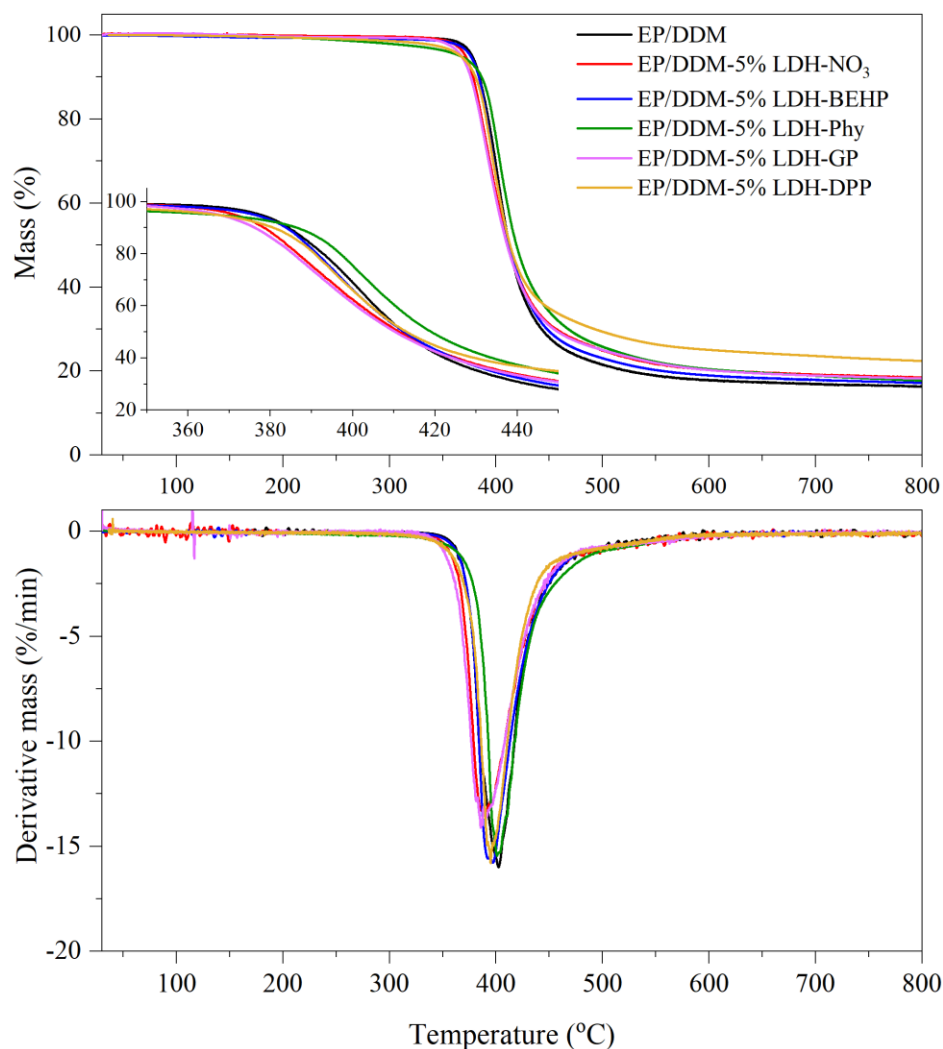


Figure 6.25 The TGA curves and their derivatives of the pure EP and the EP/LDHs nanocomposites with the different types of LDHs under N_2

Table 6.11 The $T_{10\%}$, $T_{50\%}$, T_{max} and residue at $800^\circ C$ under N_2 of the pure EP and its nanocomposites containing the different types of LDHs at 5 wt% loading

Sample	$T_{10\%}$ ($^\circ C$)	$T_{50\%}$ ($^\circ C$)	T_{max}	Mass at $800^\circ C$ (%)
EP/DDM	384.4	412.5	402.4	16.3
EP/DDM-5% LDH- NO_3	378.4	411.3	389.5	18.4
EP/DDM-5% LDH-BEHP	383.8	412.6	396.9	17.2
EP/DDM-5% LDH-Phy	386.4	419.1	400.8	17.7
EP/DDM-5% LDH-GP	376.2	410.4	385.6	18.2
EP/DDM-5% LDH-DPP	380.6	413.1	394.9	22.4

The obtained results indicated that the existence of LDHs intercalated with the NO_3 , BEHP, GP or DPP in the EP matrix could reduce the thermal decomposition temperature of the EP nanocomposites due to the decrease of $T_{10\%}$ and $T_{50\%}$ and T_{max} . The decomposition of P-O-C bonds interacting between the cured resins and the modified LDHs at the low temperature might reduce the decomposition temperature in the resin nanocomposites. Meanwhile, the LDH exfoliated with the Phy contributed to the slight increase of the T_{max} from the pure EP. It could imply that the addition of LDH-Phy increased the thermal stability of the EP nanocomposites.

Furthermore, the residues of EP nanocomposites obtained in the end of TGA increased by 0.9-6.1% with incorporating the 5 wt% pristine or modified LDHs from the pure EP/DDM (16.3%). The residual amounts with loading the LDH-BEHP, LDH-Phy or LDH-GP were not significantly different; however, they were higher than the loading of LDH- NO_3 . All of three modified LDHs induced the decomposition and volatilisation of products more than the LDH- NO_3 . According to the TGA results of LDHs in the Section 5.6.2.6, there was the decomposition of organophosphate ester compounds in the LDHs, inducing the volatilised products of phosphorus-containing compounds. Hence, the char residues reduced with loading the LDH-BEHP, LDH-Phy or LDH-GP. However, the addition of LDH-DPP provided the highest content of char residue at 22.4 %. It was due to the high thermal stability of aromatic groups in the DPP. The char residue obtained from the thermal decomposition of EP/LDH-DPP nanocomposite might contain aromatic compounds.

6.6.3.2 TGA Test under the Air Atmosphere

The thermal stability of samples in air was investigated to represent the actual environment for burning. Figure 6.26 showed the TGA curves and their derivatives of the pure EP and the EP/LDHs nanocomposites under the flowing air, and Table 6.12 presented the important TGA data of the samples. The two stages of the mass loss process were displayed in the TGA curves. The first stage took place between 250°C and 500°C and the second stage occurred in the range of 500-700°C. It was noticeable that there was a difference of thermograms run under air and N_2 . Under N_2 flow the samples possessed a single degradation temperature, while the temperature dependent degradation in air is more complex in all samples.

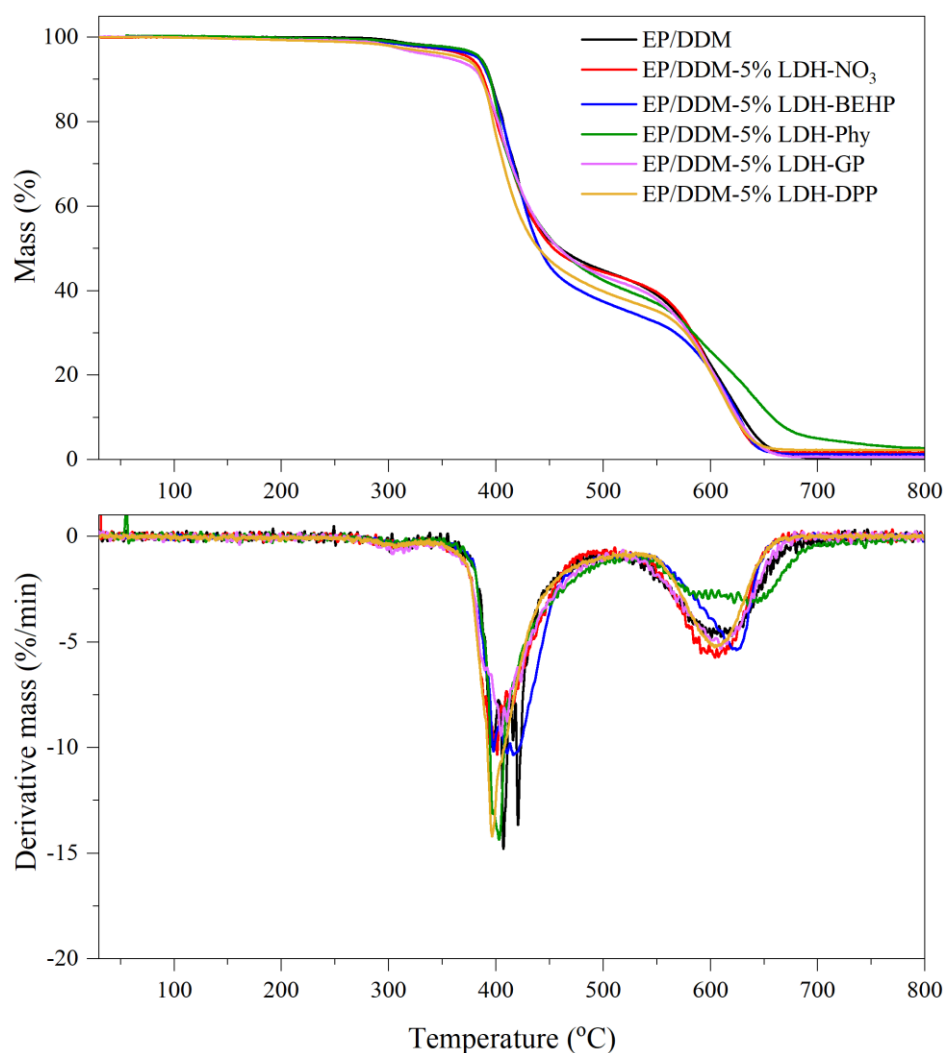


Figure 6.26 The TGA curves and their derivatives of the pure EP and the EP/LDHs nanocomposites with the different types of LDHs under air.

Table 6.12 The $T_{10\%}$, $T_{50\%}$, T_{\max} and residue at 800°C under air of the pure EP and its nanocomposites containing the different types of LDHs at 5 wt% loading.

Sample	$T_{10\%}$ ($^{\circ}\text{C}$)	$T_{50\%}$ ($^{\circ}\text{C}$)	$T_{\max 1}$ ($^{\circ}\text{C}$)	$T_{\max 2}$ ($^{\circ}\text{C}$)	Mass at 800°C (%)
EP/DDM	395.0	460.1	408.3	605.9	0.0
EP/DDM-5% LDH- NO_3	388.7	454.0	401.5	608.1	1.7
EP/DDM-5% LDH-BEHP	393.9	440.8	418.3	626.0	1.2
EP/DDM-5% LDH-Phy	394.9	459.2	402.5	642.9	2.8
EP/DDM-5% LDH-GP	386.3	458.9	403.6	611.3	0.7
EP/DDM-5% LDH-DPP	387.2	439.7	397.3	607.1	2.3

For the pure EP cured with the DDM, the first stage of the mass loss appeared in the range of 300-500°C with the maximum mass loss rate temperature at 408.3°C under air. Comparing with the analysis under N₂ atmosphere, the first stage of mass loss in the air occurred in the same temperature range. Therefore, the possibility of mass loss of the pure EP/DDM under air flow at this stage was the thermal degradation of polymer chains and cross-link networks. During the thermal decomposition of the cured EP, there was the release of gaseous fractions.

According to the previous studies, the volatile products produced from the degradation of the DDM-cured DGEBA between 380°C and 450°C under the air were derivatives of phenol and compounds containing aromatic rings, alkane, ester, ether, CO₂ and CO [24]. At the second stage of the mass loss process, it was at 500-700°C with the maximum mass loss rate temperature at 605.9°C. This process occurred in the thermal-oxidative reaction of char produced in the first stage of decomposition [25].

With the loading of LDHs, the T_{10%} and T_{50%} of the epoxy nanocomposites were shifted to the low temperature by comparison with the pure EP excluding the LDH-Phy. Both the T_{10%} and T_{50%} were in the first event of mass loss. The results indicated that the composites could decompose easier than the pure EP due to the participation of LDH decomposition.

At the temperature of 300-450°C, the LDHs lost water molecules in the interlayer regions and the dehydroxylation of metal hydroxide layers, contributing to the end products of mixed metal oxides. These characteristics could reduce the decomposition temperatures of the epoxy nanocomposites. The fillers with the highest efficiency of T_{10%} and T_{50%} reduction was the LDH-BEHP and LDH-DPP. However, the T_{max} of this decomposition stage of the EP/LDH-DPP nanocomposites was lower than that of the EP/LDH-BEHP nanocomposites. Therefore, the LDH-DPP was the highest performance for the temperature reduction in the first stage decomposition of EP nanocomposites.

For the second mass loss event, it was worth noting that the EP/LDH-Phy provided a broad temperature range of decomposition (500-700°C), whereas the other composites

decomposed between 500°C and 650°C. The T_{\max} of EP/LDH-Phy composite (604.6°C) was higher than any other nanocomposites (607.1-626.0°C). Hence, at the higher temperature, the adding of LDH-Phy could improve the thermal stability of epoxy resin.

At 800°C, the char residue of pure EP was 0, while the nanocomposites containing LDH-NO₃, LDH-BEHP, LDH-Phy, LDH-GP or LDH-DPP provided the mass at 1.7%, 1.2%, 2.8%, 0.7% and 2.3%, respectively. It can be seen that the residual mass of samples increased with incorporating the LDHs. The addition of LDH-Phy contributed to the highest amount of residues, correlating to the molecular weight used to modify the LDHs.

Overall, the TGA results under N₂ and air stated that the incorporation of LDHs accelerated the thermal decomposition of the epoxy nanocomposites at the ranges of 300-450°C, including the char formation. At the higher temperature, the char produced in the first stage of decomposition increased the thermal oxidation stability of the compositions. These phenomenon of LDHs were positive consequences for the application of flame retardant fillers.

6.7 Combustion Behaviors of Epoxy Resin Nanocomposites Cured with DDM

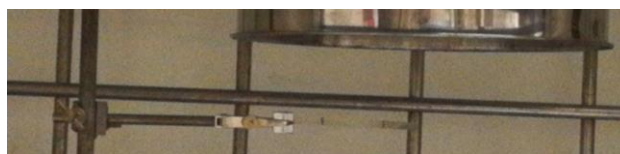
As mentioned in Chapter 2 of the background on the characterisation of combustion behaviours for plastics, the perfect technique is the cone calorimetry. It can detect heat, volatile components and smoke during combustion. The time of ignition and combustion also are measured. The initial research plan of this study was the characterization of combustion behaviours with the cone calorimeter at the University of Bolton. However, this plan has been cancelled due to a long period of COVID-19 pandemic and national lockdown. The Government and The University have announced the health and safety measures during the pandemic. They affected the travel and the working in the laboratory. Thereby, it was necessary to look for a new optional method to set the burning test in the department.

This study selected the UL-94 method because it is not complicated for the setting-up and does not need a specific instrument. Although the UL-94 test cannot provide the same result data as the cone calorimetry, it gives the ignition time, flammability and burning behaviours of the polymeric sample. This combustion test would be carried out in both horizontal and vertical directions. All the burning tests were recorded videos with a mobile phone to measure the burning time and observe the burning behaviors.

6.7.1 Burning Test in Horizontal Direction

The initial burning test was conducted in the K04 laboratory, which was the polymer composites' laboratory. It is well known that the combustion of polymers produces smoke and soot. The burning test was operated in a laboratory fume hood for the preliminary test. From the observation, it was found that large amounts of smoke and soot released during the combustion. As the contaminated air around the burning area was suctioned into the fume hood system to trap the particles and odours in the filter before all get extracted outside, the smoke and soot occurred the burning might enforce the fouling of fillers. From this problem, it had an idea to collect the soot by using a vacuum cleaner connecting to a large metal funnel.

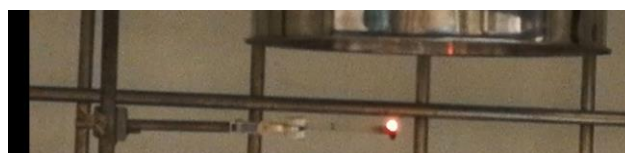
According to the ASTM D635 Standard of burning test in horizontal direction [26]. The two reference lines were marked on the surface of the sample specimen at 25 mm and 100 mm from the free end. The fire source was applied at the end side for 30 s and then moved away. If the flame passes the first marked line, the time would be stated to record. In practically, the sample was extinguished before the flame reached the first marked line. The photo snapshots of the combustion test in the horizontal position in the K04 laboratory are presented in Figure 6.27. It was expected that the suction of the vacuum cleaner might affect the air flow around the burning area because the air flowed in the vertical direction, which was the opposite direction with the flame.



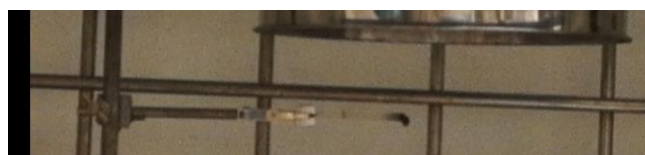
0s



After the ignition for 10s



After the ignition 20s



After the ignition 28s

Figure 6.27 The horizontal burning test in the K04 laboratory.

Although there was a reduction of specimen dimension in the width and thickness, the flame could not pass through the reference line. As the tests operated in the fume hood and under the suction, the testing area's airflow might not be appropriate for the burning test.

Due to the above-failed results in the laboratory fume hood, a new place for the burning test was an area with a fume extraction hood in the Quarrell laboratory. This place was designed for the burn of materials with a fire safety system and good ventilation. The consequence of the test showed that the flame on the sample extinguished before the first reference line, as provided in Figure 6.28.

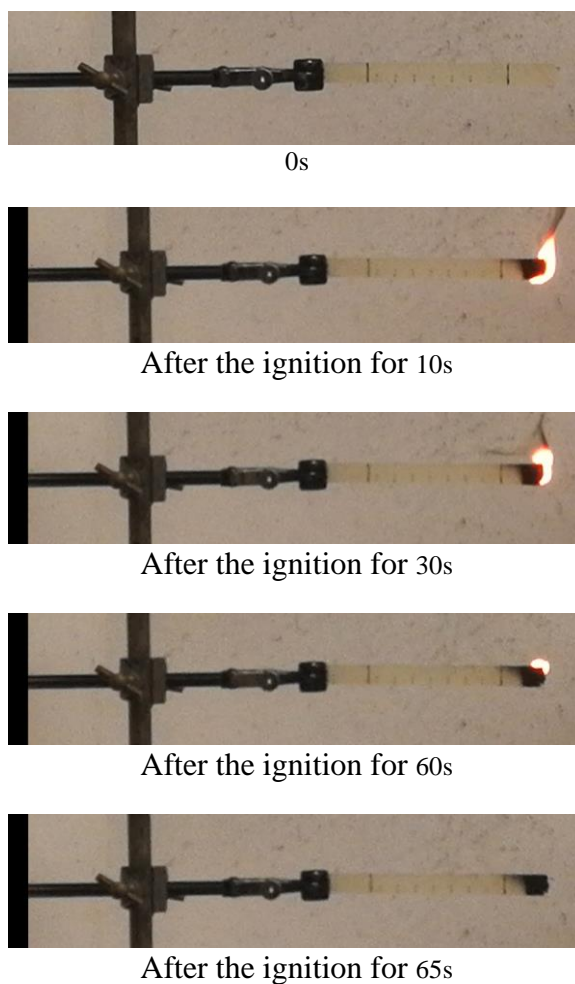


Figure 6.28 The horizontal burning test in the Quarrell Laboratory.

The results demonstrated that the horizontal burning test might not be appropriate for the flammability evaluation of the epoxy resin of DGEBA/DDM. Most of the literature did not test the flammability in the horizontal direction.

6.7.2 Burning Test in Vertical Direction

The preliminary burn test in the vertical position was in the fume hood in the K04 laboratory. The ASTM D3801 Standard has been approved to evaluate the flammability of polymers in the vertical direction [27]. The guidelines of the specimen dimension and the testing procedure in this standard were followed. The burn test of the DGEBA/DDM found that the whole specimen was entirely burned, as shown in Figure 6.29. As described in the horizontal burn test, many smokes and soots are

released during combustion. It might impair the fume extraction system. Therefore, the burning experiments should not conduct in the fume hood.

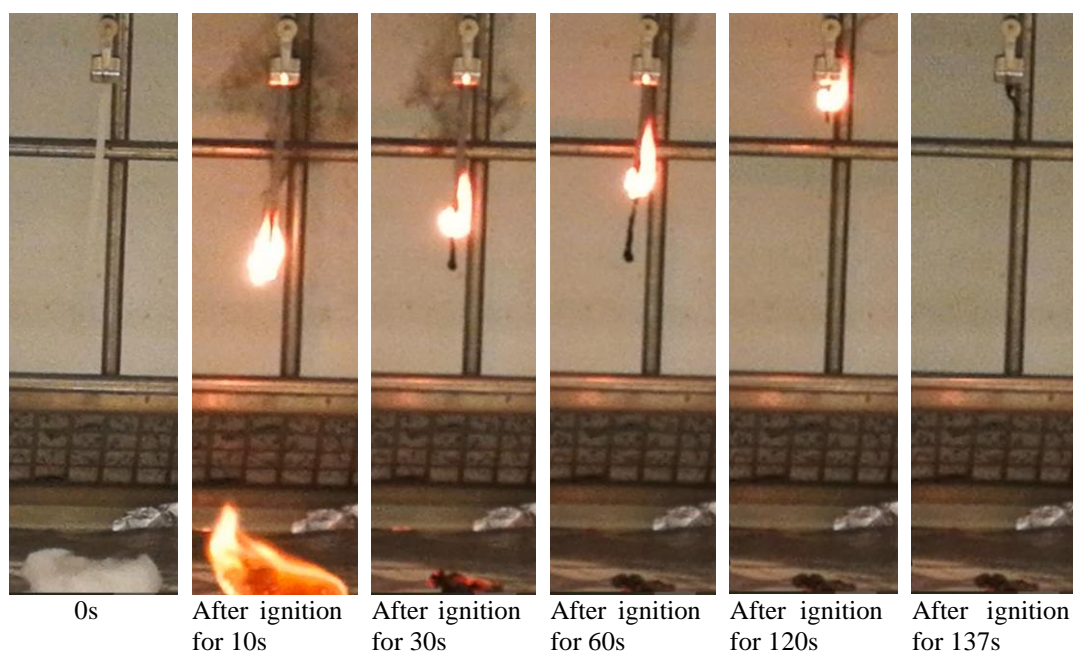


Figure 6.29 The experimental setting of vertical flammability test in the K04 laboratory.

With the test execution in the Quarrell laboratory, the fire was over the specimen of DGEBA/DDM and the gaseous and solid products generated during the combustion were suctioned to the fume extraction hood. This result indicated that the burning experiment set at the Quarrell laboratory was successful. Therefore, the Quarrell laboratory area was an appropriate place to test the cured epoxy resin's flammability.

This study investigated the combustion behaviours of pure EP and its nanocomposites with the vertical UL-94 test. The photo snapshots of representative pure EP/DDM and EP/DDM-5% LDHs nanocomposites during the UL-94 test are shown in Figure 6.30. After the first and second flame applications, the burning times were recorded in t_1 and t_2 , respectively. The five specimens of each sample were used to determine the average value and standard deviation. The testing results in the pure EP/DDM and the EP/DDM-5% LDHs nanocomposites were reported in Table 6.13.

Table 6.13 The combustion time and burning characteristics of the pure DGEBA/DDM and its nanocomposites incorporating the 5% wt LDHs.

Additives	t ₁ in each specimen (s)	t ₂ in each specimen (s)	t ₁ +t ₂ for five specimens (s)	Flame to clamp	Dripping	Rating
No fillers	89 ± 19	181 ± 18	1346	Yes	Yes	NA
5%LDH-CO ₃	38 ± 27	165 ± 14	1014	Yes	Yes	NA
5%LDH-NO ₃	47 ± 24	117 ± 46	819	Yes	Yes	NA
5%LDH-BEHP	26 ± 5	42 ± 10	340	No	No	NA
5%LDH-Phy	21 ± 13	64 ± 14	425	No	No	NA
5%LDH-GP	26 ± 7	66 ± 5	459	No	No	NA
5%LDH-DPP	27 ± 9	45 ± 10	357	No	No	NA

After the first ignition, all the samples continued burning without the fire dripping, and then the fire extinction. The average t₁ decreased significantly over 50% with the addition of 5% LDHs compared to the pure EP, especially the addition of organophosphate ester-modified LDHs. According to the TGA results of samples under air in the Section 6.6.3.2, the decomposition temperatures of the EP/DDM-5% LDHs nanocomposites were lower than the pure EP. These circumstances stated that the LDHs accelerated the decomposition of epoxy nanocomposites, leading to the volatilisation and char formation at the lower temperatures. It meant the formations of char and volatile products in the epoxy nanocomposites were more accessible than the pure EP. Both the products could obstruct the fire spread to the epoxy resins. Thereby, there was the reduction of t₁ with incorporating the LDHs. It indicated that the t₁ of the modified LDHs loading was less than the unmodified LDHs. It stated that the EP nanocomposites with adding the modified LDHs were more difficult to ignition than the epoxy samples with the loading of the unmodified LDHs.

When the first flame extinguished, the second flame application would be processed immediately. The pure EP burned vigorously until the flame reached the clamp. Besides the burning, there was appearance of fire dripping during the combustion.

This result showed that the pure EP was high flammability. For the loading of the LDH-CO₃ or LDH-NO₃, these composites' combustion behaviours were similar to the pure EP--that is, the whole specimens combusted and had the fire dripping to the ignited cotton. Nevertheless, the t_2 of the epoxy nanocomposites were less than the pure EP. It was because of the lower decomposition temperature of the EP/LDH-CO₃ or -NO₃ nanocomposites. It caused both nanocomposites decomposed quickly.

Meanwhile, the second ignition to the EP nanocomposites adding the 5% modified LDHs induced the combustion for a while, and then the fire had gone out. The flame could not get through the clamp, and the fire dripping did not present during the burning. The circumstance might result from the influence of organophosphate compounds modified in the LDHs. The literature stated that the organophosphate compounds could accelerate the char formation during the thermal degradation of polymers. The produced char layers prohibited the permeation of flame, heat and combustible gases through the burning surface.

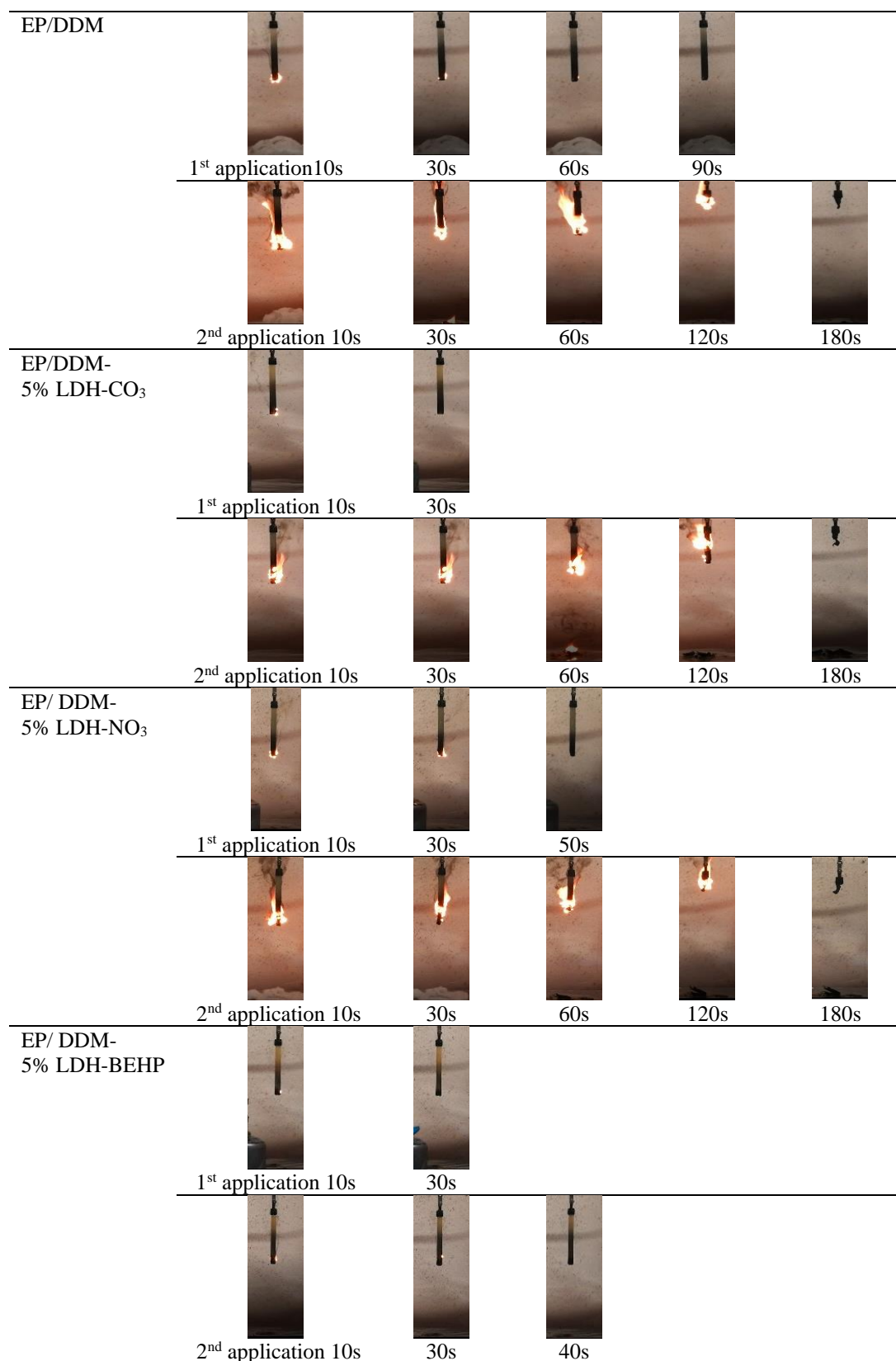


Figure 6.30 The digital photos of the pure DGEBA/DDM and its nanocomposites with the 5% LDHs during the UL-94 test.

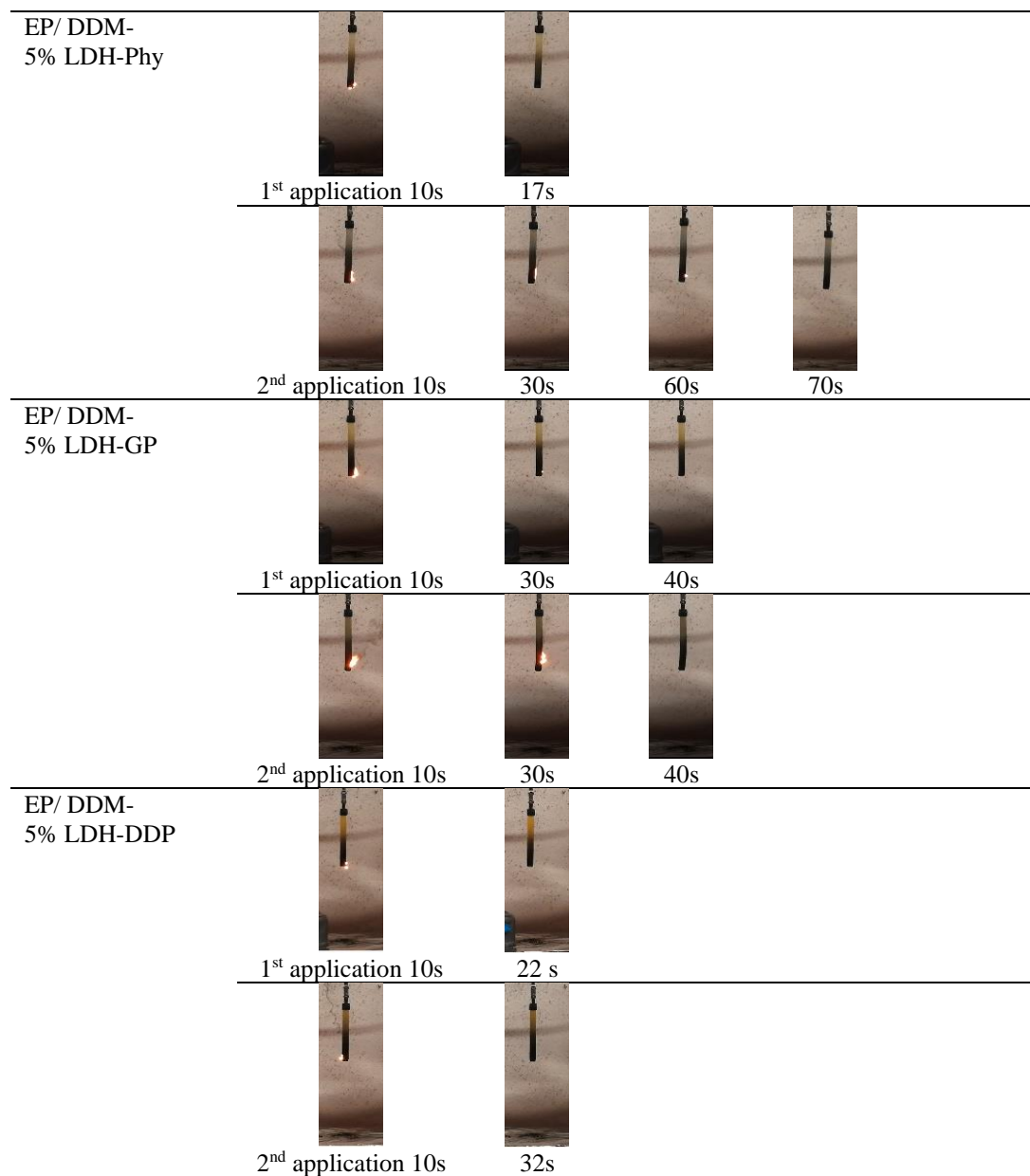


Figure 6.30 The digital photos of the pure DGEBA/DDM and its nanocomposites with the 5% LDHs during the UL-94 test. (continued)

After the burning test, the characteristics of the pure EP cured with the DDM and its nanocomposites with the 5wt% were displayed in Figure 6.31. It could be seen clearly that the additions of 5 wt% pristine LDHs were not able to stop the combustion of the EP/DDM. However, all of the modified LDHs at 5 wt% loading could retain the structural EP/DDM after the burning.

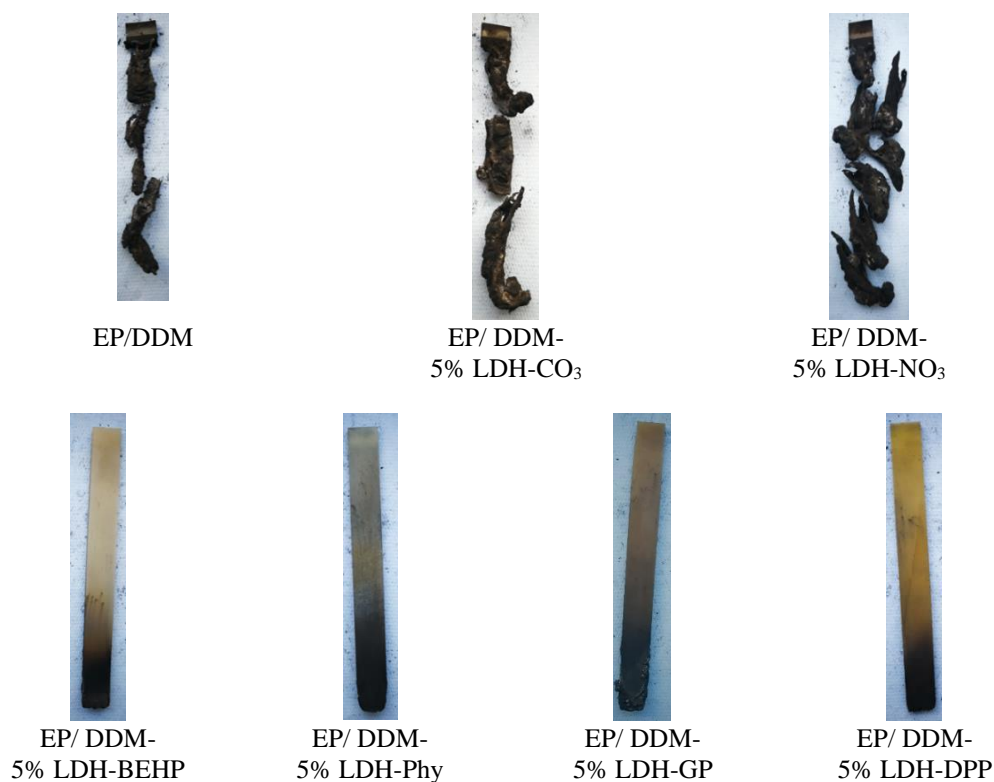


Figure 6.31 The char characteristics after the flame test of the pure DGEBA/DDM and its composites with the 5% LDHs.

For the classification of material flammability by following the criteria in the standard ASTM D3801 detailed in Table 6.14, there are categorised into three groups: V-0 (non-flammable materials), V-1 (moderately flammable materials) and V-2 (flammable materials). Considering the t_1 , t_2 and total of t_1 and t_2 and combustion behaviours of all the samples in Table 6.14, they could not be classified as the criteria in the standard.

Table 6.14 Criteria and classification of vertical burning behaviour following by ASTM:D3801 [20].

Requirement	Categories		
	V-0	V-1	V-2
t_1 for each specimen	≤ 10 s	≤ 30 s	≤ 30 s
T_2 for each specimen	≤ 30 s	≤ 60 s	≤ 60 s
Total time of t_1 and t_2 for five specimens	≤ 50 s	≤ 250 s	≤ 250 s
Burning processes to the holding clamp	No	No	No
Dropping of flame particles	No	No	Yes

Furthermore, the effect of the increasing LDHs content at 10 wt% in the epoxy matrix on the combustion behaviours was studied. The characteristics of representative samples during the burning test were shown in Figure 6.32. Besides, the data obtained from the test were presented in Table 6.15. It can be seen that the t_1 and t_2 of the EP/LDHs nanocomposites reduced significantly, comparing to the pure EP. The combustion of all nanocomposites did not provide the fire spread to the clamp, and the flame drips.

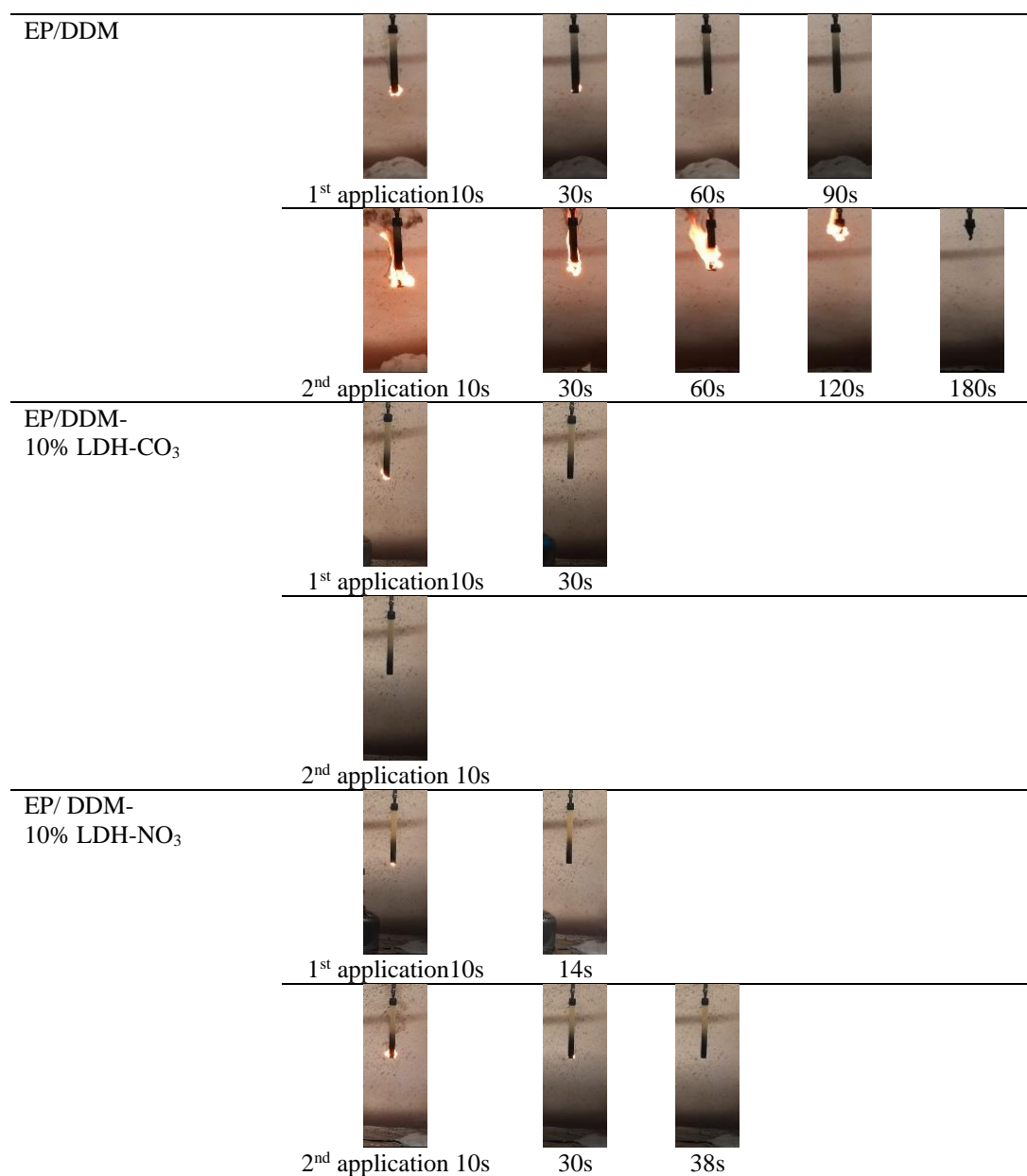


Figure 6.32 The digital photos of the pure DGEBA/DDM and its nanocomposites with the 10% LDHs during the UL-94 test.

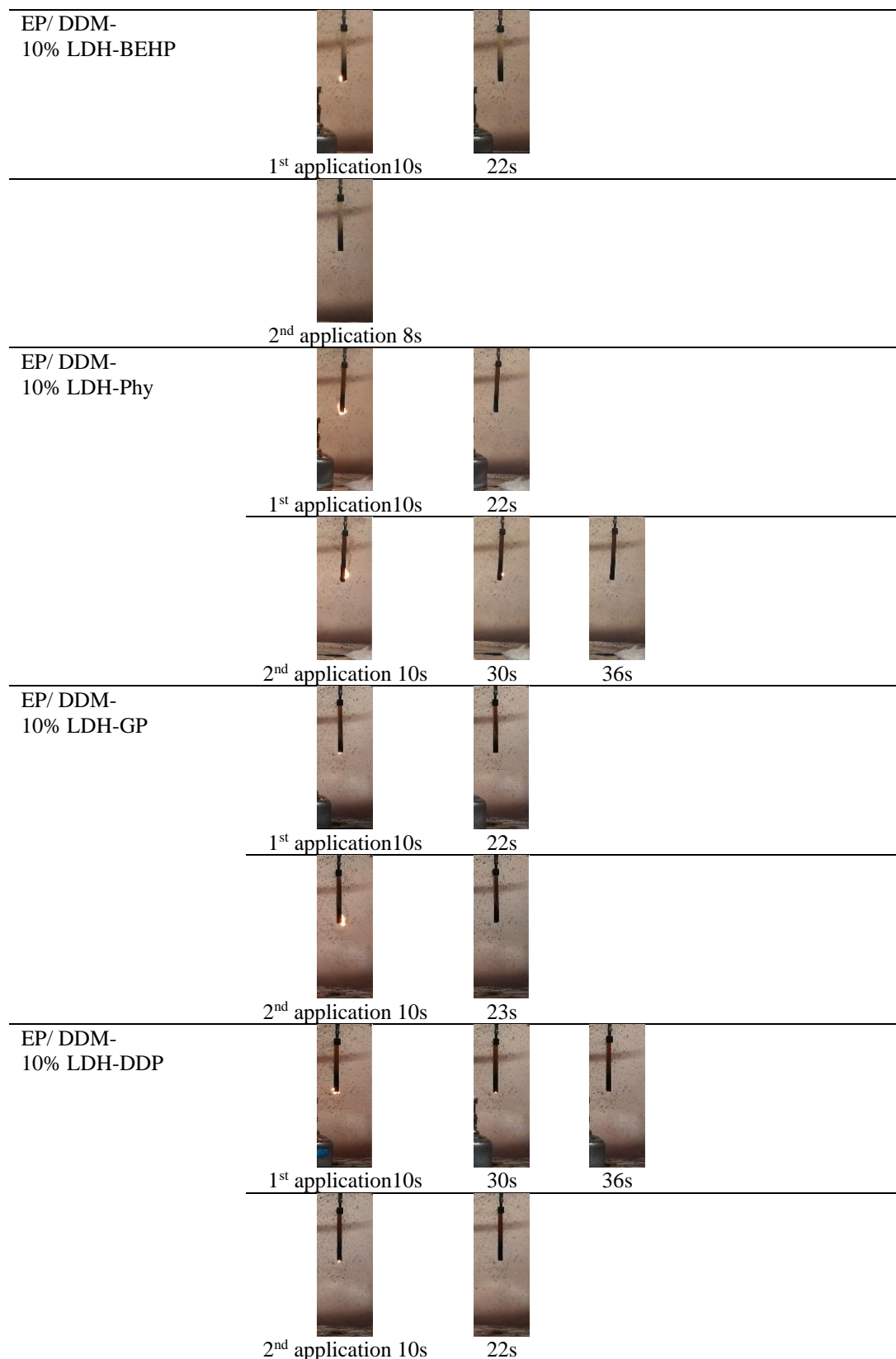


Figure 6.32 The digital photos of the pure DGEBA/DDM and it nanocomposites with the 10% LDHs during the UL-94 test. (Continued)

Table 6.15 The combustion time and burning characteristics of the pure DGEBA/DDM and its nanocomposites incorporating the 10% wt LDHs.

Additives	t ₁ in each specimen (s)	t ₂ in each specimen (s)	t ₁ +t ₂ for five specimens (s)	Flame to clamp	Dripping	Rating
No fillers	89 ± 19	181 ± 18	1346	Yes	Yes	NA
10%LDH-CO ₃	26 ± 3	15 ± 8	205	No	No	V-1
10%LDH-NO ₃	9 ± 4	40 ± 7	248	No	No	V-1
10%LDH-BEHP	12 ± 4	20 ± 8	159	No	No	V-1
10%LDH-Phy	15 ± 8	21 ± 15	176	No	No	V-1
10%LDH-GP	21 ± 2	21 ± 3	211	No	No	V-1
10%LDH-DPP	12 ± 5	23 ± 6	176	No	No	V-1

From the visual characterisation of samples after the flame test in Figure 6.33, it could be observed that both the pristine LDHs and the modified LDHs at 10 wt% loadings were able to stop the combustion of the EP/DDM. The results of burning indicated that the combustion of EP/DDM were self-extinguish with the loading at 10 wt% for the pristine LDHs or at 5 wt% for the modified LDHs.



Figure 6.33 The char characteristics after the flame test of the the pure DGEBA/DDM and its composites with the 10% LDHs

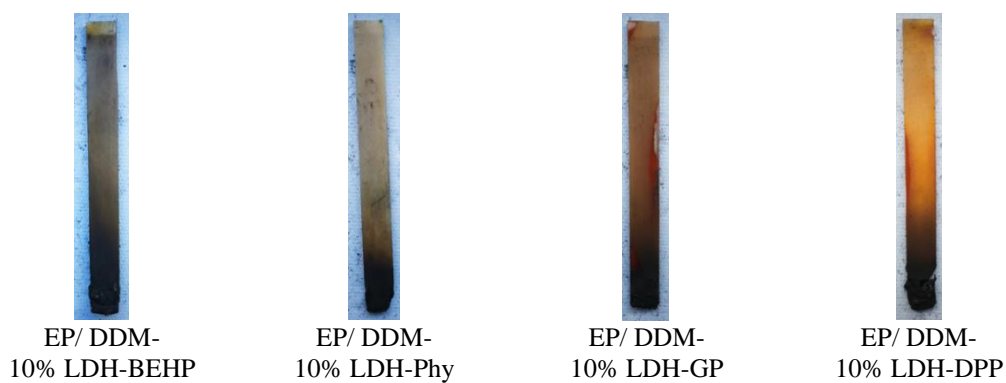


Figure 6.33 The char characteristics after the flame test of the the pure DGEBA/DDM and its composites with the 10% LDHs (continued)

As described previously, the LDHs played a vital role in decreasing the degradation temperatures and accelerating the char formation of the EP nanocomposites. The rise of LDHs loading was possible to reduce the decomposition temperature of the EP nanocomposites, enhancing the char volumes. Both the phenomena can inhibit the flammability of the thermosets. Therefore, the flame retardancy of epoxy resins enhanced with the addition of LDHs at a higher volume.

Considering the difference of LDHs, the total burning times of epoxy resin nanocomposites with the components of the organophosphate modified LDHs were less than that of the inorganic intercalated LDHs. The decomposition of the organophosphate compounds can generate phosphoric acid, acting as the accelerating agent for the char formation. The results stated that the modified LDHs were more flame retardancy efficiency than the unmodified LDHs.

With the flammability classification of the samples as the standard, all the nanocomposites were defined in the V-1 class. It expected that the epoxy nanocomposites could achieve the V-0 (non-flammable class) by incorporating the modified LDHs over 10 wt% loadings.

From the burning tests, the characterisation in the horizontal direction might be not appropriate to evaluate the flammability of epoxy resin. This study carried out the burning test in the vertical position. The results indicated that the 5 wt% loadings of LDHs decreased the burning time of the DGEBA/DDM nanocomposites, especially

the organophosphate-modified LDHs. They could improve flame retardancy. At the 10 wt% LDHs contents, the flammability of the epoxy nanocomposites reduced significantly. Hence, this study has successfully enhanced the flame retardancy of the epoxy resin cured in the DDM system with the organophosphate-modified LDHs.

6.8 Summary

The recent study aimed to enhance epoxy resin's flame retardancy by incorporating the organophosphate ester modified LDHs (LDH-BEHP, LDH-Phy, LDH-GP and LDH-DPP). This chapter concentrated on the characterisation of DGEBA resin cured with the DDM hardener and its nanocomposites containing the various LDHs at the 1, 5 and 10 wt% loading. The flexural behaviours, dynamic mechanical properties, thermal stability and burning behaviours of all samples were characterised by using the flexural testing, DMA, TGA and burning test, respectively.

From observing visual characteristics and evaluating flexural properties, the preparation of EP/LDHs nanocomposites using the solvent, sonication, and stirring was more appropriate than the only stirring. The incorporation of pristine or modified LDHs decreased the flexural strength and flexural modulus of the EP nanocomposites with the pure EP due to the agglomeration of LDHs. However, the storage modulus and loss modulus of the EP nanocomposites with adding increased with adding the LDHs.

By comparing the pure EP, the incorporation of the pristine or modified LDHs decreased the flexural strength and flexural modulus, but it increased the storage modulus and loss modulus in the glassy state. The agglomerated LDHs acted as the inorganic fillers, enhancing the stiffness of the EP nanocomposites and the friction of polymeric chain movement. The increase of filler contents led to the rise of flexural properties and dynamic mechanical properties. Furthermore, the properties of most EP nanocomposites containing the modified LDHs were more significant than the pure EP.

For the TGA results, the EP nanocomposites adding the LDHs decomposed at the lower temperature than the pure EP under N₂ or air atmospheres, especially incorporating the modified LDHs. It indicated that the LDHs accelerated the decomposition of the EP matrix, resulting in the char formation at the lower temperature. The higher contents of LDHs, the more char volumes. The volatiles and char residues produced at lower temperature could delay the combustion of the polymer materials.

Considering the burning tests of the samples cured with the DDM, it was found that the test in the horizontal direction was not suitable for the epoxy resin material. This study focused on the burning test in the vertical direction. The whole specimens of the pure EP and the EP/pristine LDHs were burned, and they showed the flame dripping during the combustion. Meanwhile, the addition of 5 and 10 wt% modified LDHs reduced the ignition time and extinct the flame without the flame dripping. Hence, the organophosphate ester-modified LDHs enhanced flame retardancy efficiency for the DGEBA cured with the DDM.

References

- [1] B. Ellis. "Introduction to the Chemistry, Synthesis, Manufacture and Characterisation of Epoxy Resins". in "Chemistry and Technology of Epoxy Resins", Springer Science+Business Media Dordrecht, Bath:, 1993
- [2] W. Xi, W. Liu, M. Yue, D. Zhang, Q. Lu, H. Zhang, Q. Wu and Y. Li, "DDM Curing Enhancement for the Epoxy Resin Binder Bonded Nd-Fe-B Magnets", IEEE Trans. Magn., 2021, **57(2)**, 1-7
- [3] C. Pagano, F. Marmottini, M. Nocchetti, D. Ramella and L. Perioli, "Effects of Different Milling Techniques on the Layered Double Hydroxides Final Properties", Appl. Clay Sci., 2018, **151**, 124-133
- [4] G. H. Michler and H.-H. K.-B. von Schmeling, "The Physics and Micro-Mechanics of Nano-Voids and Nano-Particles in Polymer Combinations", Polym., 2013, **54(13)**, 3131-3144

- [5] C. Nyambo, D. Chen, S. Su, and C. A. Wilkie, "Does Organic Modification of Layered Double Hydroxides Improve the Fire Performance of PMMA?", *Polym. Degrad. Stabil.*, 2009, **94(8)**, 1298-1306
- [6] A. Kumar and R. K. Gupta, "Mechanical Properties" in "Fundamentals of Polymer Engineering", McGraw-Hill, USA, 2003
- [7] H. P. Menard, "Dynamic Mechanical Analysis: A Practical Introduction", Taylor & Francis Groups, USA, 2008
- [8] F. Garcia, B. Soares, V. Pita, R. Sanchez and J. Rieumont, "Mechanical Properties of Epoxy Networks Based on DGEBA and Aliphatic Amines", *J. Appl. Polym. Sci.*, 2007, **106(3)**, 2047-2055
- [9] R. Hagen, L. Salmén, H. Lavebratt and B. Stenberg, "Comparison of Dynamic Mechanical Measurements and T_g Determinations with Two Different Instruments", *Polym. Test.*, 1994, **13(2)**, 113-128
- [10] P. J. Haines and C. "Thermal Analysis and Calorimetry" in "Principles of Thermal Analysis and Calorimetry", Royal Society of Chemistry, Cambridge, 2002
- [11] C.-H. Tseng, H.-B. Hsueh and C.-Y. Chen, "Effect of Reactive Layered Double Hydroxides on the Thermal and Mechanical Properties of LDHs/Epoxy Nanocomposites", *Comp. Sci. Tech.*, 2007, **67(11)**, 2350-2362
- [12] G. Mikolajczak, J. Y. Cavaille and G. P. Johari, "Dynamic Mechanical Behaviour and its Dependence on Preparation Method of Structural Epoxide Resin", *Polym.*, 1987, **28(12)**, 2023-2031
- [13] R. B. Prime, H. E. Bair, S. Vyazovkin, P. K. Gallagher and A. Riga, "Thermogravimetric Analysis (TGA)" in "Thermal Analysis of polymers", eds. J. D. Menczel and R. B. Prime, John Wiley & Sons, Canada, 2009, pp 240-317
- [14] D. Meng, Z. Ma, Q. Leng, Z. Zhang, H. Ning, X. Peng and Y. Wang, "A Flame-Retardant DOPO-MgAl-LDH was Prepared and Applied in Poly (methyl methacrylate) Resin", *Polym. Adv. Technol*, 2020, **31(1)**, 73-85
- [15] Y. Gao, Q. Wang and W. Lin, "Ammonium Polyphosphate Intercalated Layered Double Hydroxide and Zinc Borate as Highly Efficient Flame Retardant Nanofillers for Polypropylene", *Polym.*, 2018, **10(10)**, 1114
- [16] M. Rajaei, N. K. Kim, S. Bickerton and D. Bhattacharyya, "A Comparative Study on Effects of Natural and Synthesised Nano-Clays on the Fire and

- Mechanical Properties of Epoxy Composites", *Comp. B, Eng.*, 2019, **165**, 65-74
- [17] E. N. Kalali, X. Wang and D.-Y. Wang, "Functionalised Layered Double Hydroxide-Based Epoxy Nanocomposites with Improved Flame Retardancy and Mechanical Properties", *J. Mater. Chem. A*, 2015, **3(13)**, 6819-6826
- [18] A. Frache, O. Monticelli, M. Nocchetti, G. Tartaglione and U. Costantino, "Thermal Properties of Epoxy Resin Nanocomposites Based on Hydrotalcites", *Polym. Degrad. Stabil.*, 2011, **96(1)**, 164-169
- [19] C. Dong, A. Wirasaputra, Q. Luo, S. Liu, Y. Yuan, J. Zhao, Y. Fu, "Intrinsic Flame-Retardant and Thermally Stable Epoxy Endowed by a Highly Efficient, Multifunctional Curing Agent", *Mater.*, 2016, **9(12)**, 1008
- [20] F. Millange, R. I. Walton and D. O'Hare, "Time-Resolved in situ X-ray Diffraction Study of the Liquid-Phase Reconstruction of Mg-Al-Carboate Hydrotalcite-Like Compounds", *J. Mater. Chem.*, 2000, **10(7)**, 1713-1720
- [21] L. Wang, S. Su, D. Chen and C. A. Wilkie, "Variation of Anions in Layered Double Hydroxides: Effects on Dispersion and Fire Properties", *Polym. Degrad. Stabil.*, 2009, **94(5)**, 770-781
- [22] E. N. Kalali, A. Montes, X. Wang, L. Zhang, M. E. Shabestari, Z. Li and D.-Y. Wang, "Effect of Phytic Acid-Modified Layered Double Hydroxide on Flammability and Mechanical Properties of Intumescent Flame Retardant Polypropylene System", *Fire Mater.*, 2018, **42(2)**, 213-220
- [23] X. Jin, X. Gu, C. Chen, W. Tang, H. Li, X. Liu, S. Bourbigot, Z. Zhang, J. Sun and S. Zhang, "The Fire Performance of Polylactic Acid Containing a Novel Intumescent Flame Retardant and Intercalated Layered Double Hydroxides", *J. Mater. Sci. Lett.*, 2017, **52(20)**, 12235-12250
- [24] Q. Luo, Y. Yuan, C. Dong, S. Liu and J. Zhao, "Intumescent Flame Retardancy of a DGEBA Epoxy Resin Based on 5,10-dihydrophenophosphazine-10-oxide", *RSC adv.*, 2015, **5(84)**, 68476-68484
- [25] L. Zhou, G. Zhang, S. Yang, L. Yang, J. Cao and K. Yang, "The Synthesis, Curing Kinetics, Thermal Properties and Flame Retardancy of Cyclotriphosphazene-Containing Multifunctional Epoxy Resin", *Thermochim. Acta*, 2019, **680**, 178348

- [26] ASTM:D635 Standard Test Method for Rate of Burning and/or Extent and Time of Burning of Plastics in a Horizontal Position, A. International, US, 2014.
- [27] ASTM:D3801 Standard Test Method for Measuring the Comparative Burning Characteristics of Solid Plastics in a Vertical Position, A. International, US, 2010.

Chapter 7

Characterisation of Epoxy Resin/LDHs Nanocomposites Cured with DDS

Chapter 6 presented the potential of pristine and organophosphate ester-modified layered double hydroxides (LDHs) on the characteristics of diglycidyl ether of bisphenol A (DGEBA) cured with the diamino diphenyl methane (DDM). The pristine LDHs were the carbonate or nitrate intercalated LDHs, which were the abbreviations of LDH-CO₃ and LDH-NO₃, respectively. For the modified LDHs, they were the intercalation of anions of bis(2-ethyl hexyl) phosphate (BEHP), phytate (Phy), glycerophosphate (GP) and diphenyl phosphate (DPP). The abbreviations of the modified LDHs were LDH-BEHP, LDH-Phy, LDH-GP and LDH-DPP, respectively. The types and contents of LDHs employed in this chapter are similar to the previous chapter. However, there is a difference in the curing agent used for the epoxy (EP) curing. The diamino diphenyl sulfone (DDS) is the curing agent focused on this chapter.

The early chapter explains the curing mechanism of DGEBA with the DDS. Then, there is an investigation of the dispersion of LDHs in the epoxy matrix. Besides, the flexural properties, dynamic mechanical behaviours, thermal stability and combustion behaviours of the pure EP and the EP/LDHs nanocomposites in the DDS curing system will be discussed further.

7.1 Mechanism of DDS Curing with DGEBA

As mentioned previously, this chapter concentrated on the curing of epoxy nanocomposites with the DDS. The pure epoxy resin was also prepared to compare the properties with its composites containing the LDHs. For preparing the pure EP/DDS, the DGEBA and DDS were blended entirely and heated in the oven under the curing cycle. The procedures of EP/DDS curing resembled the EP/DDM curing; however, there were differences in mixing and curing temperatures.

The mixing temperature in the DDS curing system was higher than that of the DDM curing system. The probable explanation was that the melting point of DDS (146-151°C) is higher than the DDM (88-92°C), requiring the higher applied heat energy for the dissolving and blending [1]. Likewise, the curing temperature of the EP/DDS system was higher than the EP/DDM system. Ling et al. [2] suggested that the curing

temperature of DGEBA correlated to the electron density within the molecule of curing agent. For the DDS molecule, the sulfonate group ($-\text{SO}_2-$), an electron-withdrawing group, drawn electron away from the amines. It provided a negative effect on the reaction between the epoxy and amine groups. Meanwhile, the methylene group ($-\text{CH}_2-$) in the DDM corresponded to an electron-donating group, increasing the reactivity of amine groups. Therefore, the reactivity of DDS with epoxy was less than DDM being necessary to apply the higher temperature for the epoxy curing with DDS.

The curing mechanism of DGEBA/DDS was the same as the DGEBA/DDM because of the similarity of the aromatic amines in the primary chemical structure. The amine groups in the DDS interact with the epoxy groups in the resin, leading to the formation of cross-linking networks. The schematic reaction of DGEBA and DDS is presented in Figure 7.1.

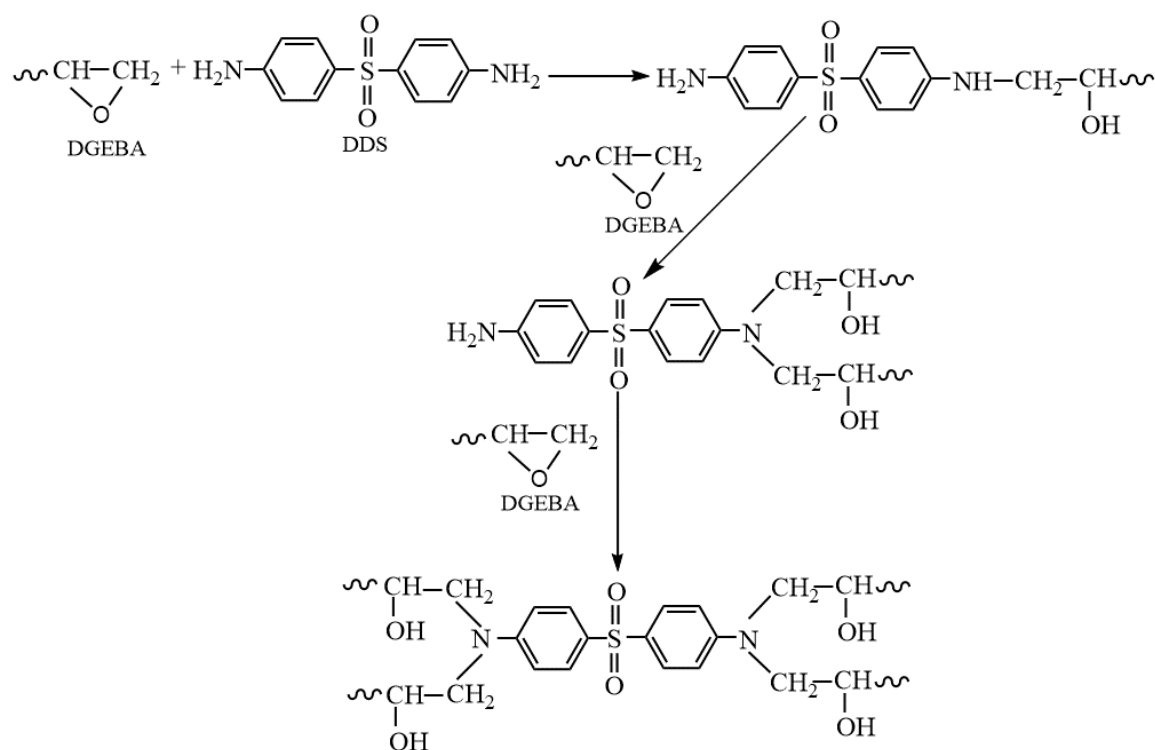


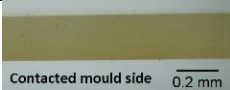
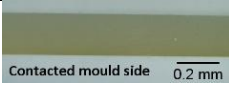
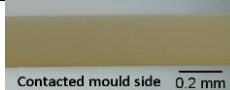
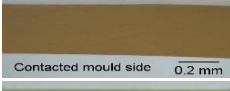
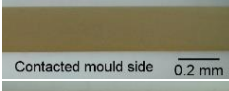
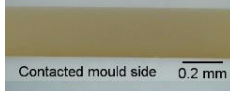
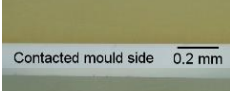
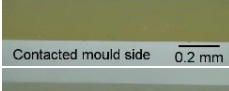
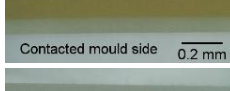
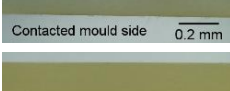
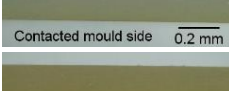
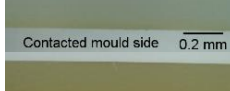
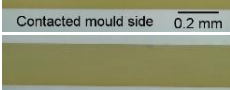
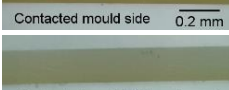
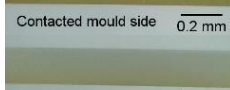
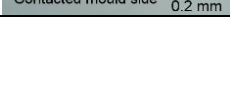
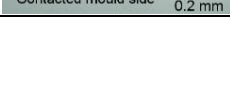
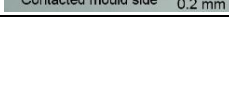
Figure 7.1 Schematic curing reaction of DGEBA monomers and DDS. [2]

7.2 Visual Characteristics of EP/DDS Nanocomposites Incorporating LDHs

The Section 6.2 stated that the preparation procedure of EP/LDHs nanocomposites using the blending solvent, sonication, and stirring was more significant than the only use of mechanical stirring. Therefore, the former was selected to prepare the EP/DDS-LDHs composites with the various types and contents LDHs.

All the cured samples were observed on the cut-edge surface to consider roughly the distribution of LDHs fillers in the epoxy matrix. Table 7.1 displays the visual photos of the cross-section surface in each sample. All the composites had a consistency of colour on the surface even if the loading contents of LDHs increased. These results were expected that the epoxy nanocomposites had a good distribution of the fillers in the matrix.

Table 7.1 The cross-sections of EP/DDS nanocomposites incorporating the various LDHs

Sample	Contents of LDHs		
	1%	5%	10%
EP/DDM-LDH-CO ₃			
EP/DDM-LDH-NO ₃			
EP/DDM-LDH-BEHP			
EP/DDM-LDH-Phy			
EP/DDM-LDH-GP			
EP/DDM-LDH-DPP			

7.2 Flexural Properties of Pure EP and EP/LDHs Nanocomposites in DDS Curing System

For the three-point bending test, it provided the flexural mechanical properties of the materials. The flexural strength and flexural modulus of the pure EP cured with DDS were 185.2 MPa and 3062.2 MPa, respectively. Table 7.2 compared the flexural strength and flexural modulus of the pure epoxy cured with the DDS or DDM. It can be seen that the average value of flexural strength of EP/DDS was slightly higher, whereas the average value of flexural modulus of EP/DDS was lower than the EP/DDM. However, the standard deviation range of flexural strength values for the EP/DDS covered the values of EP/DDM and the range of flexural modulus values for EP/DDS were in the standard deviation range of the EP/DDM. Thus, there was not much difference between two epoxy resins.

Table 7.2 The comparison of flexural properties of pure EPs cured with different aromatic diamines.

Sample	Flexural Strength (MPa)	Flexural Modulus (MPa)
EP/DDS	185.2 ± 20.0	3062.2 ± 114.5
EP/DDM	172.9 ± 10.0	3089.0 ± 171.5

The previous study of Ling et al. compared the flexural strength of DGEBA in the DDS curing system to the DDM curing system [2]. The mechanical strength of the epoxy resin with the DDS was higher than that with the DDM. The higher flexural strength in the DDS curing system might be caused by the crosslink density in the cured resin. As the sulfonate group (-SO₂-) in the DDS was more reactive than the methylene group (-CH₂-) in the DDM, the high active epoxy group in the resin could react with the former more than the latter. The amount of crosslink networks in the epoxy resin cured with the DDS should be more than that with the DDM. This reason led to the increase of strength in the DDS curing.

Meanwhile, in the theoretical polymer composites, the flexural modulus of the epoxy with the DDS is higher than the epoxy with the DDM. The DDS contains the sulfonate

group which is low flexibility. As a result, there is an increase of stiffness for the epoxy with curing of DDS, affecting the increase of flexural modulus [3].

For the epoxy nanocomposites, their flexural strength and flexural modulus were displayed in Figure 7.2 and 7.3, respectively. At the 1 wt% loading of LDHs, both the flexural strength and flexural modulus did not change significantly comparing to the pure EP cured the DDS. The 1 wt% loading of LDHs might be too small amount.

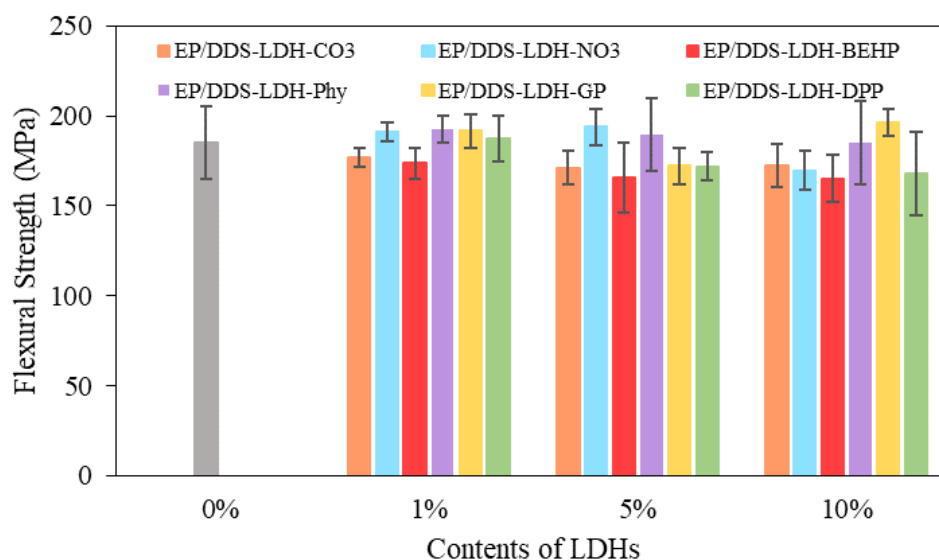


Figure 7.2 The flexural strength of the pure EP and the EP/LDHs nanocomposites cured with the DDS.

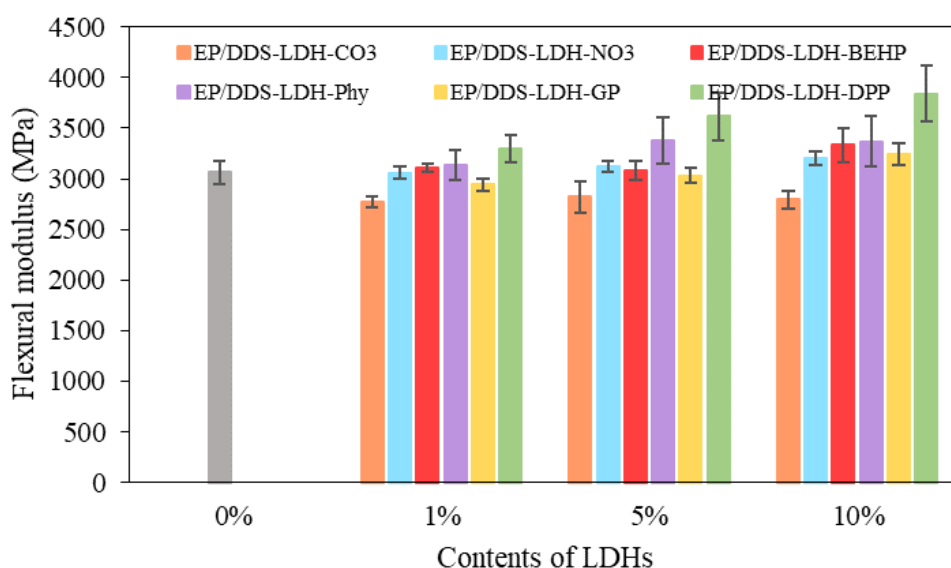


Figure 7.3 The flexural modulus of the pure EP and the EP/LDHs nanocomposites cured with the DDS.

With increasing the LDH contents to 5 wt% and 10 wt%, the average values of flexural strength decreased slightly. Due to the LDHs based on the inorganic fillers, the dispersion of LDHs into the epoxy resulted in many microvoids in the matrix. These formed microvoids are flaws in the epoxy matrix. The higher loading contents of LDHs, the more flaws in the matrix. It caused the reduction of strength. Moreover, the higher loading contents of LDHs might cause the agglomeration of LDH particles in the matrix. This circumstance accounted for the reduction of surface area for the interaction with the epoxy matrix. It might cause the decrease of flexural strength.

However, it was notice that the error ranges of the flexural strength in most EP/DDS-LDHs nanocomposites were in the error range of the pure EP/DDS. It indicated that there was not significantly difference between the pure resin and their composites containing the pristine LDHs or the modified LDHs. The trend of flexural strength for the DDS curing system was dissimilar to the DDM curing system in Chapter 6. The flexural strength of EP nanocomposites cured with the DDM reduced with incorporating the higher contents of LDHs. This circumstance might correlate the polarity of curing agents and LDHs. The DDS containing the sulfonate group was more polar than the DDM and the LDHs acting as the inorganic fillers also was high polarity. The polarity of EP/DDS might be more close to the polarity of LDHs than the EP/DDM. From this reason, the DDS curing induced more compatible between the two phases of epoxy matrix and fillers. It did not the reduction of flexural strength in the DDS system with the increase of LDHs contents.

For the flexural modulus results, the average values of flexural modulus increased gradually with the increase of LDHs contents at 5 wt% and 10 wt%. Since the LDHs incorporated to the epoxy matrix acted as the inorganic fillers, the incorporation of LDHs at the high loading resulted in the increase of stiffness to the composites. Therefore, the more the LDH loading, the higher flexural modulus, especially the addition of modified LDHs. The results stated that the adhesion between the epoxy matrix and LDHs fillers in the DDS curing were improved by the organophosphate ester anions modified on the LDHs. Comparing the flexural modulus in the two different amine curing systems, it was found that there was not resemble between the DDS curing and the DDM curing. In the DDM curing system, the flexural modulus values of most nanocompostites were less than the pure EP/DDM even though there

was the increase of LDHs loading. That could imply that the modified LDHs contributed the adhesion with the EP/DDS better than the EP/DDM. It might occur the interaction of sulfonate group in the DDS with the modified LDHs.

It was worth noting that the flexural strength and flexural modulus of the EP/DDS nanocomposites containing the LDHs modified with the BEHP, Phy, GP or DDP were higher than the loading of unmodified LDHs. These circumstances displayed the same trend as the EP/DDM system. As described in the Section 6.4, the modification of LDHs with the organophosphate ester-based anions enlarged the gallery between the layers of metal hydroxides and reduced the polarity of LDHs. For these reasons, the modified LDHs encouraged the increase of interacting area and interfacial strength between the epoxy matrix and the LDH fillers. Hence, the flexural properties of the epoxy nanocomposites were improved by adding the modified LDHs.

7.4 Dynamic Mechanical Properties of the Pure EP and the EP/LDHs Nanocomposites in DDS Curing System

The dynamic mechanical properties with the elevated temperature of the pure EP/DDS and its nanocomposites with the component of pristine and modified LDHs were characterised by the dynamic mechanical analysis (DMA). The experimental results provided the storage modulus (E'), loss modulus (E'') and ratio of E'' to E' ($\tan \delta$). The storage modulus corresponds to the elasticity of materials, whereas the loss modulus associates with the energy loss during the polymer chain movement. Besides, the $\tan \delta$ relates to the damping property [4, 5].

7.4.1 Dynamic Mechanical Behaviours of Pure EP Cured with DDS

The temperature dependence of the storage modulus, loss modulus and $\tan \delta$ of the pure cured EP/DDS was exhibited in the black line of Figure 7.4. The thermograms showed variations over the temperature range of -150°C to 230°C . The storage modulus decreased gradually between -150°C and 50°C , then plunged between 100°C and 230°C . The increase of temperature induced the rise of free volume in the polymer, decreasing the stiffness of the polymer. Therefore, it reduced storage modulus as the elevated temperature [4].

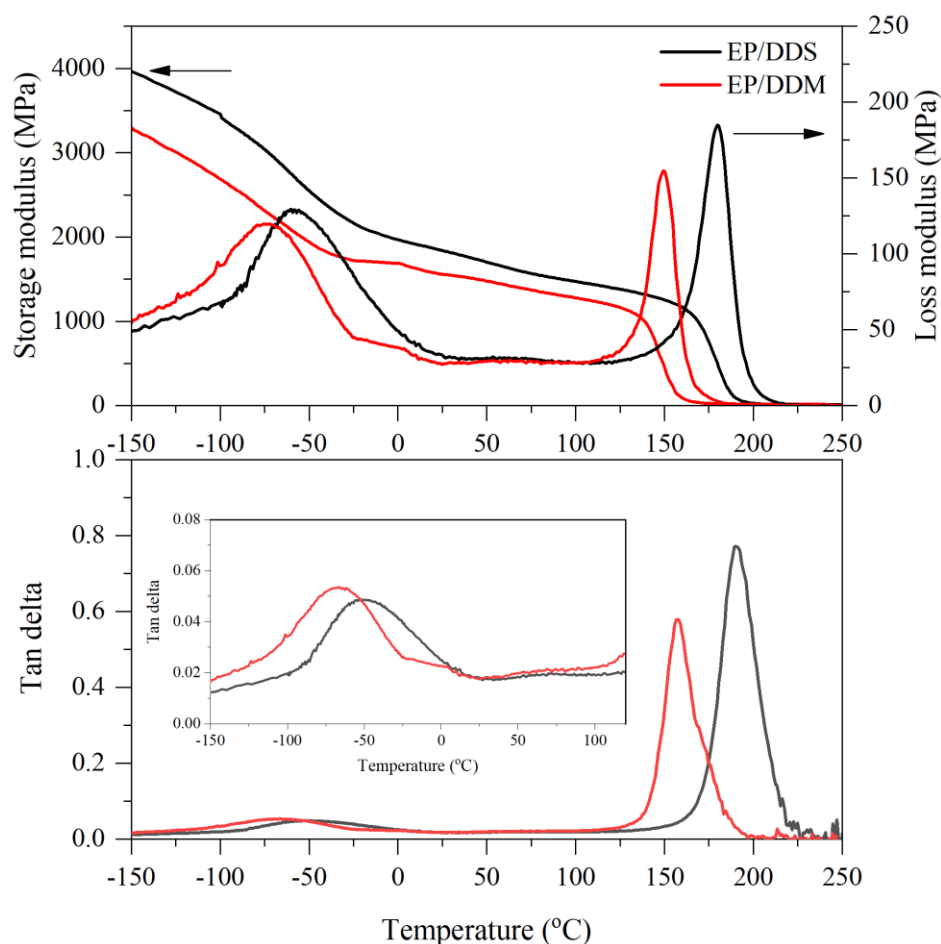


Figure 7.4 The storage modulus, loss modulus and Tan δ of the pristine EP cured with the DDS or DDM.

Due to the relaxation transition of the polymer as the increase of temperature, the loss modulus and Tan δ curves of the pure EP/DDS provided the peaks at approximate -48°C and 190°C , respectively. In the Tan δ curve, the peak at the lower temperature was attributed to the beta transition (T_{β}), whereas the peak at the higher temperature was the characteristic of the glass transition (T_g). As described in the Section 6.5.1, the T_{β} was associated with the local motions of small segments on the polymer chains such as hydroxyl ethers, phenyl rings or tertiary amine groups, while the T_g responded to the mobility of polymer backbone chains.

However, by comparison the pure EP/DDS with the pure EP/DDM (the red line in Figure 7.4), it can be seen that the E' of the epoxy cured with the DDS was higher than that with the DDM. As the storage modulus reflected the elastic behaviours of the cured epoxy, the stiffness of epoxy curing with the DDS was higher than that with

the DDM. It was because the steric and/or the polarity effects. In term of the steric effect, it related to space filling in the matrix. The difference of two curing agents was the main chain; that is, the DDS and DDM contained the functional groups of sulfonate and methylene, respectively. The size of sulfonate group was larger than the methylene group, resulting in the DDS stiffer than the DDM. Regarding the polarity, as described previously, the DDS was more polar than the DDM. The sulfonate group in the DDS restricted the mobility of the polymer chains, accounting for the increase of stiffness of the EP/DDS.

In the meantime, the peaks of loss modulus and the $\text{Tan } \delta$ curves in the pure EP/DDS shifted toward higher temperatures comparing to the pure EP/DDM. The T_{β} and T_g of the pure EP/DDS were higher than that of the pure EP/DDM by 3.8°C and 30.8°C , respectively. The motions of the small groups on the polymer chains and the backbone chains of polymer were probably obstructed due to the existence of the sulfonate groups in the DDS. It could rise the friction during the mobility, contributing to the increase of the energy loss in the DDS curing system. Therefore, the movement of molecules or polymer chains in the DDS curing system took place at the higher temperature.

7.4.2 Dynamic Mechanical Behaviors of EP/Pristine LDHs Nanocomposites Cured with DDS

The incorporation of the pristine LDHs intercalated with carbonate (LDH-CO_3) or nitrate (LDH-NO_3) into the epoxy matrix influenced on the dynamic thermal characteristics of EP/DDS nanocomposites. Figure 7.5 and 7.6 provide the DMA thermograms of the nanocomposites of EP/LDH- CO_3 and EP/LDH- NO_3 cured with the DDS, respectively. With the comparison with the pure EP, the storage modulus and loss modulus increased with the loading of the pristine LDHs.

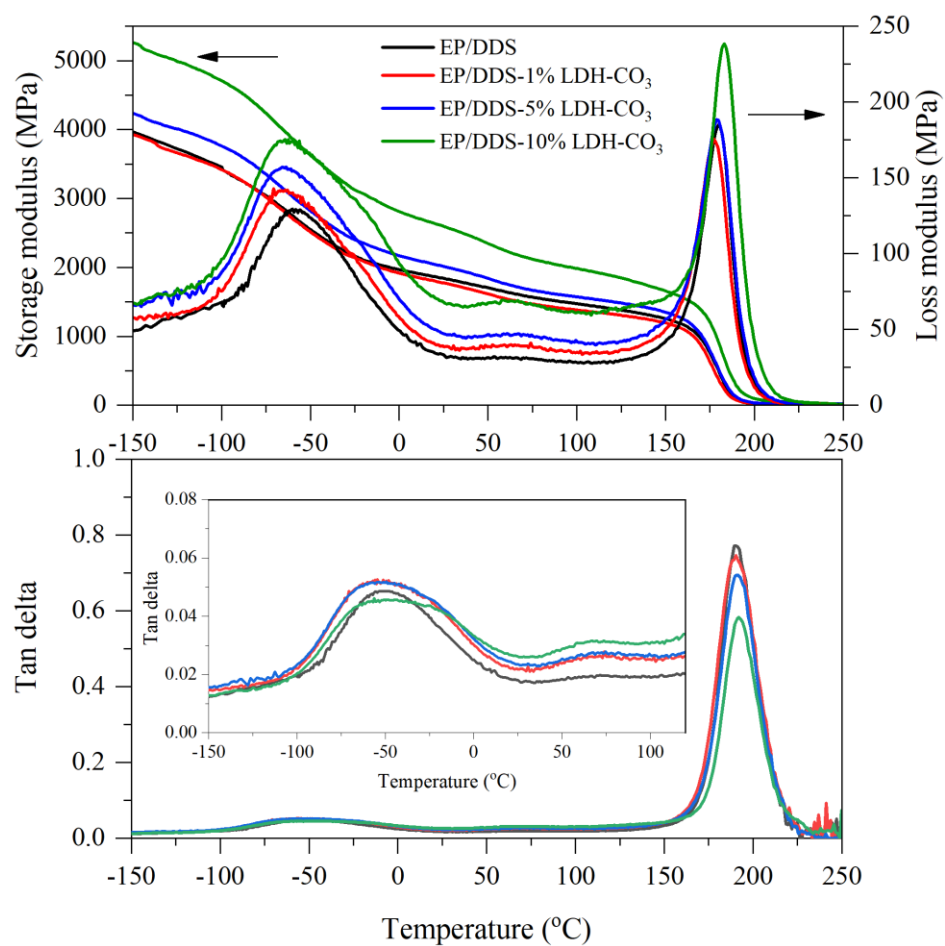


Figure 7.5 The storage modulus, loss modulus and Tan δ of the DGEBA/DDS and its nanocomposites containing the variation of LDH-CO₃ contents.

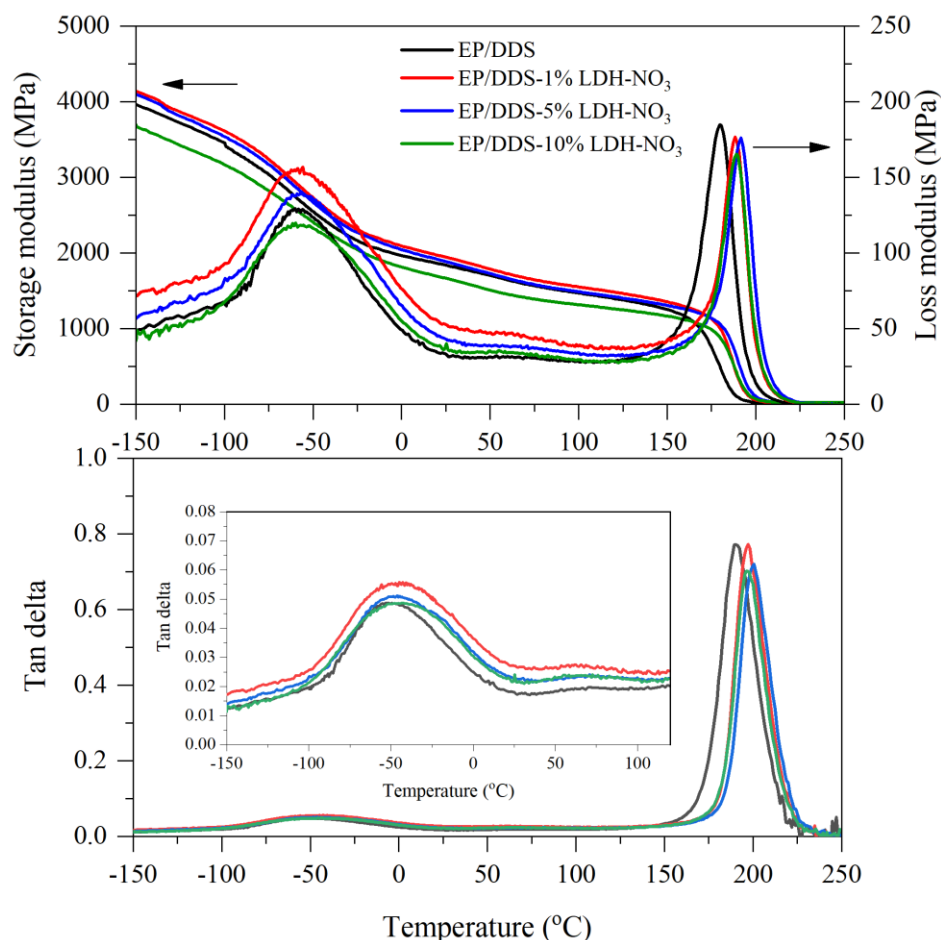


Figure 7.6 The storage modulus, loss modulus and $\text{Tan } \delta$ of the DGEBA/DDS and its nanocomposites containing the variation of LDH-NO₃ contents.

For the incorporation of LDH-CO₃, the higher loading percentage of the LDH-CO₃, the higher E' and E'' of the EP nanocomposites. Meanwhile, the additions of LDH-NO₃ at the higher contents (5 wt% and 10 wt%) were similar to the 1wt% LDH-NO₃ loading. As the LDHs are rigid nano-layered clay, the dispersion of LDHs in the epoxy matrix enhanced the stiffness to the EP nanocomposites [6, 7]. Hence, the storage modulus increased by adding the pristine LDHs. Besides, the layered structure of LDHs could be intercalated by the epoxy matrix, increasing the interaction surface area. This circumstance raised the friction of polymer mobility between the epoxy matrix and the LDH layers, affecting the increase of loss modulus.

Table 7.3 summarises the T_{β} and T_g of the pure EP/DDS and their nanocomposites containing the different contents of the LDH-CO₃ or LDH-NO₃. Both the transition temperatures shifted to the positive temperature with the pristine LDHs in the epoxy

matrix. The movement of molecules in the polymer matrix could be restricted due to the existence of LDH layers in the epoxy matrix. It was necessary to apply the higher thermal energy for the relaxation transition in the EP/pristine LDHs nanocomposites.

Table 7.3 The T_{β} , T_g , storage modulus at the rubbery state and cross-link density of the pure EP, EP/LDH- CO_3 and EP/LDH- NO_3 cured with the DDS in the different contents of LDHs.

Sample	T_{β} (°C)	T_g (°C)	E' at T_g+30 (MPa)	Cross-link density (mol/m ³)
Pure EP/DDS	-47.9 ± 2.8	190.0 ± 1.0	13.0 ± 0.4	1058.9 ± 30.8
EP/DDS-1% LDH- CO_3	-54.8 ± 0.1	191.1 ± 0.2	15.3 ± 0.6	1244.1 ± 46.6
EP/DDS-5% LDH- CO_3	-54.5 ± 1.4	192.9 ± 0.2	18.9 ± 0.0	1527.2 ± 2.5
EP/DDS-10% LDH- CO_3	-53.2 ± 5.0	196.3 ± 0.3	17.6 ± 3.5	1606.5 ± 20.0
EP/DDS-1% LDH- NO_3	-46.1 ± 1.8	197.52 ± 0.5	17.6 ± 3.8	1408.9 ± 36.5
EP/DDS-5% LDH- NO_3	-46.8 ± 1.7	200.3 ± 0.2	23.5 ± 0.8	1872.4 ± 67.4
EP/DDS-10% LDH- NO_3	-42.7 ± 2.8	196.9 ± 0.5	24.7 ± 0.4	2003.8 ± 32.4

Furthermore, the increase of T_g with incorporating the pristine LDHs might relate to the enhancement of the cross-link density in the epoxy matrix. The calculated cross-link density in the rubbery state (T_g+30) also are presented in Table 7.3. It can be seen that the cross-link density of the EP nanocomposites had an increasing trend with loading the LDH- CO_3 or LDH- NO_3 , which agreed with the expectation. This means that both the pristine LDHs could bond with the cured epoxy resin.

7.4.3 Dynamic Mechanical Behaviors of EP/Modified LDH Nanocomposites Cured with DDS

The influence of the organophosphate ester modified LDHs on the dynamic thermal behaviours of the EP/DDS nanocomposites were also investigated. Figure 7.7-7.10 present the DMA thermograms of the EP/DDS nanocomposites incorporating the varied contents of LDH-BEHP, LDH-Phy, LDH-GP or LDH-DPP, respectively.

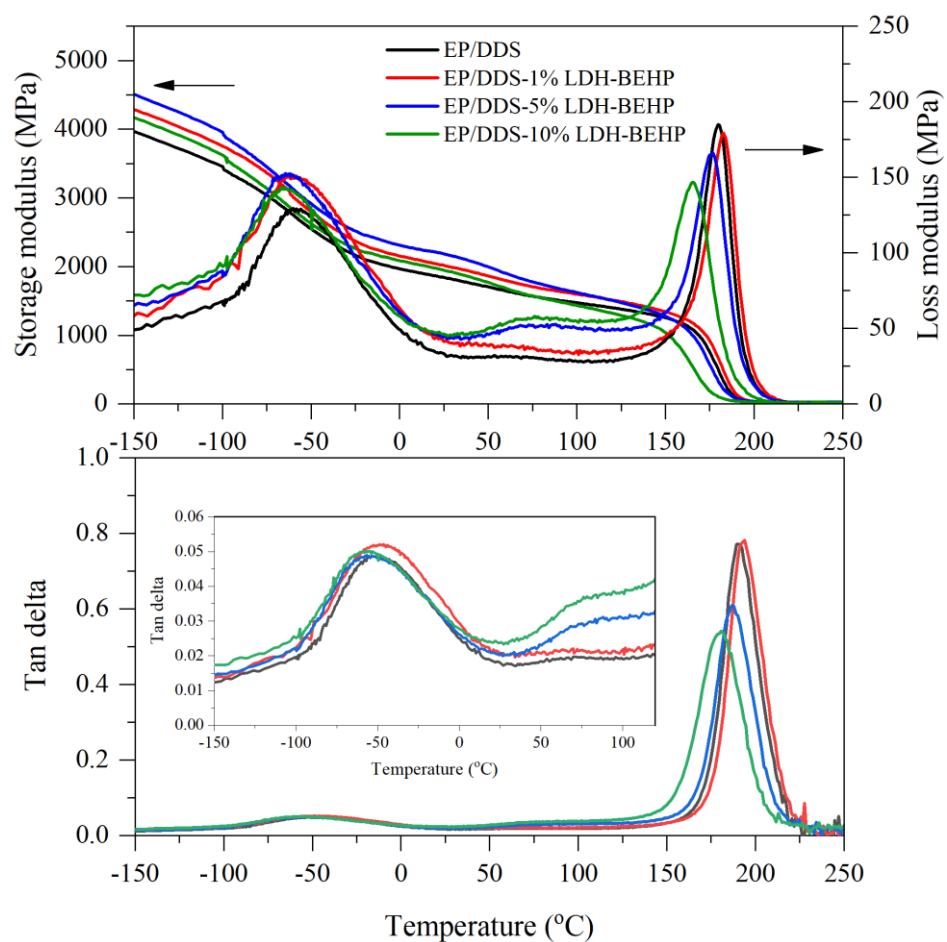


Figure 7.7 The storage modulus, loss modulus and $\text{Tan } \delta$ of the DGEBA/DDS and its nanocomposites containing the variation of LDH-BEHP contents.

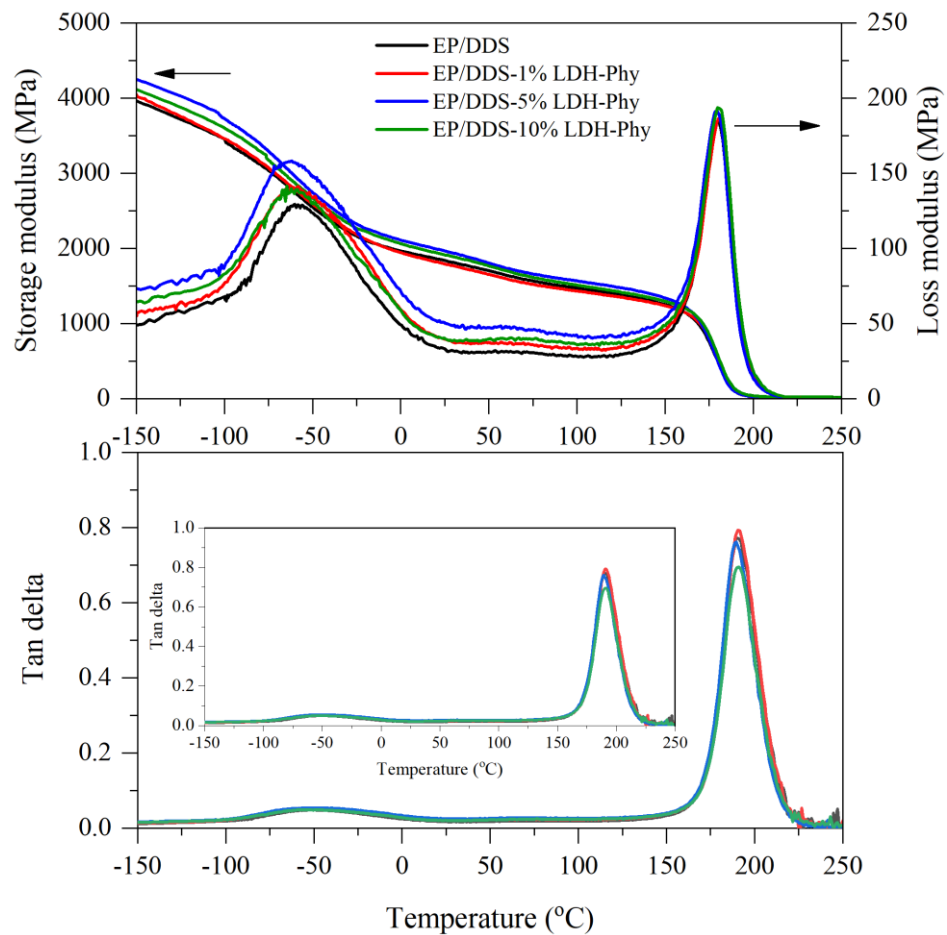


Figure 7.8 The storage modulus, loss modulus and $\text{Tan } \delta$ of the DGEBA/DDS and its nanocomposites containing the variation of LDH-Phy contents.

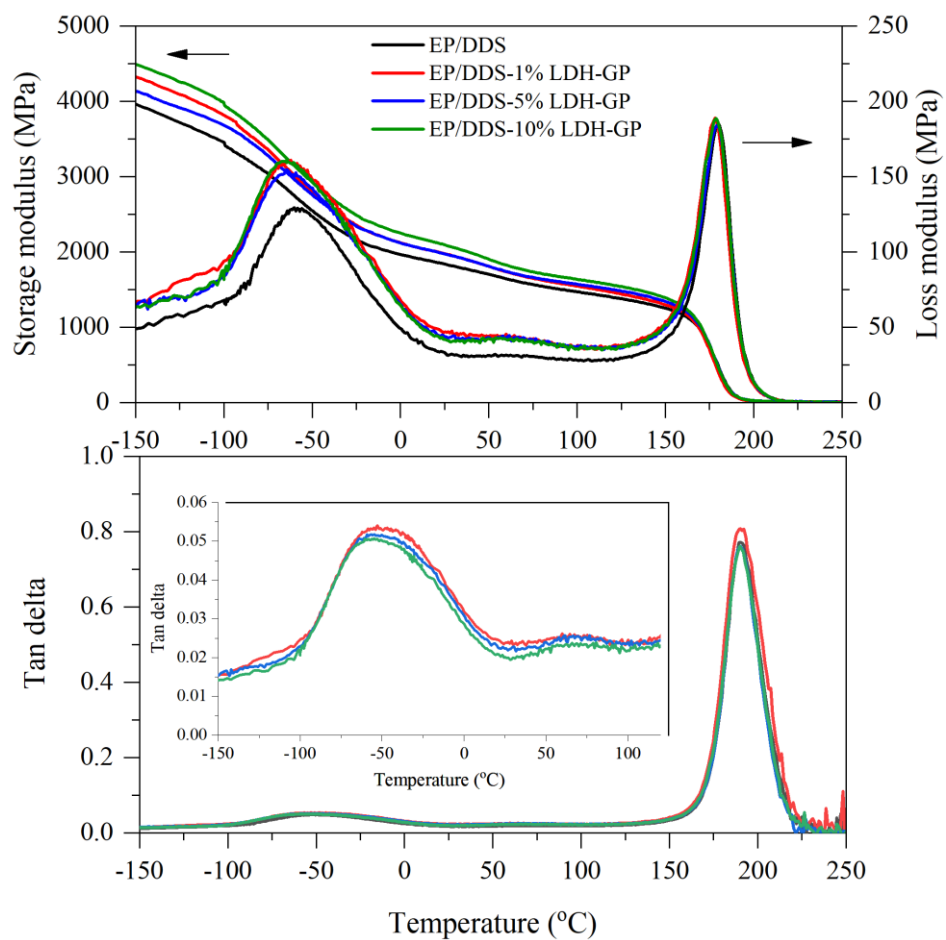


Figure 7.9 The storage modulus, loss modulus and $\text{Tan } \delta$ of the DGEBA/DDS and its nanocomposites containing the variation of LDH-GP contents.

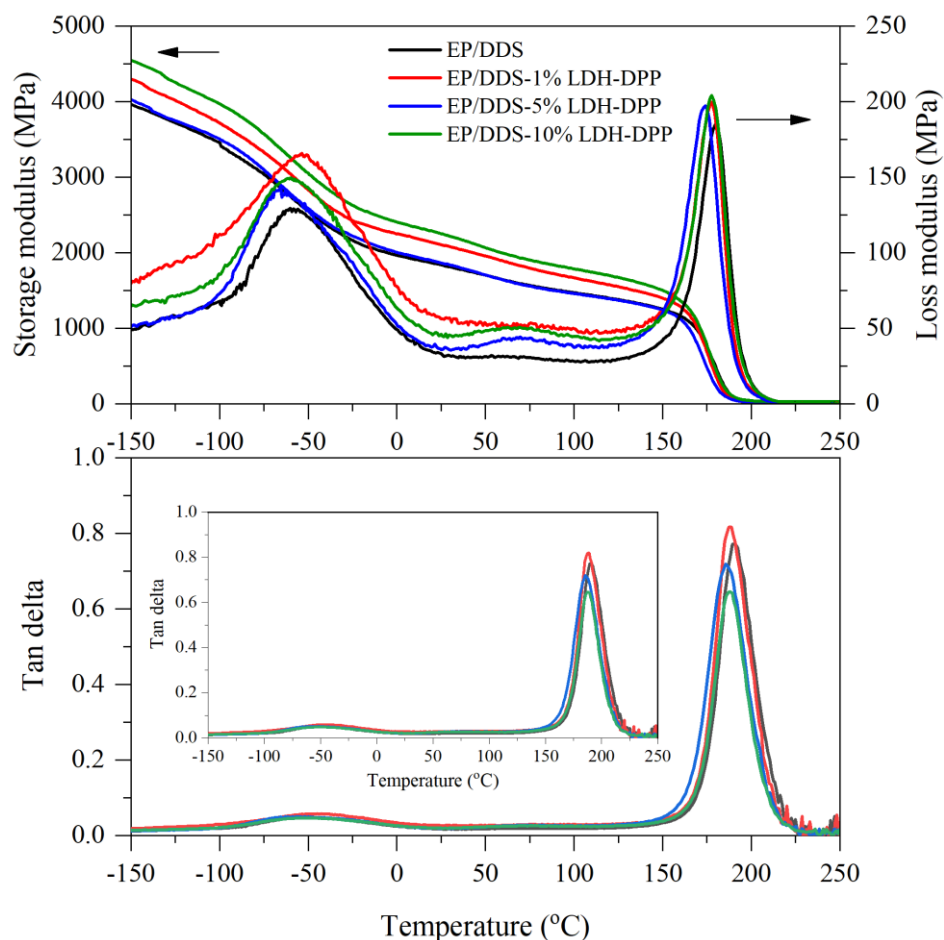


Figure 7.10 The storage modulus, loss modulus and $\text{Tan } \delta$ of the DGEBA/DDS and its nanocomposites containing the variation of LDH-DPP contents.

At the 1 wt% loading of the modified LDHs loading, all the EP nanocomposites had the increase of E' and E'' in the glassy state, compared to the pure EP/DDS. As mentioned previously, the addition of LDHs enhanced the stiffness of the composites accounting for the increase of the storage modulus. Besides, the mobility of the molecules and backbone chains in the epoxy matrix was impeded by incorporating the LDHs. It affected the increase of loss energy to encourage the motions of the molecules and backbone chains in the epoxy matrix, thereby the enhanced loss modulus.

When the proportion of the modified LDHs in the epoxy matrix increased to 5 wt% and 10 wt%, both the E' and E'' of the EP nanocomposites increased. However, this trend did not present in the EP nanocomposites containing the LDH-BEHP and LDH-Phy. The addition of the LDH-BEHP at 5 wt% contributed to the E' higher than at

1 wt% filler loading. At the higher loading (10 wt%) of LDH-BEHP, it affected the decrease of E' for the epoxy nanocomposite because the LDH-BEHP might be able to interfere in the EP/DDS curing reaction. The phosphate ester group in the BEHP might bond to the amine group in the epoxy. For this reason, the interaction of the LDH-BEHP nano-layered particles and the matrix was weaker at the higher loading content of the nano-filler. With the LDH-Phy addition, the E' , E'' and $\tan \delta$ behaviours of the EP nanocomposites did not seem to alter with increasing the LDH-Phy contents. It might occur the good dispersion of the LDH-Phy in the epoxy matrix. Thus, the LDH-Phy had not affected the DMA behaviours of the composites at the higher volume of the filler.

The T_{β} and T_g values of each epoxy nanocomposites with the variation of LDH types and loading contents are presented in Table 7.4. Most of the EP nanocomposites cured with the DDS possessed the reduction of the T_{β} and T_g compared to the pure EP. Both the transition temperatures increased with the higher loading contents of the nanolayered fillers. The research of Li et al. [8] explained that the reduction of the relaxation temperatures was associated with the molecular flexibility of modifying agents in the LDHs. This reason showed that the molecules of BEHP, Phy, GP and DPP were highly flexible, increasing the flexibility of the epoxy networks. Moreover, the calculated cross-link densities of the EP nanocomposites were higher than the pure EP and were likely to increase with rising the modified LDHs. This might correlate to the increase of stiffness.

Table 7.4 The T_{β} , T_g and cross-link density of the pure EP and its nanocomposites containing the BEHP, Phy, GP or DPP modified LDHs cured with the DDS in the different contents of LDHs.

Sample	T_{β} (°C)	T_g (°C)	E' at T_g+30 (MPa)	Cross-link density (mol/m ³)
Pure EP/DDS	-47.9 ± 2.8	190.0 ± 1.0	13.0 ± 0.4	1058.9 ± 30.8
EP/DDS-1% LDH-BEHP	-48.2 ± 0.7	193.2 ± 1.0	15.1 ± 0.2	1221.4 ± 19.4
EP/DDS-5% LDH- BEHP	-54.2 ± 3.2	188.2 ± 1.7	25.7 ± 1.8	2096.6 ± 140.7
EP/DDS-10% LDH- BEHP	-56.0 ± 0.5	182.6 ± 2.0	25.9 ± 1.3	2133.8 ± 101.0
EP/DDS-1% LDH-Phy	-50.6 ± 3.0	190.6 ± 0.4	14.7 ± 0.5	1196.3 ± 37.4
EP/DDS-5% LDH-Phy	-47.9 ± 0.2	189.9 ± 0.6	17.7 ± 3.0	1440.6 ± 245.0
EP/DDS-10% LDH-Phy	-52.3 ± 0.9	190.7 ± 0.2	21.6 ± 4.8	1753.6 ± 388.9
EP/DDS-1% LDH-GP	-52.4 ± 0.5	189.7 ± 0.6	12.1 ± 3.6	980.8 ± 295.0
EP/DDS-5% LDH-GP	-53.9 ± 2.4	190.7 ± 0.9	15.9 ± 0.2	1291.6 ± 19.4
EP/DDS-10% LDH-GP	-54.3 ± 2.8	189.7 ± 0.1	16.4 ± 0.6	1335.1 ± 48.1
EP/DDS- 1%LDH-DPP	-47.2 ± 3.5	190.7 ± 2.7	13.0 ± 0.5	1054.8 ± 31.0
EP/DDS-5% LDH-DPP	-50.5 ± 2.2	189.1 ± 4.9	18.3 ± 2.5	1622.8 ± 40.0
EP/DDS-10% LDH-DPP	-51.2 ± 1.0	187.7 ± 0.4	31.3 ± 1.6	2557.9 ± 134.6

Figure 7.11-7.13 compared the DMA performance of the pure EP/DDS and its nanocomposites with the composition of various LDHs at 5 wt% loading for the storage modulus, loss modulus and $\tan \delta$, respectively. As observing the thermograms, it was found that the storage modulus and loss modulus of all the EP/LDHs nanocomposites exceeded the pure EP since the dispersion of LDHs layers increased the stiffness of the EP nanocomposites, and the restriction of polymer chain motions. Most of the LDHs reduced the T_{β} , but did not affect the change of T_g , comparing the pure EP/DDS.

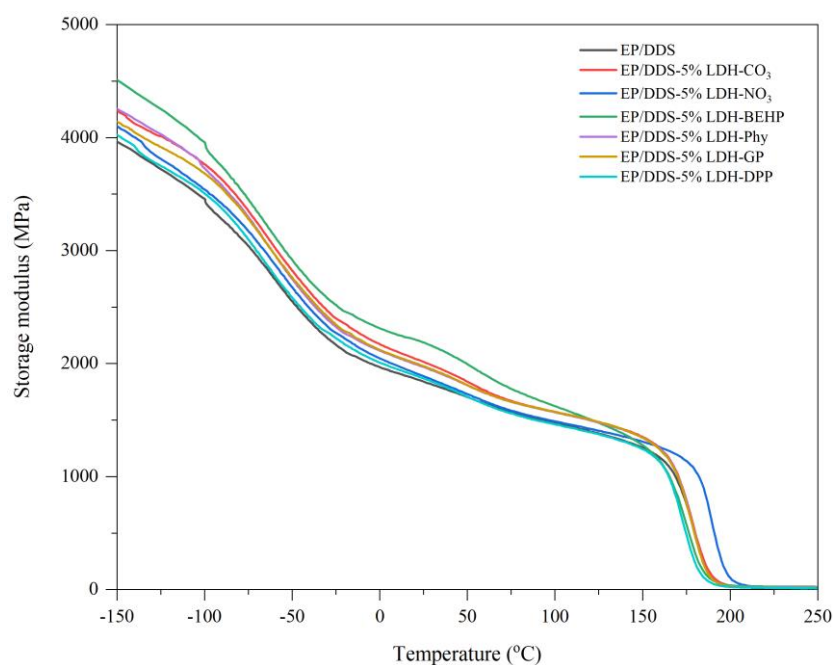


Figure 7.11 The storage modulus of the pure EP and its nanocomposites containing the 5 wt% loading contents of LDH-CO₃, LDH-NO₃, LDH-BEHP, LDH-Phy, LDH-GP and LDH-DPP in the curing system of DDS.

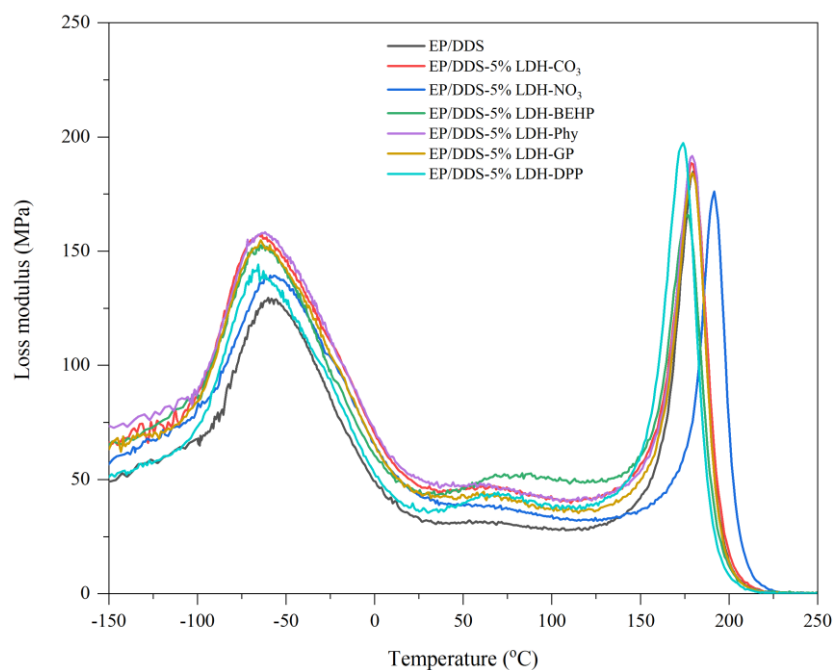


Figure 7.12 The loss modulus of the pure EP and its nanocomposites containing the 5 wt% loading contents of LDH-CO₃, LDH-NO₃, LDH-BEHP, LDH-Phy, LDH-GP and LDH-DPP in the curing system of DDS.

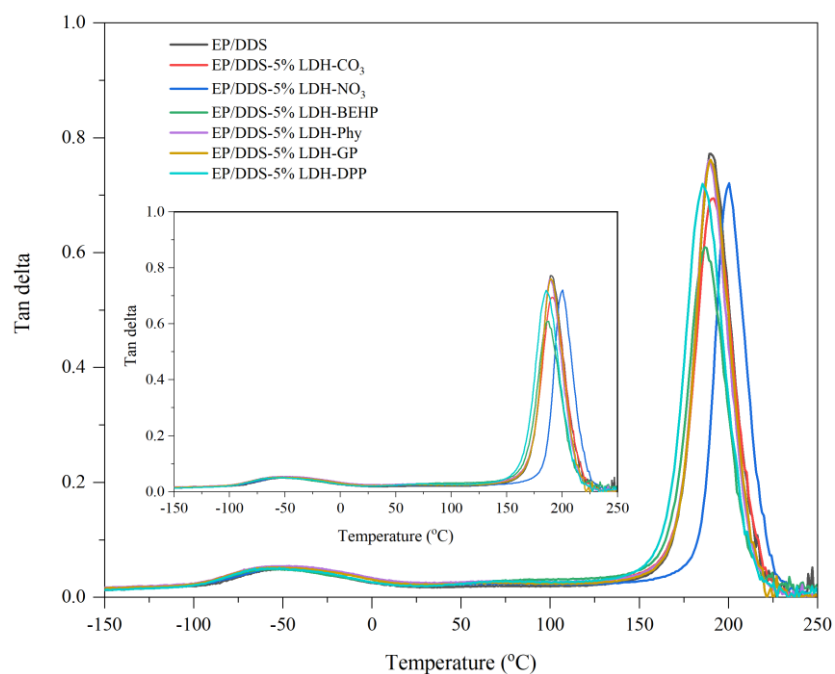


Figure 7.13 The Tan δ of the pure EP and its nanocomposites containing the 5 wt% loading contents of LDH-CO₃, LDH-NO₃, LDH-BEHP, LDH-Phy, LDH-GP and LDH-DPP in the curing system of DDS.

In Figure 7.11, it can be seen that the storage modulus of the EP/LDH-GP and EP/LDH-BEHP nanocomposites was higher than any other the EP nanocomposites. Meanwhile, the storage modulus of the EP/LDH-DPP and EP/LDH-Phy was between the EP/LDH-NO₃ and EP/LDH-CO₃. From the results, it was expected that the particles of LDH-DPP and LDH-Phy might agglomerate in the EP/DDS matrix were more than the pristine LDHs.

Over the temperature range of glassy state (-150°C to 150°C), the storage modulus and the loss modulus of the EP/LDH-BEHP and EP/LDH-GP nanocomposites were higher than any other the EP nanocomposites. Meanwhile, the storage modulus and loss modulus of the EP/LDH-Phy and EP/LDH-DPP were between the EP/LDH-CO₃ and the EP/LDH-NO₃.

From the DMA results, it was expected that both the LDH-BEHP and LDH-GP well dispersed in the EP/DDS, whereas the particles of LDH-Phy and LDH-DPP might agglomerate in the matrix were more than the pristine LDHs. As described previously, the pristine LDHs and the modified LDHs had an influence on the only T_β, but did not alter the T_g of the epoxy nanocomposites. These results indicated that the LDHs induced the increase of flexibility of the side groups on the epoxy chains.

7.5 Thermal Stability of Epoxy Resin/LDHs Nanocomposites in DDS Curing System

The thermal stability of EP/LDHs nanocomposites cured with the DDS was investigated via the thermal gravimetric analysis (TGA) under N₂ or air atmosphere. The temperature at 10% and 50% mass loss (T_{10%} and T_{50%}), temperature at maximum mass loss (T_{max}) and char yield at 800°C of the pure EP-LDHs and its nanocomposites were considered for estimating the thermal decomposition behaviours.

7.5.1 Thermal Stability of Pure EP Cured with DDS under N₂ Atmosphere

The TGA curve and its derivative of the pure EP/DDS under N₂ flow as the elevated temperature were presented in the black line of Figure 7.14. It can be seen that the

thermogram exhibited one stage of mass loss in the temperature range of 350-500°C with the maximum mass loss rate at 429.9°C.

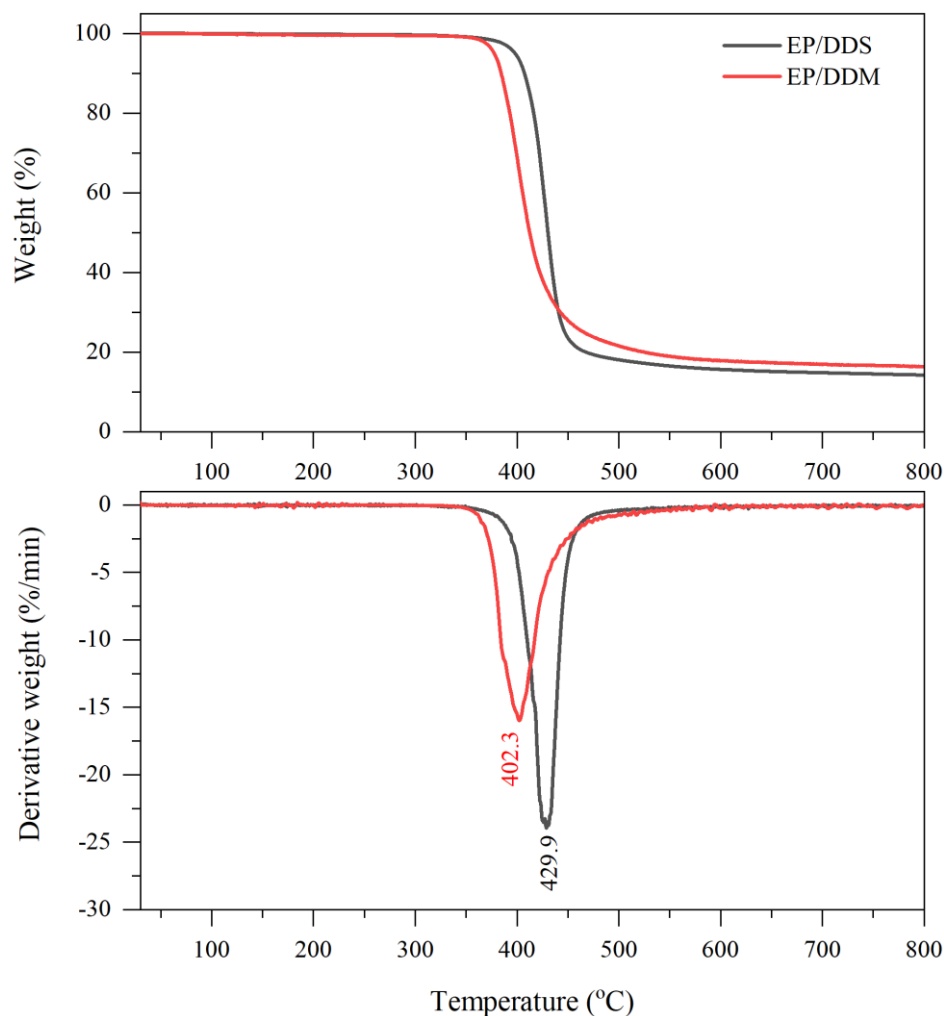


Figure 7.14 The TGA and DTG curves of the pure EP cured with the DDS and DDM.

The previous research reported that the TGA curve of the DGEBA cured with the DDS possessed the single step of the thermal degradation process. The pure EP decomposed between 380°C and 500°C with the maximum degradation rate at 416-425°C [9-11]. Although there was a similarity between the epoxy and curing agent types, the cured epoxy had a difference in the degradation temperature. Several parameters might account for the variation of thermal decomposition behaviours, such as the purity of chemicals, the proportion between the epoxy and curing agent, the curing conditions (e.g. temperature and time). The literature established that there was scission of C-N and C-O bonds in the structure of DGEBA cured with the DDS. This led to the evaporation of sulfur dioxide (SO₂), carbon monoxide (CO) and methane

(CH₄) and the formation of aromatic compounds containing oxygen or nitrogen [12-14].

By comparison with the pure EP/DDM (the black line in Figure 7.14), the EP/DDS had a high decomposed temperature. From the DMA results, the T_g of the DDS curing (190°C) was higher than that of the DDM curing (159.2°C). Due to the high strength of the sulfonate group in the DDS structure, the epoxy cured with the DDS was high thermal stability. In addition to the degradation temperature, the residue at 800°C of the EP/DDS (14.2 %) was less than the EP/DDM (16.3%). This event occurred the dehydration of the macro networks and the volatility of SO₂ in the DDS.

7.5.2 Thermal Stability of EP/Pristine LDHs Nanocomposites in the DDS Curing System under N₂ Atmosphere

The effect of LDH-CO₃ and LDH-NO₃ incorporation on the thermal decomposition behaviours of the EP/DDS nanocomposites is presented in Figures 7.15 and 7.16, respectively. The essential data obtained from the TGA characterisation are also listed in Table 7.5. The TGA thermograms of the EP/LDH-CO₃ and the EP/LDH-NO₃ nanocomposites cured with the DDS displayed the one stage of thermal degradation, which resembled the TGA curve of the pure EP/DDS.

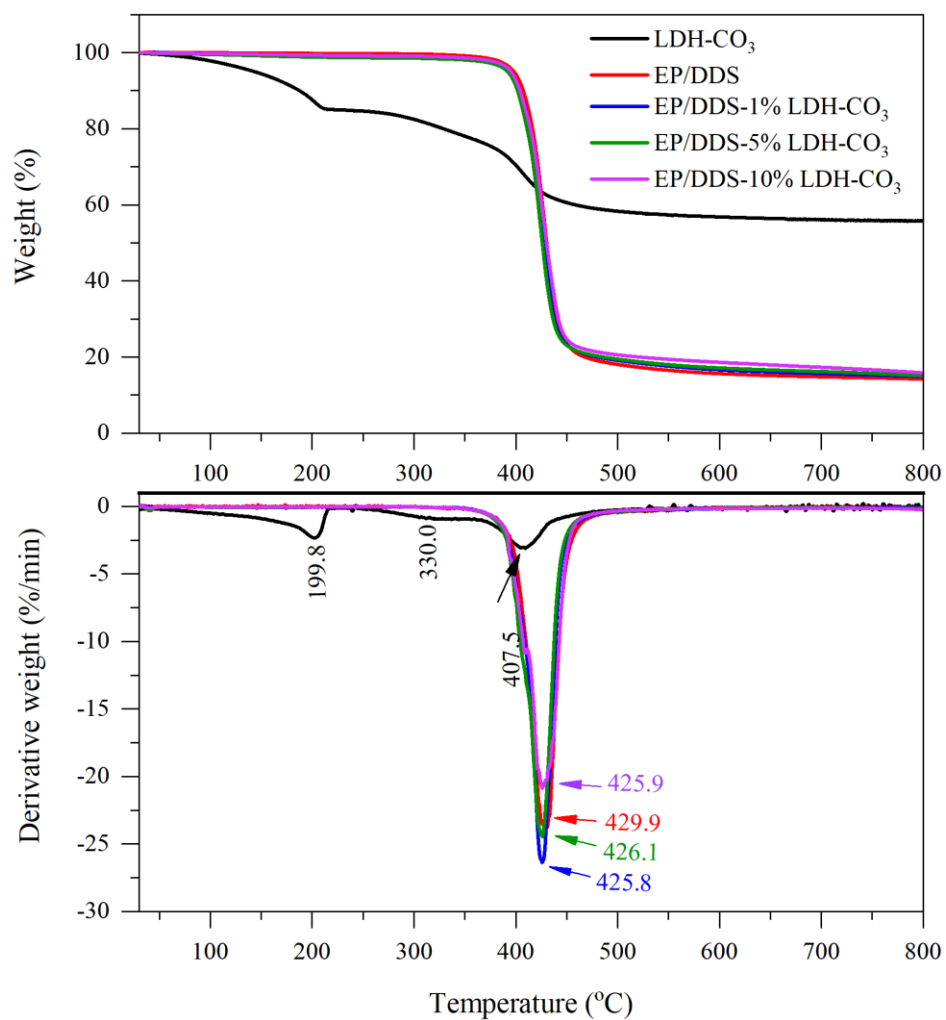


Figure 7.15 The TGA curves and their derivatives of LDH-CO₃, pure EP/DDS and EP/LDH-CO₃ nanocomposites with the variation of LDH-CO₃ contents under N₂ flow.

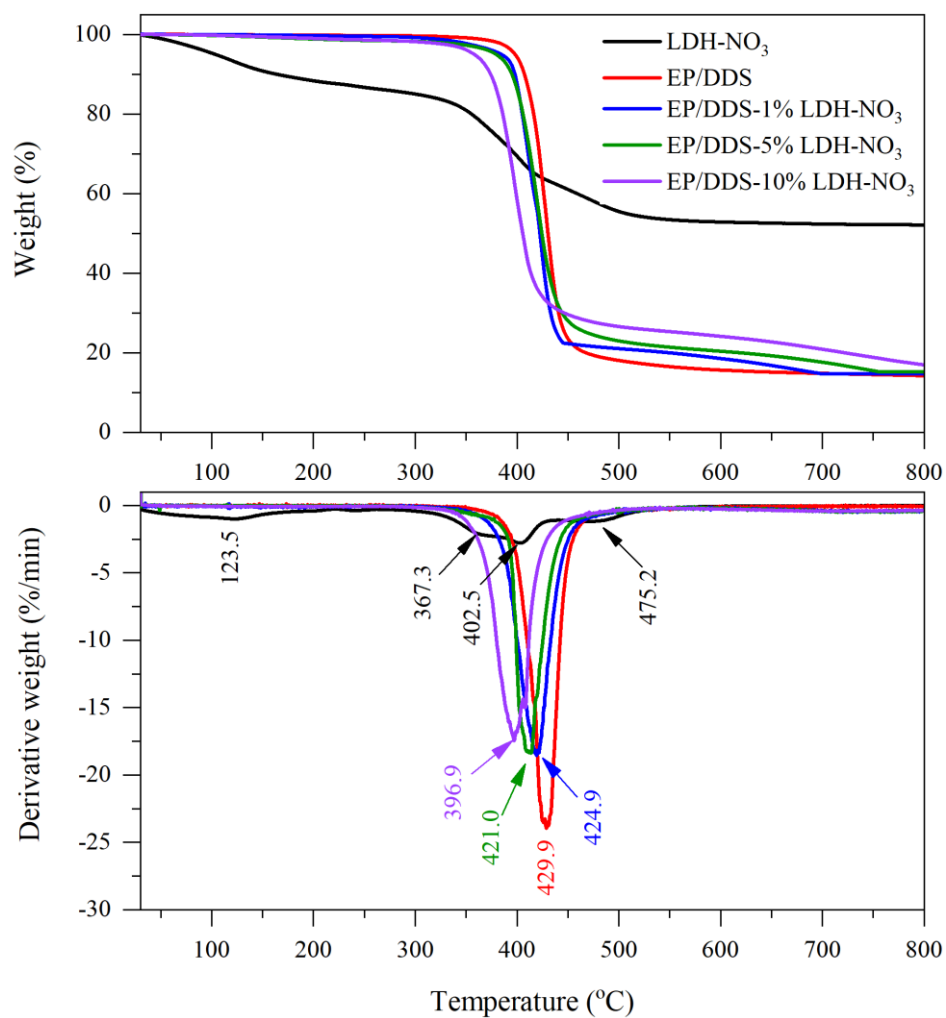


Figure 7.16 The TGA curves and their derivatives of LDH-NO₃, pure EP/DDS and the EP/LDH-NO₃ nanocomposites with the variation of LDH-NO₃ contents under N₂ flow.

Table 7.5 The $T_{10\%}$, $T_{50\%}$, T_{\max} and residue at 800°C of the pure EP/DDS and its nanocomposites with the variation of LDH-CO₃ or LDH-NO₃ contents under N₂ flow.

Sample	$T_{10\%}$ (°C)	$T_{50\%}$ (°C)	T_{\max} (°C)	Mass at 800°C (%)
EP/DDS	407.2	430.3	429.9	14.2
EP/DDS-1% LDH-CO ₃	384.4	411.2	425.8	17.1
EP/DDS-5% LDH-CO ₃	382.1	410.4	426.1	18.4
EP/DDS-10% LDH-CO ₃	382.4	410.8	425.9	22.5
EP/DDS-1% LDH-NO ₃	397.9	422.4	424.9	14.8
EP/DDS-5% LDH-NO ₃	394.9	424.3	421.0	15.3
EP/DDS-10% LDH-NO ₃	374.0	405.5	396.9	16.9

Both the LDH-CO₃ and LDH-NO₃ declined the $T_{10\%}$, $T_{50\%}$ and T_{\max} of the EP nanocomposites compared to the pure EP, summarised in Table 7.5. The increase of the pristine LDHs contents also reduced those properties. These results indicated that the loading of the LDH-CO₃ and LDH-NO₃ accelerated the thermal decomposition of the EP nanocomposites, corresponding to the prior studies [9, 10].

Moreover, the char yields at 800°C of all the EP/pristine LDHs nanocomposites were higher than that of the pure EP, as displayed in Table 7.5. The probable components of residues produced from the decomposition of the EP/pristine LDHs nanocomposites were the char and metal oxides. The increase of the filler contents in the epoxy matrix also enhanced the content of residues. This phenomenon could inhibit the dispersion of flame, heat and combustible gas to the burning region, which was a powerful mechanism for fire retardancy.

7.5.3 Thermal Stability of EP/modified LDHs Nanocomposites in the DDS Curing System under the N₂ Atmosphere

When the organophosphate ester modified LDHs were used as the fillers in the EP/DDS nanocomposites, they influenced the thermal stability performance of EP matrix. Under N₂ atmosphere of TGA characterisation, the TGA curves and their derivatives of organophosphate-ester reactants, modified LDHs, pure EP/DDS and EP nanocomposites containing the LDHs modified with the BEHP, Phy, GP or DPP were presented in Figure 7.17-7.20, respectively. Besides, the important TGA results are summarised in Table 7.6.

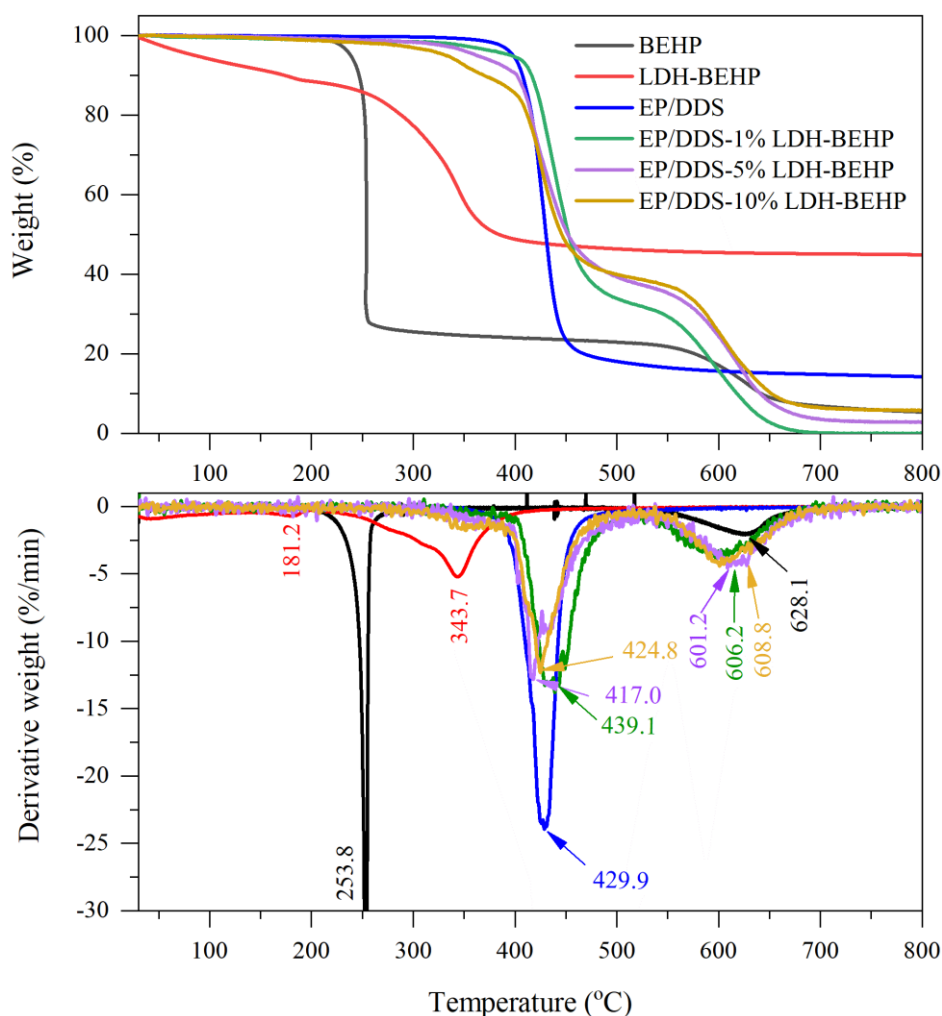


Figure 7.17 The TGA curves and their derivatives of BEHP reactant, LDH-BEHP, pure EP/DDS and the EP/LDH-BEHP nanocomposites with the variation of LDH-BEHP contents under N₂ flow.

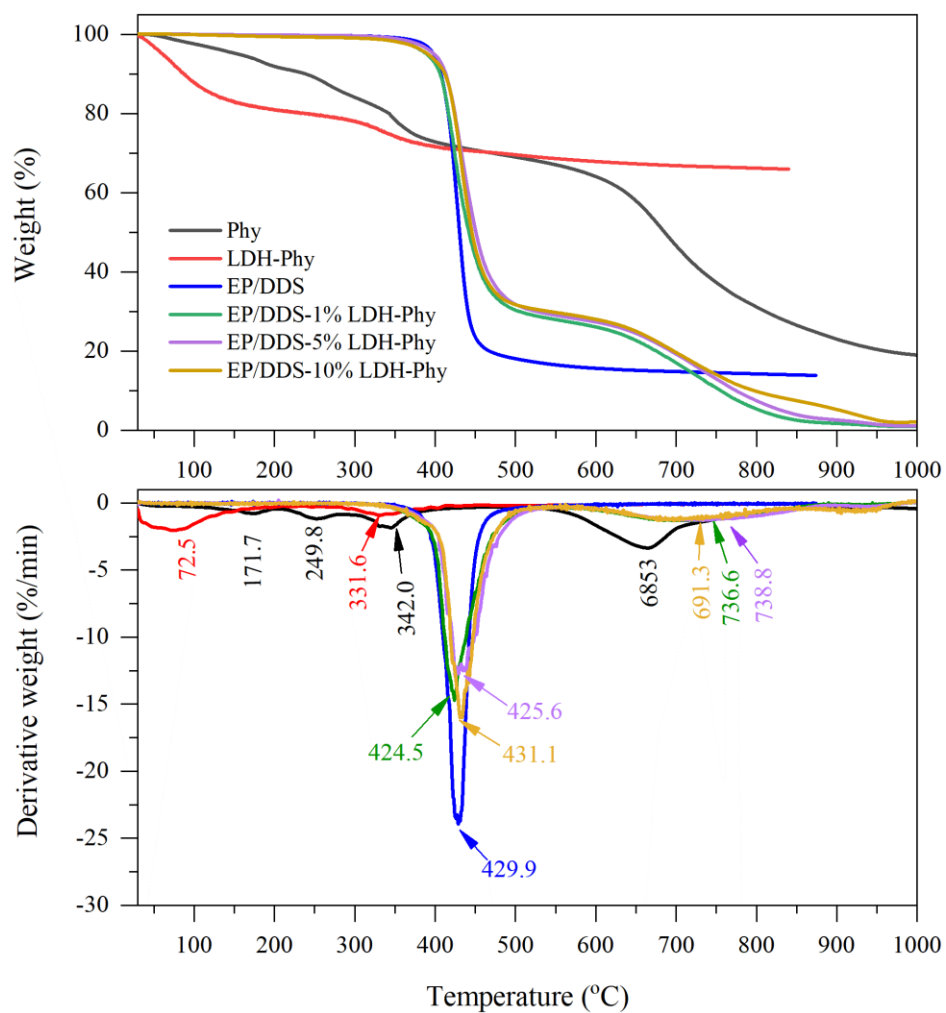


Figure 7.18 The TGA curves and their derivatives of Phy reactant, LDH-Phy, pure EP/DDS and the EP/LDH-Phy nanocomposites with the variation of LDH-Phy contents under N₂ flow.

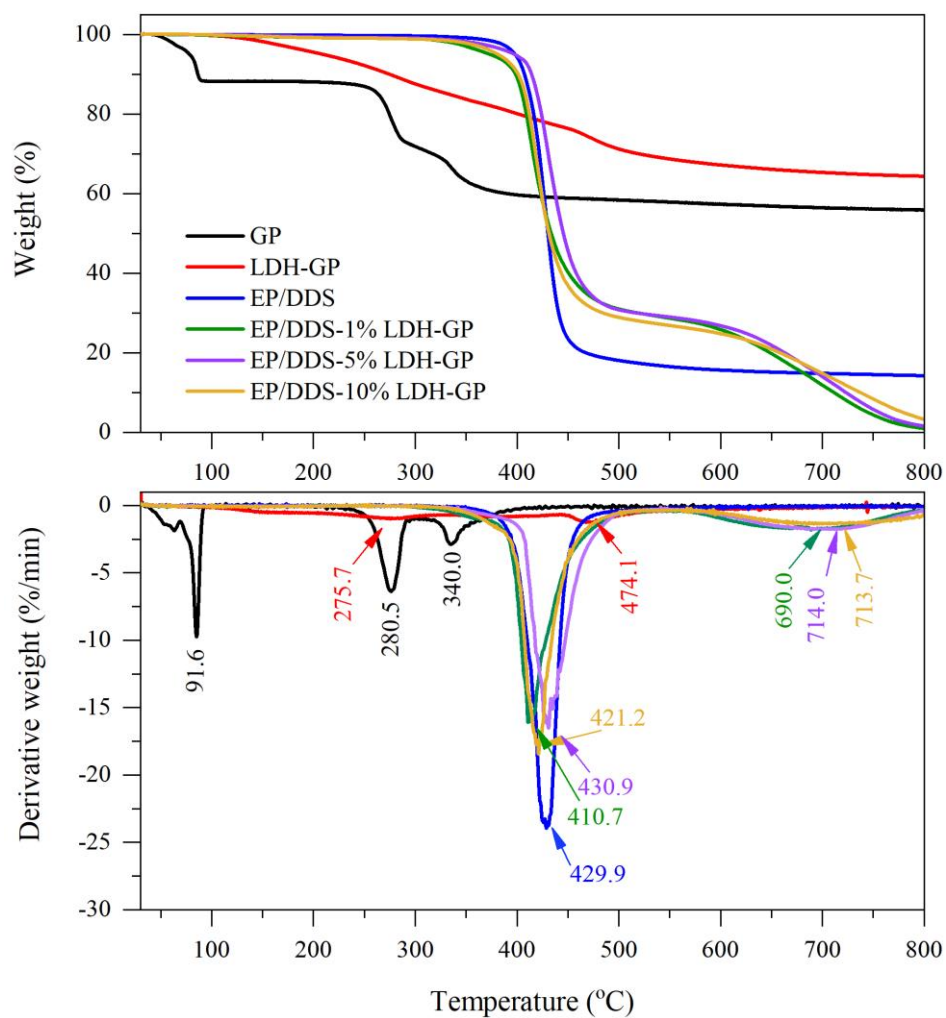


Figure 7.19 The TGA curves and their derivatives of GP reactant, LDH-GP, pure EP/DDS and the EP/LDH-GP nanocomposites with the variation of LDH-GP contents under N_2 flow.

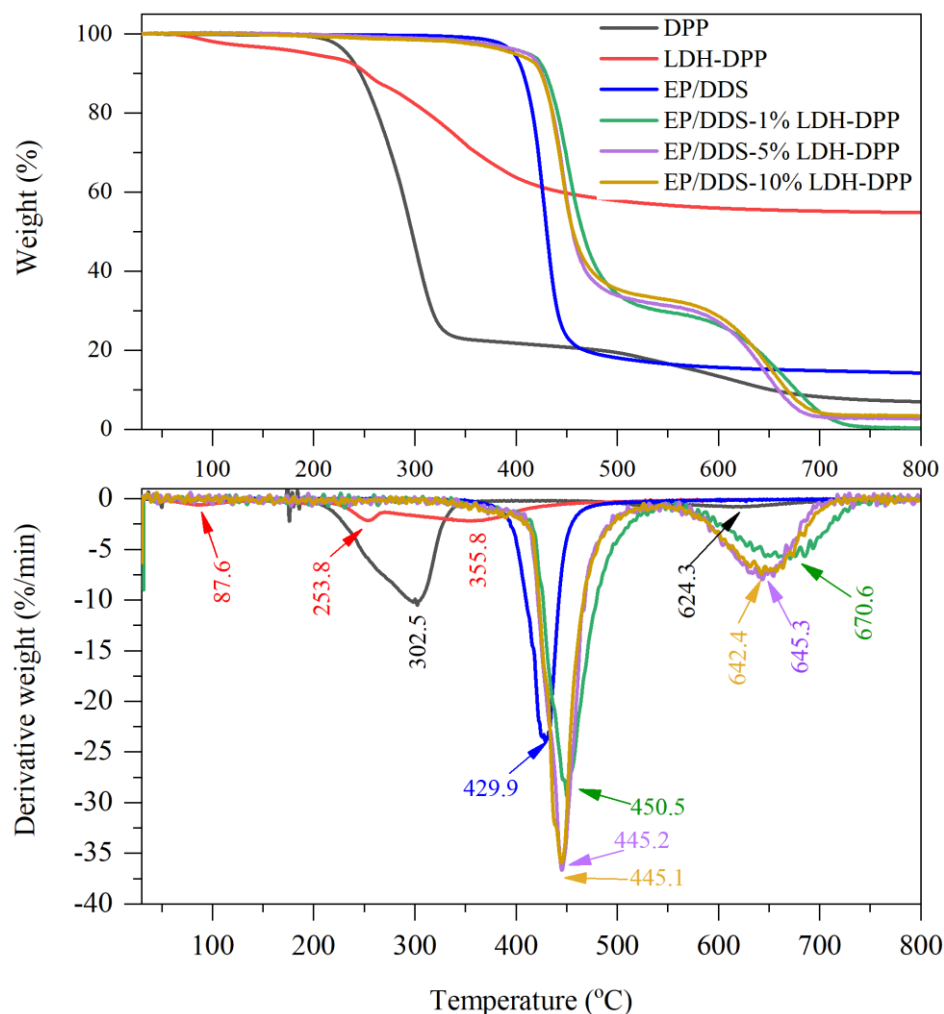


Figure 7.20 The TGA curves and their derivatives of DPP reactant, LDH-DPP, pure EP/DDS and the EP/LDH-DPP nanocomposites with the variation of LDH-DPP contents under N_2 flow.

As observed in the thermograms, it can be seen that all the EP nanocomposites degraded two stages in the temperature range of 30-800°C. The first stage occurred at approximately 200-500°C. Since this decomposition temperature range was equivalent to the degradation of pure EP, the decomposition of the EP/LDHs composites at this stage can be ascribed to the degradation of epoxy matrix. However, the initial decomposition temperature of all the EP nanocomposites was lower than that of the pure EP, excluding the incorporation of LDH-DPP. It indicated that the LDHs modified with the organophosphate ester-based anions could accelerate the degradation of epoxy matrix. Meanwhile, the decomposition temperature of the EP nanocomposite with the addition of LDH-DPP was higher than the pure EP. These

results state that the addition of LDH-DPP enhanced the thermal stability of the EP/DDS nanocomposites.

For the second decomposition stage of the EP/DDS- nanocomposites, it took place at the higher temperature than 500°C. This decomposition LDHs stage did not appear in the pure EP; however, it was observed in the thermogram of organophosphate ester-based reactant. According to the proposed thermal decomposition of organic phosphate reactants in the Section 5.4, the liquid phase of P₂O₅ volatile at 350-800°C. The possibility of decomposition of the EP nanocomposites at over 500°C was the thermal decomposition of phosphorus compounds.

From the TGA data in Table 7.6, the incorporation of 1 wt% LDHs-BEHP, -Phy, or -DPP increased the temperature at 10% mass loss (T_{10%}) and at 50% mass loss (T_{50%}) from the pure EP. These results stated that the thermal stability of the EP nanocomposites enhanced with the loading of 1 wt% LDHs modified BEHP, Phy or DPP. With increasing the loading percentage of the modified LDHs at 5 wt% and 10 wt%, the T_{10%} and T_{50%} were likely to decline by the comparison with the 1w% LDHs loading. Meanwhile, the addition of 1 wt% LDH-GP resulted in the slight decrease of T_{10%}, but the small increase of T_{50%} compared with the pure EP. With the loading of 5% LDH-GP, the EP nanocomposites revealed the rise of T_{10%} and T_{50%}, which were higher than the pure EP and EP/1% LDH-GP nanocomposite.

Table 7.6 The $T_{10\%}$, $T_{50\%}$, T_{\max} and residue percentage at 800°C of the pure EP/DDS and its nanocomposites incorporating the variation contents of modified LDHs

Sample	$T_{10\%}$ (°C)	$T_{50\%}$ (°C)	$T_{\max 1}$ (°C)	$T_{\max 2}$ (°C)	Mass at 800°C (%)
EP/DDS	407.2	430.3	429.9	-	14.2
EP/DDS-1% LDH-BEHP	416.2	452.4	439.1	606.2	0.0
EP/DDS-5% LDH-BEHP	401.9	451.8	417.0	601.2	2.8
EP/DDS-10% LDH-BEHP	369.1	445.8	424.8	608.8	5.7
EP/DDS-1% LDH-Phy	407.8	442.6	424.5	736.6	5.3
EP/DDS-5% LDH-Phy	413.3	450.8	425.6	738.8	7.5
EP/DDS-10% LDH-Phy	412.2	445.7	431.1	691.3	9.8
EP/DDS-1% LDH-GP	398.5	433.5	410.7	689.0	1.0
EP/DDS-5% LDH-GP	414.3	445.5	430.9	714.0	1.6
EP/DDS-10% LDH-GP	401.1	431.4	421.2	713.7	3.3
EP/DDS-1% LDH-DPP	429.5	465.9	450.5	670.6	0.3
EP/DDS-5% LDH-DPP	425.6	456.0	445.2	643.3	2.7
EP/DDS-10% LDH-DPP	424.6	456.3	445.1	642.4	3.4

Moreover, the TGA data in Table 7.6 indicated that the amount of residue at 800°C reduced significantly with loading the modified LDHs by comparison with the pure EP/DDS. The consequences indicated that the thermal decomposition of the EP nanocomposites containing the modified LDHs was more volatile than the pure EP due to the decomposition process of phosphorus compounds at the higher 500°C. However, the higher loading of the fillers, the higher content of residues.

As considered the TGA results under N_2 , it could be seen that the LDH modified with the various organophosphate-ester anions influenced the thermal decomposition behaviours of the EP nanocomposites. The loading of LDH-BEHP, LDH-Phy and LDH-GP played an important role in accelerating the thermal decomposition of the EP nanocomposites. These phenomena induced the formation of gaseous products and solid residues. It was speculated that both the released gases and the produced residues could restrict the combustion of epoxy resin. Meanwhile, the loading of LDH-DPP

enhanced the thermal stability of the EP nanocomposites, affecting the ignition of the EP nanocomposites.

7.5.4 Comparison of Thermal Behaviours of EP/DDS Nanocomposites with the Addition of LDHs Modified Different Organophosphate Compounds

The estimation of thermal behaviours of the EP/DDS nanocomposites containing the different LDHs under the N₂ or air atmosphere was discussed in this section by using the 5% wt loading of LDHs.

7.5.4.1 TGA Test under the N₂ Atmosphere

At the same loading contents of 5 wt% LDHs, the TGA thermograms and their derivatives of the EP/DDS nanocomposites were compared in Figure 7.21. As described in the above section, the thermogram of the EP nanocomposite containing the LDH-NO₃ exhibited the one stage of decomposition, which was similar to the pure EP. The mass loss at this stage was attributed to the cleavage of the polymer chain and the cross-linking networks.

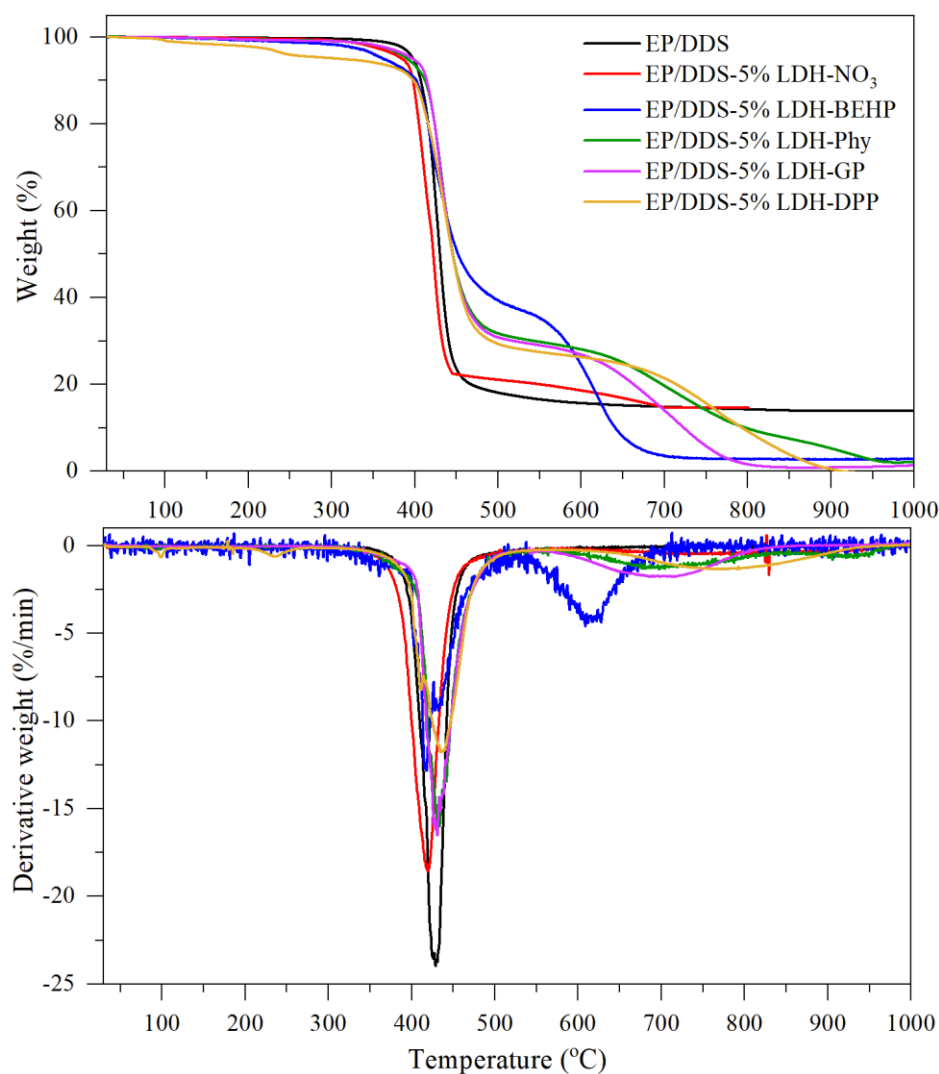


Figure 7.21 The TGA curves and their derivatives of the pure EP/DDS and the EP/DDS LDHs nanocomposites containing the 5 wt% loading of the various LDHs under N₂ atmosphere.

On the other hand, the TGA curves of all the EP nanocomposites with the BEHP, Phy, GP or DDP modified LDHs displayed two decomposition stages. The first stage of mass loss might be the degradation of polymer fraction, cross-linking networks, metal hydroxides, and organophosphate ester-based compounds in the LDHs. The second stage of mass loss corresponded to the decomposition of char produced from the first decomposition stage, which might be the decomposition of phosphate-based compounds.

With the consideration of introducing decomposition in the thermograms, it could be seen that the EP/DDS nanocomposites containing the 5 wt% LDH-NO₃, LDH-BEHP,

LDH-Phy, LDH-GP or LDH-DPP decomposed at the lower temperature than the pure EP/DDS. Table 7.7 notes the T_{max} and residue at 800°C from the TGA results of the EP/DDS nanocomposites with the different LDHs under N_2 . The maximum mass loss rate temperature at the first stage (T_{max1}) of all the EP/LDHs nanocomposites was less than the pure EP except for the addition of LDH-DPP. The results indicated that the thermal decomposition process of the EP nanocomposites could be accelerated by adding the LDHs due to the decomposition of phosphate-based composites in the LDHs. This phenomenon induced the fast char formation.

Table 7.7 The thermal degradation of the pure EP/DDS and the EP/LDHs nanocomposites

under N_2 atmosphere.

Sample	$T_{10\%}$ (°C)	$T_{50\%}$ (°C)	T_{max1} (°C)	T_{max2} (°C)	Mass at 800°C (%)
EP/DDS	407.2	430.3	429.9	-	14.2
EP/DDS-5% LDH- NO_3	394.9	424.3	421.0	-	15.3
EP/DDS-5% LDH-BEHP	401.9	451.8	417.0	601.2	2.8
EP/DDS-5% LDH-Phy	413.3	450.8	425.6	738.8	7.5
EP/DDS-5% LDH-GP	414.3	445.5	430.9	714.0	1.6
EP/DDS-5% LDH-DPP	425.6	456.0	445.2	643.3	2.7

In case of the addition of 5 wt% LDH-DPP, it provided the higher T_{max1} of the EP/DDS nanocomposites compared to the pure EP/DDS because of the increase of interaction between the epoxy matrix and the LDH-DPP. This action contributed to the enhancement of thermal stability in the composites.

Since there was the second decomposition stage in the EP nanocomposites with the composition of 5 wt% organophosphate ester modified LDHs, the residual content at 800°C of those composites was less than the pure EP and the EP/pristine LDHs.

7.5.4.2 TGA Test under the Air Atmosphere

As mentioned in the Section 6.6.3.2, the TGA characterisation under air was the simulation of the combustion process with O₂. The thermal oxidation behaviours of the pure EP and its nanocomposites cured with the DDS curing agent under the air atmosphere were presented in Figure 7.22 and Table 7.8. All the thermograms presented two steps of mass change at the ranges of 300-500°C and 500-700°C. Compared to the test under N₂ as described in the previous section, there was a dissimilarity of decomposition pattern.

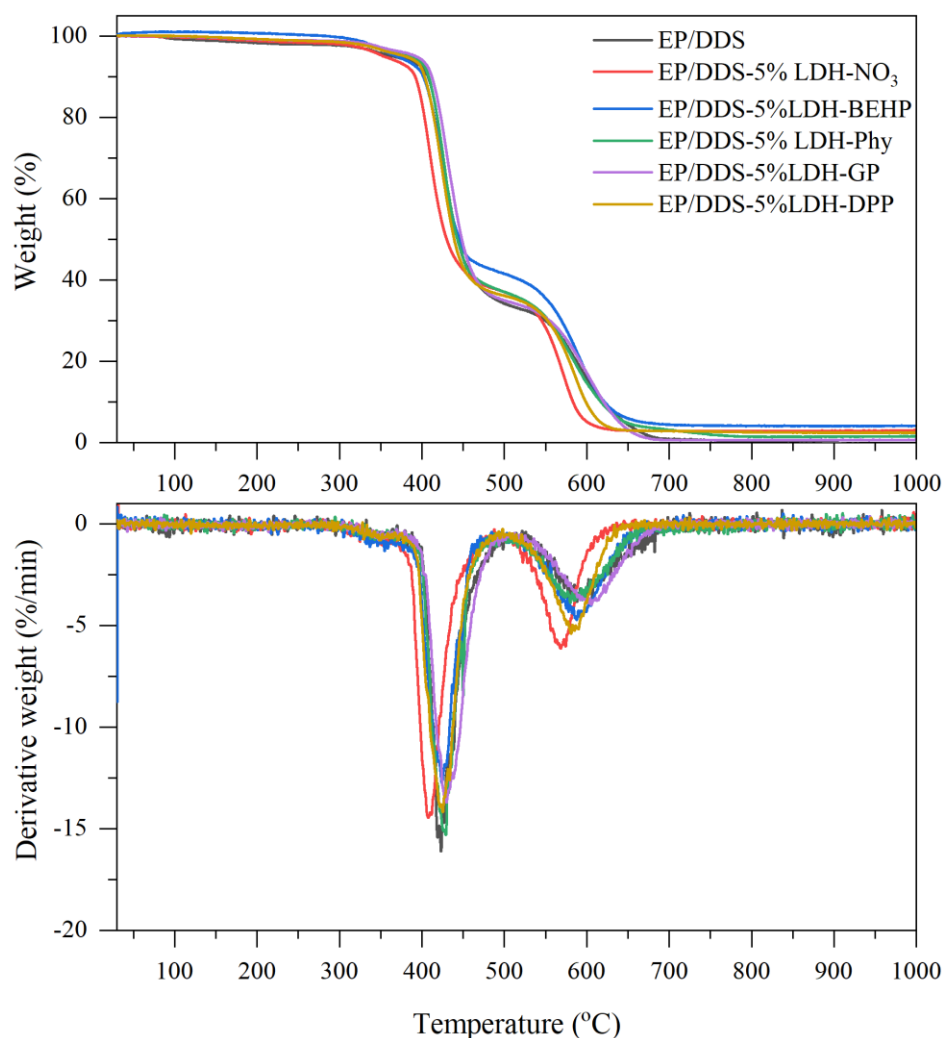


Figure 7.22 The TGA curves and their derivatives of the pure EP/DDS and its nanocomposites with the 5 wt% loading of the various LDHs under air

Table 7.8 The thermal oxidative degradation of the pure EP/DDS and the EP/LDHs nanocomposites under air.

Sample	T _{10%} (°C)	T _{50%} (°C)	T _{max1} (°C)	T _{max2} (°C)	Mass at 800°C (%)
EP/DDS	407.4	443.0	423.2	600.3	0.4
EP/DDS-5% LDH-NO ₃	391.8	430.0	407.5	568.2	2.8
EP/DDS-5% LDH-BEHP	401.7	445.6	424.3	587.7	4.1
EP/DDS-5% LDH-Phy	408.1	443.0	428.8	579.7	1.4
EP/DDS-5% LDH-GP	412.0	448.3	429.9	605.3	0.6
EP/DDS-5% LDH-DPP	403.2	439.0	425.8	581.1	2.5

The pure EP derived from the mixture of DGEBA and DDS showed the T_{max1} at 423.2°C for the test under air. This decomposition occurred at the same temperature range of test under N₂; however, the decomposition under air took place at the lower temperature. The previous section explained that this stage was the scission of C-O and C-N in the DDS cured DGEBA. It produced SO₂, CO and acetone gases and the char residues of aromatic-O and aromatic -N compounds [14, 15]. The second step was in 500-700°C with the maximum mass loss rate (T_{max2}) at 600.3°C. This step was attributed to the thermal oxidative degradation of the char produced in the first step [14, 15]. The mass of char residue at 800°C was almost 0%.

For the EP/DDS-LDHs nanocomposites, the thermograms under air revealed two decomposition stages, resembling the pure EP. When the different LDHs were loaded to the epoxy matrix, the T_{10%} of nanocomposites decreased with incorporating the LDH-NO₃, LDH-BEHP or LDH-DPP; however, it increased with the addition of LDH-Phy or LDH-GP by comparison with the pure EP/DDS. Observing the T_{50%}, the LDH-NO₃ and LDH-DPP contributed to the gradual reduction, but the LDH-BEHP, LDH-Phy and LDH-GP resulted in the slight increase. Both the T_{10%} and T_{50%} of the nanocomposites were in the first stage of decomposition.

The thermal oxidative process in the first decomposition stage occurred at 424.3-429.9°C. It was probably due to the degradation of the cross-linked polymer fractions and the LDHs fractions combined with the epoxy matrix. The T_{max1} increased slightly

with the addition of 5 wt% LDHs modified the organophosphate ester-based anions. It stated that the modified LDHs enhanced the thermal oxidative stability of the EP nanocomposites.

At the second stage of decomposition, it was attributed to the decomposition of compounds formed in the first decomposition stage. Most $T_{\max 2}$ of the EP/LDHs nanocomposites reduced by approximately 12-20°C from the 600.3°C of the pure EP/DDS. Furthermore, the char residues at 800°C of the nanocomposites increased slightly with the loading of LDHs. This included the decomposition of metal hydroxides in the LDH layers and organic compounds intercalated or exfoliated in the LDHs.

7.6 Combustion Behaviors of Epoxy Resin Nanocomposites Cured with DDS

As mentioned in the previous chapter, the burning test in the horizontal direction was not suitable for the epoxy resin. This chapter focused on the vertical burning test for the epoxy resins cured with the DDS, carried out at the Quarrell Laboratory.

7.6.1 Burning Test in Vertical Direction

The combustion times of samples after the first and second flame application (t_1 and t_2) were recorded, and their combustion behaviours were observed to evaluate the flammability. The results of the burning test for the pure EP and the EP nanocomposites containing the 5 wt% loading of LDHs were noted in Table 7.9.

Table 7.9 The combustion time and burning characteristics of the pure DGEBA/DDS and its nanocomposites with the 5 wt % LDHs.

Additives	t ₁ in each specimen (s)	t ₂ in each specimen (s)	t ₁ +t ₂ for five specimens (s)	Flame to clamp	Dripping	Ratting
No fillers	246 ± 17	-	1232	Yes	Yes	NA
5%LDH-CO ₃	98 ± 25	156 ± 43	1269	Yes	Yes	NA
5%LDH-NO ₃	66 ± 23	139 ± 6	1025	Yes	Yes	NA
5%LDH-BEHP	69 ± 20	130 ± 14	995	Yes	Yes	NA
5%LDH-Phy	86 ± 37	204 ± 43	1446	Yes	Yes	NA
5%LDH-GP	99 ± 45	216 ± 3	1574	Yes	Yes	NA
5%LDH-DPP	68 ± 18	187 ± 11	1276	Yes	Yes	NA

The obtained data found that the pure EP (the DDS cured DGEBA) did continually burn after remove the first ignition without the self-extinguish. Besides, there was the dripping of flame during the combustion. With the comparison of pure EP burning behaviours between the DDS and the DDM curing system after the first ignition, the EP/DDS could be burned spontaneously; on the other hand; the EP/DDM continued to burn and extinguished. Considering the TGA results of the Section 7.5.1, the char residue of the EP/DDS (14.2%) was less than the EP/DDM (16.3%). The charring layer acted as the layered barrier to protect the dispersion of flame, gases, and heat to the combusting area. Hence, the flammability of EP/DDS was higher than the EP/DDM.

When the 5 wt% LDHs were loaded to the EP matrix, they influenced the flame retardancy performance of the EP nanocomposites. After the first ignition, the EP/DDS-5 wt% LDHs continued to burn and extinguished without the fire dripping. The incorporation of LDHs led to the remarkable decrease of the burning time after the first ignition (t₁) by 59-73% from the pure EP/DDS. As mentioned in the Section 7.5.4.2 about the thermal oxidative degradation of the EP/DDS-5% LDHs

nanocomposites, the decomposition temperatures of most nanocomposites were lower than that of the pure EP resulting in the accessibility of volatilisation and char formation. Both of them could inhibit the spreading of flame, gases, and heat to the combusting surface of materials. For this reason, it accounted for the reduction of t_1 for the EP/DDS nanocomposites containing the 5 wt% LDHs. The different LDHs did not significantly affect the t_1 burning time.

Then, the flame was applied to the extinguished specimen again. The nanocomposites did not stop burning after the second ignition and were accompanied by the fire dripping. The burning time after applying the second flame was in the range of 130-216 s. The ignition of EP/DDS nanocomposites with the 5 wt% LDHs was more than the pure EP/DDS. The results indicated that the LDHs restricted the ignition of the EP nanocomposites. It was noticeable that the t_2 of EP nanocomposites with the organophosphate ester modified LDHs were longer than that with the pristine LDHs. It might associate with the thermal oxidative decomposition. From the TGA results under air atmosphere, the thermal oxidative stability of EP nanocomposites with the modified LDHs was more than that with the pristine LDHs. Therefore, the burning time at this stage was delayed by adding the 5 wt% modified LDHs. The photo representatives of the pure EP/DDS and their nanocomposites with the 5 wt% LDHs during the UL-94 test were displayed in Figure 7.23.

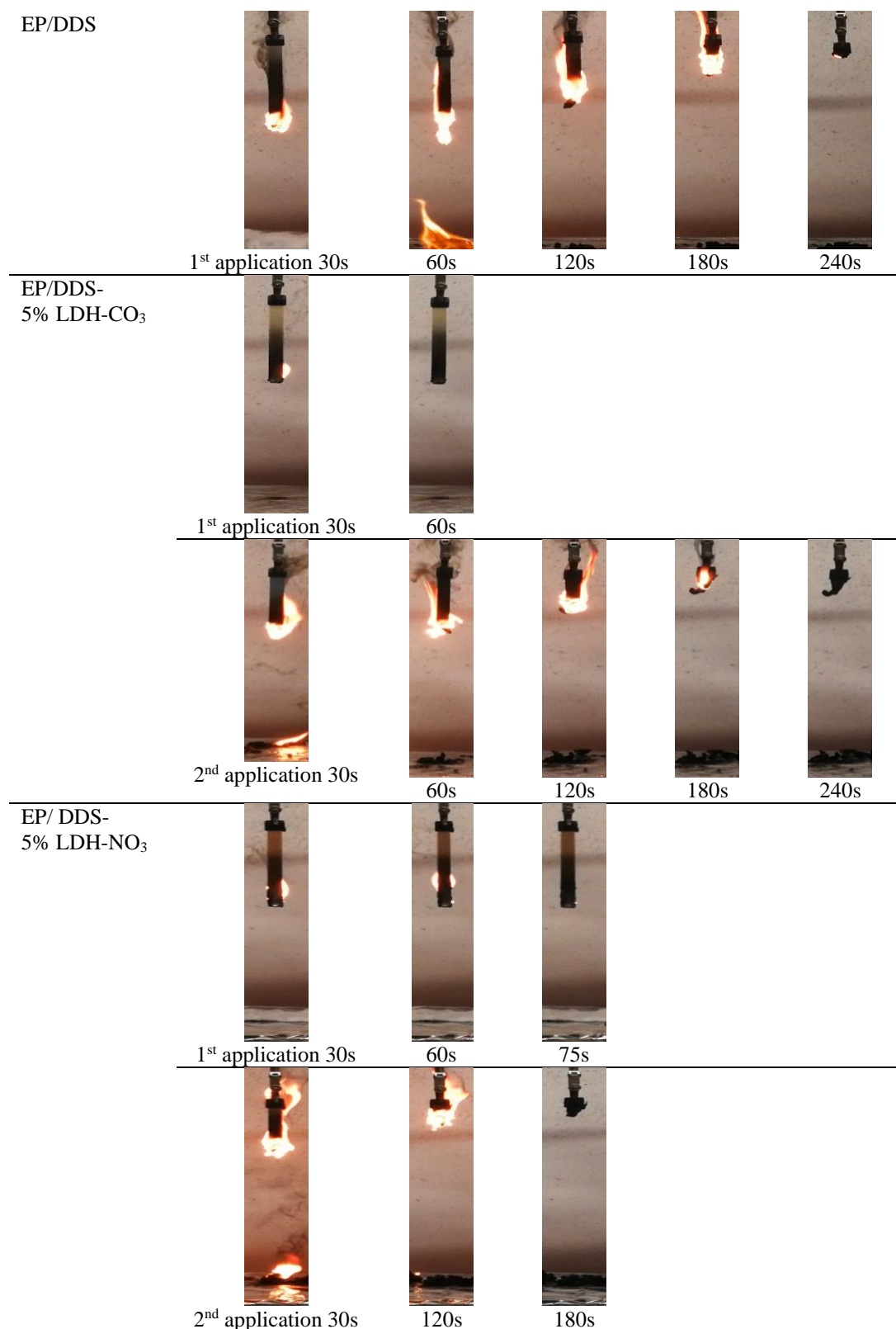


Figure 7.23 The digital photos of the pure DGEBA/DDS and its nanocomposites with the 5 wt% LDHs during the UL-94 test.

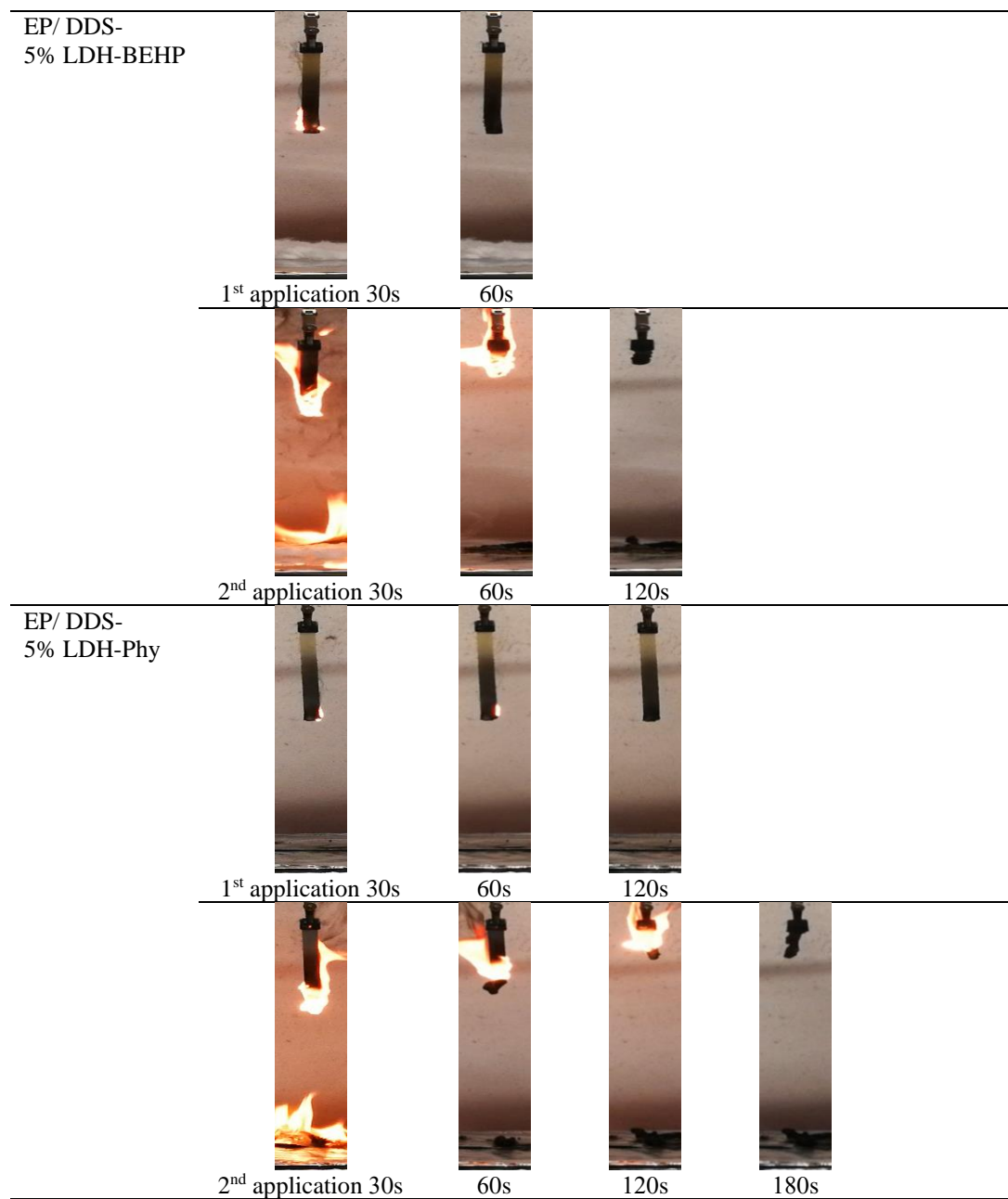


Figure 7.23 The digital photos of the pure DGEBA/DDS and it nanocomposites with the 5 wt% LDHs during the UL-94 test. (continued)

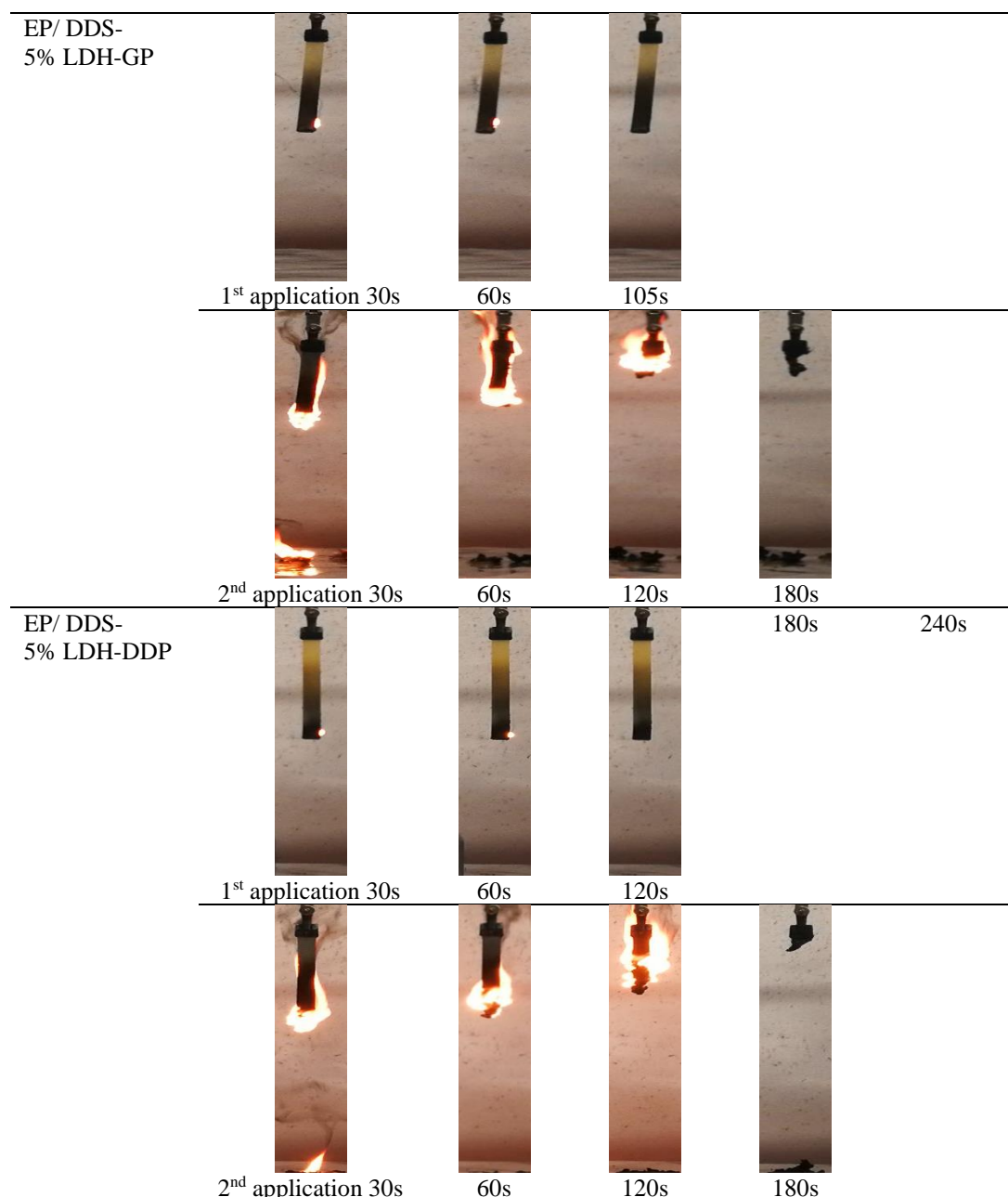


Figure 7.23 The digital photos of the pure DGEBA/DDS and it nanocomposites with the 5 wt% LDHs during the UL-94 test. (continued)

The characteristics of sample after the burning test were presented in Figure 7.24. It could be seen obviously that all the nanocomposites containing the 5 wt% LDHs were burn completely after applying the flame. The results indicated that the loading of 5 wt% pristine LDHs or modified LDHs was not able to stop the combustion of EP/DDS.

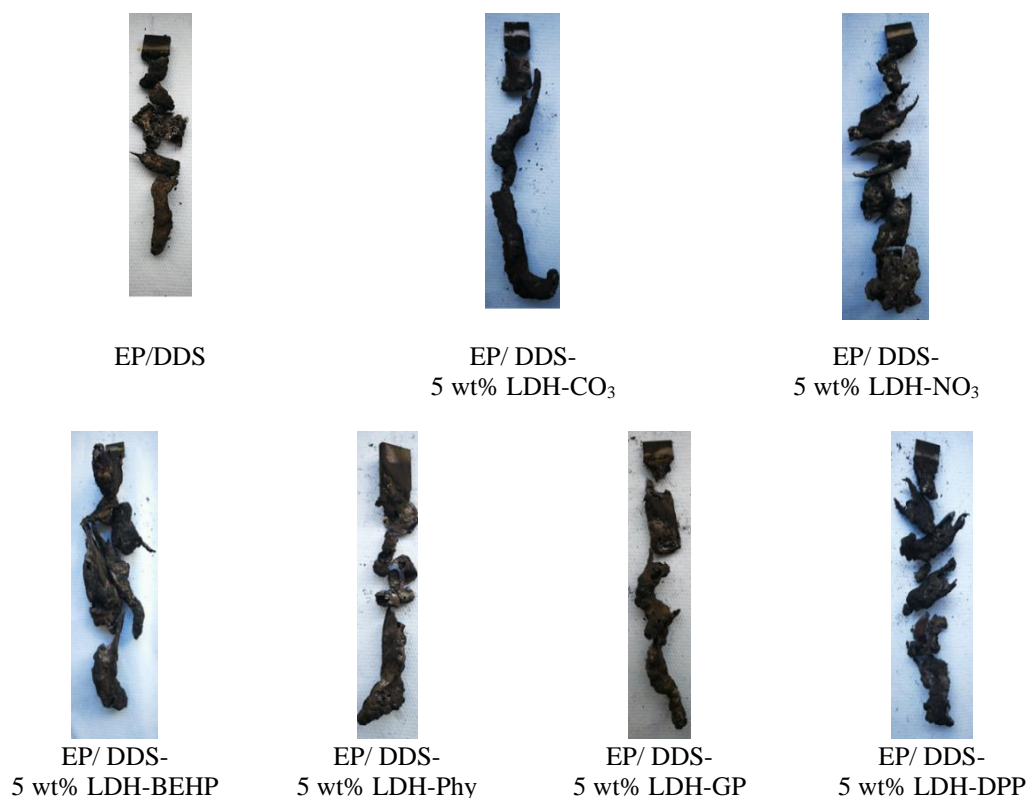


Figure 7.24 The char characteristics after the flame test of the pure DGEBA/DDS and its nanocomposites with the 5 wt% LDHs.

Considering the rating criteria in the standard ASTM D3801 described in Table 6.14, the burning times (t_1 and t_2) of the EP nanocomposites containing the 5 wt% LDHs were longer than the determined standard. Moreover, there were the dripping of fire during the burning of EP/DDS nanocomposites with the 5 wt% LDHs. Therefore, the burning behaviours of the samples did not match with the criteria determined in the standard. That meant the incorporation of 5% LDHs could not enhance the flame retardancy to the EP/DDS.

The 10 wt% LDHs were loaded to the epoxy matrix to investigate the combustion behaviours to verify the expectation. The crucial data obtained from the burning test were reported in Table 7.10. The addition of 10 wt% LDHs decreased the t_1 by comparison with the pure EP, especially the organophosphate ester modified LDHs. These results were the same decreasing trend as the loading of 5 wt% LDHs. However, the t_1 of 10 wt% LDHs loading was lower than that of 5 wt% LDHs loading more than one time. The increase of LDHs contents led to the rise of char residues during the combustion, restricting the dispersion of flame, gas and heat to the combusting area.

Thus, the increase of LDH contents reduced the flammability of EP composites. As the organophosphate ester compounds in the LDHs accelerate the thermal oxidative degradation of the EP nanocomposites to the lower temperature, the volatilised and char products produced during the combustion could delay the combustion of composites. Hence, the t_1 burning times of composites with the modified LDHs were less than that with the pristine LDHs.

Table 7.10 The combustion time and burning characteristics of the pure DGEBA/DDS and its nanocomposites incorporating the 10 wt % LDHs.

Additives	t_1 in each specimen (s)	t_2 in each specimen (s)	t_1+t_2 for five specimens (s)	Flame to clamp	Drippin g	Rating
No fillers	246 ± 17	-	1232	Yes	Yes	NA
10%LDH-CO ₃	57 ± 18	161 ± 73	1091	Yes	Yes	NA
10%LDH-NO ₃	50 ± 21	171 ± 84	1103	Yes	Yes	NA
10%LDH-BEHP	24 ± 20	219 ± 4	1215	No	No	NA
10%LDH-Phy	14 ± 3	199 ± 10	1065	No	No	NA
10%LDH-GP	27 ± 7	16 ± 11	214	No	No	V-1
10%LDH-DPP	26 ± 7	159 ± 16	927	No	No	NA

After the flame applied to the samples in the second times, the t_2 burning time of each composite with adding the 10 wt% modified LDHs was not different significantly. Nevertheless, the total burning times of EP nanocomposites containing the modified LDHs were less than that containing the pristine LDH particular to the LDH-GP loading. As explained in the previous paragraph, the organophosphate ester compounds could accelerate the formation of gases and char. They acted as the insulators to protect the spreading of flame, gases, and heat to the materials. Therefore, the total burning times and fire distribution of EP nanocomposites declined with incorporating the modified LDHs. The combustion was stopped with the addition of

modified LDHs without the dripping of flame. All the results insisted that the flame retardancy of thermoset materials increased with the loading of modified LDHs at higher contents. The behaviours of materials during the burning test were displayed in Figures 7.25.



Figure 7.25 The digital photos of the pure DGEBA/DDS and its nanocomposites with the 10% LDHs during the UL-94 test.

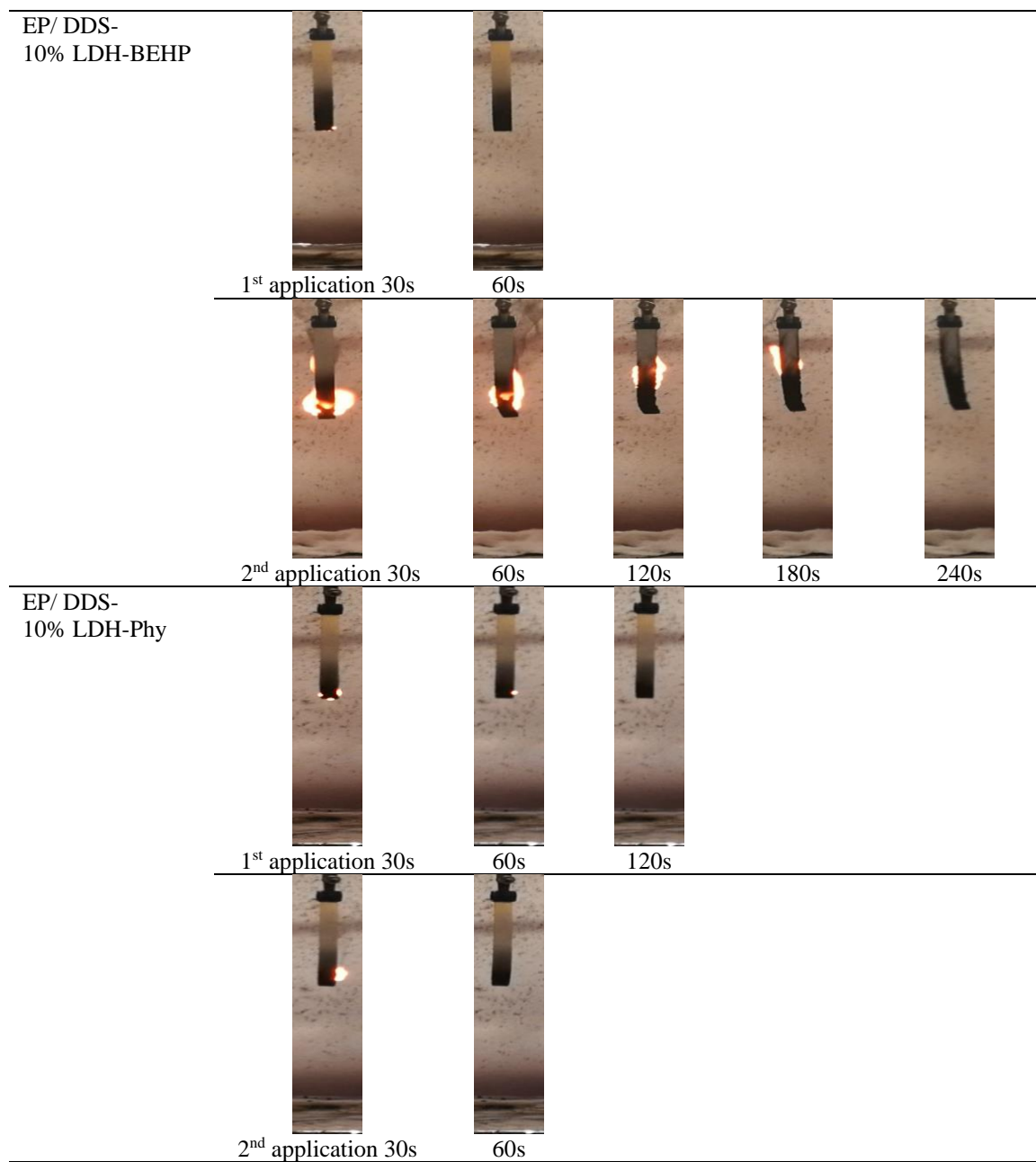


Figure 7.25 The digital photos of the pure DGEBA/DDS and its nanocomposites with the 10% LDHs during the UL-94 test. (continued)

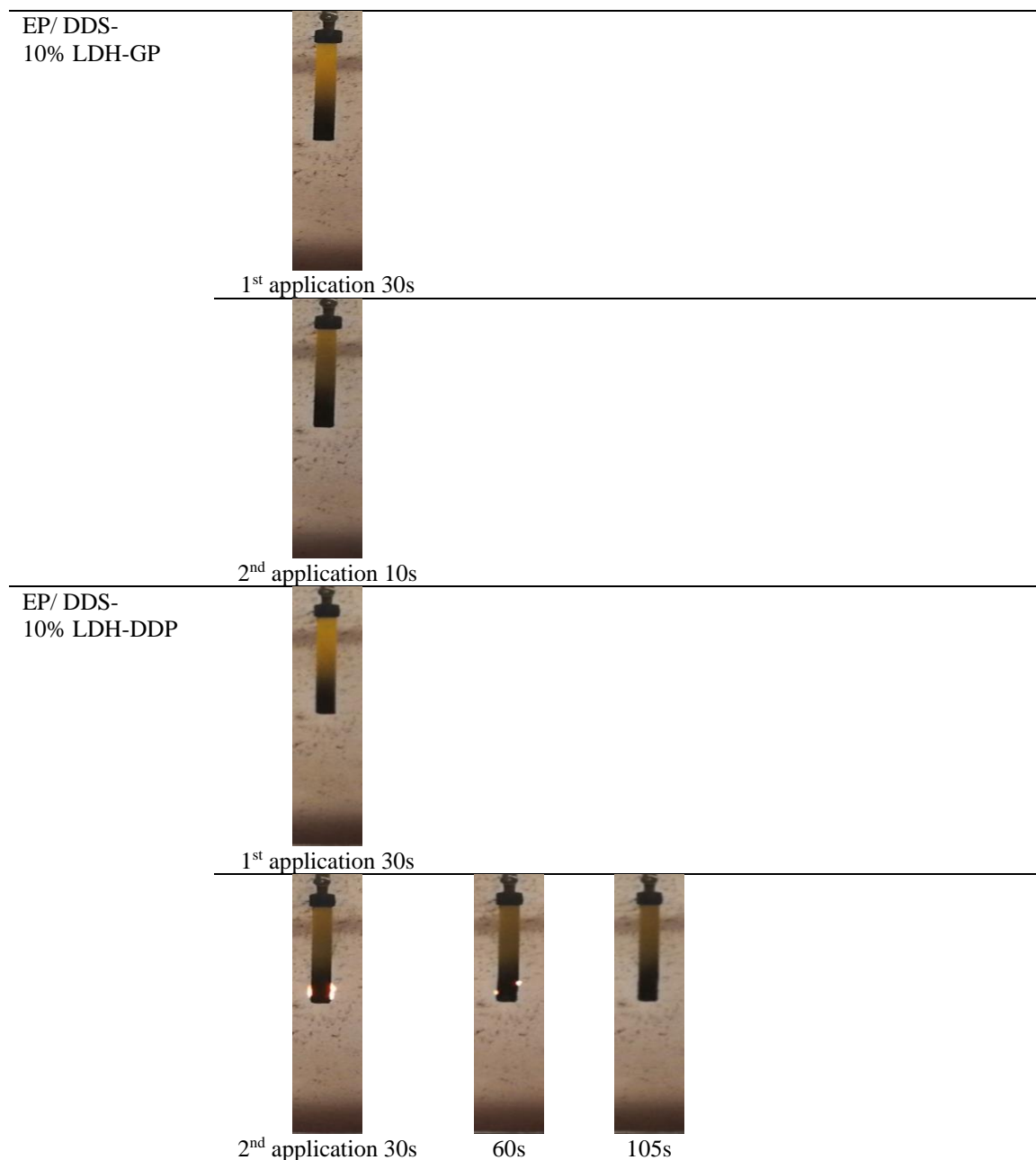


Figure 7.25 The digital photos of the pure DGEBA/DDS and its nanocomposites with the 10% LDHs during the UL-94 test. (continued)

Observing the characteristics of samples after the burning test in Figure 7.26, the epoxy nanocomposites with adding the 10 wt% unmodified LDHs did not survive from the combustion. However, the incorporation of 10 wt% modified LDHs was able to inhibit the combustion of EP/DDS.

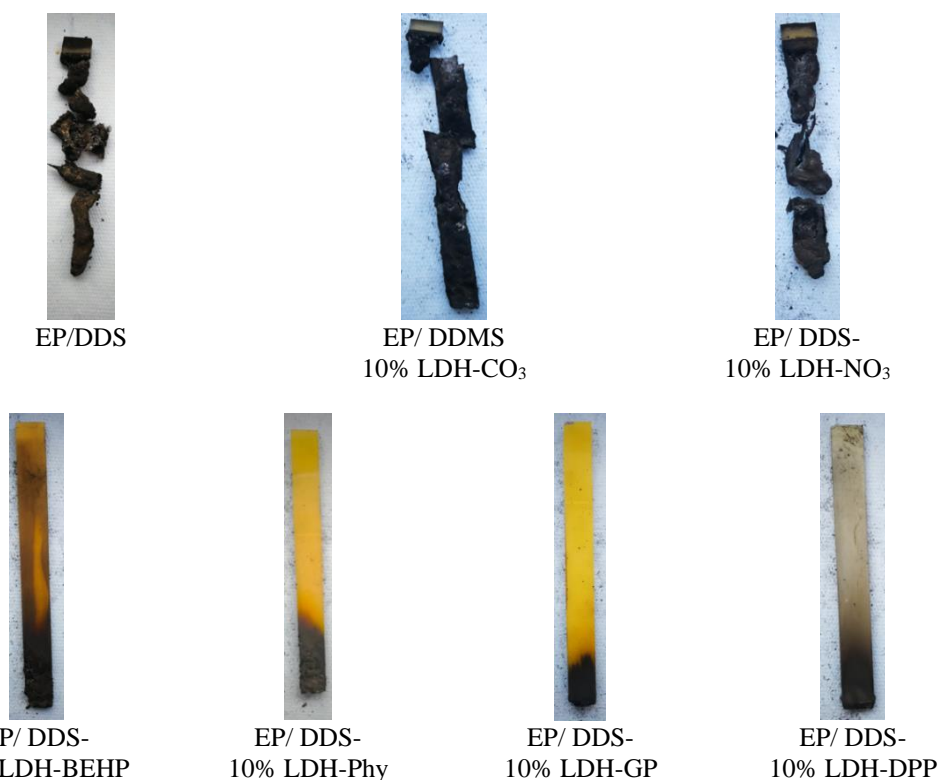


Figure 7.26 The char characteristics after the flame test of the pure DGEBA/DDS and its nanocomposites with the 10 wt% LDHs.

With the classification of material flammability as following the criteria in the standard, the only EP nanocomposites containing the 10 wt% LDH-GP was defined in the moderately flammable materials (V-1), whereas the other composites could not still determine in any classes. As the flame retardancy of EP/DDS tended to enhance with increasing the contents of LDHs, the incorporation of LDHs over 10 wt% is interesting for studying in future work.

Overall, the addition of 5 wt% pristine or modified LDHs was not able to extinguish the EP/DDS. With the loading contents of LDHs increased to 10 wt%, the EP/DDS with the pristine LDHs were not still burnt through their whole specimens. However, the loading of 10 wt% organophosphate ester modified LDHs could induce the EP/DDS nanocomposites to extinguish. Although the EP/DDS-10% modified LDHs were extinguished, their burning times were longer than the criteria in the standard. They could not be classified in any type except the EP nanocomposite with the 10 wt% LDH-GP.

7.7 Summary

This chapter studied the effect of LDHs addition on the properties of the DDS cured with the DGEBA. The LDHs used as the fillers were the pristine LDHs (LDH-CO₃ and LDH-NO₃) and the organophosphate ester modified LDHs (LDH-BEHP, LDH-Phy, LDH-GP and LDH-DPP). All the LDHs at 1, 5 and 10 wt% loadings were well dispersed in the epoxy matrix. The addition of LDHs did not significantly decrease the flexural properties. The modified LDHs improved the flexural modulus more than the pristine LDHs. As the addition of LDHs enhanced the stiffness and the friction of polymer chain movement, both the pristine and modified LDHs increased the storage modulus and loss modulus in the glassy state compared to the pure EP/DDS. However, the T_g of EP nanocomposites did not change by incorporating the LDHs. It was because the LDHs did not interfere with the polymer.

Furthermore, the pristine and modified LDHs influenced the thermal decomposition behaviours of the EP/DDS nanocomposites under N₂ and air. All the LDHs accelerated the decomposition, resulting in the volatilisation and char formation at lower temperatures than the pure EP/DDS. The rise of LDHs loading contributed to the decrease of decomposition temperature but the increase of char residues. Some gases and char produced during the heating could inhibit the combustion. These circumstances were advantages of LDHs for flame retardant applications.

For the burning test, the addition of 5 wt% LDHs reduced the flammability of polymer. After applying the second ignition, however, they could not stop the combustion of EP/DDS. To enhance the flame retardancy performance of the EP/DDS, the 10 wt% LDHs were incorporated into the epoxy matrix. The EP nanocomposites with the 10 wt% organophosphate ester modified LDHs extinguished and did not result in the fire dripping during the combustion. Therefore, the LDH-BEHP, LDH-Phy, LDH-GP and LDH-DPP could be used as the flame retardants for the epoxy resin.

References

- [1] M. L. Costa, L. C. Pardini and M. C. Rezende, "Influence of Aromatic Amine Hardeners in the Cure Kinetics of an Epoxy Resin Used in Advanced Composites", *Mat. Res.*, 2005, **8(1)**, 65-70
- [2] Q. Ling, D. Wang, Y. Zhang, X. Lu, S. Zhao and F. Sun, "Morphology, Thermal and Mechanical Performance of Epoxy/Polysulfone Composites Improved by Curing with Two Different Aromatic Diamines", *J. Appl. Polym. Sci.*, 2020, **137(41)**, 49265
- [3] R. Ebwewele, "Polymer Science and Technology", Taylor & Francis Group, USA, 2000.
- [4] H. P. Menard, "Dynamic Mechanical Analysis: A Practical Introduction", Taylor & Francis Groups 2 ed. USA:, 2008.
- [5] R. B. Prime, H. E. Bair, S. Vyazovkin, P. K. Gallagher, and A. Riga, "Thermogravimetric Analysis (TGA)," in *Thermal Analysis of polymers*, J. D. Menczel and R. B. Prime Eds. John Wiley & Sons, Canada, 2009, pp. 240-317
- [6] P. J. Haines and F. W. Wilburn, "Differential Thermal Analysis and Differential Scanning Calorimetry" in "Principles of Thermal Analysis and Calorimetry", eds. P.J.Haines, Royal Society of Chemistry, Cambridge, 2002, pp 63-122
- [7] C.-H. Tseng, H.-B. Hsueh and C.-Y. Chen, "Effect of Reactive Layered Double Hydroxides on the Thermal and Mechanical Properties of LDHs/Epoxy Nanocomposites", *Comp. Sci. Tech.*, 2007, **67(11)**, 2350-2362
- [8] C. Li, J. Wan, E. Kalali, H. Fan and D.-Y. Wang, "Synthesis and Characterization of Functional Eugenol Derivative based Layered Double Hydroxide and Its Use as a Nanoflame-Retardant in Epoxy Resin", *J. Mater. Chem. A.*, 2015, **3(7)**, 3471-3479
- [9] E. N. Kalali, X. Wang and D.-Y. Wang, "Functionalized Layered Double Hydroxide-Based Epoxy Nanocomposites with Improved Flame Retardancy and Mechanical Properties", *J. Mater. Chem. A.*, 2015, **3(13)**, 6819-6826
- [10] P. Zhu, Z. Gu, S. Hong and H. Lian, "Preparation and cCharacterization of Microencapsulated LDHs with Melamine-Formaldehyde Resin and Its Flame

- Retardant Application in Epoxy Resin", *Polym. Adv. Tech.*, 2018, **29(7)**, 2147-2160
- [11] J. Meng, P. Chen, R. Yang, L. Dai, C. Yao, Z. Fang and K. Guo, "Thermal Stable Honokiol-Derived Epoxy Resin with Reinforced Thermal Conductivity, Dielectric Properties and Flame Resistance", *Chem. Eng. J.*, 2021, **412**, 128647
- [12] F. Yeasmin, A. K. Mallik, A. H. Chisty, F. N. Robei, M. Shahruzzaman, P. Haque, M. M. Rahman, N. Hano, M. Takafuji and H. Ihara "Remarkable Enhancement of Thermal Stability of Epoxy Resin Through the Incorporation of Mesoporous Silica Micro-Filler", *Heliyon*, 2021, **7(1)**, e05959
- [13] J. Macan, I. Brnardić, S. Orlić, H. Ivanković and M. Ivanković, "Thermal Degradation of Epoxy-Silica Organic-Inorganic Hybrid Materials", *Polym. Degrad. Stabil.*, 2006, **91(1)**, 122-127
- [14] U. Braun, A.I. Balabanovich, B. Schartel, U. Knoll, J. Artner, M. Ciesielski, M. Döring, R. Perez, J. K. W. Sandler, V. Altstädt, T. Hoffmann, D. Pospiech, "Influence of the Oxidation State of Phosphorus on the Decomposition and Fire Behaviour of Flame-Retarded Epoxy Resin Composites", *Polym.*, 2006, **47(26)**, 8495-8508
- [15] G. You, Z. Cheng, H. Peng and H. He, "Synthesis and Performance of a Novel Nitrogen-Containing Cyclic Phosphate for Intumescent Flame Retardant and its Application in Epoxy Resin", *J. Appl. Polym. Sci.*, 2015, **132(16)**, 41859

Chapter 8
**Conclusions and Suggestions
for Future Work**

This is a final chapter of the dissertation concluding the results obtained from the experiments relating to the aim and objectives of the research. Besides, the following section provides suggestions for future works.

8.1 Conclusions

In recent years, polymer composite materials have received an increase in attention across a number of industries due to their high mechanical properties, good chemical resistance and lightweight. Although there are many advantages of polymer composites, one of their common disadvantages needing to improve is high flammability. The combustion of polymers produces an extensive amount of flame, heat and smoke, leading to health impacts, environmental problems and property damages. Several researches have attempted to inhibit the flammability of polymers by incorporating flame retardant fillers such as compounds containing halogen, phosphate and/or nitrogen, mineral fillers and nano-fillers.

Layered double hydroxides (LDHs) have attracted significant attention as flame retardants for polymers due to the unique structure of LDHs. The thermal decomposition of LDHs results in volatilised gases and char residues. All products produced from the burning of LDHs can prohibit the dispersion of fuels, e.g. flame, heat and flammable gases, to combusting areas. Therefore, the aim of this dissertation was to develop the flame retardancy performance of polymers by the addition of LDHs fillers. The intercalated anions in LDHs were modified with four anionic compounds consisting of the organophosphate ester groups: bis(2-ethyl hexyl)phosphate (BEHP), phytate (Phy), glycerophosphate (GP) or diphenyl phosphate (DPP). The epoxy resins of bisphenol A diglycidyl ether (DGEBA) cured with the 4,4-diamino diphenyl methane (DDM) or 4,4-diamino diphenylsulfone (DDS) were employed as the representatives of polymers.

8.1.1 Synthesis and Characterisation of LDHs

For the synthesis of LDHs, the co-precipitation method was more suitable than the calcination-rehydration method. The N_2 flow within the reaction chamber and the

decarbonation of used distilled water and precipitating agents were conducted during the LDHs synthesis so as to protect the disruption of desired anion intercalation from the intercalation of high-affinity carbonate anions in the interlayer space. The characterisations of all synthesised LDHs were analysed by the X-rays diffractometry (XRD), Fourier transform infrared spectroscopy (FTIR), thermogravimetric analysis (TGA).

This study showed that the preparing conditions affecting the crystallinity and crystal size of LDHs were pH, precipitating agent, and aging time. The optimum conditions for the LDHs preparation were the aging at pH 9 for 24 h. The NaOH solution was used to prepare LDH-NO₃, LDH-BEHP, LDH-Phy and LDH-GP, whereas the NH₄OH solution was employed to prepare LDH-DPP. The anions of nitrate, BEHP, GP or DPP intercalated between the metal hydroxide layers. Meanwhile, the layer structure of LDHs was exfoliated by the anions of Phy.

From the TGA results, the pristine LDHs (LDHs intercalated with the CO₃ or NO₃) displayed the loss of water adsorbed on the surface and intercalated between the layered space at the below 250°C and the dehydration of metal hydroxide layers in the range of 250-500°C. The residues were metal oxides, such as MgO and Al₂O₃. In the case of the organophosphate ester modified LDHs, not only the loss of water but the organophosphate ester anions also decomposed. The modified LDHs had more thermal stability than the pristine LDHs. The residual yields of the modified LDHs also were higher than the pristine LDHs.

As the synthesised LDHs acted as the fillers for the polymers, there was necessary to reduce and control the particle sizes of the LDHs. The use of attrition milling could reduce the particle size distribution. Both the rotating speed and milling time influenced the particle size distribution. The higher rotating speed and/or the longer milling time caused the agglomeration of particles. Thus, the optimum conditions for the milling were at 250 rpm for 2 h with the 100 µm of particulate LDHs as the initial substance.

8.1.2 Preparation and Characterisation of DGEBA/LDHs Nanocomposites

The performance of the pristine LDHs (LDH-CO₃ and LDH-NO₃) and the modified LDHs (LDH-BEHP, LDH-Phy, LDH-GP and LDH-DPP) was estimated by preparing the nanocomposites based on the pure epoxy of DGEBA cured with the DDM or DDM. The 1 wt%, 5 wt% and 10 wt% of LDHs were incorporated into the epoxy matrix.

The two methods used for the preparation of nanocomposites were the only stirring and the use of solvent, sonication, and mechanical stirring. From the investigation of the cut edge of the nanocomposites, they had the consistency of colour. The results implied that the LDHs were well distributed in the epoxy matrix. However, the flexural properties of nanocomposites prepared from the use of solvent, sonication, and mechanical stirring were slightly higher than those prepared from the only stirring method. Hence, the suitable procedure for the blend between the DGEBA, LDHs and curing agent was the use of solvent, sonication, and mechanical stirring. All the pure resins and their nanocomposites were investigated the flexural properties, dynamic mechanical properties, thermal stability and flammability by the three-point bending tester, dynamic mechanical analyser, thermogravimetric analyser and UL-94 burning testing, respectively.

For the DDM curing system, the loading of LDHs resulted in the slight reduction of flexural strength and flexural modulus of nanocomposites by comparison with the pure epoxy resin. The reduction of mechanical properties might occur the miscibility of matrix and fillers or the agglomeration of fillers in the matrix, accounting for the flaws in the nanocomposites. The mechanical properties of the epoxy nanocomposites with the additions of organophosphate ester modified LDHs were higher than that with the addition of pristine LDHs due to the increase of interaction between the epoxy resins and the modified LDHs.

Moreover, the storage modulus and loss modulus of the epoxy nanocomposites with incorporating the pristine LDHs or the modified LDHs were higher than that of the pure DGEBA/DDM. Since the components of LDHs lamellae were inorganic compounds, they increased the stiffness of the polymer matrix and the friction of polymer chain movement. These circumstances affected the increases of the storage modulus and loss modulus for the epoxy nanocomposites. Besides, the storage

modulus and loss modulus of the nanocomposites enhanced with the high loading contents. Nevertheless, the LDHs did not influence the temperatures of beta transition (T_{β}) and glass transition (T_g). The T_{β} and T_g are related to the movements of the side groups on the backbone polymer chains and the polymeric backbone chains, respectively. The results stated that the mobility of both was not restricted with the loading of LDHs.

With the thermal stability test under N_2 atmospheres, the TGA thermograms of the pure DGEBA/DDM presented the single stage of mass change in between 300°C and 500°C. It occurred the cleavage of polymer chains and crosslinked networks, releasing the gaseous compounds containing the phenol, amine, ester, ether, hydrocarbon, water, carbon dioxide and carbon monoxide. As a result, there was the formation of char residues. The addition of 10 wt% LDHs-Phy or LDH-GP led to the increase of thermal stability of the nanocomposites. The residual assay increased with the high loading content of LDHs.

For the thermal stability test under air, both the pure epoxy and its nanocomposites presented two stages of mass loss. The first decomposition stage reflected the degradation of the polymer, and the second decomposition stage showed the thermal-oxidative decomposition of residues produced from the first decomposition stage. The decomposition temperatures of the nanocomposites reduced with the incorporation of LDHs. The epoxy nanocomposite containing the LDH-Phy provided the highest residual contents at 800°C.

Furthermore, the pure epoxy of DGEBA/DDM and its nanocomposites with the loading of LDHs had been tested the burning, which was the key of research. As the thermal decompositions of the modified LDHs provided the volatilisation of non-flammable gases and the formation of char, the epoxy nanocomposites presented the decrease of ignition times and the increase of combustion resistance with the 5 and 10 wt% loadings of the modified LDHs.

8.1.3 Preparation and Characterisation of DGEBA/DDS-LDHs nanocomposites

In case of the DDS curing system, the LDHs could well distribute in the epoxy matrix, observed from the colour consistency of the cut edge. The incorporation of LDHs did

not significantly affect the flexural properties; however, it affected the dynamic mechanical properties. For the same reasons mentioned in the DDM curing system, the stiffness of the epoxy nanocomposites and the friction between the epoxy and fillers increased with the loading of LDHs. As a result, there were the increases in the storage modulus and loss modulus. Meanwhile, the LDHs did not influence the change of T_{β} and T_g , excluding the loading of LDH-BEHP. It might correspond to the interaction between epoxy matrix and fillers.

For the study of thermal behaviours under N_2 atmosphere, the pure DGEBA/DDS decomposed to the gases of SO_2 , CO and CH_4 and the char solids of aromatic-O and aromatic-N compounds at between $350^{\circ}C$ and $500^{\circ}C$. The thermal decomposition characteristics of the nanocomposites were similar to the pure epoxy resin; however, the initial decomposition of the nanocomposites took place at the lower temperature. Additionally, the composites containing the organophosphate ester modified LDHs appeared the mass loss at the temperature over $500^{\circ}C$, occurring the decomposition of phosphorus compounds.

Under the air atmosphere, all the pure resin and its nanocomposites with the LDHs displayed two stages of mass loss: the thermal decomposition of resin and the thermal-oxidative decomposition of solid compounds produced in the first stage. The thermal behaviours of the epoxy nanocomposites under air resembled under N_2 atmosphere; that was, the LDHs acted as the accelerators for the degradation of the resin. Besides, the LDHs increased the content of residues.

The flammability of epoxy nanocomposites reduced with the incorporation of 5 wt% LDHs since there were the increase of ignition number and the decrease of burning time after applying the first flame by comparison with the pure DGEBA/DDS. Besides, the combustion of nanocomposites was delayed by incorporating the organophosphate ester modified LDHs, causing the increase of total burning time. However, the addition of 5 wt% modified LDHs could not stop the burning of epoxy nanocomposites by using the DDS curing agent.

Moreover, the flame retardancy of epoxy nanocomposites in the DDS curing system enhanced with loading the 10 wt% LDHs particular to the organophosphate ester

modified LDHs. The burning time after the first ignition with the incorporation of 10 wt% LDHs was shorter than the addition of 5 wt% LDHs. All the epoxy nanocomposites containing the 10 wt% modified LDHs were self-extinguish. The 10 wt% LDH-GP was the highest efficiency of flame retardancy for the DDS cured DGEBA.

To conclude, this research stated that the LDHs modified with the organophosphate ester anions, namely the BEHP, Phy, GP and DPP, enhanced the flame retardancy of the DGEBA cured with the DDM or DDS. The modified LDHs accelerated the thermal degradation of the epoxy nanocomposites, resulting in the volatilisation of water and gases and the formation of char at the low temperature. These products could restrict the dispersion of flame, heat and combustible gases. Nevertheless, the incorporation of modified LDHs did not result in the changes of mechanical properties and phase transition temperatures. Hence, the organophosphate ester modified LDHs can be employed as the flame retardants for the epoxy resins.

8.1.4 Overall Summary of Discussed Results

The modifications of LDHs with the four different types of organophosphate compounds (BEHP, Phy, GP and DPP) prepared by the co-precipitation method were successful in this study. The conditions being proper for the synthesis of modified were the aging at pH 9 for 24 h under the N₂ atmosphere and the decarbonation. The molecules of BEHP, GP and DPP could be intercalated between the metal hydroxide layers whereas the modification with the Phy could exfoliate the layers. In addition to the presence of organophosphate anions in the interlayer regions, there was the intercalation of water molecules adsorbed on the surface of LDHs and intercalated between the layers in the structure of LDHs.

For the thermal decomposition of modified LDHs, the below 250°C presented the decomposition of water molecules adsorbed on the LDH surface and intercalated in the interlayers and the temperature range of 250-500°C provided the dehydrogenation of layered metal hydroxides and the degradation of organophosphate molecules in the

structure of LDHs. The decomposition temperatures of the modified LDHs were lower than the pristine LDHs.

For the preparation of EP/LDHs nanocomposites cured with the DDM or DDS, the use of acetone solvent, sonication and mechanical stirring for blending the epoxy resin and the LDHs fillers provided the flexural properties more than the only use of mechanical stirring. Both the pristine and modified LDHs well dispersed in the EP matrix as observing the cut edge of the samples. With the incorporation of 1 wt%, 5 wt% and 10 wt% LDHs in the EP matrix, there were not the significant difference of flexural properties and the dynamic mechanical properties. Besides, the incorporation of LDHs reduced the initial decomposition temperature of the nanocomposites comparing to the pure EP. However, the thermal stability of the nanocomposites at the high temperature was more than the pure EP. The higher content of LDHs also increased the thermal stability of the nanocomposites and the char residues.

Compared the flame retardancy performance of pristine LDHs with the modified LDHs, the modified LDHs were higher performance than the pristine LDHs. In the DDM curing system, the incorporation of 5 wt% modified LDHs was enough content to retard the combustion of epoxy resin. Meanwhile, the DDS curing system need to apply the 10 wt% modified LDHs for inhibiting the flame retardancy for epoxy resin. Hence, the organophosphate-modified LDHs could be used as the flame retardants for the epoxy resin.

8.2 Future works

From the experimental results, the organophosphate ester modified LDHs did not induce the significant increase of mechanical properties and the glass transition temperature of epoxy nanocomposites. These characteristics might correlate to the interaction between resin and LDHs. Future studies should attempt to improve the compatibility of polymer and fillers and the dispersion of LDHs in the matrix by functionalising the LDHs surface with interface modifiers such as stearic acid and organosilane coupling agents. The interface modifiers consist of the carboxylate or inorganic fraction and the hydrocarbon fraction. The former can connect to the

inorganic fillers, while the latter can bond to the epoxy resin. The modification of LDH surface can also adjust polarity close to the polarity of epoxy resin. Furthermore, the modified LDHs may be added in other resins or curing agents.

Many researchers have investigated the crystal morphology of LDHs by using a scanning electron microscope (SEM). It would be interesting to comprehend the crystal shapes and particle size of LDHs. Further study is needed to determine the dispersion of LDHs in the polymer matrix using a transmission electron microscope (TEM). As the crosslinking densities of the cured resins in this study were examined from the calculation of DMA data, this method might not be appropriate for determining the crosslinking densities for the epoxy resins. Future work should look for the proper techniques of crosslinking density measurement such as use of infrared spectrometry or swelling method.

This study proposed the thermal decomposition mechanisms of organophosphate ester reactants using the mass loss data and the molecular weight from the TGA. In addition, there was speculation of the products produced from the thermal decomposition of LDHs modified organophosphate ester anions and epoxy resins. The obtained results were just the estimation based on the literature and the conversion of mass loss to molecular weight, which might account for the error in the speculation. To achieve the accuracy of results, the study of thermal stability should be investigated by using the TGA connecting to FTIR and mass spectrometry so as to detect the structure of gas phases released during the increase of heat. It is useful to the study of combustion behaviours for polymer nanocomposites containing the LDHs.

As mentioned in Chapter 2 and Chapter 6, the cone calorimetry is the excellent technique used intensively to study the combustion behaviours for polymers since it can analyse ignition and total combustion times, heat release, volatile components and amount of smoke. In the research plan, the cone calorimetry test would be carried out at The University of Bolton. Due to the COVID-19 pandemic, this plan was disrupted. The UL-94 test was considered to estimate the flammability of the polymer. Therefore, it is recommended that the cone calorimetry test is investigated in the future work.

Appendix I

Flexural Behaviours of DGEBA/DDM and Its Nanocomposites Containing LDHs

Table I-1 The flexural strength of the pure DGEBA and its nanocomposites containing the LDH-CO₃ in the DDM curing system prepared with the mechanical stirring.

Sample	Flexural Strength (MPa)			
	No filler	1% LDH-CO ₃	5% LDH-CO ₃	10% LDH-CO ₃
1	183.88	133.40	106.61	84.14
2	160.06	140.02	100.39	142.57
3	171.08	128.38	126.92	100.29
4	176.55	143.08	132.74	89.74
5	173.02	128.65	126.12	65.65
Average	172.92	134.71	118.56	96.48
SD	8.69	6.65	14.15	28.67

Table I-2 The flexural modulus of the pure DGEBA and its nanocomposites containing the LDH-CO₃ in the DDM curing system prepared with the mechanical stirring.

Sample	Flexural Modulus (MPa)			
	No filler	1% LDH-CO ₃	5% LDH-CO ₃	10% LDH-CO ₃
1		3182.54	3167.46	2481.60
2		3167.46	2676.26	2579.13
3		3173.92	2520.29	2657.00
4		2831.96	2521.81	2680.17
5		3087.04	2609.57	2657.99
Average		3088.58	2699.08	2611.18
SD		148.48	269.86	81.96

Table I-3 The flexural strength of the pure DGEBA and its nanocomposites containing the LDH-NO₃ in the DDM curing system prepared with the mechanical stirring.

Sample	Flexural Strength (MPa)			
	No filler	1% LDH-NO ₃	5% LDH-NO ₃	10% LDH-NO ₃
1	183.88	116.07	126.97	148.23
2	160.06	140.28	119.30	149.59
3	171.08	146.32	122.74	129.05
4	176.55	146.17	143.30	120.42
5	173.02	139.52	117.64	136.85
Average	172.92	137.67	125.99	136.83
SD	8.69	12.49	10.32	12.48

Table I-4 The flexural modulus of the pure DGEBA and its nanocomposites containing the LDH-NO₃ in the DDM curing system prepared with the mechanical stirring.

Sample	Flexural Modulus (MPa)			
	No filler	1% LDH-NO ₃	5% LDH-NO ₃	10% LDH-NO ₃
1	3182.54	2531.53	2826.54	2909.32
2	3167.46	2591.80	2562.00	2826.44
3	3173.92	2561.96	2670.28	2802.71
4	2831.96	2610.97	2717.42	2841.13
5	3087.04	2556.24	2622.79	2843.18
Average	3088.58	2570.50	2679.81	2844.56
SD	148.48	31.17	100.21	39.65

Table I-5 The flexural strength of the pure DGEBA and its nanocomposites containing the LDH-BEHP in the DDM curing system prepared with the mechanical stirring.

Sample	Flexural Strength (MPa)			
	No filler	1% LDH-BEHP	5% LDH-BEHP	10% LDH-BEHP
1	183.88	138.60	110.00	110.23
2	160.06	130.73	123.80	122.33
3	171.08	120.57	125.13	94.98
4	176.55	120.41	106.64	111.79
5	173.02	121.16	145.44	117.36
Average	172.92	126.29	122.20	111.34
SD	8.69	8.14	15.35	10.32

Table I-6 The flexural modulus of the pure DGEBA and its nanocomposites containing the LDH-BEHP in the DDM curing system prepared with the mechanical stirring.

Sample	Flexural Modulus (MPa)			
	No filler	1% LDH-BEHP	5% LDH-BEHP	10% LDH-BEHP
1	3182.54	2614.53	2449.47	2356.28
2	3167.46	2536.18	2414.09	2398.34
3	3173.92	2606.22	2585.15	2354.26
4	2831.96	2558.55	2568.54	2130.87
5	3087.04	2621.91	2468.47	2232.94
Average	3088.58	2587.48	2497.14	2294.54
SD	148.48	37.87	75.55	110.38

Table I-7 The flexural strength of the pure DGEBA and its nanocomposites containing the LDH-Phy in the DDM curing system prepared with the mechanical stirring.

Sample	Flexural Strength (MPa)			
	No filler	1% LDH-Phy	5% LDH-Phy	10% LDH-Phy
1	183.88	2543.02	3209.93	3131.06
2	160.06	2603.21	2952.71	2924.35
3	171.08	2265.27	2958.57	3074.17
4	176.55	2507.83	2912.51	3237.09
5	173.02	2409.25	2926.49	2993.1
Average	172.92	2465.72	2992.04	3071.95
SD	8.69	132.31	123.25	121.22

Table I-8 The flexural modulus of the pure DGEBA and its nanocomposites containing the LDH-Phy in the DDM curing system prepared with the mechanical stirring.

Sample	Flexural Modulus (MPa)			
	No filler	1% LDH-Phy	5% LDH-Phy	10% LDH-Phy
1	3182.54	182.38	145.46	118.98
2	3167.46	174.65	154.55	147.53
3	3173.92	132.78	134.3	120.03
4	2831.96	171.41	149.16	127.12
5	3087.04	161.15	130.61	114.81
Average	3088.58	164.47	142.82	125.69
SD	148.48	19.29	10.08	12.99

Table I-9 The flexural strength of the pure DGEBA and its nanocomposites containing the LDH-GP in the DDM curing system prepared with the mechanical stirring.

Sample	Flexural Strength (MPa)			
	No filler	1% LDH-GP	5% LDH-GP	10% LDH-GP
1	183.88	155.51	170.08	137.03
2	160.06	149.00	165.47	131.99
3	171.08	161.36	168.43	164.11
4	176.55	154.79	166.25	167.05
5	173.02	154.63	142.67	161.75
Average	172.92	155.02	162.61	155.41
SD	8.69	3.92	10.09	16.53

Table I-10 The flexural modulus of the pure DGEBA and its nanocomposites containing the LDH-GP in the DDM curing system prepared with the mechanical stirring.

Sample	Flexural Modulus (MPa)			
	No filler	1% LDH-GP	5% LDH-GP	10% LDH-GP
1	3182.54	2669.01	2488.01	2824.31
2	3167.46	2651.48	2560.84	2880.37
3	3173.92	2602.83	2502.22	2774.00
4	2831.96	2626.10	2538.72	2735.24
5	3087.04	2525.73	2526.80	2875.64
Average	3088.58	2615.51	2522.88	2803.76
SD	148.48	49.99	25.90	66.40

Table I-11 The flexural strength of the pure DGEBA and its nanocomposites containing the LDH-DPP in the DDM curing system prepared with the mechanical stirring.

Sample	Flexural Strength (MPa)			
	No filler	1% LDH-DPP	5% LDH-DPP	10% LDH-DPP
1	183.88	137.15	141.20	124.03
2	160.06	130.61	111.30	136.07
3	171.08	142.01	117.01	112.01
4	176.55	137.27	122.88	115.26
5	173.02	132.56	109.84	102.45
Average	172.92	135.92	120.45	117.96
SD	8.69	4.47	12.69	12.73

Table I-12 The flexural modulus of the pure DGEBA and its nanocomposites containing the LDH-DPP in the DDM curing system prepared with the mechanical stirring.

Sample	Flexural Modulus (MPa)			
	No filler	1% LDH-DPP	5% LDH-DPP	10% LDH-DPP
1	3182.54	2518.63	2848.03	2733.80
2	3167.46	2612.27	2794.86	2756.95
3	3173.92	2594.10	2814.40	2718.16
4	2831.96	2584.21	2905.49	2748.31
5	3087.04	2636.38	2756.86	2703.54
Average	3088.58	2589.12	2823.93	2732.15
SD	148.48	44.12	56.27	21.75

Table I-13 The flexural strength of the pure DGEBA and its nanocomposites containing the LDH-CO₃ in the DDM curing system prepared with the solvent, sonication and mechanical stirring.

Sample	Flexural Strength (MPa)			
	No filler	1% LDH-CO ₃	5% LDH-CO ₃	10% LDH-CO ₃
1	183.88	165.71	112.73	77.99
2	160.06	140.01	143.39	120.56
3	171.08	153.41	129.63	119.33
4	176.55	145.93	132.64	107.10
5	173.02	134.64	128.87	94.22
Average	172.92	147.94	129.45	103.84
SD	8.69	12.14	11.00	17.96

Table I-14 The flexural modulus of the pure DGEBA and its nanocomposites containing the LDH-CO₃ in the DDM curing system prepared with the solvent, sonication and mechanical stirring.

Sample	Flexural Modulus (MPa)			
	No filler	1% LDH-CO ₃	5% LDH-CO ₃	10% LDH-CO ₃
1	3182.54	2542.95	2688.02	2687.90
2	3167.46	2525.64	2666.12	2785.35
3	3173.92	2514.36	2603.89	2891.79
4	2831.96	2558.41	2537.45	2605.78
5	3087.04	2594.46	2625.00	2737.82
Average	3088.58	2547.16	2624.10	2741.73
SD	148.48	31.31	58.67	107.03

Table I-15 The flexural strength of the pure DGEBA and its nanocomposites containing the LDH-NO₃ in the DDM curing system prepared with the solvent, sonication and mechanical stirring.

Sample	Flexural Strength (MPa)			
	No filler	1% LDH-NO ₃	5% LDH-NO ₃	10% LDH-CO ₃
1	183.88	127.16	154.50	146.19
2	160.06	160.42	138.75	145.45
3	171.08	164.82	135.00	143.87
4	176.55	155.98	136.35	122.52
5	173.02	125.29	134.91	116.12
Average	172.92	146.73	139.90	134.83
SD	8.69	19.00	8.31	14.36

Table I-16 The flexural modulus of the pure DGEBA and its nanocomposites containing the LDH-NO₃ in the DDM curing system prepared with the solvent, sonication and mechanical stirring.

Sample	Flexural Modulus (MPa)			
	No filler	1% LDH-NO ₃	5% LDH-NO ₃	10% LDH-NO ₃
1	3182.54	2668.90	3166.05	3180.24
2	3167.46	2748.55	2972.21	3056.48
3	3173.92	2643.07	3191.46	2976.37
4	2831.96	2745.99	2971.01	2943.47
5	3087.04	2732.71	2862.56	3005.97
Average	3088.58	2707.85	3032.66	3032.50
SD	148.48	48.59	140.89	92.44

Table I-17 The flexural strength of the pure DGEBA and its nanocomposites containing the LDH-BEHP in the DDM curing system prepared with the solvent, sonication and mechanical stirring.

Sample	Flexural Strength (MPa)			
	No filler	1% LDH-BEHP	5% LDH-BEHP	10% LDH-BEHP
1	183.88	144.12	123.39	105.03
2	160.06	124.41	126.63	119.29
3	171.08	122.26	136.78	98.67
4	176.55	134.37	117.41	110.09
5	173.02	103.95	95.98	111.06
Average	172.92	125.82	120.04	108.83
SD	8.69	15.01	15.17	7.64

Table I-18 The flexural modulus of the pure DGEBA and its nanocomposites containing the LDH-BEHP in the DDM curing system prepared with the solvent, sonication and mechanical stirring.

Sample	Flexural Modulus (MPa)			
	No filler	1% LDH-BEHP	5% LDH-BEHP	10% LDH-BEHP
1	3182.54	2532.47	2491.41	2559.57
2	3167.46	2438.49	2599.84	2343.43
3	3173.92	2669.68	2472.60	2728.68
4	2831.96	2683.84	2486.13	2602.76
5	3087.04	2518.81	2343.93	2682.42
Average	3088.58	2568.66	2478.78	2583.37
SD	148.48	105.13	90.96	149.53

Table I-19 The flexural strength of the pure DGEBA and its nanocomposites containing the LDH-Phy in the DDM curing system prepared with the solvent, sonication and mechanical stirring.

Sample	Flexural Strength (MPa)			
	No filler	1% LDH-Phy	5% LDH-Phy	10% LDH-Phy
1	183.88	170.08	163.35	138.37
2	160.06	168.73	155.26	145.43
3	171.08	175.72	148.37	163.33
4	176.55	181.16	168.36	131.96
5	173.02	157.91	165.16	143.22
Average	172.92	170.72	160.10	144.46
SD	8.69	8.70	8.15	11.75

Table I-20 The flexural modulus of the pure DGEBA and its nanocomposites containing the LDH-Phy in the DDM curing system prepared with the solvent, sonication and mechanical stirring.

Sample	Flexural Modulus (MPa)			
	No filler	1% LDH-Phy	5% LDH-Phy	10% LDH-Phy
1	3182.54	3052.21	2773.46	2983.07
2	3167.46	2644.36	2690.68	3152.26
3	3173.92	2795.87	2881.42	2990.31
4	2831.96	2731.99	3153.38	3178.14
5	3087.04	2647.13	3043.22	3045.83
Average	3088.58	2774.31	2908.43	3069.92
SD	148.48	167.74	190.09	90.76

Table I-21 The flexural strength of the pure DGEBA and its nanocomposites containing the LDH-GP in the DDM curing system prepared with the solvent, sonication and mechanical stirring.

Sample	Flexural Strength (MPa)			
	No filler	1% LDH-GP	5% LDH-GP	10% LDH-GP
1	183.88	175.49	167.52	175.10
2	160.06	172.72	152.23	172.33
3	171.08	178.89	169.41	172.70
4	176.55	169.94	175.74	170.31
5	173.02	165.37	177.04	169.90
Average	172.92	172.48	168.39	172.07
SD	8.69	5.18	9.90	2.09

Table I-22 The flexural modulus of the pure DGEBA and its nanocomposites containing the LDH-GP in the DDM curing system prepared with the solvent, sonication and mechanical stirring.

Sample	Flexural Modulus (MPa)			
	No filler	1% LDH-GP	5% LDH-GP	10% LDH-GP
1	3182.54	2802.72	2676.98	2813.52
2	3167.46	2756.52	2742.90	2804.81
3	3173.92	2821.42	2861.69	2723.90
4	2831.96	2672.43	2778.30	2764.28
5	3087.04	2830.83	2755.95	2847.28
Average	3088.58	2776.78	2763.16	2790.76
SD	148.48	64.98	66.76	47.65

Table I-23 The flexural strength of the pure DGEBA and its nanocomposites containing the LDH-DPP in the DDM curing system prepared with the solvent, sonication and mechanical stirring.

Sample	Flexural Strength (MPa)			
	No filler	1% LDH-DPP	5% LDH-DPP	10% LDH- DPP
1	183.88	178.85	168.63	117.46
2	160.06	163.72	153.41	151.42
3	171.08	177.76	164.75	149.62
4	176.55	174.62	139.63	146.88
5	173.02	175.75	159.15	135.97
Average	172.92	174.14	157.11	140.27
SD	8.69	6.06	11.34	14.09

Table I-24 The flexural strength and flexural modulus of the pure DGEBA and its nanocomposites containing the LDH-DPP in the DDM curing system prepared with the solvent, sonication and mechanical stirring.

Sample	Flexural Modulus (MPa)			
	No filler	1% LDH-DPP	5% LDH-DPP	10% LDH-DPP
1	3182.54	2670.27	2920.24	3802.89
2	3167.46	2866.27	2704.29	3796.61
3	3173.92	2718.86	2818.13	3725.92
4	2831.96	2660.93	2798.81	3857.53
5	3087.04	2788.16	2857.57	3788.80
Average	3088.58	2740.90	2819.81	3794.35
SD	148.48	86.34	79.53	46.86

Appendix II

Burning Test of DGEBA/DDM and Its Nanocomposites Containing LDHs

Table II-1 The combustion time and characteristics of the pure DGEBA cured with the DDM.

Sample	Combustion time after the first ignition (s)	Combustion time after the second ignition (s)	Total time of combustion (s)	Flame to clamp	Dripping
1	97	153	250	Yes	Yes
2	88	200	288	Yes	Yes
3	116	180	296	Yes	Yes
4	72	176	248	Yes	Yes
5	70	194	264	Yes	Yes
Average	89	181		Yes	Yes
SD	19	18		Yes	Yes

Table II-2 The combustion time and characteristics of the DGEBA/5% LDH-CO₃ cured with the DDM.

Sample	Combustion time after the first ignition (s)	Combustion time after the second ignition (s)	Total time of combustion (s)	Flame to clamp	Dripping
1	20	149	169	Yes	Yes
2	25	180	205	Yes	Yes
3	16	153	169	Yes	Yes
4	82	176	258	Yes	Yes
5	47	166	213	Yes	Yes
Average	38	165		Yes	Yes
SD	27	14		Yes	Yes

Table II-3 The combustion time and characteristics of the DGEBA/10% LDH-CO₃ cured with the DDM.

Sample	Combustion time after the first ignition (s)	Combustion time after the second ignition (s)	Total time of combustion (s)	Flame to clamp	Dripping
1	22	10	32	No	No
2	25	8	33	No	No
3	30	10	40	No	No
4	28	26	54	No	No
5	27	19	46	No	No
Average	26	15			
SD	3	8			

Table II-4 The combustion time and characteristics of the DGEBA/5% LDH-NO₃ cured with the DDM

Sample	Combustion time after the first ignition (s)	Combustion time after the second ignition (s)	Total time of combustion (s)	Flame to clamp	Dripping
1	66	70	136	Yes	Yes
2	22	119	141	Yes	Yes
3	79	156	235	Yes	Yes
4	35	168	203	Yes	Yes
5	33	71	104	Yes	Yes
Average	47	117			
SD	24	46			

Table II-5 The combustion time and characteristics of the DGEBA/10% LDH-NO₃ cured with the DDM.

Sample	Combustion time after the first ignition (s)	Combustion time after the second ignition (s)	Total time of combustion (s)	Flame to clamp	Dripping
1	14	48	62	No	No
2	5	34	39	No	No
3	7	39	46	No	No
4	12	46	58	No	No
5	9	34	43	No	No
Average	9	40			
SD	4	7			

Table II-6 The combustion time and characteristics of the DGEBA/5% LDH-BEHP cured with the DDM.

Sample	Combustion time after the first ignition (s)	Combustion time after the second ignition (s)	Total time of combustion (s)	Flame to clamp	Dripping
1	21	55	76	No	No
2	28	37	65	No	No
3	19	29	48	No	No
4	31	41	72	No	No
5	29	50	79	No	No
Average	26	42			
SD	5	10			

Table II-7 The combustion time and characteristics of the DGEBA/10% LDH-BEHP cured with the DDM.

Sample	Combustion time after the first ignition (s)	Combustion time after the second ignition (s)	Total time of combustion (s)	Flame to clamp	Dripping
1	8	29	37	No	No
2	10	27	37	No	No
3	16	13	29	No	No
4	18	16	34	No	No
5	9	13	22	No	No
Average	12	20			
SD	4	8			

Table II-8 The combustion time and characteristics of the DGEBA/5% LDH-Phy cured with the DDM

Sample	Combustion time after the first ignition (s)	Combustion time after the second ignition (s)	Total time of combustion (s)	Flame to clamp	Dripping
1	17	70	87	No	No
2	12	78	90	No	No
3	16	46	62	No	No
4	15	52	67	No	No
5	44	75	119	No	No
Average	21	64			
SD	13	14			

Table II-9 The combustion time and characteristics of the DGEBA/10% LDH-Phy cured with the DDM.

Sample	Combustion time after the first ignition (s)	Combustion time after the second ignition (s)	Total time of combustion (s)	Flame to clamp	Dripping
1	14	38	52	No	No
2	28	8	36	No	No
3	15	35	50	No	No
4	9	10	19	No	No
5	7	12	19	No	No
Average	15	21			
SD	8	15			

Table II-10 The combustion time and characteristics of the DGEBA/5% LDH-GP cured with the DDM.

Sample	Combustion time after the first ignition (s)	Combustion time after the second ignition (s)	Total time of combustion (s)	Flame to clamp	Dripping
1	20	58	78	No	No
2	20	66	86	No	No
3	38	66	104	No	No
4	26	71	97	No	No
5	25	69	94	No	No
Average	26	66			
SD	7	5			

Table II-11 The combustion time and characteristics of the DGEBA/10% LDH-GP cured with the DDM.

Sample	Combustion time after the first ignition (s)	Combustion time after the second ignition (s)	Total time of combustion (s)	Flame to clamp	Dripping
1	23	19	42	No	No
2	23	17	40	No	No
3	20	24	44	No	No
4	22	23	45	No	No
5	18	22	40	No	No
Average	21	21			
SD	2	3			

Table II-12 The combustion time and characteristics of the DGEBA/5% LDH-DPP cured with the DDM.

Sample	Combustion time after the first ignition (s)	Combustion time after the second ignition (s)	Total time of combustion (s)	Flame to clamp	Dripping
1	22	32	54	No	No
2	24	60	84	No	No
3	43	43	86	No	No
4	23	45	68	No	No
5	22	43	65	No	No
Average	27	45			
SD	9	10			

Table II-13 The combustion time and characteristics of the DGEBA/10% LDH-DPP cured with the DDM

Sample	Combustion time after the first ignition (s)	Combustion time after the second ignition (s)	Total time of combustion (s)	Flame to clamp	Dripping
1	12	16	28	No	No
2	15	22	37	No	No
3	8	18	26	No	No
4	19	31	50	No	No
5	7	28	35	No	No
Average	12	23			
SD	5	6			

Appendix III
**Flexural Behaviours of
DGEBA/DDS and
Its Nanocomposites
Containing LDHs**

Table III-1 The flexural strength of the pure DGEBA and its nanocomposites containing the LDH-CO₃ in the DDM curing system prepared with the solvent, sonication and mechanical stirring.

Sample	Flexural Strength (MPa)			
	No filler	1% LDH-CO ₃	5% LDH-CO ₃	10% LDH-CO ₃
1	183.88	168.81	167.65	165.42
2	160.06	180.09	172.78	185.77
3	171.08	174.63	176.47	161.71
4	176.55	177.39	181.62	163.43
5	173.02	182.43	156.88	185.90
Average	172.92	176.67	171.08	172.44
SD	8.69	5.28	9.44	12.29

Table III-2 The flexural modulus of the pure DGEBA and its nanocomposites containing the LDH-CO₃ in the DDM curing system prepared with the solvent, sonication and mechanical stirring.

Sample	Flexural Modulus (MPa)			
	No filler	1% LDH-CO ₃	5% LDH-CO ₃	10% LDH-CO ₃
1	3182.54	2794.65	2819.98	2854.37
2	3167.46	2747.81	2583.50	2849.02
3	3173.92	2742.88	2935.91	2741.86
4	2831.96	2862.91	2958.94	2669.01
5	3087.04	2716.26	2794.65	2871.74
Average	3088.58	2772.90	2818.59	2797.20
SD	148.48	57.69	149.42	88.04

Table III-3 The flexural strength of the pure DGEBA and its nanocomposites containing the LDH-NO₃ in the DDM curing system prepared with the solvent, sonication and mechanical stirring.

Sample	Flexural Strength (MPa)			
	No filler	1% LDH-NO ₃	5% LDH-NO ₃	10% LDH-NO ₃
1	183.88	196.84	200.738	176.41
2	160.06	193.86	204.7866	152.36
3	171.08	191.26	196.1311	177.23
4	176.55	182.56	179.2991	176.86
5	173.02	190.97	188.0886	164.74
Average	172.92	191.10	193.81	169.52
SD	8.69	5.33	10.21	10.93

Table III-4 The flexural modulus of the pure DGEBA and its nanocomposites containing the LDH-NO₃ in the DDM curing system prepared with the solvent, sonication and mechanical stirring.

Sample	Flexural Modulus (MPa)			
	No filler	1% LDH-NO ₃	5% LDH-NO ₃	10% LDH-NO ₃
1	3182.54	2983.15	3162.3075	3131.62
2	3167.46	3140.96	3149.98311	3213.83
3	3173.92	3090.08	3143.17833	3302.95
4	2831.96	3049.56	3119.30335	3204.62
5	3087.04	3038.85	3027.85691	3166.48
Average	3088.58	3060.52	3120.53	3203.90
SD	148.48	58.99	54.12	64.29

Table III-5 The flexural strength of the pure DGEBA and its nanocomposites containing the LDH-BEHP in the DDS curing system prepared with the solvent, sonication and mechanical stirring.

Sample	Flexural Strength (MPa)			
	No filler	1% LDH-BEHP	5% LDH-BEHP	10% LDH-BEHP
1	183.88	171.03	151.5163	151.0413
2	160.06	178.0237	142.5	167.43
3	171.08	178.345	173.3	152.87
4	176.55	181.4433	168	181.23
5	173.02	159.7245	192.1	173.94
Average	172.92	173.71	165.48	165.30
SD	8.69	8.70	19.36	13.14

Table III-6 The flexural modulus of the pure DGEBA and its nanocomposites containing the LDH-BEHP in the DDS curing system prepared with the solvent, sonication and mechanical stirring.

Sample	Flexural Modulus (MPa)			
	No filler	1% LDH-BEHP	5% LDH-BEHP	10% LDH-BEHP
1	3182.54	3100.62	3002.13	3577.02
2	3167.46	3098.20	3299.06	3203.83
3	3173.92	3074.80	3149.21	3403.76
4	2831.96	3030.21	3283.58	3149.21
5	3087.04	3150.56	3300.82	3328.90
Average	3088.58	3090.88	3206.96	3332.54
SD	148.48	43.73	130.82	169.58

Table III-7 The flexural strength of the pure DGEBA and its nanocomposites containing the LDH-Phy in the DDM curing system prepared with the solvent, sonication and mechanical stirring.

Sample	Flexural Strength (MPa)			
	No filler	1% LDH-Phy	5% LDH-Phy	10% LDH-Phy
1	183.88	180.743	159.0875	207.38
2	160.06	195.4227	202.6106	194.15
3	171.08	191.5682	211.3999	200.09
4	176.55	199.5624	191.7665	149.70
5	173.02	196.047	181.7963	174.44
Average	172.92	192.67	189.33	185.15
SD	8.69	7.244892	20.25314	23.2919

Table III-8 The flexural modulus of the pure DGEBA and its nanocomposites containing the LDH-Phy in the DDM curing system prepared with the solvent, sonication and mechanical stirring.

Sample	Flexural Modulus (MPa)			
	No filler	1% LDH-Phy	5% LDH-Phy	10% LDH-Phy
1	3182.54	3133.02	3378.03	3368.87
2	3167.46	145.6387	224.7247	246.8514
3	3173.92	3133.02	3378.03	3368.87
4	2831.96	145.6387	224.7247	246.8514
5	3087.04	3133.02	3378.03	3368.87
Average	3088.58	3133.02	3378.03	3368.87
SD	148.48	145.6387	224.7247	246.8514

Table III-9 The flexural strength and flexural modulus of the pure DGEBA and its nanocomposites containing the LDH-GP in the DDM curing system prepared with the solvent, sonication and mechanical stirring.

Sample	Flexural Strength (MPa)			
	No filler	1% LDH-GP	5% LDH-GP	10% LDH-GP
1	183.88	179.91	173.98	204.04
2	160.06	196.08	163.69	199.65
3	171.08	201.92	178.86	198.08
4	176.55	188.96	160.19	183.89
5	173.02	190.92	184.42	196.17
Average	172.92	191.56	172.23	196.37
SD	9.49	10.17	7.55	9.49

Table III-10 The flexural strength and flexural modulus of the pure DGEBA and its nanocomposites containing the LDH-GP in the DDM curing system prepared with the solvent, sonication and mechanical stirring.

Sample	Flexural Modulus (MPa)			
	No filler	1% LDH-GP	5% LDH-GP	10% LDH-GP
1	3182.54	2924.61	2983.15	3291.53
2	3167.46	3024.24	3075.36	3298.81
3	3173.92	2942.29	3003.88	3131.18
4	2831.96	2879.03	3136.83	3365.21
5	3087.04	2940.89	2947.64	3124.59
Average	3088.58	2942.21	3029.37	3242.26
SD	148.48	60.64	76.04	108.31

Table III-11 The flexural strength of the pure DGEBA and its nanocomposites containing the LDH-DPP in the DDM curing system prepared with the solvent, sonication and mechanical stirring.

Sample	Flexural Strength (MPa)			
	No filler	1% LDH-DPP	5% LDH-DPP	10% LDH-DPP
1	183.88	196.33	204.58	182.19
2	160.06	185.97	160.51	200.49
3	171.08	202.05	150.79	148.69
4	176.55	169.19	190.24	145.78
5	173.02	183.96	170.38	161.66
Average	172.92	187.50	175.30	167.76
SD	8.69	12.65	23.46	23.26

Table III-12 The flexural modulus of the pure DGEBA and its nanocomposites containing the LDH-DPP in the DDM curing system prepared with the solvent, sonication and mechanical stirring.

Sample	Flexural Modulus (MPa)			
	No filler	1% LDH-DPP	5% LDH-DPP	10% LDH-DPP
1	3182.54	3184.67	3519.69	3488.79
2	3167.46	3379.20	3955.41	3625.03
3	3173.92	3200.66	3587.98	3979.46
4	2831.96	3482.48	3405.96	3953.51
5	3087.04	3229.28	3619.23	4148.43
Average	3088.58	3295.26	3617.65	3839.04
SD	148.48	130.03	205.78	272.50

Appendix IV

Burning Test of DGEBA/DDS and Its Nanocomposites Containing LDHs

Table IV-1 The combustion time and characteristics of the pure DGEBA cured with the DDS.

Sample	Combustion time after the first ignition (s)	Combustion time after the second ignition (s)	Total time of combustion (s)	Flame to clamp	Dripping
1	271	-		Yes	Yes
2	230	-		Yes	Yes
3	256	-		Yes	Yes
4	242	-		Yes	Yes
5	233	-		Yes	Yes
Average	246	-			
SD	17	-			

Table IV-2 The combustion time and characteristics of the DGEBA/5% LDH-CO₃ cured with the DDS.

Sample	Combustion time after the first ignition (s)	Combustion time after the second ignition (s)	Total time of combustion (s)	Flame to clamp	Dripping
1	121	129	250	Yes	Yes
2	60	116	176	Yes	Yes
3	86	142	228	Yes	Yes
4	114	225	339	Yes	Yes
5	107	169	276	Yes	Yes
Average	98	156			
SD	25	43			

Table IV-3 The combustion time and characteristics of the DGEBA/10% LDH-CO₃ cured with the DDS.

Sample	Combustion time after the first ignition (s)	Combustion time after the second ignition (s)	Total time of combustion (s)	Flame to clamp	Dripping
1	39	214	253	Yes	Yes
2	53	108	161	Yes	Yes
3	69	207	276	Yes	Yes
4	81	60	141	Yes	Yes
5	43	217	260	Yes	Yes
Average	57	161			
SD	18	73			

Table IV-4 The combustion time and characteristics of the DGEBA/5% LDH-NO₃ cured with the DDS.

Sample	Combustion time after the first ignition (s)	Combustion time after the second ignition (s)	Total time of combustion (s)	Flame to clamp	Dripping
1	36	147	183	Yes	Yes
2	94	136	230	Yes	Yes
3	78	132	210	Yes	Yes
4	73	143	216	Yes	Yes
5	49	137	186	Yes	Yes
Average	66	139			
SD	23	6			

Table IV-5 The combustion time and characteristics of the DGEBA/10% LDH-NO₃ cured with the DDS.

Sample	Combustion time after the first ignition (s)	Combustion time after the second ignition (s)	Total time of combustion (s)	Flame to clamp	Dripping
1	30	201	231	Yes	Yes
2	60	24	84	Yes	Yes
3	80	193	273	Yes	Yes
4	45	202	247	Yes	Yes
5	33	235	268	Yes	Yes
Average	50	171			
SD	21	84			

Table IV-6 The combustion time and characteristics of the DGEBA/5% LDH-BEHP cured with the DDS

Sample	Combustion time after the first ignition (s)	Combustion time after the second ignition (s)	Total time of combustion (s)	Flame to clamp	Dripping
1	89	148	237	Yes	Yes
2	72	112	184	Yes	Yes
3	68	121	189	Yes	Yes
4	81	132	213	Yes	Yes
5	37	135	172	Yes	Yes
Average	69	130			
SD	20	14			

Table IV-7 The combustion time and characteristics of the DGEBA/10% LDH-BEHP cured with the DDS.

Sample	Combustion time after the first ignition (s)	Combustion time after the second ignition (s)	Total time of combustion (s)	Flame to clamp	Dripping
1	17	213	230	No	No
2	15	224	239	No	No
3	8	217	225	No	No
4	59	221	280	No	No
5	23	218	241	No	No
Average	24	219			
SD	20	4			

Table IV-8 The combustion time and characteristics of the DGEBA/5% LDH-Phy cured with the DDS.

Sample	Combustion time after the first ignition (s)	Combustion time after the second ignition (s)	Total time of combustion (s)	Flame to clamp	Dripping
1	103	151	254	Yes	Yes
2	116	200	316	Yes	Yes
3	117	215	332	Yes	Yes
4	57	184	241	Yes	Yes
5	35	268	303	Yes	Yes
Average	86	204			
SD	37	43			

Table IV-9 The combustion time and characteristics of the DGEBA/10% LDH-Phy cured with the DDS

Sample	Combustion time after the first ignition (s)	Combustion time after the second ignition (s)	Total time of combustion (s)	Flame to clamp	Dripping
1	17	211	228	No	No
2	12	198	210	No	No
3	14	192	206	No	No
4	17	207	224	No	No
5	10	187	197	No	No
Average	14	199			
SD	3	10			

Table IV-10 The combustion time and characteristics of the DGEBA/5% LDH-GP cured with the DDS

Sample	Combustion time after the first ignition (s)	Combustion time after the second ignition (s)	Total time of combustion (s)	Flame to clamp	Dripping
1	52	220	272	Yes	Yes
2	105	215	320	Yes	Yes
3	59	216	275	Yes	Yes
4	117	217	334	Yes	Yes
5	161	212	373	Yes	Yes
Average	99	216			
SD	45	3			

Table IV-11 The combustion time and characteristics of the DGEBA/10% LDH-GP cured with the DDS

Sample	Combustion time after the first ignition (s)	Combustion time after the second ignition (s)	Total time of combustion (s)	Flame to clamp	Dripping
1	30	28	58	No	No
2	18	29	47	No	No
3	32	10	42	No	No
4	21	8	29	No	No
5	32	6	38	No	No
Average	27	16			
SD	7	11			

Table IV-12 The combustion time and characteristics of the DGEBA/5% LDH-DPP cured with the DDS.

Sample	Combustion time after the first ignition (s)	Combustion time after the second ignition (s)	Total time of combustion (s)	Flame to clamp	Dripping
1	45	187	232	Yes	Yes
2	90	172	262	Yes	Yes
3	68	182	250	Yes	Yes
4	80	191	271	Yes	Yes
5	59	202	261	Yes	Yes
Average	68	187			
SD	18	11			

Table IV-13 The combustion time and characteristics of the DGEBA/10% LDH-DPP cured with the DDS.

Sample	Combustion time after the first ignition (s)	Combustion time after the second ignition (s)	Total time of combustion (s)	Flame to clamp	Dripping
1	21	164	185	No	No
2	18	133	151	No	No
3	26	156	182	No	No
4	34	169	203	No	No
5	31	175	206	No	No
Average	26	159			
SD	7	16			